Fugitive Dust and Other Source Contributions to PM$_{10}$ in Nevada's Las Vegas Valley

Volume II – Final Report

DRI Document No. 4039.2F1

April 18, 1997

PRINCIPAL INVESTIGATORS:

Dr. Judith C. Chow
Dr. John G. Watson

Desert Research Institute
P.O. Box 60220
Reno, NV 89506

PREPARED FOR:

Mr. Will Cates
Clark County Department of Comprehensive Planning
Clark County Government Center
500 South Grand Central Parkway
Las Vegas, NV 89155

ADDITIONAL CONTRIBUTORS:

Dr. Mark C. Green
Mr. Richard T. Egami
Dr. Douglas H. Lowenthal
Dr. John A. Gillies
Dr. C. Fred Rogers
Mr. David DuBois

Mr. Clifton L. Frazier
Mr. Jerry Derby
Mr. Daniel L. Freeman
Mr. Steven Kohl
Mr. Timothy Minor

ACKNOWLEDGEMENTS

TABLE OF CONTENTS

ii

LIST OF TABLES

vi

LIST OF TABLES (continued)

LIST OF TABLES (continued)

LIST OF FIGURES

1.0 INTRODUCTION

1.1 Background

The Las Vegas Valley is located within Clark County in the southern part of Nevada. The valley comprises approximately 3,745 square kilometers (1,463 square miles) and includes three incorporated cities (Las Vegas, North Las Vegas, and Henderson) and five unincorporated towns.

Geographically, the Las Vegas Valley lies in the southwestern part of the Great Basin; extends in a northwest to southeast direction, draining toward the south through the Las Vegas Wash into Lake Mead; and ranges in elevation from 550 to 760 meters above mean sea level (m amsl). It is surrounded by sharp, rugged mountain ranges that range in elevation up to 3,600 m amsl. The valley is bounded on the northeast by the Nellis Air Force Base Ground Gunnery Range, on the west by the Spring Mountains, on the south by the McCullough Mountains and Spring Mountains, and on the east by the River Mountains and Frenchman Mountain.

The climate in the valley is generally arid and warm. The Sierra Nevada Mountain Range of California and the Spring Mountains to the west of the Las Vegas Valley act as effective barriers to moisture-laden storms moving eastward from the Pacific Ocean (National Climatic Data Center, 1995). The movement of these dry air masses results in clear to partially cloudy skies with 85% sunshine for an average year. Temperature typically ranges from 75 to 105 °F in the summer and 35 to 60 °F in the winter. Annual precipitation averages 0.1 m (4 inches) per year with a variation of 0.05 to 0.25 m (2 to 10 inches) in the past decade in the Las Vegas Valley. Most of the precipitation occurs during the winter and summer months.

Surface wind patterns in the valley are characterized by prevailing southwesterly winds with average wind speeds of 4 to 7 meters per second (m/s) (9 to 16 miles per hour [mph]). High hourly wind speeds often occur during the spring and summer with maximum wind speeds of 10 to 15 m/s (23 to 34 mph). During winter, persistent surface-based radiation inversions are frequently observed with low to stagnant winds.

Clark County is the fastest-growing county in the nation. The 1995 U.S. Census reports a population of over 1 million (60% of Nevada's total population). Its major industries are tourism, gaming, government/defense, chemical manufacturing, quarry operations, and construction. Growing population and expanding industry in the Las Vegas Valley have resulted in elevated concentrations of PM_{10} (particles with aerodynamic diameters less than 10 microns). Measured PM_{10} levels often exceed the National

of 150 $\mu g/m^3$ for PM_{10} 24-hour averages and/or 50 $\mu g/m^3$ for PM_{10} annual averages. Table 1-1 presents the annual statistics of PM_{10} concentrations in the Las Vegas Valley between 1988 and 1995. Fugitive dust suspended by high winds or other mechanical forces in the atmosphere is the major cause of these elevated PM_{10} concentrations.

In 1991, the U.S. Environmental Protection Agency (EPA) designated the Las Vegas Valley as a "moderate" PM_{10} non-attainment area (Federal Register, 1991). The area was subsequently designated as a "serious" PM_{10} non-attainment area in 1993 (Federal Register, 1993). As shown in Figure 1-1, the air quality non-attainment area in the Las Vegas Valley, which coincides with Hydrographic Basin 212, encompasses 15,000 square kilometers (5,859 square miles) in size, and includes the cities of Las Vegas, North Las Vegas, and Henderson, as well as unincorporated areas in Clark County.

The 1990 Clean Air Act Amendments (CAAA) (U.S. Government Printing Office, 1991) requires states to develop and submit State Implementation Plans (SIPs) that specify the technologies, activities, and strategies that will be applied in each PM_{10} non-attainment area to achieve compliance with the PM_{10} standards. A Las Vegas Valley PM_{10} SIP was submitted to the U.S. EPA by the State of Nevada, Department of Conservation and Natural Resources, Division of Environmental Protection on 01/10/95 to address the "serious" non-attainment status. A revised PM_{10} SIP will be submitted to the U.S. EPA during the summer of 1997 that proposes attainment of the national PM_{10} standards by 2001 (Jacquart, 1997).

The purpose of this study is to measure and model fugitive dust and other source contributions to PM_{10} in the an urban portion of the Las Vegas Valley nonattainment area in order to provide additional information for Las Vegas Valley PM_{10} SIP development.

1.2 Study Objectives

The objectives of this study are:

- To acquire a data base of specified precision, accuracy, and validity which is suitable to determine source contributions of elevated PM_{10} concentrations.

- To estimate the spatial and temporal distributions of PM_{10} concentrations, especially near fugitive dust sources.

- To apportion PM_{10} concentrations to source emissions, with emphasis on specific sources of fugitive dust.

- To estimate fugitive dust contributions based on existing PM_{10} emissions information.

Table 1-1
Annual Statistics of PM$_{10}$ Concentrations in the Las Vegas Valley[a]

Year	Sampling Site[b]	Maximum 24-Hour PM$_{10}$ ($\mu g/m^3$)	Annual Arithmetic Avg. ($\mu g/m^3$)	Number of Values $>150\mu g/m^3$	Number of Values $>50\mu g/m^3$	Total Number of Observations
1988	Frias	41	18	0	0	57
	McDaniel Post Office	93	40	0	37	169
	Bonanza	94	35	0	6	58
	Wengert	161	58	1	28	58
	Burkholder	84	38	0	0	46
1989	Frias	86	23	0	6	52
	McDaniel Post Office	359	60	3	69	167
	Bonanza	104	39	0	9	59
	Wengert	159	69	1	33	58
	Burkholder	91	36	0	12	54
1990	Frias	125	22	0	14	46
	McDaniel Post Office	362	70	3	26	57
	Bonanza	135	39	0	26	57
	Wengert	368	64	3	26	59
	Burkholder	227	33	1	8	58
1991	Frias	345	26	1	3	55
	McDaniel Post Office	110	55	0	25	52
	Bonanza	184	35	1	6	53
	Wengert	122	57	0	31	54
	Burkholder	157	36	1	10	58
1992	Frias	66	18	0	1	51
	McDaniel Post Office	121	53	0	27	49
	Bonanza	58	29	0	0	58
	Wengert	101	46	0	17	53
	Burkholder	53	24	0	1	58
1993	Frias	68	20	0	2	60
	McDaniel Post Office	117	41	0	9	54
	Bonanza	76	29	0	6	58
	Wengert	112	43	0	3	57
	Burkholder	51	22	0	0	60
1994	Frias	46	21	0	0	59
	McDaniel Post Office	117	47	0	23	57
	Bonanza	89	35	0	4	56
	Wengert	122	47	0	21	55
	Burkholder	46	21	0	0	56
1995	Frias	NA[c]	NA[c]	NA[c]	NA[c]	NA[c]
	McDaniel Post Office	126	47	0	17	49
	Bonanza	56	25	0	1	11[d]
	Wengert	58	31	0	2	15[d]
	Burkholder	NA[c]	NA[c]	0	NA[c]	NA[c]
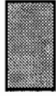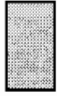
[a] Courtesy of Clark County Health Department.
[b] Only the high-volume size-selective inlet (HIVOL-SSI) PM$_{10}$ sites are included.
[c] Monitoring discontinued in January 1995.
[d] Monitoring discontinued in March 1995.

CLARK COUNTY
WITHIN NON-ATTAINMENT AREA

- NON-ATTAINMENT AREA
- LAKE MEAD
- CLARK COUNTY
- BLM DISPOSAL AREA
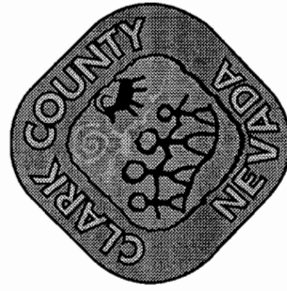
COMPREHENSIVE PLANNING
Advanced Planning Division

This information is for display only. No liability is assumed as to accuracy of the data delineated hereon.
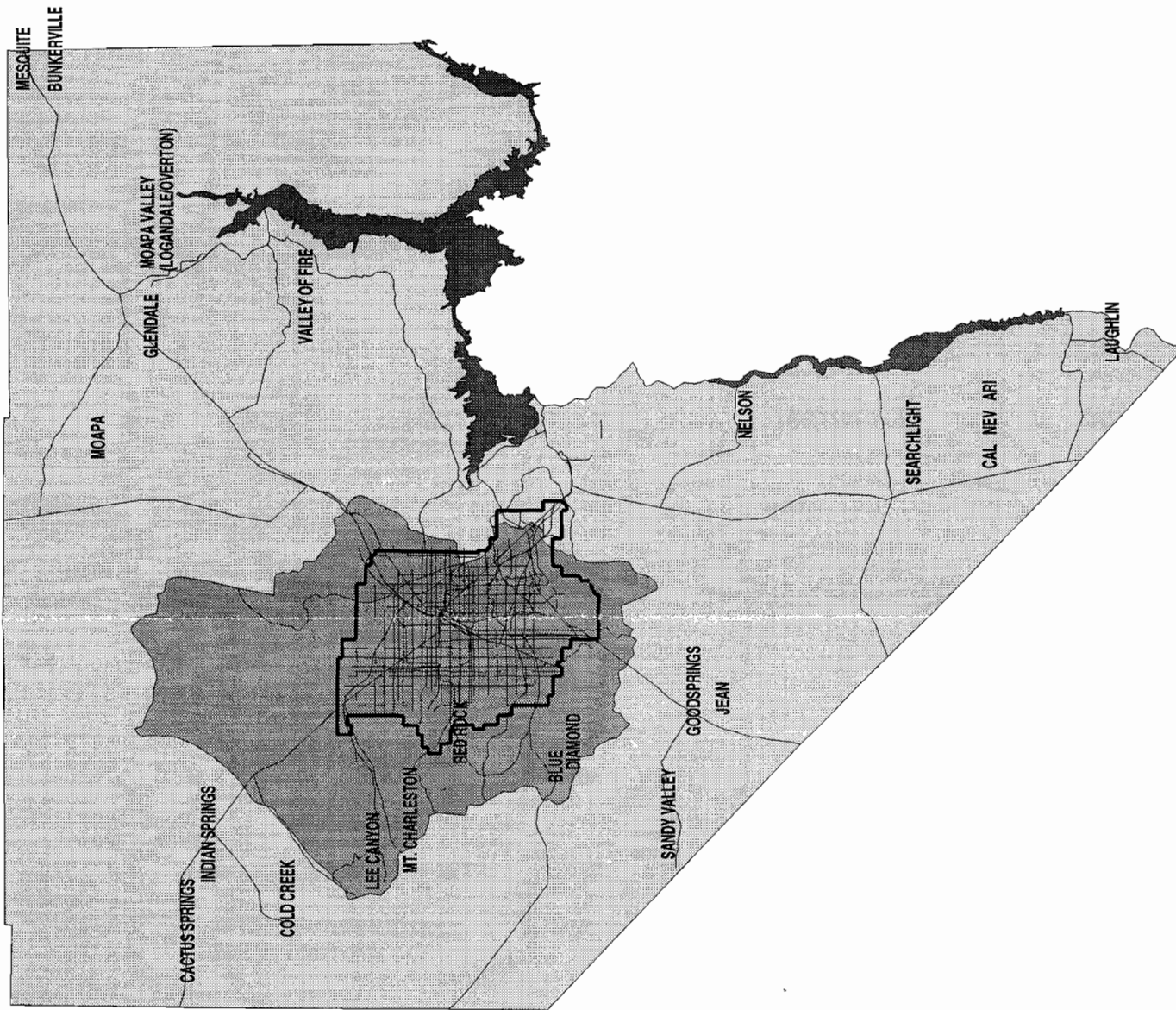
Figure 1-1 PM_{10} nonattainment area in the Las Vegas Valley.

- To reconcile differences between source and receptor models.

- To evaluate and recommend long-term monitoring and data analysis methods which allow the effects of emissions reductions on ambient PM_{10} concentrations to be detected.

Concurrent efforts were made to evaluate the effectiveness of potential fugitive dust control measures that could be implemented in the Las Vegas Valley to reduce PM_{10} concentrations.

1.3   Technical Approach

This study is designed to better understand the source and nature of the elevated PM_{10} levels in the Las Vegas Valley. Both source- and receptor-oriented modeling approaches were taken to apportion PM_{10} to emission sources. Source and receptor models are complementary, with each type having strengths which compensate for the weaknesses of the other. Source models simulate the emissions, transport, dispersion, and chemical transformations of pollutants to calculate the concentrations contributed by each source to a receptor. Receptor models use the chemical and physical characteristics of gases and particles measured at source and receptor to identify and quantify source contributions to the measured receptor concentrations.

Several air quality models were applied in this study. They are: 1) the Chemical Mass Balance (CMB) source apportionment receptor model (Watson *et al.*, 1984, 1990a, 1990b, 1991a), 2) the Cluster Analysis receptor model (a multivariate statistical analysis tool), 3) the Geographical Information System (GIS) emission data base model (Chow and Watson, 1994a), and 4) the Industrial Source Complex dispersion model (ISC3, Winges, 1990a, 1990b; Winges and Gombar, 1990a, 1990b).

In the receptor-oriented source apportionment approach, chemical properties are measured at sources to develop a fingerprint of each major emissions source type. These "source profiles" are then used in receptor models to calculate the amount which each source type contributes to PM_{10} concentrations measured at receptors. Since fugitive dust was suspected of being a major contributor to suspended particles, and since the source profiles for fugitive dust sources are too similar to allow their separation, other receptor- and source-oriented approaches were included in the study design. Several intensive monitoring periods were superimposed on the annual monitoring period to characterize seasonal emissions under different meteorological conditions. During these periods, 24-hour average samples were taken at 30 sampling sites located within, nearby, and far away from different fugitive emissions source types. These data were intended to support the use of spatial and temporal receptor models, in addition to the well-established CMB model (U.S. Environmental

1-5

Protection Agency, 1987a, 1987b; Watson *et al.*, 1984, 1990a, 1990b, 1991a) that is commonly used to support SIP development.

As complements to receptor models, the source-oriented ISCST-3 dispersion model was also applied to simulate meteorological transport and diffusion and to estimate the fugitive dust impacts to PM_{10} from different geological source types. The dispersion model results are compared to the ambient measurements taken at the receptor sites to evaluate the adequacy of the current emissions inventory and to reconcile the differences in source and receptor modeling.

Existing emissions inventories were evaluated with respect to their emissions factors and activity levels. Microinventories surrounding the two base monitoring sites were developed. Fugitive dust emission data bases were assembled. A geographical information system (GIS) emission data base model was developed to calculate the fugitive dust emission rates for paved and unpaved roads, construction activities, and disturbed/undisturbed vacant land. Other potential particulate matter emission sources such as on-road and off-road vehicle exhaust, residential wood combustion, sand and gravel plants, natural gas combustion, aircraft operations, and natural desert background were investigated. Information on emission factors and/or activity levels from these other potential sources were incomplete, so their estimated emissions were not included in the GIS emissions data base model. The relative abundance of major fugitive dust emission sources identified in this report may be positively biased due to the omission of some other potential sources.

In the ambient sampling program, the Desert Research Institute (DRI) acquired PM_{10} measurements at two base sites in the cities of Las Vegas (i.e., East Charleston) and North Las Vegas (i.e., Bemis) between 01/03/95 and 01/28/96 on an every-sixth-day sampling schedule, as well as during mini-intensive (12/23/95 to 01/04/96) and five intensive monitoring periods on a daily basis. DRI operated a saturation monitoring network consisting of 30 satellite sites during the spring (04/15/95 to 04/21/95 and 05/12/95 to 05/16/95), summer (06/05/95 to 06/07/95), fall (09/07/95 to 09/12/95), and winter (01/26/96 to 01/30/96) intensive monitoring periods. These periods of intensive monitoring were chosen based on meteorological forecasting for high wind and typical conditions.

Source emissions for fugitive dust, motor vehicle exhaust, and residential wood combustion were sampled and chemically characterized. Ambient and source PM_{10} samples were analyzed for mass, elements (i.e., sodium [Na] to uranium [U]), ions (i.e., chloride [Cl⁻], nitrate [NO_3^-], sulfate [$SO_4^=$], ammonium [NH_4^+], soluble potassium [K⁺]), and carbon (organic carbon [OC] and elemental carbon [EC]).

These data were supplemented with: 1) hourly average beta-attenuation measurements of PM_{10} mass concentrations, and 2) hourly meteorological data acquired in

the Las Vegas Valley by the Clark County Health District (CCHD). All of these data were assembled into a documented data base in common units, available in PC-DOS-compatible Xbase formats. The study design is described in greater detail by Chow *et al.* (1995).

1.4   Guide to Report

This section has stated the background and objectives of the Las Vegas Valley PM_{10} Study. Section 2 documents the ambient monitoring network, the supplemental data acquired from existing CCHD monitoring networks, and the unified data base compiled from these measurements. Validity and uncertainty of the PM_{10} fugitive dust emission rates are evaluated in Section 3, and the emissions inventory of the Las Vegas Valley and microinventories of the two base monitoring sites are assembled. Emission source characterization is summarized in Section 4, from which the chemical source profiles for fugitive dust, motor vehicle exhaust, and residential wood combustion used in CMB modeling are derived. The ambient and source data bases are assembled, validated, and documented in Section 5. Section 6 examines the temporal and spatial variations of PM_{10} and evaluates the representativeness of the base monitoring sites. Source and receptor modeling approaches and results are shown in Section 7, in which fugitive dust zones of influence are evaluated. Transport of fugitive dust and the relationships between PM_{10} and meteorology are shown in Section 8. Fugitive dust demonstration studies are reviewed and the effectiveness of control measures are evaluated. Control measures applicable in the Las Vegas Valley to reduce PM_{10} fugitive dust emissions are discussed in Section 9. Summary, conclusions, and recommendations are contained in Section 10. The bibliography and references are assembled in Section 11. Details about the ambient and source data base and dispersion model input are included in a series of appendices.

2.0   AMBIENT MEASUREMENTS

The program plan (Chow *et al.*, 1995) provides justification for the observables, sampling durations, sampling frequency, and monitoring periods for the Las Vegas Valley PM_{10} Study measurements.   This section describes the particulate and meteorological networks, documents the measurement methods, and evaluates the measurements themselves.

2.1   Aerosol and Meteorological Sampling Networks

The ambient particulate and meteorological monitoring network for this study consisted of 63 sampling sites, including:

- 2 PM_{10} base monitoring sites in Las Vegas (i.e., East Charleston) and North Las Vegas (i.e., Bemis) with sequential filter samplers (SFS) operated by the Desert Research Institute (DRI).

- 30 PM_{10} satellite monitoring sites with battery-powered portable PM_{10} samplers operated by DRI.

- 14 PM_{10} monitoring sites (including 1 compliance monitoring site with high-volume samplers equipped with PM_{10} size-selective inlets [HIVOL-SSI], 6 compliance monitoring sites with beta attenuation monitors [BAM], and 7 special-purpose sites with BAMs) operated by the Clark County Health District (CCHD),
.

- 17 meteorological monitoring sites with 10-m-height meteorological towers operated by CCHD.

Table 2-1 documents the sampling site locations, descriptions, coordinates, elevations, and measurements acquired by the CCHD air quality and meteorology monitoring network since 1985. Existing PM_{10} (i.e., compliance and special-purpose) and meteorological sampling site locations are shown in Figure 2-1.

With respect to the Las Vegas Valley PM_{10} Study, the filter-based PM_{10} measurements, averaging times, sampling frequency/periods, and measurement methods are detailed in Table 2-2. The layout of the monitoring locations for this study is illustrated in Figure 2-2. These sampling sites were selected to represent different commercial, residential, construction, and vacant land uses, and to characterize source emissions transport and impact in the Las Vegas Valley.

PM_{10} measurements were made at the base and satellite sites from 01/03/95 to 01/30/96. Ambient PM_{10} sampling consisted of the following elements:

Table 2-1

PM$_{10}$ Air Quality and Meteorological Monitoring Network in the Non-Attainment Area of the Las Vegas Valley

Site Location	Start Year	End Year	Air Quality Observable	Air Quality Instrument Type	Meteorological Measurements	UTM East	UTM North	Elev. (m) Above Ground	Above MSL	Description
Frias 10245 S. Schuster Las Vegas, NV 89118 (FRIC)	1987	1994	PM$_{10}$ Fine (0-2.5 µm) Coarse (2.5-10 µm)	PM$_{10}$ (SSI) Particulate Monitor (Graseby-Andersen) Dichotomous Particulate Monitor (Graseby-Andersen)		662781	3998018	1.5	716	This site is located in a rural residential area. Traffic is light. Freeway I-15 is nearby with moderate to heavy traffic.
Flamingo 366 E. Flamingo Las Vegas, NV 89110 (FLAC)	1992		PM$_{10}$ O$_3$	Beta-Attenuation Monitor (Graseby-Andersen) Ultraviolet Absorption Ozone Analyzer (Dasibi 1003H)	Temperature Wind Speed Wind Direction Relative Humidity	665976	3998058	3.5	600	This site is located in an urban commercial area. Traffic is heavy.
Bemis (A.K.A Craig) 4701 Mitchell St. North Las Vegas, NV 89031 (BEMC)	1992 1991 1991		PM$_{10}$ NO$_x$/NH$_3$ O$_3$	Beta-Attenuation Monitor (Graseby-Andersen) Chemiluminescent NO$_x$ Analyzer (Monitor Labs 8840) Ultraviolet Absorption Ozone Analyzer (Dasibi 1003H)	Temperature Wind Speed Wind Direction Relative Humidity	671439	4012654	3.5	625	This site is located amongst commercial development. Traffic from nearby Craig Rd. and Interstate 5 is moderate.

Table 2-1 (continued)
PM$_{10}$ Air Quality and Meteorological Monitoring Network
in the Non-Attainment Area of the Las Vegas Valley

Site Location	Start Year	End Year	Air Quality Observable	Air Quality Instrument Type	Meteorological Measurements	UTM East	UTM North	Elev. (m) Above Ground	Above MSL	Description
McDaniel Post Office 1414 E. Lake Mead Blvd. North Las Vegas, NV 89115 (MPOC)	1985		PM$_{10}$	PM$_{10}$ (SSI) Particulate Monitor (Wedding & Associates)		668716.8	4007135	7	588	This site is located in a suburban commercial area. Traffic is heavy.
Bonanza 215 E. Bonanza Las Vegas, NV 89101 (CCEC)	1989		PM$_{10}$	PM$_{10}$ (SSI) Particulate Monitor (Wedding & Associates)		667440.3	4004817	7	616	This site is located in an urban commercial area. Nearby traffic is heavy and Freeway I-95 is nearby.
City Center 559 N. 7th St. Las Vegas, NV 89101 (CCWC)	1993		PM$_{10}$	Beta-Attenuation Monitor (Graseby-Andersen)	Temperature Wind Speed Wind Direction	656382.9	40040170	3.5	616	This site is located in an urban commercial area. Nearby traffic is heavy and Freeway I-95 is nearby.
	1987		CO	Infrared CO Analyzer (Dasibi 3008)						
	1987		NO$_2$	Chemiluminescent NO$_x$ Analyzer (Monitor Labs 8840)						
	1987		O$_3$	Ozone Analyzer (Environics)						

Table 2-1 (continued)

PM$_{10}$ Air Quality and Meteorological Monitoring Network
in the Non-Attainment Area of the Las Vegas Valley

Site Location	Start Year	End Year	Air Quality Observable	Air Quality Instrument Type	Meteorological Measurements	UTM East	UTM North	Elev. (m) Above Ground	Elev. (m) Above MSL	Description
Maycliff 4001 Sahara Ave. Las Vegas, NV 89104 (MAYC)	1991		PM$_{10}$	Beta-Attenuation Monitor (Graseby-Andersen)	Temperature Relative Humidity Wind Speed Wind Direction	672246	4001458	3.5	516	This site is located in an urban residential/commercial area. Traffic is moderate to heavy.
	1989		CO	Infrared CO Analyzer (Dasibi 3008)						
Wengert 2001 Winterwood Blvd. Las Vegas, NV 89122 (WENC)	1987		PM$_{10}$	PM$_{10}$ (SSI) Particulate Monitor (Graseby-Andersen)		674818.5	4002068	5	524	This site is located in a suburban residential area. Traffic is moderate to light with heavy traffic on Nellis Blvd.
Burkholder 335 W. Van Wagenen Henderson, NV 89015 (BURC)	1988	1994	PM$_{10}$	PM$_{10}$ (SSI) Particulate Monitor (Wedding & Associates)		667200	3989000	4	579	This site is located in a suburban residential area of Henderson. Traffic is light to moderate.
Powerline 545 W. Lake Mead Dr. Henderson, NV 89015 (POWC)	1990		PM$_{10}$	Beta-Attenuation Monitor (Graseby-Andersen)	Temperature Wind Speed Wind Direction	681200	398800	3.5	570	This site is located in an urban residential/commercial area. Traffic is moderate.
	1980		O$_3$	Ultraviolet Ozone Analyzer (Dasibi 1003H)						

Table 2-1 (continued)
PM$_{10}$ Air Quality and Meteorological Monitoring Network in the Non-Attainment Area of the Las Vegas Valley

Site Location	Start Year	End Year	Air Quality Observable	Air Quality Instrument Type	Meteorological Measurements	UTM East	UTM North	Elev. (m) Above Ground	Above MSL	Description
Kerr McGee 8000 W. Lake Mead Henderson, NV (KMGC)	1980		NO$_x$/NH$_3$	Chemiluminescent NO$_x$ Analyzer (Monitor Labs 8840)						
	1982	1994	NO$_x$/NH$_3$	Chemiluminescent NO$_x$ Analyzer (Monitor Labs 8840)	Temperature Wind Speed Wind Direction	680128.5	3990233	NA	560	This site is located in a suburban/commercial area. Traffic is moderate.
Health District 625 Shadow Ln. Las Vegas, NV 89106 (CHDC)	1989		CO	Infrared CO Analyzer (Dasibi 3008)	Temperature Wind Speed Wind Direction	665303.5	4003473	6.5	590	This site is located in a suburban residential area. Traffic is light.
	1989		O$_3$	Ultraviolet Ozone Analyzer (Dasibi 1003H)						
Pittman 1137 N. Boulder Wy. Las Vegas, NV 89015 (PITC)	1994		PM$_{10}$	Beta-Attenuation Monitor (Graseby-Andersen)	Temperature Relative Humidity Wind Speed Wind Direction	680390	3991640	4.5	NA	This site is located in a commercial storage area. Traffic is light.
	1994		NO$_x$/NH$_3$	Chemiluminescent NO$_x$ Analyzer (Monitor Labs 8840)						

Table 2-1 (continued)
PM$_{10}$ Air Quality and Meteorological Monitoring Network in the Non-Attainment Area of the Las Vegas Valley

Site Location	Start Year	End Year	Air Quality Observable	Air Quality Instrument Type	Meteorological Measurements	UTM East	UTM North	Elev. (m) Above Ground	Above MSL	Description
Microscale E.L. 2801 E. Charleston Las Vegas, NV 89104 (MICC)	1994		PM$_{10}$	Beta-Attenuation Monitor (Graseby-Andersen)		669947.5	4002997	4.0	567	This site is located in a suburban commercial area. Traffic is heavy.
	1994		CO	Ultraviolet CO Analyzer (Dasibi 3003)						
McMillan 7000 Walt Lott Dr. Las Vegas, NV	1993		PM$_{10}$	PM$_{10}$ (SSI) Particulate Monitor (Wedding & Associates)		657666	4006537	5.0	NA	This site is located in a suburban commercial/ residential area. Traffic is moderate.
Diskin 4200 Ravenwood Drive Las Vegas, NV 89117	1993	1994	PM$_{10}$	PM$_{10}$ (SSI) Particulate Monitor (Wedding & Associates)		657830	3997516	5.0	NA	This site is located in a suburban commercial/ residential area. Traffic is moderate.
Dime III 2908 Gavilan Lane Las Vegas, NV 89122	1993		NO$_x$/NH$_3$	Chemiluminescent NO$_x$ Analyzer (Monitor Labs 8840)	Temperature Wind Speed Wind Direction	675429	4000654	NA	NA	NA
East Charleston 2850 East Charleston Las Vegas, 89104	1989		CO	Ultraviolet CO Analyzer (Dasibi 3008)		670092.1	4003036	NA	NA	This site is located in a suburban commercial area. Traffic is heavy.

Table 2-1 (continued)
PM$_{10}$ Air Quality and Meteorological Monitoring Network
in the Non-Attainment Area of the Las Vegas Valley

Site Location	Start Year	End Year	Air Quality Observable	Air Quality Instrument Type	Meteorological Measurements	UTM East	UTM North	Elev. (m) Above Ground	Above MSL	Description
	1989		NO$_x$/NO	Chemiluminescent NO$_x$ Analyzer	Temperature Wind Speed Wind Direction				.	
McDaniel 1600 Lake Mead Blvd. Las Vegas, NV 89115	1994		PM$_{10}$	Beta-Attenuation Monitor (Graseby-Andersen)	Temperature Wind Speed Wind Direction	668832	400721	NA	NA	
Meyer 4525 New Forest Dr. Las Vegas, NV 89117			PM$_{10}$	Beta-Attenuation Monitor (Graseby-Andersen)	Temperature Wind Speed Wind Direction	657191	3997118	NA	NA	
Walter John 7701 Ducharme Ave. Las Vegas, NV	1995		PM$_{10}$	Beta-Attenuation Monitor (Graseby-Andersen)	Temperature Wind Speed Wind Direction	656382.9	4004017	NA	NA	
Winterwood 5483 Club House Dr. Las Vegas, NV 89122	1989		CO	Ultraviolet CO Analyzer (Dasibi 3008)	Temperature Wind Speed Wind Direction	675024.9	4001446			
	1989		O$_3$	Ultraviolet Ozone Analyzer						
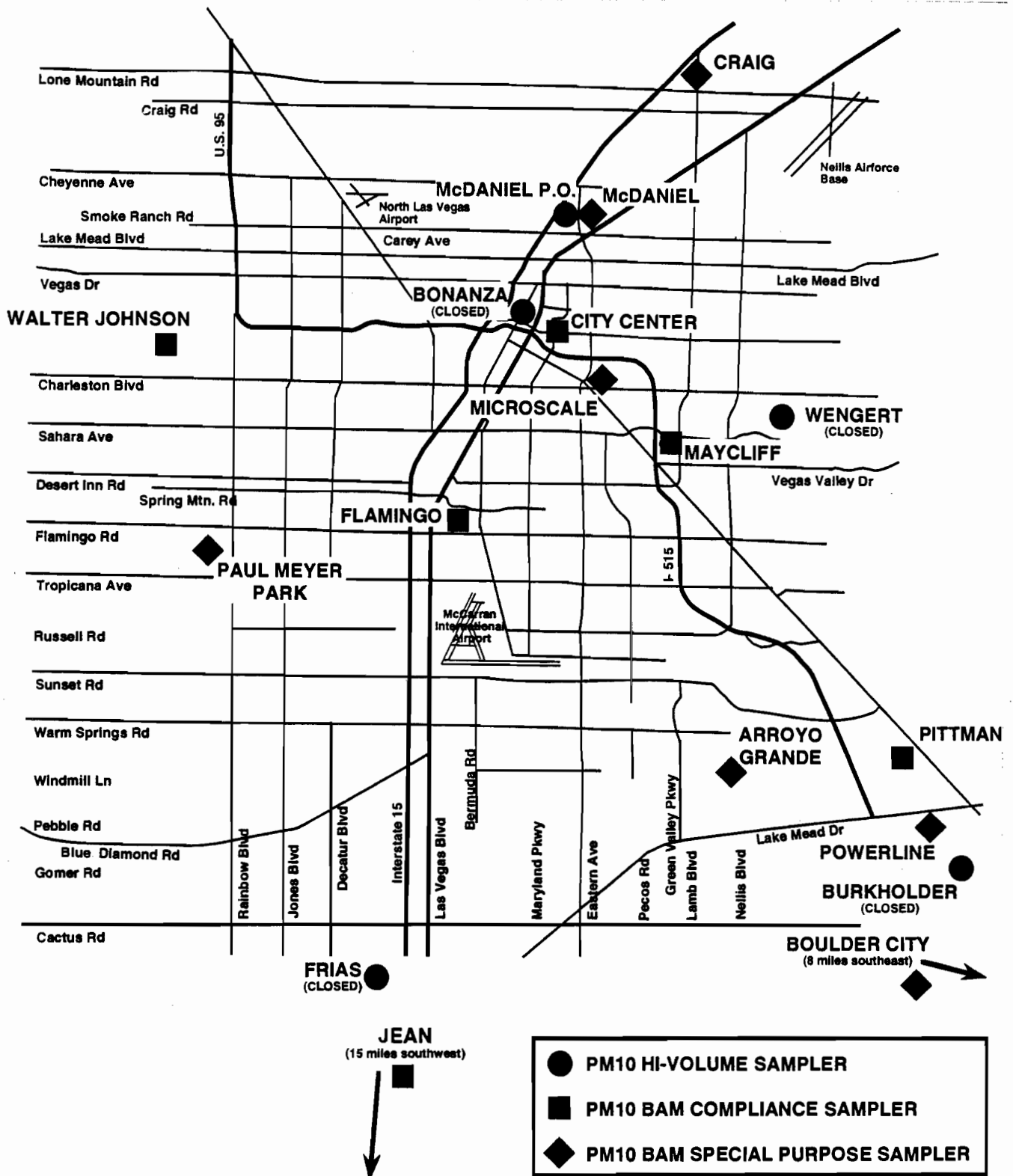
Figure 2-1   PM$_{10}$ and meteorological sampling site locations.

Table 2-2
Filter Pack Aerosol Measurements for the Las Vegas Valley PM$_{10}$ Study

Ambient Measurement	Sampling Site	Averaging Time	Sampling Frequency and Period	Measurement Instrument
PM$_{10}$	2 base sites (East Charleston and Bemis)	24-hour	Every-sixth-day between 01/03/95 and 01/28/96	DRI Sequential Filter Sampler (SFS) with SA 254I PM$_{10}$ medium-volume inlet and nitric acid denuders
		24-hour	Daily between 12/23/95 and 01/04/96	DRI Sequential Filter Sampler (SFS) with SA 254I PM$_{10}$ medium-volume inlet and nitric acid denuders
PM$_{10}$	30 satellite sites	24-hour	Daily for the periods of spring (04/15/95 to 04/21/95 and 05/12/95 to 05/16/95), summer (06/05/95 to 06/07/95), fall (09/07/95 to 09/12/95), and winter (01/26/96 to 01/30/96)	Battery-Powered Portable PM$_{10}$ Sampler
PM$_{10}$ Mass	Base and satellite sites	24-hour	All periods	Gravimetric analysis on Teflon-membrane filters (Cahn 31 electromicrobalance)
PM$_{10}$ Particle Light Absorption	Base and satellite sites	24-hour	All periods	Light transmission on Teflon-membrane filters (Tobias TBX-10 densitometer)
PM$_{10}$ Elements	Base sites (SFS samples only)	24-hour	During selected intensive[a] and nonintensive[b] 14-day periods	X-Ray Fluorescence analysis on Teflon-membrane filters (Kevex 0700/0800 XRF analyzer)[c]
PM$_{10}$ Elements	Satellite sites	24-hour	During selected intensive[a] and nonintensive[b] 14-day periods	X-Ray Fluorescence analysis on Teflon-membrane filters (Kevex 0700/0800 XRF analyzer)[c]

Table 2-2 (continued)
Filter Pack Aerosol Measurements for the Las Vegas Valley PM$_{10}$ Study

Ambient Measurement	Sampling Site	Averaging Time	Sampling Frequency and Period	Measurement Instrument
PM$_{10}$ Water-Soluble Chloride (Cl⁻), Nitrate (NO$_3^-$), and Sulfate (SO$_4^=$) Ions	Base sites (SFS samples only)	24-hour	During selected intensive[a] and nonintensive[b] 14-day periods	Ion Chromatographic analysis on quartz-fiber filter extracts (Dionex 2020i ion chromatograph)
PM$_{10}$ Volatilized Nitrate (NO$_3^-$)	Base sites (SFS samples only)	24-hour	During selected intensive[a] and nonintensive[b] 14-day periods	Ion Chromatographic analysis on nylon-membrane filter extracts (Dionex 2020i ion chromatograph)
PM$_{10}$ Water-Soluble Potassium (K⁺)	Base sites (SFS samples only)	24-hour	During selected intensive[a] and nonintensive[b] 14-day periods	Atomic Absorption Spectrophotometry on quartz-fiber filter extracts (Perkin-Elmer Model 2380 System)
PM$_{10}$ Water-Soluble Ammonium (NH$_4^+$)	Base sites (SFS samples only)	24-hour	During selected intensive[a] and nonintensive[b] 14-day periods	Technicon Automatic Colorimetry on quartz-fiber filter extracts (TRAACS 800 System)
PM$_{10}$ Organic and Elemental Carbon (OC, EC)	Base sites (SFS samples only)	24-hour	During selected intensive[a] and nonintensive[b] 14-day periods	Thermal/Optical Reflectance Carbon Analysis on pre-fired quartz-fiber filters (DRI/OGC Thermal/Optical Reflectance Carbon Analyzer)

---

[a] 14 intensive days are: 06/05/95 to 06/07/95, 09/07/95 to 09/12/95, and 01/26/96 to 01/30/96.

[b] 14 nonintensive days are: 04/09/95, 04/27/95, 11/23/95, 12/24/95 to 01/02/96, and 01/16/96.

[c] For six elements: aluminum (Al), silicon (Si), sulfur (S), potassium (K), calcium (Ca), and iron (Fe).
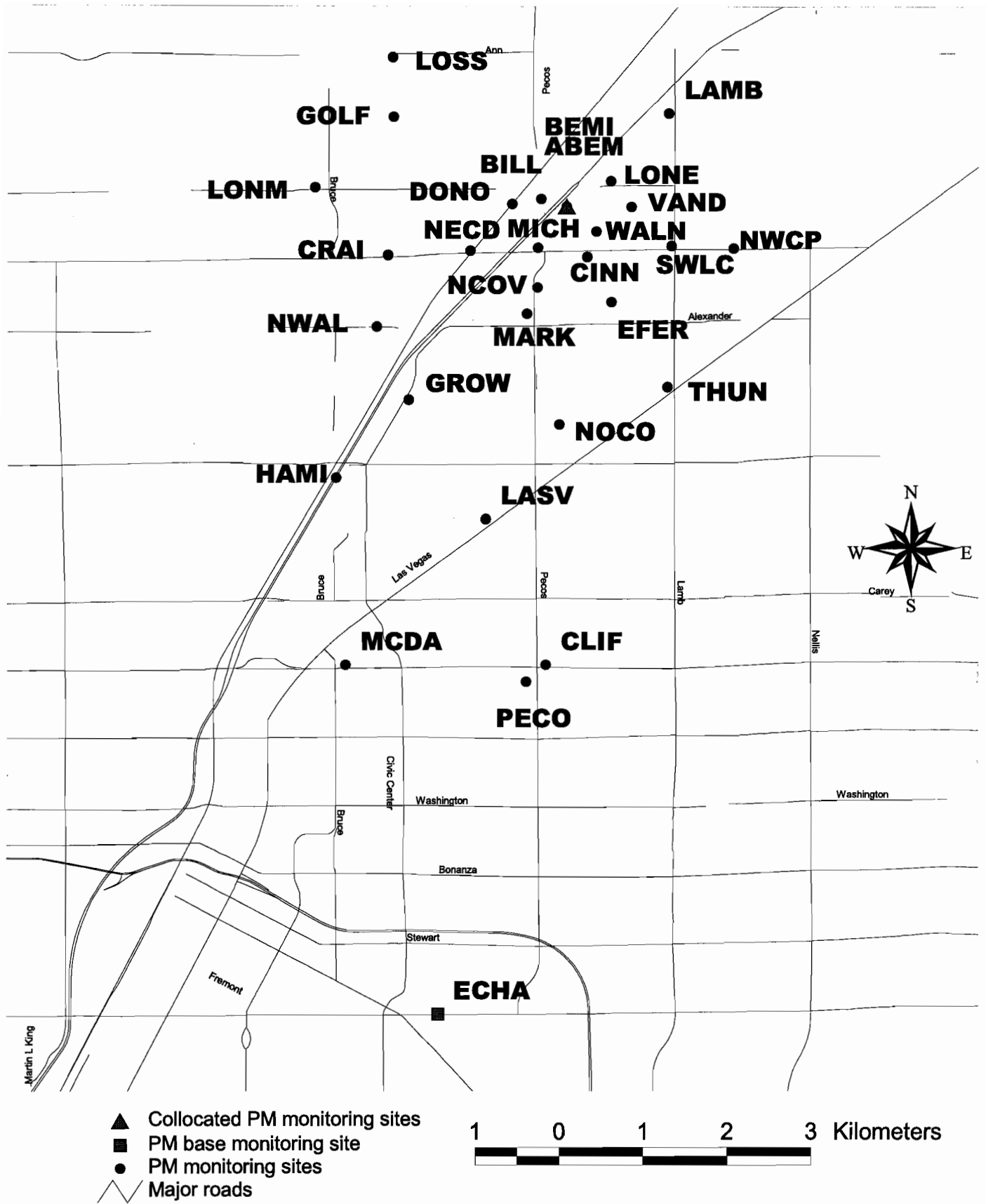
Figure 2-2   Layout of monitoring locations for the Las Vegas Valley PM$_{10}$ Study.

- *Annual Sampling:* Every-sixth-day sampling of PM_{10} was conducted at the two base sites between 01/03/95 and 01/28/96 for a total of 59 sampling days, with sequential filter samplers (SFSs). This sampling period was intended to correspond to the schedule normally followed by the U.S. EPA compliance monitoring network, and to calculate annual average PM_{10} concentrations. Unusually low PM_{10} concentrations were found during January 1995; consequently, the monitoring period was extended through January 1996.

- *Intensive Sampling*: Daily, once-per-day sampling of PM_{10} was conducted at the two base sites and thirty satellite sites during spring (04/15/95 to 04/21/95 and 05/12/95 to 05/16/95), summer (06/05/95 to 06/07/95), fall (09/07/95 to 09/12/95), and winter (01/26/96 to 01/30/96) periods, for a total of 26 sampling days with SFSs and portable PM_{10} survey samplers. The intensive sampling periods were selected to characterize high PM_{10} that corresponded to unique emissions and meteorological situations. The spring, summer, and fall intensives characterized local fugitive dust over prolonged dry periods with occasional high winds. The winter intensive captured particle emissions from motor vehicles, residential wood combustion, and resuspended dust during typical winter conditions.

- *Mini-Intensive Sampling*: Daily, once-per-day sampling of PM_{10} was conducted at the two base sites between 12/23/95 and 01/04/96, for a total of 13 sampling days with SFSs, to characterize increased anthropogenic activities during the holiday season.

The satellite monitoring sites were chosen to measure and evaluate the near-field fugitive dust impact on PM_{10} concentrations in the Las Vegas Valley. Portable PM_{10} survey samplers were located adjacent to or around specific fugitive dust emission sources. Table 2-3 summarizes the site locations and surrounding land use types for the 30 satellite sites. Detailed site maps are provided in Appendix A of the program plan (Chow *et al.*, 1995).

2.2 Ambient Particulate Measurements

Twenty-four-hour filter-based PM_{10} measurements acquired with high-volume, medium-volume, and low-volume sampling systems along with hourly PM_{10} measurements acquired with beta-attenuation monitors were examined. The measurement methods are described below.

Table 2-3
Descriptions of the Satellite Monitoring Sites for the Las Vegas Valley PM$_{10}$ Study[a]

Site ID/Code	Site Location	Site Description
1. PECO	Samplers located on light pole on Pecos Rd. directly opposite the eastern end of Hickey Ave.	A residential neighborhood lies to the west of the site. Immediately adjacent to the east of this site is a construction area for a large apartment complex.
2. CLIF	Samplers located on a light pole at the corner of Lake Mead Blvd. and Clifford St.	Across the Lake Mead Blvd. to the southwest is a construction area for residential apartment units. Directly north of the site is an established residential community.
3. NCOV	Samplers located on a light pole on the south side of Carey Street by an unnamed dirt access road. Pole is between Pecos Rd. and North Covey Lane across from Ed Von Tobel Middle School.	Directly south of the site is a construction area. Across Carey Ave. to the north is a school which is within an established residential neighborhood.
4. MARK	Samplers are located on a light pole in the median area of Market Center Drive. Market Center Drive/Alexander Rd. intersects Civic Center Drive west of Pecos Rd.	This area is a new commercial district. Site is located on the median of a wide paved street. Immediately to the east and west are large warehouse-size buildings. At the end of the buildings on the west side there is ongoing construction to complete the commercial developments.
5. CINN	Samplers are located on a light pole at the corner of Fernwood and Toothwood.	This site is located in a newly developed residential area. Front yards of properties have been landscaped, while back yards are mostly bare or being landscaped. Within close proximity of the site to the southwest is a construction area for more residential properties.
6. EFER	Samplers located on a light pole on Fernleaf Dr. directly across from the eastern end of Adirondack Ave. Pole is located in front of #4090 Fernleaf.	This site is located in a well established residential neighborhood. There are no construction activities or vacant lots within visible distance of the site.

Site ID/Code	Site Location	Site Description
7. LONE	Samplers located on a light pole at the corner of Lone Mountain Rd. and Vandenburg Dr.	This site is located in a light commercial area with large warehouse-like buildings and appears to be of recent development. Roads are new and beyond the curbs is usually bare soil. Across Lone Mountain Rd. to the northwest of the site is a ready-mix sand and gravel operation.
8. BEMI[b,c]	Samplers located on the meteorological tower operated by Clark County Health District (CCHD). The site is located on the west side of Mitchell St. across from the western terminus of Andrews St.	This site is located amongst commercial developments. Directly to the south is an open undeveloped area. To the east are established commercial enterprises and a sand and gravel operation is 0.5 km to the northwest. Traffic from nearby Craig Rd. and Interstate 15 is moderate.
9. LAMB	Samplers located on a light pole on the south west corner of the intersection of Lamb Blvd. and Smiley St.	This site is quite open with a large undeveloped parcel of land directly to the southwest. A truck yard and a sand and gravel operation are located across Smiley St. to the northwest of the samplers. To the north and northeast are open fields with bare to scrubby vegetation. To the east and southeast are some commercial properties with a junkyard and a used car parts/wrecking yard.
10. MICH	Samplers are located on a light pole on Mitchell St. beside the entrance to a gas station located at the Corner of Mitchell and Craig Rd.	This site is located near a busy intersection in a commercial district. Directly to the west of the site is a large truck stop frequently traveled by semi-trailer size vehicles.
11. DONO	Samplers are located on a light pole at the terminus of Donovan Way.	This site is located beside a large truck yard to the south and a major land development project in all other directions.
12. BILL	Samplers are located on the western stanchion of a large billboard adjacent to Interstate 15 just north of the Craig Rd. exit.	This site is located adjacent to Interstate 15 and is bordered by an extensive land development operation on the north, west, and south. To the east is Interstate 15, with commercially-developed land beyond.

Site ID/Code	Site Location	Site Description
13. GOLF	Samplers are located on the last light pole at the terminus of Washburn Rd. off Losee Rd.	Directly to the north of the site is a newly developed golf course. Directly to the south is an extensive area of land under development. There is some land to the west and northwest that was not graded prior to the study.
14. LOSS	Samplers are located on a light pole at the north west corner of the golf course at the point where Losee Rd. becomes unpaved.	An unpaved road is located to the east of this site. To the northeast is a heavy equipment training center. The golf course bounds the site to the east and southeast. Across the street to the west is open, scrubby disturbed land.
15. CRAI	Samplers are located on the south side of Craig Rd. on the fourth light pole west of the intersection of Craig Rd. and Losee Rd.	Directly to the south of the samplers is a large open field covered with short, dry grass. Across Craig Rd. to the north are commercial properties. To the northeast at the intersection of Craig Rd. and Losee Rd. is undeveloped scrubby, open land.
16. LONM	Samplers are located on the third light pole past the construction company trailer on the south side of Lone Mountain Rd. just west of Bruce St.	To the south of the site is an extensive housing development area. The surface has been graded in preparation for building construction and the roads are unpaved. To the north is low-density residential housing. At this location Lone Mountain Rd. is unpaved.
17. NWAL	Samplers are located on the fourth light pole from the beginning of Alexander St. on the north side of the street.	Directly north of the site is a large area covered with coarse gravel. To the west and northwest is a sand and gravel operation. Dirt piles are situated on a generally unmaintained area south of Alexander St.
18. GROW	Samplers are located on a pole at the west entrance to the parking lot of Lois Craig School off of Gowan St.	Directly west of the site is a section of Gowan St. and Civic Center Dr. that is being reconstructed (04/15/95). A section of open disturbed land is lies to the north. The school yard encompasses all the land directly east and south of the site.

Table 2-3 (continued)
Descriptions of the Satellite Monitoring Sites for the Las Vegas Valley PM$_{10}$ Study[a]

Site ID/Code	Site Location	Site Description
19. HAMI	Samplers are located on a light pole in front of the residence at 1609 N. Hamilton St.	Directly south of the site is an older established residential area, with Cheyenne Ave. to the north and Interstate 15 to the west.
20. NOCO	Samplers are located on a light pole at the northeast corner of the intersection of Colton Ave. and Covey St.	This site is located in a residential district. Family dwellings are located in all directions except for a vacant lot with some evidence of disturbance to the southwest of the site.
21. LASV	Samplers are located on a light pole on the east side of Van der Meer St. just north of the intersection with Las Vegas Blvd.	Directly south of the site across Las Vegas Blvd. are open scrubby fields. Similar conditions are found to the east and west. North of the site are some light/commercial and residential properties.
22. WALN	Samplers are located on a light pole north of the railway tracks that cross Walnut St. before it joins Mitchell St.	The area surrounding this site consists of large commercial buildings of warehouse size with some open disturbed land between properties.
23. MCDA	Samplers are located on a pole adjacent to the air quality monitoring station. Entrance to the site is just west of a Wendy's restaurant west of the intersection of Lake Mead Blvd. and McDaniel St.	The area surrounding the site is paved open lots directly north and south. A large building is located to the west and a Wendy's restaurant to the east with the drive-through lane adjacent to the site.
24. ECHA[b]	Samplers are located on a pole in the compound containing a Clark County Health District air quality monitoring station. Entrance is off East Charleston Blvd., west of the intersection of E. Charleston Blvd. and 25th St.	South of the site is a large paved parking lot for a commercial mall. Directly to the east of the samplers is a McDonalds Restaurant and drive-through lane. West of the samplers is a fire department substation with a paved storage lot. The site is surrounded in the immediate vicinity by a scrubby grassed area within a 3 × 3 m fenced area.

Table 2-3 (continued)
Descriptions of the Satellite Monitoring Sites for the Las Vegas Valley PM$_{10}$ Study[a]

Site ID/Code	Site Location	Site Description
25. SWLC	Samplers are located on a light pole that identifies the area as a bus stop at the northeast corner of the intersection of Lamb Blvd. and Craig Rd.	The site is surrounded by open fields with disturbed scrubby vegetative surface. There are some moderate size commercial buildings to the northwest along Lamb Blvd.
26. THUN	Samplers are located on the second light pole past the entrance to Thunderbird Plaza from Lamb Blvd. The intersection of Lamb Blvd. and Las Vegas Blvd. is to the north and northwest.	Directly west of the site is an open gravel-covered area, and then a paved parking lot and a shopping mall. Beyond the mall to the northwest is a residential construction area behind a high brick wall. Directly east is Lamb Blvd. Across Lamb Blvd. to the east are open scrubby disturbed lands extending to the northeast.
27. ABEM[c]	Samplers are collocated with Bemis site samplers on the same meteorological tower.	Refer to the BEMI site description (site number 8).
28. NWCP	Samplers are located on the first light pole on the west side of Puebla St. where it intersects with Craig Rd.	North of the site across Craig Rd. is an area of open scrubby land. To the south is a residential area. To the west is a small area with gravel and barren soil.
29. VAND	Samplers are located on a light pole in the median area of Vandenburg Dr. between Craig Rd. and Lone Mountain Rd.	The site is located beside the drain/median dividing Vandenburg Dr. To the east are open scrubby disturbed lands. To the west are large commercial buildings.
30. NECD	Samplers are located on the first light pole on the east side of Donovan Wy. north of Craig Rd.	To the east is a vacant area with scrubby vegetation, with Interstate 15 beyond. Immediately west are train tracks, and further west is a major construction/development project that extends to the northwest. To the north and northeast are vacant lots, with a large truck yard beyond.

[a] See Appendix A of the Las Vegas PM$_{10}$ Study Program Plan (Chow *et al.*, 1995) for detailed site maps.

[b] Locations of the two base monitoring sites.

[c] BEMI (site number 8) and ABEM (site number 27) are collocated with portable PM$_{10}$ survey samplers.

2.2.1 Filter-Based PM_{10} Measurements

PM_{10} measurements were acquired on several substrates configured both in series and in parallel with sequential filter samplers (SFSs). Single Teflon-membrane substrates were used in the portable PM_{10} survey samplers. The sampling system configurations, filter substrates, and chemical analyses applied to the filter-pack measurements are described below.

2.2.1.1 Filter-Based PM_{10} Sampling System

Two types of filter-based aerosol samplers were operated by DRI as part of this study: 1) medium-volume SFSs at the East Charleston and Bemis base sites, and 2) low-volume or mini-volume battery-powered portable PM_{10} survey samplers at the 30 satellite sites. PM_{10} measurements with HIVOL-SSI at the McDaniel Post Office site operated by CCHD were also acquired. The sampling methods are discussed below.

2.2.1.1a PM_{10} Sequential Filter Sampler

The medium-volume sequential filter sampler (SFS) was equipped with an SA-254 size-selective inlet that sampled PM_{10} with a flow rate of 113 L/min. The SFS was configured to take two simultaneous samples (i.e., Teflon-membrane/drain disk and quartz-fiber/nylon-membrane filter packs) at 20 L/min through each sampling port. Aluminum-oxide-coated nitric acid denuders were installed between the inlets and the filters to remove gaseous nitric acid. The remaining 73 L/min required for the 113 L/min total inlet flow was drawn through a makeup air sampling port inside the plenum. The timer was set to take: 1) one 24-hour sample set during the annual monitoring period, 2) up to five 24-hour sample sets during the mini-intensive or intensive monitoring period. Solenoid valves, controlled by a timer, switched between one to five sets of filters at pre-set time intervals. A vacuum pump drew air through the paired filter packs when the valves were open. The flow rate was controlled by maintaining a constant pressure across a valve with a differential pressure regulator.

The filters were loaded in a laboratory into modified Nuclepore filter holders that were plugged into quick-disconnect fittings on the SFS. One filter pack contained a 47-mm-diameter Teflon-membrane filter with a backup drain disc to ensure a homogeneous sample deposit and substrate integrity. The other filter pack contained a 47-mm diameter quartz-fiber filter with a nylon-membrane backup filter.

2.2.1.1b Battery-Powered PM_{10} Portable Survey Sampler

The low-volume, portable PM_{10} survey samplers were equipped with an impactor inlet which sampled PM_{10} at a flow rate of 5 L/min. These samplers were hung from a hook

or hanging bracket attached to utility poles, lamp posts, or roof stands at the satellite sites. Flow rates were determined with a calibrated external rotameter and verified by an in-line rotameter. An internal timer kept clock time and turned the samplers on and off at preset times. Two removable battery packs accompanied each sampler so that one was charging while the other was sampling. Every time a filter was changed, the spent battery was replaced with a fresh one. Several battery chargers were used during this study to assure that batteries were fully charged for the next sampling period. Two survey samplers were located at each saturation site, so one was sampling while the other was being serviced.

Multistage 47-mm-diameter Nuclepore filter holders were used on this sampler. Teflon-membrane filter packs and greased impactors were prepared in the laboratory for placement in the survey sampler. Inlets were cleaned and re-greased between every sample to minimize overloading of the impactor plate and particle reentrainment.

2.2.1.1c   High-Volume PM_{10} Measurements

High-volume PM_{10} samplers equipped with size-selective inlets draw air through the inlet through a 20.3×25.4-cm filter at a flow rate of 1,132 L/min (Chow, 1995). General Metal Works (GMW) IP10-70 mass-flow-controlled high-volume samplers with GMW G-1200 size-selective inlets were used to collect PM_{10} at the McDaniel Post Office site with quartz-fiber filters. The high-volume size-selective PM_{10} samples were acquired at this site between 01/03/95 and 01/28/96 on the U.S. EPA every-sixth-day sampling schedule with 24-hour sample durations.

2.2.1.2 Filter Media

Lippmann (1989), Lee and Ramamurthi (1993), Watson and Chow (1993; 1994), and Chow (1995) evaluate substrates for different sampling and analyses. Based on these evaluations, the 47-mm filters used for PM_{10} sampling were: 1) Gelman (Ann Arbor, MI) polymethylpentane ringed, 2.0-μm pore size, PTFE Teflon-membrane filters (#R2PJ047) for particle mass, light absorption, and elements, 2) Pallflex (Putnam, CT) quartz-fiber filters (#2500 QAT-UP) for carbon and ions, and 3) Schleicher and Schull (Keene, NH) grade 66 nylon-membrane filters (#00440) for volatilized particulate nitrate.

2.2.1.3 Chemical Analysis

For the two base sites, the Teflon-membrane filters were analyzed for mass by gravimetry; for light absorption (b_{abs}) by densitometry; and for 40 elements (Na to U) by x-ray fluorescence (XRF) (Watson *et al.*, 1997). The front quartz-fiber filters were analyzed for chloride (Cl⁻), nitrate (NO_3^-), and sulfate ($SO_4^=$) by ion chromatography (Chow and Watson, 1997a); for ammonium (NH_4^+) by automated colorimetry; for soluble potassium (K^+) by atomic absorption spectrophotometry; and for organic carbon (OC) and elemental carbon

carbon (EC) by thermal/optical reflectance carbon analysis (Chow *et al.*, 1993b; Watson and Chow, 1993; 1994). The backup nylon-membrane filters were analyzed for nitrate by ion chromatography.

For the 30 satellite sites, the Teflon-membrane filters were analyzed for mass by gravimetry, for light absorption (b_{abs}) by densitometry, and for six elements (i.e., aluminum [Al], silicon [Si], sulfur [S], potassium [K], calcium [Ca], and iron [Fe]) by XRF scanning. Detailed chemical analyses are documented in the program plan (Chow *et al.*, 1995) following U.S. EPA guidelines for PM_{10} sampling and analysis (Chow and Watson, 1994b; Chow, 1995).

2.2.2 Continuous PM_{10} Measurements with Beta-Attenuation Monitors (BAMs)

Beta-attenuation monitors (BAM) (e.g., Lillienfeld and Dulchinos, 1972; Husar, 1974; Lillienfeld, 1975; Macias and Husar, 1976; Lillienfeld, 1979) attenuate beta rays (moderately-high-energy electrons) emitted by a radioactive source when they pass through particles deposited on a filter. Beta ray attenuation is related to the particulate mass collected on the filter. PM_{10} monitors draw a filter tape across the path between the beta emitter and a detector to measure blank attenuation, then across a sampling area where particles are collected on the tape, and finally through the detector area to measure the attenuation of the filter and the deposit.

Sierra-Andersen beta-attenuation monitors (BAMs) (Model FH62I-N) were installed by CCHD to monitor hourly PM_{10} mass at the six compliance monitoring sites and seven special-purpose sites as shown in Figure 2-1. The Sierra-Andersen FH62I-N BAM has passed the sampling and reproducibility protocol required by the U.S. EPA and has received a PM_{10} equivalency designation for the 24-hour sample durations (Chow, 1995). This type of beta-attenuation monitor has been used in field comparisons with both high-volume samplers equipped with PM_{10} size-selective inlets as well as PM_{10} dichotomous samplers (Chow and Watson, 1997b). Hourly PM_{10} data was acquired for the period of 01/01/95 to 01/31/96 for assessing the diurnal variation of the PM_{10} concentrations and for comparison with collocated medium-volume and low-volume PM_{10} measurements.

2.2.3 Meteorological Measurements

Data from the existing 17 meteorological monitoring stations operated by CCHD were assembled for the period of 01/01/95 to 01/31/96. Hourly wind speed, wind direction, temperature, and relative humidity measurements were acquired with 10-m-height meteorological towers as documented in Table 2-1.

3.0 EMISSIONS INVENTORY

According to the preliminary 1995 emissions inventory compiled for the Las Vegas Valley (Jacquart, 1997), fugitive dust sources (construction activities, paved and unpaved road dust, and windblown dust) account for nearly 97% of primary PM_{10} emissions, while other processes (e.g., residential wood combustion, stationary sources) account for 2% and on-road vehicle exhaust accounts for 1% of primary emissions. These preliminary annual PM_{10} emission estimates for 1995 were compared to the emission estimates for 1989 in Table 3-1. Annual PM_{10} emission estimates varied fivefold between 1989 and 1995. Figure 3-1 compares the 1989 and 1995 PM_{10} emission estimates from both natural and manmade sources. Dust from active construction sites is the largest source of primary PM_{10}, constituting 48% of the fugitive dust emissions. Undisturbed vacant lands account for 18%, other forms of disturbed vacant lands without active construction projects account for 14%, reentrained paved road dust accounts for 15%, and unpaved road dust accounts for 8% in the preliminary 1995 inventory.

The windblown dust category is often called "natural dust" owing to its origin from non-urban areas that are subject only to suspension by the wind. These sources are episodic rather than continuous emitters. The majority of these emitting areas were disturbed by anthropogenic activities at one time or another, however, and the level of suspendable dust would be much smaller had this disturbance not occurred. Paved road dust and construction/demolition activities are also major emitters of primary PM_{10}. Efforts were made in this study to better estimate the emissions rates for the major source categories shown in Figure 3-1.

Emissions factors for primary particles from fugitive dust sources are difficult to measure or model (Chow and Watson, 1994a). Several emissions data bases were evaluated in this study in order to provide the best available emission factors to represent sources in the Las Vegas Valley. The compiled emissions data base is used in the application of dispersion models for this study to estimate the spatial and temporal variations of fugitive dust source emissions.

This section assembles and evaluates the fugitive dust emission data bases, compares the emission factors with U.S. EPA AP-42 estimates, documents the microinventories surrounding the two base monitoring sites, and utilizes the information from geographical information system (GIS) data bases to compile the final emission data base for this study.

3.1 Comparison of Fugitive Dust Emission Factors

Emission factors for different categories of fugitive dust were acquired and assembled. A mixture of land uses was found within the study domain (12 km [7.5 mi]

Table 3-1
Preliminary Annual PM$_{10}$ Emission Estimates for the Las Vegas Valley Non-Attainment Area[a]

Category	1989			1995		
	Megagrams	Tons	% of Total	Megagrams	Tons	% of Total
Paved Roads						
Local Streets	753	683	5.08%	2,192	2,416	3.31%
Collectors	440	399	2.97%	1,443	1,591	2.18%
Arterials	1,816	1,647	12.26%	1,461	1,610	2.21%
Freeways	156	142	1.05%	1,036	1,142	1.57%
Total	2,871	3,165	19.38%	6,132	6,759	9.27%
Mobile						
Local Streets	134	148	0.91%	79	87	0.12%
Collectors	98	108	0.66%	97	107	0.15%
Arterials	598	659	4.04%	260	287	0.39%
Freeways	120	132	0.81%	310	342	0.47%
Total	949	1,046	6.40%	747	823	1.13%
Unpaved Roads	1,941	2,140	13.10%	5,590	6,162	8.45%
Construction						
Activities	3,309	3,648	22.34%	23,385	25,778	35.34%
Track-Out	0	0	0.00%	4,553	5,019	6.88%
Wind Erosion	0	0	0.00%	3,676	4,052	5.56%
Off-Road Exhaust	111	122	0.75%	0	0	0.00%
Total	3,421	3,771	23.09%	31,614	34,849	47.78%
Non-Construction Disturbed Land (Wind Erosion)	1,269	1,399	8.57%	8,970	9,888	13.56%
Urban Undisturbed Land (Wind Erosion)	0	0	0.00%	2,263	2,494	3.42%
Rural/Background Undisturbed Land (Wind Erosion)	3,704	4,083	25.00%	9,432	10,397	14.26%
Other						
Residential Wood Burning	247	272	1.67%	279	308	0.42%
Stationary Sources	362	399	2.44%	1,138	1,254	1.72%
Natural Gas Combustion	16	18	0.11%	0	0	0.00%
Aircraft Operations	36	40	0.24%	0	0	0.00%
Total	661	729	4.46%	1,417	1,562	2.14%

[a] Jacquart, 1997.

Wood/Natural Gas
Combustion, Stationary
Sources, Aircraft
Operations
4%

Paved Roads
19%

Rural/Background
Undisturbed Land
26%

Mobile
6%

Urban Undisturbed Land
0%

Unpaved Roads
13%

Non-Construction
Disturbed Land
9%

Construction
23%

1989

Wood/Natural Gas
Combustion, Stationary
Sources, Aircraft
Operations
2%

Paved Roads
9% Mobile
1%

Rural/Background
Undisturbed Land
14%

Unpaved Roads
8%

Urban Undisturbed Land
3%

Non-Construction
Disturbed Land
14%

1995

Construction
49%

Figure 3-1   Estimated PM_{10} emission rates in the Las Vegas Valley Nonattainment Area
for 1989 and 1995.

east-west × 13 km [8.1 mi] north-south). Desert surfaces (in various states of disturbance), commercial/residential districts, industrial/construction activities, and paved and unpaved roadways are the potential sources that contribute to the atmospheric loading of PM_{10}.

Table 3-2 presents calculated emission factors for each major source type using various emissions models and empirically-derived functions. In the following subsections, the variability and uncertainty of these emission factors are evaluated and compared to the emissions estimated by U.S. EPA AP-42 (U.S. EPA, 1994).

3.1.1 Emissions from Vacant Lands and Desert Surfaces

Particle suspension from vacant land or desert surfaces can be induced by natural wind erosion or external mechanical forcing processes. These surfaces may range from relatively undisturbed desert with varying degrees of vegetative cover, to vacant lands disturbed by anthropogenic activities. In the Las Vegas Valley, plant cover on desert land ranges from insignificant to an average of 30% for undisturbed areas, and 15% for disturbed areas (James, 1996).

Very few studies have investigated wind-generated particle emissions from vacant lands and desert surfaces. Nickling and Gillies (1989) reported the emission factors of total suspended particles (TSP, particles with aerodynamic diameters in the range of 30 to 50 μm) for disturbed and undisturbed desert surfaces in Arizona, and James (1996) derived PM_{10} emission factors in the Las Vegas Valley. Both studies used portable wind tunnels to establish the relationships between wind speeds and suspended particle concentrations as a function of different land-use surface types. Emission factors are derived from these measurements.

Grain size analysis of the TSP samples collected by Nickling and Gillies (1989) showed that greater than 95% of the particles were less than 10 μm in geometric diameter. Nickling and Gillies (1989) found average TSP emission factors ranged from 1×10^{-5} g/m^2-s to 6.5×10^{-3} g/m^2-s (0.12 to 76.26 tons/acre-month) for different surface types in Arizona. With respect to the undisturbed and disturbed desert surfaces, the average TSP emission factors were 1.83×10^{-4} g/m^2-s (2.15 tons/acre-month) and 9.76×10^{-4} g/m^2-s (11.45 tons/acre-month), respectively. These values are comparable to the PM_{10} emission factors reported by James (1996) for undisturbed and disturbed desert surfaces in the Las Vegas Valley, which ranged from 2.40×10^{-3} g/m^2-s to 5.0×10^{-3} g/m^2-s (28.16 to 58.66 tons/acre-month). Both of these studies show that the emission flux is dependent on wind speed, or friction velocity (u_*, m/s), and the degree of surface disturbance.

Past studies have shown that the dimensions of a wind tunnel largely determine its ability to simulate the saltation process (Shao *et al.*, 1993) and to model the transport of

Table 3-2
Comparison of Existing Fugitive Dust Emission Factors

Fugitive Dust Source Type	U.S. EPA AP-42 (U.S. EPA, 1994)	MRI (1996)	Nickling and Gillies (1989)	James (1996)	Shao et al. (1993)	Gillette and Passi (1988)	Flocchini et al. (1994)	Watson et al. (1996)	Stevens (1991)	THIS STUDY
Windblown dust, general area $u_t = 0.3$ m/s $u_* = 0.5$ m/s	1.1×10^{-7} g/m²-s or 1.3×10^{-3} tons/acre-month	NA	6.3×10^{-8} g/m²-s or 7.4×10^{-4} tons/acre-month (TSP)	3.4×10^{-3} g/m²-s or 4×10^{1} tons/acre-month (PM$_{10}$)	1.1×10^{-6} g/m²-s or 1.3×10^{-2} tons/acre-month (TSP)	3.0×10^{-5} g/m²-s or 3.5×10^{-1} tons/acre-month (TSP)	NA	NA	NA	3.4×10^{-3} g/m²-s or 4×10^{1} tons/acre-month (PM$_{10}$)
Windblown dust, undisturbed desert	NA	NA	1.83×10^{-4} g/m²-s or 2.15×10^{0} tons/acre-month (TSP)	2.4×10^{-3} g/m²-s or 2.8×10^{1} tons/acre-month (PM$_{10}$)	NA	NA	NA	NA	NA	2.4×10^{-3} g/m²-s or 2.8×10^{1} tons/acre-month (PM$_{10}$)
Windblown dust, disturbed desert	NA	NA	9.76×10^{-4} g/m²-s or 1.15×10^{1} tons/acre-month (PM$_{10}$)	5.0×10^{-3} g/m²-s or 5.9×10^{1} tons/acre-month (PM$_{10}$)	NA	NA	NA	NA	NA	5.0×10^{-3} g/m²-s or 5.9×10^{1} tons/acre-month (PM$_{10}$)
Construction sites	2.6×10^{-5} g/m²-s or 3.1×10^{-1} tons/acre-month	9.22×10^{-6} g/m²-s or 1.08×10^{-1} tons/acre-month average; 3.52×10^{-5} g/m²-s or 4.13×10^{-1} tons/acre-month industrial; 2.68×10^{-5} g/m²-s or 3.14×10^{-1} tons/acre-month residential	5.65×10^{-4} g/m²-s [a] or 6.63×10^{0} tons/acre-month[a]; 1.83×10^{-3} g/m²-s [b] or 2.15×10^{1} tons/acre-month[b]	NA	NA	NA	NA	NA	NA	9.22×10^{-6} g/m²-s or 1.08×10^{-1} tons/acre-month for active construction, 3.52×10^{-5} g/m²-s or 4.07×10^{-1} tons/acre-month for inactive construction

Table 3-2 (continued)
Comparison of Existing Fugitive Dust Emission Factors

Fugitive Dust Source Type	U.S. EPA AP-42 (U.S. EPA, 1994)	MRI (1996)	Nickling and Gillies (1989)	James (1996)	Shao et al. (1993)	Gillette and Passi (1988)	Flocchini et al. (1994)	Watson et al. (1996)	Stevens (1991)	THIS STUDY
Paved roads	1.7×10^{-3} kg/VKT or 6.0×10^{-3} lb/VMT	5.1×10^{-4} kg/VKT or 1.8×10^{-3} lb/VMT; 1.31×10^{-3} kg/VKT or 4.65×10^{-3} lb/VMT	NA	NA	NA	NA	NA	NA	NA	0.2×10^{-3} to 1.91×10^{-3} kg/VKT[a] or 0.7×10^{-3} to 6.8×10^{-3} lb/VMT[a]
Unpaved roads (assuming % silt = 6.3, speed = 40 km/hr [25 mi/hr], weight = 1.36 Mg [1.5 tons], #wheels = 4)	0.18 kg/VKT or 0.64 lb/VMT	NA	NA	NA	NA	NA	0.45 kg/VKT or 1.6 lb/VMT	0.29 kg/VKT or 1.0 lb/VMT[c]	0.29 kg/VKT[c] or 1.0 lb/VMT[c]	0.556 kg/VKT or 1.956 lb/VMT

[a] Based on U.S. EPA Part 5 Model.
[b] Based on vehicle speed only.

suspended particles (Owen and Gillette, 1985; White and Mounla, 1991). Dimensional limitations may cause particles traveling through the wind tunnel to behave differently than natural wind-blown particles. Even though a small wind tunnel was used by James (1996), similar emission factors were reported by Nickling and Gillies (1989) and James (1996). This implies that the study results were not affected by dimensional limitations of the wind tunnels.

James (1996) corrected the measured emission factors to account for the presence of vegetation and the depletion of the particle reservoir during wind erosion. The presence of vegetation reduces the vertical flux of particles due to the plants' sheltering effect and their direct absorption of momentum. Momentum absorption reduces the energy in the wind near the surface and, therefore, reduces the ability of the wind to entrain loose particles. The corrections for vegetative cover adapted by James (1996) are based on measurements of soil erosion from rough agricultural fields (Fryrear, 1985) rather than from desert surfaces. Leys (1991) examined the correction factors reported by Fryrear (1985) and found an overestimation of soil loss as vegetative coverage exceeded 30%. In addition, the correction factors are not applicable to vacant land with sparse vegetation.

Gillies *et al.* (1996a, 1996b) discussed the theory of emission decay and evaluated empirical studies. It was concluded that the application of emission factors without a decay function will lead to an overestimation of the particle contribution, especially over long time intervals. Theoretical and empirical research has suggested that dust emissions may follow an inverse time (i.e., 1/*time*) decay function (Nicholson, 1988). James (1996) derived the reservoir depletion correction factor based on analysis of observed changes in PM_{10} concentrations recorded during 10-minute wind tunnel runs. James (1996) derived the two-hour correction factor based on observed changes in dust concentrations over time during high wind events. The limited data set used by James (1996) for the two-hour correction factor may not be representative of the actual decay of particle emissions from a desert surface as conceptualized by Haun (1995). In theory, PM_{10} emissions should be decreased by 0.1% over a two-hour period, but James (1996) data suggests PM_{10} emissions can be decreased by approximately 35%.

Table 3-3 summarizes the equations reported by James (1996) to derive PM_{10} emission factors for undisturbed and disturbed desert surfaces. The effects of vegetative cover, emission decay, and wind speed were included. These equations were formulated using least-squares regressions of averages calculated from sets of PM_{10} emissions measured as a function of average 10-meter-height wind speed. Figures 3-2 to 3-9 display the scatter plots of the averages of the sets of measurements from which the regression statistics were derived. The standard deviations for the average PM_{10} emission values reported by James (1996) have not been included in these figures. Since near-surface wind speed is measured in

Table 3-3
Equations to Derive PM_{10} Emission Factors for Vacant Lands in the Las Vegas Valley[a]

Category	Base[b] Emission Factor	Corrected for Vegetative Cover[b]	Corrected for Vegetative Cover and Reservoir Depletion[b]	Corrected for Vegetative Cover and Emission Decay after a Two-Hour Period[b]
Undisturbed Surface	$1.3 \times 10^{-5} (U_{10})^{1.97}$ [c] g/m²-s or $0.15 (U_{10})^{1.97}$ [c] tons/acre-month	$2.9 \times 10^{-5} (U_{10})^{1.97}$ [d] g/m²-s or $0.34 (U_{10})^{1.97}$ [d] tons/acre-month	$3.6 \times 10^{-6} (U_{10})^{1.50}$ [e] g/m²-s or $0.04 (U_{10})^{1.50}$ [e] tons/acre-month	$1.3 \times 10^{-6} (U_{10})^{1.50}$ [f] g/m²-s or $0.02 (U_{10})^{1.50}$ [f] tons/acre-month
Disturbed Surface	$5.75 \times 10^{-6} (U_{10})^{2.56}$ [g] g/m²-s or $0.07 (U_{10})^{2.56}$ [g] tons/acre-month	$4.1 \times 10^{-6} (U_{10})^{2.55}$ [h] g/m²-s or $0.05 (U_{10})^{2.55}$ [h] tons/acre-month	$4.34 \times 10^{-6} (U_{10})^{2.2}$ [i] g/m²-s or $0.05 (U_{10})^{2.2}$ [i] tons/acre-month	$1.45 \times 10^{-6} (U_{10})^{2.28}$ [j] g/m²-s or $0.02 (U_{10})^{2.28}$ [j] tons/acre-month

[a] James (1996).

[b] U_{10} is the estimated wind speed acquired at the 10 m meteorological tower.

[c] See Figure 3-2.

[d] See Figure 3-3.

[e] See Figure 3-4.

[f] See Figure 3-5.

[g] See Figure 3-6.

[h] See Figure 3-7.

[i] See Figure 3-8.

[j] See Figure 3-9.
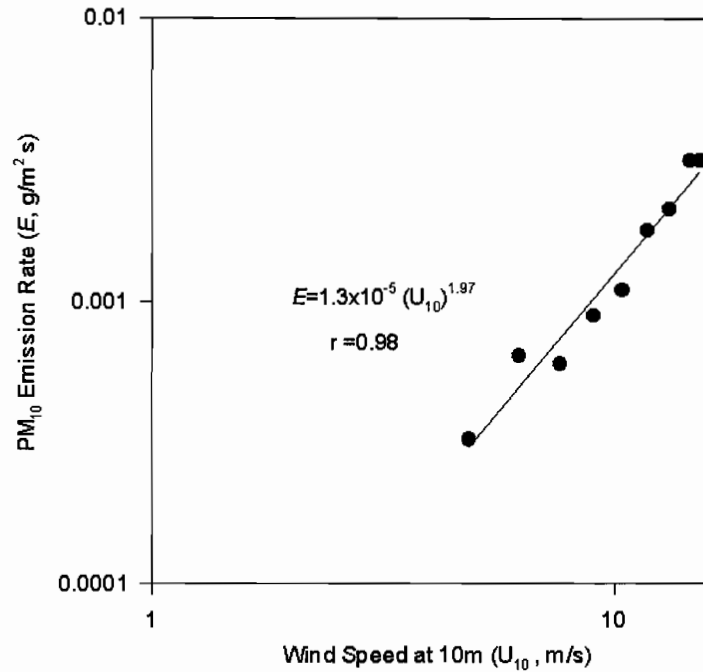
Figure 3-2 PM_{10} emission rate as a function of wind speed at 10 m height for undisturbed vacant lands without vegetative cover (James, 1996).
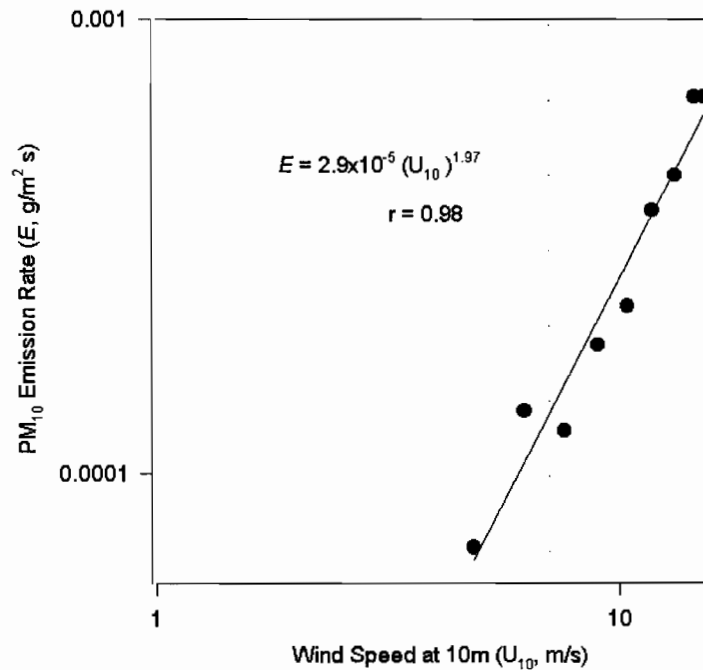
Figure 3-3 PM_{10} emission rate as a function of wind speed at 10 m height for undisturbed vacant lands (rate corrected for 31% average vegetative cover [James, 1996]).
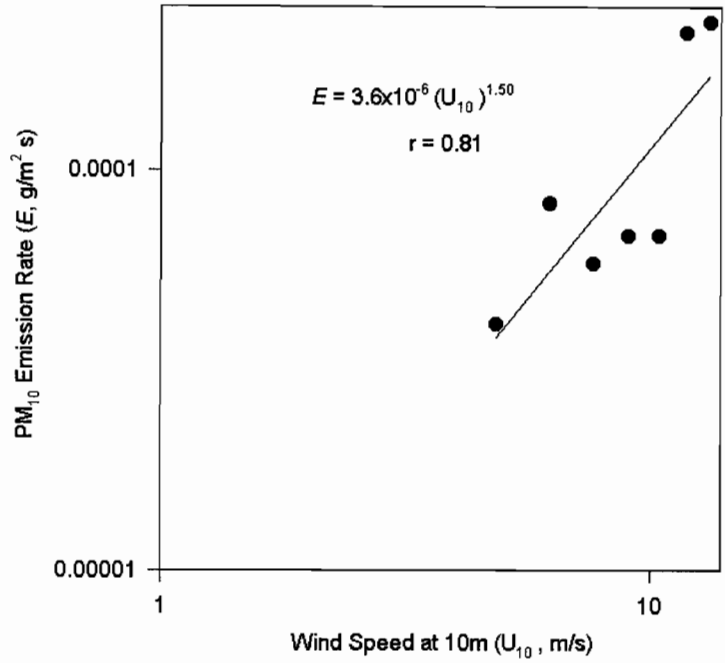
Figure 3-4 PM_{10} emission rate as a function of wind speed at 10 m height for undisturbed vacant lands (rate corrected for 31% average vegetative cover and reservoir depletion [James, 1996]).
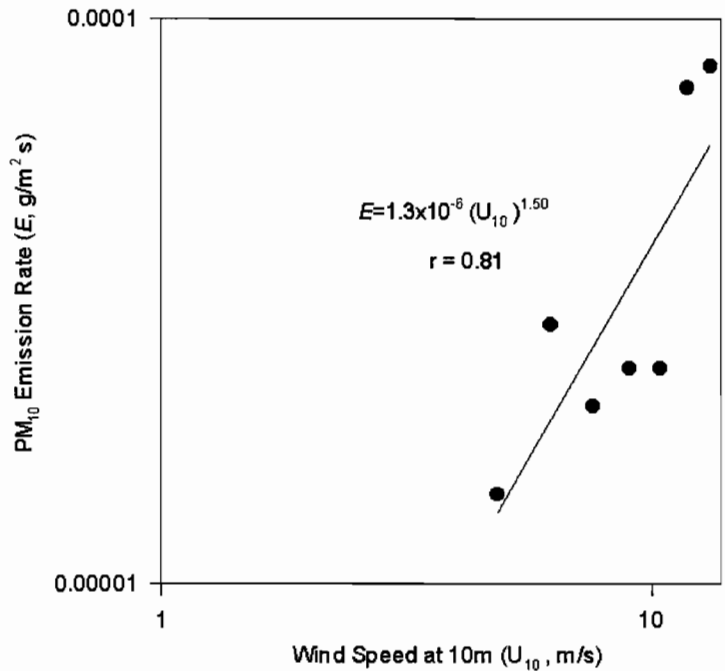
Figure 3-5 PM_{10} emission rate as a function of wind speed at 10 m height for undisturbed vacant lands (rate corrected for 31% average vegetative cover and reservoir depletion after a two-hour period [James, 1996]).
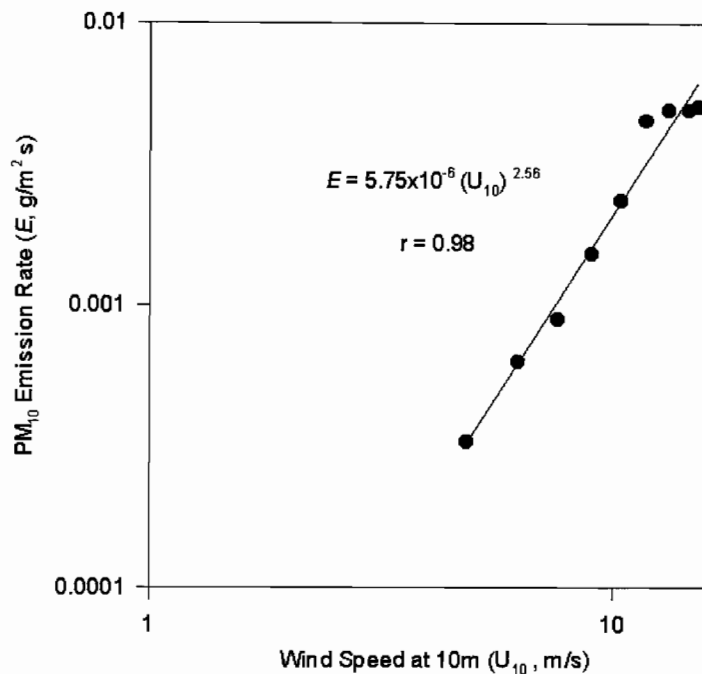
Figure 3-6 PM_{10} emission rate as a function of wind speed at 10 m height for disturbed vacant lands without vegetative cover (James, 1996).
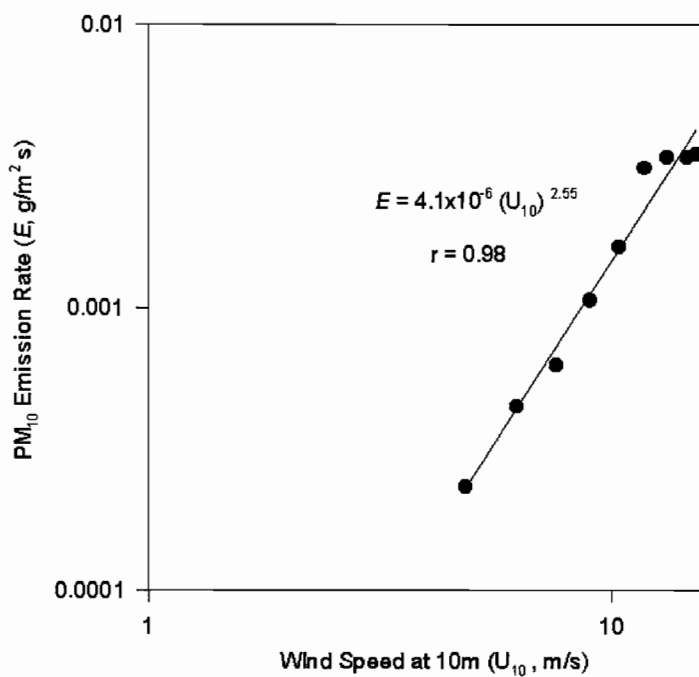
Figure 3-7 PM_{10} emission rate as a function of wind speed at 10 m height for disturbed vacant lands (rate corrected for 14.8% average vegetative cover [James, 1996]).
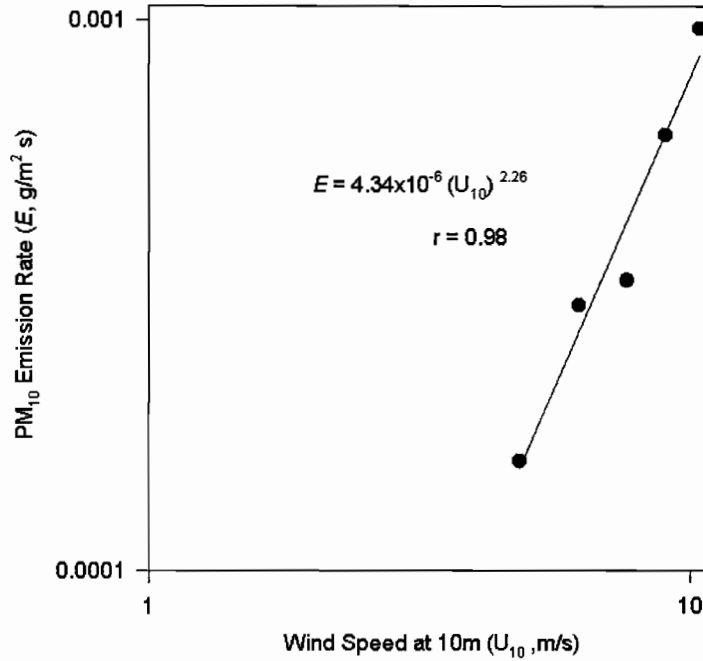
Figure 3-8 PM_{10} emission rate as a function of wind speed at 10 m height for disturbed vacant lands (rate corrected for 14.8% average vegetative cover and reservoir depletion [James, 1996]).
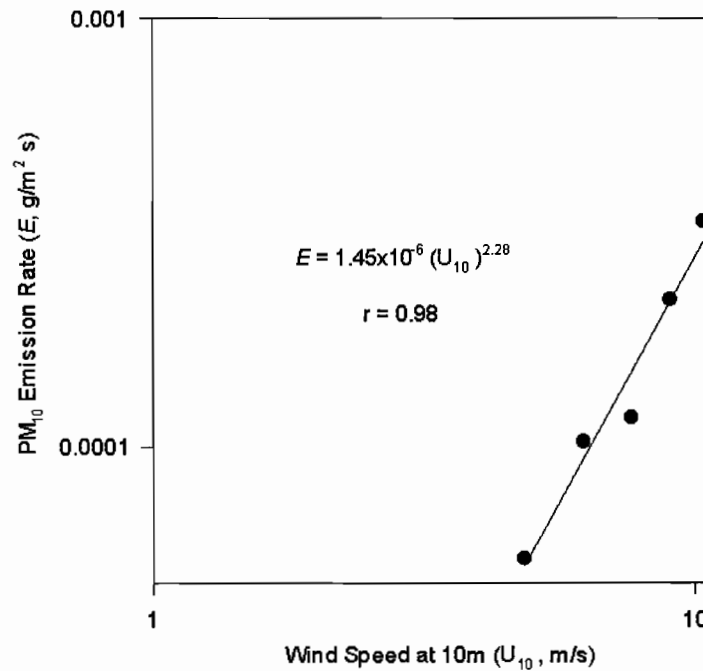
Figure 3-9 PM_{10} emission rate as a function of wind speed at 10 m height for disturbed vacant lands (rate corrected for 14.8% average vegetative cover and reservoir depletion after a two-hour period [James, 1996]).

the wind tunnel, these values are extrapolated to the 10-m height using surface-boundary-layer wind-speed profiles (Chow and Watson, 1994a).

For vacant land, the relationship between PM_{10} emission factors and wind speed can be illustrated by a power function, with particle emissions increasing as 10-m-height wind speed is raised to the third power (Shao et al., 1993). When the source of suspended particles is not a limiting factor (i.e., unlimited particle reservoir, as found in disturbed vacant land), the exponent in the regression equation approaches the theoretical value of three. For undisturbed vacant land, where the source of suspended particles may be limited, the exponent is considerably less than three. Similar magnitude exponents from desert and agricultural surfaces were reported by Gillies (1987) and Nickling and Gillies (1989).

As shown in Table 3-2, PM_{10} or TSP emission factors for vacant land can vary by three orders of magnitude. This difference would be even greater as wind speed increased due to the power function relationships, which illustrates the uncertainty in the measurement and modeling of PM_{10} emissions caused by wind erosion. In addition, the site-specific nature of soil textures and surface characteristics makes it difficult to extrapolate the empirical relationships to other areas.

Haun (1995) also found that correlations between fugitve dust abundance and wind-tunnel-measured PM_{10} emission rates for seven of the nine major soil groups occurring in the Las Vegas Valley were not statistically significant at the 0.05 confidence level. Both the sample collection methodology and the particle size analysis technique employed to determine silt and PM_{10} fractions in the soil warrant further examination. Potential sources of wind erosion particles include: 1) loose surface sediment that can be injected into the atmosphere by the saltation process, 2) sandblasting of the surface by the saltating particles that can liberate and carry particles upwards by turbulent diffusion processes, and 3) breakdown of particles during transport by the wind. In addition, the abundance of suspendable particles in the surface material is also a key factor related to the quantity of reentrainment.

In a series of laboratory wind tunnel experiments, Hagen et al. (1995) found that PM_{10} emissions from simulated agricultural fields were related to the textural qualities of the soils. Measured aggregate size distributions were used to estimate the abundance of PM_{10} in the loose surface layer. Hagen et al. (1995) concluded that PM_{10} emissions differ significantly among soils, with abrasion processes being the largest source of PM_{10}. James (1996) did not show significant PM_{10} emission variations due to different soil types in the Las Vegas Valley, however.

Shao et al. (1993) suggest two main sources of errors in modeling particle wind-erosion emissions. The first type of uncertainty is related to the prediction of horizontal

3-13

soil drift and dust entrainment from different surfaces. Current understanding on the physics of the erosion process is limited. Difficulties include: 1) measuring the threshold wind velocity (u_*) within the saltation layer, 2) deriving the relationship between the saltation process and dust emission, 3) estimating the effects of surface roughness and vegetative cover, 4) measuring and characterizing particle size distributions, 5) modeling source-limited saltation conditions, and 6) characterizing complex roughness and its effects on aerodynamics and erosion. The second type of uncertainty is concerned with the evolution of the surface over time under the influence of the wind erosion process, weathering, or anthropogenic activities. More research is needed to better understand the mechanisms of windblown dust from vacant lands and desert surfaces and to better estimate its emissions.

3.1.2 Emissions from Construction Sites

As a result of economic expansion and population growth, construction of urban housing developments and commercial properties is increasing in the Las Vegas Valley. Construction activities can be large sources of fugitive dust emissions when wind of sufficient strength (i.e., above 6.7 m/sec [15 mph]) blows over the disturbed soil surfaces and causes particle entrainment. On-site activities such as vehicle movement, earth-moving, cut and fill operations, and hauling can also induce significant quantities of dust emissions.

The most commonly-used emission factors for construction sites are from AP-42 reported in the U.S. EPA Trends Inventory (U.S. EPA, 1994). A recent study was conducted by the Midwest Research Institute (MRI, 1996) to reevaluate fugitive dust emissions from construction sources in the southwest U.S., including the Las Vegas Valley. This study showed that construction site emission factors vary from 3.27×10^{-7} to 3.6×10^{-5} g/m^2-s (0.0039 to 0.43 ton/acre-month). The reported geometric mean is 9.22×10^{-6} g/m^2-s (0.11 ton/acre-month), which is approximately one-third of the AP-42 value (2.6×10^{-5} g/m^2-s or 0.31 ton/acre-month). In the Las Vegas Valley, emission factors at construction sites can vary by more than a factor of ten depending on the extent of the earth-moving activities as shown in Table 3-4 (MRI, 1996). An adjusted factor of 3.52×10^{-5} g/m^2-s (0.42 ton/acre-month) was derived to account for large-scale earth-moving activities. This adjusted value is closer to the AP-42 factor of 2.6×10^{-5} g/m^2-s (0.31 ton/acre-month).

Nickling and Gillies (1989) reported PM$_{10}$ emission factors in construction sites ranged from 5.65×10^{-4} g/m^2-s to 1.83×10^{-3} g/m^2-s (6.63 to 21.47 tons/acre-month) in Phoenix, AZ. These emission factors are one to two orders of magnitude higher than the factors derived in the Las Vegas Valley (MRI, 1996). These discrepancies could be attributed to the high silt content (fraction of particles with geometric diameters less than 75 μm) in the Phoenix soils (14% to 25%) and to lack of correction for surface particle emission decay by Nickling and Gillies (1989). As the inverse time ($1/time$) decay function is applied, the

Table 3-4
Empirically-Derived PM_{10} Emission Factors from Construction Sites in the Las Vegas Valley[a]

Source Category	PM_{10} Emission Rate (tons/acre-month)	PM_{10} Emission Rate (g/m^2-s)	Comments
General construction (without any activity)	0.11	9.22×10^{-6}	
General construction (with earth-moving activity)	0.42	3.52×10^{-5}	
Commercial/industrial construction	0.032	2.68×10^{-6}	Measurements were taken from the North Las Vegas construction site located at Craig Rd. between Donovan Way and Loose Rd. and extending north past Washburn St.
Residential construction	0.32	2.68×10^{-5}	Measurements were taken from the southwest Las Vegas construction site near Russell Rd. and Rainbow Rd.
AP-42[b]	0.31	2.6×10^{-5}	From AP-42.

[a] MRI (1996)

[b] U.S. Environmental Protection Agency (1994)

emission factors are reduced to between 4.71×10^{-6} g/m^2-s and 1.53×10^{-3} g/m^2-s (0.06 to 17.95 tons/acre-month) after two hours of active erosion.

The MRI (1996) report recommended a construction emission factor of 9.22×10^{-6} g/m^2-s (0.11 ton/acre-month) be used when information about the construction activities is not available. If earth-moving activities dominate the construction site, the value of 3.52×10^{-5} g/m^2-s (0.42 ton/acre-month) should be applied (MRI, 1996). To improve estimates of construction emissions, it is essential to account for differences in activity levels (e.g., the amount of cut/fill, the number and type of earth-moving vehicles, the length of average round-trip distances traveled, and the density of the earth-material being handled). Guidelines need to be developed for permitting construction activities in order to provide additional information needed to calculate the emissions from construction activities (MRI, 1996).

Since one-half of the commercial district, parks, public buildings, and residential construction activities involve large amounts of earth movement, the Clark County Department of Comprehensive Planning adapted an emission factor of 9.22×10^{-6} g/m^2-s (0.11 ton/acre-month) excluding earthmoving emissions and an emission factor of 3.52×10^{-5} g/m^2-s (0.42 ton/acre-month) including earthmoving emissions. These result in an average emission factor of 2.26×10^{-5} g/m^2-s (0.27 ton/acre-month) which is similar to that recommended in AP-42. Since large amounts of earthmoving occurred during airport construction, flood control, highway construction, public works, and installation of underground utilities, the emission factor of 3.52×10^{-5} g/m^2-s (0.42 ton/acre-month) was used to estimate these emissions. PM$_{10}$ emission estimates from vehicle track-out and wind erosion from construction sites were also estimated in CCDCP's inventory (Jacquart, 1997). These values were used to estimate the emissions from construction activities.

3.1.3 Emissions from Paved Roads

Based on the Clark County emissions inventory, particle resuspension from paved roads accounts for 23% of the emissions within the Las Vegas Valley. The most recent AP-42 equation (U.S. EPA, 1994) to calculate PM$_{10}$ emissions from paved roads is:

$$e = k\left(\frac{sL}{2}\right)^{0.65}\left(\frac{W}{3}\right)^{1.5} \tag{3-1}$$

where:

e = PM$_{10}$ emission factor (mass/vehicle kilometer traveled, g/VKT)

sL = surface silt loading (loose road surface material < 75 μm in geometric diameter) expressed in mass/area

W = mean weight of vehicles traveling the road (tons)

k = base emission factor for different particle size ranges (e.g., for PM_{10}, k = 7.3 g/VKT)

The default surface silt loadings provided by AP-42 (U.S. EPA, 1994) vary from 0.022 g/m^2 (freeway/expressway) to 2.1 g/m^2 (collector streets) in five selected cities. To provide better paved-road emission estimates, AP-42 suggests the input of the area-specific surface silt loading.

A recent study (MRI, 1996) showed that the measured silt loading on paved streets were a factor of 5 to 10 lower than those derived from AP-42 criteria. Taking the silt loading of 0.04 to 0.58 g/m^3 in the Las Vegas Valley (MRI, 1996) into consideration, the paved road PM_{10} emission factor for the Las Vegas Valley ranges from 0.2×10^{-3} to 1.91×10^{-3} kg/VKT as shown in Table 3-5. These PM_{10} emission factors are comparable to the AP-42 estimates of 1.7×10^{-3} kg/VKT as shown in Table 3-2. Both site-specific silt loading and average vehicle data should be taken into account to increase the reliability of the paved-road PM_{10} emission estimates.

3.1.4 Emissions from Unpaved Roads

The Clark County emissions inventory estimated that unpaved road dust accounts for 10% of the fugitive dust emissions in the Las Vegas Valley. The AP-42 equation for calculating emissions from unpaved roads is:

$$e = 0.61 \left(\frac{s}{12}\right)\left(\frac{S}{48}\right)\left(\frac{W}{2.7}\right)^{0.7}\left(\frac{w}{4}\right)^{0.5}\left(\frac{365-p}{365}\right) \tag{3-2}$$

where:

e = PM_{10} emission factor (mass/vehicle kilometer traveled, kg/VKT)

s = silt content (percent of loose road surface material < 75 μm in geometric diameter)

S = mean vehicle speed (km/hr)

W = mean vehicle weight (megagrams, Mg)

w = mean number of wheels (dimensionless)

p = number of days with ≥ 0.254 mm (0.01 inches) of precipitation

Table 3-5

1995 PM$_{10}$ Emission Estimates from Paved Roads in the Las Vegas Valley

Roadway Classification	Daily VMT (miles)	Paved Road Emission Factor (g/mi)	Paved Road Emissions (tons)	Mobile Emission Factor (g/mi)	Mobile Emissions (tons)	1995 Total Emissions (tons/year)
Major Arterials and Freeways	7,685,022.9	0.37	1,142	0.111	342	1,484
Minor Arterials	6,464,776.0	0.62	1,610	0.111	287	1,897
Collectors and Ramps	2,414,930.3	1.64	1,591	0.111	107	1,698
Local and Transit	1,965,767.0	3.06	2,416	0.111	87	2,503
Total	18,530,496.2		6,759		823	7,582

The PM_{10} unpaved-road emission factor is 0.18 kg/VKT in AP-42. This empirical equation has been utilized to calculate emission rates in many geographically-diverse areas (e.g., Cowherd *et al.*, 1988, 1990). Recent studies reported PM_{10} emission factors on unpaved private agricultural roads (Flocchini *et al.*, 1994) and unpaved public roads (Watson *et al.*, 1996) in California's San Joaquin Valley to be factors of 2.5 and 1.6 greater, respectively, than AP-42 estimates. Zimmer *et al.* (1992) cautions the uncertainties of using AP-42 beyond the range for which the variables were defined. Actual emissions depend on the relationship between the road surface PM_{10} loading and the processes or surficial conditions that control their resuspension either by reentrainment in turbulent vehicle wakes or by the shearing action of tires.

CCDCP adapted an unpaved road emission factor of 0.556 kg/VKT (1.956 lbs/VMT) which was based on an average silt content of 12%, mean vehicle speed of 47.8 km/hour (29.9 mi/hour) (which corresponds to the Washoe County Regional Transportatation Commission's (RTC) TRANSPLAN model speed for the "collector street" classification), mean vehicle (i.e., passenger car) weight of 1.82 Mg (4,000 lbs), mean number of wheels equals four, and number of days with at least 0.254 mm (0.01 inch) of precipitation equals 23 (as indicated by NOAA weather reports) (Jacquart, 1997). These values were adapted to the GIS emissions data base.

3.2   Geological Material Size Fractions in the Las Vegas Valley

Particle size analysis should focus on the loose surface material which can be collected with a sweeping or vacuuming technique (Zobeck, 1989). The top few millimeters of soil can also be collected to compare the surface material with soil matrix. Several particle sizing methodologies have been developed, such as micromesh sieving (Hagen *et al.*, 1995), resuspension chambers (Ashbaugh *et al.*, 1995), and vertical settling and sonic sieving (Fryrear *et al.*, 1995), to determine the amount of PM_{10} in geological material. Fryrear *et al.* (1995) reported good correlations for the particle size distributions obtained with sonic sieving and vertical settling techniques, whereas James and Haun (1994) found particle size distributions with a factor of 2.6 higher silt content than those measured by the Wind Erosion Research Laboratory (WERL) for the same soil samples. These differences in silt content can be attributed to the fact that James and Haun (1994) used particle sizing methods (hard sieving and hydrometer analysis) that were more aggressive than the microsieving technique employed by WERL. James and Haun (1994)'s technique was more likely to break up soil aggregates, whereas WERL's technique was more likely to leave some soil aggregates intact.

James and Haun (1994) characterized the particle size distributions of 79 soil samples acquired in the Las Vegas Valley. Using a combination of hard sieving and hydrometer analysis techniques, the study reported silt content ranged from 2% to 82% (James and Haun,

1994). Even though particle sizes calculated by the hydrometer method (i.e., measuring change in solution density with time) do not give equivalent aerodynamic particle sizes (Carvacho *et al.*, 1995), this study illustrates the variations in particle sizes within the Las Vegas Valley.

Percent silt content is used in AP-42 to calculate unpaved road dust emissions (Equation 3-2). Grab samples from the Las Vegas Valley were analyzed for the silt content. Samples from paved and unpaved roads, paved parking lots, windblown soil, construction sites, and material from storage piles were collected by: 1) sweeping the loose surface sediment, 2) scraping off the top 5 mm of material if the sampling surface was crusted, or 3) vacuuming 0.5 to 1.0 kg of material into a plastic bag for transport to the laboratory (Chow, 1987; Houck *et al.*, 1989a). Bulk and soil samples are often mixed together to reduce the total number of individual samples. A total of 22 samples were air-dried in a low-relative-humidity (20% to 30%) environment prior to sample sieving.

A "hard sieving" procedure is applied in this study (Cowherd *et al.*, 1990; Chow and Watson, 1994a) which submits the bulk samples to vigorous shaking in a mechanical sieve. This method determines the maximum amount of fugitive dust potentially available for resuspension when disaggregating activities (e.g., high wind, vehicle traffic) occur. Bulk samples were well-mixed and separated into two parts with sample splitter. Half of the bulk samples were sieved through a 4,000 μm woven wire mesh to remove large particles prior to mass determination. These samples were then sieved again into 600, 300, 150, 75, 38, and 25 μm size fractions. Three out of 22 samples contained a factor of two higher silt content when a 4,000 μm sieve was used. To determine adequate silt content, the set of samples with 4,000 μm sieve is used to normalize the mass abundance.

Figure 3-10 displays the mass size distribution found in dust from paved and unpaved roads, paved parking lots, storage piles, construction sites, and desert surfaces. High variabilities were found for all source types. The percent silt content as well as the silt subfractions (e.g., 38 to 75 μm, 25 to 38 μm, < 25 μm) are presented in Table 3-6. The percent silt content is in the range of 0.9 ± 0.2% in paved road dust to 52.4 ± 0.01% in paved parking lot dust.

Figure 3-11 shows that the average silt content varied from 5.8 ± 3.6% in paved road dust to 36.5 ± 22.5% in paved parking lot dust. Similar compositions are found for the 25-to-38-μm and 38-to-75-μm size fractions. The paved parking lot samples reported 21.0 ± 13.7% of particles less than 25 μm, which is a factor of 10 to 20 higher than was found in other soil types. The difference in silt contents between paved parking lot and other soil types can be attributed to the < 25 μm size fraction. Different sample collection methods (grab versus vacuum sampling) might be the cause of variations. The average silt content for
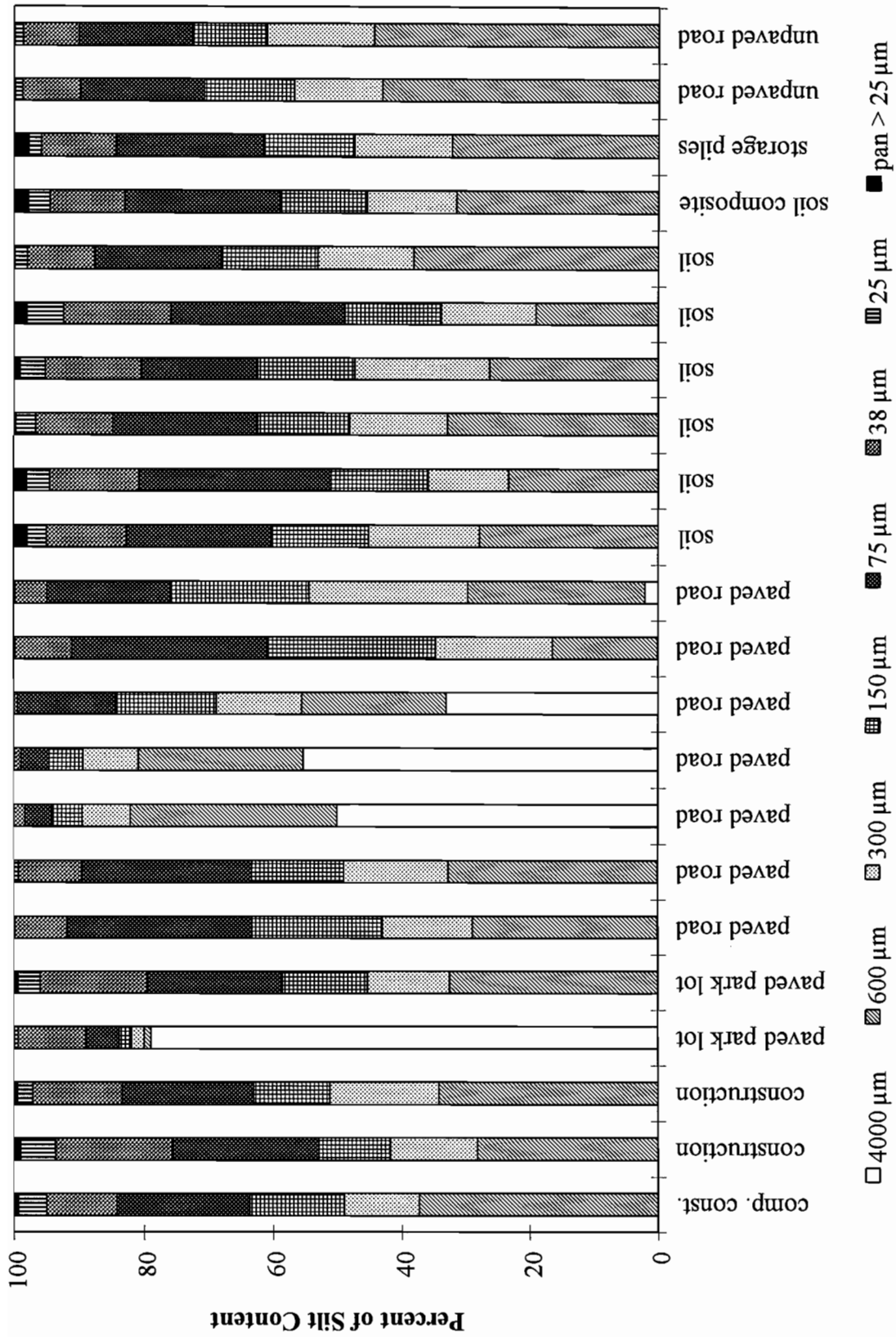
Figure 3-10   Comparison of mass size distributions from various geological materials in the Las Vegas Valley.

Table 3-6
Geological Material Silt Analysis Results in the Las Vegas Valley PM$_{10}$ Study

Geological Source Type	Sampling Location	Individual Samples				Averages by Source Type				
		>75μm (%)	Total Silt <75μm (%)	38 to 75μm (%)	25 to 38μm (%)	>75 μm (%)	Total Silt <75μm (%)	38 to 75μm (%)	25 to 38μm (%)	<25μm (%)
Construction Composite	CINN/NCOV	84.1	15.9 ± 5.0	10.7	4.4					
Construction Soil	PECO	75.6	24.4 ± 0.1	18.0	5.4					
Construction Soil	LONM	83.2	16.8 ± 0.1	13.8	2.3	81.0 ± 4.7	19.0 ± 4.7	14.2 ± 6.1	4.0 ± 1.6	0.8 ± 4.5
Paved Parking Lot Dust	BEMIS	88.9	52.4 ± 0.1	10.4	0.6					
Paved Parking Lot Dust	East Charleston	79.4	20.6 ± 5.0	16.4	3.5	84.2 ± 4.0	36.5 ± 22.5	13.4 ± 7.1	2.0 ± 2.0	21.0 ± 13.7
Paved Road Dust	LSVB @ Spring Mt.	91.7	8.3 ± 0.1	8.1	0.2					
Paved Road Dust	Lake Mead @ Civic	89.4	10.6 ± 0.1	9.8	0.8					
Paved Road Dust	Craig @ PECOS	98.2	3.7 ± 0.1	1.7	0.1					
Paved Road Dust	Mitchell @ BEMIS	98.8	2.7 ± 0.1	1.1	0.1					
Paved Road Dust	East Charleston @ ECHA	99.4	0.9 ± 0.2	0.6	0.1					
Paved Road Dust	East Charleston @ Eastern Ave.	91.0	9.0 ± 0.2	8.8	0.2					
Paved Road Dust	I-95	94.8	5.3 ± 0.1	5.0	0.2	94.8 ± 4.1	5.8 ± 3.6	5.0 ± 3.6	0.2 ± 0.2	2.6 ± 2.9
Soil	NOCO	82.6	17.4 ± 0.1	12.3	3.0					
Soil	GOLF	80.7	19.3 ± 0.1	13.7	3.6					
Soil	NECD	84.7	15.3 ± 0.3	11.9	3.1					
Soil	BEMIS	80.4	19.6 ± 4.4	14.7	3.9					
Soil	LONE	75.8	24.2 ± 0.1	16.5	5.7					
Soil	ECHA	87.6	12.4 ± 0.1	10.3	1.9					
Soil Composite	THUN/LOSS/GROW/LAMB	83.0	17.0 ± 0.1	11.4	3.3	82.1 ± 3.7	17.9 ± 3.7	13.0 ± 2.1	3.5 ± 1.1	1.4 ± 2.5
Storage Pile	LONE	84.4	15.6 ± 0.1	11.5	1.9	84.8	16	12	1.9	2.2
Unpaved Road Dust	LOSS	89.9	10.1 ± 0.9	8.9	1.2					
Unpaved Road Dust	DONO	90.0	10.0 ± 0.3	8.6	1.3	89.9 ± 0.1	10.1 ± 0.1	8.8 ± 0.2	1.2 ± 0.1	0.1 ± 0.1
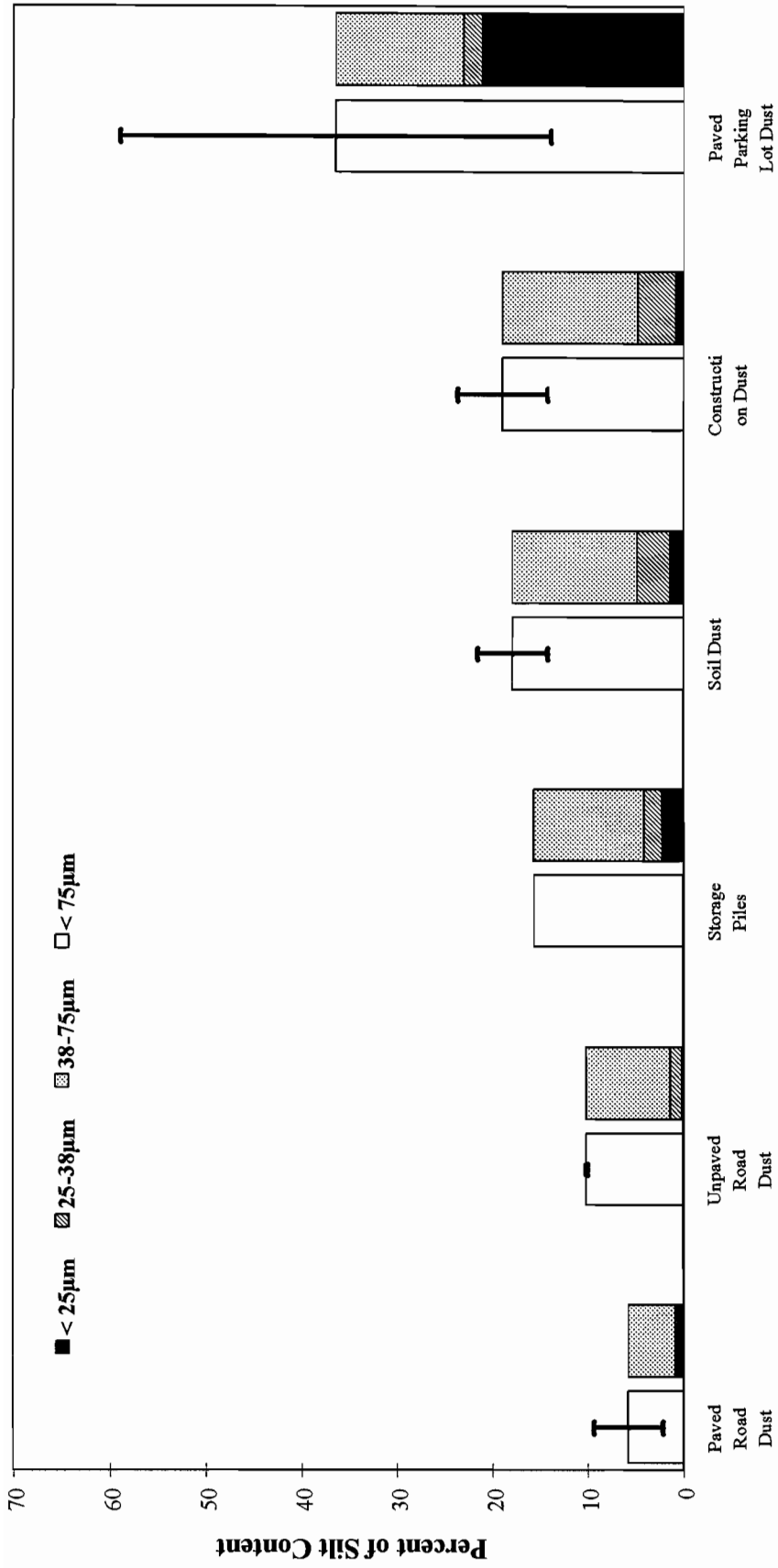
Figure 3-11   Comparison of mass size distributions within the silt content in the Las Vegas Valley.

soils, construction dust, and unpaved road dust is $15.7 \pm 4.0\%$. This value is similar to the 18% silt content of Las Vegas soils determined by the Wind Erosion Research Laboratory (WERL) in Manhattan, KS, using a micromesh sieving technique (Hagen *et al.*, 1995; James and Haun, 1994).

3.3   Emission Activities Surrounding the Ambient Monitoring Sites

Development of a PM_{10} fugitive dust emissions inventory requires the input of: 1) emission factors, 2) source activity levels, and 3) applicable control measures. Section 3.1 summarizes and compares the emission factors for various source types. These emission factors often require the input of additional parameters such as soil type, soil surface conditions, frequency and type of natural and anthropogenic disturbances, equipment/vehicle characteristics, and climate factors. In addition, information on source extent (e.g., activity level, vehicle kilometers traveled), is required to calculate the emission rate.

This subsection examines the activity levels for unpaved roads/parking lots, disturbed/undisturbed vacant lands, construction activities, and industrial operations for the two base sites and 30 satellite sites. Emphasis was given to tracking the progress/completion of each construction project located in close proximity to a satellite monitoring site.

3.3.1   The Bemis and East Charleston Base Site Microinventory

To identify the potential sources that contribute to the PM_{10} concentrations within close proximity (i.e., 4 km^2 or 1.5 mi^2) to the two base sites (i.e., Bemis and East Charleston), a detailed site survey by video camera was undertaken. The dominant land use patterns identified within the study areas were:

- Industrial operations (e.g., sand and gravel operations);

- Commercial construction;

- Residential construction;

- Disturbed desert/vacant land;

- Undisturbed desert/vacant land;

- Recreational areas (e.g., parks, golf courses);

- Commercial districts; and

- Residential areas.

Figure 3-12 shows different land uses in the vicinity of the Bemis monitoring site. Although the land-use units designated on the map are not scaled, the relative land-use types and locations of the different areas are discernible.

In the immediate vicinity of the Bemis monitoring site (100 m radius), there are bare, relatively-heavily-crusted soils to the south, east, and west extending to I-15. Directly north of the sampling site is a paved parking lot and a large commercial building. Mitchell Street, which lies approximately 75 m to the east, is a four-lane paved road that is frequently traveled by medium- to heavy-duty trucks. A large development construction project is situated one kilometer to the west of the monitoring site and extends to the northwest. The area to the northeast is mainly open, undisturbed desert soil that is subdivided by paved roads (i.e., McGuire Street, Walnut Road, Andrews Street, Vandenberg Drive, and Eaker Street). Some commercial buildings along these roads extend back up to 150 m. The undisturbed desert soils are covered with varying amounts of scrubby desert vegetation. Owing to the high surface roughness and vegetative cover, wind-blown dust from these surfaces are minimized. To the north, past Lone Mountain Road, is also undisturbed desert land with a much higher percentage of vegetative cover. Potential fugitive dust sources within the microinventory area include a sand and gravel operation 0.75 km to the northwest at Lone Mountain Road and Vandenberg Drive, and some small-scale commercial construction projects. Traffic from nearby Craig Road and I-15 is moderate with heavy-duty vehicles.

The microinventory of the East Charleston base site is shown in Figure 3-13. The dominant land use in this area is residential housing with some commercial properties along East Charleston Boulevard. Most of the residential houses have established grass yards, while the commercial properties are largely surrounded by paved parking lots. South of the monitoring site is a large paved commercial parking lot. Across East Charleston Boulevard to the southeast is a large undeveloped vacant property that shows signs of disturbance by anthropogenic activity. In addition, 0.5 to 1.0 km (0.3 to 0.6 mi) south of East Charleston Boulevard behind a vacant lot and extending towards Olive Street lies a residential housing construction project that was active throughout the study period. Traffic on East Charleston Boulevard is heavy with a mixture of light- and heavy-duty vehicles.

3.3.2 Activities Surrounding the Satellite Sites

Similar to the microinventory approach at the two base monitoring sites, site surveys were conducted for the 30 satellite monitoring sites during each of the five intensive monitoring periods. Video cameras were used to document the environment surrounding the satellite monitoring site during each intensive monitoring period. Written records further document any changes that occurred on a day-to-day and/or long-term basis. A list of
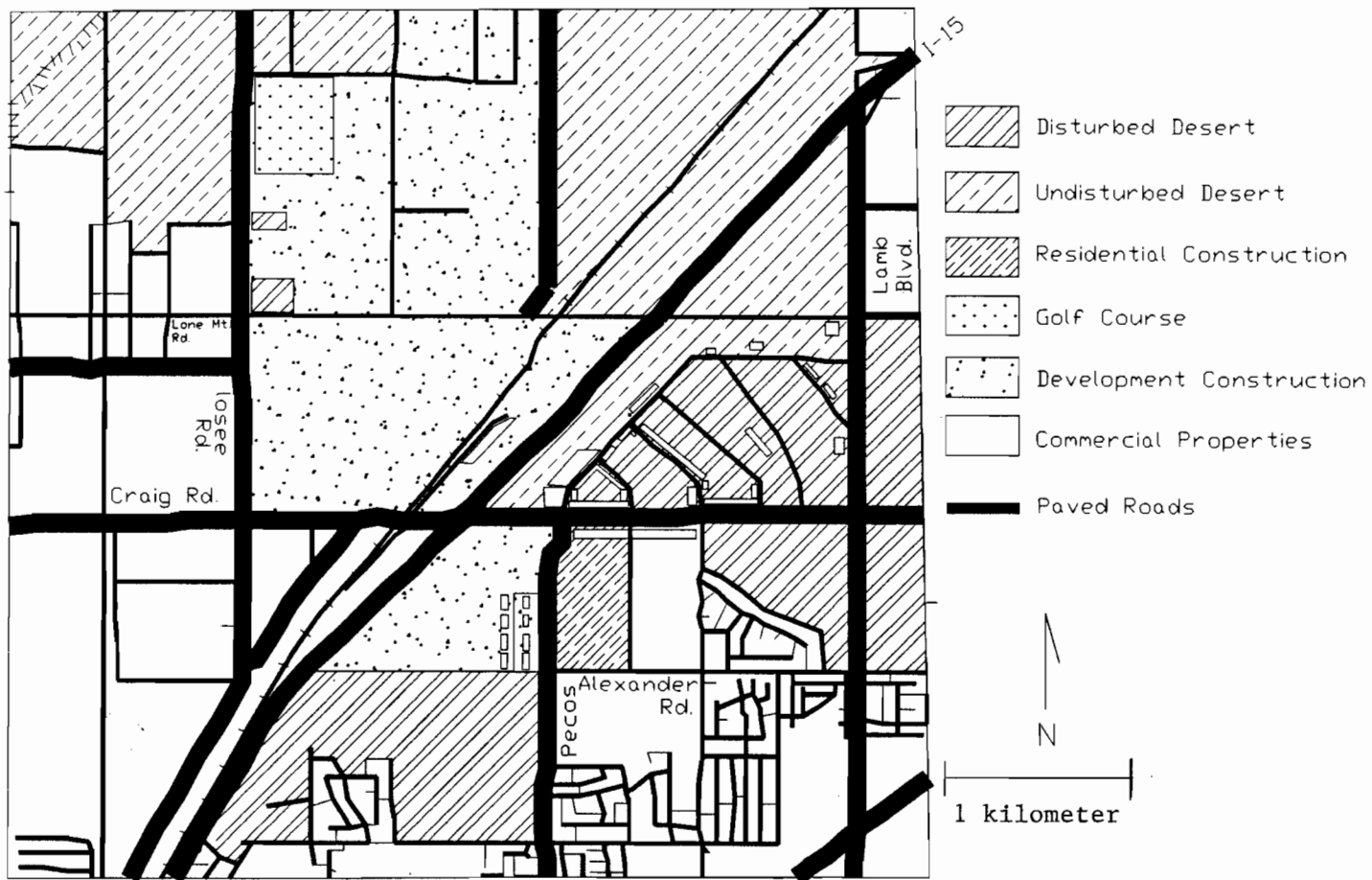
Figure 3-12   Microinventory map of land use patterns surrounding the Bemis base site.
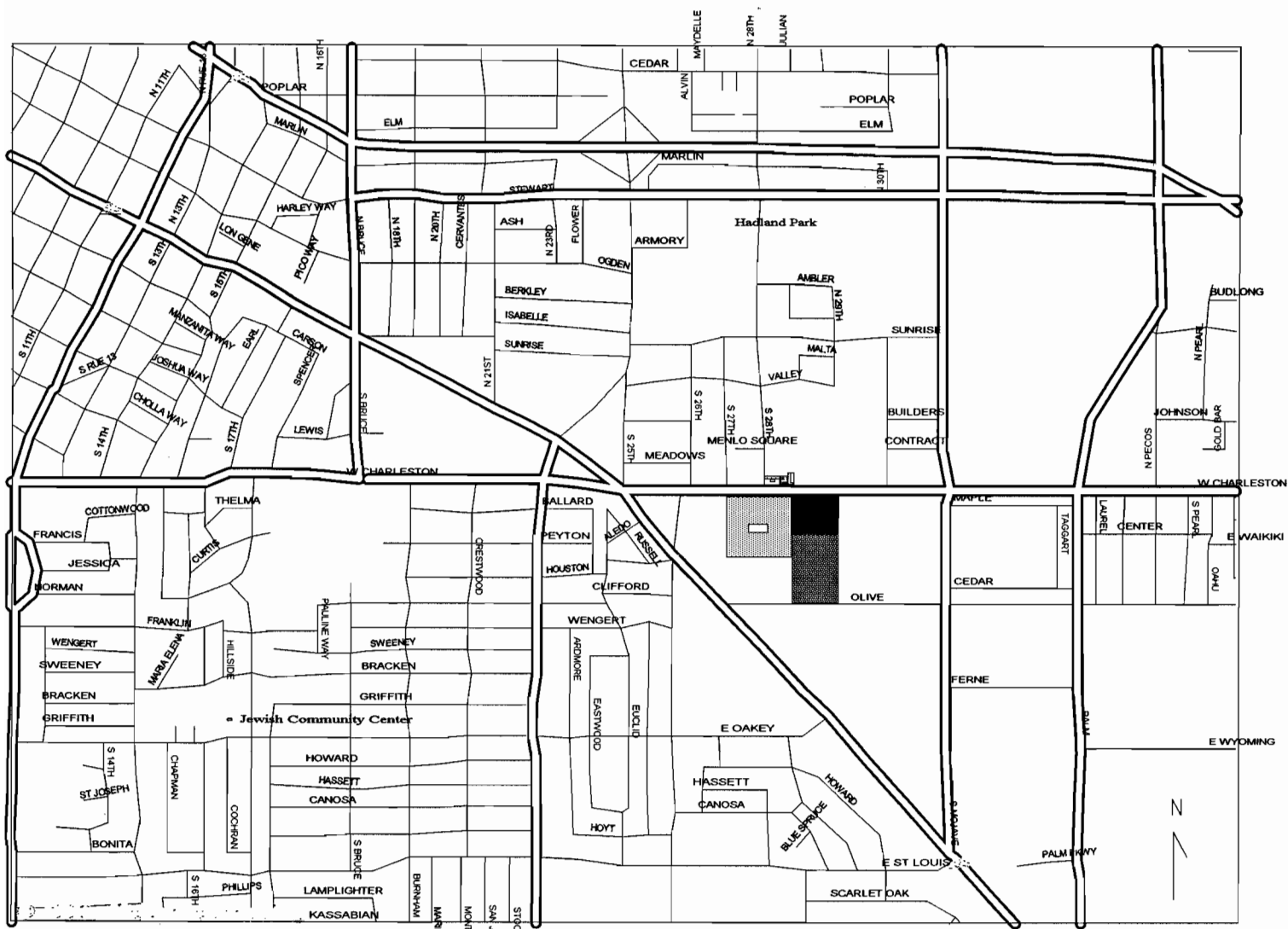
Legend

☐ Commercial Buildings

■ Disturbed Vacant Land

▨ Paved Parking Lot

▨ Residential Construction

▦ Grassed Area

1 kilometer

Figure 3-13 Microinventory map of land use patterns surrounding the East Charleston base site (unmarked areas are predominantly residential with commercial properties lining the major streets).

satellite monitoring site descriptions and locations are presented in Table 2-3. Detailed site maps with identification of the land uses in the vicinity of the monitoring site can be found in the study plan (Chow *et al.*, 1995).

Site surveys were conducted at the beginning of each intensive monitoring period. Activity measurements included a 360-degree video tape of each site, as well as recording the locations and descriptions of surrounding activities on the site survey log book. Documented emission activity records for the 30 satellite sites during each intensive are summarized in Table 3-7.

As noted in the site surveys, most of the anthropogenic activities in the commercial districts, residential neighborhoods, and industrial operations remained consistent, while activity levels at residential/commercial development projects and paving/oiling of roads varied from one intensive monitoring period to another. These activity records, along with the land uses surrounding each site, are the basis for site-type classification. General source types of interest were used to categorize the satellite sites into the following six site-types:

- Industrial (mainly sand and gravel operations);

- Construction activities for commercial building, residential housing, or roadway development;

- Commercial district (e.g., small shopping centers, restaurants);

- Residential neighborhoods;

- Disturbed and undisturbed vacant land; and

- Motor-vehicle-related suspended road dust.

Each satellite monitoring site is classified according to its dominant activities during each intensive monitoring period. As shown in Table 3-8, classifications are prioritized into primary, secondary, and tertiary sources which represent the degree of activity level among different source categories. The primary source type is used to determine the ultimate site-type classification. Among the 30 satellite monitoring sites, the site-type distribution is: three industrial, ten construction, five commercial (excluding one collocated site), three residential, and eight disturbed/undisturbed vacant land sites. These site-type classifications are used for data analysis and modeling presented in Sections 6 and 7.

Table 3-7

Documented Activities Surrounding the Saturation Monitoring Sites during Intensive Monitoring Periods

Site ID/Code	Spring Intensive 1 (04/15/95 to 04/21/95)	Spring Intensive 2 (05/12/95 to 05/16/95)	Summer Intensive (06/05/95 to 06/07/95)	Fall Intensive (09/07/95 to 09/12/95)	Winter Intensive (01/26/96 to 01/30/96)
1. PECO	Active construction to the E, NE and SE.	Active construction to the E, NE and SE.	Active construction to the E, NE and SE.	Housing construction is near completion. Site still requires landscaping. Bare, disturbed, exposed soil adjacent to buildings.	Construction is completed to the south. Open area in front of condos has been paved. Dirt tracks adjacent to samplers.
2. CLIF	Construction activity to the S and SW across Lake Mead Blvd.	Construction activity to the S and SW across Lake Mead Blvd.	Construction activity to the S and SW across Lake Mead Blvd. Open stockpiles of soil situated between apartments and road.	Across Lake Mead Blvd. to the southwest the construction site for residential apartment units is almost completed.	Construction and landscaping is completed. No visible construction activity in any direction.
3. NCOV	Construction activity during weekdays.	Unpaved road providing track-out to Carey St. Construction activity during weekdays.	Unpaved road providing track-out to Carey St. Construction activity during weekdays.	Street running N-S nearby the site has been paved. Seven-foot wall has been erected around construction site. No change on vacant lot to the SE.	Housing construction is completed. No change on vacant lot to the SE.
4. MARK	Construction activity to the W and NW.	Construction activity to the W and NW. Market Center Dr. is unpaved one "block" past the site.	Construction activity to the W and NW. Market Center Dr. is unpaved one "block" past the site.	Building complex directly west of site is completed. Dead end road is now paved. Open area to the northwest.	Completed building instead of open field to the NW. Only a small piece of land left between new building and Craig Rd.

Table 3-7 (continued)

Documented Activities Surrounding the Saturation Monitoring Sites during Intensive Monitoring Periods

Site ID/Code	Spring Intensive 1 (04/15/95 to 04/21/95)	Spring Intensive 2 (05/12/95 to 05/16/95)	Summer Intensive (06/05/95 to 06/07/95)	Fall Intensive (09/07/95 to 09/12/95)	Winter Intensive (01/26/96 to 01/30/96)
5. CINN	Active housing construction phase.	Active construction phase.	Active construction phase. Framing of houses in immediate vicinity of site is almost completed. Yard areas are still bare with disturbed soil.	Houses directly south are finished and landscaped. No more visible construction activities in the vicinity. Construction activity located 0.25 km south of the site.	Construction and landscaping in the neighborhood is finished. Small scale curb repairs nearby with concrete cutting operations creating some dust.
6. EFER	Well established residential area, light vehicle traffic.	No observable changes in the vicinity of the site.	No observable changes in the vicinity of the site.	No observable changes in the vicinity of the site.	No observable changes in the vicinity of the site.
7. LONE	Weekday activity at the sand and gravel operation. Vacant land to the S and SE.	Weekday activity at the sand and gravel operation. Open areas are unchanged.	Weekday activity at the sand and gravel operation. Open areas are unchanged.	Active construction in the vicinity (new building construction at Mitchell St. and Lone Mountain Rd.). Weekday activity at the sand and gravel operation. Open areas are unchanged.	Construction noted in September is finished. Weekday activity at the sand and gravel operation. Open areas are unchanged.

Table 3-7 (continued)

Documented Activities Surrounding the Saturation Monitoring Sites during Intensive Monitoring Periods

Site ID/Code	Spring Intensive 1 (04/15/95 to 04/21/95)	Spring Intensive 2 (05/12/95 to 05/16/95)	Summer Intensive (06/05/95 to 06/07/95)	Fall Intensive (09/07/95 to 09/12/95)	Winter Intensive (01/26/96 to 01/30/96)
8. BEMI	Vacant land to the S and W. Commercial properties to the N and E. Sand and gravel operation 0.75 km to NW. Construction site is 1 km to the W.	No discernible change in the open areas.	No discernible change in the open areas.	No discernible change in the open areas. Visible dust plumes observed as heavy-duty vehicles pass by.	No discernible change in the open areas. Visible dust plumes are observed as heavy-duty vehicles pass by.
9. LAMB	Truck traffic entering/exiting sand and gravel operation creates visible dust from road surface. Commercial properties to the N to NE, E to S with vacant land in between.	Truck traffic entering/exiting sand and gravel operation creates visible dust from road surface. Open field remains unchanged.	Truck traffic entering/exiting sand and gravel operation creates visible dust from road surface. Open field remains unchanged.	Truck traffic entering/exiting sand and gravel operation creates visible dust from road surface. Open field remains unchanged. Plume was observed from sand and gravel hopper.	Truck traffic entering/exiting sand and gravel operation creates visible dust from road surface. Open field remains unchanged.
10. MICH	Daily activity of heavy-duty trucks passing by the site.	Daily activity of heavy-duty trucks passing the site at low speed.	Daily activity of heavy-duty trucks passing the site at low speed.	Daily activity of heavy-duty trucks passing the site at low speed. Grass was added around the site in front of the warehouse. Small vacant lot directly to the SE adjacent to the convenience store.	Grassed area around building has been replaced with gravel. New building has been completed in the lot adjacent to the convenience store.

Table 3-7 (continued)
Documented Activities Surrounding the Saturation Monitoring Sites during Intensive Monitoring Periods

Site ID/Code	Spring Intensive 1 (04/15/95 to 04/21/95)	Spring Intensive 2 (05/12/95 to 05/16/95)	Summer Intensive (06/05/95 to 06/07/95)	Fall Intensive (09/07/95 to 09/12/95)	Winter Intensive (01/26/96 to 01/30/96)
11. DONO	Construction activity west of the site.	Activity noted on the construction site to the west of the site.	Activity noted on the construction site to the west of the site.	Activity noted on the construction site to the west of the site.	No evidence of activity on the construction site. Site has been prepared and is awaiting next development phase.
12. BILL	Flat, graded vacant land surrounds the site. I-15 is 150 m to the E.	No observable changes.	No observable changes.	No observable changes.	No observable changes.
13. GOLF	Activity noted on the construction site to the S and SE of the site. Impacted by the same development as NECD (site ID number 30).	Activity noted on the construction site to the S and SE of the site. Impacted by the same development as NECD (site ID number 30).	Active construction of sewer installation directly south of site.	Sewer installation is completed. Active construction with water truck on the road. Visible dust loading on the street surface.	No evidence of activity on the construction site. Site has been prepared and is awaiting next development phase.
14. LOSS	Vacant land with scrubby vegetation to the W and NW. Golf course to the E around to the S. Unpaved road to the N.	No observable changes in the surrounding open fields.	No observable changes in the surrounding open fields.	No observable changes in the surrounding open fields. More visible dust loading on the street surface.	No observable changes in the surrounding open fields.

Table 3-7 (continued)

Documented Activities Surrounding the Saturation Monitoring Sites during Intensive Monitoring Periods

Site ID/Code	Spring Intensive 1 (04/15/95 to 04/21/95)	Spring Intensive 2 (05/12/95 to 05/16/95)	Summer Intensive (06/05/95 to 06/07/95)	Fall Intensive (09/07/95 to 09/12/95)	Winter Intensive (01/26/96 to 01/30/96)
15. CRAI	Construction on N side of Craig Rd. Commercial building site is surrounded by open disturbed surfaces. Road construction at Craig Rd. and Losee Rd. Vacant land to the S.	Construction on N side of Craig Rd. Commercial building site is surrounded by open disturbed surfaces. Road construction at Craig Rd. and Losee Rd. No change in open fields.	Construction on N side of Craig Rd. Commercial building site is surrounded by open disturbed surfaces. No change in open fields.	Construction of large building to the N is completed. Large, flat, open area surrounding new building. No change in open fields to S. No more stockpiles of soil to the N.	No observable changes.
16. LONM	Area south of the site is being prepared for a housing development.	Area south of the site is being prepared for a housing development. Two lanes of the unpaved road adjacent to the site to the N have been oiled.	No housing construction yet. Roads within the developing area have been paved. North half of Lone Mountain Rd. remains unpaved.	Active construction of houses to the S. North half of Lone Mountain Rd. remains unpaved.	Active construction of houses to the S. North half of Lone Mountain Rd. remains unpaved.
17. NWAL	Sand and gravel operation directly to the E. Vacant lot to the N. Stockpiles of soils to the S.	No observable changes.	No observable changes.	Noticeable dust loading on street surface.	No observable changes.

Table 3-7 (continued)

Documented Activities Surrounding the Saturation Monitoring Sites during Intensive Monitoring Periods

Site ID/Code	Spring Intensive 1 (04/15/95 to 04/21/95)	Spring Intensive 2 (05/12/95 to 05/16/95)	Summer Intensive (06/05/95 to 06/07/95)	Fall Intensive (09/07/95 to 09/12/95)	Winter Intensive (01/26/96 to 01/30/96)
18. GROW	Road construction around the intersection of Gowan St. and Civic Center Dr.	Road construction around the intersection of Gowan St. and Civic Center Dr.	Road construction around the intersection of Gowan St. and Civic Center Dr.	Road construction is completed. Bare, disturbed soil on all corners of the intersection.	Road construction is completed. Bare, disturbed soil on all corners of the intersection.
19. HAMI	Established residential area. I-15 is ~100 m to the W. Cheyenne Ave is ~ 50 m to the N.	No observable changes.	No observable changes.	No observable changes.	No observable changes.
20. NOCO	Residential area, vacant lot to the SW.	No observable changes.	No observable changes.	No observable changes.	No observable changes.
21. LASV	Vacant land to the E & S. Light commercial/ residential to the N.	No observable changes.	No observable changes.	No observable changes.	No observable changes.
22. WALN	Surrounded by commercial properties, with some vacant land between properties.	No observable changes.	No observable changes.	No observable changes.	No observable changes.
23. MCDA	Surrounded by paved open surfaces. Large building to the W and a Wendy's restaurant to the E.	No observable changes.	No observable changes.	No observable changes.	No observable changes.

Table 3-7 (continued)

Documented Activities Surrounding the Saturation Monitoring Sites during Intensive Monitoring Periods

Site ID/Code	Spring Intensive 1 (04/15/95 to 04/21/95)	Spring Intensive 2 (05/12/95 to 05/16/95)	Summer Intensive (06/05/95 to 06/07/95)	Fall Intensive (09/07/95 to 09/12/95)	Winter Intensive (01/26/96 to 01/30/96)
24. ECHA	Site is surrounded by grassy area. McDonalds restaurant to the E. Paved parking lot to the S. Housing construction far to the S (approx. 0.5 to 1.0 km).	Construction is active past the vacant land 0.5 to 1.0 km to the SE.	Construction is active past the vacant land 0.5 to 1.0 km to the SE.	Construction is active past the vacant land 0.5 to 1.0 km to the SE.	McDonalds has closed. Housing development is completed 0.5 to 1.0 km to the SE.
25. SWLC	Surrounded by vacant land.	No observable changes.	No observable changes.	No observable changes.	Construction activity 0.5 to 1.0 km to the SE.
26. THUN	Open gravel-covered surface to the S and W before paved parking lot begins. Housing construction to the N and NW.	No observable changes to the S. Housing construction 0.5 to 1.0 km behind the wall to the N.	No observable changes to the S. Housing construction 0.5 to 1.0 km behind the wall to the N.	No observable changes to the S. More housing has been completed behind the wall to the N.	No observable changes to the S. Housing construction is almost complete.
27. ABEM	Collocated site with BEMI (site ID number 8).	Collocated site with BEMI (site ID number 8).	Collocated site with BEMI (site ID number 8).	Collocated site with BEMI (site ID number 8).	Collocated site with BEMI (site ID number 8).
28. NWCP	Established residential to the S. Across Craig Rd is vacant land.	No observable changes.	No observable changes.	No observable changes.	No observable changes.

Table 3-7 (continued)

Documented Activities Surrounding the Saturation Monitoring Sites during Intensive Monitoring Periods

Site ID/Code	Spring Intensive 1 (04/15/95 to 04/21/95)	Spring Intensive 2 (05/12/95 to 05/16/95)	Summer Intensive (06/05/95 to 06/07/95)	Fall Intensive (09/07/95 to 09/12/95)	Winter Intensive (01/26/96 to 01/30/96)
29. VAND	Vacant land to the E and W. Large commercial buildings past the vacant land to the W.	No observable changes.	No observable changes.	Active earth moving activity noted to the E (0.5 km away).	No observable changes in the immediate surroundings. No activity noted.
30. NECD	Vacant land with scrubby vegetation to the E. Active development construction to the W.	Active development construction to the W.	Active development construction to the W.	Not much activity noted on construction site.	No activity noted on construction site.

Table 3-8

Source Type Classifications during Each Intensive Monitoring Period

Site ID/Code	Residential Neighborhood	Commercial District	Industrial	Residential Development	Commercial/ Roadway	Undisturbed	Disturbed	Motor-Vehicle-Related Suspended Road Dust	Comments
1. PECO	S S S S S							T T T T T	
2. CLIFF	T T T T T							S S S S P	
3. NCOV	S S S S P							T T T T T	
4. MARK		T T P P P		P P S S S				S S T T T	
5. CINN	S S S S P							T T T T T	
6. EFER	P P P P P							S S S S S	
7. LONE			P P P P P				S S S S S	T T T T T	Sand and gravel operation
8. BEMI		P P P P P					T T T T T	S S S S S	
9. LAMB			$P^aP^bP^cP^dP^e$				T T T T T	S S S S S	Sand and gravel operation
10. MICH		P P P P P					S S S S S	S S S S S	3 service centers
11. DONO				P P P P S			S S S S P		
12. BILL						P P P P S		S S S S P	Adjacent to I-15
13. GOLF				P P P P			T T T T P	S S S S S	

Table 3-8 (continued)
Source Type Classifications during Each Intensive Monitoring Period

Site ID/Code	Residential Neighborhood	Commercial District	Residential	Industrial	Development	Commercial/ Roadway	Undisturbed	Disturbed	Motor-Vehicle-Related Suspended Road Dust	Comments
14. LOSS								PPPPP	SSSSS	Unpaved road to the north
15. CRAI		TTTTT					PPPPP		SSSSS	
16. LONM			PPPPP						SSSSS	
17. NWAL				PPPPP			TTTTT		SSSSS	Sand and gravel operation
18. GROW					PPPTT[a]			SSSPP	TTTSS	Road construction
19. HAMI	SSSSS	TTTTT				PPPPP				
20. NOCO	PPPPP						TTTTT		SSSSS	Adjacent to I-15
21. LASV		SSSSS					PPPPP		TTTTT	
22. WALN		PPPPP					PPPPP		SSSSS	
23. MCDA		PPPPP					TTTTT		SSSSS	
24. ECHA	TTTTT	PPPPP							SSSSS	
25. SWLC							PPPPP		SSSSS	
26. THUN			TTTTT					PPPPP	SSSSS	

Table 3-8 (continued)
Source Type Classifications during Each Intensive Monitoring Period

Site ID/Code	Residential Neighborhood	Commercial District	Industrial	Residential	Development	Commercial/ Roadway	Undisturbed	Disturbed	Motor-Vehicle-Related Suspended Road Dust	Comments
27. ABEM		P P P P P						T T T T T	S S S S S	
28. NWCP	T T T T T						P P P P P		S S S S S	
29. VAND		T T T T T						P P P P P	S S S S S	
30. NECD					P P P P S			T T T T T	S S S S P	

a   Representing spring intensive between 04/15/95 and 04/21/95.

b   Representing spring intensive between 05/12/95 and 05/16/95.

c   Representing summer intensive between 06/05/95 and 06/07/95.

d   Representing fall intensive between 09/07/95 and 09/12/95.

e   Representing winter intensive between 01/26/96 and 01/30/96.

3.4 Fugitive Dust Emission Data Base

Clark County Department of Comprehensive Planning (CCDCP) provided the 1995 emission estimates in the form of dBase files for each source type (Jacquart, 1997). These data base files were integrated into an Arc/Info coverage of township-range-section as part of the Las Vegas PM_{10} Study dispersion modeling effort. The resulting Arc/Info coverage contained emission estimates for each section in tons per year for unpaved roads, paved roads, mobile sources, residential wood combustion, disturbed land, controlled construction, controlled construction track-out, controlled construction wind erosion, and stationary sources. Table 3-9 summarizes the calculated emissions for each source type.

Table 3-9
Summary of Fugitive Dust Emission Rates in the Modeling Domain

| | Valley-wide Annual Emission Rate | |
Source Type	(tons/year)	(Mg/year)
Paved Road	6,766	6,138
Unpaved Road	6,162	5,590
Mobile Sources	822	746
Residential Wood Combustion	309	280
Wind Erosion from Disturbed Vacant Land	4,881	4,428
Controlled Construction Activities	25,778	23,385
Controlled Construction Site Track-Out	5,019	4,553
Controlled Construction Site Wind Erosion	4,052	3,676
Stationary Sources	1,855	1,683

4.0 SOURCE MEASUREMENTS

Source apportionment requires information about the chemical and physical characteristics of the emissions sources that are likely to affect pollutant concentrations at a receptor. For the Chemical Mass Balance (CMB) receptor model (Watson *et al.*, 1990b), the required information is the fractional composition of each chemical species in the source emissions and an estimate of the variability of those compositions.

In a study to evaluate the feasibility of source apportionment of utility emissions, Javitz and Watson (1988) concluded that the major weakness of all receptor models is inadequate source composition data. They identified the following deficiencies in currently available source profiles: 1) the species measured are more often those that are convenient rather those which differentiate among sources; 2) the types of species and size fractions measured are not the same for different source types and are not equivalent to the types of measurements made at receptors; 3) measurement methods are non-standard and do not give equivalent results for the same species; 4) source characteristics, fuels, and operating parameters are inadequately documented; 5) data are of poor or unknown quality; 6) source profile uncertainties are not reported or realistic; 7) source samples are not representative of source profiles as they appear at the receptor; and 8) data are not available in formats which can be conveniently interfaced to modeling software.

Javitz and Watson (1988) recommended the development of a standardized approach to sampling and analyzing particulate and gaseous emissions that would minimize these concerns with respect to future source profile measurements. Such a protocol was developed (Core and Houck, 1987) and adapted for the California Air Resources Board's (ARB) source characterization studies (Chow, 1987; Houck *et al.*, 1989a, 1989b, 1989c, 1989d, 1989e) in addition to several other recent studies (e.g., Chow and Watson, 1994b; Chow and Watson, 1997b; Heisler *et al.*, 1995). This section describes the source profiles that were measured in the Las Vegas Valley for use in receptor modeling.

4.1 Source Types and Characterization Methods

The potential source types that contribute to PM_{10} in the Las Vegas Valley are: 1) fugitive dust from paved and unpaved roads, disturbed and undisturbed vacant land, and construction as well as sand and gravel operations (termed geological material); 2) motor vehicle exhaust from passenger cars, buses, and trucks; 3) residential wood combustion; and 4) secondary aerosols (i.e., ammonium nitrate and ammonium sulfate particles that form from gaseous ammonia, oxides of nitrogen, and sulfur dioxide emissions).

There are many source sub-types within some of these categories that cannot be distinguished by commonly measured chemical species. The source contribution from each

category is a composite of these different sub-types, and the derived profile must represent this mixture. For example, with currently measured chemical species, it is not possible to distinguish contributions from resuspended road dust, windblown dust, and construction dust from each other. These sources are therefore grouped together into a source type known as geological material.

A number of methods have evolved over the past decade to extract samples from sources that have chemical and physical properties similar to those found at a receptor. Several of these methods are described in detail by Chow *et al.* (1986), Gordon *et al.* (1984), and Houck (1991), and the methods selected for this study were described in the program plan (Chow *et al.*, 1995). In each of these methods, emitted particulate matter is collected on substrates that are then submitted to chemical analyses as described in Section 2 for ambient samples.

More than 100 size-fractionated source samples were collected using the following specialized approaches:

- Sweeping or grab sampling of soil, unpaved-road dust, and bulk material using a trowel and brush.

- Vacuum sampling of paved-road and paved parking lots using a high-volume road dust sampler (Houck, 1991).

- Laboratory resuspension sampling of sieved soil samples using a parallel impactor sampling device (Chow *et al.*, 1994a).

- Ground-based source sampling of motor vehicle exhaust in source-dominated environments using portable fine-particle samplers.

- Diluted exhaust sampling of emissions from residential chimneys using a portable fine particle sampler and extended sampling probe.

The individual source profiles compiled for the Las Vegas Valley PM_{10} Study are assembled in the data base and presented in Section 5.2 and in Appendix B. Not all of the species that contribute to PM_{10} were measured (i.e. oxygen associated with mineral oxides and hydrogen associated with organic carbon compounds), and the abundances do not sum to 100%. Many of these profiles were not used in the CMB source apportionments, but all profiles were made available for model sensitivity tests. Mnemonics and brief descriptions for each of these profiles are summarized. Profiles used for source apportionment are often composites derived from several individual sample profiles. Such composites provide a better estimate of the average abundances and their variability than is available from a single source sample

with an analytical uncertainty. The rationale for selecting certain samples used in the composites is documented in the following subsections.

4.2   Geological Source Profiles

Since soils vary chemically due to their geological origin and amendment, local soil types and land uses were examined prior to obtaining samples using maps from the U.S. Department of Agriculture Soil Conservation Service. Site surveys were made around sampling sites to determine the surface loadings on nearby streets and the locations of construction activities. Sampling locations included road-fills and cuts, sidewalks, shoulders, parking lots, fields in close proximity to the receptor sites (base and satellite sites), highways, busy traffic intersections, unpaved roads, storage piles, and construction sites.

A total of 40 geological samples were collected using grab sampling and vacuum sampling techniques. The top 1 or 2 cm of surface material was collected from unpaved surfaces, since this represents the reservoir available for suspension by wind or vehicle movement. Unpaved road dust was collected across the road from shoulder to shoulder. Samples from highways, paved roads, gutters, sidewalks, and paved parking lots were collected using a "vacuum cleaner" high-volume road dust samplers owing to the relatively small amounts of dust on paved surfaces. The vacuum sampler consisted of a modified high-volume sampler filter housing with a 20.3 × 25.4 cm quartz-fiber filter to trap all particles. Each paved surface sample included several traverses across the pavement.

Table 4-1 lists each of the geological source samples along with a description of sampling location. The locations from which geological material was collected are shown in Figure 4-1. To reduce the total number of individual samples, bulk and soil samples were composited to represent individual source types. Twenty-two of the 40 samples were composited and submitted for resuspension and chemical analysis. These samples are identified in Table 4-1 under the "composited sample ID" column. In the laboratory, the soil samples were air-dried in a low-relative-humidity (approximately 20% to 30%) environment and sieved through a Tyler 400-mesh screen (< 38 μm geometric diameter) prior to resuspension in the laboratory chamber following the procedures described by Chow *et al.* (1994a).

Filter samples were drawn through PM_{10} inlets. Most of the mass of geological material is in the coarse particle portion of PM_{10} (Houck *et al.*, 1989a), and similar compositions were found for the $PM_{2.5}$ and PM_{10} geological profiles (Chow and Watson, 1994c). As shown in Table 4-2, 22 of the individual geological source profiles were used to form six composite source profiles by calculating the average and standard deviation of each chemical abundance.

Table 4-1
Geological Material Source Profiles Acquired for the Las Vegas Valley PM$_{10}$ Study

Composited Sample ID	Sample ID	Laboratory /Map[a] ID	Sample Type	Collection Date	Description	Mnemonic in Composited Profile
LVGCONS1	LVSS025	RS285	Construction Soil	06/06/95	Soil from south of CINN site	LVGCONSC
	LVSS027	RS287	Construction Soil	06/06/95	Soil adjacent to NCOV site	
LVGCONS2	LVSS028	RS288	Construction Soil	06/06/95	Soil from east of PECO site	LVGCONSC
LVGCONS3	LVSS032	RS292	Graded Surface/Construction	06/07/95	Soil from graded surface west of NECD site	LVGCONSC
	LVSS033	RS293	Graded Surface/Construction	06/07/95	Soil from graded surface west of DONO site	
	LVSS034	RS294	Graded Surface/Construction	06/07/95	Soil from graded surface west of BILL site	
LVGCONS4	LVSS035	RS295	Soil/Graded Surface	06/07/95	Soil from graded surface south of GOLF site	LVGCONSC
LVGCONS5	LVSS037	RS297	Construction Soil	06/07/95	Soil from south of LONM site	LVGCONSC
LVGPLOT1	LVSS007	RS268	Paved Parking Lot Dust	09/10/95	Paved parking lot dust at the McDonalds parking lot north of East Charleston Blvd.	LVGPLOTC
LVGPLOT2	LVSS010	RS271	Paved Parking Lot Dust	09/10/95	Paved parking lot dust from east of Bemis site	LVGPLOTC
LVGPVRD1	LVSS008	RS269	Paved Road Dust	09/10/95	Paved road and soil dust from the median at East Charleston Blvd. (motor vehicle exhaust source sampling site)	LVGPVRDC
	LVSS004	RS265	Paved Road Dust	09/10/95	Paved road dust from westbound lane of East Charleston Blvd.	
LVGPVRD2	LVSS006	RS267	Gutter and Sidewalk Road Dust	09/10/95	Gutter and sidewalk road dust from westbound lane of East Charleston Blvd.	LVGPVRDC
LVGPVRD3	LVSS009	RS270	Paved Road Dust	09/10/95	Paved road dust from Mitchell St. in front of the Bemis site	LVGPVRDC
LVGPVRD4	LVSS011	RS272	Paved Road Dust	09/10/95	Paved road dust from the intersection of Craig Rd. and Pecos Rd. (motor vehicle exhaust source sampling site)	LVGPVRDC

Table 4-1 (continued)
Geological Material Source Profiles Acquired for the Las Vegas Valley PM$_{10}$ Study

Composited Sample ID	Sample ID	Laboratory /Map[a] ID	Sample Type	Collection Date	Description	Mnemonic in Composited Profile
LVGPVRD5	LVSS012	RS273	Paved Road Dust	09/10/95	Paved road dust from the intersection of Las Vegas Blvd. and Spring Mountain Rd. (motor vehicle exhaust source sampling site)	LVGPVRDC
	LVSS013	RS274	Paved Road Dust	09/10/95	Paved road dust from the intersection of Las Vegas Blvd. and Sahara Ave. (motor vehicle exhaust source sampling site)	
	LVSS019	RS280	Paved Road Dust	09/11/95	Paved road dust from Las Vegas Blvd. in front of the El Rancho Hotel (motor vehicle exhaust source sampling site)	
	LVSS020	RS281	Paved Road Dust	09/11/95	Paved road dust from the intersection of Flamingo Blvd. and Las Vegas Blvd. (motor vehicle exhaust source sampling site)	
LVGPVRD6	LVSS014	RS275	Paved Road Dust	09/11/95	Paved road dust from the intersection of Lake Mead Blvd. and Civic Center Dr. (motor vehicle exhaust source sampling site)	LVGPVRDC
	LVSS015	RS276	Paved Road Dust	09/11/95	Paved road dust from the intersection of Lake Mead Blvd. and Pecos Rd. (motor vehicle exhaust source sampling site)	
	LVSS016	RS277	Paved Road Dust	09/11/95	Paved road dust from the intersection of Cheyenne Ave. and Civic Center Dr. (motor vehicle exhaust source sampling site)	
LVGPVRD7	LVSS001	RS262	Paved Highway Dust	09/10/95	Paved highway dust from I-15 near Sahara Ave. exit	LVGPVRDC
	LVSS002	RS263	Paved Highway Dust	09/10/95	Paved highway dust from I-15 near Sahara Ave. exit	
	LVSS003	RS264	Paved Highway Dust	09/10/95	Paved highway dust from intersection of Highway 93 and Interstate 15	
LVGDDES1	LVSS031	RS291	Disturbed Desert Soil	06/07/95	Soil from median and open fields north of NWCP site	LVGSOILC
	LVSS036	RS296	Disturbed Desert Soil	06/07/95	Soil from vacant area west of LOSS site	
	LVSS039	RS299	Disturbed Desert Soil	06/07/95	Soil from west of GROW site	
	LVSS040	RS300	Disturbed Desert Soil	06/07/95	Soil from east of LAMB site	

Table 4-1 (continued)
Geological Material Source Profiles Acquired for the Las Vegas Valley PM$_{10}$ Study

Composited Sample ID	Sample ID	Laboratory /Map[a] ID	Sample Type	Collection Date	Description	Mnemonic in Composited Profile
LVGSOIL1	LVSS005	RS266	Soil	09/10/95	Soil from East Charleston site inside of the air quality monitoring station fence	LVGSOILC
	LVSS029	RS289	Soil	06/06/95	Soil from vacant lot southeast of East Charleston site	
LVGSOIL2	LVSS021	RS282a	Soil	06/06/95	Soil from open area east of Bemis site	LVGSOILC
	LVSS022	RS282b	Soil	06/06/95	Soil from open area south of Bemis site	
LVGSOIL3	LVSS023	RS283	Soil	06/06/95	Soil from open area southwest of Lone Mountain Rd.	LVGSOILC
	LVSS038	RS298	Soil	06/07/95	Soil from open area south of CRAI site	
LVGSOIL4	LVSS026	RS286	Soil	06/06/95	Soil from vacant lot southwest of NOCO site	LVGSOILC
	LVSS030	RS290	Soil	06/07/95	Soil from bare area around the THUN site	
LVGSOIL5	LVSS024	RS284	Storage Piles	06/06/95	Soil from storage piles north of Lone Mountain Rd.	None
LVGUPRD1	LVSS017	RS278	Unpaved Road Dust	09/11/95	Unpaved road dust from north end of Donovan Way	LVGUPRDC
LVGUPRD2	LVSS018	RS279	Unpaved Road Dust	09/11/95	Unpaved road dust from north end of Losee Rd.	LVGUPRDC

[a] See Figure 4-1 for locations in which geological samples were collected.

Figure 4-1   Locations of geological material samples collected during the Las Vegas Valley PM$_{10}$ Study.

Table 4-2

Composite Geological Material Source Profiles Calculated for the Las Vegas Valley PM₁₀ Study

Mnemonic of Composited Profile	Description	Samples Included in Composite		
LVGCONSC	Construction Soil	LVGCONS1 LVGCONS3 LVGCONS5	LVGCONS2 LVGCONS4	
LVGPLOTC	Paved Parking Lot Dust	LVGPLOT1	LVGPLOT2	
LVGPVRDC	Paved Road Dust	LVGPVRD1 LVGPVRD3 LVGPVRD5 LVGPVRD7	LVGPVRD2 LVGPVRD4 LVGPVRD6	
LVGSOILC	Desert Soil	LVGDDES1 LVGSOIL2 LVGSOIL4	LVGSOIL1 LVGSOIL3	
LVGUPRDC	Unpaved Road Dust	LVGUPRD1	LVGUPRD2	
LVGEOLC	Composite of Las Vegas Geological Material	LVGCONSC LVGPVRDC LVGUPRDC	LVGPLOTC LVGSOILC	

4-8

Figures 4-2 and 4-3 show the chemical abundances of these profiles. In each of the illustrations, the height of each bar indicates the average fractional abundance for the indicated chemical, while the dot shows the standard deviation of the average. When the height of the bar exceeds the position of the dot, and when the height of the bar is much higher than it is in other profiles, the corresponding species is considered as a good marker for that source type.

Though there are slight differences among these profiles, they are not sufficient to distinguish one geological subgroup from other subgroups by CMB receptor modeling. In each of these profiles, aluminum (Al), silicon (Si), potassium (K), calcium (Ca), and iron (Fe) have large abundances with low variabilities. The abundance of total potassium (K) is six to seven times the abundance of soluble potassium (K^+). The abundances of aluminum (Al), silicon (Si), potassium (K), and iron (Fe) are similar among the profiles.

Calcium (Ca) abundance is enriched in the unpaved road dust (20.4 ± 3.4%), desert soil (17.0 ± 2.0%), and construction soil (16.8 ± 1.4%) profiles. It is a few percent less abundant in the paved road (15.0 ± 2.7%) and paved parking lot (13.4 ± 2.6%) profiles. These abundances are a factor of four to six higher than those observed in southern and central California (Chow et al., 1992a; Watson et al., 1994a). It is suspected that geological material in the Las Vegas Valley contains gypsum ($CaSO_4$) which elevates the abundances of both calcium and sulfate. The gypsum mine southwest of the valley, along with frequent construction activity in the Las Vegas Valley, might result in such a calcium-rich geological material.

Lead (Pb) is most abundant in paved road dust (0.021 ± 0.006%) and paved parking lot dust (0.019 ± 0.014%), and is as low as 0.003% in the construction soil and unpaved road profiles. Elemental carbon (EC) abundances range from 0% to 9% in individual profiles (Appendix B), with an average of 2.7 ± 2.3% in the composite geological profile (LVGEOLC). Organic carbon (OC) abundances vary among the composite profiles, ranging from 8.2 ± 2.8% (desert soil) to 14.2 ± 5.0% (paved parking lot), with an overall composite of 10.0 ± 1.2% (LVGEOLC). The organic-to-total-carbon (sum of organic and elemental carbon), OC/TC, ratios are similar among all samples with an average ratio of 0.80. The effect of motor vehicle emissions (e.g., brake and tire wear, oil drips) could result in greater abundances of Pb, EC, and OC in these source profiles.

Soluble ions such as nitrate (NO_3^-) and ammonium (NH_4^+) are generally low, in the range of 0.1% to 0.2%. Sulfate abundance ranges from 0.71 ± 0.5% (desert soil) to 1.8 ± 0.7% (paved parking lot), which is also a factor of three to nine higher than those found in central and southern California (Chow et al., 1992a; Watson et al., 1994a) Elemental sodium (Na) and chloride (Cl^-) are also low, with less than 0.2% in abundance.

Figure 4-2 Composite paved and unpaved road dust profiles acquired in the Las Vegas Valley PM$_{10}$ Study.

4-10
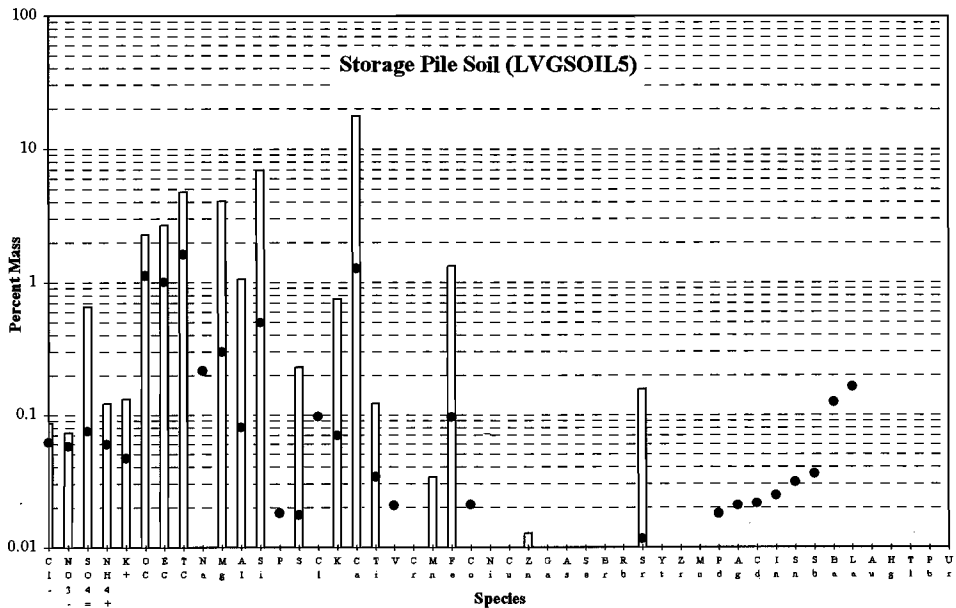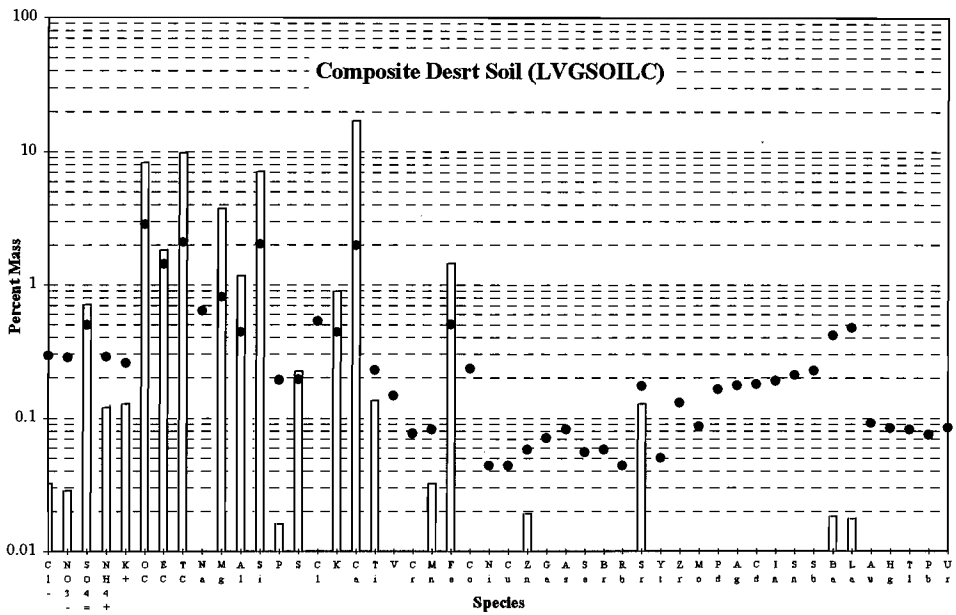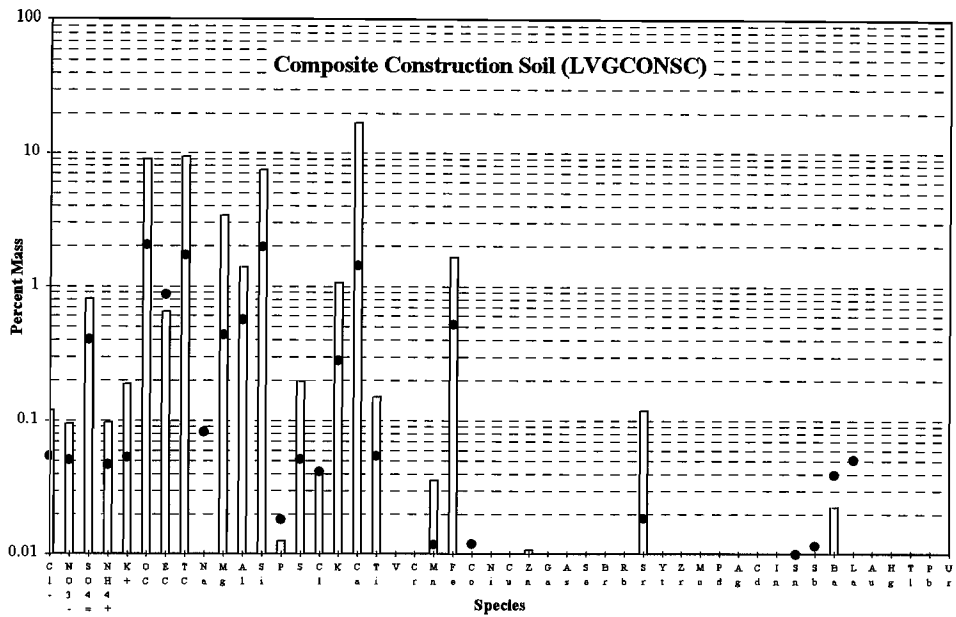
Figure 4-3 Composite soil dust source profiles acquired in the Las Vegas Valley PM₁₀ Study.

4-11

Previous source apportionment studies (e.g., Chow *et al.*, 1992b; Watson *et al.*, 1994a) show that the chemical abundances and variabilities of the commonly measured elements, ions, and carbon in geological source profiles are sufficient to separate geological source contributions from other source types. These commonly measured components are insufficient to distinguish paved road, unpaved road, construction soil, and desert soil contributions from each other. This is a reflection of insufficient model input data rather than inadequacies of the Chemical Mass Balance (CMB) model. A major research study is being initiated as part of the California Regional Particulate Air Quality Study (Roth and Watson, 1993) to evaluate particle morphology, specific organic compounds, isotopic abundances, microorganism content, and other markers for geological subtypes. The results of this research will be available by the end of 1998.

4.3   Motor Vehicle Exhaust

Mobile source particulate emissions are among the most difficult to measure with respect to emission rates and chemical composition. This difficulty arises from: 1) different mobile source types (e.g., passenger cars, light-duty gasoline-fueled trucks, heavy-duty diesel-fueled trucks, diesel buses); 2) inadequate characterization of the high emitters within the motor vehicle fleet; 3) a large number of individual emitters within each mobile source subcategory; 4) yearly changes in fuel composition and emission control technology; 5) undefined operating conditions; 6) several emission points on each vehicle (i.e., tailpipe, fuel evaporation, tire wear, brake wear, resuspended dust); and 7) a mixture of primary particles, semivolatile organic compounds, and secondary particle precursors.

To obtain a representation of all of these variables for conditions in the Las Vegas Valley, 32 samples with approximately two-hour sampling durations were obtained between 09/07/95 and 09/10/95 during morning (0800-1000 PST), noon (1200-1400 PST), and afternoon (1600-1800 PST) rush hours at ten locations in the valley. These ten sites were selected to represent different motor vehicle fleets, traffic patterns, traffic volumes, and vehicle operating conditions. Figure 4-4 shows motor vehicle source sampling locations. The sample identification codes, sampling dates, sampling periods, and locations are presented in Table 4-3. Mnemonics were assigned to indicate the 20 validated motor vehicle samples that were submitted to chemical analysis.

The portable ground-based sampling system was located on the median, sidewalk or shoulder within 2 m of the nearest high density traffic lane, with the sampling inlet placed at 1.5 m above ground level. The system itself included a Bendix/Sensidyne 240 cyclone, 1.2 cm diameter copper tube in the shape of an inverted U, a 4 cm diameter by 50 cm homogenizing chamber, a 5 cm diameter flow splitter, two 47-mm filter holders, two flow
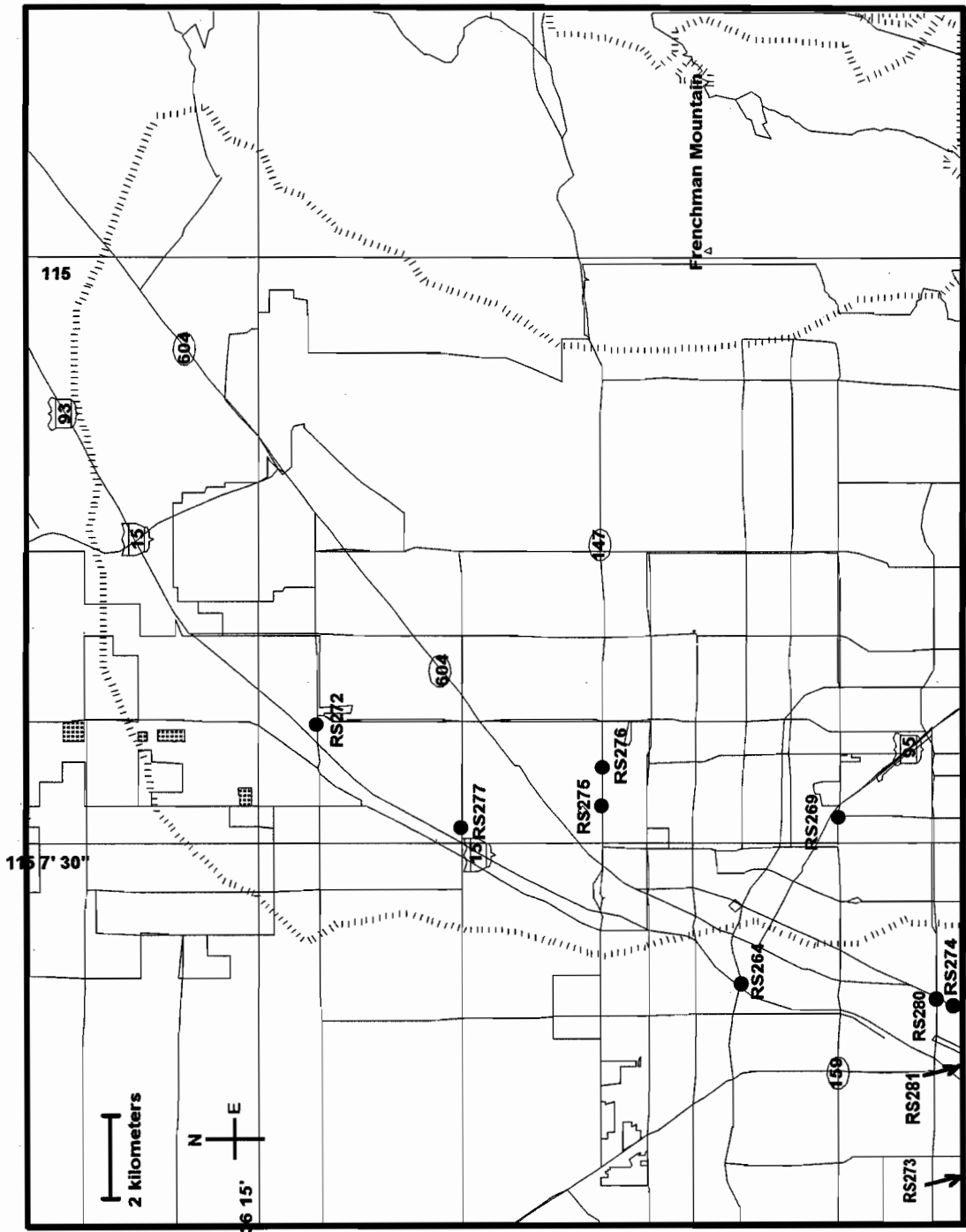
Figure 4-4   Locations of roadside motor vehicle samples collected during the Las Vegas Valley PM_{10} Study.

Table 4-3

Roadside Motor Vehicle Source Samples Collected during the Las Vegas Valley PM$_{10}$ Study

Mnemonic	Sample ID	Site Name		Sampling Date	Sampling Period Start Time (PST)	Stop Time (PST)	Sampling Duration	Wind Direction	Approximate Wind Speed (m/s)
LVMVECH1	LVST007	Cheyenne Ave. and Civic Center Dr.	RS277	09/07/95	07:45	09:45	2:00	East	1-2
LVMVECH2	LVST034	Cheyenne Ave. and Civic Center Dr.		09/07/95	11:31	13:31	2:00	East	0-5
LVMVEPE1	LVST004	Craig Rd. and Pecos Rd.	RS272	09/07/95	07:21	09:21	2:00	East	1-2
LVMVEPE2	LVST010	Craig Rd. and Pecos Rd.		09/07/95	12:07	14:07	2:00	East	3-5
LVMVEPE3	LVST032	Craig Rd. and Pecos Rd.		09/07/95	16:38	18:38	2:00	East	8-10
LVMVEEC1	LVST008	E. Charleston Blvd. and Eastern Ave.	RS269	09/07/95	12:25	14:25	2:00	East	3-5
LVMVEEC2	LVST011	E. Charleston Blvd. and Eastern Ave.		09/07/95	16:40	18:40	2:00	Southeast	4-5
	LVST012	E. Charleston Blvd. and Eastern Ave.		09/08/95	08:28	10:28	2:00	Calm	0-2
	LVST022	E. Charleston Blvd. and Eastern Ave.		09/09/95	16:21	18:21	2:00	Southwest	5-10
LVMVESA1	LVST015	Northwest corner of East Sahara Ave. and Las Vegas Blvd.	RS274	09/09/95	09:07	11:07	2:00	Southeast	0-1
LVMVESA2	LVST017	Northwest corner of East Sahara Ave. and Las Vegas Blvd.		09/09/95	15:38	17:38	2:00	Southwest	10-13
	LVST018	Northwest corner of East Sahara Ave. and Las Vegas Blvd.		09/10/95	11:50	13:50	2:00		Calm
	LVST020	Northwest corner of East Sahara Ave. and Las Vegas Blvd.		09/10/95	14:05	16:11	2:06	Southwest	1-2
	LVST021	Northwest corner of East Sahara Ave. and Las Vegas Blvd.		09/10/95	16:20	18:20	2:00	Southwest	3
LVMVESA3	LVST025	Northwest corner of East Sahara Ave. and Las Vegas Blvd.		09/09/95	11:10	13:10	2:00	Calm	Calm
	LVST026	Northwest corner of East Sahara Ave. and Las Vegas Blvd.		09/09/95	13:20	15:20	2:00	Calm	Calm
LVMVELV1	LVST003	Flamingo Rd. and Las Vegas Blvd.	RS281	09/08/95	12:35	14:35	2:00	East	5-6
	LVST002	Flamingo Rd. and Las Vegas Blvd.		09/08/95	17:00	19:00	2:00	West by SW	10

4-14

Table 4-3 (continued)

Roadside Motor Vehicle Source Samples Collected during the Las Vegas Valley PM$_{10}$ Study

Mnemonic	Sample ID	Site Name	Sampling Date	Sampling Period Start Time (PST)	Stop Time (PST)	Sampling Duration	Wind Direction	Approximate Wind Speed (mph)
LVMVELV2	LVST009	Las Vegas Blvd. in front of El Rancho Hotel	09/09/95	11:28	13:38	2:10	Southwest	Calm
LVMVELV3	LVST001	Lake Mead Blvd. and Pecos Rd.	09/08/95	07:30	09:30	2:00	Calm	Calm
	LVST030	Lake Mead Blvd. and Pecos Rd.	09/08/95	11:16	12:16	1:00	Southeast	5
	LVST016	Spring Mountain Rd. and Las Vegas Blvd.	09/09/95	11:55	13:55	2:00	East	0-3
LVMVELV4	LVST019	Spring Mountain Rd. and Las Vegas Blvd.	09/09/95	16:17	18:17	2:00	South	2-5
	LVST023	Spring Mountain Rd. and Las Vegas Blvd.	09/10/95	11:55	13:55	2:00	South	1-3
	LVST028	Spring Mountain Rd. and Las Vegas Blvd.	09/10/95	13:58	15:58	2:00	Southeast	1-5
	LVST014	Spring Mountain Rd. and Las Vegas Blvd.	09/10/95	16:04	18:04	2:00	Southeast	1-5
LVMVELV5	LVST031	Las Vegas Blvd. in front of El Rancho Hotel	09/09/95	09:05	11:05	2:00	Southeast	Calm
LVMVELV6	LVST033	Northwest corner of East Sahara Ave. and Las Vegas Blvd.	09/08/95	16:23	18:48	2:25	West by SW	7-10
LVMVE951	LSVT013	Highway 93 and Interstate 15	09/08/95	17:05	19:05	2:00	West	8
LVMVELM1	LVST006	Lake Mead Blvd. and Civic Center Dr.	09/07/95	16:48	18:48	2:00	Southeast	1-3
LVMVELM2	LVST005	Lake Mead Blvd. and Civic Center Dr.	09/08/95	08:10	10:06	2:00	Calm	Calm
LVMVELM3	LVST029	Lake Mead Blvd. and Civic Center Dr.	09/08/95	11:03	12:41	1:38	East	7-10

control valves, and a Gast 1023 0.75-horsepower carbon-vane vacuum pump. Fine particle Teflon-membrane and quartz-fiber filter samples were collected at ~60 L/min flow rate (per channel) to collect particles less than 2.5 μm.

The vehicle fleet was determined by counting vehicles during ten minutes out of each hour of the sampling interval to allow differences in vehicle mixture to be determined. Motor vehicle counts are provided for the following seven categories: 1) passenger cars, 2) light-duty pickup trucks, 3) taxis, 4) heavy-duty diesel-powered trucks, 5) commuter buses, 6) motorcycles, and 7) miscellaneous (e.g., RV campers). The average traffic counts ranged from 500 to over 2,000 vehicles per hour, and 95% of the vehicles were fueled by gasoline. A summary of vehicles counts by vehicle category for each of the motor vehicle sampling locations is shown in Table 4-4. Table 4-5 compares the average counting results at all sites with Clark County vehicle registration records. Observed vehicle statistics were similar to vehicle registration data, with approximately 75% gasoline-powered cars, 20% light-duty trucks, and less than 2% diesel-powered vehicles. This comparison demonstrates that the motor vehicle samples were acquired from a vehicle fleet representative of Clark County as a whole.

Though dominated by motor vehicle emissions, roadside samples also contain suspended road dust and particles from other sources in the background air. These samples are likely to be affected by vehicle-related resuspended road dust. The geological contribution was minimized by using a $PM_{2.5}$ inlet on the sampling system to remove coarse particles. The remaining geological contribution was removed from each sample by applying the CMB model with Al, Si, K, and Ca as fitting species for the LVGEOLC profile, then subtracting the calculated geological contribution from each chemical species and the measured mass. Ammonium and nitrate were also used as CMB fitting species with secondary ammonium nitrate and sulfate as sources to remove background concentrations of secondary aerosol from these samples. Individual motor vehicle exhaust profiles were calculated based on the remaining concentrations of mass and chemical species. Table 4-6 lists the seven composite source profiles for motor vehicle emissions. The overall motor vehicle exhaust composite profile (LVMVC2) was constructed as the average of six composited profiles listed in Table 4-6 and the highway profile (LVMVE951). The chemical abundances in four of these composite profiles are presented in Figure 4-5.

Organic carbon (OC) and elemental carbon (EC) are the most abundant species in motor vehicle exhaust, accounting for over 85% of the total mass. OC abundances in the composite motor vehicle profiles range from 42.7 ± 8.9% (LVMVEPEC) to 60.7 ± 14.6% (LVMVEECC). Organic-to-total-carbon (OC/TC) ratios range from 0.48 for the LVMVEPEC profile to 0.67 for the LVMVEECC profile, with an average ratio of 0.59 (LVMVC2). Watson *et al.* (1994a)

Table 4-4

Average Vehicle Counting Statistics during Motor Vehicle Sampling in the Las Vegas Valley PM_{10} Study

Site	Passenger Cars (%)	Light-Duty Gasoline Trucks (%)	Taxis (%)	Heavy-Duty Diesel Trucks (%)	Diesel Bus (%)	Motorcycles (%)	Miscellaneous (%)
Cheyenne Ave. and Civic Center Dr.	67	28	0	3	1	0	0
Craig Rd. and Pecos Rd.	56	32	0	11	1	1	0
E. Charleston Blvd. and Eastern Ave.	66	28	0	2	1	0	2
Northwest corner of East Sahara Ave. and Las Vegas Blvd.	76	18	3	1	1	1	0
Flamingo Rd. and Las Vegas Blvd.	43	25	17	5	7	2	0
Las Vegas Blvd. in front of El Rancho Hotel	71	20	6	0	2	0	0
Spring Mountain Rd. and Las Vegas Blvd.	66	28	0	2	1	0	2
Lake Mead Blvd. and Civic Center Dr.	63	34	0	2	0	0	0
Lake Mead Blvd. and Pecos Rd.	61	30	0	6	1	1	0
Highway 93 and Interstate 15	65	33	0	1	0	0	0
All Sites	64	28	3	3	1	1	1

4-17

Table 4-5

Comparison of Vehicle Counts during the Motor Vehicle Source Sampling Period with Clark County Vehicle Registration Records

	Passenger Cars (%)	Light-Duty Gasoline Trucks (%)	Taxis (%)	Diesel Trucks (%)	Diesel Bus (%)	Motorcycles (%)	Miscellaneous (%)
DRI Traffic Counting[a]	76.3	17.8	3.1	1.1	1.1	0.5	0.1
Registration Records	77.3	20.1	NA	0.9	NA	1.7	NA

[a] Based on 22,874 vehicles counted between 09/07/95 and 09/10/95.

Table 4-6
Composite Roadside Motor Vehicle Source Profiles Calculated
for the Las Vegas Valley PM$_{10}$ Study

Mnemonic	Sampling Location	Samples Included in Composite	
LVMVECHC	Cheyenne Ave. and Civic Center Dr.	LVMVECH1	LVMVECH2
LVMVEPEC	Craig Rd. and Pecos Rd.	LVMVEPE1 LVMVEPE3	LVMVEPE2
LVMVECEC	E. Charleston Blvd. and Eastern Ave.	LVMVEEC1	LVMVEEC2
LVMVESAC	East Sahara Ave. and Las Vegas Blvd.	LVMVESA1 LVMVESA3	LVMVESA2
LVMVELVC	Las Vegas Blvd. at El Rancho Hotel, Flamingo Rd., and Spring Mountain Rd.	LVMVELV1 LVMVELV3 LVMVELV5	LVMVELV2 LVMVELV4 LVMVELV6
LVMVELMC	Lake Mead Blvd. and Civic Center Dr.	LVMVELM1 LVMVELM3	LVMVELM2
LVMVC2	Las Vegas Roadside Motor Vehicle Composite	LVMVECHC LVMVEECC LVMVELVC LVMVE951	LVMVEPEC LVMVESAC LVMVELMC
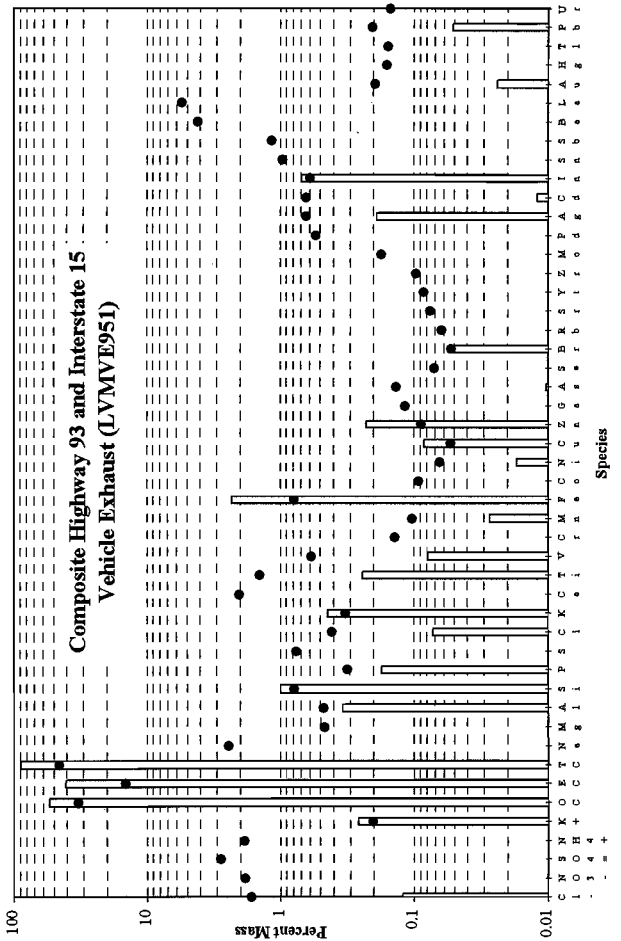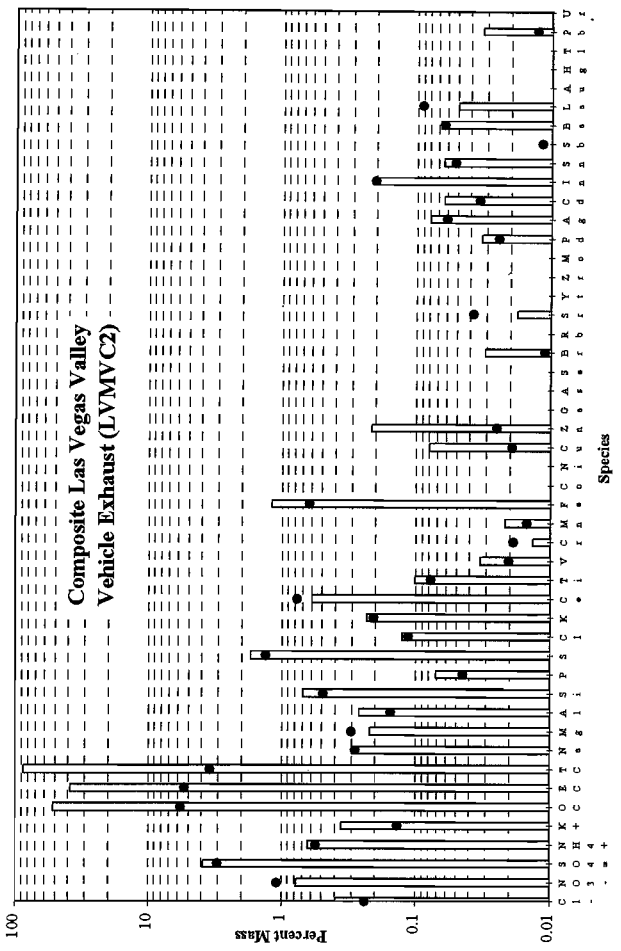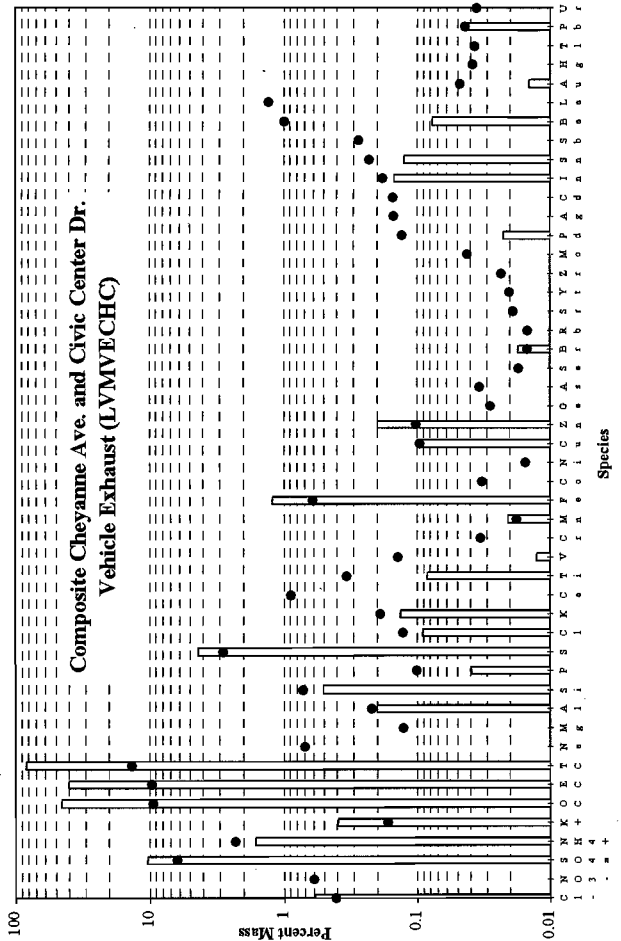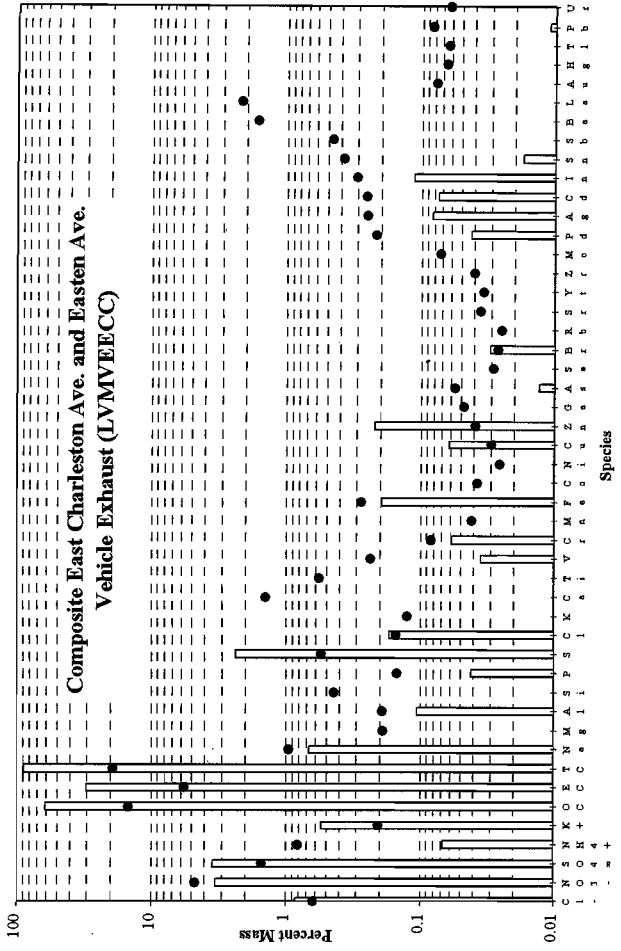
Figure 4-5 Composite motor vehicle exhaust source profiles acquired in the Las Vegas Valley PM$_{10}$ Study.

reported OC/TC ratios of 0.69 for gasoline-fueled vehicle exhaust (PHAUTO), 0.55 for diesel-fueled vehicle exhaust (PHDIES), and 0.52 for a mixture of vehicle types in roadside tests (PHRD) in Phoenix, AZ. These ratios are similar to the range of OC/TC ratios in the Las Vegas motor vehicle profiles.

The lead (Pb) abundance is negligible (0.032 ± 0.013%) in the LVMVC2 overall composite profiles. The abundance of bromine (Br) is also low, in the range of 0.02% to 0.04%. Zinc (Zn) is present in most of these profiles, usually at levels between 0.18% and 0.25%. The abundance of chloride (Cl⁻) is 0.2% to 0.8%.

4.4 Residential Wood Combustion

The chemical composition of residential wood combustion (RWC) emissions are expected to vary owing to: 1) differences in appliance types and installation factors (e.g., appliance types, catalyst/noncatalyst, damper control, airtight/nonairtight, chimney system); 2) wood compositions (e.g., species/density/size, moisture content, seasoned/nonseasoned, extent of decomposition); 3) burning practices (e.g., burning rate/duration, load, frequency of fueling, kindling procedure, household trash); and 4) burn conditions (e.g., kindling/charcoal phase, cool/hot burn, damper settings) (Houck, 1991).

Sampling methods for exhaust from residential chimneys also introduce variability owing to: 1) tar-like emissions adhering to chimneys and sampler inlets; 2) low exit velocities; 3) large ranges of particle concentrations in effluents; and 4) large water vapor contents that condense upon contact with cold ambient air (Houck, 1991).

A proficient means of obtaining chemical profiles for residential wood combustion (RWC) in the Las Vegas Valley is by directly sampling the chimney plumes of burning fireplaces or wood stoves. This method provides RWC samples that are relatively free from contamination of other sources. The sampling system used consisted of a 4- to 5-meter stainless steel sampling probe joined to a Bendix/Sensidyne 240 cyclone, a 4-cm-diameter-by-50-cm homogenizing chamber, a 5-cm-diameter flow splitter, two 47-mm filter holders, two flow control valves, and a Gast 1023 0.75-horsepower carbon-vane vacuum pump. Each sample was collected by placing the probe and cyclone 0.3 to 0.5 meters above the smoke plume.

Five sampling sites were selected in the study area. A total of 30 Teflon-membrane and quartz-fiber filter samples were collected for 2 to 20 minute periods at ~60 L/min flow rates (per channel). The collection times varied depending on observed filter loadings. The samples were collected at night (1900 to 0300 PST) during the seasonably cold (~40 °F) period of 12/21/95 to 12/25/95 (the holiday season), when radiation inversions are intense,

local traffic and industrial source emissions are low, and people are likely to burn wood. Table 4-7 lists the 22 RWC source samples collected for the Las Vegas Valley PM_{10} Study.

A total of four fireplaces and one wood stove were sampled. The combustible material used during RWC sampling included mesquite, ponderosa pine, lumber (two by fours), and Dura Logs®. Ponderosa pine is the most popular firewood in the Las Vegas Valley for residential fireplaces and wood stoves mainly due to its abundant availability.

Because none of the five chimney exhausts sampled in this study can be considered representative of the valley at large, it is more useful to group source samples based on chemical similarity rather than by sampling location. Four RWC composite profiles were constructed based on similarities in the composition of soluble potassium (K^+), organic carbon (OC), and elemental carbon (EC). The individual samples used to construct these composites are listed in Table 4-8. As illustrated in Figure 4-6, the majority of emissions from RWC emissions are composed of carbonaceous material. Organic carbon (OC) is generally the most abundant constituent, followed by elemental carbon. In these profiles, average OC abundance ranged from 5.5 ± 2.4% in two Race Track Road wood stove profiles (LVRWCC4) to 57 ± 13% in the Washington Avenue fireplace profile (LVRWCC1). Elemental carbon (EC) ranged from 4.4 ± 1.3% (LVRWCC1) to 26 ± 8% (LVRWCC3, Valley Glen Court fireplace profile). The OC/TC ratios varied by almost a factor of five, from 0.21 to 0.93.

Unusual chemical abundances were found in the LVRWCC4 wood stove profile, which contained very low OC (5.5 ± 2.4%) and high Si (32.0 ± 2.4%) levels. The key feature of the RWC profiles are that soluble potassium (K^+) is mostly (>50%) in water-soluble form, approaching an average abundance of 1% in these emissions. The abundance of chloride (Cl^-) is highly variable, ranging from 0.40 ± 0.14% (LVRWCC4) to 7.4 ± 3.4% (LVRWCC3). On average, the abundances of sulfate ($SO_4^=$), nitrate (NO_3^-), and ammonium (NH_4^+), are less than 1% in the composite RWC profiles. The abundances of trace elements (aluminum [Al], silicon [Si], calcium [Ca], iron [Fe]) are low, in the range of 0.1% to 0.5%, except for Si in LVRWCC4 (32.0 ± 2.4%).

4.5   Secondary Aerosol Profiles

Because species such as NO_3^-, $SO_4^=$, and OC can be formed through gas-to-particle transformation in the atmosphere, they cannot be entirely accounted for by primary emissions profiles. Secondary source profiles are also included in Appendix B which consist of "pure" ammonium bisulfate (NH_4HSO_4), ammonium nitrate (NH_4NO_3), and ammonium sulfate ($[NH_4]_2SO_4$).

Table 4-7

Residential Wood Combustion Source Profiles Collected for the Las Vegas Valley PM$_{10}$ Study

Mnemonic	Sampling Date	Site Location	Sample ID	Start Time (PST)	Duration (minutes)	Stove Type	Description of the Firewood
LVRWCPI1	12/21/95	1693 Valley Glen Ct., Las Vegas	LVST041	20:56	5	fireplace	2 pine logs, fire starting
LVRWCPI2	12/21/95	1693 Valley Glen Ct., Las Vegas	LVST042	21:14	5		2 pine logs, fire hot
LVRWCPI3	12/21/95	1693 Valley Glen Ct., Las Vegas	LVST044	21:40	5		adding scap wood (2 x 4's)
LVRWCPI4	12/21/95	1693 Valley Glen Ct., Las Vegas	LVST045	21:51	10		fire burning down
LVRWCAD1	12/22/95	7743 Washington Ave., Las Vegas	LVST047	20:14	5	fireplace	mesquite and pine
LVRWCAD2	12/22/95	7743 Washington Ave., Las Vegas	LVST048	20:25	5		mesquite and pine
LVRWCAD3	12/22/95	7743 Washington Ave., Las Vegas	LVST051	20:45	2		mesquite and pine
LVRWCAD4	12/22/95	7743 Washington Ave., Las Vegas	LVST052	20:55	3		mesquite and pine
LVRWCAD5	12/22/95	7743 Washington Ave., Las Vegas	LVST053	21:00	3		mesquite and pine
LVRWCCA1	12/22/95	6525 Burlwood Ave., Las Vegas	LVST054	00:36	15	fireplace	pine, probe out of visible plume
LVRWCCA2	12/22/95	6525 Burlwood Ave., Las Vegas	LVST056	01:15	8		pine
LVRWCCA3	12/22/95	6525 Burlwood Ave., Las Vegas	LVST057	01:28	8		pine
LVRWCCA4	12/22/95	6525 Burlwood Ave., Las Vegas	LVST058	02:12	10		Duralog added to pine
LVRWCCA5	12/22/95	6525 Burlwood Ave., Las Vegas	LVST059	03:15	6		pine and Duralog
LVRWCSI1	12/23/95	113 S. Race Track Rd., Las Vegas	LVST060	20:15	15	wood stove	fire very hot, burning all day, pine
LVRWCSI2	12/23/95	113 S. Race Track Rd., Las Vegas	LVST062	21:00	20		pine, fire burning down
LVRWCSI3	12/23/95	113 S. Race Track Rd., Las Vegas	LVST063	21:30	10		new log added
LVRWCSI4	12/23/95	113 S. Race Track Rd., Las Vegas	LVST065	21:50	10		fire very hot, pine
LVRWCCH1	12/24/95	corner of Robin and St. Anderson, Las Vegas	LVST066	18:30	5	fireplace	baywood and pine
LVRWCCH2	12/24/95	corner of Robin and St. Anderson, Las Vegas	LVST067	18:35	5		baywood and pine
LVRWCCH3	12/24/95	corner of Robin and St. Anderson, Las Vegas	LVST068	18:45	5		baywood and pine
LVRWCCH4	12/24/95	corner of Robin and St. Anderson, Las Vegas	LVST069	18:55	5		baywood and pine

Table 4-8
Residential Wood Combustion Source Profile Composites
Calculated for the Las Vegas Valley PM$_{10}$ Study

Composite ID	Sampling Location	Mnemonic	
LVRWCC1	7743 Washington Ave., Las Vegas	LVRWCAD1 LVRWCAD3 LVRWCAD5	LVRWCAD2 LVRWCAD4
LVRWCC2	6525 Burlwood Ave., Las Vegas	LVRWCCA1 LVRWCCA3 LVRWCCA5	LVRWCCA2 LVRWCCA4
	corner of Robin and St. Anderson, Las Vegas	LVRWCCH1 LVRWCCH3	LVRWCCH2 LVRWCCH4
	1693 Valley Glen Ct., Las Vegas	LVRWCPI1	
	113 S. Race Track Rd., Las Vegas	LVRWCSI1	LVRWCSI2
LVRWCC3	1693 Valley Glen Ct., Las Vegas	LVRWCPI2 LVRWCPI4	LVRWCPI3
LVRWCC4	113 S. Race Track Rd., Las Vegas	LVRWCSI3	LVRWCSI4
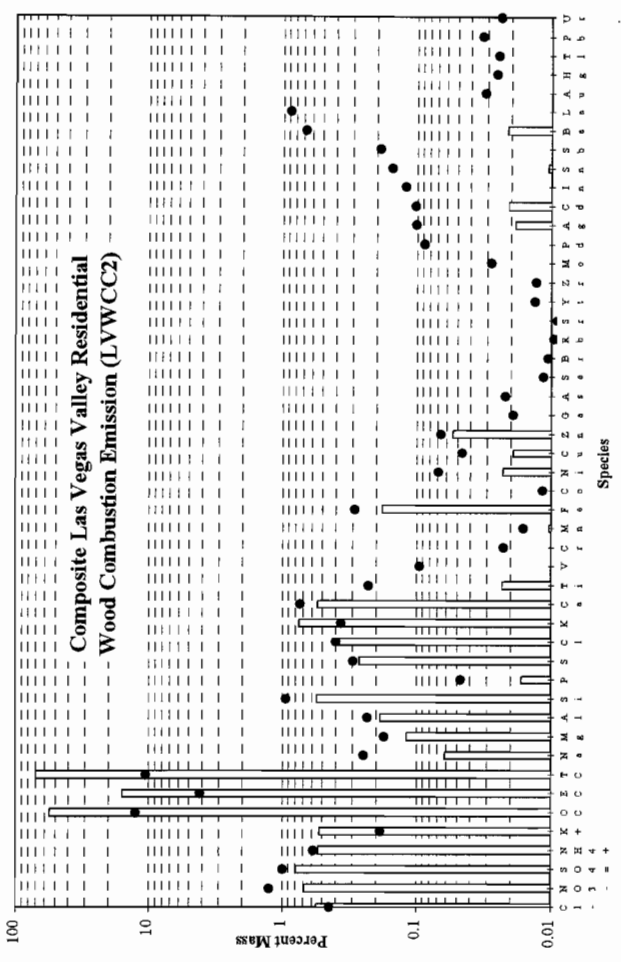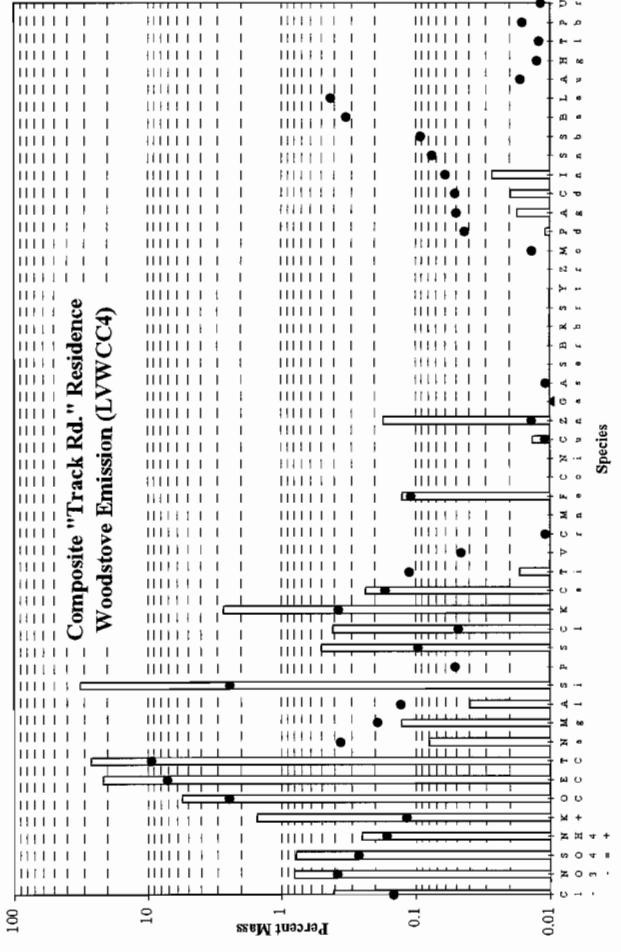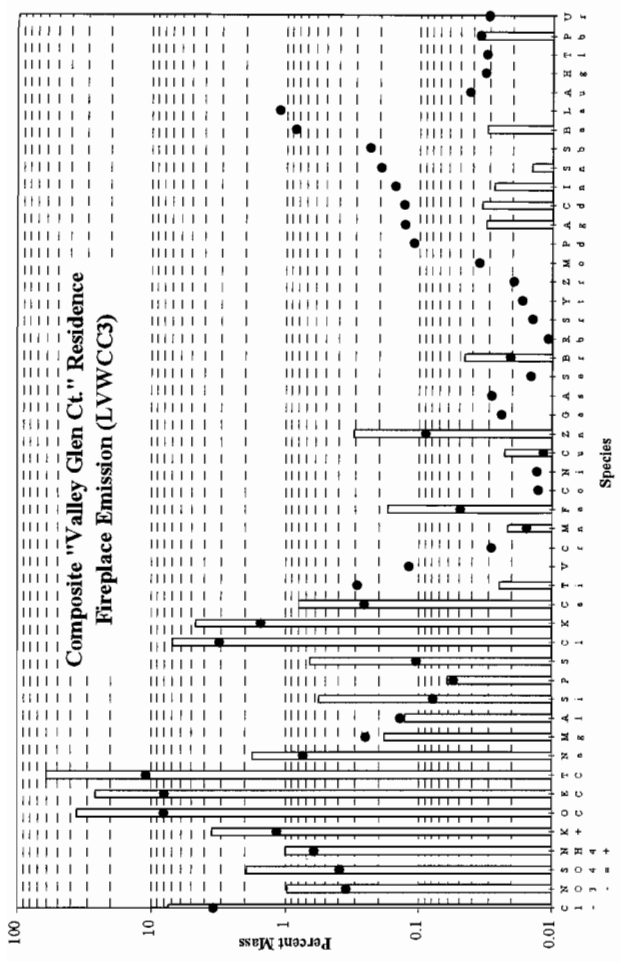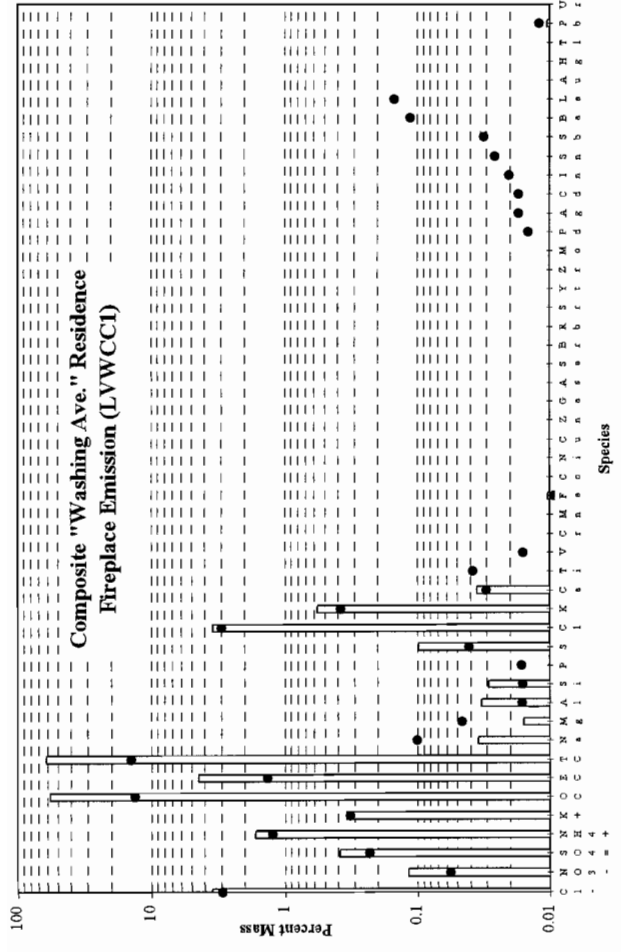
Figure 4-6 Composite residential wood combustion source profiles acquired in the Las Vegas Valley PM₁₀ Study.

4.6   Source Profile Summary

This *a priori* examination of source profiles for the study cannot determine which profiles will be distinguishable by CMB modeling. Current modeling software contains diagnostic tests to allow the degree of "collinearity" (or similarity among profiles) to be evaluated for each combination of source and receptor data. This examination indicates the following expectations:

- Geological profiles are too similar to be distinguished from one another. It is unlikely that CMB receptor modeling by itself and without measurement of additional unique species will distinguish different geological source profiles from each other.

- The same is true for motor vehicle exhaust from leaded-, unleaded-, and diesel-fueled vehicles. While these general source categories can probably be distinguishable from each other with receptor modeling, individual source types within the categories probably cannot be separated by the modeling.

- Sulfate, nitrate, and organic carbon are present in nearly all of the primary emissions from these sources, though the majority of the sulfate, nitrate, and organic carbon measured in ambient samples in the Las Vegas area will be of secondary origin.

5.0   DATA BASE AND DATA VALIDATION

One of the objectives of this study is to acquire a data base of ambient PM_{10} concentrations, source profiles, and meteorological measurements with specified precision, accuracy, and validity. Numerous air quality studies have been conducted over the past decade, but the data obtained are often not available or applicable for source assessment because the data bases lack documentation with regard to sampling and analysis methods, quality control/quality assurance procedures, accuracy specifications, precision calculations, and data validity. Lioy *et al.* (1980), Chow and Watson (1989), and Watson and Chow (1992) summarize the requirements, limitations, and current availability of ambient and source data bases in the United States. The Las Vegas Valley PM_{10} Study aerosol and meteorological data base attempts to meet these requirements. The data base files for this study have the following attributes:

- They contain the ambient and source observables needed to assess source/receptor relationships;

- They are available in a well-documented, computerized form accessible by personal computers;

- Measurement methods, locations, and schedules are documented;

- Quality control and quality audits are documented;

- Precision and accuracy estimates are reported;

- Validation flags are assigned; and

- Feedback from data base users has been solicited and incorporated into the data files.

Documentation files include project and data description files, a site description file, and site maps. Data files include base site PM_{10} mass and chemical concentrations, satellite site PM_{10} mass and chemical concentrations, source profiles for geological material, motor vehicle exhaust, and residential wood combustion, as well as supplemental data from hourly beta-attenuation monitor (BAM) PM_{10} and hourly meteorological measurements from the Clark County Health District (CCHD) monitoring network.

This section introduces the features, data structures, and contents of the Las Vegas Valley PM_{10} Study data archive. The approach that was followed to obtain the final data files is illustrated in Figure 5-1. Detailed data processing and data validation procedures are documented in Sections 5.3 and 5.4. These data are available on floppy diskettes for convenient distribution to data base users. Detailed file structures are presented in Appendix A and are referred to below as Tables A-1 through A-13. The file extension identifies the file type according to the following definitions:
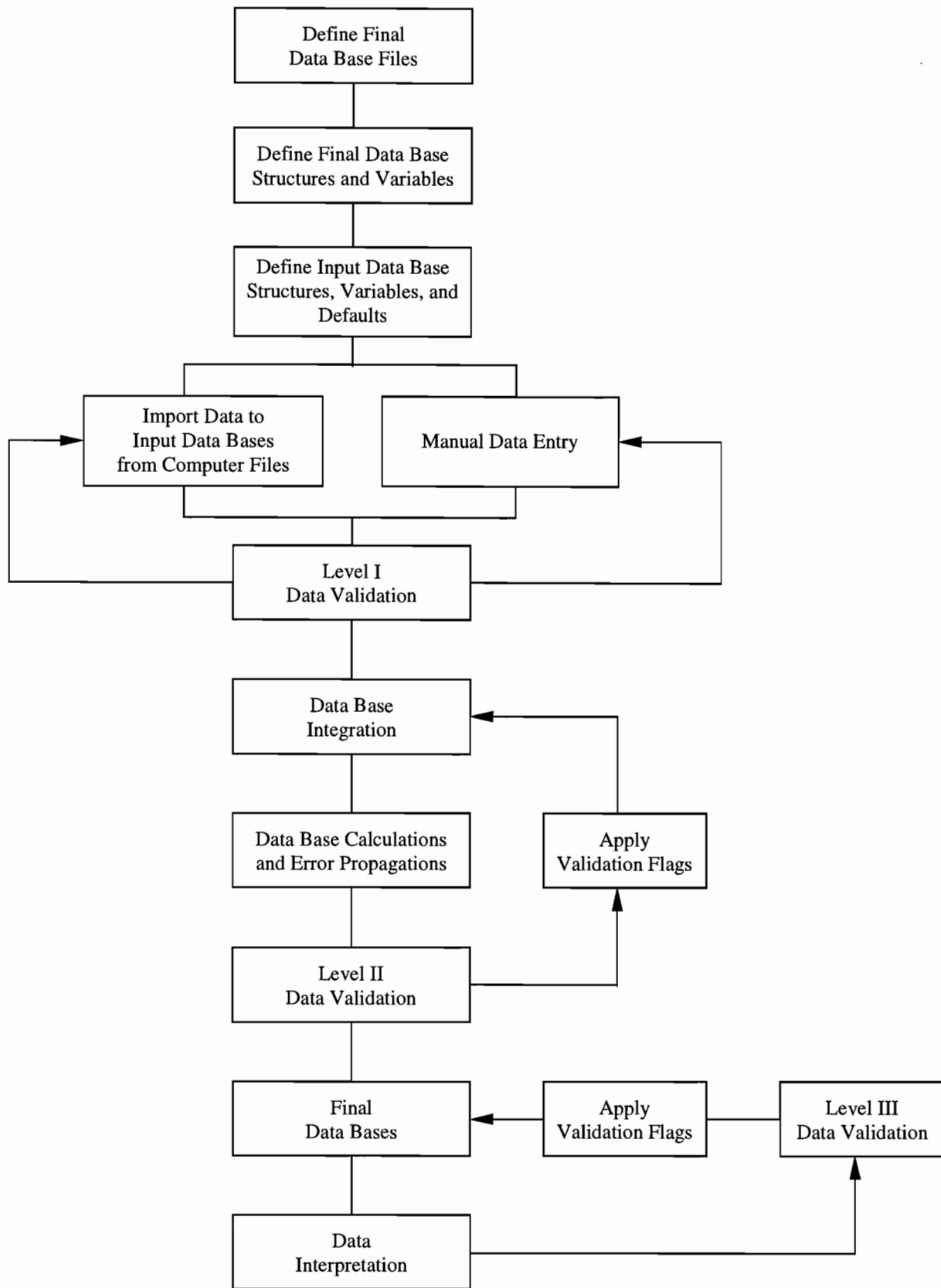
Figure 5-1   Flow diagram of the data base management system.

- TXT = ASCII text file

- DOC = Microsoft Word 6 document

- XLS = Microsoft Excel 5 spreadsheet file

- DBF = Xbase (i.e., dBase, FoxPro) data base file

- FPT = FoxPro memo field file

- GSM = Map Viewer map file

- ZIP = File or set of files compressed with PKZIP. Decompress with PKUNZIP.

5.1 Project Documentation Files

Five files contain project documentation for this study:

- File "README.DOC" presents a brief overview of the scope of the project and the study objectives. It also specifies, in tabular form, the ambient measurement periods as well as their locations. Additionally, this file defines the directory structure and file structures, and lists the data base files with brief descriptions of the data contained in each file.

- File "LVSITE.DBF" documents the site names, addresses, UTM coordinates, characteristics of the aerosol sampling locations, and the observables collected at each site. The structure of this file is shown in Table A-1.

- File "LVSITES.GSM" contains the map of the study area in a MAPVIEWER software package.

- File "LVFLDNAM.DBF" provides the field descriptions, naming conventions, and measurement units utilized in the FoxPro-generated data base files. The structure of this file is shown in Table A-2.

- File "LVSOURCE.DOC" explains the source profile identification codes.

5.2 Data Base Structures and Features

FoxPro for Windows 2.5 (Fox Software, Inc., 1991), is a commercially-available relational data base management system that can be used to manipulate the data acquired in this study. FoxPro can handle 256 fields of up to 4,000 characters per record and up to one billion records per file. This system can be implemented on most IBM PC-compatible

desktop computers. The data base files (*.DBF) can also be read directly into a variety of popular statistical, plotting, data base, and spreadsheet programs without having to use any specific conversion software.

Each file structure was established by defining the fields for data to be stored. One of five field types, character, date, numerical, logical, or memo, can be assigned to each observable. Sampling sites and particle size fractions are defined as "Character" fields, sampling dates are defined as "Date" fields, and measured data are defined as "Numeric" fields. "Logical" fields are used to represent a "yes" or "no" value applied to a variable, and "Memo" fields accommodate large blocks of textual information and can be used to document the data validation results.

Data contained in different XBase files can be linked by indexing on and relating to common attributes in each file. Sampling site, sampling hour, sampling period, particle size, and sampling substrate IDs are, in general, the common fields among various data files which can be used to relate data in one file to the corresponding data in another file.

To assemble the final data files, information was merged from many data sets derived from field monitoring and laboratory analyses by relating information on the common fields cited above. Detailed explanations and programming techniques for manipulation of this data base in FoxPro are presented by Christensen *et al.* (1989).

5.2.1 Data Base Description

Table 5-1 summarizes the validated data files that constitute the Las Vegas ambient PM_{10} and meteorological data base. Tables A-3 through A-11 identify the number of records, file dates, missing value codes, and data precisions for the ambient and source data. The field sequence, field name, data type and format, and description of each field name are also documented. Documentation for the FoxPro field descriptions, naming conventions, and measurement units used in the ambient PM_{10} and the meteorological data bases is given in the file "LVFLDNAM.DBF" (Table A-2). Tables A-12 and A-13 are field and laboratory validation flags for the 24-hour PM_{10}.

The data base structures and their definitions for ambient and source filter-based measurements are contained in the data documentation files entitled "AMBSTRU.DOC" and "SRCSTRU.DOC," respectively. Data base structures for the meteorological data are documented in "METSTRU.DOC." These documentation files are updated when changes are made in the data base. Users should review the current documentation on the set of disks containing the data base since this documentation may differ from the tables presented in Appendix A.

5-4

Table 5-1
Summary of Las Vegas Valley PM$_{10}$ Study Data Bases

Category	Data Base File	Data Base Description	Number of Records	Reference Table Numbers
I. DATA BASE DOCUMENTATION				
	README.DOC	Project and data description file.	NA	NA
	LVSITE.DBF	Site description, location, and data collected.	48	Table A-1
	LVSITE.GSM	Site map.	1	NA
	LVFLDNAM.DBF	Defines the FoxPro fields and measurement units used in the ambient and meteorological data bases.	167	Table A-2
	AMBSTRU.DOC	Ambient data base structure documentation.	NA	NA
	SRCSTRU.DOC	Source data base structure documentation.	NA	NA
	LVSOURCE.DOC	Source identification codes.	NA	NA
	METBAMST.DOC	Meteorological and beta attenuation monitor (BAM) data base structure documentation.	NA	NA

Table 5-1 (continued)
Summary of Las Vegas Valley PM$_{10}$ Study Data Bases

Category	Data Base File	Data Base Description	Number of Records	Reference Table Numbers
II. PM$_{10}$ MASS AND CHEMICAL DATA				
PM$_{10}$	AMB_SFS1.DBF	Contains 24-hour PM$_{10}$ mass and light absorption (b_{abs}) data collected at the Bemis and East Charleston sites on: 1) every sixth day between 01/03/95 to 01/28/96; 2) daily spring (04/15/95 to 04/21/95) and 05/12/95 to 05/16/95), summer (06/05/95 to 06/07/95), fall (09/07/95 to 09/12/95), and winter (01/26/96 to 01/30/96) five intensive periods; and 3) daily between 12/23/95 and 01/04/96 with sequential filter samplers.	194	Table A-3
PM$_{10}$	AMB_SFS2.DBF	Contains 24-hour PM$_{10}$ mass, light absorption (b_{abs}), elements (Na to U), organic and elemental carbon, and ions[a], collected at the Bemis and East Charleston sites for the selected 14 days	37	Table A-4
PM$_{10}$	AMB_POR1.DBF	Contains 24-hour PM$_{10}$ mass and light absorption (b_{abs}) collected at the 30 satellite sites for daily spring (04/15/95 to 04/21/95) and 05/12/95 to 05/16/95), summer (06/05/95 to 06/07/95), fall (09/07/95 to 09/12/95), and winter (01/26/96 to 01/30/96) intensive monitoring periods with portable PM$_{10}$ samplers.	781	Table A-5

Table 5-1 (continued)
Summary of Las Vegas Valley PM$_{10}$ Study Data Bases

Category	Data Base File	Data Base Description	Number of Records	Reference Table Numbers
II. PM$_{10}$ MASS AND CHEMICAL DATA (CONT'D)				
PM$_{10}$	AMB_POR2.DBF	Contains 24-hour PM$_{10}$ mass, light absorption (b$_{abs}$), and elements (Al, Si, S, K, Ca, and Fe) collected daily at 30 satellite sites for the periods: summer (06/05/95 to 06/07/95), fall (09/07/95 to 09/12/95), and winter (01/26/96 to 01/30/96) intensive monitoring periods with portable PM$_{10}$ samplers.	424	Table A-6
III. SOURCE PROFILE DATA				
Source	LVSORPCT.DBF	Contains the source composition of PM$_{2.5}$ or PM$_{10}$, elements (Na to U), organic and elemental carbon, and ions[a] in percent of total mass for the composite and individual source measurements profiles.	88	Table A-7
Source	LVSORFRC.DBF	Contains the source composition of PM$_{2.5}$ or PM$_{10}$, elements (Na to U), organic and elemental carbon, and ions[a] in fraction of total mass for the composite and individual source profiles.	88	Table A-8
Source	LVSORCMB.DBF	Contains the source composition of PM$_{2.5}$, coarse (PM$_{2.5}$ minus PM$_{10}$), and PM$_{10}$ elements (Al to U), organic and elemental carbon, and ions[a] in fraction of total mass for the composite and individual source profiles as CMB model input format.	88	Table A-9

Table 5-1 (continued)
Summary of Las Vegas Valley PM$_{10}$ Study Data Bases

Category	Data Base File	Data Base Description	Number of Records	Reference Table Numbers
IV. METEOROLOGICAL AND PM$_{10}$ DATA				
Met. & PM$_{10}$	LVMETBAM.DBF	Contains hourly meteorological data for 17 sites[b] and hourly PM$_{10}$ beta attenuation monitor (BAM) data for 14 sites[b] collected for the period from 01/01/95 to 01/31/96.	182,016	Table A-10
PM$_{10}$	LVBAM24H.DBF	Contains 24-hour PM$_{10}$ mass collected at 10 stations from 01/01/95 to 01/31/96 with a beta attenuation monitor.	7584	Table A-11
V. DATA VALIDATION FLAGS				
	AMBFLAG.DOC	Contains the field sampling data validation flags.	NA	Table A-12
	CHEMFLAG.DOC	Contains the chemical analysis data validation flags.	NA	Table A-13

[a] Chloride, nitrate, sulfate, ammonium, and soluble potassium.
[b] See Table 5-3 for meteorological measurements.

5.2.2 Ambient Data Base

A prefix "AMB" is assigned to the primary Las Vegas particulate data files. The particulate data files are classified at a second level that is dependent upon the instrumentation used to collect the sample. Separated from the "AMB" prefix with an underscore, two additional identification naming conventions are used to indicate the type of instrument used to collect the data. These conventions are: 1) SFS to represent a sequential filter sampler, and 2) POR to represent a portable battery-powered PM_{10} survey sampler. Each observable is identified by a field name which follows a pattern for that type of observable. For example, in the ambient particle concentration file, the first two characters represent the measurement species (e.g., AL for aluminum, SI for silicon, CA for calcium), the third character designates the analysis method (i.e., "G" for gravimetric weighing, "D" for optical densitometry, "X" for x-ray fluorescence analysis, "T" for ion chromatography, "A" for atomic absorption spectrophotometry, "C" for automated colorimetry, "T" for thermal/optical carbon analysis), and the last character uses a "C" to identify a species concentration or a "U" to identify the uncertainty (i.e., precision) of the corresponding measurement. Each measurement method is associated with a separate validation field to document the sample validity for that method. These flags, as well as the comments, are recorded in a validation flags summary that accompanies each record.

Table 5-2 summarizes the ambient 24-hour PM_{10} measurements acquired for this study. Four files are included in the mass and chemical concentration data bases:

- Twenty-four-hour (0001 to 2400 PST) ambient PM_{10} mass and light absorption for all samples collected at the two base sites are in the file "AMB_SFS1.DBF." The structure of this file is shown in Table A-3.

- Twenty-four-hour (0001 to 2400 PST) ambient PM_{10} mass, light absorption, and chemical speciation for all samples selected for chemical analysis at the two base sites are in the file "AMB_SFS2.DBF." The structure of this file is shown in Table A-4.

- Twenty-four-hour (0001 to 2400 PST) PM_{10} mass and light absorption for all samples collected at the satellite sites are in the file "AMB_POR1.DBF." The structure of this file is shown in Table A-5.

- Twenty-four-hour (0001 to 2400 PST) PM_{10} mass, light absorption, and chemical speciation for all samples collected at the satellite sites are in the file "AMB_POR2.DBF." The structure of this file is shown in Table A-6.

Table 5-2
Ambient PM_{10} Measurements Collected during the Las Vegas Valley PM_{10} Study

Ambient Measurements	Start Date	End Date	Sampling Frequency	Sampling Period	Filename
• Annual Sampling					
Bemis	01/03/95	01/28/96	every sixth day	24 hour	AMB_SFS1.DBF
East Charleston	01/03/95	01/28/96	every sixth day	24 hour	AMB_SFS1.DBF
• Intensive Sampling					
Spring Intensive					
Bemis	04/15/95	04/21/95	daily	24-hour	AMB_SFS1.DBF
East Charleston	04/15/95	04/21/95	daily	24-hour	AMB_SFS1.DBF
Bemis	05/12/95	05/16/95	daily	24-hour	AMB_SFS1.DBF
East Charleston	05/12/95	05/16/95	daily	24-hour	AMB_SFS1.DBF
30 satellite sites	04/15/95	04/21/95	daily	24 hour	AMB_POR1.DBF
30 satellite sites	05/12/95	05/16/95	daily	24 hour	AMB_POR1.DBF
Summer Intensive					
Bemis	06/05/95	06/07/95	daily	24-hour	AMB_SFS1.DBF
East Charleston	06/05/95	06/07/95	daily	24-hour	AMB_SFS1.DBF
30 satellite sites	06/05/95	06/07/95	daily	24-hour	AMB_POR1.DBF
Fall Intensive					
Bemis	09/07/95	09/12/95	daily	24 hour	AMB_SFS1.DBF
East Charleston	09/07/95	09/12/95	daily	24 hour	AMB_SFS1.DBF
30 satellite sites	09/07/95	09/12/95	daily	24 hour	AMB_POR1.DBF
Winter Intensive					
Bemis	01/26/96	01/30/96	daily	24 hour	AMB_SFS1.DBF
East Charleston	01/26/96	01/30/96	daily	24 hour	AMB_SFS1.DBF
30 satellite sites	01/26/96	01/30/96	daily	24 hour	AMB_POR1.DBF
• Mini-intensive Sampling					
Bemis	12/23/95	01/04/96	daily	24 hour	AMB_SFS1.DBF
East Charleston	12/23/95	01/04/96	daily	24 hour	AMB_SFS1.DBF

5.2.3 Source Data Base

Tables 4-1 to 4-8 summarize the source profiles described in Section 4, as well as those profiles extracted from other source apportionment studies. The source profiles and the data from which they were derived are contained in the "LVSORPCT.DBF" file which contains the percent of total mass and the uncertainty associated with each source measurement for the elements (Na to U), carbon (OC and EC), and ions (Cl^-, NO_3^-, $SO_4^=$, NH_4^+, and K^+) for each of the individual source samples and the composite source profiles acquired in this study. This file includes all the source samples acquired for this study. The structure of this data base file is shown in Table A-7. Individual and composite source profiles in fraction of total mass and in CMB Version 7 model input format are documented in the "LVSORFRC.DBF" file (Table A-8) and the "LVSORCMB.DBF" file (Table A-9), respectively.

5.2.4 Hourly Meteorological and PM_{10} Data Base

Table 5-3 lists the hourly meteorological and PM_{10} beta-attenuation monitor (BAM) sampling sites, sampling periods, sampling frequency, and filenames for each station's hourly meteorological and PM_{10} BAM data. Hourly meteorological and PM_{10} BAM data were acquired from CCHD's network. File "LVMETBAM.DBF" contains hourly meteorological data from 17 stations and hourly PM_{10} BAM data from 14 stations in the CCHD network. The structure of this file is shown in Table A-10. Hourly PM_{10} BAM data are averaged to obtain 24-hour PM_{10} concentrations for each day. These 24-hour PM_{10} averages are contained in the "LVBAM24H.DBF" file. The structure of this file is shown in Table A-11.

5.3 Analytical Specifications

Every measurement consists of four attributes: 1) a value; 2) a precision; 3) an accuracy; and 4) a validity (Hidy, 1985; Watson et al., 1989). The measurement methods described by Chow and Richards (1990) and in this volume are used to obtain the value. Performance testing via regular submission of standards, blank analysis, and replicate analysis are used to estimate precision. These precisions are reported in the data files described in Section 5.2 so that they can be propagated through air quality models and used to evaluate how well different values compare with one another. The submission and evaluation of independent standards through quality audits are used to estimate accuracy. Validity applies both to the measurement method and to each measurement taken with that method. The validity of each measurement is indicated by appropriate flagging within the data base, while the validity of the methods has been evaluated in this study by a number of tests.

Table 5-3
Supplemental Meteorological and PM_{10} (BAM) Data
from the Clark County Health District for the Las Vegas Valley PM_{10} Study

ID	Site Name	Start Date	End Date	Temp	RH	Wind	BAM	Number of Records
BC	Boulder City	01/01/95	01/31/96				*	9504
BS	Bemis/Craig	01/01/95	01/31/96	*		*	*	9504
CC	City Center	01/01/95	01/31/96	*		*	*	9504
DM	Dime III	01/01/95	01/31/96			*		9504
EC	East Charleston	01/01/95	01/31/96	*		*		9504
FL	Flamingo	01/01/95	01/31/96	*		*	*	9504
GR	Green Valley (Arroyo Grande)	01/01/95	01/31/96	*		*	*	8016
JN	Jean	01/01/95	01/31/96	*		*	*	9504
LM	Lake Mead (McDaniel)	01/01/95	01/31/96	*		*	*	9504
MC	Maycliff (East Sahara)	01/01/95	01/31/96	*	*	*	*	9504
MS	East Charleston (Microscale)	01/01/95	01/31/96				*	9504
PL	Powerline (Southeast Valley)	01/01/95	01/31/96	*		*	*	9504
PM	Paul Meyer Park	01/01/95	01/31/96	*		*	*	9504
PT	Pittman	01/01/95	01/31/96	*	*	*	*	8706
PX	Proximity	01/01/95	01/31/96	*		*		9504
SL	Shadow Lane (Health District)	01/01/95	01/31/96	*		*		9504
VS	Varity School	01/01/95	01/31/96	*		*		5088
WJ	Walter Johnson	03/01/95	01/31/96	*		*	*	9405
WS	Warm Springs (Arroyo Grande)	01/01/95	01/31/96				*	9504
WW	Winterwood	01/01/95	11/30/95	*	*	*		9504

The precision, accuracy, and validity of the Las Vegas Valley aerosol measurements are defined as follows:

- A measurement is an observation at a specific time and place which possesses four attributes: 1) value – the center of the measurement interval; 2) precision – the width of the measurement interval; 3) accuracy – the difference between measured and reference values; and 4) validity – the compliance with assumptions made in the measurement method.

- A measurement method is the combination of equipment, reagents, and procedures which provide the value of a measurement. The full description of the measurement method requires substantial documentation. For example, two methods may use the same sampling systems and the same analysis systems. These are not identical methods, however, if one performs acceptance testing on filter media and the other does not. Seemingly minor differences between methods can result in major differences between measurement values.

- Measurement method validity is the identification of measurement method assumptions, the quantification of effects of deviations from those assumptions, the evaluation that deviations are within reasonable tolerances for the specific application, and the creation of procedures to quantify and minimize those deviations during a specific application. A substantial effort was expended in the Las Vegas PM_{10} Study to establish the validity of measurement methods, especially for the measurements of elemental carbon, light absorption, and particle nitrate.

- Sample validation is accomplished by procedures which identify deviations from measurement assumptions and the assignment of flags to individual measurements for potential deviations from assumptions.

- The comparability and equivalence of sampling and analysis methods are established by the comparison of values and precisions for the same measurement obtained by different measurement methods. Interlaboratory and intralaboratory comparisons are usually made to establish this comparability. Simultaneous measurements of the same observable are considered equivalent when more than 90% of the values differ by no more than the sum of two one-sigma precision intervals for each measurement.

- Completeness measures how many environmental measurements with specified values, precisions, accuracies, and validities were obtained out of the total number attainable. It measures the practicability of applying the selected measurement

processes throughout the measurement period. Data bases which have excellent precision, accuracy, and validity may be of little use if they contain so many missing values that data interpretation is impossible.

Approximately 1,000 PM_{10} samples were acquired for the Las Vegas Valley PM_{10} Study. Samples were submitted for comprehensive chemical analyses which resulted in over 20,000 data points, as documented in Section 5.2.

A data base with numerous data points, such as the one used in this study, requires detailed documentation of precision, accuracy, and validity of the measurements. This section addresses the procedures followed to define these quantities and presents the results of those procedures.

5.3.1 Precision

Measurement precisions reported in the Las Vegas Valley filter-based measurement data bases are propagated from precisions of the volumetric measurements, the chemical composition measurements, and the field blank variability using the methods of Bevington (1969). The following equations are used to calculate the precision associated with filter-based measurements:

$$C_i = (M_i - B_i)/V \tag{5-1}$$

$$V = F \times t \tag{5-2}$$

$$B_i = \frac{1}{n}\sum_{j=1}^{n} B_{ij} \quad \text{for } B_i > \sigma_{Bi} \tag{5-3}$$

$$B_i = 0 \quad \text{for } B_i \le \sigma_{Bi} \tag{5-4}$$

$$\sigma_{Bi} = STD_{Bi} = [\frac{1}{n-1}\sum_{j=1}^{n}(B_{ij} - B_i)^2]^{1/2} \quad \text{for } STD_{Bi} > SIG_{Bi} \tag{5-5}$$

$$\sigma_{Bi} = SIG_{Bi} = [\frac{1}{n}\sum_{j=1}^{n}(\sigma_{Bij})^2]^{1/2} \quad \text{for } STD_{Bi} \le SIG_{4Bi} \tag{5-6}$$

$$\sigma_{Ci} = [\frac{\sigma_{Mi}^2 + \sigma_{Bi}^2}{V^2} + \frac{\sigma_V^2(M_i - B_i)^2}{V^4}]^{1/2} \tag{5-7}$$

$$\sigma_{RMS_i} = (\frac{1}{n}\sum_{j=1}^{n}\sigma_{Ci}^2)^{1/2} \tag{5-8}$$

$$\sigma_V/V = 0.05 \tag{5-9}$$

where:

B_i = average amount of species i on field blanks

B_{ij} = the amount of species i found on field blank j

C_i = the ambient concentration of species i

F = flow rate throughout sampling period

M_i = amount of species i on the substrate

M_{ijf} = amount of species i on sample j from original analysis

M_{ijr} = amount of species i on sample j from replicate analysis

n = total number of samples in the sum

SIG_{Bi} = the root mean square error (RMSE), the square root of the averaged sum of the squared of σ_{Bij}.

STD_{Bi} = standard deviation of the blank

σ_{Bi} = blank precision for species i

σ_{Bij} = precision of the species i found on field blank j

σ_{Ci} = propagated precision for the concentration of species i

σ_{Mi} = precision of amount of species i on the substrate

σ_{RMSi} = root mean square precision for species i

σ_V = precision of sample volume

t = sample duration

V = volume of air sampled

Dynamic field blanks were periodically placed in each sampling system without air being drawn through them to estimate the magnitude of passive deposition for the period of time which filter packs remained in a sampler (typically five days). Three to four field blanks were obtained per site per sampler. No significant inter-site differences in field blank

concentrations were found for any species after removal of outliers (i.e., concentration exceeding three times the standard deviations of the field blanks). The average field blank concentrations (with outliers removed) were calculated for each species on each substrate (i.e., Teflon-membrane, quartz-fiber), irrespective of the sites. It was found in this study that inter-site differences are not statistically significant.

Blank precisions (σ_{Bi}) are defined as the higher value of the standard deviation of the blank measurements, STD_{Bi}, or the square root of the averaged squared uncertainties of the blank concentrations, SIG_{Bi}. If the average blank for a species was less than its precision, the blank was set to zero (as shown in Equation 5-4). Dynamic field blank concentrations are given in Tables 5-4 and 5-5 for PM_{10} samples in μg/filter collected with SFS and portable PM_{10} survey samplers, respectively.

The precisions (σ_{Mi}) for x-ray fluorescence analysis were determined from counting statistics unique to each sample. Hence, the σ_{Mi} is a function of the energy-specific peak area, the background, and the area under the baseline.

As shown in Table 5-4, the standard deviation of the field blank is a factor of two or greater than its corresponding root mean square error (RMSE) for PM_{10} volatilized nitrate, soluble potassium, organic carbon, calcium, iron, and zinc. Some of these field blanks may have been contaminated during the passive deposition period and during sample changing while the plenum was wide open. Examining the individual field blank values shows that these values are well within the range of the standard deviation of the average blank concentrations.

In Tables 5-4 and 5-5, PM_{10} mass blank values for SFS and portable PM_{10} survey samplers were less than their precisions. The largest variation is found for organic carbon, with an average of 23 ± 7 μg/47-mm filter. It is apparent that adsorption of gaseous organic carbon is enhanced over the five-day passive sampling period while filter substrates are left in the sampler. These values are comparable with those reported in other studies (e.g., Watson *et al.*, 1988; Chow and Watson, 1997b), however.

Table 5-6 summarizes the analytical specifications for the 24-hour PM_{10} measurements from the SFS and portable PM_{10} survey samplers. Minimum detectable limits (MDL), root mean squared (RMS) precisions, and lower quantifiable limits (LQL) are given. The LQL is defined as a concentration corresponding to two times the precision of the dynamic field blank. The LQLs in Table 5-6 were divided by 28.8 m^3 for SFSs and 7.2 m^3 for portable PM_{10} survey samplers. These are the nominal sample volumes of 24-hour samples. Actual volumes varied from sample to sample, typically within $\pm 5\%$ of the pre-set volume. The LQLs should always be equal to or larger than the analytical MDLs because they include the standard deviation of the field blank and flow rate precision

Species	Blank[a] Subtracted (B_i)	Blank[b] Precision (σ_{Bi})	Average Field Blank	Field Blank Std. Dev. (STD_{Bi})	Root Mean Squared Blank Precision (σ_{RMS})[c]	Total No. of Blanks in Average
Mass	0.0000	11.1910	3.7143	11.1910	8.5640	7
b_{abs} (Mm^{-1})	0.0000	1.1366	-0.4193	1.0152	1.1366	9
Chloride (Cl$^-$)	0.0000	0.5003	0.3767	0.1072	0.5003	9
Nonvolatilized Nitrate (NO$_3^-$)	1.2733	0.5000	1.2733	0.1832	0.5000	9
Volatilized Nitrate (NO$_3^-$)	1.9200	0.7390	1.9200	0.7390	0.1675	9
Sulfate (SO$_4^=$)	0.0000	0.5000	0.4700	0.3665	0.5000	9
Ammonium (NH$_4^+$)	0.5657	0.5000	0.5657	0.1362	0.5000	9
Soluble Potassium (K$^+$)	0.0000	0.0972	0.0539	0.0972	0.0550	9
Organic Carbon (OC)	22.6444	7.4159	22.6444	7.4159	3.8224	9
Elemental Carbon (EC)	0.0000	1.4873	0.9778	1.4873	0.9000	9
Sodium (Na)	0.8315	0.5945	0.8315	0.4605	0.5945	9
Magnesium (Mg)	0.0000	0.3335	0.2480	0.1932	0.3335	9
Aluminum (Al)	0.0000	0.4527	0.4233	0.2796	0.4527	9
Silicon (Si)	0.9595	0.5901	0.9595	0.5901	0.3615	9
Phosphorus (P)	0.0000	0.1236	0.1167	0.0808	0.1236	9
Sulfur (S)	0.1232	0.0733	0.1232	0.0733	0.0536	9
Chlorine (Cl)	0.0000	0.1515	0.0320	0.0981	0.1515	9
Potassium (K)	0.0000	0.1352	0.0498	0.0845	0.1352	9
Calcium (Ca)	1.1836	0.6891	1.1836	0.6891	0.2268	9
Titanium (Ti)	0.0000	0.4735	-0.0462	0.0751	0.4735	9
Vanadium (V)	0.0000	0.2456	-0.0591	0.0673	0.2456	9
Chromium (Cr)	0.0000	0.0705	-0.0190	0.0304	0.0705	9
Manganese (Mn)	0.0000	0.0356	0.0047	0.0075	0.0356	9
Iron (Fe)	0.0000	0.4268	0.3200	0.4268	0.0146	9
Cobalt (Co)	0.0000	0.0225	0.0006	0.0065	0.0225	9
Nickel (Ni)	0.0000	0.0207	-0.0002	0.0058	0.0207	9
Copper (Cu)	0.0000	0.0193	0.0123	0.0104	0.0193	9
Zinc (Zn)	0.0285	0.0202	0.0285	0.0202	0.0156	9
Gallium (Ga)	0.0000	0.0348	0.0051	0.0143	0.0348	9
Arsenic (As)	0.0000	0.0419	-0.0017	0.0092	0.0419	9
Selenium (Se)	0.0000	0.0218	-0.0035	0.0066	0.0218	9
Bromine (Br)	0.0000	0.0194	-0.0005	0.0065	0.0194	9
Rubidium (Rb)	0.0000	0.0186	-0.0030	0.0042	0.0186	9
Strontium (Sr)	0.0000	0.0211	0.0039	0.0069	0.0211	9
Yttrium (Y)	0.0000	0.0260	0.0024	0.0054	0.0260	9
Zirconium (Zr)	0.0000	0.0305	0.0001	0.0071	0.0305	9
Molybdenum (Mo)	0.0000	0.0556	0.0009	0.0109	0.0556	9
Palladium (Pd)	0.0000	0.1723	-0.0440	0.0541	0.1723	9
Silver (Ag)	0.0000	0.1900	0.0885	0.0739	0.1900	9
Cadmium (Cd)	0.0000	0.2050	0.0271	0.0849	0.2050	9
Indium (In)	0.0000	0.2376	-0.0632	0.0756	0.2376	9
Tin (Sn)	0.0000	0.2978	0.0180	0.1309	0.2978	9
Antimony (Sb)	0.0000	0.3514	-0.0383	0.0691	0.3514	9
Barium (Ba)	0.0000	1.2602	0.0420	0.3332	1.2602	9
Lanthanum (La)	0.0000	1.6523	0.4213	0.5069	1.6523	9
Gold (Au)	0.0000	0.0593	0.0174	0.0206	0.0593	9
Mercury (Hg)	0.0000	0.0491	-0.0012	0.0131	0.0491	9
Thallium (Tl)	0.0000	0.0461	0.0070	0.0126	0.0461	9
Lead (Pb)	0.0000	0.0622	0.0054	0.0208	0.0622	9
Uranium (U)	0.0000	0.0469	-0.0089	0.0096	0.0469	9

[a] Values used in data processing. Non-zero average blank concentrations are subtracted when the average blank exceeds its standard deviation.

[b] Larger of either the analytical precision or standard deviation from the field.

[c] RMS precision is the square root of the sum of the squared uncertainties of the observations divided by the number of observations.

Table 5-5
Las Vegas Valley PM$_{10}$ Study Field Blank Concentrations and Precisions (µg/filter) at the 30 Satellite Sites
Acquired with Portable PM$_{10}$ Survey Samplers

Species	Blank[a] Subtracted (B_i)	Blank[b] Precision (σ_{Bi})	Average Field Blank	Field Blank Std. Dev. (STD_{Bi})	Root Mean Squared Blank Precision (σ_{RMS})[c]	Total No. of Blanks in Average
Mass	0.0000	21.9628	-0.5222	21.9628	8.5640	90
b_{abs} (Mm^{-1})	0.0000	4.5465	2.8692	4.3700	4.5465	60
Aluminum (Al)	0.0000	0.4832	0.1130	0.2324	0.4832	89
Silicon (Si)	0.0000	0.7640	0.2082	0.7640	0.3252	89
Sulfur (S)	0.0000	0.1200	0.0220	0.0741	0.1200	90
Potassium (K)	0.0000	0.2034	0.0064	0.1438	0.2034	89
Calcium (Ca)	0.0000	0.2641	-0.0562	0.2435	0.2641	89
Iron (Fe)	0.0000	0.9976	0.1147	0.8107	0.9976	89

[a] Values used in data processing. Non-zero average blank concentrations are subtracted when the average blank exceeds its standard deviation.

[b] Larger of either the analytical precision or standard deviation from the field.

[c] RMS precision is the square root of the sum of the squared uncertainties of the observations divided by the number of observations.

Table 5-6
Analytical Specification of 24-Hour PM$_{10}$ Measurements for the Las Vegas Valley PM$_{10}$ Study

Species	Analysis Method[a]	Sequential Filter Sampler					Portable PM$_{10}$ Survey Sampler				
		MDL[b] [µg/m³]	RMS[c] [µg/m³]	LQL[d] [µg/m³]	No.[e] Values	No. > LQL	MDL[b] [µg/m³]	RMS[c] [µg/m³]	LQL[d] [µg/m³]	No.[e] Values	No. > LQL
Mass	Gravimetry	0.2429	3.0961	0.7772	27	27	0.9718	3.0154	6.1008	422	420
b$_{abs}$ (Mm^{-1})	Densitometry	2.1	3.5578	2.2247	53	53	8.4	6.7397	4.5465	423	415
Chloride (Cl$^-$)	IC	0.0521	0.0367	0.0347	54	53					
Nonvolatilized Nitrate (NO$_3^-$)	IC	0.0521	0.0910	0.0347	54	54					
Volatilized Nitrate (NO$_3^-$)	IC	0.0521	0.0553	0.0513	40	36					
Sulfate (SO$_4^=$)	IC	0.0521	0.1067	0.0347	54	54					
Ammonium (NH$_4^+$)	AC	0.0521	0.0389	0.0347	54	51					
Soluble Potassium (K$^+$)	AAS	0.0104	0.0109	0.0068	54	54					
Organic Carbon (OC)	TOR	0.0958	0.7554	0.5150	54	54					
Elemental Carbon (EC)	TOR	0.0958	0.7427	0.1033	54	54					
Sodium (Na)	XRF	0.0052	0.1280	0.0413	53	18					
Magnesium (Mg)	XRF	0.0031	0.0652	0.0232	53	53					
Aluminum (Al)	XRF	0.0048	0.4731	0.0314	53	53	0.0192	0.4668	0.1342	423	421
Silicon (Si)	XRF	0.0030	2.1293	0.0410	53	53	0.0121	1.8660	0.2122	423	422
Phosphorus (P)	XRF	0.0027	0.0182	0.0086	53	31					
Sulfur (S)	XRF	0.0024	0.2978	0.0051	53	53	0.0096	0.2681	0.0333	423	421
Chlorine (Cl)	XRF	0.0048	0.0704	0.0105	53	50					
Potassium (K)	XRF	0.0029	0.1346	0.0094	53	53	0.0117	0.0948	0.0565	423	420
Calcium (Ca)	XRF	0.0022	1.6214	0.0479	53	53	0.0086	1.2194	0.0734	423	422
Titanium (Ti)	XRF	0.0014	0.0253	0.0329	53	37					
Vanadium (V)	XRF	0.0012	0.0167	0.0171	53	1					
Chromium (Cr)	XRF	0.0009	0.0045	0.0049	53	14					
Manganese (Mn)	XRF	0.0008	0.0022	0.0025	53	51					
Iron (Fe)	XRF	0.0007	0.0606	0.0296	53	53	0.0029	0.1614	0.2771	423	373
Cobalt (Co)	XRF	0.0004	0.0178	0.0016	53	0					
Nickel (Ni)	XRF	0.0004	0.0015	0.0014	53	18					
Copper (Cu)	XRF	0.0005	0.0013	0.0013	53	53					
Zinc (Zn)	XRF	0.0005	0.0025	0.0014	53	53					
Gallium (Ga)	XRF	0.0009	0.0025	0.0024	53	1					
Arsenic (As)	XRF	0.0008	0.0039	0.0029	53	3					
Selenium (Se)	XRF	0.0006	0.0016	0.0015	53	0					
Bromine (Br)	XRF	0.0005	0.0011	0.0013	53	46					

Table 5-6 (continued)
Analytical Specification of 24-Hour PM$_{10}$ Measurements for the Las Vegas Valley PM$_{10}$ Study

Species	Analysis Method[a]	MDL[b] [µg/m³]	RMS[c] [µg/m³]	LQL[d] [µg/m³]	No.[e] Values	No. > LQL
Rubidium (Rb)	XRF	0.0005	0.0010	0.0013	53	31
Strontium (Sr)	XRF	0.0005	0.0024	0.0015	53	53
Yttrium (Y)	XRF	0.0006	0.0018	0.0018	53	2
Zirconium (Zr)	XRF	0.0008	0.0022	0.0021	53	25
Molybdenum (Mo)	XRF	0.0013	0.0039	0.0039	53	5
Palladium (Pd)	XRF	0.0053	0.0126	0.0120	53	0
Silver (Ag)	XRF	0.0058	0.0141	0.0132	53	0
Cadmium (Cd)	XRF	0.0058	0.0151	0.0142	53	0
Indium (In)	XRF	0.0062	0.0171	0.0165	53	1
Tin (Sn)	XRF	0.0081	0.0214	0.0207	53	0
Antimony (Sb)	XRF	0.0086	0.0252	0.0244	53	0
Barium (Ba)	XRF	0.0249	0.0845	0.0875	53	4
Lanthanum (La)	XRF	0.0297	0.1168	0.1147	53	0
Gold (Au)	XRF	0.0015	0.0046	0.0041	53	0
Mercury (Hg)	XRF	0.0012	0.0035	0.0034	53	0
Thallium (Tl)	XRF	0.0012	0.0034	0.0032	53	0
Lead (Pb)	XRF	0.0014	0.0033	0.0043	53	34
Uranium (U)	XRF	0.0011	0.0034	0.0033	53	0

[a] IC: Ion Chromatography
   AC: Automated Colorimetry
   AAS: Atomic Absorption Spectrophotometry
   TOR: Thermal/Optical Reflectance
   XRF: X-Ray Fluorescence

[b] Minimum Detectable Limits (MDL) is the concentration at which instrument response equals three times the standard deviation of the response to a known concentration of zero. Typical sample volumes are 28.8 m³ with sequential filter sampler and 7.2 m³ for portable PM$_{10}$ survey sampler with a sampling period of 24-hours.

[c] RMS or root mean squared precision is the square root of the sum of the square uncertainties of the field blank. The LQL is expressed here in terms of mass per cubic meter, after dividing by 28.8 m³, (the nominal volume of a 24-hour sample at 20 L/min) for sequential filter sampler and dividing by 7.2 m³ (the nominal volume of a 24-hour sample at 5 L/min).

[d] LQL or lower quantifiable limit is equal to two times the uncertainty of the field blank. The LQL is expressed here in terms of mass per cubic meter, after dividing by 28.8 m³, (the nominal volume of a 24-hour sample at 20 L/min) for sequential filter sampler and dividing by 7.2 m³ (the nominal volume of a 24-hour sample at 5 L/min).

[e] Number of non-voided (with -99) values reported.

[f] Not applicable.

(Watson *et al.*, 1995). This is the case for most of the chemical compounds noted in Table 5-6. This table indicates that the RMS precisions are comparable in magnitude to the LQLs for most species.

The number of reported (nonvoid, nonmissing) concentrations for each species and the number of reported concentrations greater than the LQLs are also summarized in Table 5-6. For the SFS samples, PM_{10} mass, light absorption, ions (e.g., chloride, nonvolatilized nitrate, sulfate, ammonium, soluble potassium), and organic and elemental carbon were detected in almost all cases except for volatilized nitrate, which was only detected in 90% of the cases. PM_{10} bromine (Br) and lead (Pb) were detected in 87% and 64% of the samples, respectively. Several rare-earth XRF elements (e.g., Co, Ga, Y, Mo, Pd, In, Sn, Sb, Tl) were not detected in most cases, which is typical for urban sites in most regions. PM_{10} nickel (Ni) and vanadium (V) concentrations were detected in 33% and 2% of the cases, respectively, indicating insignificant residual oil combustion in the study area. Industrial-source-related toxic species such as PM_{10} Se, Cd, and Hg were not detected in any of the cases with the exception of As, which was found above the LQLs in 6% of the cases. PM_{10} Mg, Al, Si, S, K, Ca, Mn, Fe, Cu, Zn, and Sr were found above the LQLs in over 95% of the cases, and most of these are abundant in resuspended dust. The maximum arsenic concentration of 0.0052 $\mu g/m^3$ was far below those levels that might be hazardous to human health.

The RMS precisions and LQLs for the portable PM_{10} survey samples were higher than those of the SFSs due to their greater variations in field blank concentrations. Similar to the SFS samples, most of the crustal species concentrations for the portable survey samples were above the LQLs in over 90% of the cases.

These analytical specifications imply that PM_{10} samples acquired in this study possess adequate sample loading for various chemical analyses. In addition, the MDLs of the selected chemical analysis methods were sufficiently low to establish a valid measurement with associated uncertainties.

5.4   Quality Assurance

Both system and performance audits are performed in the analytical laboratory during the spring of 1996 as samples for the Las Vegas Valley PM_{10} Study were processed. Auditors acquired and reviewed the standard operating procedures and examined all phases of measurement activities to assure that procedures were being followed and that operators were properly trained. All procedures reviewed by the auditors were acceptable and proved to be adequate for the study.

Performance audits establish whether or not predetermined specifications are being achieved in practice. For laboratory performance audits, both XRF thin-film standards and

laboratory spiked filters were submitted to independent laboratories for x-ray fluorescence, ion chromatographic, automated colorimetric, and carbon analyses. The following subsections summarize the audit results.

5.4.1 Thin-Film Standards Comparison for Elements

Table 5-7 summarizes the audit results for the 20 thin-film standards obtained by the auditor from MicroMatter Company (Deer Harbor, WA). The samples flagged "x" (i.e., S127, S139, and S142) are those which MicroMatter Co. specified as having "variable stoichiometry" with deposit concentrations certified for the sum of both elements, but not for each individual element. Therefore, only the sum of the elemental concentrations are used to compare with these standards.

The manufacturer's accuracy specifications for these thin-film standards are ±5% at best. Table 5-7 shows that over 90% of the comparisons are within ±15% of the standard value, with 64% of the elemental analyses reporting percent differences within ±10%. This yielded an overall average difference of -9%.

Poor comparisons were found for titanium (Ti) (-20.5%), vanadium (V) (-19.8%), sulfur (S) (-19.0%), and copper (Cu) (15.5%). Past experience in analyzing different batches of MicroMatter standards indicates substantial variability among individual standards for given elements. Figure 5-2 gives an example of a recent calibration in which sulfur concentrations varied by up to 160% (based on manufacturer's specifications) for the twelve MicroMatter sulfur standards. Multiple standards for each element are used in the normal XRF calibration process.

Table 5-8 summarizes the comparisons of recent (04/04/96) XRF standard calibrations with the National Institute of Standards and Technology (NIST) thin-film XRF standards. These comparisons report 1.0 ± 10.2% and 5.2 ± 11.1% differences for vanadium (V), 0 ± 14.4% and -1.3 ± 14.3% differences for titanium (Ti), and 4.7 ± 8.0%, -4.3 ± 8.0%, 7 ± 6.8%, and -5.0 ± 6.8% differences for copper (Cu). The standard deviation associated with the "percent difference" is propagated with XRF counting errors as well as the standard deviation of the NIST standard value. Standard deviations exceed the differences between measurements and standards most of the time in these comparisons, indicating that the average percent error is not significantly difference from zero. These values show that comparisons with NIST standards result in 10% to 15% fewer discrepancies than comparisons with MicroMatter standards.

Table 5-7
X-Ray Fluorescence Audit Results

(concentrations in $\mu g/cm^2$)

ID	Flag[a]	Element	Standard Concentration	Measured Concentration[b]			Absolute Difference[c]	% Difference[d]
S125		Al	42.60	40.39	±	0.11	-2.21	-5.19
S126		Si	33.70	31.03	±	0.07	-2.67	-7.92
S127	f3,x	P	n/a	10.92	±	0.03	n/a	n/a
S127	f3,x	Ga	n/a	32.15	±	0.03	n/a	n/a
S127		Sum of P and GA	48.50	43.07	±	0.03	-5.43	-11.20
S128		S	17.80	14.42	±	0.03	-3.38	-18.99
S128		Cu	42.40	35.83	±	0.02	-6.57	-15.50
S129		Cl	21.66	19.75	±	0.09	-1.91	-8.82
S129		K	23.84	22.28	±	0.05	-1.56	-6.54
S130		Ca	23.24	20.72	±	0.04	-2.52	-10.84
S131		Ti	48.40	38.46	±	0.05	-9.94	-20.54
S132		V	46.60	37.39	±	0.04	-9.21	-19.76
S133		Cr	47.00	45.27	±	0.04	-1.73	-3.68
S134		Mn	45.80	40.40	±	0.04	-5.4	-11.79
S135	n9	Fe	46.80	41.72	±	0.03	-5.08	-10.85
S136		Ni	44.50	48.11	±	0.03	3.61	8.11
S137		Cu	43.90	41.40	±	0.02	-2.5	-5.69
S138	i	Zn	30.00	29.80	±	0.02	-0.2	-0.67
S139	x	Ga	n/a	9.88	±	0.02	n/a	n/a
S139	x	As	n/a	34.43	±	0.04	n/a	n/a
S139		Sum of Ga and As	47.80	44.31	±	0.03	-3.49	-7.30
S140		Se	40.80	37.66	±	0.03	-3.14	-7.70
S141		Br	17.29	17.18	±	0.02	-0.11	-0.64
S142	x	Se	n/a	17.73	±	0.02	n/a	n/a
S142	x	Cd	n/a	24.07	±	0.06	n/a	n/a
S142		Sum of Se and Cd	46.70	41.80	±	0.04	-4.9	-10.49
S143		Ba	38.29	37.71	±	0.15	-0.58	-1.51
S144		Pb	49.20	46.96	±	0.05	-2.24	-4.55

[a] f3 = Filter wrinkled.

   i = Inhomogeneous sample deposit.

   n9 = Discoloration on deposit.

   x = Non-stoichiometric standard.

[b] Based on counting statistics from the x-ray fluorescence analysis.

[c] Absolute difference = Measured concentration - Standard concentration.

[d] % difference = [(Measured concentration - Standard concentration) * 100] / Standard concentration.
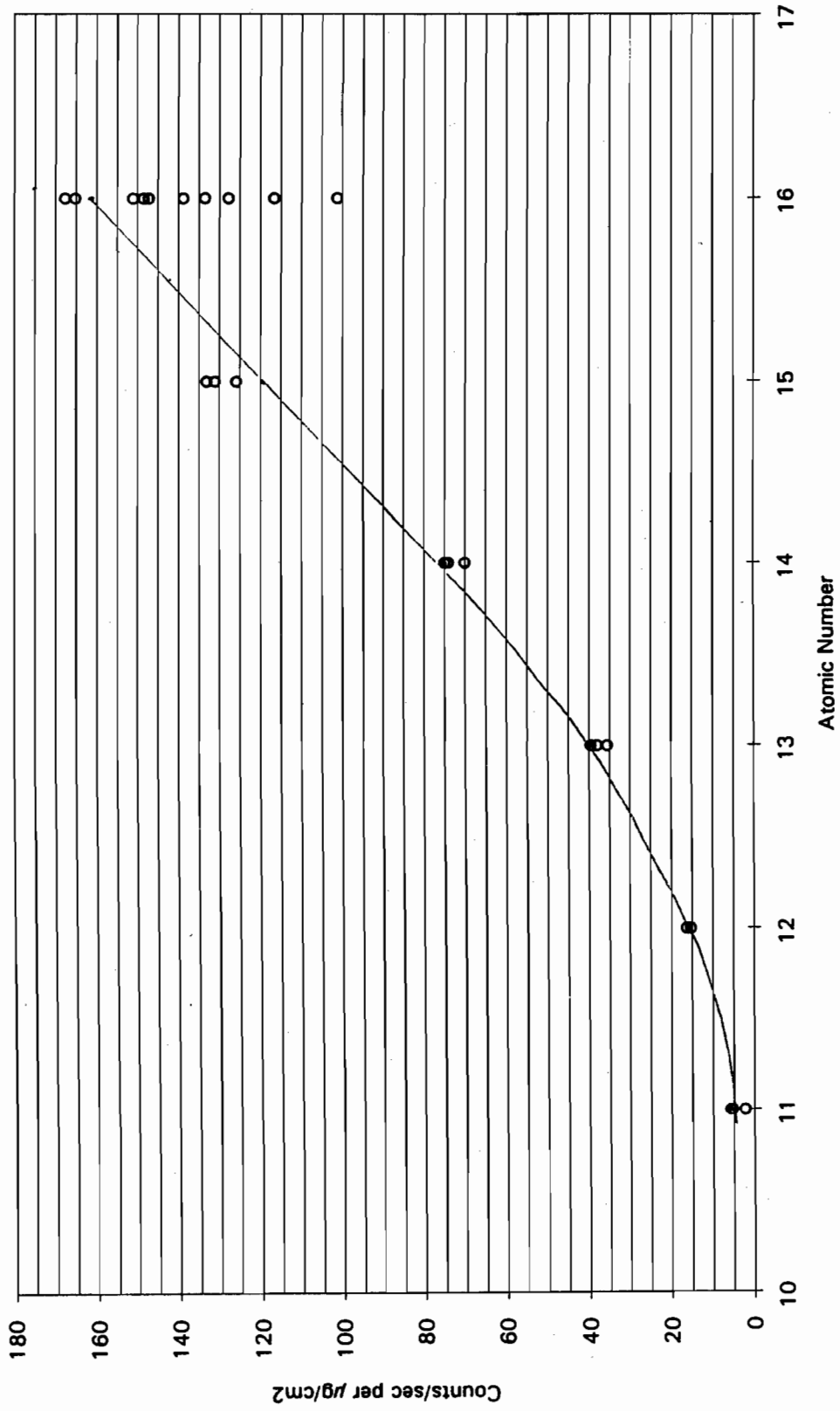
Figure 5-2   Instrument responses from calibrating twelve MicroMatter thin-film sulfur standards.

5-24

Table 5-8
Verification of XRF Calibration with NIST Thin-Film Standards

Element	Nominal µg/cm²		Excitation Condition	True Concentration at Surface (µg/cm²)		04/04/96 Calibration Measured Results		% Error	
SRM 1832									
S044									
Na[a]	11.50		5	7.1639		7.5149 ± 0.1799		4.9 ±	2.5
Al	15.20	± 1.00	5	11.4931	± 0.7561	11.4326 ± 0.0692		-0.5 ±	6.6
Al	15.20	± 1.00	4	12.3853	± 0.8148	12.3573 ± 0.1920		-0.2 ±	6.8
Si	36.20	± 1.20	5	28.1082	± 0.9318	30.2542 ± 0.0680		7.6 ±	3.3
Si	36.20	± 1.20	4	30.3141	± 1.0049	31.6614 ± 0.1501		4.4 ±	3.4
Ca	21.50	± 1.40	4	20.2162	± 1.3164	22.3008 ± 0.0421		10.3 ±	6.5
Ca	21.50	± 1.40	3	20.7131	± 1.3488	22.7814 ± 0.0507		10.0 ±	6.5
V	4.90	± 0.50	3	4.7683	± 0.4866	4.8166 ± 0.0166		1.0 ±	10.2
Mn	4.90	± 0.50	3	4.8018	± 0.4900	5.1587 ± 0.0138		7.4 ±	10.2
Co	1.08	± 0.07	3	1.0630	± 0.0689	1.1919 ± 0.0058		12.1 ±	6.6
Co	1.08	± 0.07	2	1.0671	± 0.0692	1.0860 ± 0.0085		1.8 ±	6.5
Cu	2.50	± 0.20	3	2.4693	± 0.1975	2.5853 ± 0.0065		4.7 ±	8.0
Cu	2.50	± 0.20	2	2.4786	± 0.1983	2.3728 ± 0.0095		-4.3 ±	8.0
SRM 1833									
S043									
Si	32.40	± 2.10	5	25.6435	± 1.6621	28.2156 ± 0.0854		10.0 ±	6.5
Si	32.40	± 2.10	4	27.7375	± 1.7978	30.6059 ± 0.2035		10.3 ±	6.6
K	16.90	± 1.70	4	15.5479	± 1.5640	16.4669 ± 0.0422		5.9 ±	10.1
K	16.90	± 1.70	3	15.9516	± 1.6046	17.4583 ± 0.0547		9.4 ±	10.1
Ti	12.50	± 1.80	3	12.0087	± 1.7292	12.0109 ± 0.0314		0.0 ±	14.4
Fe	14.10	± 0.45	3	13.7809	± 0.4398	14.9435 ± 0.0205		8.4 ±	3.2
Fe	14.10	± 0.45	2	13.8439	± 0.4418	14.3133 ± 0.0344		3.4 ±	3.2
Zn	3.80	± 0.30	3	3.7385	± 0.2951	4.1755 ± 0.0076		11.7 ±	8.0
Zn	3.80	± 0.30	2	3.7556	± 0.2965	3.5830 ± 0.0120		-4.6 ±	7.9
Pb	15.90	± 0.80	2	15.8039	± 0.7952	16.6711 ± 0.0286		5.5 ±	5.0
SRM 1832									
S112									
Na[a]	11.40		5	7.1653 ±		7.5013 ± 0.1821		4.7 ±	2.5
Al	14.90	± 1.00	5	11.3160	± 0.7595	11.9361 ± 0.0696		5.5 ±	6.7
Al	14.90	± 1.00	4	12.1957	± 0.8185	12.8174 ± 0.1971		5.1 ±	6.9
Si	36.60	± 1.20	5	28.5268	± 0.9353	30.4367 ± 0.0680		6.7 ±	3.3
Si	36.60	± 1.20	4	30.7682	± 1.0088	33.0386 ± 0.1530		7.4 ±	3.3
Ca	20.00	± 1.30	4	18.8282	± 1.2238	21.5239 ± 0.0413		14.3 ±	6.6
Ca	20.00	± 1.30	3	19.2787	± 1.2531	21.8541 ± 0.0496		13.4 ±	6.6
V	4.53	± 0.50	3	4.4125	± 0.4870	4.6407 ± 0.0163		5.2 ±	11.1
Mn	4.53	± 0.50	3	4.4429	± 0.4904	4.9242 ± 0.0135		10.8 ±	11.1
Co	0.99	± 0.07	3	0.9752	± 0.0660	1.1422 ± 0.0056		17.1 ±	6.9
Co	0.99	± 0.07	2	0.9786	± 0.0662	1.0057 ± 0.0081		2.8 ±	6.8
Cu	2.52	± 0.17	3	2.4908	± 0.1680	2.6656 ± 0.0066		7.0 ±	6.8
Cu	2.52	± 0.17	2	2.4997	± 0.1686	2.3745 ± 0.0095		-5.0 ±	6.8
SRM 1833									
S113									
Si	32.60	± 2.20	5	25.7073	± 1.7349	28.3727 ± 0.0861		10.4 ±	6.8
Si	32.60	± 2.20	4	27.8422	± 1.8789	30.5942 ± 0.2052		9.9 ±	6.8
K	16.80	± 1.70	4	15.4368	± 1.5621	16.2967 ± 0.0421		5.6 ±	10.1
K	16.80	± 1.70	3	15.8429	± 1.6032	17.3085 ± 0.0546		9.3 ±	10.2
Ti	12.60	± 1.80	3	12.0992	± 1.7285	11.9445 ± 0.0315		-1.3 ±	14.3
Fe	14.00	± 0.46	3	13.6800	± 0.4495	14.8728 ± 0.0205		8.7 ±	3.3
Fe	14.00	± 0.46	2	13.7428	± 0.4515	14.2539 ± 0.0344		3.7 ±	3.3
Zn	3.85	± 0.31	3	3.7872	± 0.3049	4.2160 ± 0.0077		11.3 ±	8.1
Zn	3.85	± 0.31	2	3.8046	± 0.3063	3.6231 ± 0.0121		-4.8 ±	8.1
Pb	16.30	± 0.77	2	16.2003	± 0.7653	16.9506 ± 0.0288		4.6 ±	4.7

[a] Uncertified value.

5.4.2 Laboratory Audit and Intercomparison for Carbon

Known amounts of aqueous potassium hydrogen phthalate (KHP) solution were deposited on nine pre-fired, acceptance-tested, quartz-fiber filter punches (each with a disc area of 0.536 cm^2) with a microsyringe (accuracy ±0.54%) to obtain audit standards. These spiked samples along with three method blanks were submitted to the thermal/optical reflectance carbon analysis method.

Table 5-9 summarizes the performance of carbon analysis on the spiked samples. More than 50% of the samples differed by more than 5% from the spiked concentrations. The average difference was 10% of the amount present. The largest percent variations of 25.9% (sample C5) and 18.9% (sample C4) were found on the lowest-concentration (1.43 μg/punch) samples, though the absolute differences were no more than those found for the higher concentrations; the maximum absolute difference was 0.37 μg/punch of organic carbon (sample C5) for these samples.

The largest absolute difference was 0.58 μg/punch (sample C3), equivalent to 0.75 μg/m^3 of organic carbon with nominal six-hour samples. Audit results with spiked samples reported by Chow *et al.* (1993b) showed an absolute difference of 1.1 to 5.3 μg/punch and an average ±7% relative difference, which is comparable to the findings in this study.

Method blanks (samples C2, C8, and C11) reported an average of 0.2 ± 0.3 μg/punch organic carbon and zero elemental carbon. These values indicated minimal contamination of these spiked samples during standard preparation, sample shipping, and refrigerator storage.

During the spring of 1996, a laboratory intercomparison was conducted by analyzing separate, identically-prepared punches of each of the 20 samples acquired in the Mt. Zirkel Visibility Study in the laboratories at DRI and at the South Coast Air Quality Management District (SCAQMD). Table 5-10 summarizes the results of these analyses. In these comparisons, 50% of the samples reported less than ±10% variations and 75% of the samples reporting less than ±20% variations. The correlation coefficients were 0.84 for organic or total carbon. For elemental carbon, the correlation coefficient is 0.43. The absolute differences in measured elemental carbon concentrations range from -6.1 to +10.9 μg/filter with large (~22%) average percent differences. Since the average elemental carbon concentrations are at or below three times the minimum detection level of 8.3 μg/filter, large uncertainties are not unusual for these comparisons.

5.4.3 Laboratory Audit for Ions

Known amounts of aqueous chloride, nitrate, sulfate, and ammonium solution were deposited on nine acceptance-tested quartz-fiber filters with a microsyringe (accuracy

Table 5-9
Carbon Audit Results of Laboratory-Spiked Samples

(carbon concentrations in µg/punch[a])

ID	Flag	Spike Value	Measured Organic Carbon			Spike Value	Measured Elemental Carbon			Absolute Difference[c] (µg/punch)	% Difference[d]
C1		2.69	2.4	±	0.3[b]	0.0	0.0	±	0.1	-0.29	-10.78
C2		0.00	0.1	±	0.3	0.0	0.0	±	0.1	0.10	n/a[e]
C3		4.48	3.9	±	0.3	0.0	0.0	±	0.1	-0.58	-12.95
C4		1.43	1.7	±	0.3	0.0	0.0	±	0.1	0.27	18.88
C5		1.43	1.8	±	0.3	0.0	0.0	±	0.1	0.37	25.87
C6		2.69	2.8	±	0.3	0.0	0.0	±	0.1	0.11	4.09
C7		1.43	1.5	±	0.3	0.0	0.1	±	0.1	0.07	4.90
C8		0.00	0.2	±	0.3	0.0	0.0	±	0.1	0.20	n/a[e]
C9		4.48	4.4	±	0.3	0.0	0.1	±	0.1	-0.08	-1.79
C10		2.69	2.7	±	0.3	0.0	0.0	±	0.1	0.01	0.37
C11		0.00	0.3	±	0.3	0.0	0.0	±	0.1	0.30	n/a[e]
C12		4.48	4.4	±	0.3	0.0	0.0	±	0.1	-0.08	-1.79

[a] Punch size is 0.536 cm^2.

[b] Uncertainty estimates are based on the instrument detection limits.

[c] Absolute difference = Measured value - Spike value.

[d] % difference = [(Measured value - Spike value) * 100] / Spike value.

[e] Not applicable.

Table 5-10

Results of the DRI / SCAQMD Laboratory Intercomparison for Thermal/Optical Reflectance Carbon Analysis

I.D. #	DRI Organic Carbon Mean ± Unc (µg/filter)	SCAQMD Organic Carbon Mean ± Unc (µg/filter)	Absolute[a] Difference (µg/filter)	Average Percent[b] Difference	DRI Elemental Carbon Mean ± Unc (µg/filter)	SCAQMD Elemental Carbon Mean ± Unc (µg/filter)	Absolute[a] Difference (µg/filter)	Average Percent[b] Difference	DRI Total Carbon Mean ± Unc (µg/filter)	SCAQMD Total Carbon Mean ± Unc (µg/filter)	Absolute[a] Difference (µg/filter)	Average Percent[b] Difference
BBFQ153	103.5 ± 8.3	96.75 ± 9.783	6.75	6.74	8.8 ± 1.6	11 ± 6.534	-2.20	-22.22	112.3 ± 9.7	108.65 ± 5.882	3.65	3.30
BBFQ154	81.7 ± 7.0	94.35 ± 9.359	-12.65	-14.37	11.1 ± 1.9	8.65 ± 6.292	2.45	24.81	92.8 ± 8.4	103.45 ± 5.639	-10.65	-10.85
BPFQ228	90.9 ± 7.5	111.95 ± 10.183	-21.05	-20.75	13.2 ± 2.2	11.95 ± 6.365	1.25	9.94	104.1 ± 9.1	123.45 ± 6.004	-19.35	-17.01
BPFQ281	71.2 ± 6.3	85.3 ± 9.338	-14.10	-18.02	4.3 ± 1.1	5.95 ± 6.188	-1.65	-32.20	75.5 ± 7.2	91.5 ± 5.601	-16.00	-19.16
BPFQ348	45.8 ± 5.0	43.3 ± 7.579	2.50	5.61	4.4 ± 1.1	6.05 ± 6.323	-1.65	-31.58	50.2 ± 5.8	48.3 ± 4.935	1.90	3.86
BPFQ384	62.1 ± 10.4	48.9 ± 8.529	13.20	23.78	12.3 ± 9.9	5.05 ± 6.266	7.25	83.57	74.4 ± 6.2	53.1 ± 5.292	21.30	33.41
BPFQ391	46.5 ± 8.2	43.25 ± 7.717	3.25	7.24	12.3 ± 9.9	10.5 ± 6.710	1.80	15.79	58.8 ± 5.6	56.85 ± 5.113	1.95	3.37
HSFQ104	62.4 ± 5.8	65.1 ± 8.914	-2.70	-4.24	16.3 ± 2.6	6.5 ± 6.162	9.80	85.96	78.7 ± 7.4	71.7 ± 5.418	7.00	9.31
HSFQ130	80.3 ± 6.9	80.25 ± 9.591	0.05	0.06	8.7 ± 1.6	6.2 ± 6.243	2.50	33.56	88.9 ± 8.1	86.95 ± 5.722	1.95	2.22
HSFQ153	59.8 ± 5.7	71.9 ± 8.762	-12.10	-18.38	0.2 ± 0.9	6.25 ± 6.301	-6.05	-187.60	60.0 ± 6.3	77.3 ± 5.396	-17.30	-25.20
HSFQ182	65.0 ± 8.6	62.7 ± 8.404	2.30	3.60	12.0 ± 4.4	5.95 ± 6.228	6.05	67.41	77.0 ± 10.5	68.2 ± 5.230	8.80	12.12
HSFQ184	45.2 ± 5.0	56.35 ± 8.683	-11.15	-21.96	4.2 ± 1.1	6.7 ± 6.376	-2.50	-45.87	49.4 ± 5.7	64.35 ± 5.386	-14.95	-26.29
HVFQ129	118.1 ± 9.3	93.9 ± 9.489	24.20	22.83	10.2 ± 1.8	7.75 ± 6.271	2.45	27.30	128.4 ± 10.8	102.1 ± 5.687	26.30	22.82
HVFQ152	112.2 ± 8.9	87.8 ± 9.102	24.40	24.40	6.1 ± 1.3	7 ± 6.198	-0.90	-13.74	118.4 ± 10.1	94.6 ± 5.506	23.80	22.35
HVFQ161	62.2 ± 5.8	67.45 ± 8.688	-5.25	-8.10	9.3 ± 1.7	4.55 ± 6.156	4.75	68.59	71.5 ± 7.0	71.75 ± 5.324	-0.25	-0.35
HVFQ174	97.4 ± 7.9	89.55 ± 9.620	7.85	8.40	21.1 ± 3.3	10.2 ± 6.265	10.90	69.65	118.5 ± 10.1	99.95 ± 5.740	18.55	16.98
HVFQ181	74.6 ± 9.6	76.8 ± 8.895	-2.20	-2.91	10.2 ± 3.8	4.05 ± 6.123	6.15	86.32	84.8 ± 11.4	81 ± 5.399	3.80	4.58
HVFQ198	72.4 ± 9.3	62.95 ± 8.422	9.45	13.96	4.2 ± 1.8	6.45 ± 6.258	-2.25	-42.25	76.5 ± 10.5	69.95 ± 5.246	6.55	8.95
JUFQ345	46.4 ± 6.7	47.9 ± 8.519	-1.50	-3.18	5.0 ± 2.0	5.9 ± 6.253	-0.90	-16.51	51.4 ± 7.7	54.4 ± 5.284	-3.00	-5.67
JUFQ361	45.4 ± 6.6	47.45 ± 7.827	-2.05	-4.42	3.5 ± 1.5	5.5 ± 6.188	-2.00	-44.44	49.0 ± 7.5	53.25 ± 4.989	-4.25	-8.31
Average	72.2 ± 22.7	71.7 ± 20.340	0.46	0.64	8.9 ± 5.0	7.1 ± 2.2	1.76	22.06	81.0 ± 24.9	79.0 ± 21.5	1.99	2.49

[a] Absolute difference = DRI minus SCAQMD measured concentration.

[b] Average percent difference = DRI minus SCAQMD, divided by their average, times 100%.

±0.54%). These triplicate spiked samples, at three different concentration levels, along with three method blanks, were submitted for ion chromatography (IC) analysis of chloride, nitrate, and sulfate, and for automated colorimetry (AC) analysis of ammonium.

Table 5-11 summarizes the performance of the IC and AC analyses. The best comparisons were found for sulfate, with a percent difference of less than ±3% for the spiked samples and zero (0 ± 0.25 µg/filter) for the filter blanks.

The percent differences for nitrate range from 0.9% to 7.8% with measured concentrations exceeding the spiked concentration by 0.07 to 0.58 µg/filter. This positive bias can be attributed to the slightly elevated blank values which averaged 0.52 ± 0.02 µg/filter. This positive bias has a negligible effect (less than 0.03 µg/m³ of nitrate) on the nitrate concentrations in the data base.

Chloride comparisons are generally within ±10% of the spiked amount, except for the lowest concentration level (0.86 µg/filter) where DRI's measurement shows a positive bias of 0.09 and 0.16 µg/filter. DRI's measurements on the blank filters also showed similar positive biases of 0.09 to 0.15 µg/filter. It is suspected that a slight baseline shift occurred during IC analysis which resulted in this positive bias for chloride and nitrate concentrations.

Table 5-11 shows positive ammonium biases of 0.27 to 0.56 µg/filter for blank filters and negative biases of 0.36 to 3.96 µg/filter were found for spiked filters, resulting in average percent differences -7.7% to -13.4% at three concentration levels. It is suspected that ammonia was liberated from the basic extraction solution due to vigorous shaking and sonicating procedures. This phenomenon is not expected to occur on the ambient samples, however, since the aerosols in the study region are expected to be either neutral or acidic, rather than basic as is the case for the spiked samples.

5.5   Data Validation

Data acquired from the Las Vegas Valley PM_{10} Study were submitted to four data validation levels:

Level 0 sample validation designates data as they come off the instrument. This process ascertains that the field or laboratory instrument is functioning properly.

Level I sample validation: 1) flags samples when significant deviations from measurement assumptions have occurred; 2) verifies computer file entries against data sheets; 3) eliminates values for measurements which are known to be invalid because of instrument malfunctions; 4) replaces data from a backup data acquisition system in the event

Table 5-11
Ion Analysis Results for Laboratory Spiked Samples

(concentrations in µg/filter)

ID	Element	Standard[a] Concentration			Measured[b] Concentration			Absolute Difference[e]	% Difference[f]
1	Cl^-	Filter blank			0.15	±	0.25	0.15	n/a
2	Cl^-	Filter blank			0.09	±	0.25	0.09	n/a
3	Cl^-	Filter blank			0.11	±	0.25	0.11	n/a
Average[c]	Cl^-	Filter blank			0.12	±	0.03	0.12	n/a
6	Cl^-	0.86	±	0.04	1.02	±	0.26	0.16	18.60
8	Cl^-	0.86	±	0.04	0.95	±	0.26	0.09	10.47
10	Cl^-	0.86	±	0.04	0.93	±	0.26	0.07	8.14
Average	Cl^-				0.97	±	0.05	0.11	12.40
Analyzed[d]	Cl^-	0.92							
5	Cl^-	1.43	±	0.07	1.44	±	0.27	0.01	0.70
9	Cl^-	1.43	±	0.07	1.55	±	0.27	0.12	8.39
12	Cl^-	1.43	±	0.07	1.50	±	0.27	0.07	4.90
Average	Cl^-				1.50	±	0.06	0.07	4.66
Analyzed[d]	Cl^-	1.46							
4	Cl^-	2.58	±	0.13	2.78	±	0.31	0.20	7.75
7	Cl^-	2.58	±	0.13	2.63	±	0.30	0.05	1.94
11	Cl^-	2.58	±	0.13	2.64	±	0.30	0.06	2.33
Average	Cl^-				2.68	±	0.08	0.10	4.01
Analyzed[d]	Cl^-	2.51							
1	NO_3^-	Filter blank			0.50	±	0.25	0.50	n/a
2	NO_3^-	Filter blank			0.51	±	0.25	0.51	n/a
3	NO_3^-	Filter blank			0.54	±	0.25	0.54	n/a
Average[c]	NO_3^-	Filter blank			0.52	±	0.02	0.52	n/a
6	NO_3^-	4.64	±	0.23	4.94	±	0.27	0.30	6.47
8	NO_3^-	4.64	±	0.23	4.94	±	0.27	0.30	6.47
10	NO_3^-	4.64	±	0.23	5.00	±	0.27	0.36	7.76
Average	NO_3^-				4.96	±	0.03	0.32	6.90
Analyzed[d]	NO_3^-	4.64							
5	NO_3^-	7.73	±	0.39	7.80	±	0.31	0.07	0.91
9	NO_3^-	7.73	±	0.39	8.21	±	0.31	0.48	6.21
12	NO_3^-	7.73	±	0.39	8.19	±	0.31	0.46	5.95
Average	NO_3^-				8.07	±	0.23	0.34	4.36
Analyzed[d]	NO_3^-	7.63							
4	NO_3^-	13.91	±	0.70	14.40	±	0.41	0.49	3.52
7	NO_3^-	13.91	±	0.70	14.37	±	0.41	0.46	3.31
11	NO_3^-	13.91	±	0.70	14.49	±	0.41	0.58	4.17
Average	NO_3^-				14.42	±	0.06	0.51	3.67
Analyzed[d]	NO_3^-	13.90							

Table 5-11 (continued)
Ion Analysis Results for Laboratory Spiked Samples

(concentrations in μg/filter)

ID	Element	Standard[a] Concentration			Measured[b] Concentration			Absolute Difference[e]	% Difference[f]
1	$SO_4^=$	Filter blank			0.00	±	0.25	0.00	n/a
2	$SO_4^=$	Filter blank			0.00	±	0.25	0.00	n/a
3	$SO_4^=$	Filter blank			0.00	±	0.25	0.00	n/a
Average[c]	$SO_4^=$	Filter blank			0.00	±	0.00	0.00	n/a
6	$SO_4^=$	34.31	±	1.72	35.10	±	0.80	0.79	2.30
8	$SO_4^=$	34.31	±	1.72	34.38	±	0.79	0.07	0.20
10	$SO_4^=$	34.31	±	1.72	34.74	±	0.79	0.43	1.25
Average	$SO_4^=$				34.74	±	0.36	0.43	1.25
Analyzed[d]	$SO_4^=$	33.87							
5	$SO_4^=$	57.18	±	2.86	55.50	±	1.32	-1.68	-2.94
9	$SO_4^=$	57.18	±	2.86	57.90	±	1.32	0.72	1.26
12	$SO_4^=$	57.18	±	2.86	58.20	±	1.33	1.02	1.78
Average	$SO_4^=$				57.20	±	1.48	0.02	0.03
Analyzed[d]	$SO_4^=$	56.49							
4	$SO_4^=$	102.90	±	5.15	104.70	±	2.62	1.80	1.75
7	$SO_4^=$	102.90	±	5.15	105.30	±	2.62	2.40	2.33
11	$SO_4^=$	102.90	±	5.15	104.10	±	2.62	1.20	1.17
Average	$SO_4^=$				104.70	±	0.60	1.80	1.75
Analyzed[d]	$SO_4^=$	101.51							
1	NH_4^+	Filter blank			0.27	±	0.25	0.27	n/a
2	NH_4^+	Filter blank			0.44	±	0.25	0.44	n/a
3	NH_4^+	Filter blank			0.56	±	0.25	0.56	n/a
Average[c]	NH_4^+	Filter blank			0.42	±	0.15	0.42	n/a
6	NH_4^+	5.57	±	0.28	5.06	±	0.26	-0.51	-9.16
8	NH_4^+	5.57	±	0.28	5.16	±	0.26	-0.41	-7.36
10	NH_4^+	5.57	±	0.28	5.21	±	0.26	-0.36	-6.46
Average	NH_4^+				5.14	±	0.08	-0.43	-7.66
Analyzed[d]	NH_4^+	5.49							
5	NH_4^+	16.70	±	0.84	13.56	±	0.30	-3.14	-18.80
9	NH_4^+	16.70	±	0.84	14.69	±	0.30	-2.01	-12.04
12	NH_4^+	16.70	±	0.84	15.16	±	0.31	-1.54	-9.22
Average	NH_4^+				14.47	±	0.82	-2.23	-13.35
Analyzed[d]	NH_4^+	15.57							
4	NH_4^+	27.83	±	1.39	23.87	±	0.37	-3.96	-14.23
7	NH_4^+	27.83	±	1.39	25.14	±	0.39	-2.69	-9.67
11	NH_4^+	27.83	±	1.39	24.67	±	0.38	-3.16	-11.35
Average	NH_4^+				24.56	±	0.64	-3.27	-11.75
Analyzed[d]	NH_4^+	26.80							

[a] Spike values from AtmAA.

[b] As measured by DRI.

[c] Average of the triplicate spike samples.

[d] As measured by Global Labs, an independent laboratory.

[e] Absolute difference = Measured concentration - Standard concentration.

[f] % difference = [(Measured concentration - Standard concentration) * 100] / Standard concentration.

of failure of the primary system; and 5) adjusts values for quantifiable calibration or interference biases.

Level II sample validation takes place after data from various measurement methods have been assembled in the master data base, and it is the first data analysis task. Level II applies consistency tests to the assembled data based on known physical relationships between variables.

Level III sample validation is part of the data interpretation process. The first assumption upon finding a measurement which is inconsistent with physical expectations is that the unusual value is due to a measurement error. If, upon tracing the path of the measurement nothing unusual is found, the value can be assumed to be a valid result of an environmental cause. Unusual values are identified during the data interpretation process as: 1) extreme values; 2) values which would otherwise normally track the values of other variables in a time series; and 3) values for observables which would normally follow a qualitatively predictable spatial or temporal pattern.

Level I validation flags and comments are included with each data record in the data base and are defined by Chow *et al.* (1994b). Level II validation tests and results are described in the following subsections.

Level II tests evaluate the chemical data for internal consistency. In this study, Level II data validations were made for: 1) comparison of collocated PM_{10} precisions, 2) sum of chemical species versus PM_{10} mass, 3) physical consistency, 4) cation and anion balance, and 5) nitrate volatilization. Correlations and linear regression statistics were computed and scatter plots prepared to examine the data. Suspect data were flagged and data validation summary was documented in the "Memo" field of the data base described in Section 5.2.

5.5.1 Collocated Precision

Three different aerosol samplers were used to measure PM_{10} at the Bemis and East Charleston sites: 1) the medium-volume Sequential Filter Sampler (SFS); 2) the low-volume Portable PM_{10} Survey Sampler (POR); and 3) the low-volume PM_{10} Beta-Attenuation Monitor (BAM). This provided an opportunity to compare the measurements for these different samplers. This comparison included 24-hour average PM_{10} mass concentrations ($\mu g/m^3$) from each sampler during the period from 01/03/95 and 01/28/96. PM_{10} BAM data was averaged to obtain 24-hour PM_{10} concentrations.

Comparisons were done on a pairwise basis. All concurrent samples for each pair of samplers were used in the comparisons. Four pairwise comparisons were made at the Bemis site and three at the East Charleston site. There are several empirical and statistical

approaches which may be used to make these comparisons although conclusions about sampler equivalence are ultimately subjective. The results of several tests are shown in Table 5-12 and Figure 5-3. For each pairwise comparison, one sampler is designated as the X sampler and the other as the Y sampler. These designations are unrelated to the U.S. EPA's designation of medium-flow SFSs as a "reference" method or the designation of the BAM as an "equivalent" method for PM_{10} (Chow and Watson, 1997b). (The portable PM_{10} sampler has no official designation.)

Linear regression can be used to infer equivalence between the X and Y samplers as well as predictability of one sampler's measurement from that of another sampler (King, 1977). Regression slope and intercept for each sample pair, along with their standard errors, are given in Table 5-12. For each comparison, the X-sampler PM_{10} measurement was the independent variable and the Y-sampler PM_{10} measurement was the dependent variable. When the slope equals unity to within three standard errors, the intercept is equal to zero within three standard errors, and the correlation coefficient is greater than 0.9, the selection of independent and dependent variables is often considered to be equivalent (Berkson, 1950; Madansky, 1959; Kendall, 1951; 1952). If the correlation coefficient is greater than 0.9 but the slope and intercept criteria are not met, the compared measurements are said to be predictable from the independent variable.

Table 5-12 indicates that in most cases, the correlation coefficients were less than 0.9. and these sampler measurements are not equivalent to each other. The intercepts are quite large, ranging from 2.2 ± 2.5 $\mu g/m^3$ from collocated portable PM_{10} survey sampler pairs to 23.9 ± 5.3 $\mu g/m^3$ for the BAM versus SFS pair. Figure 5-3 confirms that the BAM concentrations were generally higher than those obtained from the SFS or portable PM_{10} survey samplers. For the collocated portable sampler comparison (i.e., POR(A) versus POR(B) pair), the slope was within three standard errors of unity, the intercept was equal to zero within three standard errors, and the correlation was 0.87, so these two samplers can be considered to be equivalent.

Table 5-12 also presents the average ratios and standard deviation of "Y to X" and the percent distribution of the data pairs whose difference (X minus Y) is less than 1σ, between 1σ and 2σ, between 2σ and 3σ, and greater than 3σ. Here, σ is the measurement uncertainty of "X-Y", which is the square root of the sum of the squared uncertainties ($\sigma^2_x + \sigma^2_y$), where σ_x and σ_y are the PM_{10} measurement uncertainties for the X and Y samplers, respectively. The individual sampler uncertainties were estimated from replicate analyses for the SFS and portable PM_{10} survey samplers and is assumed to be 10% of the mass concentration for the BAM samplers. Table 5-12 shows that over 80% of all the pair comparisons lie within $\pm 1\sigma$ for POR(A) versus POR(B) at the Bemis site and for POR versus SFS and BAM versus POR at the East Charleston site, with more than 90% of the pair comparisons lying within $\pm 1\sigma$ for

Table 5-12
Intersampler Comparison of PM$_{10}$ Concentrations at the Bemis and East Charleston Sites

| Sampler[a] | | Slope[b] (µg/m³) | Intercept[c] (µg/m³) | Correlation[d] Coefficient (r) | No. of Pairs | Avg. Ratio[e] | % Distribution[f] <1σ | 1-2σ | 2-3σ | >3σ | Avg.[g] Diff. (µg/m³) | Precision (µg/m³) Collocated[h] | RMS[i] | P>|T|[j] |
Y	X													
I. Bemis Site														
POR	SFS	0.72 ± 0.09	4.95 ± 2.49	0.85	24	1.00 ± 0.48	83	17	0	0	1.61	6.95	3.26	0.27
BAM	SFS	0.66 ± 0.14	23.92 ± 5.28	0.44	91	1.61 ± 0.92	54	28	8	10	-13.61	29.28	5.70	0.0001
BAM	POR	1.78 ± 0.59	1.65 ± 15.00	0.52	26	2.06 ± 1.78	73	19	0	8	-19.30	34.69	6.40	0.0089
POR(A)	POR(B)	0.83 ± 0.10	2.22 ± 2.47	0.87	26	1.00 ± 0.42	96	0	4	0	1.57	5.85	4.26	0.18
II. East Charleston Site														
POR	SFS	1.29 ± 0.18	-7.31 ± 4.75	0.83	25	0.97 ± 0.52	80	12	8	0	0.50	10.61	3.39	0.82
BAM	SFS	0.71 ± 0.09	16.40 ± 3.67	0.64	93	1.30 ± 0.51	72	18	2	8	-6.21	20.00	11.03	0.0035
BAM	POR	0.54 ± 0.19	19.97 ± 5.61	0.50	25	1.70 ± 0.64	92	8	0	0	-9.34	18.64	4.84	0.0194

[a] POR=Low-volume Portable PM$_{10}$ Survey Sampler; SFS=Medium-volume Sequential Filter Sampler; POR(A)=PM$_{10}$ samples from collocated ABEM site; POR(B)=PM$_{10}$ samples from collocated BEMI site; BAM=Beta Attenuation Monitor.
[b] Regression slope with standard error.
[c] Regression intercept with standard error.
[d] Correlation coefficient.
[e] Average of Y/X and standard deviation of this ratio.
[f] Percentage of data pairs falling into the specified precision intervals, where each precision interval is equal to root mean square (RMS) of the sum of the squared precisions of the X and Y samplers.
[g] Average of X minus Y.
[h] Collocated precision or standard deviation of X minus Y.
[i] RMS precision of the difference between X and Y, the root mean square (RMS) of the sum of the squared precisions of X and Y.
[j] Probability of a greater absolute value for Student's T under the hypothesis that the difference between X and Y is zero.

(I) Bemis Site

Portable (A) vs. Portable (B)

Slope = 0.83 ± 0.10
Intercept = 2.22 ± 2.47 μg/m³
r = 0.87
n = 26

BAM vs. Portable

Slope = 1.78 ± 0.59
Intercept = 1.65 ± 15.0 μg/m³
r = 0.52
n = 26
Y/X = 2.06 ± 1.78

BAM vs. SFS

Slope = 0.66 ± 0.14
Intercept = 23.92 ± 5.28 μg/m³
r = 0.44
n = 91
Y/X = 1.61 ± 0.92

Portable vs. SFS

Slope = 0.72 ± 0.09
Intercept = 4.95 ± 2.49 μg/m³
r = 0.85
n = 24
Y/X = 1.00 ± 0.48

(II) East Charleston Site

BAM vs. Portable

Slope = 0.54 ± 0.19
Intercept = 19.97 ± 5.61 μg/m³
r = 0.50
n = 25

BAM vs. SFS

Slope = 0.71 ± 0.09
Intercept = 16.40 ± 3.67 μg/m³
r = 0.64
n = 93

Portable vs. SFS

Slope = 1.29 ± 0.18
Intercept = -7.31 ± 4.75 μg/m³
r = 0.83
n = 25
Y/X = 0.97 ± 0.52

Figure 5-3 Scatter plot of collocated precisions for the PM$_{10}$ samples acquired in the Las Vegas Valley PM$_{10}$ study.

POR(A) versus POR(B) at the Bemis site and for BAM versus POR at the East Charleston site. In all cases, over 80% of the paired differences lie within $\pm 2\sigma$, and over 90% of the measurements differ by no more than $\pm 3\sigma$. That is, in most cases, the differences between samplers are within the measurement errors.

Table 5-12 also shows that in all but two cases (BAM versus POR at the Bemis and East Charleston sites), the average Y/X ratio is equal to unity within one standard deviation of the average.

Table 5-12 gives the average of the paired differences (X-Y) between the X and Y sampler; the collocated precision, which is the standard deviation of the paired differences; and the root mean squared (RMS) precision (the square root of the mean squared precisions), which is essentially the average measurement uncertainty of "X-Y." The average differences and collocated precisions can be used to test the statistical hypothesis that the difference between samplers X and Y is zero. Statistical equivalence can be established when the RMS precision is less than 5 $\mu g/m^3$ or 7% of the PM_{10} mass, whichever is greater (Mathai *et al.*, 1990). Table 5-12 indicates statistical equivalence based on the pair-difference test which is only valid for four cases (POR versus SFS and POR(A) versus POR(B) at the Bemis sites, POR versus SFS and BAM versus POR at the East Charleston site). However, this rigorous test does not account for measurement uncertainty (i.e., if the samplers are different to within some multiple of the measurement uncertainty, they cannot realistically be considered different).

A parametric test (Student's T-test) is performed for each pair of samplers to illustrate the paired differences. Table 5-12 gives the probability (P) for a greater absolute value of Student's T statistic. If P is less than 0.05, one can infer that one of the samplers gives a concentration which is greater or smaller than the other, depending on the sign of the average difference. Table 5-12 shows that BAM data is systematically higher than the SFS and POR data in every case.

Because measurement uncertainty should be considered when making these comparisons, there is no rigorous statistical test or standard by which two samplers can be considered equivalent. However, the combined weight of the indices shown in Table 5-12 and the near one-to-one relationships shown in Figure 5-3 support the general conclusion that SFS and POR samplers measured the same mass concentration of PM_{10} during this study. The BAM sampler systematically gives higher values than the other samplers (in the order of 30% to 100% on average).

5.5.2　Sum of Chemical Species versus Mass

The sum of the individual chemical concentrations for PM_{10} should be less than or equal to the corresponding gravimetrically measured mass concentrations. This sum includes chemicals quantified on the Teflon-membrane and quartz-fiber filters for SFS samples and includes only Teflon-membrane filters for the portable PM_{10} samples. Total sulfur (S), soluble chloride (Cl^-), and soluble potassium (K^+) were excluded from the sum using SFS samples to avoid double counting. Measured concentrations do not account for unmeasured metal oxides in crustal material, cations, or hydrogen in organic carbon. Figure 5-4 shows a scatter plot of the PM_{10} sum of species versus mass at the two base sites using SFS PM_{10} samplers. This plot contains a dashed line indicating the slope with a nonzero intercept and a solid line with zero intercept. The correlation coefficient is generally lower with regression line forcing zero. Measurement uncertainties associated with the X- and Y-axes are shown for comparison. Regression statistics with mass as the independent variable (X) and sum of species as the dependent variable (Y) are also calculated. The average ratio of Y over X is also shown for comparison. As intercepts are low compared to the measured concentrations, the slope closely represents the ratio of Y over X. Suspect data were examined and removed from future statistical analyses if sampling or analytical anomalies were identified.

Figure 5-4 shows that the sum of species is always less than the corresponding PM_{10} mass within the measurement uncertainties. An excellent relationship is found between the sum of species and PM_{10} mass with correlation coefficients exceeding 0.97 for the two sites. Approximately 66% of the PM_{10} mass can be explained by the chemical species measured in this study. Similar sum-of-species-to-PM_{10}-mass ratios were found in California's Imperial Valley, where geological material was found to be one of the major PM_{10} sources (Chow and Watson, 1997b). It is suspected that unmeasured metal oxides in crustal material constitutes a major portion of the unaccounted mass.

5.5.3　Physical Consistency

The composition of chemical species concentrations measured by different chemical analysis methods can be examined. Physical consistency was tested for: 1) sulfate versus total sulfur, 2) chloride versus chlorine, 3) soluble potassium versus total potassium, and 4) light absorption versus elemental carbon.

5.5.3a　Sulfate versus Total Sulfur

Sulfate ($SO_4^=$) was acquired by ion chromatography (IC) analysis on quartz-fiber filters, and total sulfur (S) was obtained by x-ray fluorescence (XRF) analysis on Teflon-membrane filters of the SFSs. The ratio of sulfate to total sulfur should equal "three" if all of the sulfur was present as soluble sulfate. Figure 5-5 shows scatter plots of sulfate
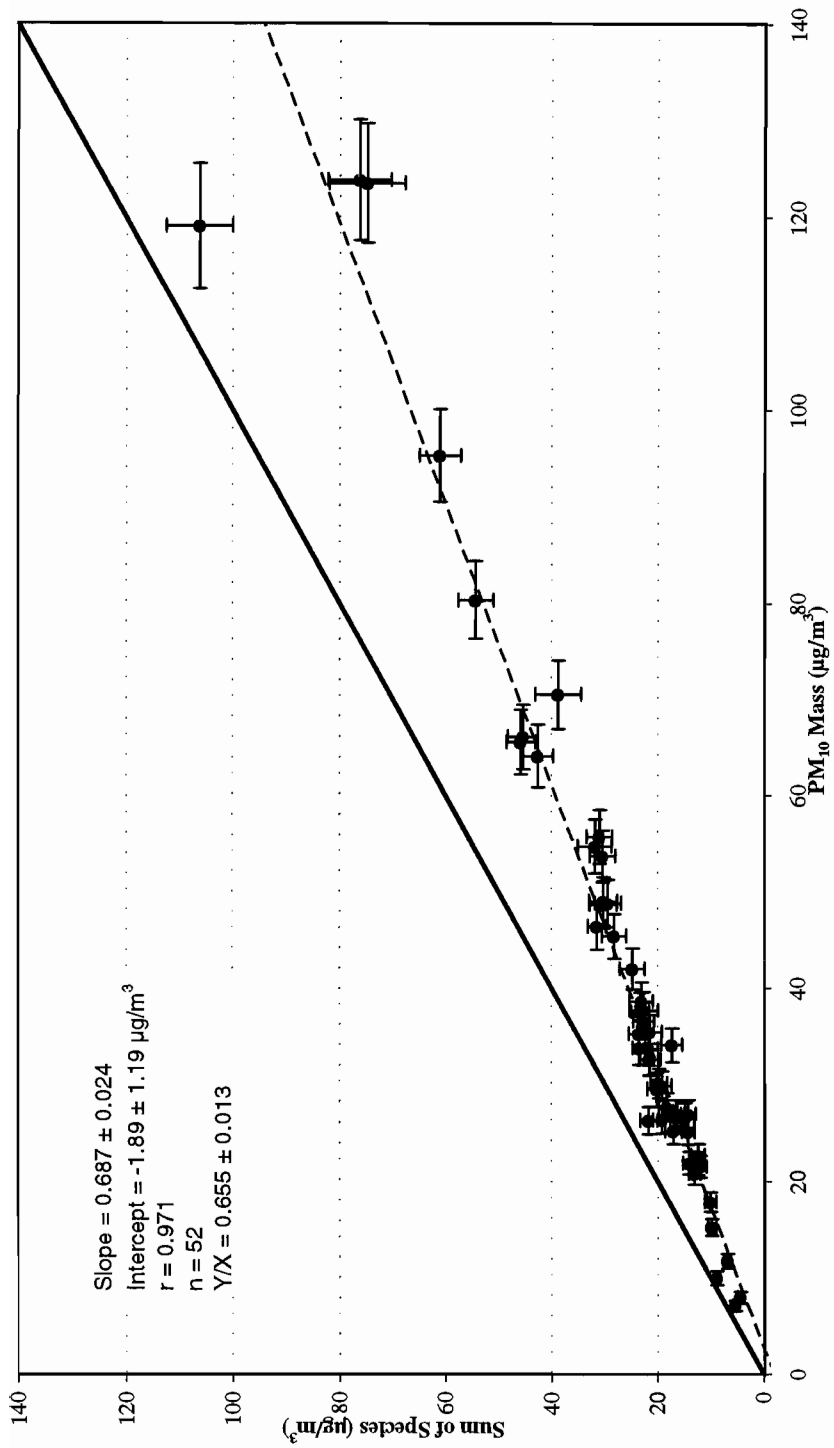
Figure 5-4 Scatter plot of PM$_{10}$ sum of species versus mass for PM$_{10}$ measurements collected at the Bemis and East Charleston sites between 01/03/95 and 01/28/96.

Slope = 0.687 ± 0.024
Intercept = -1.89 ± 1.19 µg/m^3
r = 0.971
n = 52
Y/X = 0.655 ± 0.013
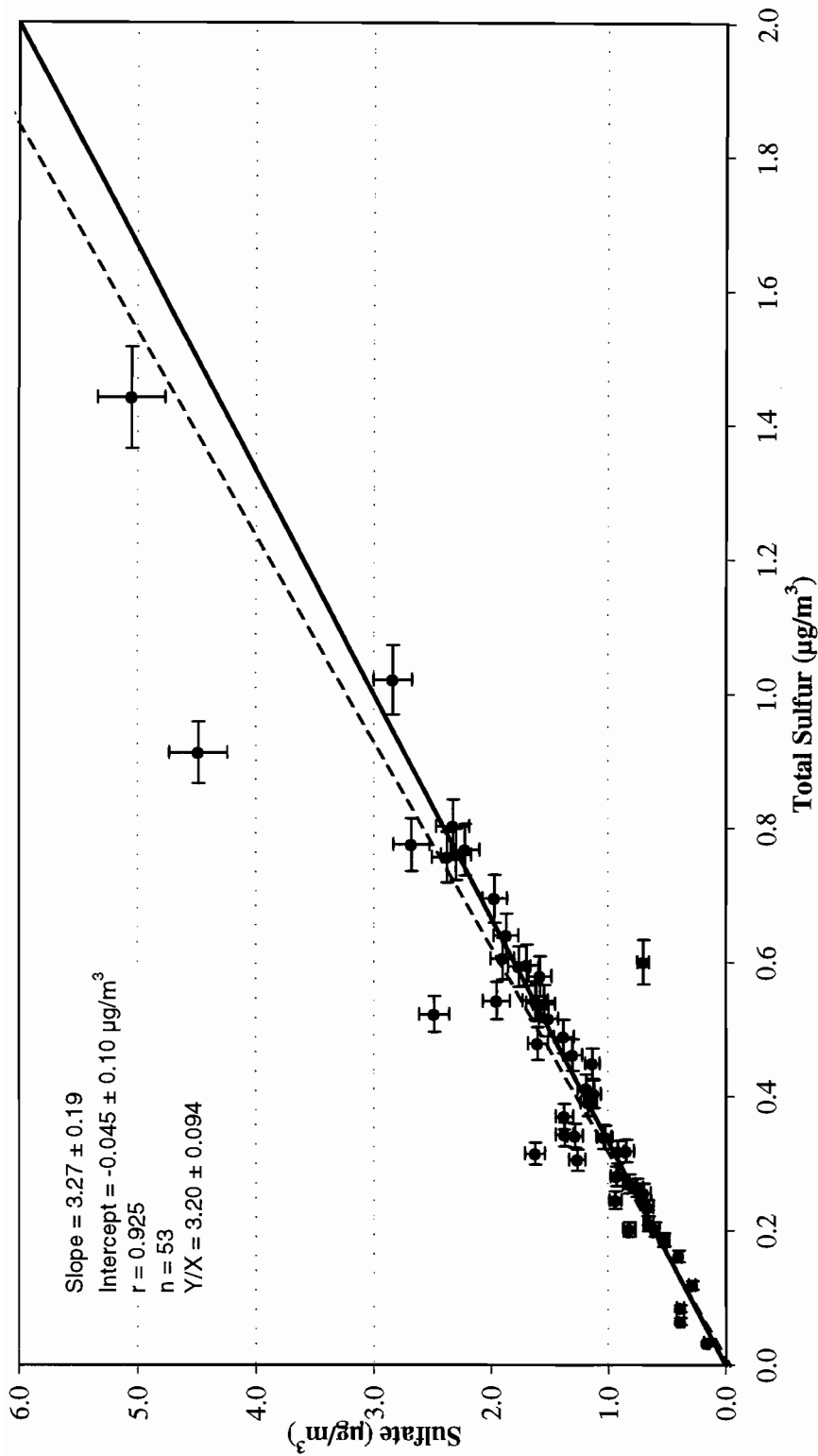
Figure 5-5 Scatter plot of sulfate versus total sulfur for PM_{10} measurements collected at the Bemis and East Charleston sites between 01/03/95 and 01/28/96.

Slope = 3.27 ± 0.19
Intercept = -0.045 ± 0.10 µg/m³
r = 0.925
n = 53
Y/X = 3.20 ± 0.094

Total Sulfur (µg/m³)

Sulfate (µg/m³)

versus sulfur of the PM_{10} measurements at the two base sites. Good correlations $(r = 0.93)$ were found for these measurements with a slope of 3.3 ± 0.2 and an intercept of -0.045 ± 0.1 $\mu g/m^3$ for the 53 measurement pairs. Forcing zero regression gives a sulfate-to-sulfur ratio of 3.0 within two standard deviations. There is some scattering in the data sets, especially at higher concentrations, indicating the presence of nonsoluble sulfur at these sites. This analysis implies that there are some discrepancies between the standard calibrations of the XRF and IC analyses, but the data are well within the measurement uncertainties.

5.5.3b Chloride versus Chlorine

Chloride (Cl^-) was acquired by IC analysis on quartz-fiber filters and chlorine (Cl) was acquired by XRF analysis on Teflon-membrane filters of the SFSs. Since chloride is the water-soluble portion of chlorine, it is expected that the chloride-to-chlorine ratio should be less than unity. Figure 5-6 shows that a high correlation coefficient $(r = 0.91)$ was found between chloride and chlorine with a slope of 0.91 ± 0.06 and a high intercept of 0.04 ± 0.01 $\mu g/m^3$. When calculated precisions are applied to Figure 5-6, a majority of the measurements fall within the one-to-one regression line within two standard deviations of the measurement intervals. Several of the data points above the regression line shows that Cl^- concentrations were higher than the corresponding Cl concentrations. These data pairs were checked against their standard calibration curves and replicates, but no suspects were found. The uncertainties of chloride measurement increase at low concentrations since chloride's elution peak in ion chromatography analysis is too close to the distilled water dip which, in turn, shifts the baseline of the chromatogram (Chow and Watson, 1997a).

5.5.3c Soluble Potassium versus Total Potassium

Soluble potassium (K^+) was acquired by atomic absorption spectrophotometry (AAS) analysis on quartz-fiber filters, and total potassium (K) was acquired by XRF analysis on Teflon-membrane filters of the SFSs. Since potassium concentrations are often used as an indicator of vegetative burning, it is important to assure the validity of the K^+ measurement. Figure 5-7 displays the scatter plot of soluble potassium versus total potassium concentrations.

The data pairs are scattered, especially at low concentrations, with high measurement uncertainties, but they are well within the measurement uncertainties. The regression statistics reported a correlation coefficient of 0.90 and insignificant intercept ($a = 0.039 \pm 0.013$ $\mu g/m^3$). It is apparent that some of the K^+/K ratios are quite low, especially as K concentrations are above 1 $\mu g/m^3$. Forcing zero intercepts gives a K^+/K ratio of 0.23 ± 0.01. This analysis shows that K^+ concentrations are quite low in the study area and approximately 25% of the total potassium is in its soluble state.

Slope = 0.912 ± 0.061
Intercept = 0.039 ± 0.012 µg/m³
r = 0.901
n = 53
Y/X = 1.06 ± 0.044
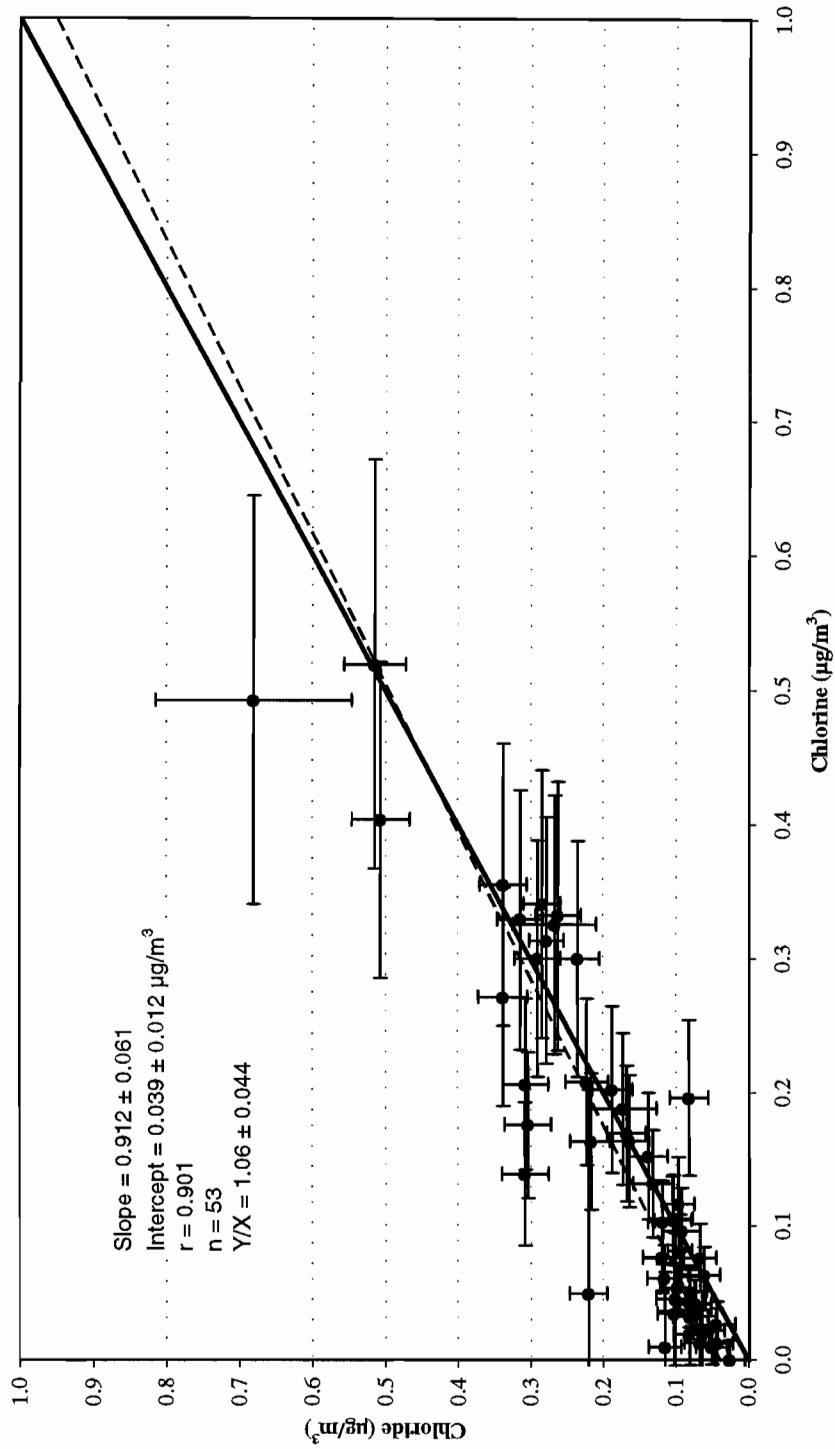
Figure 5-6 Scatter plot of chloride versus chlorine for PM_{10} measurements collected at Bemis and East Charleston sites between 01/03/95 and 01/28/96.
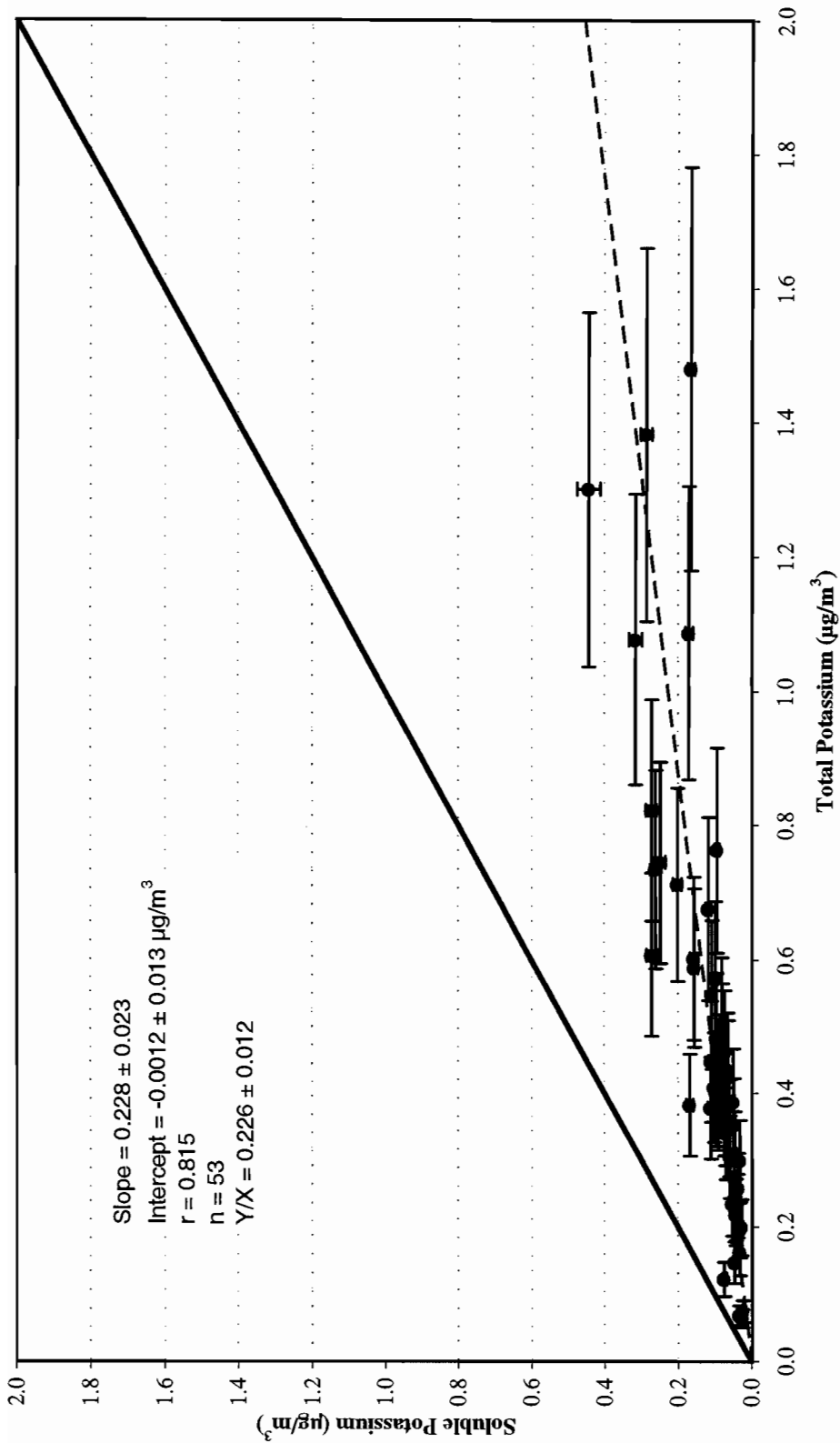
Figure 5-7 Scatter plot of soluble potassium versus total potassium for PM_{10} measurements collected at the Bemis and East Charleston sites between 01/03/95 and 01/28/96.

The plot shows:
- Slope = 0.228 ± 0.023
- Intercept = -0.0012 ± 0.013 µg/m³
- r = 0.815
- n = 53
- Y/X = 0.226 ± 0.012

X-axis: Total Potassium (µg/m³)
Y-axis: Soluble Potassium (µg/m³)

5.5.3d Light Absorption versus Elemental Carbon

Teflon-membrane filters from SFS PM_{10} samplers were submitted to light absorption (b_{abs}) measurement before and after sampling using a densitometer. The b_{abs} measurement on the Teflon-membrane filters is compared to elemental carbon (EC) measured with thermal/optical reflectance (TOR) analysis (Chow *et al.*, 1993b) on the quartz-fiber filter for each sample. Figure 5-8 illustrates the relationships between the b_{abs} and EC with an excellent correlation coefficient ($r = 0.96$). Data points above the regression lines are the values with high b_{abs} and low EC, that is, some nonelemental carbon light absorbing particles. If the filter samples contain significant amounts of crustal material, nonwhite, yellowish quartz-fiber filter punches are often obtained after the TOR analysis. It is likely these soil particles absorb light during the absorption measurement. Figure 5-8 shows that with zero intercept, the slope is 8.6 ± 0.3 m^2/g, a value lower than the empirically-derived absorption coefficient of 10 m^2/g (Trijonis *et al.*, 1988).

5.5.4 Anion and Cation Balance

Ammonium sulfate (($NH_4)_2SO_4$), ammonium bisulfate (NH_4HSO_4), and ammonium nitrate (NH_4NO_3) are the most common water-soluble compounds that are usually found in continental air. The ammonium concentrations can be calculated based on the sulfate and nitrate measurements by assuming that all the particulate nitrate is in the form of ammonium nitrate and all the particulate sulfate is either in the form of ammonium sulfate (i.e., calculated ammonium = $0.38 \times$ sulfate + $0.29 \times$ nitrate) or in the form of ammonium bisulfate (i.e., calculated ammonium = $0.192 \times$ sulfate + $0.29 \times$ nitrate). Measured ammonium concentrations should equal those calculated from ammonium nitrate and ammonium sulfate or ammonium bisulfate on a mole-to-mole basis. These comparisons assume that nitrate lost by volatilization of ammonium nitrate from the front quartz-fiber filters depletes both particulate nitrate and ammonium.

Scatter plots of calculated versus measured ammonium in Figure 5-9 show that the majority of ammonium sulfate or ammonium bisulfate points are above the one-to-one line with reasonable correlation ($r = 0.8$). Some of the sulfate is probably in the form of ammonium bisulfate, rather than ammonium sulfate. This implies that aerosol in the study area is acidic or trace amounts of some mineral products (such as calcium sulfate [$CaSO_4$], sodium sulfate [Na_2SO_4], magnesium sulfate [$MgSO_4$], or sodium nitrate [$NaNO_3$]) were present in the atmosphere. Given that sulfur emissions are low in the Las Vegas Valley, and there is little moisture to engender conversion to sulfuric acid, the excess sulfur is probably of geological origin (e.g., $CaSO_4$). Potassium chloride (KCl) and sodium chloride (NaCl) may also be present in the study region, but probably not in significant quantities due to the low chlorine and soluble potassium concentrations shown in Figures 5-6 and 5-7, respectively.
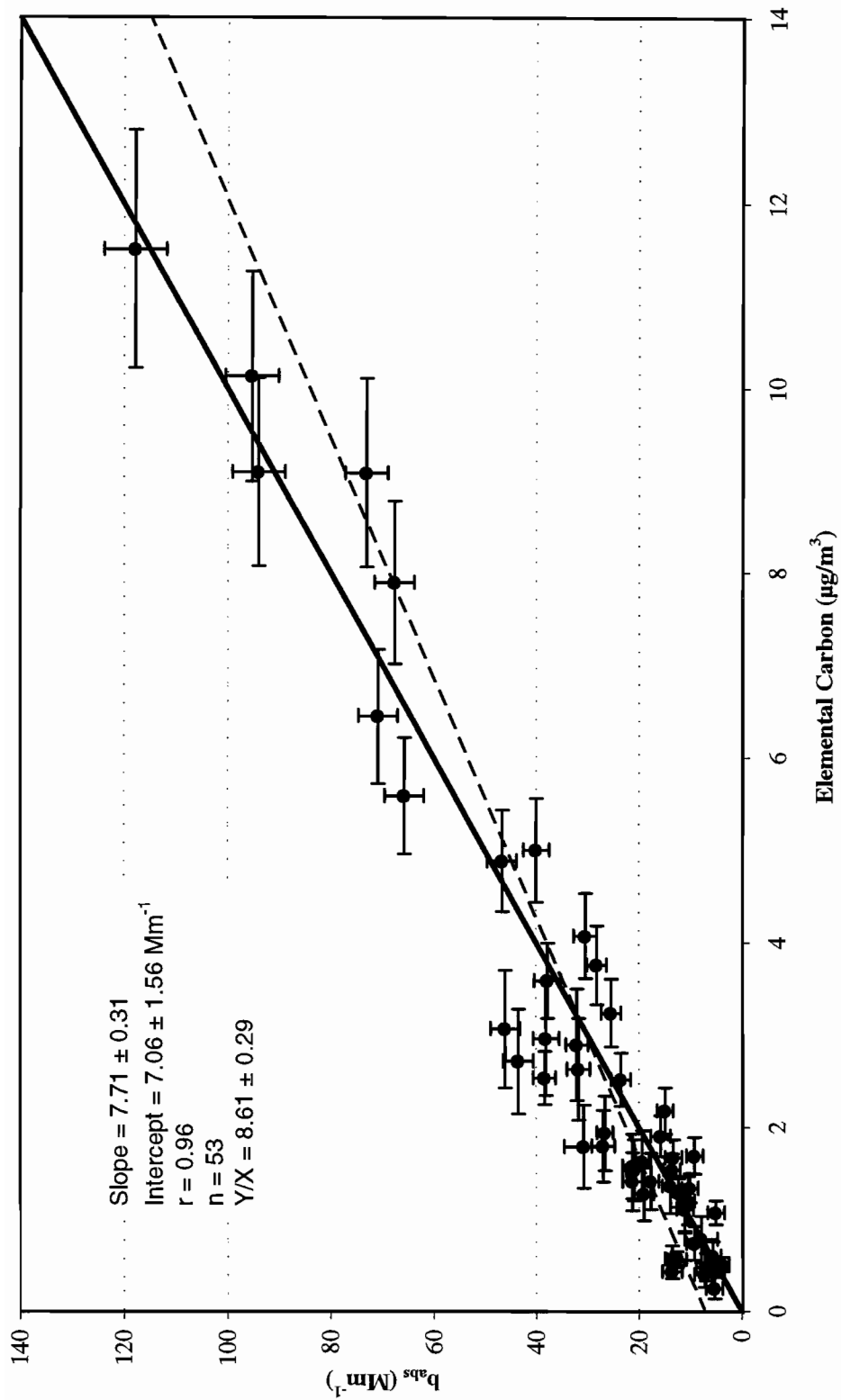
Figure 5-8 Scatter plot of light absorption (b_{abs}) versus elemental carbon for PM_{10} measurements collected at the Bemis and East Charleston sites between 01/03/95 and 01/28/96.

Slope = 7.71 ± 0.31
Intercept = 7.06 ± 1.56 Mm^{-1}
r = 0.96
n = 53
Y/X = 8.61 ± 0.29

Elemental Carbon ($\mu g/m^3$)

b_{abs} (Mm^{-1})
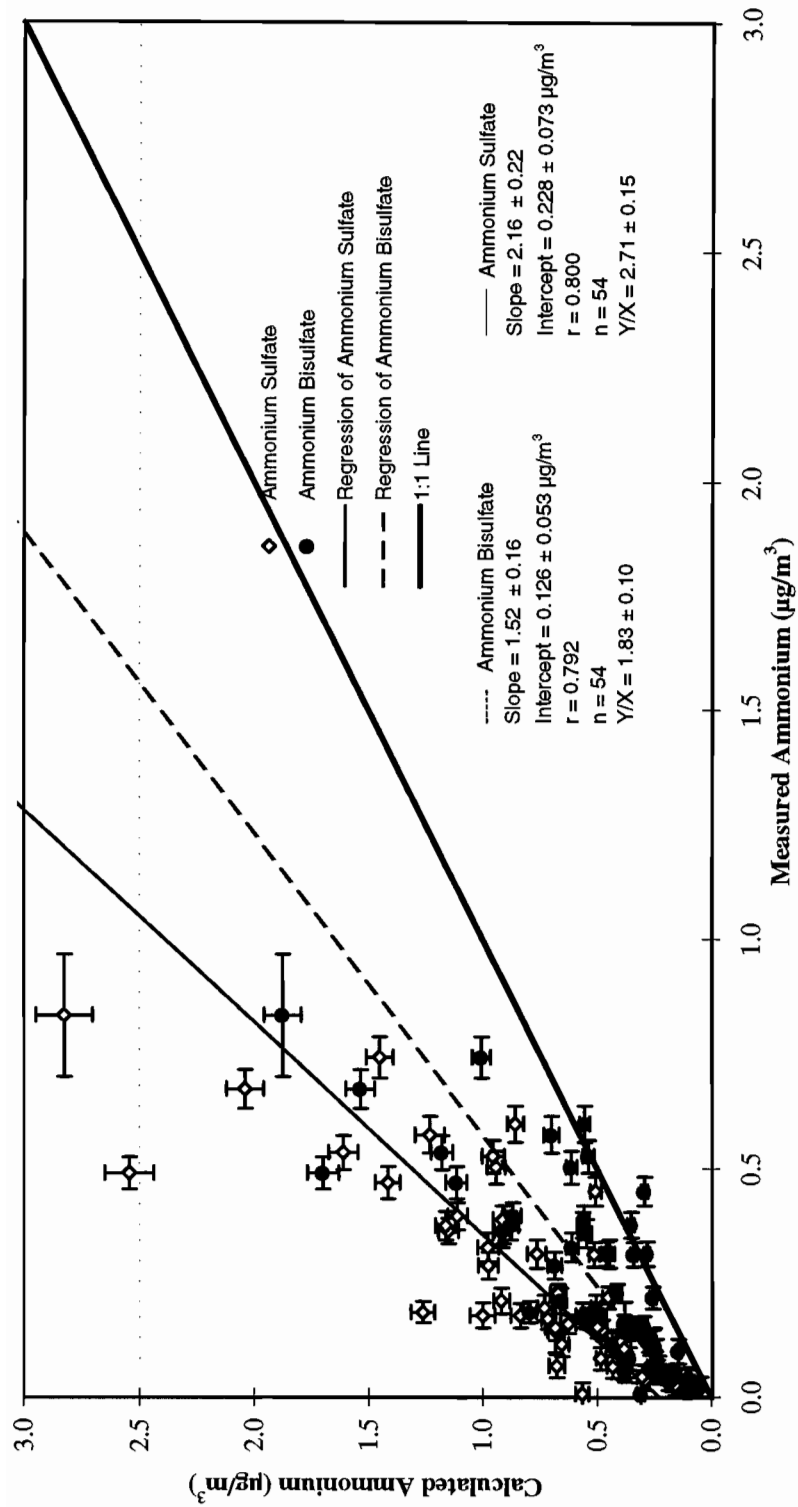
Figure 5-9 Comparison between measured and calculated ammonium for PM_{10} measurements collected at the Bemis and East Charleston sites between 01/03/95 and 01/28/96.

The equivalent amount of anions and cations are expected if the correct species were identified and measured accurately. In this study, all the anions (Cl^-, NO_3^-, $SO_4^=$) were acquired by IC analysis on quartz-fiber filters of the SFSs. Ammonium (NH_4^+) was obtained by automated colorimetry (AC) analysis, whereas K^+ was obtained by AAS analysis of quartz-fiber filters of the SFSs.

Figure 5-10 illustrates that these ionic measurements are reasonably correlated (r = 0.84), with all of the data points falling below the one-to-one regression line. Only 35% of the anions can be balanced with cations on a molar equivalent basis. Since fugitive dust is one of the major contributors to PM_{10} concentrations, it is suspected that some traceable quantities of soluble magnesium (Mg^{++}) and soluble calcium (Ca^{++}) might provide the needed cations from soluble fractions of magnesium sulfate ($MgSO_4$), gypsum ($CaSO_4$), and/or lime (CaO). Soluble magnesium and calcium were not measured in this study. Since good correlations were found, this anion and cation balance provides confidence, in that the ionic measurements made by IC, AC, and AAS are in good agreement among each other.

5.5.5 Nitrate Volatilization

The quartz/nylon filter pack in the SFS, preceded by an anodized aluminum nitric acid denuder, measures PM_{10} nitrate (i.e., nonvolatilized nitrate) from the front quartz-fiber filter and captures the volatilized particulate nitrate dissociated from the front quartz-fiber filter with a backup nylon-membrane filter. The sum of these two nitrate measurements in the quartz/nylon filter pack gives total PM_{10} particulate nitrate. The nitric-acid-denuded total PM_{10} particulate nitrate should be greater than or equal to the PM_{10} nonvolatilized nitrate, depending on the extent of volatilization.

Figure 5-11 displays scatter plots of PM_{10} nonvolatilized particulate nitrate versus nitric-acid-denuded total PM_{10} particulate nitrate. As discussed in Watson *et al.* (1994b), secondary ammonium nitrate is not a stable compound. Its equilibrium with gaseous ammonia and nitric acid is strongly influenced by temperature and relative humidity. The dissociation of particulate nitrate from the front quartz-fiber filter is expected to be more prevalent when ambient temperatures exceed 25 °C. Figure 5-11 shows an excellent correlation (r = 0.93) between the PM_{10} nonvolatilized nitrate and nitric-acid-denuded total PM_{10} particulate nitrate with a slope of 0.65 ± 0.04 with negligible intercept (-0.055 ± 0.06 $\mu g/m^3$). On average, approximately 40% of the particulate nitrate volatilized from the front quartz-fiber filter.

Major losses due to nitrate volatilization were also found in other studies (e.g., Chow *et al.*, 1994b; Chow, 1995). Volatilized nitrate is not part of the measured PM_{10} mass, so this loss does not show up in the sum of species comparison shown in Figure 5-4. Without a backup absorbent filter, particulate nitrate would be greatly underestimated.
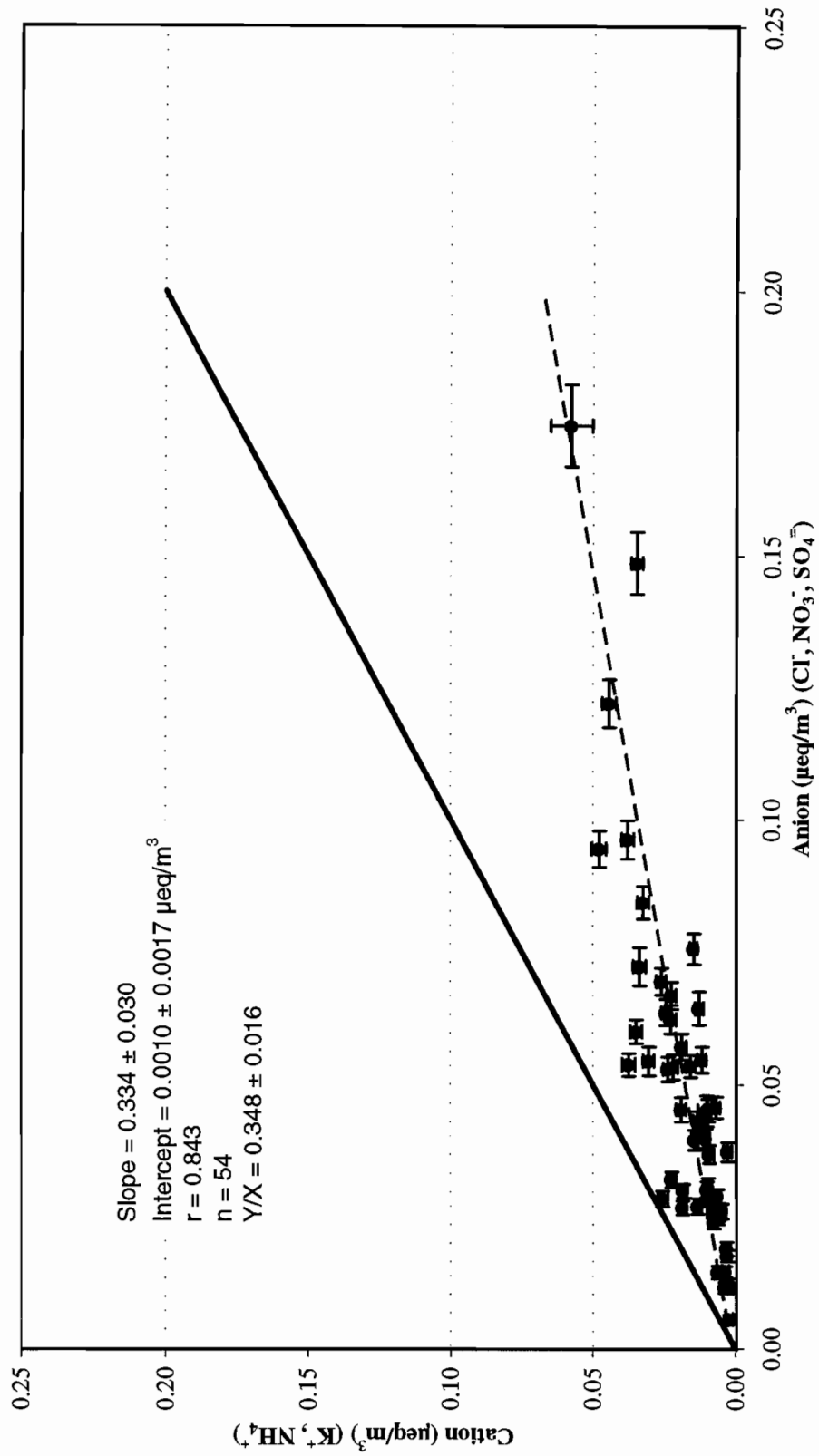
Figure 5-10 Scatter plot of cations versus anions for PM_{10} measurements collected at the Bemis and East Charleston sites between 01/03/95 and 01/28/96.

Slope = 0.334 ± 0.030

Intercept = 0.0010 ± 0.0017 $\mu eq/m^3$

r = 0.843

n = 54

Y/X = 0.348 ± 0.016

Anion ($\mu eq/m^3$) (Cl^-, NO_3^-, $SO_4^=$)

Cation ($\mu eq/m^3$) (K^+, NH_4^+)
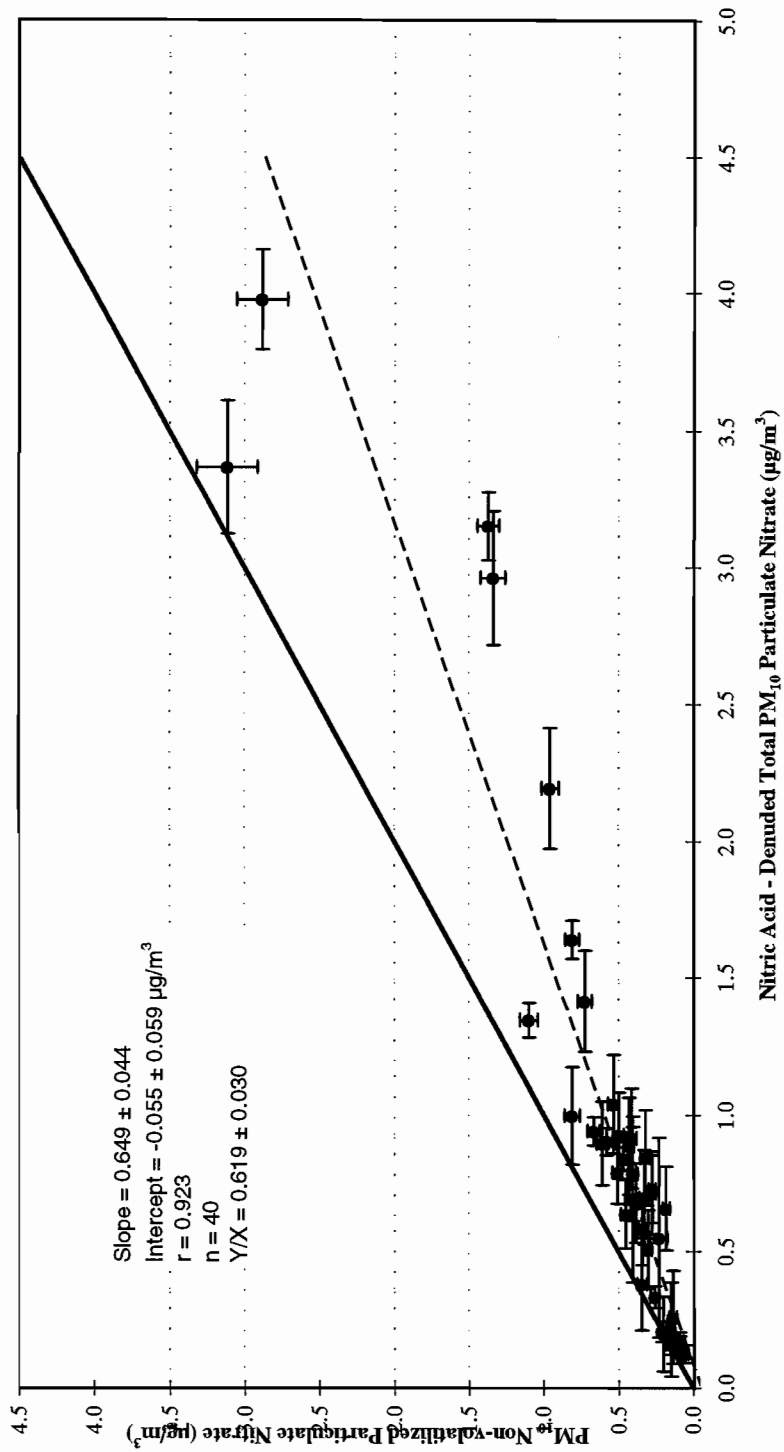
Figure 5-11 Scatter plot of PM_{10} non-volatilized particulate nitrate versus nitric acid-denuded total PM_{10} particulate nitrate for PM_{10} measurements collected at the Bemis and East Charleston sites between 01/03/95 and 01/28/96.

6.0 TEMPORAL AND SPATIAL VARIATIONS OF PM_{10}

The most rudimentary form of receptor modeling consists of examination of spatial and temporal distributions of atmospheric constituents and relative abundances of certain chemical species. When coupled with a conceptual understanding of the emissions sources, meteorology, and chemical transformation mechanisms, this receptor-oriented analysis provides qualitative, and even semi-qualitative, evidence of relationships between source emissions and receptor concentrations. This section examines the temporal and spatial distribution of PM_{10} and its chemical components.

6.1 Exceedances of Federal 24-Hour PM_{10} Standards

Table 6-1 summarizes the number of cases which exceeded the federal 24-hour PM_{10} standard of 150 $\mu g/m^3$ between 01/03/95 and 01/28/96 at the Clark County beta attenuation compliance monitoring network. Hourly PM_{10} beta-attenuation monitoring data are averaged to obtain 24-hour PM_{10} concentrations. For the 17 standard exceedance days, 24-hour PM_{10} concentrations were exceeded 12 times at the Green Valley site, six times at the Craig/Bemis site, four times each at the Maycliff, McDaniel, and City Center sites, three times each at the East Charleston (microscale) and Pittman sites, and once each at the Powerline and Flamingo sites. The highest PM_{10} concentration of 388 $\mu g/m^3$ was reported at the McDaniel site on 01/17/96. In fact, 24-hour PM_{10} concentrations exceeded 300 $\mu g/m^3$ (two times the 24-hour PM_{10} NAAQS) nine times during the study period.

Except for samples acquired on 04/13/95 and 10/04/95, PM_{10} mass concentrations varied by more than a factor of five among the ten sampling locations on a given standard exceedance day. In most cases, elevated PM_{10} concentrations at one site did not necessarily correspond with high concentrations at the other sites. This implies that local sources superimposed upon surface meteorology are the driving forces for these standard exceedances. Twenty-four-hour average and maximum hourly wind speeds, along with their maximum gust winds are listed in Table 6-1. Meteorological analysis showed that most of the PM_{10} standard exceedance days are associated with high winds. Maximum wind speed exceeded 10 m/s on over 80% of the standard exceedance days.

These high wind events were not the only cause of 24-hour PM_{10} standard exceedance, however. Table 6-1 showed that average daily wind speeds were below 6 m/s on 08/09/95, 08/15/95, 09/01/95, and 10/05/95, with hourly maximum wind speeds below 10 m/s.

Valley-wide elevated PM_{10} concentrations were observed on 11/26/95, 01/16/96, and 01/17/96 with PM_{10} concentrations exceeding 150 $\mu g/m^3$ at 60% to 80% of the monitoring sites. Meteorological analyses indicate strong winds were observed on these days. On

Table 6-1
Summary of 24-Hour PM$_{10}$ Exceedances in the Clark County Monitoring Network between 01/03/95 and 01/28/96
(one or more beta gauge sites >150 µg/m^3)

Date	PM$_{10}$ Concentration (µg/m^3) [a]										Meteorology [b]		
	Craig/Bemis	E. Charleston Microscale	Arroyo Grande	Powerline	Maycliff	McDaniel	City Center	Pittman	Flamingo	Jean	Average Wind Speed (m/s)	Maximum Wind Speed (m/s)	Maximum Wind Gust (m/s)
04/09/95	176	78	170	142	270	165	97	137	48	32	9.5	13.2	19.4
04/13/95	213	78	NA [c]	91	65	97	86	120	85	52	11.5	15.7	21.3
04/27/95	61	58	157	67	32	66	56	58	89	24	9.3	14.5	18.0
05/04/95	92	54	196	90	37	50	48	84	50	24	5.5	10.6	14.1
06/01/95	57	63	226	51	48	47	55	57	58	30	5.4	11.4	16.3
06/05/95	186	104	342	236	122	117	116	149	111	47	9.9	15.4	21.1
08/09/95	74	47	155	NA [c]	40	46	48	98	56	19	4.0	9.2	8.8
08/12/95	84	77	158	28	55	55	59	90	55	28	5.8	9.7	13.2
08/15/95	62	55	185	43	48	59	55	69	47	31	5.4	7.5	11.0
09/01/95	83	163	219	57	85	98	89	108	109	19	2.6	11.0	15.8
10/04/95	115	79	226	84	110	116	111	138	81	51	7.0	11.0	15.4
10/05/95	55	45	174	29	56	41	40	41	34	19	4.0	6.2	9.2
10/22/95	121	110	129	47	127	117	177	74	90	67	8.2	12.3	16.7
11/26/95	219	160	366	149	315	260	276	258	134	56	9.0	13.6	17.2
12/12/95	318	121	NA [c]	40	NA [c]	109	89	NA [c]	94	25	5.4	13.2	15.4
01/16/96	385	193	NA [c]	120	270	310	219	386	339	37	5.9	16.7	21.6
01/17/96	148	108	NA [c]	94	229	388	242	184	149	96	9.3	16.3	21.6

[a] Averaged from hourly beta-attenuation monitoring data.

[b] Data acquired at the McCarran Airport. Maximum wind speed is the maximum of the 24 hourly observations taken each day. The hourly observation is a one-minute average ten minutes before the hour. Maximum wind gust is the maximum gust over the 24 hourly observations.

[c] Data not available.

11/26/95, PM_{10} exceeded 150 $\mu g/m^3$ at seven sites. A cold front from the Pacific Northwest passed through Las Vegas between 0800 and 0900 PST. Late in the previous day, winds from the southwest began increasing in strength. After the frontal passage, winds became northwesterly and remained strong for several hours. After 1500 to 1600 PST on 11/26/95, wind speeds rapidly diminished.

Figure 6-1 shows the relationships between hourly PM_{10} concentrations at the Craig/Bemis site and Green Valley site for 11/26/95. The Green Valley site reported the highest 24-hour PM_{10} concentration for 1995, at 366 $\mu g/m^3$. The 24-hour average at the Craig/Bemis site was 219 $\mu g/m^3$. The Green Valley site exhibited three distinct wind speed peaks which corresponded to the hourly PM_{10} peak concentrations. At the Craig/Bemis site, peak PM_{10} concentrations occurred at 1000 and 1200 PST with hourly wind speed over 8 m/s during the same period. Winds at McCarran airport (not shown) stayed high throughout the 0100 to 1600 PST period, and did not decrease in the early morning as they did at the Craig/Bemis site. Thus, even during windy conditions, winds at different locations across the valley can vary considerably. PM_{10} at the Green Valley site was higher than the Craig/Bemis site for a given wind speed. At the Craig/Bemis site, wind speed peaked at 12 m/s with PM_{10} of about 1,000 $\mu g/m^3$ at 1000 PST; at the Green Valley site, wind speed peaked at less than 10 m/s, but PM_{10} reached over 1,400 $\mu g/m^3$. This suggests that a greater fugitive dust source is in the close vicinity of the Green Valley site.

Average and maximum wind speeds at the McCarran Airport and Bemis sites are shown in Figure 6-2 for 01/16/96 and 01/17/96. Similar patterns in hourly wind speed are found at both sites. On 01/16/96, wind speeds were low during the morning, began increasing after 1500 PST, and peaked at 17 m/s with gusts to 22 m/s at 2300 PST. Winds decreased somewhat after 0200 PST on 01/17/96, then increased again to between 10 and 15 m/s later in the morning before gradually tapering off. These winds were in response to a strong surface low that developed rapidly over the central Rocky Mountains on 01/16/96. A strong west to east pressure gradient between the low and high pressure center over the eastern Pacific Ocean caused the high winds. The highest winds were associated with the passage of a cold front of moderate intensity near midnight. A strong west-northwest jet stream was also located over southern Nevada, contributing to the high wind speeds. This period experienced highest hourly wind speed and gust at the McCarran Airport for the study period. Because the high winds spanned portions of two days, multiple exceedances of the PM_{10} standard occurred on both days.

Twenty-four-hour PM_{10} concentrations exceeded 150 $\mu g/m^3$ on six days at the Bemis/Craig site during the 13-month study period. Detailed meteorological analysis on these days is discussed in Section 8.4. Three of these days (i.e., 04/09/95, 06/05/95, and 01/16/96) were on the U.S. EPA compliance monitoring network sampling schedule in which
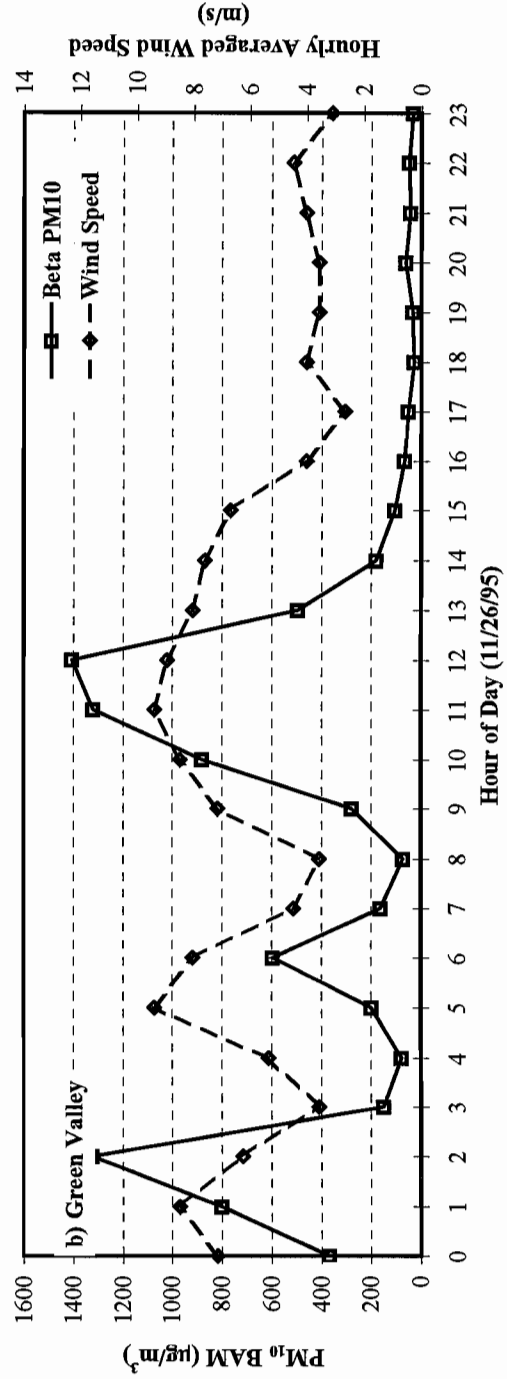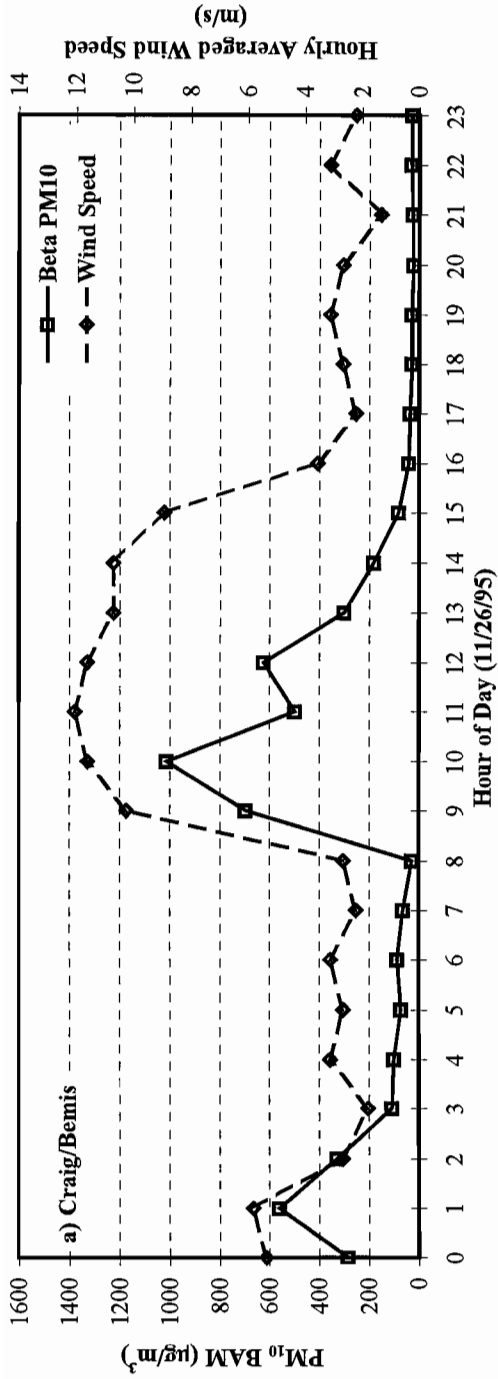
Figure 6-1 Comparison of hourly wind speed and PM$_{10}$ concentrations at: a) Craig/Bemis, and b) Green Valley site on 11/26/95.

6-4
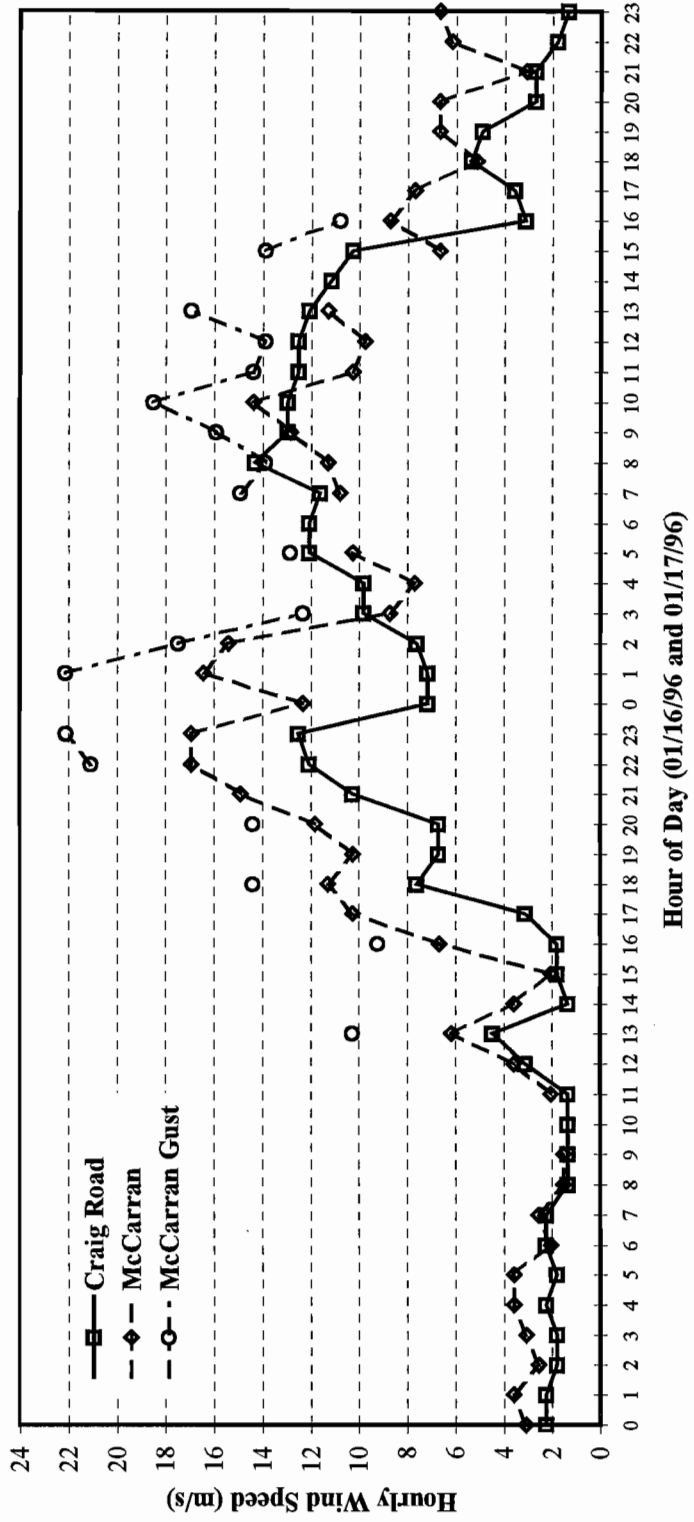
Figure 6-2 Hourly wind speed observed at the McCarran Airport and Craig/Bemis sites on 01/16/96 and 01/17/96.

concurrent PM_{10} measurements were acquired with the BAM and SFS. Even though both the BAM (with a low-volume SA246 inlet) and the SFS (with a medium-volume SA254I inlet) are U.S.-EPA-approved equivalent and reference methods to monitor PM_{10}, respectively, PM_{10} levels acquired by BAM were a factor of two higher on these days. The collocated comparison in Section 5.3 shows that BAM samplers systematically give 30% to 100% higher values than the other samplers for the Craig/Bemis and East Charleston sites. It is suspected that some bias in the calibration of the BAM instruments resulted in these discrepancies.

6.2   Temporal and Spatial Variations of PM_{10} at the Two Base Sites

Table 6-2 summarizes the quarterly and annual averages of PM_{10} mass and b_{abs} concentrations acquired between 01/03/95 and 12/29/95 on the U.S. EPA's every-sixth-day sampling schedule. No 24-hour PM_{10} standard violation was found at the two base sites during the study period. Both quarterly stratified and unstratified annual averages are reported in Table 6-2, and there are few differences between them.

At the Bemis site, quarterly-averaged PM_{10} mass ranks highest (36.6 ± 14.3 $\mu g/m^3$) during the third quarter (July to September) and lowest (23.1 ± 14.1 $\mu g/m^3$) during the second quarter (April to June). The time series plots in Figure 6-3 show insignificant seasonal variations. More pronounced differences were found for the East Charleston site where quarterly-averaged PM_{10} varied by over a factor of two, ranging from 24.4 ± 7.8 $\mu g/m^3$ in the second quarter to 42.4 ± 23.3 $\mu g/m^3$ in the fourth quarter (October to December). It is apparent from the time series plots that PM_{10} concentrations increased during the winter period. In 1995, seasonally-stratified annual averages at the two base sites were well below the annual PM_{10} standard of 50 $\mu g/m^3$, with 28.8 ± 0.5 $\mu g/m^3$ at the Bemis site and 32.4 ± 7.1 $\mu g/m^3$ at the East Charleston site. On an annual basis, PM_{10} mass at the East Charleston site is approximately 13% higher than at the Bemis site.

Even though the two base sites are less than 10 km apart, their PM_{10} and b_{abs} concentrations are not well correlated. The correlation coefficients (r) were 0.56 and 0.27 for the SFS PM_{10} mass and b_{abs} measurements, respectively. As discussed in Section 3.3, the surrounding environments of these two base sites are quite different. Local sources within a few kilometers of one or both of the sampling sites have a major impact on measured PM_{10} and b_{abs} concentrations.

Similar patterns were found in Figure 6-4 for b_{abs} measurements, with more pronounced seasonal variations at the East Charleston site. Analogous to PM_{10}, seasonally stratified annual-average b_{abs} (33.5 ± 9.4 Mm^{-1}) at the East Charleston site is almost twice as high as the Bemis site (17.4 ± 2.5 Mm^{-1}). Impacts from motor vehicle exhaust resulted in consistently higher light absorption concentrations at the East Charleston site.

Table 6-2

Seasonal and Annual Averages of PM_{10} and b_{abs} Concentrations for Samples Acquired between 01/03/95 and 12/29/95

Bemis Site

	Average ± Std. Dev.	Minimum Conc.	Minimum Date	Maximum Conc.	Maximum Date	Total No. in Average
Mass ($\mu g/m^3$)						
First Quarter (January-March 1995)	24.2 ± 14.6	9.4	02/04/95	50.3	02/02/95	14
Second Quarter (April-June 1995)	23.1 ± 14.1	0.0	06/14/95	54.7	04/09/95	14
Third Quarter (July-September 1995)	36.6 ± 14.3	13.8	08/13/95	57.3	07/26/95	16
Fourth Quarter (October-December 1995)	31.4 ± 15.2	7.8	12/24/95	50.5	10/12/95	15
Unstratified Annual Average	29.1 ± 15.2	0.0		57.3		59
Seasonally-Stratified Annual Average	28.8 ± 0.5	0.0		57.3		4
b_{abs} (Mm^{-1})						
First Quarter (January-March 1995)	16.9 ± 10.3	5.7	01/15/95	37.5	01/09/95	14
Second Quarter (April-June 1995)	14.1 ± 5.9	3.5	06/14/95	23.8	05/09/95	14
Third Quarter (July-September 1995)	20.6 ± 6.9	9.2	09/30/95	37.2	07/26/95	16
Fourth Quarter (October-December 1995)	18.1 ± 10.8	1.9	12/17/95	42.3	10/30/95	15
Unstratified Annual Average	17.6 ± 8.8	1.9		42.3		59
Seasonally-Stratified Annual Average	17.4 ± 2.5	1.9		42.3		4

East Charleston Site

	Average ± Std. Dev.	Minimum Conc.	Minimum Date	Maximum Conc.	Maximum Date	Total No. in Average
Mass ($\mu g/m^3$)						
First Quarter (January-March 1995)	29.6 ± 18.4	6.5	02/14/95	69.1	01/09/95	15
Second Quarter (April-June 1995)	24.4 ± 7.8	12.0	04/21/95	36.7	04/27/95	13
Third Quarter (July-September 1995)	33.4 ± 10.6	18.1	07/02/95	53.0	08/01/95	15
Fourth Quarter (October-December 1995)	42.4 ± 23.3	11.2	12/17/95	72.8	10/18/95	7
Unstratified Annual Average	31.2 ± 15.6	6.5		72.8		50
Seasonally-Stratified Annual Average	32.4 ± 7.1	6.5		72.8		4
b_{abs} (Mm^{-1})						
First Quarter (January-March 1995)	40.1 ± 26.9	7.0	02/26/95	90.6	01/09/95	15
Second Quarter (April-June 1995)	23.2 ± 11.4	7.9	04/21/95	47.4	04/03/95	13
Third Quarter (July-September 1995)	30.7 ± 9.4	16.8	06/08/95	46.1	09/12/95	15
Fourth Quarter (October-December 1995)	39.8 ± 26.3	7.9	12/17/95	71.8	10/18/95	7
Unstratified Annual Average	32.8 ± 19.9	7.0		90.6		50
Seasonally-Stratified Annual Average	33.5 ± 9.4	7.0		90.6		4

Figure 6-3 Time series plot of PM_{10} mass concentrations acquired at the Bemis and East Charleston sites between 01/03/95 and 01/28/96.

6-8
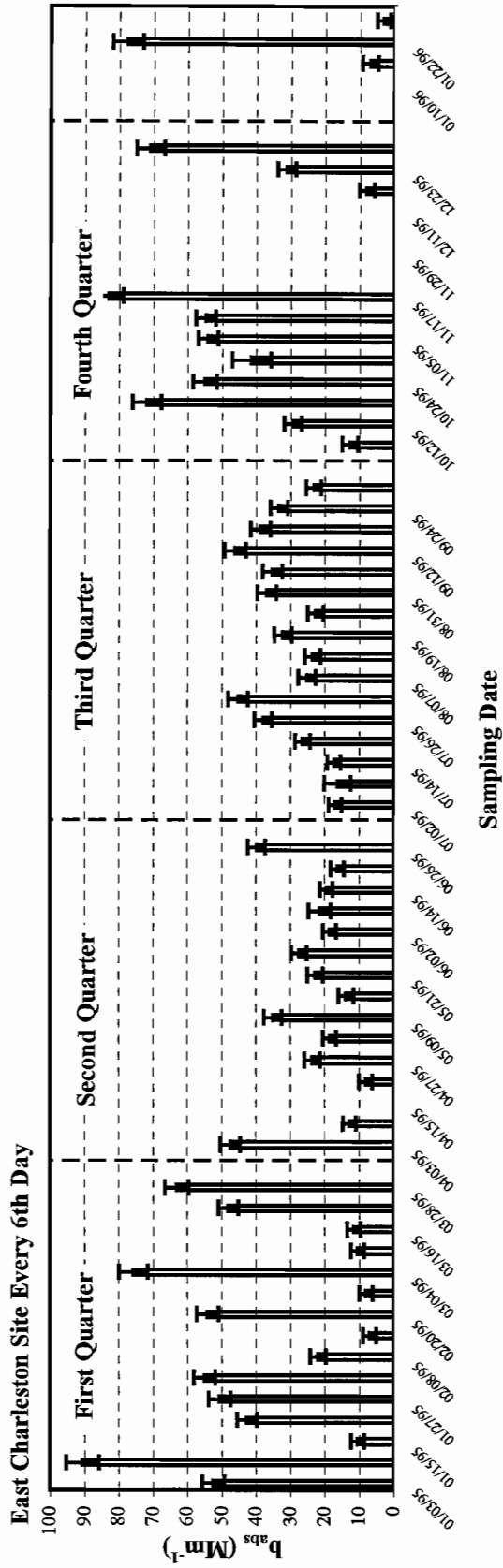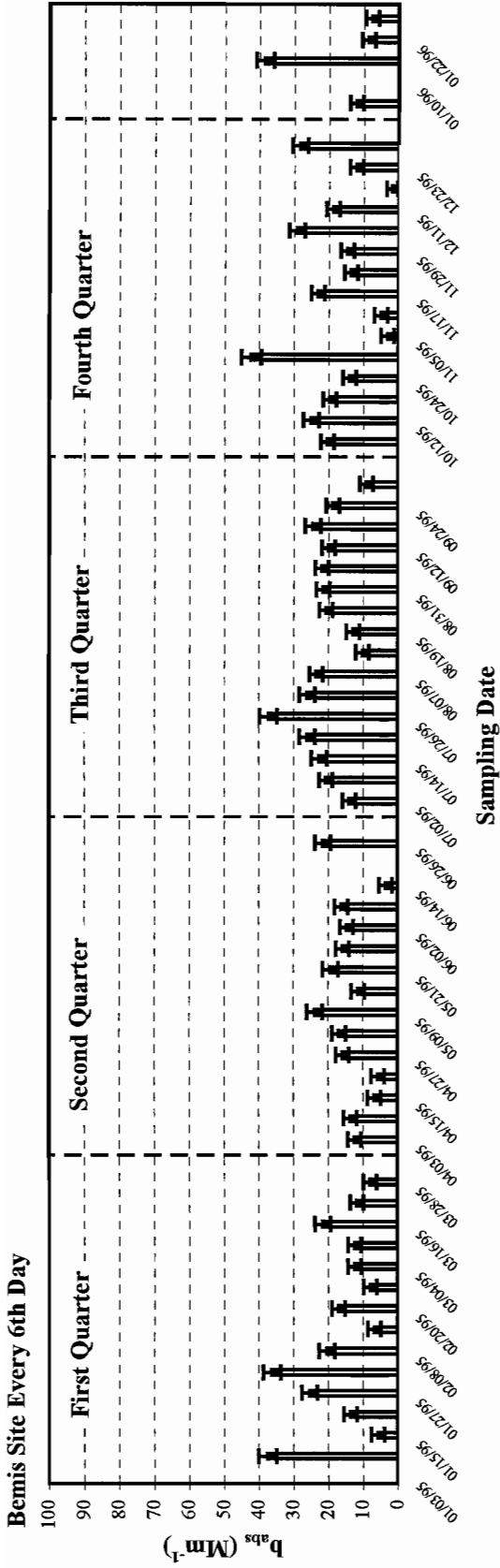
Figure 6-4 Time series plot of b_{abs} measurements acquired at the Bemis and East Charleston sites

A histogram of the PM_{10} concentrations during the mini-intensive monitoring period (12/23/95 to 01/04/96) is presented in Figure 6-5. There is an apparent pollution build-up around the Christmas/holiday season between 12/23/95 and 12/27/95, especially at the East Charleston site. PM_{10} concentrations gradually decreased between 12/28/95 and 01/01/96.

Table 6-3 presents the three highest PM_{10} concentrations observed during the study period. These high concentrations could serve as design values for source identification and control strategy development. Source emissions from the major contributors must be reduced if the Las Vegas Valley is to attain the National Ambient Air Quality Standard (NAAQS) for PM_{10}. It is interesting to note that only on one occasion (i.e., 01/16/96) were concurrent elevated PM_{10} concentrations observed at both sites, with PM_{10} mass being 123.6 ± 6.2 $\mu g/m^3$ at the Bemis site and 123.9 ± 6.2 $\mu g/m^3$ at the East Charleston site. PM_{10} mass varied by a factor of two to four at the two base sites on other elevated PM_{10} days.

High values of light absorption (b_{abs}) measurements are also summarized in Table 6-3 for comparison. Elevated b_{abs} measurements were found after the Christmas holiday at the East Charleston site. This suggests increases in motor vehicle exhaust, restaurant emissions, and/or residential wood combustion during this period. Table 6-3 also shows that the three highest b_{abs} values at the East Charleston site are 3 to 7 times higher than the concurrent measurements at the Bemis site. Local source emissions impacted the East Charleston site and resulted in high b_{abs} values.

For the five forecasted intensive monitoring periods, temporal variations of PM_{10} mass concentrations acquired with SFSs are illustrated in Figure 6-6. PM_{10} concentrations were low during the two spring intensive monitoring periods. These concentrations gradually increased during the other intensive periods. The highest PM_{10} concentrations were 70.5 ± 3.6 $\mu g/m^3$ at the Bemis site on 06/05/95, and 48.7 ± 2.5 $\mu g/m^3$ and 48.8 ± 2.5 $\mu g/m^3$ at the East Charleston site on 09/12/95 and 01/27/96, respectively.

6.3   Sample Selection for Chemical Analysis

PM_{10} mass concentrations were measured on all valid samples taken at each site. A total of 59 sets of every-sixth-day samples, 26 sets of intensive samples, and 13 sets of mini-intensive samples were examined. The sample selection process for the nonintensive (i.e., every-sixth-day and mini-intensive) monitoring periods consisted of the following criteria:

- The sampling day with the highest PM_{10} concentration at the Bemis and East Charleston sites (i.e., 01/16/96);

- The sampling day with highest gust wind or on a windy day (i.e., 04/09/95);
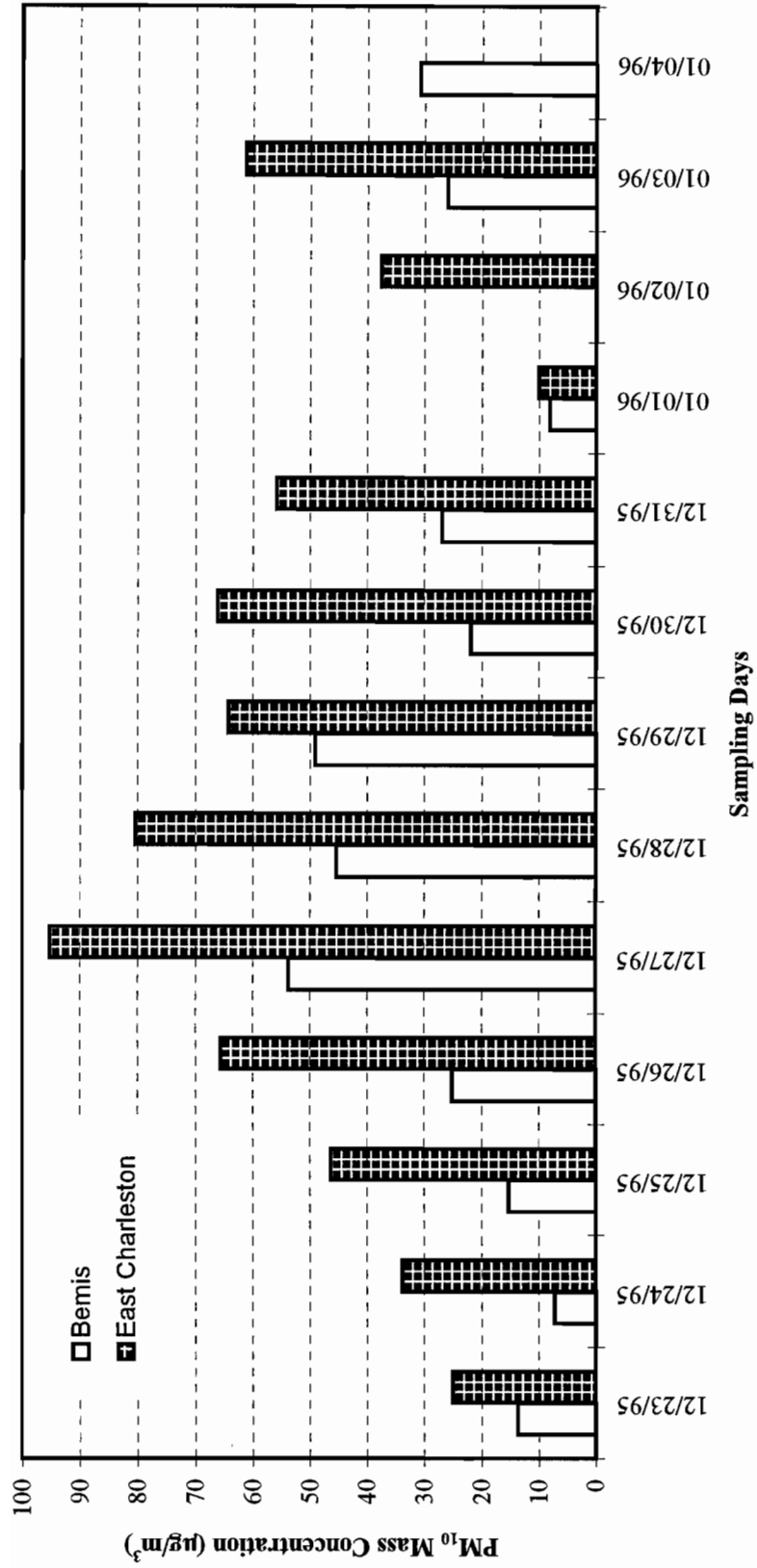
Figure 6-5 Histogram of PM_{10} mass concentrations acquired at the Bemis and East Charleston sites during the mini-intensive monitoring period between 12/23/95 and 01/04/96.

Table 6-3
Elevated PM_{10} and b_{abs} Concentrations at the Two Base Sites
between 01/03/95 and 01/28/96

Date	Bemis Site Mass ($\mu g/m^3$)	East Charleston Site Mass ($\mu g/m^3$)
I. Three Highest PM_{10} Measurements at the Bemis Site		
01/16/96	123.6 ± 6.2	123.9 ± 6.2
06/05/95	70.5 ± 3.6	37.7 ± 1.9[a]
07/26/95	57.3 ± 2.9	37.8 ± 1.9
II. Three Highest PM_{10} Measurements at the East Charleston Site[b]		
01/16/96	123.6 ± 6.2	123.9 ± 6.2
11/23/95	27.0 ± 1.4	119.1 ± 6.6
12/27/95	53.7 ± 2.7	95.3 ± 4.8

Date	Bemis Site b_{abs} (Mm^{-1})	East Charleston Site b_{abs} (Mm^{-1})
III. Three Highest b_{abs} Measurements at the Bemis Site		
10/30/95	42.3 ± 2.9	41.3 ± 5.7
01/16/96	38.5 ± 2.5	7.0 ± 2.2
01/09/96	37.5 ± 2.5	90.6 ± 4.8
IV. Three Highest b_{abs} Measurements at the East Charleston Site		
12/27/95	25.4 ± 2.2	117.9 ± 6.4
12/28/95	30.5 ± 2.2	95.3 ± 5.1
12/26/95	13.3 ± 1.9	94.1 ± 5.1

[a] Sampling duration beyond 24 ± 4.8 hours and excluded from the average value calculations.
[b] Short sampling duration was found for the 11/23/95 samples at the East Charleston site. The elevated PM_{10} concentration (119.1 ± 6.6 $\mu g/m^3$) was excluded from further data analysis.
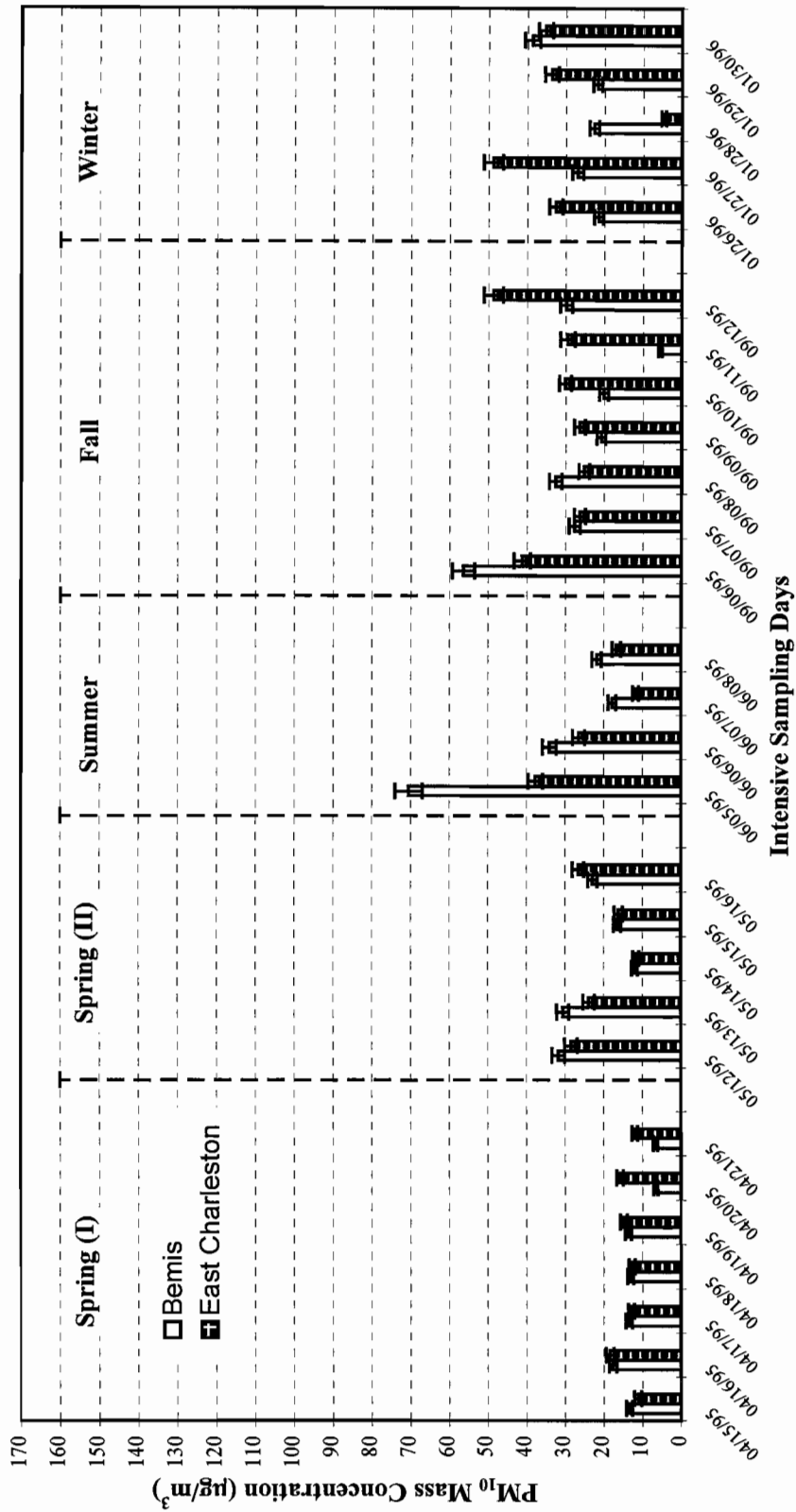
Figure 6-6 Histogram of PM$_{10}$ mass concentrations acquired at the Bemis and East Charleston sites during the five intensive monitoring periods between 04/15/95 and 01/30/96.

- An every-sixth-day sampling day corresponding with an exceedance day observed in the CCHD monitoring network (i.e., 04/27/95);

- A sampling day representing fall stagnation conditions (i.e., 11/23/95); and

- Sampling days representing winter stagnation and cold front passing through (i.e., 12/24/95 to 01/02/96).

For the intensive monitoring periods, the sample selection process consisted of the following criteria:

- A monitoring period experiencing high wind events (i.e., 06/05/95 to 06/07/95);

- A monitoring period representing typical late-summer meteorological conditions in the Las Vegas Valley (i.e., 09/07/95 to 09/12/95); and

- A monitoring period representing typical winter conditions (i.e., 01/26/96 to 01/30/96).

As a result, a total of 14 days were selected from the nonintensive monitoring periods to represent all days with high concentrations at any site, and another 14 days were selected from the intensive monitoring periods to represent a mixture of meteorological conditions. The following subsection focuses on the discussion of PM_{10} mass and chemical characteristics acquired by the SFSs. Statistics from the portable PM_{10} survey samples during the intensive monitoring periods are also summarized for comparison.

6.4   Characteristics of PM_{10} Chemical Composition at the Two Base Sites

Table 6-4 presents averages, standard deviations, as well as minimum and maximum PM_{10} concentrations for the 14 sets of SFS samples selected for chemical speciation during the non-intensive (i.e., every-sixth-day and mini-intensive) monitoring periods, and the 14 sets of samples from the intensive (summer, fall and winter) monitoring periods. Statistical summaries for each site as well as the average of both sites are presented for comparison.

Thirteen-month average PM_{10} mass was 28.4 ± 17.8 $\mu g/m^3$ at the Bemis site and 33.0 ± 21.0 $\mu g/m^3$ at the East Charleston site, with a two-site average of 30.7 ± 19.5 $\mu g/m^3$. The large standard deviations associated with the averages suggest that a wide range of PM_{10} concentrations were observed. Since the selected subset of samples were intended to represent days with high PM_{10} concentrations, their average values are expected to be higher than the average for the entire data set. As shown in Table 6-4, average PM_{10} concentrations on these 28 days are 22% and 34% higher than the corresponding overall averages obtained at the Bemis and East Charleston sites, respectively.

Table 6-4

Statistical Summary of PM_{10} Mass and Chemical Compositions ($\mu g/m^3$) Acquired at the Two Base Sites during Intensive and Non-Intensive Monitoring Periods between 01/03/95 and 01/28/96[a]

Species	Average of the Two Base Sites					Bemis Site					East Charleston Site				
	Average	Std. Dev.	No. in Average	Minimum	Maximum	Average	Std. Dev.	No. in Average	Minimum	Maximum	Average	Std. Dev.	No. in Average	Minimum	Maximum
PM_{10} Mass (97 days)[b]	30.66	19.48	172	0	123.89	28.35	17.89	92	0.00	123.55	33.31	20.97	80	4.71	123.89
PM_{10} Mass (28 days)[c]	39.76	25.04	51	7.15	123.89	34.59	23.85	25	7.15	123.55	44.73	25.60	26	10.00	123.89
b_{abs} (Mm^{-1}) (97 days)[d]	24.41	20.16	173	0	117.91	15.93	8.72	93	0.00	42.27	34.26	24.77	80	3.18	117.91
b_{abs} (Mm^{-1}) (28 days)[d]	28.55	25.56	52	3.81	117.91	14.78	8.63	26	3.81	38.46	42.32	29.39	26	7.31	117.91
Chloride (Cl⁻)	0.16	0.11	53	0.026	0.51	0.12	0.106	26	0.03	0.51	0.21	0.11	27	0.077	0.51
Nonvolatilized Nitrate (NO_3^-)	0.80	0.82	53	0.054	3.52	0.61	0.57	26	0.05	2.31	1.00	0.97	27	0.092	3.52
Volatilized Nitrate (NO_3^-)	0.41	0.41	39	0	1.78	0.25	0.20	19	0.00	0.83	0.55	0.50	20	0.005	1.78
Sulfate ($SO_4^=$)	1.35	0.79	53	0.16	4.49	1.04	0.60	26	0.16	2.48	1.64	0.84	27	0.39	4.49
Ammonium (NH_4^+)	0.25	0.19	53	0.0071	0.74	0.21	0.15	26	0.02	0.53	0.28	0.22	27	0.0071	0.74
Soluble Potassium (K⁺)	0.10	0.08	53	0.024	0.32	0.063	0.039	26	0.02	0.17	0.14	0.09	27	0.031	0.32
Organic Carbon (OC)	5.55	4.34	53	0.84	18.20	3.64	3.03	26	0.84	16.34	7.40	4.65	27	1.49	18.20
Elemental Carbon (EC)	2.68	2.65	53	0.25	11.51	1.50	0.99	26	0.25	4.08	3.82	3.22	27	0.40	11.51
Total Carbon (TC)	8.22	6.76	53	1.25	28.79	5.12	3.53	26	1.25	18.85	11.20	7.78	27	1.89	28.79
Sodium (Na)	0.039	0.059	52	0	0.26	0.014	0.033	26	0.00	0.12	0.064	0.068	26	0	0.26
Magnesium (Mg)	0.73	0.52	52	0.094	3.16	0.71	0.61	26	0.09	3.16	0.74	0.42	26	0.18	2.06
Aluminum (Al)	1.16	0.77	52	0.20	3.81	1.07	0.86	26	0.20	3.76	1.26	0.69	26	0.27	3.81
Silicon (Si)	4.81	3.07	52	0.61	16.64	4.44	3.43	26	0.61	16.64	5.19	2.68	26	1.15	14.87
Phosphorus (P)	0.014	0.014	52	0	0.055	0.007	0.011	26	0.00	0.053	0.021	0.014	26	0.06	0.055
Sulfur (S)	0.43	0.23	52	0.032	1.02	0.32	0.17	26	0.03	0.77	0.55	0.22	26	0.06	1.02
Chlorine (Cl)	0.14	0.12	52	0	0.52	0.070	0.084	26	0.00	0.40	0.21	0.12	26	0.037	0.52
Potassium (K)	0.46	0.30	52	0.065	1.48	0.38	0.31	26	0.06	1.48	0.55	0.27	26	0.12	1.38
Calcium (Ca)	6.24	4.37	52	0.83	27.43	6.30	5.10	26	0.83	27.43	6.18	3.61	26	1.29	17.94
Titanium (Ti)	0.049	0.036	52	0	0.18	0.044	0.037	26	0.00	0.18	0.054	0.035	26	0.0008	0.18
Vanadium (V)	0.0016	0.0021	52	0	0.008	0.0019	0.0021	26	0.00	0.0075	0.0012	0.0021	26	0	0.008
Chromium (Cr)	0.0048	0.0074	52	0	0.031	0.0082	0.0092	26	0.00	0.031	0.0014	0.0014	26	0	0.0056
Manganese (Mn)	0.016	0.010	52	0.0023	0.051	0.015	0.011	26	0.00	0.051	0.017	0.009	26	0.0024	0.047
Iron (Fe)	0.77	0.49	52	0.11	2.37	0.60	0.44	26	0.11	2.20	0.94	0.50	26	0.16	2.37
Cobalt (Co)	0	0	52	0	0	0	0	26	0	0	0	0	26	0	0
Nickel (Ni)	0.0030	0.0049	52	0	0.020	0.0053	0.0062	26	0	0.020	0.00070	0.00054	26	0	0.0021
Copper (Cu)	0.010	0.007	52	0.0015	0.032	0.0065	0.0044	26	0.0015	0.017	0.013	0.008	26	0.0024	0.032
Zinc (Zn)	0.028	0.019	52	0.0044	0.08	0.021	0.014	26	0.0044	0.056	0.035	0.021	26	0.0048	0.08
Gallium (Ga)	0.00023	0.00032	52	0	0.0011	0.00022	0.00027	26	0	0.0011	0.00025	0.0004	26	0	0.0011
Arsenic (As)	0.0008	0.0008	52	0	0.0035	0.00055	0.00046	26	0	0.0018	0.0011	0.0010	26	0	0.0035
Selenium (Se)	0.00020	0.00023	52	0	0.0008	0.00015	0.00021	26	0	0.0008	0.00025	0.00025	26	0	0.0008
Bromine (Br)	0.0033	0.0019	52	0.0002	0.009	0.0024	0.0012	26	0.0002	0.0052	0.0043	0.0020	26	0.0002	0.009
Rubidium (Rb)	0.0016	0.0013	52	0	0.0066	0.0014	0.0014	26	0	0.0066	0.0018	0.0011	26	0.0001	0.0056

Table 6-4 (continued)

Statistical Summary of PM$_{10}$ Mass and Chemical Compositions ($\mu g/m^3$) Acquired at the Two Base Sites during Intensive and Non-Intensive Monitoring Periods between 01/03/95 and 01/28/96[a]

Species	Average of the Two Base Sites					Bemis Site					East Charleston Site				
	Average	Std. Dev.	No. in Average	Minimum	Maximum	Average	Std. Dev.	No. in Average	Minimum	Maximum	Average	Std. Dev.	No. in Average	Minimum	Maximum
Strontium (Sr)	0.027	0.021	52	0.0026	0.13	0.028	0.026	26	0.0026	0.13	0.027	0.015	26	0.006	0.080
Yttrium (Y)	0.00054	0.00050	52	0	0.0026	0.00052	0.00049	26	0	0.0026	0.00057	0.00052	26	0.0000	0.0025
Zirconium (Zr)	0.0023	0.0016	52	0.0003	0.0087	0.0020	0.0017	26	0.0005	0.0087	0.0027	0.0014	26	0.0003	0.0067
Molybdenum (Mo)	0.0016	0.0029	52	0	0.015	0.0022	0.0039	26	0	0.015	0.0009	0.0008	26	0	0.0027
Palladium (Pd)	0.00024	0.00060	52	0	0.0026	0.00025	0.00060	26	0	0.0026	0.00023	0.00060	26	0	0.0023
Silver (Ag)	0.0019	0.0022	52	0	0.007	0.0017	0.0021	26	0	0.0061	0.0021	0.0024	26	0	0.007
Cadmium (Cd)	0.0017	0.0020	52	0	0.0079	0.0017	0.0019	26	0	0.0079	0.0016	0.0020	26	0	0.0076
Indium (In)	0.00128	0.0028	52	0	0.0166	0.00083	0.0016	26	0	0.006	0.00173	0.0036	26	0	0.0166
Tin (Sn)	0.0021	0.0028	52	0	0.013	0.0014	0.0018	26	0	0.0059	0.0027	0.0034	26	0	0.013
Antimony (Sb)	0.0023	0.0038	52	0	0.014	0.0018	0.0031	26	0	0.013	0.0027	0.0044	26	0	0.014
Barium (Ba)	0.039	0.035	52	0	0.13	0.021	0.017	26	0	0.058	0.056	0.039	26	0	0.13
Lanthanum (La)	0.015	0.016	52	0	0.061	0.0070	0.0086	26	0	0.030	0.022	0.018	26	0	0.061
Gold (Au)	0.00039	0.00051	52	0	0.0022	0.00037	0.00049	26	0	0.0018	0.00040	0.00054	26	0	0.0022
Mercury (Hg)	0.00031	0.00042	52	0	0.0019	0.00025	0.00031	26	0	0.0011	0.00038	0.00049	26	0	0.0019
Thallium (Tl)	0.00044	0.00049	52	0	0.0020	0.00041	0.00040	26	0	0.0016	0.00048	0.00056	26	0	0.0020
Lead (Pb)	0.0075	0.0060	52	0	0.026	0.0045	0.0034	26	0	0.013	0.010	0.0066	26	0.0023	0.026
Uranium (U)	0.00021	0.00027	52	0	0.00090	0.00022	0.00028	26	0	0.0009	0.00020	0.00026	26	0	0.0009

[a] Acquired with sequential filter samplers (SFS).
[b] Entire data set including every-sixth-day, mini-intensive, and intensive monitoring periods.
[c] The 14 days are 04/09/95, 04/27/95, 11/23/95, 12/24/95 to 01/02/96, and 01/16/96.
[d] Concentration in Mm^{-1}.

6-16

The most abundant (> 1 $\mu g/m^3$) species were found to be ions (e.g., NO_3^-, $SO_4^=$), carbon (OC, EC), and soil-related crustal species (e.g., Al, Si, Ca). Relative proportions of soil-related species were similar at the two base sites. The sums of these soil-related crustal species (e.g., Al, Si, K, Ca, Ti, Fe, Zn) were approximately 37% and 32% of the average PM_{10} mass concentrations at the Bemis and East Charleston sites, respectively, though their absolute concentrations were about 10% higher at the East Charleston site than at the Bemis site. Average PM_{10} silicon concentrations varied from 4.4 ± 3.4 $\mu g/m^3$ at the Bemis site, to 5.2 ± 2.7 $\mu g/m^3$ at the East Charleston site. The highest observed PM_{10} silicon concentrations were found on 01/16/96 with 16.6 ± 5.3 $\mu g/m^3$ (13% of PM_{10} mass) at the Bemis site, and 14.9 ± 4.7 $\mu g/m^3$ (12% of PM_{10} mass) at the East Charleston site. PM_{10} calcium concentrations were also high, averaging 6.3 ± 5.1 $\mu g/m^3$ at the Bemis site and 6.2 ± 3.6 $\mu g/m^3$ at the East Charleston site. The highest PM_{10} calcium concentrations were also found on 01/16/96, with 27.4 ± 4.6 $\mu g/m^3$ (22% of PM_{10} mass) at the Bemis site and 17.9 ± 3.0 $\mu g/m^3$ (15% of PM_{10} mass) at the East Charleston site.

While PM_{10} silicon concentrations were comparable to or higher than those observed in other urban areas (e.g., Chow *et al.*, 1992a, 1992b, 1993a), PM_{10} calcium concentrations are a factor of two to three higher than those observed in the Imperial Valley, CA (Chow and Watson, 1997b) and Tucson, AZ (Chow *et al.*, 1992c), and a factor of seven to eight higher than those observed in the San Joaquin Valley, CA (Chow *et al.*, 1992a, 1993a). Elevated calcium concentrations were found at Rubidoux, CA, during the Southern California Air Quality Study, with an average of 12 $\mu g/m^3$ in the fall and 3 $\mu g/m^3$ in the summer (Chow *et al.*, 1994c). Annual PM_{10} calcium in the Rubidoux/Riverside area ranged from 2 to 6 $\mu g/m^3$ (Chow *et al.*, 1992b). These PM_{10} calcium concentrations in Rubidoux, CA, are similar in magnitude to the 6 or 7 $\mu g/m^3$ found in the Las Vegas Valley. The gypsum mine in the southwestern part of the Valley, along with frequent construction activities in Las Vegas, and widespread alkaline soils may have contributed to these elevated calcium concentrations.

Concentrations of motor-vehicle-exhaust-related species, such as PM_{10} bromine (Br) and lead (Pb), were also a factor of two to four higher at the East Charleston site than those found at the Bemis site. Similar to elevated b_{abs} concentrations, impact from motor vehicle exhaust are much greater at the East Charleston site than at the Bemis site. Average PM_{10} Pb concentrations were 0.0045 ± 0.003 $\mu g/m^3$ at the Bemis site and 0.010 ± 0.007 $\mu g/m^3$ at the East Charleston site. PM_{10} Pb concentrations are not expected to be high since leaded gasoline was phased out of the U.S. market during the late 1980s, and no other lead sources were recorded in the current Clark County emissions inventory.

Concentrations of residential-oil-combustion-related species, such as PM_{10} vanadium (V) and nickel (Ni), were low with an average of 0.002 ± 0.002 $\mu g/m^3$ of PM_{10} for V and 0.003 ± 0.005 $\mu g/m^3$ for Ni. These PM_{10} concentrations were detected on 4% and 39% of the

samples for V and Ni, respectively, as shown in Table 5-6. These low concentrations reflect an absence or insignificant level of residential oil combustion in the study area.

Besides the Ni, V, and Pb levels, the average and maximum concentrations of several potentially-toxic species such as manganese (Mn), copper (Cu), zinc (Zn), arsenic (As), selenium (Se), strontium (Sr), barium (Ba), and mercury (Hg) noted in Table 6-4 were typically at or below their respective minimum detection limits stated in Table 5-6.

Besides the 1.5 $\mu g/m^3$ quarterly average standard for lead (in TSP, not in PM_{10}), air quality standards have not been set for the other metals. However, concentrations of these toxic elements have often been considered in analyses of cancer risk. Since the maximum concentrations for these metals shown in Table 6-4 are very low, the risk from exposure to these concentrations is probably minimal.

With regard to secondary aerosol, NO_3^-, $SO_4^=$, and NH_4^+ that were formed from gaseous precursors such as nitrogen oxides, sulfur dioxide, and ammonia, respectively, accounted for 5% to 7% of the average PM_{10} mass at the two base sites. The absolute difference in average ion concentrations between the two sites was more pronounced than in soil-related species, typically a factor of two higher at the East Charleston site. Ammonium concentrations are low as compared to the stoichiometric ratios of ammonium sulfate and ammonium nitrate. Since Section 5.5 shows that approximately 65% of the measured anions cannot be explained by the measured cations in this study on a molar-to-molar basis, it is assumed that some form of ammonium bisulfate, calcium sulfate, or calcium nitrate may be present in the valley at detectable levels.

The greatest differences were found in average PM_{10} OC concentrations, which varied from 3.6 ± 3.0 $\mu g/m^3$ at the Bemis site to 7.4 ± 4.7 $\mu g/m^3$ at the East Charleston site, and accounted for 11% and 17% of the average PM_{10} mass, respectively. The large standard deviations associated with these averages indicate that high OC concentrations only occurred on a few days and the averages were positively biased. Examination of the data base shows that elevated OC concentrations (i.e., exceeding 50% of the average) were found on 04/09/95 and 01/16/96 at the Bemis site, and on 12/27/95 and 01/16/96 at the East Charleston site. The highest PM_{10} OC concentrations were both found on 01/16/96 with 16.3 ± 1.0 $\mu g/m^3$ (13% of PM_{10} mass) at the Bemis site and 18.2 ± 1.1 $\mu g/m^3$ (15% of PM_{10} mass) at the East Charleston site. The average ratios of organic to total carbon (TC = OC + EC) were similar, however, with 0.71 at the Bemis site and 0.66 at the East Charleston site.

Elemental carbon concentrations also varied by a factor of three, averaging 1.5 ± 1.0 $\mu g/m^3$ at the Bemis site and 4.5 ± 4.9 $\mu g/m^3$ at the East Charleston site. Elevated PM_{10} EC concentrations (i.e., exceeding 50% of the average) were found on 12/27/95 to 12/29/95 at the Bemis site, and on 11/23/95, 12/27/95, and 12/28/95 at the East Charleston site. All of

these days occurred during fall or winter stagnation periods when transport was expected to be minimal.

PM$_{10}$ Cl$^-$ and K$^+$ concentrations were well below 1 μg/m^3, typically in the range of 0.05 to 0.2 μg/m^3. As discussed in Section 4, residential wood combustion or other vegetative burning could potentially be the sources of these species in the study area.

6.5   Temporal and Spatial Variations of PM$_{10}$ at the Satellite Sites

PM$_{10}$ mass and chemical concentration data, acquired at 30 satellite sites during the spring, summer, fall, and winter intensive monitoring periods over a small geographical area, was examined to estimate the zones of influence of pollution sources. Figure 2-2 displays the sampling locations for the two base and 30 satellite sites. The saturation monitoring network was designed to:

- Examine the spatial variations of PM$_{10}$ concentrations within the study domain (12 km east-west × 13 km north-south);

- Identify potential pollutant transport following the prevailing wind direction;

- Determine the zones of influence of specific fugitive dust emitters on PM$_{10}$ loadings in a mixed-land-use area; and

- Evaluate the representativeness of a single site measurement.

Section 3.3 classified the satellite monitoring sites based on the primary land uses in the close vicinity of each site. As a result, the saturation monitoring network was divided into five site types. The sampling locations within each site type were arranged, to the extent possible, in sequence from north to south and from west to east. Table 6-5 summarizes the site-type classifications. The collocated measurements at the ABEM (i.e., Bemis) site were excluded from the following analysis to avoid double-counting in average calculations. Consequently, the saturation monitoring network includes three industrial sites (mainly sand/gravel operations), ten active/inactive construction sites, five commercial sites, three residential sites, and eight disturbed/undisturbed vacant land sites.

6.5.1   Temporal Variations of PM$_{10}$ Mass at the Satellite Sites

Average PM$_{10}$ mass for each of the satellite sites for the entire sampling period as well as for each intensive monitoring period is summarized in Table 6-6. Over 80% of the highest PM$_{10}$ concentrations were found during the fall intensive monitoring period, with average PM$_{10}$ concentrations being 40% to 60% above their site averages. Average PM$_{10}$ concentrations are lowest during the first spring intensive monitoring period, which are often

Table 6-5
Classification of the Saturation Monitoring Network

Dominant Source Type	Number of Sites	Inclusive Satellite Sites
Industrial (sand/gravel operation)	3	LAMB LONE NWAL
Active/Inactive Construction	10	GOLF LONM DONO NECD CINN NCOV MARK GROW CLIF PECO
Commercial	5	BEMI[b] WALN MICH MCDA ECHA
Residential	3	EFER NOCO HAMI
Disturbed/Undisturbed Vacant Land/Desert Surface	8	LOSS BILL VAND SWLC NWCP CRAI THUN LASV

[a] See Figure 2-2 for site locations and Table 2-3 for site descriptions.

[b] BEMI and ABEI are collocated satellite sites. Only BEMI site is used in the data analysis.

Table 6-6

Average PM$_{10}$ Mass Concentrations (μg/m³) for Five Intensive Periods in the Saturation Monitoring Network

Site Type	Site	Total Average	StdDev	No.	Spring (first intensive) Average	StdDev	No.	Spring (second intensive) Average	StdDev	No.	Summer Average	StdDev	No.	Fall Average	StdDev	No.	Winter Average	StdDev	No.
Industrial	LAMB	36.94	± 21.63	26	18.41	± 3.94	7	32.16	± 24.23	5	37.60	± 7.23	3	55.58	± 20.78	6	44.91	± 22.75	5
	LONE	33.74	± 18.87	25	18.88	± 6.21	7	29.73	± 24.75	5	48.82	± 6.31	2	51.24	± 17.19	6	31.50	± 9.99	5
	NWAL	47.41	± 28.87	26	26.99	± 15.98	7	35.53	± 14.12	5	53.89	± 54.13	3	68.56	± 28.44	6	58.61	± 19.61	5
Construction	GOLF	23.88	± 18.57	25	9.70	± 5.53	7	18.98	± 3.18	4	40.70	± 37.25	3	41.58	± 11.27	6	16.34	± 5.77	5
	LONM	52.18	± 33.86	26	23.45	± 8.37	7	24.46	± 11.08	5	41.75	± 18.83	3	75.48	± 19.15	6	98.44	± 18.01	5
	DONO	35.68	± 38.48	26	15.38	± 4.65	7	21.09	± 12.40	5	108.64	± 86.67	3	42.62	± 9.92	6	26.57	± 5.72	5
	NECD	29.82	± 16.96	26	13.59	± 5.75	7	35.82	± 21.65	5	47.06	± 26.53	3	34.32	± 4.94	6	30.80	± 11.67	5
	CINN	26.05	± 14.51	26	23.59	± 20.44	7	29.19	± 19.17	5	20.51	± 12.90	3	29.56	± 6.95	6	25.47	± 10.61	5
	NCOV	31.97	± 27.71	26	10.50	± 3.52	7	16.85	± 7.62	5	29.57	± 20.01	3	66.57	± 35.23	6	37.07	± 6.70	5
	MARK	25.00	± 13.11	25	20.72	± 11.47	6	18.26	± 17.50	5	23.69	± 15.52	3	32.96	± 5.51	6	28.10	± 14.50	5
	GROW	27.26	± 13.40	25	21.20	± 14.20	6	17.94	± 7.75	5	31.12	± 23.38	3	36.01	± 8.83	6	31.02	± 9.35	5
	CLIF	31.85	± 20.73	26	18.62	± 12.95	7	33.09	± 27.28	5	39.94	± 39.64	3	44.83	± 11.76	6	28.72	± 10.47	5
	PECO	28.11	± 18.33	26	10.64	± 1.30	7	17.83	± 10.16	5	26.98	± 14.60	3	46.80	± 17.88	6	41.09	± 9.25	5
Commercial	BEMI	22.67	± 11.58	26	11.01	± 4.38	7	19.58	± 9.59	5	30.05	± 18.52	3	33.51	± 4.65	6	24.66	± 6.83	5
	WALN	24.29	± 12.27	26	16.29	± 8.45	7	17.77	± 6.78	5	30.09	± 24.06	3	32.24	± 5.39	6	28.98	± 12.22	5
	MICH	29.92	± 14.82	26	16.84	± 4.85	7	27.33	± 17.73	5	45.38	± 20.87	3	36.76	± 7.53	6	33.35	± 12.72	5
	MCDA	23.64	± 12.65	26	11.46	± 2.84	7	15.61	± 5.11	5	25.57	± 17.95	3	36.24	± 9.15	6	32.49	± 4.07	5
	ECHA	23.01	± 17.97	25	10.65	± 2.82	7	15.13	± 6.90	5	23.28	± 15.34	3	34.29	± 11.37	6	37.35	± 33.80	4
Residential	EFER	20.20	± 9.77	26	10.90	± 3.27	7	16.55	± 7.57	5	28.20	± 15.03	3	28.55	± 4.91	6	22.02	± 7.45	5
	NOCO	23.57	± 12.35	26	11.32	± 3.40	7	18.12	± 8.24	5	22.94	± 14.55	3	37.90	± 7.10	6	29.34	± 6.98	5
	HAMI	26.64	± 12.67	26	11.41	± 3.41	7	23.46	± 9.45	5	31.20	± 13.65	3	34.19	± 6.29	6	39.33	± 5.76	5
Vacant Land	LOSS	29.78	± 21.50	26	17.91	± 12.52	7	20.40	± 8.30	5	40.52	± 25.08	3	52.93	± 26.81	6	21.56	± 6.43	5
	BILL	20.62	± 10.37	26	10.79	± 2.28	7	16.49	± 6.81	5	21.97	± 12.01	3	32.66	± 9.03	6	23.25	± 5.06	5
	VAND	21.87	± 12.15	25	10.04	± 2.63	7	16.27	± 9.45	4	29.08	± 10.92	3	31.03	± 9.58	6	27.59	± 12.34	5
	SWLC	19.06	± 9.10	26	11.98	± 4.21	7	15.41	± 7.32	5	22.54	± 12.76	3	24.75	± 10.98	6	23.70	± 4.01	5
	NWCP	19.38	± 9.87	26	11.53	± 1.94	7	15.01	± 4.82	5	25.64	± 22.54	3	27.45	± 6.17	6	21.27	± 3.94	5
	CRAI	28.08	± 15.38	26	13.93	± 2.89	7	25.40	± 19.74	5	36.87	± 18.26	3	40.49	± 9.28	6	30.41	± 12.08	5
	THUN	21.36	± 12.34	26	10.64	± 3.18	7	16.63	± 9.14	5	32.35	± 26.49	3	30.42	± 4.77	6	23.63	± 4.92	5
	LASV	23.53	± 13.11	26	9.77	± 2.65	7	16.84	± 5.97	5	26.87	± 18.67	3	34.00	± 7.89	6	34.94	± 7.33	5

6-21

40% to 50% below their corresponding site averages. Meteorological conditions for each of the five intensive monitoring periods are characterized in Section 8.5.

Temporal variations of 24-hour PM_{10} mass during the five intensive monitoring periods are shown in Figure 6-7. Peak concentrations were observed on 06/05/95, 09/11/95, and 09/12/95. Daily average PM_{10} concentrations varied by a factor of five, ranging from 9.6 ± 3.9 $\mu g/m^3$ on 05/14/95 to 52.8 ± 19.1 $\mu g/m^3$ on 06/05/95, whereas daily maximum concentrations varied by a factor of ten, ranging from 21.3 ± 3.5 $\mu g/m^3$ on 04/18/95 at the NWAL industrial site to 208.4 ± 11.7 $\mu g/m^3$ on 06/06/95 at the DONO construction site.

As shown in Figure 6-7, peak concentrations occurred 14 times at the construction sites (especially at the LONM site), 10 times at the industrial sites (especially at the NWAL site), and twice at the disturbed vacant land sites (i.e., LOSS). This illustration demonstrates that no peak concentrations were found at the residential or commercial sites where the general population resides.

Daily PM_{10} concentrations at the Bemis base site are superimposed on Figure 6-7 for comparison. The concentrations at the Bemis site (a commercial site close to a mixture of industrial operations, construction activities, and vacant land) are approximately 10% to 20% below the daily averages, but closely coincided with the pattern of daily averages.

Temporal variations of average PM_{10} concentrations by site type are presented in Figure 6-8. Industrial and construction sites tend to deviate from the general pattern with elevated PM_{10} concentrations, while the commercial, residential, and vacant land sites overlapped one another within one standard deviation of the average. This analysis shows that meteorology is the major driving force for the temporal variations of commercial, residential, and vacant land sites. Temporal variations of industrial and construction sites are dominated by local fugitive dust sources, irrespective of changes in daily meteorology.

Time series plots of PM_{10} concentrations, grouped by site type (i.e., industrial, construction, commercial, residential, vacant land) are presented in Figures 6-9a to 6-13a. With the exception of a few industrial and construction sites, the peaks and valleys of PM_{10} concentrations tend to coincide with each other. These plots show that, in most cases, meteorological conditions are a major driving force controlling PM_{10} concentrations during the study period. Within each site type, the variations among the sites are smallest for the residential sites and largest for the construction sites.

An analysis of variance (ANOVA) is performed for each of the five site types. Table 6-7 gives the statistical summary of the results. This analysis shows that there is a significant difference between the industrial and all other site types except for construction sites. There is no difference between any of the other site types. This statistical analysis confirms the

Figure 6-7 Temporal variations of PM$_{10}$ concentrations acquired at the saturation monitoring network between 04/15/95 and 01/30/96.

6-23

Figure 6-8 Temporal variations of PM_{10} concentrations among five different site types acquired at the saturation monitoring network between 04/15/95 and 01/30/96.
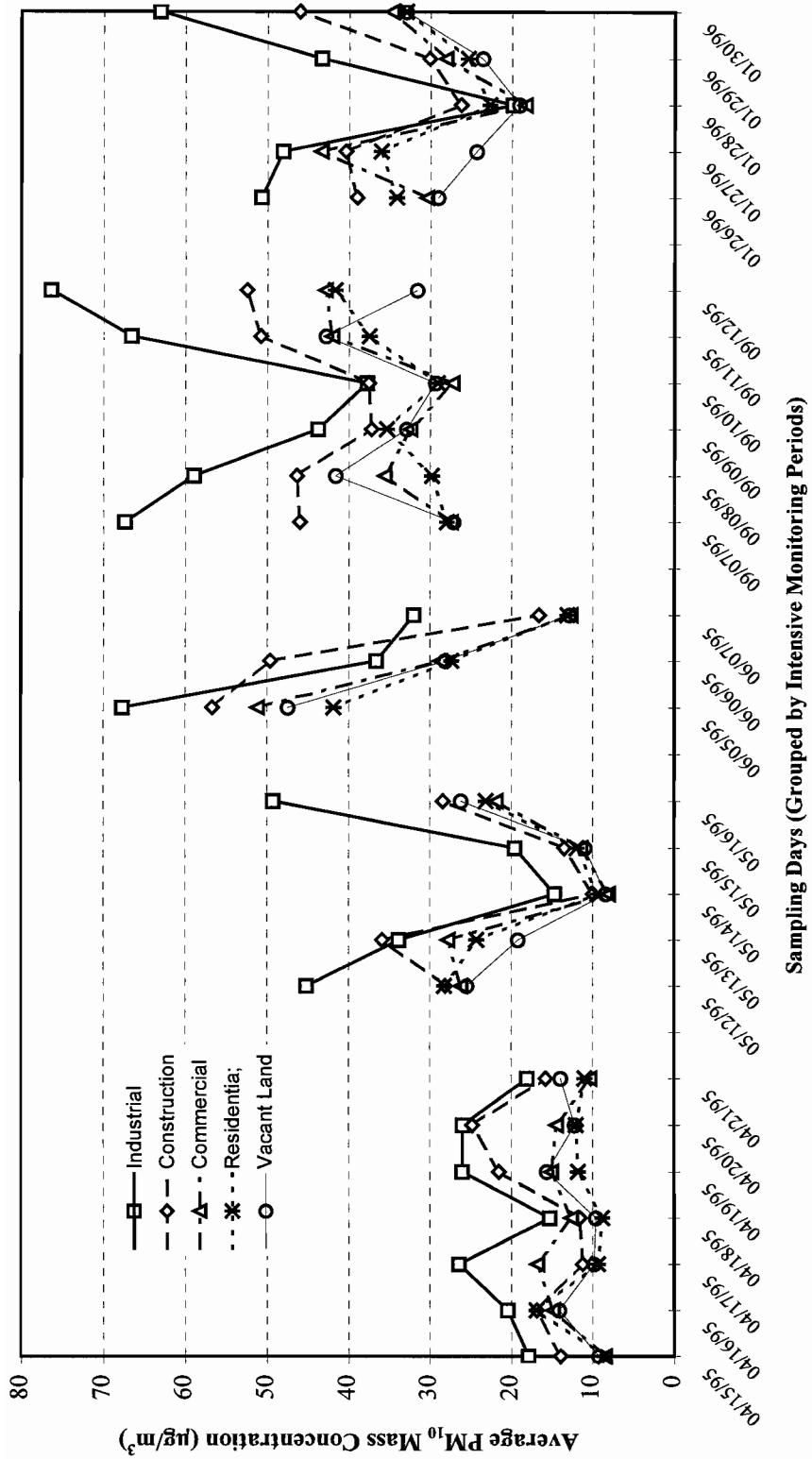
Table 6-7
Statistical Summary of Analysis of Variance (ANOVA) for Five Site Types

		Industrial	Construction	Commercial	Residential	Vacant Land
Industrial	f^{a}					
	$F_{0.05}{}^{b}$					
	β^{c}					
Construction	f^{a}	1.18				
	$F_{0.05}{}^{b}$	4.84				
	β^{c}	30.1%				
Commercial	f^{a}	17.10	1.59			
	$F_{0.05}{}^{b}$	5.99	4.67			
	β^{c}	0.6%	23.0%			
Residential	f^{a}	10.40	1.29	0.33		
	$F_{0.05}{}^{b}$	7.71	4.84	5.99		
	β^{c}	3.2%	28.0%	58.5%		
Vacant Land	f^{a}	21.80	3.94	0.81	0.06	
	$F_{0.05}{}^{b}$	5.12	4.49	4.84	5.12	
	β^{c}	0.1%	6.4%	38.7%	81.3%	

[a] The calculated f-value for two groups of samples.

[b] The critical f-value with a confidence level of 95%. For sample group A and B, if f is less than $F_{0.05}$, A and B are statistically equivalent to each other with a confidence level of 95%.

[c] The possibility at which two groups of samples are indistinguishable to each other.

findings in the time series analysis that PM_{10} concentrations observed at the industrial sites are somewhat similar to those of construction sites, but significantly different from the commercial, residential, and vacant land sites.

Average as well as maximum and minimum concentrations, as a function of intensive monitoring days, for each site-type are shown in Figures 6-9b to 6-13b to represent the temporal pattern within each site type. Large variations among the industrial or construction sites reflect the potential impact on PM_{10} from local fugitive dust emission activities. Daily concentration variations (maximum minus minimum) are substantially reduced at the commercial and residential sites.

Notice that in Figure 6-10a, PM_{10} concentrations at the LONM construction site during the fall and winter intensive monitoring periods are much higher than those found for the two spring intensives. The average PM_{10} concentrations during the winter intensive is over a factor of four higher than the average of the two spring intensives. The site log in Table 3-6 indicated that road oil was applied on the nearby Lone Mountain Road during the second spring intensive, with the road being completely paved during the summer intensive monitoring period. Active housing construction directly south of the site took place during the fall and winter intensive monitoring periods. This increment in ambient PM_{10} concentrations is in the same magnitude as estimated by MRI (1996) which reported the ratio of active to inactive construction emission factors to be 3.8.

Active housing construction east and northeast of the PECO site, and south and southeast of the CLIF site, were completed prior to the winter intensive monitoring period. Figure 6-10a shows that while the PM_{10} concentrations were comparable ($\sim$45 $\mu g/m^3$) during the fall intensive at these two sites, the completion of the nearby housing construction reduced the PM_{10} concentrations at the CLIF site by approximately 60% as compared to a 15% reduction at the PECO site. It is suspected that some residual soil from the construction site was carried over to the frequently-traveled Pecos Road, which might have resulted in less PM_{10} reduction at the PECO site. While these two sites are less than 0.25 km from each other with similar site averages (i.e., 31.8 ± 20.7 $\mu g/m^3$ at the CLIF site and 28.1 ± 18.3 $\mu g/m^3$ at the PECO site), the effect of construction activity can result in a difference in PM_{10} concentrations by 40 to 50 $\mu g/m^3$ on a given day depending on wind direction and activity level.

Active sewer construction at the GOLF construction site was noted in Table 3-6 for the summer and fall intensive monitoring periods. Visible dust loading was recorded on the nearby Losee Road and Washburn Road during the fall intensive monitoring period. The construction site was inactive during the winter intensive monitoring period. Table 6-6 shows that average PM_{10} mass concentrations were 70% and 74% above their site averages during the summer and fall intensive monitoring periods, respectively. In contrast, average
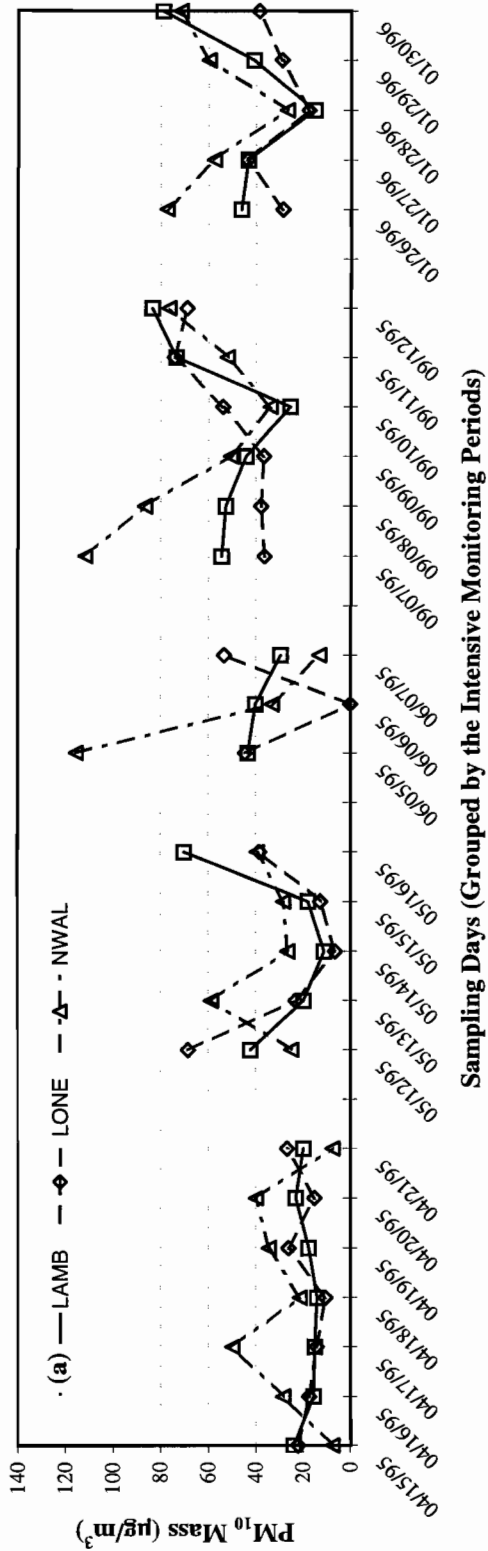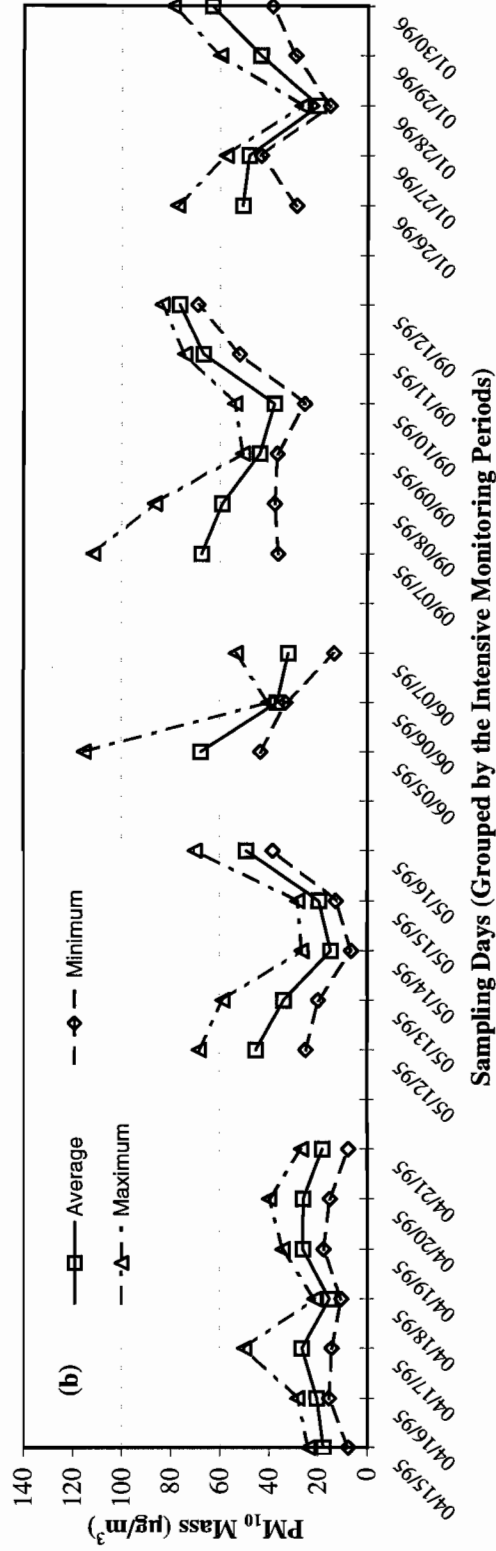
Figure 6-9 Temporal variations of PM$_{10}$ concentrations at the industrial sites for: a) concentrations at the individual sites, and b) average, minimum, and maximum concentrations between 04/15/95 and 01/30/96.

6-27
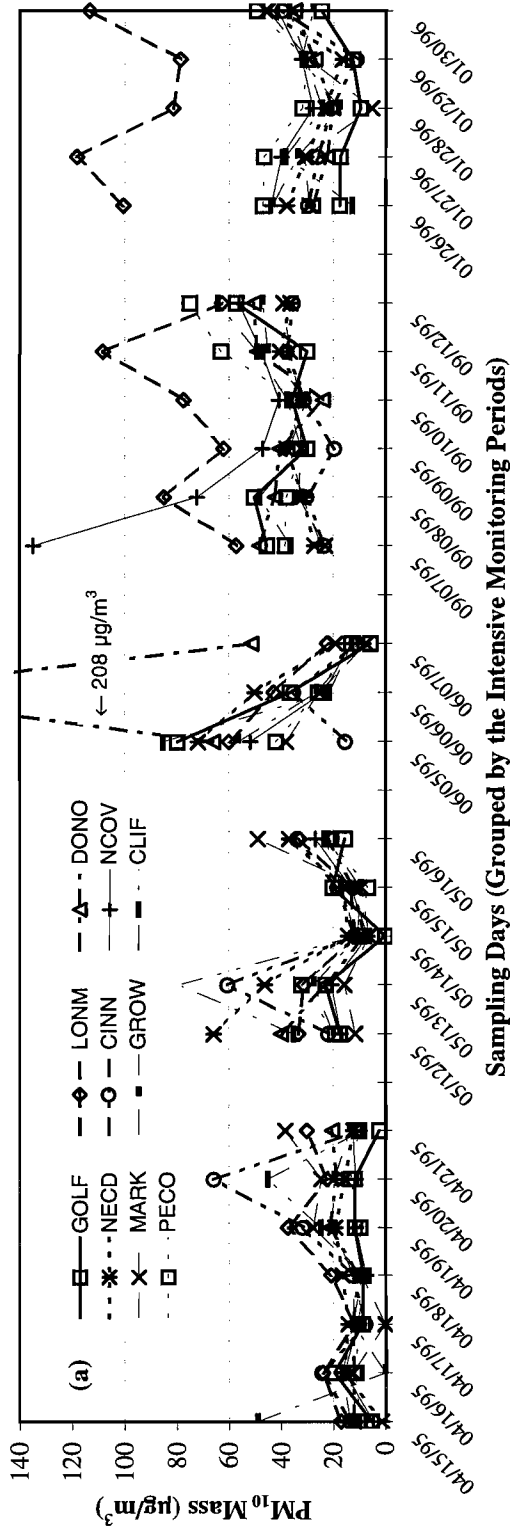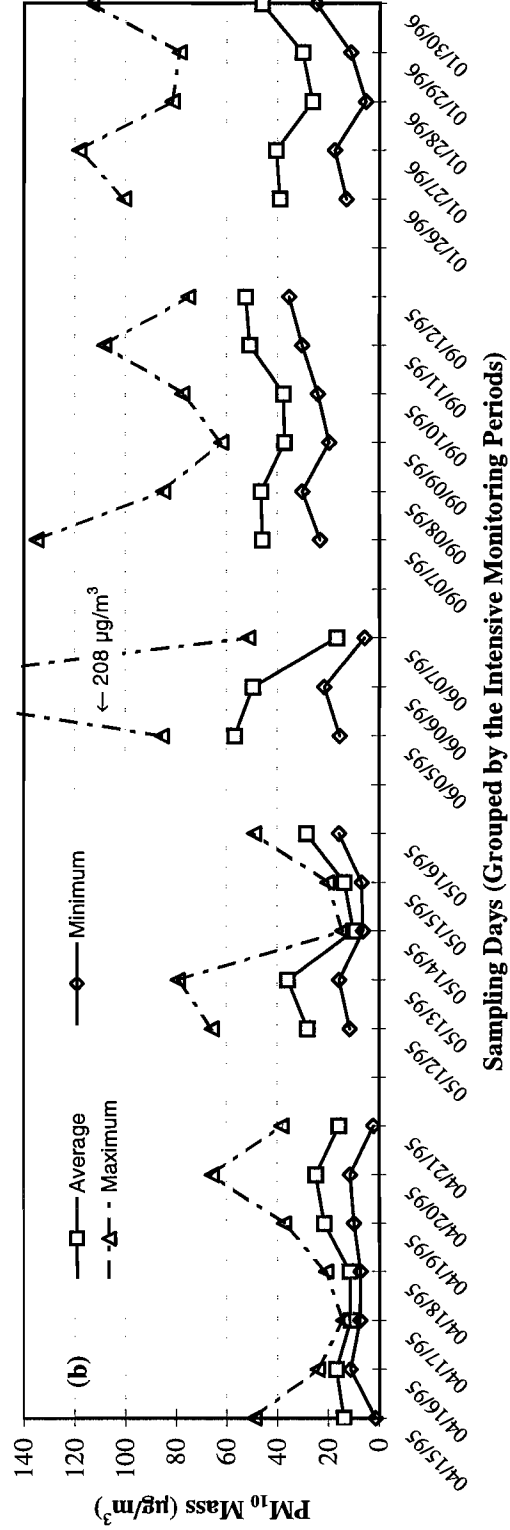
Figure 6-10 Temporal variations of PM$_{10}$ concentrations at the construction sites for: a) concentrations at the individual sites, and b) average, minimum, and maximum concentrations between 04/15/95 and 01/30/96.

6-28
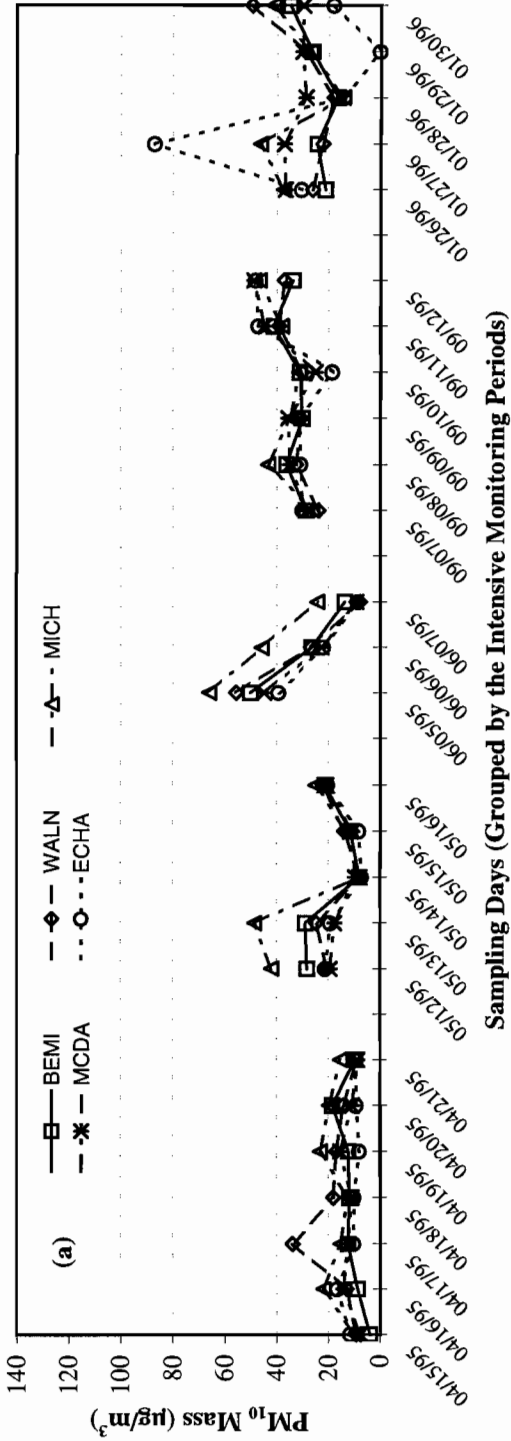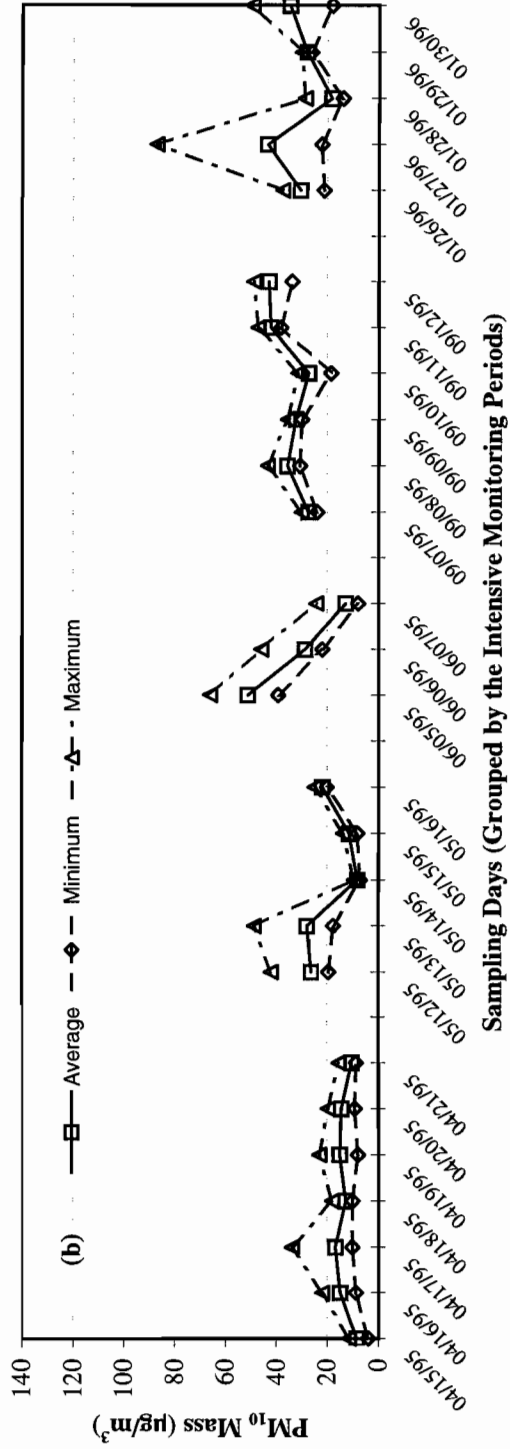
Figure 6-11 Temporal variations of PM_{10} concentrations at the commercial sites for: a) concentrations at the individual sites, and b) average, minimum, and maximum concentrations between 04/15/95 and 01/30/96.

6-29

Figure 6-12 Temporal variations of PM$_{10}$ concentrations at the residential sites for: a) concentrations at the individual sites, and b) average, minimum, and maximum concentrations between 04/15/95 and 01/30/96.
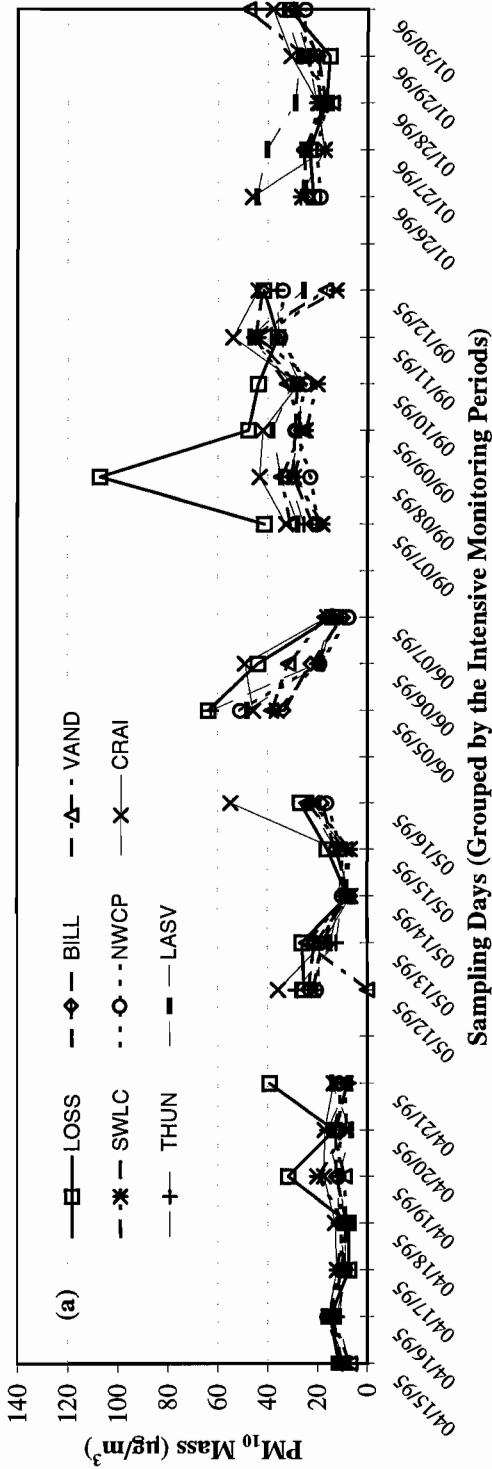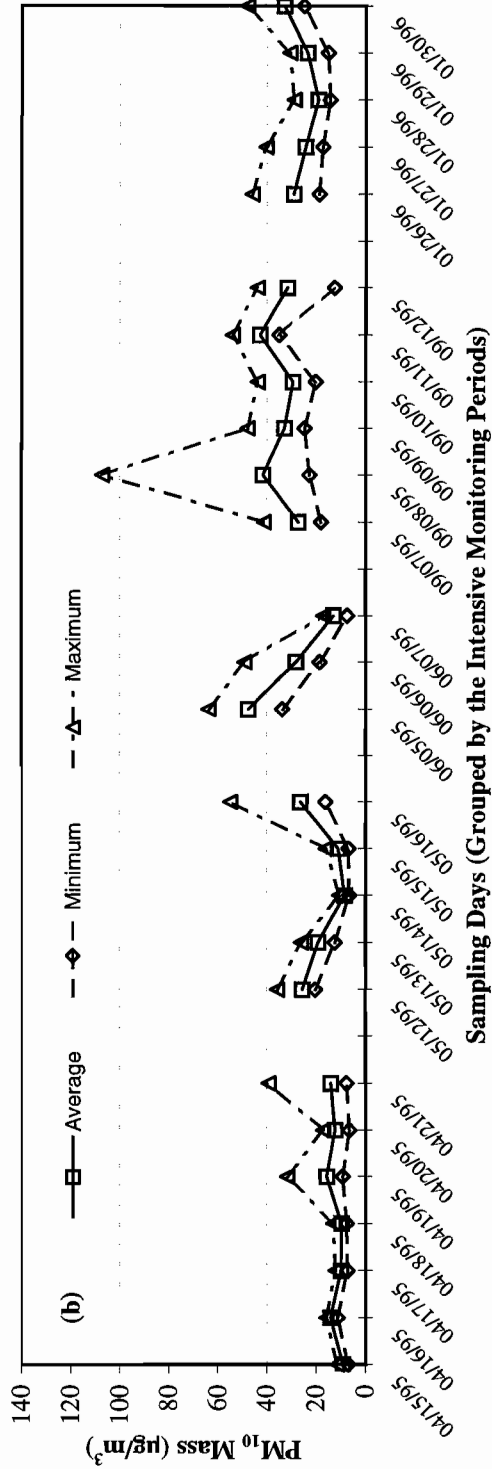
Figure 6-13 Temporal variations of PM_{10} concentrations at the vacant land sites for: a) concentrations at the individual sites, and b) average, minimum, and maximum concentrations between 04/15/95 and 01/30/96.

6-31

PM_{10} concentrations for the winter intensive monitoring period were 32% below the corresponding site average as construction activity ceased.

Similarly to the GOLF site, no construction activities were found at the DONO construction site during the winter intensive monitoring period. Table 6-6 shows that average PM_{10} concentrations during this period were 25% below the site average. No apparent construction activity was noted at the NECD construction site during the winter intensive monitoring period. Average PM_{10} concentrations for the winter intensive monitoring period were similar to the site averages with significantly lower PM_{10} concentrations than the second spring and summer intensive monitoring periods, when active development construction immediately (0.05 km) south of the site was recorded. Railroad tracks located 0.05 km west of this site may have also contributed to the PM_{10} loadings measured at the NECD site.

Road construction around the intersection of Gowan Street and Civic Center Drive 0.2 km northeast of the GROW site were recorded for all but the winter intensive monitoring period. Elevated (15% to 30%) PM_{10} concentrations were found during the fall and winter intensive monitoring periods when road construction was in progress. However, the site log recorded visible dust loading on all corners of the intersection between Gowan Street and Civic Center Drive. Since this site is located adjacent to the parking lot of Lois Craig School off Gowan Street, the traffic on this road increased after school started in the fall. Track-off of soil on the street surface may have resulted in these elevated PM_{10} concentrations.

Figure 6-9a shows that elevated PM_{10} concentrations were found at the NWAL industrial site during the summer (i.e., 06/05/95) and fall (i.e., 09/07/95, 09/08/95) intensive monitoring periods. The site log in Table 3-6 confirmed the observation that noticeable dust loading was present on Alexander Street adjacent to the NWAL site during the fall intensive monitoring period. Average PM_{10} mass concentration at the NWAL site during the fall intensive monitoring period is 45% above its site average. Track-out from the sand and gravel operation to the nearby access road apparently had a major effect on the measured PM_{10} concentrations.

Figure 6-13a shows an abrupt peak PM_{10} concentration (107.1 ± 5.6 μg/m^3) at the LOSS vacant land site on 09/08/95. The site log in Table 3-6 recorded visible dust loading on Losee Road adjacent to the LOSS site during the fall intensive. Since this was not a windy day, track-out or carry-out from the nearby GOLF or LONM construction sites or anthropogenic disturbance in the nearby vacant land are suspected as possible causes of this elevated PM_{10} concentration.

PM_{10} concentrations at the VAND vacant land site were elevated by 10 to 25 μg/m^3 or 42% above the site average (21.9 ± 12.3 μg/m^3) during the fall intensive monitoring period.

The site log in Table 3-6 noted that active earth-moving activity was found 0.5 km east of the site during this period. Even though no construction activity was noted during the winter intensive monitoring period, average PM_{10} mass concentrations were 26% above the site average.

Weekend/weekday comparisons were also made. Since there are hardly any activities at the sand and gravel operation or at construction sites on weekends, these sites experience the greatest weekend/weekday variations among all source types, with the lowest PM_{10} concentrations occurring on Sundays (i.e., 04/16/95, 05/14/95, 09/10/95, 01/28/96).

This analysis shows that temporal variations of PM_{10} concentrations are more pronounced in the industrial, construction, and disturbed vacant land sites than in residential and commercial sites. Elevated PM_{10} concentrations were found to be associated with local construction activities, industrial processes, or excessive surface street dust loadings. When potential fugitive dust sources were identified within 0.5 km from the sampling site, PM_{10} concentrations were often up to four times higher than PM_{10} at nearby sites that were not adjacent to the sources. Most of the elevated PM_{10} concentrations occurred when dust-generating activities were identified in the site log during each of the intensive monitoring periods. For these intermittent fugitive dust sources, a survey of activity levels and surface street dust loading is essential to understanding the transport and deposition of resuspended particles.

6.5.2 Chemical Characteristics of the Five Site Types

With respect to the saturation monitoring network, a total of 14 days from the summer, fall, and winter intensive periods were selected for x-ray fluorescence (XRF) scanning for aluminum (Al), silicon (Si), sulfur (S), potassium (K), calcium (Ca), and iron (Fe). Table 6-8 provides a statistical summary for all sites, and for each of the five site types.

The average PM_{10} mass concentration is 27.9 ± 19.7 $\mu g/m^3$ for the 26 intensive monitoring days and 36.6 ± 20.9 $\mu g/m^3$ for the selected 14 chemical analysis days. PM_{10} and b_{abs} concentrations from this subset of samples are 31% and 8% higher, respectively, than the overall average. Among the five site types, the average PM_{10} mass concentrations are: 39.4 ± 24.0 $\mu g/m^3$ for the industrial sites, 31.3 ± 24.1 $\mu g/m^3$ for the construction sites, 24.7 ± 14.1 $\mu g/m^3$ for the commercial sites, 23.5 ± 11.8 $\mu g/m^3$ for the residential sites, and 23.0 ± 13.8 $\mu g/m^3$ for the vacant land sites. Note that the standard deviations for the industrial and commercial sites are approximately a factor of two higher than those of other site types, indicating a greater extent of day-to-day and/or site-to-site variabilities within each these two site types. For the selected 14 days, PM_{10} mass varied from 30.2 ± 13.6 $\mu g/m^3$ at the vacant land site to 51.2 ± 23.8 $\mu g/m^3$ at the industrial sites, with a site-type average of 36.6 ± 20.9

Table 6-8
Statistical Summary of Average PM_{10} Mass and Chemical Composition ($\mu g/m^3$)
Acquired in the Saturation Monitoring Network

		Average	Std. Dev.	Maximum	Date with Maximum
Average of	Mass (26 days)[a]	27.86	19.66	208.36	06/06/95
Five Site Types	Mass (14 days)[b]	36.60	20.86	208.36	06/06/95
	b_{abs} (Mm^{-1}) (26 days)[a]	21.01	10.24	69.60	01/27/96
	b_{abs} (Mm^{-1}) (14 days)[b]	22.62	10.53	69.60	01/27/96
	Aluminum	1.31	0.81	5.94	01/26/96
	Silicon	5.02	3.12	23.55	09/07/95
	Sulfur	0.43	0.24	1.22	09/07/95
	Potassium	0.39	0.23	1.77	09/07/95
	Calcium	6.06	4.10	28.55	09/07/95
	Iron	0.69	0.39	2.67	01/26/96
Industrial	Mass (26 days)[a]	39.44	23.98	115.33	06/05/95
	Mass (14 days)[b]	51.21	23.78	115.33	06/05/95
	b_{abs} (Mm^{-1}) (26 days)[a]	24.23	11.39	56.25	09/12/95
	b_{abs} (Mm^{-1}) (14 days)[b]	26.59	11.81	56.25	09/12/95
	Aluminum	1.82	0.88	4.28	09/07/95
	Silicon	7.35	3.55	16.85	09/07/95
	Sulfur	0.53	0.26	1.12	09/07/95
	Potassium	0.50	0.27	1.33	09/07/95
	Calcium	10.59	5.42	22.07	01/26/96
	Iron	0.90	0.44	1.97	09/07/95
Construction	Mass (26 days)[a]	31.25	24.11	208.36	06/06/95
	Mass (14 days)[b]	41.09	26.55	208.36	06/06/95
	b_{abs} (Mm^{-1}) (26 days)[a]	21.01	10.29	60.70	09/12/95
	b_{abs} (Mm^{-1}) (14 days)[b]	23.18	10.20	60.70	09/12/95
	Aluminum	1.45	0.96	5.94	01/26/96
	Silicon	5.53	3.72	23.55	09/07/95
	Sulfur	0.43	0.23	1.22	09/07/95
	Potassium	0.44	0.27	1.77	09/07/95
	Calcium	6.69	4.58	28.55	09/07/95
	Iron	0.75	0.44	2.67	01/26/96
Commercial	Mass (26 days)[a]	24.72	14.05	86.95	01/27/96
	Mass (14 days)[b]	32.58	13.27	86.95	01/27/96
	b_{abs} (Mm^{-1}) (26 days)[a]	22.03	10.82	69.60	01/27/96

Table 6-8 (continued)

Statistical Summary of Average PM$_{10}$ Mass and Chemical Composition (μg/m^3)
Acquired in the Saturation Monitoring Network

		Average	Std. Dev.	Maximum	Date with Maximum
	b$_{abs}$ (Mm^{-1}) (14 days)[b]	23.79	11.91	69.60	01/27/96
	Aluminum	1.11	0.62	3.12	01/27/96
	Silicon	4.25	2.20	11.90	01/27/96
	Sulfur	0.45	0.25	1.17	09/07/95
	Potassium	0.34	0.17	1.00	01/27/96
	Calcium	4.70	2.31	12.40	01/27/96
	Iron	0.66	0.33	2.24	01/27/96
Residential	Mass (26 days)[a]	23.47	11.82	46.80	01/26/96
	Mass (14 days)[b]	31.05	9.54	46.80	01/26/96
	b$_{abs}$ (Mm^{-1}) (26 days)[a]	21.71	11.45	67.38	01/26/96
	b$_{abs}$ (Mm^{-1}) (14 days)[b]	24.06	12.52	67.38	01/26/96
	Aluminum	1.14	0.49	2.73	06/05/95
	Silicon	4.25	1.65	9.20	06/05/95
	Sulfur	0.42	0.21	1.00	09/07/95
	Potassium	0.35	0.14	0.79	06/05/95
	Calcium	4.76	1.88	8.17	09/12/95
	Iron	0.64	0.28	1.37	06/05/95
Vacant Land	Mass (26 days)[a]	22.97	13.79	107.08	09/08/95
	Mass (14 days)[b]	30.19	13.60	107.08	09/08/95
	b$_{abs}$ (Mm^{-1}) (26 days)[a]	18.87	8.31	50.53	04/19/95
	b$_{abs}$ (Mm^{-1}) (14 days)[b]	19.18	7.55	41.00	01/26/96
	Aluminum	1.14	0.66	4.36	09/08/95
	Silicon	4.28	2.47	18.96	09/08/95
	Sulfur	0.40	0.22	1.04	09/07/95
	Potassium	0.33	0.18	1.14	09/08/95
	Calcium	4.96	2.96	25.59	09/08/95
	Iron	0.58	0.33	1.89	09/08/95

[a] Includes 5 intensive monitoring periods: 04/15/95 to 04/21/95, 05/12/95 to 05/16/95, 06/05/95 to 06/07/95, 09/07/95 to 09/12/95, and 01/26/95 to 01/30/95.

[b] Includes 3 intensive monitoring periods: 06/05/95 to 06/07/95, 09/07/95 to 09/12/95, and 01/26/95 to 01/30/95.

$\mu g/m^3$. PM_{10} b_{abs} concentrations are less variable, with 19.2 ± 7.6 Mm^{-1} at the vacant land site to 26.6 ± 11.8 Mm^{-1} at the industrial sites.

For the five site types, industrial sites ranked highest in concentrations of PM_{10} crustal components (e.g., Al, Si, K, Ca, Fe), followed by construction sites. The enrichment of crustal species is similar among the commercial, residential, and vacant land sites.

PM_{10} sulfur concentrations were more homogeneously distributed within the study domain, with an average of 0.40 ± 0.22 $\mu g/m^3$ at the vacant land sites to 0.53 ± 0.26 $\mu g/m^3$ at the industrial sites. This finding was expected since the majority of sulfur should be in the form of sulfate, a secondary aerosol that does not originate on the neighborhood scale (Chow *et al.*, 1992b; Chow and Watson, 1997b).

6.5.3 Material Balance of PM_{10} Chemical Compositions

Material balances (Solomon *et al.*, 1989; Chow *et al.*, 1994b) for crustal material, sulfate, elemental carbon, and unexplained mass abundances in PM_{10} were constructed by: 1) summing the aluminum, silicon, calcium, and iron oxides (i.e., [1.89 × aluminum] + [2.14 × silicon] + [1.4 × calcium] + [1.43 × iron]) to estimate the crustal or geological material; 2) deriving the elemental carbon concentration based on the relationship between b_{abs} and elemental carbon (i.e., $b_{abs} \div 8.6$, see Section 5.5) as a surrogate to estimate combustion byproducts, and 3) calculating the sulfate concentration (i.e., 3 × sulfur) to estimate secondary sulfate.

Average material balance for each site type is displayed in Figure 6-14. Similar abundances were found among the five site types, with the exception of the industrial sites, which show approximately 10% higher crustal components. Overall, crustal material was the largest contributor, accounting for 60% to 70% of PM_{10} mass. Combustion byproducts accounted for 7% to 10%, and secondary sulfate accounted for 3% to 4%.

Figure 6-15 displays the scatter plot of the sum of the crustal compounds (accounting for their corresponding oxides) versus PM_{10} mass for over 400 samples acquired and chemically analyzed during the summer, fall, and winter intensive monitoring periods. High correlation (r = 0.90) was found between the crustal component and PM_{10} mass, with an average ratio of 0.62 ± 0.01. This implies that, on average, over 60% of the PM_{10} mass consists of crustal components. In addition to the crustal component, material balance was constructed based on an absorption coefficient of 8.6 m^2/g to derive elemental carbon (EC = $b_{abs} \div 8.6$) which represents combustion byproducts, and the sulfur/sulfate stoichiometric ratio (sulfate = 3 × sulfur) to estimate secondary sulfate. A scatter plot of material balance versus PM_{10} mass is shown in Figure 6-16. Similar correlation (r = 0.92) was found in this comparison, with an average ratio of 0.72 ± 0.01. This illustration indicates that over 70% of

Industrial Sites

Crustal
34.4 ± 17.6 μg/m³
(70.7%)

Others
10.0 ± 9.87 μg/m³
(19.2%)

Sulfate
1.54 ± 0.81 μg/m³
(3.4%)

Combustion
3.02 ± 1.44 μg/m³
(6.8%)

Construction Sites

Crustal
25.2 ± 16.4 μg/m³
(62.8%)

Others
11.0 ± 13.7 μg/m³
(25.3 %)

Sulfate
1.31 ± 0.69 μg/m³
(3.8%)

Combustion
2.70 ± 1.18 μg/m³
(8.1%)

Commercial Sites

Crustal
18.7 ± 9.02 μg/m³
(59.9%)

Others
8.33 ± 4.28 μg/m³
(26.2 %)

Sulfate
1.36 ± 0.76 μg/m³
(4.6%)

Combustion
2.77 ± 1.38 μg/m³
(9.3%)

Residential Sites

Crustal
18.8 ± 6.77 μg/m³
(62.9%)

Others
7.17 ± 4.52 μg/m³
(23.0%)

Sulfate
1.27 ± 0.64 μg/m³
(4.42%)

Combustion
2.80 ± 1.46 μg/m³
(9.7%)

Vacant Land Sites

Crustal
19.1 ± 10.6 μg/m³
(64.5%)

Others
6.72 ± 4.01 μg/m³
(22.7%)

Sulfate
1.19 ± 0.67 μg/m³
(4.3%)

Combustion
2.23 ± 0.88 μg/m³
(8.5%)

Figure 6-14 Average material balance for PM$_{10}$ measurements aquired at the saturation monitoring network for each of the five site types between 04/15/95 and 01/30/96.
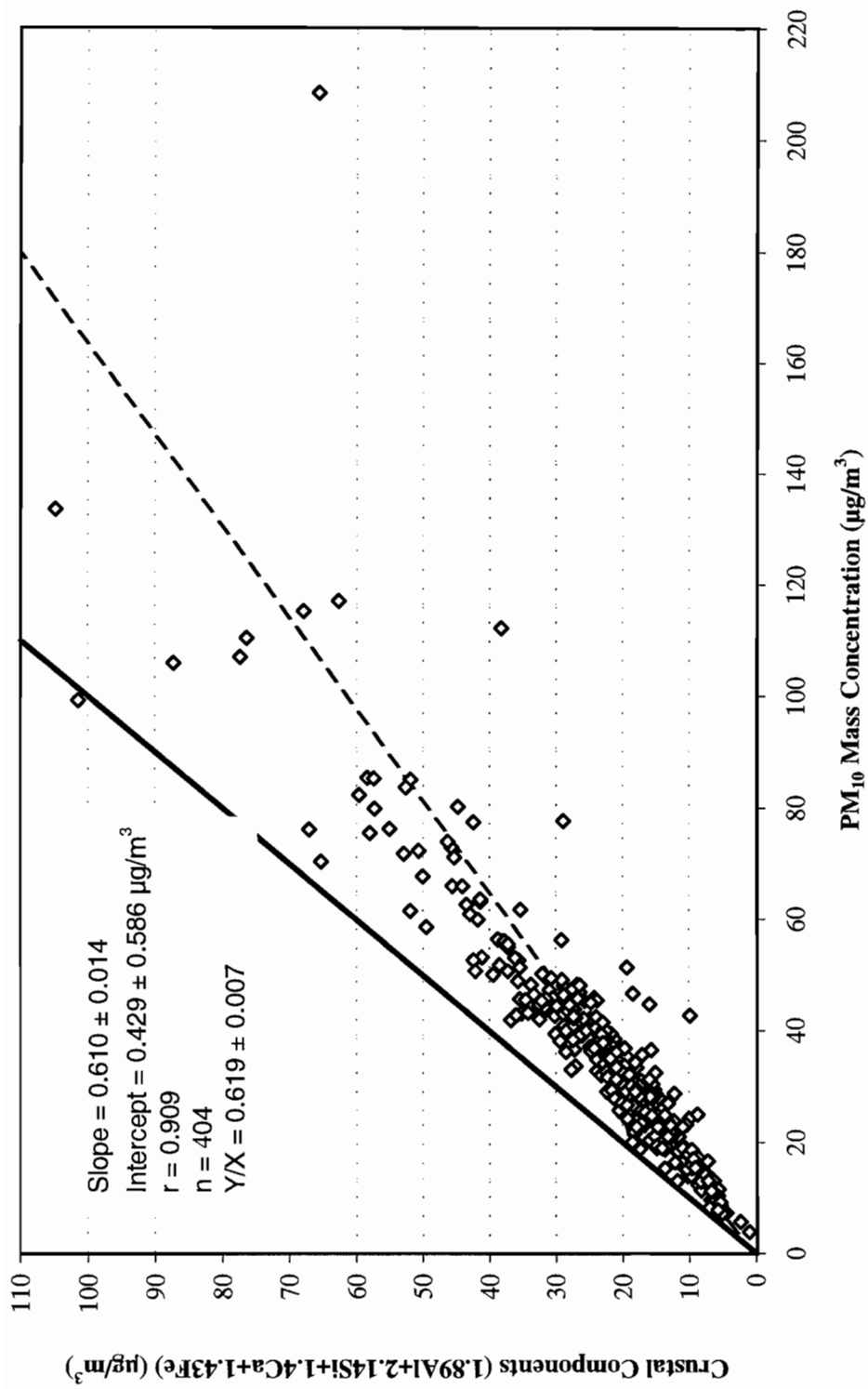
Figure 6-15 Sum of the crustal components versus PM_{10} mass for the samples acquired during the summer, fall, and winter intensive monitoring periods between 06/05/95 and 01/30/96.
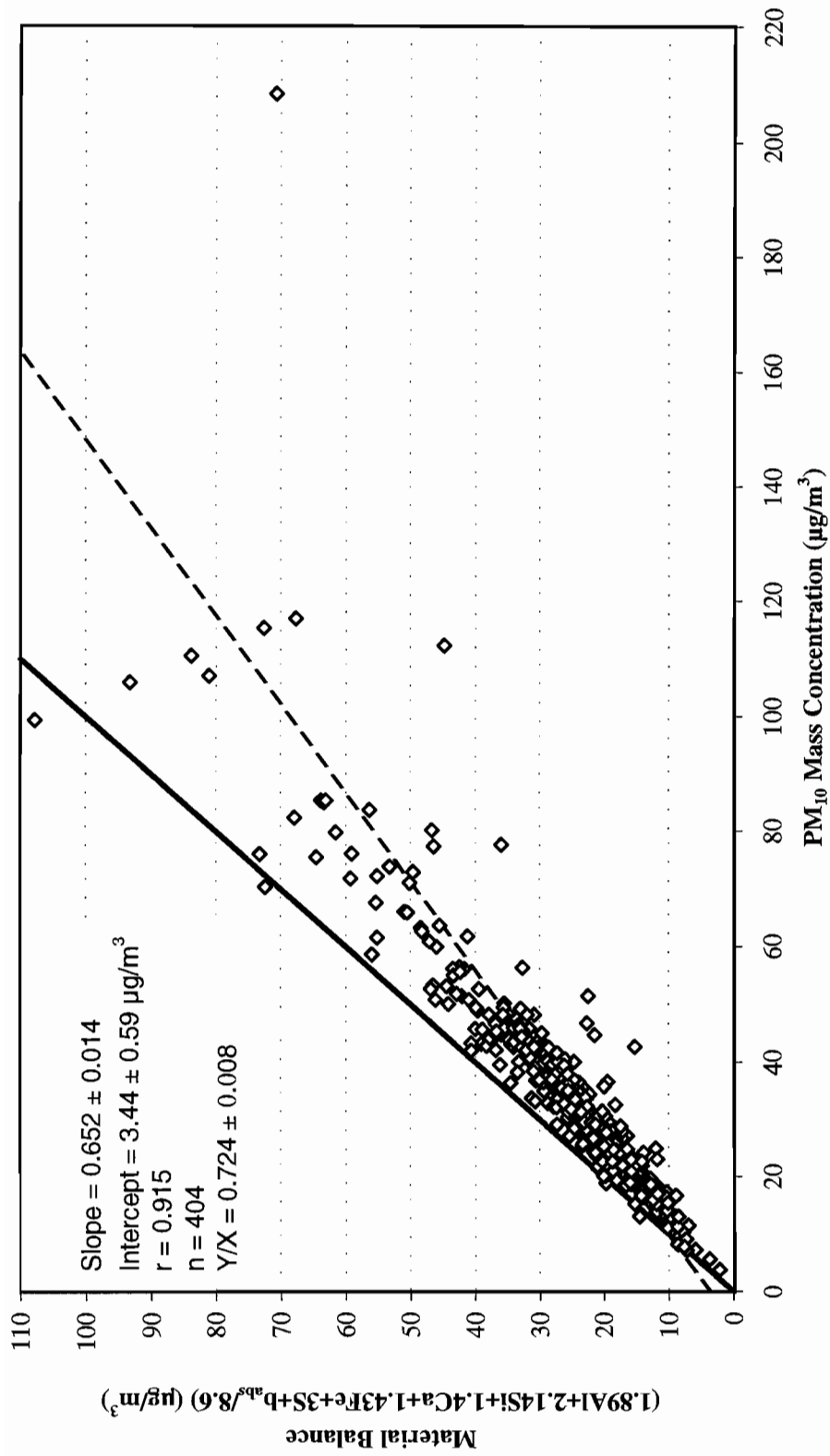
Figure 6-16 Material balance versus PM$_{10}$ mass for PM$_{10}$ measurements collected at the saturation monitoring network between 04/15/95 and 01/30/96.

Slope = 0.652 ± 0.014
Intercept = 3.44 ± 0.59 µg/m^3
r = 0.915
n = 404
Y/X = 0.724 ± 0.008

PM$_{10}$ Mass Concentration (µg/m^3)

Material Balance
(1.89Al+2.14Si+1.4Ca+1.43Fe+3S+b$_{abs}$/8.6) (µg/m^3)

the PM_{10} mass can be explained by crustal material, combustion byproducts, and secondary sulfate. Combustion byproducts and secondary sulfate constitute approximately 10% of PM_{10} mass.

6.5.4 Spatial Variations of the Satellite Sites

Averages of PM_{10} mass were computed over the 26 intensive monitoring days to compare site-to-site variations as shown in Table 6-9. During the intensive monitoring periods, average PM_{10} mass concentrations varied by a factor of three from site to site. The LONM site, which experienced the greatest impact from nearby construction activities, reported the highest average PM_{10} concentration (52.2 ± 33.9 $\mu g/m^3$), and the undisturbed desert site (SWLC) reported the lowest PM_{10} average (19.1 ± 9.1 $\mu g/m^3$).

PM_{10} concentrations at the 90th percentile are associated with either construction or industrial sites. Similarly, PM_{10} concentrations from sites closest to the residential and vacant land sites appear in the 10th percentile. The standard deviations of these averages are very high, with coefficients of variation ranging from 47% to 108% from site to site. This is higher than the day-to-day coefficients of variation which ranged from 27% to 96%. The greatest site-to-site variations are found with industrial and construction sites, and the least with residential and commercial sites. Table 6-9 also shows that maximum concentrations occurred sporadically at different locations on different days. The site-specific maximum PM_{10} concentrations varied by a factor of five during the intensive monitoring periods, ranging from 43.8 ± 2.7 $\mu g/m^3$ at the SWLC vacant land site on 09/11/95, to 208.4 ± 11.7 $\mu g/m^3$ at the DONO construction site on 06/06/95.

Even though the sampling sites are located close to each other, PM_{10} concentrations on any given day (e.g., 06/06/95) can vary by over one order of magnitude, from 18.4 ± 3.3 $\mu g/m^3$ at the LASV vacant land site to 208.4 ± 11.7 $\mu g/m^3$ at the DONO construction site. Since these two sites are less than 4 km from each other, it confirms that local sources in close proximity to the sampling site had a greater effect on PM_{10} loadings, and the zone of influence from a particular fugitive dust source is likely to be small. Meteorological data show that average and maximum wind speeds were 6 and 12 m/s with maximum gusts of 16 m/s on 06/06/95.

Figure 6-17 displays the spatial variations among the 30 satellite sites on this windy day. PM_{10} concentrations are generally low on 06/06/95 in the study area, ranging from 25 to 35 $\mu g/m^3$ with the exception of the DONO construction site. The NECD construction site (approximately 0.75 km southwest of the DONO site) and CRAI vacant land site (approximately 1.5 km southwest-south of the DONO site) reported PM_{10} concentrations 70% and 74% above their corresponding site averages, respectively. The MICH commercial site (approximately 0.6 km southeast of the DONO site) experienced PM_{10} concentrations

Table 6-9

Statistical Summary of PM$_{10}$ Mass Concentrations in the Saturation Monitoring Network

Site Type	Site	Maximum ($\mu g/m^3$)	Date with Maximum Value	Minimum ($\mu g/m^3$)	Average ($\mu g/m^3$)	Std. Dev. ($\mu g/m^3$)	Coefficient of Variation (%)	Total No. in Average
Industrial	LAMB	83.54	09/12/95	10.991	36.943 ±	21.629	0.585	26
	LONE	74.27	09/11/95	6.421	33.738 ±	18.867	0.559	25
	NWAL	115.33	06/05/95	7.530	47.411 ±	28.868	0.609	26
Construction	GOLF	79.86	06/05/95	2.165	23.882 ±	18.567	0.777	25
	LONM	118.18	01/27/96	11.408	52.185 ±	33.857	0.649	26
	DONO	208.36	06/06/95	8.069	35.677 ±	38.477	1.078	26
	NECD	71.87	06/05/95	1.530	29.823 ±	16.957	0.569	26
	CINN	65.68	04/20/95	7.495	26.049 ±	14.507	0.557	26
	NCOV	134.93	09/07/95	4.774	31.972 ±	27.706	0.867	26
	MARK	48.96	05/16/95	5.176	24.998 ±	13.114	0.525	25
	GROW	56.48	06/05/95	9.411	27.255 ±	13.403	0.492	25
	CLIF	85.44	06/05/95	8.635	31.854 ±	20.732	0.651	26
	PECO	75.17	09/12/95	6.689	28.108 ±	18.328	0.652	26
Commercial	BEMI	50.14	06/05/95	3.955	22.672 ±	11.579	0.511	26
	WALN	55.65	06/05/95	7.875	24.289 ±	12.268	0.505	26
	MICH	66.02	06/05/95	7.987	29.920 ±	14.816	0.495	26
	MCDA	48.76	09/12/95	7.638	23.645 ±	12.646	0.535	26
	ECHA	86.95	01/27/96	7.092	23.008 ±	17.967	0.781	25
Residential	EFER	43.13	06/05/95	8.069	20.195 ±	9.771	0.484	26
	NOCO	45.92	09/12/95	7.365	23.569 ±	12.345	0.524	26
	HAMI	46.80	01/26/96	7.373	26.636 ±	12.670	0.476	26
Vacant Land	LOSS	107.08	09/08/95	7.234	29.780 ±	21.501	0.722	26
	BILL	45.08	09/11/95	6.678	20.622 ±	10.368	0.503	26
	VAND	47.92	01/30/96	6.956	21.870 ±	12.151	0.556	25
	SWLC	43.81	09/11/95	6.817	19.059 ±	9.096	0.477	26
	NWCP	50.78	06/05/95	7.234	19.375 ±	9.872	0.509	26
	CRAI	54.81	05/16/95	6.539	28.082 ±	15.376	0.548	26
	THUN	62.74	06/05/95	7.092	21.360 ±	12.336	0.578	26
	LASV	48.27	06/05/95	6.397	23.534 ±	13.115	0.557	26
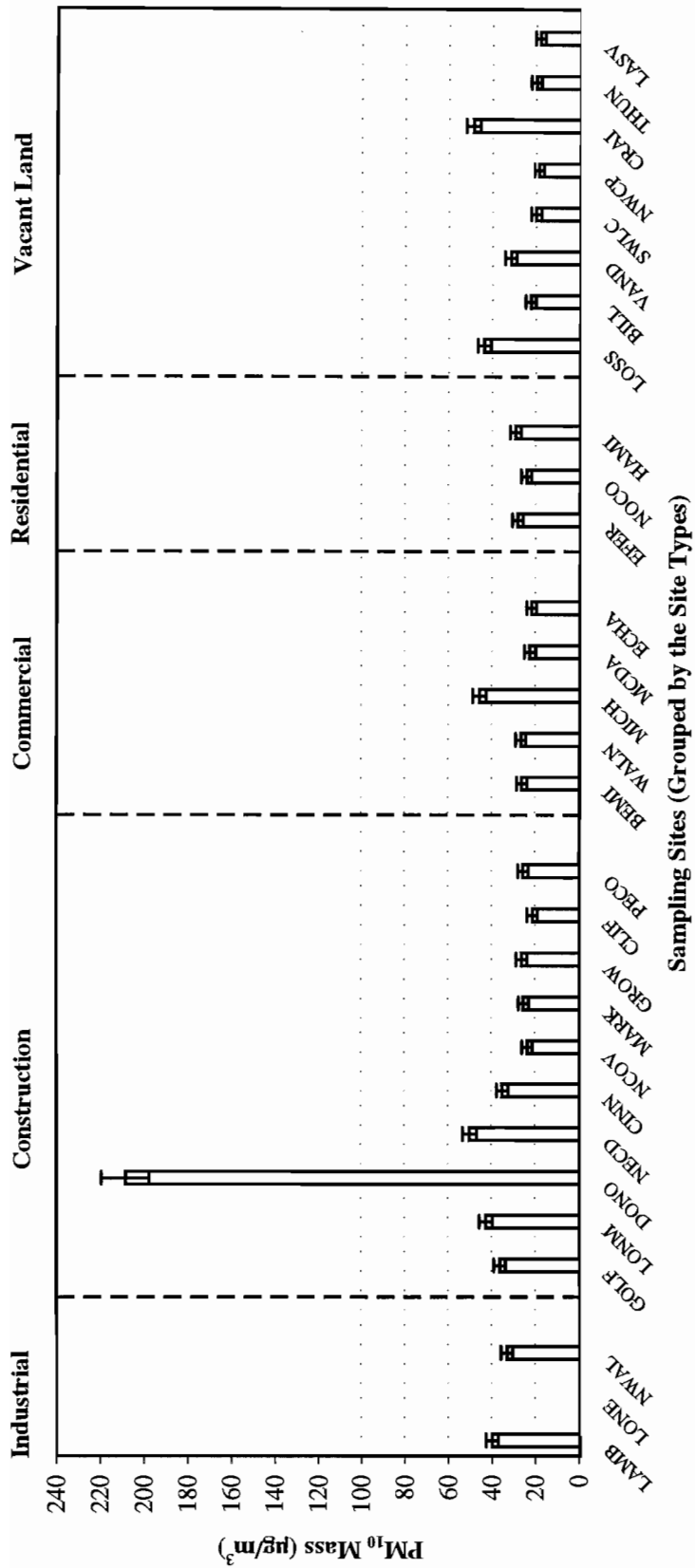
Figure 6-17 Histogram of PM_{10} mass concentrations acquired at the saturation monitoring network on 06/06/95.

53% above its site average (29.9 ± 14.8 μg/m^3). The construction site influence did not extend further south, however. Higher-than-average PM$_{10}$ concentrations were not found at the NCOV and MARK construction sites located south of the MICH site, approximately 1.0 to 1.2 km south from the DONO site.

Slightly-higher PM$_{10}$ concentrations were found at the BILL vacant land site (approximately 0.35 km northeast-east of the DONO site on the east side of Interstate 15) and at the BEMI construction site (approximately 0.6 km east of the DONO site) with PM$_{10}$ concentrations exceeding their site averages by 9% and 16%, respectively. Meteorological analysis shows that winds were east to northeast in the early morning between 0000 and 0900 PST at approximately 2 to 5 m/s. Wind direction shifted to the northwest for the remainder of the day. Wind speeds are high at night, exceeding 8 m/s after 2100 PST.

This analysis shows that elevated PM$_{10}$ concentrations, ranging between 9% to 70% above their site averages, were found within a 0.75 km radius from the DONO construction site. On a windy day such as 06/06/95, this source impact might extend to 1.5 km downwind of the source (e.g., CRAI site) over relatively flat terrain without any wind barriers. It is suspected that most of the wind-blown dust from construction activities consist of large coarse particles. These particles tend to settle out rapidly within a short distance from the source and they do not travel over long distances. The zone of influence did not apply to upwind sites (e.g., NCOV and MARK sites) 1.5 km from the construction activity.

During the intensive monitoring period, 24-hour PM$_{10}$ concentrations exceeding 100 μg/m^3 (three to four times higher than the corresponding site-type averages) were recorded at only one industrial site (NWAL on 06/05/95 and 09/07/95), three construction sites (LONM on 09/11/95, 01/26/96, 01/27/96, and 01/30/96, DONO on 06/06/95, and NCOV on 09/07/95), and one vacant land site (LOSS on 09/08/95). Meteorological analysis on these days shows that high winds occurred on only 50% of the site-days (06/05/95, 06/06/95, 09/07/95, and 09/08/95). Four elevated (> 100 μg/m^3) PM$_{10}$ concentrations, observed at the LONM construction site on 09/11/95, 01/26/96, 01/27/96, and 01/30/96, all occurred during low-to-moderate wind periods. The 24-hour average wind speeds at the Bemis site were 2 to 4 m/s and maximum hourly wind speeds were 4 to 5 m/s on these days. Active construction adjacent to the south side of the LONM site during the fall and winter intensive monitoring periods (noted in Table 3-6) apparently had a major impact on these elevated PM$_{10}$ concentrations.

The zones of influence of these construction activities were further examined. Elevated PM$_{10}$ concentrations were found at the CRAI vacant land site, approximately 1.2 km southeast of the LONM construction site, on three out of four days with PM$_{10}$ mass being 36% to 92% higher than the corresponding site average (28.1 ± 15.4 μg/m^3). These influences decreased by 10% to 40% at the NECD construction site, approximately 2 km

southeast-east of the LONM site. Elevated PM_{10} concentrations at the NECD construction site on 09/11/95, 01/26/96, and 01/30/96 were found to be 27% to 54% above the site average (29.8 ± 16.9 μg/m^3). The MICH commercial site, approximately 0.8 km east of the NECD construction site, experienced similar elevations in PM_{10} concentrations, ranging from 25% to 56% above the site average (29.9 ± 14.8 μg/m^3).

The NWAL industrial site, approximately 1.8 km south-southeast of the LONM site, also reported 10% to 62% higher-than-average PM_{10} concentrations (47.4 ± 28.9 μg/m^3) on these days. It is interesting to note that sites 1 to 2 km northeast of the LONM site (GOLF construction site and LOSS vacant land site) suffered no apparent impact on PM_{10} concentrations during these days. Meteorological data at the Bemis site shows similar wind patterns on those days with prevailing northwesterly winds during the morning (0000 to 0700 PST) and night (1800 to 2400 PST) at 1 to 2 m/s. Winds were from the east and southeast during the daytime with wind speeds in the range of 2 to 4 m/s.

This analysis shows that on a nonwindy day, the zone of influence from an active construction site was mainly within one kilometer downwind from the source. The zone of influence could extend up to 2 km from a dust source, with the concentration gradient decreasing by 10% to 40%, during low wind periods.

A statistical summary of PM_{10} chemical compositions acquired during the summer, fall, and winter intensive periods from the saturation monitoring network is presented in Table 6-10. Average and maximum crustal abundances varied by a factor of two to four among all site types. For the crustal component being measured, the average concentrations measured at the industrial and construction sites often exceeded the maximum concentrations found at the commercial and residential sites.

The highest concentrations of silicon (23.6 ± 7.5 μg/m^3), sulfur (1.9 ± 0.7 μg/m^3), potassium (1.8 ± 0.4 μg/m^3), and calcium (28.6 ± 4.8 μg/m^3) were found on 09/07/95 at the NCOV construction site. The highest concentrations of aluminum (5.9 ± 1.8 μg/m^3) and iron (2.7 ± 0.2 μg/m^3) were found on 01/26/96 at the LONM construction site. Elevated crustal components were also found on 09/08/95. Average wind speeds of 4 to 7 m/s, maximum wind speeds of 11 to 13 m/s, and wind gusts up to 12 m/s were recorded on 09/07/95 and 09/08/95. It is suspected that some crustal material was dislodged from the ground surface and became airborne. Low wind speeds (2.3 m/s on average) were recorded on 01/26/96, however. Construction activities within the close proximity of the LONM site may have contributed to the high level of crustal components.

Average PM_{10} sulfur concentrations exhibited very little spatial variation, ranging from 0.36 ± 0.23 μg/m^3 at the CINN construction site to 0.57 ± 0.28 μg/m^3 at the NWAL

Table 6-10

Statistical Summary of PM$_{10}$ Mass and Chemical Compositions
Acquired during Intensive Monitoring Periods at Saturation Monitoring Sites

Site Type	Site	Mass (μg/m³)					b$_{abs}$ (Mm⁻¹)					Aluminum (μg/m³)				
		Average	Std. Dev.	Minimum	Maximum	No. in Average	Average	Std. Dev.	Minimum	Maximum	No. in Average	Average	Std. Dev.	Minimum	Maximum	No. in Average
Industrial	LAMB	47.92	19.71	15.25	83.54	14	30.78	15.61	0.00	56.25	14	1.61	0.58	0.61	2.71	14
	LONE	43.28	15.95	17.60	74.27	13	21.10	6.55	8.90	33.37	13	1.41	0.47	0.70	2.32	13
	NWAL	61.86	30.33	13.22	115.33	14	27.49	9.78	17.48	45.13	14	2.42	1.12	0.48	4.28	14
Construction	GOLF	32.38	20.65	5.70	79.86	14	14.60	4.88	8.58	23.52	14	1.18	0.86	0.21	3.61	14
	LONM	76.45	27.56	22.40	118.18	14	24.22	11.03	8.90	47.67	14	2.86	1.18	0.60	5.94	14
	DONO	51.03	47.25	20.32	208.36	14	31.17	14.26	9.85	60.70	14	1.27	0.75	0.55	3.15	14
	NECD	35.80	14.12	16.54	71.87	14	24.06	8.57	9.85	38.46	14	1.22	0.68	0.60	3.30	14
	CINN	26.16	9.58	10.97	39.76	14	17.18	5.61	8.90	30.19	14	0.83	0.31	0.35	1.45	14
	NCOV	48.11	28.92	13.12	134.93	14	25.52	7.70	12.39	36.23	14	1.82	1.28	0.53	5.67	14
	MARK	29.24	11.29	5.18	45.52	14	20.09	8.44	8.26	39.41	14	1.10	0.58	0.09	2.32	14
	GROW	33.18	12.14	10.43	56.48	14	20.86	9.55	8.90	45.13	14	1.16	0.58	0.33	2.86	14
	CLIF	38.03	19.60	12.86	85.44	14	25.52	9.22	9.85	42.59	14	1.46	0.90	0.33	4.09	14
	PECO	40.51	15.58	12.99	75.17	14	28.60	10.25	8.26	47.67	14	1.54	0.59	0.56	2.72	14
Commercial	BEMI	29.61	9.59	13.64	50.14	14	16.59	6.04	4.45	25.11	14	1.04	0.60	0.43	2.84	14
	WALN	30.62	12.18	7.87	55.65	14	17.41	6.01	8.90	29.56	14	1.02	0.57	0.23	2.57	14
	MICH	37.39	12.64	14.45	66.02	14	32.35	7.53	19.70	49.58	14	1.23	0.61	0.46	2.82	14
	MCDA	32.61	10.22	9.19	48.76	14	27.24	9.39	12.39	44.18	14	1.17	0.55	0.26	2.64	14
	ECHA	32.69	20.23	8.66	86.95	14	25.33	18.46	4.45	69.60	14	1.11	0.79	0.00	3.12	14
Residential	EFER	26.14	8.44	13.08	43.13	14	15.37	7.70	0.00	31.46	14	1.08	0.60	0.38	2.73	14
	NOCO	31.64	10.23	7.76	45.92	14	21.38	6.90	12.71	31.46	14	1.19	0.39	0.43	2.03	14
	HAMI	35.38	8.05	18.50	46.80	14	35.44	12.60	21.61	67.38	14	1.16	0.48	0.49	2.51	14
Vacant Land	LOSS	39.07	24.35	13.91	107.08	14	16.75	6.94	8.26	34.01	14	1.53	1.12	0.48	4.36	14
	BILL	27.01	9.35	9.69	45.08	14	15.98	5.45	8.58	26.06	14	0.99	0.46	0.37	2.20	14
	VAND	29.38	10.15	14.25	47.92	14	14.35	5.49	4.45	26.38	14	0.97	0.46	0.41	2.02	14
	SWLC	23.90	8.78	11.13	43.81	14	21.20	9.43	8.58	35.28	14	0.89	0.49	0.36	2.23	14
	NWCP	24.85	10.28	7.23	50.78	14	18.02	5.01	8.58	26.38	14	1.04	0.71	0.37	3.33	14
	CRAI	36.11	12.28	15.86	53.91	14	22.54	7.88	8.58	36.23	14	1.35	0.59	0.54	2.46	14
	THUN	28.41	11.76	14.19	62.74	14	21.36	6.62	8.90	34.32	14	1.09	0.58	0.31	2.83	14
	LASV	32.81	10.23	13.91	48.27	14	23.25	8.70	8.58	41.00	14	1.27	0.50	0.47	2.52	14

6-45

Table 6-10 (continued)
Statistical Summary of PM$_{10}$ Mass and Chemical Compositions
Acquired during Intensive Monitoring Periods at Saturation Monitoring Sites

Site Type	Site	Silicon (µg/m³)					Sulfur (µg/m³)					Potassium (µg/m³)				
		Average	Std. Dev.	Minimum	Maximum	No. in Average	Average	Std. Dev.	Minimum	Maximum	No. in Average	Average	Std. Dev.	Minimum	Maximum	No. in Average
Industrial	LAMB	6.54	2.52	2.31	11.78	14	0.46	0.25	0.17	1.03	14	0.41	0.14	0.19	0.64	14
	LONE	5.97	2.04	2.74	9.52	13	0.55	0.26	0.19	1.10	13	0.37	0.12	0.19	0.63	13
	NWAL	9.43	4.61	1.64	16.85	14	0.57	0.28	0.17	1.12	14	0.71	0.35	0.13	1.33	14
Construction	GOLF	4.43	3.26	0.58	13.27	14	0.40	0.25	0.11	1.00	14	0.33	0.23	0.03	0.95	14
	LONM	11.01	4.57	2.60	22.81	14	0.44	0.20	0.20	1.03	14	0.80	0.32	0.14	1.62	14
	DONO	5.37	3.42	2.30	14.39	14	0.39	0.21	0.15	0.91	14	0.38	0.22	0.19	0.93	14
	NECD	4.61	2.62	2.07	12.15	14	0.41	0.21	0.15	0.84	14	0.37	0.19	0.18	0.91	14
	CINN	3.31	1.24	1.36	5.43	14	0.36	0.23	0.13	0.95	14	0.26	0.11	0.07	0.45	14
	NCOV	7.05	5.29	1.74	23.55	14	0.53	0.30	0.19	1.22	14	0.61	0.40	0.14	1.77	14
	MARK	4.21	1.98	0.26	7.79	14	0.40	0.24	0.01	0.93	14	0.34	0.16	0.00	0.66	14
	GROW	4.27	1.91	1.19	9.49	14	0.44	0.22	0.14	0.83	14	0.35	0.14	0.10	0.72	14
	CLIF	5.38	3.18	1.07	14.28	14	0.49	0.26	0.07	1.04	14	0.46	0.26	0.12	1.20	14
	PECO	5.70	2.06	1.78	9.73	14	0.49	0.21	0.17	0.88	14	0.47	0.18	0.13	0.85	14
Commercial	BEMI	4.05	2.03	1.63	9.98	14	0.41	0.24	0.15	1.04	14	0.31	0.17	0.12	0.81	14
	WALN	3.94	2.03	1.30	9.44	14	0.40	0.20	0.16	0.73	14	0.31	0.16	0.08	0.73	14
	MICH	4.82	2.24	2.10	10.70	14	0.44	0.22	0.15	0.96	14	0.36	0.16	0.15	0.76	14
	MCDA	4.33	1.76	1.18	8.72	14	0.47	0.23	0.17	1.05	14	0.36	0.14	0.09	0.70	14
	ECHA	4.10	2.98	0.03	11.90	14	0.54	0.35	0.01	1.17	14	0.35	0.24	0.02	1.00	14
Residential	EFER	3.93	1.94	1.47	9.20	14	0.41	0.23	0.15	0.97	14	0.33	0.17	0.12	0.79	14
	NOCO	4.47	1.45	1.25	7.06	14	0.41	0.22	0.17	0.97	14	0.36	0.12	0.11	0.63	14
	HAMI	4.35	1.61	2.10	8.66	14	0.45	0.21	0.20	1.00	14	0.34	0.12	0.18	0.71	14
Vacant Land	LOSS	6.04	4.51	1.82	18.96	14	0.37	0.21	0.12	0.88	14	0.45	0.29	0.17	1.14	14
	BILL	3.80	1.59	1.48	7.17	14	0.37	0.19	0.15	0.79	14	0.29	0.12	0.09	0.58	14
	VAND	3.74	1.62	1.60	6.72	14	0.38	0.26	0.11	1.04	14	0.28	0.13	0.11	0.56	14
	SWLC	3.27	1.74	1.30	7.49	14	0.37	0.23	0.12	0.93	14	0.26	0.15	0.08	0.64	14
	NWCP	3.74	2.31	1.13	11.08	14	0.40	0.22	0.13	0.96	14	0.30	0.19	0.10	0.92	14
	CRAI	4.98	2.12	1.90	8.62	14	0.43	0.25	0.09	0.99	14	0.39	0.17	0.13	0.69	14
	THUN	4.14	2.21	1.84	11.22	14	0.41	0.23	0.15	1.00	14	0.33	0.16	0.14	0.83	14
	LASV	4.54	1.73	1.74	8.72	14	0.42	0.23	0.16	1.01	14	0.38	0.13	0.16	0.69	14

Table 6-10 (continued)

Statistical Summary of PM$_{10}$ Mass and Chemical Compositions

Acquired during Intensive Monitoring Periods at Saturation Monitoring Sites

Site Type	Site	Calcium (µg/m³)					Iron (µg/m³)				
		Average	Std. Dev.	Minimum	Maximum	No. in Average	Average	Std. Dev.	Minimum	Maximum	No. in Average
Industrial	LAMB	9.61	4.51	2.80	19.51	14	0.77	0.32	0.19	1.35	14
	LONE	9.39	4.69	3.35	17.21	13	0.82	0.33	0.21	1.28	13
	NWAL	12.68	6.51	2.20	22.07	14	1.12	0.55	0.27	1.97	14
Construction	GOLF	5.79	4.03	0.55	14.18	14	0.56	0.36	0.00	1.52	14
	LONM	13.64	5.93	4.55	26.87	14	1.27	0.53	0.36	2.67	14
	DONO	7.54	4.23	3.12	19.40	14	0.69	0.34	0.31	1.54	14
	NECD	5.66	2.51	2.59	12.96	14	0.70	0.37	0.31	1.71	14
	CINN	3.93	1.85	1.56	7.00	14	0.43	0.22	0.03	0.74	14
	NCOV	8.14	6.40	2.18	28.55	14	0.97	0.58	0.22	2.63	14
	MARK	4.69	2.35	0.22	9.49	14	0.60	0.31	0.00	0.93	14
	GROW	5.32	2.49	1.50	9.11	14	0.62	0.30	0.23	1.29	14
	CLIF	5.89	3.25	1.76	12.58	14	0.82	0.42	0.09	1.70	14
	PECO	6.28	3.02	2.12	13.30	14	0.84	0.30	0.34	1.46	14
Commercial	BEMI	4.72	1.72	2.13	7.73	14	0.59	0.30	0.15	1.32	14
	WALN	4.61	2.35	1.61	10.20	14	0.58	0.24	0.15	1.12	14
	MICH	5.70	2.10	2.96	9.94	14	0.70	0.27	0.36	1.36	14
	MCDA	4.60	1.99	1.38	8.08	14	0.68	0.26	0.31	1.08	14
	ECHA	3.87	3.11	0.07	12.40	14	0.73	0.53	0.10	2.24	14
Residential	EFFER	4.01	1.68	1.67	6.62	14	0.57	0.34	0.00	1.37	14
	NOCO	4.90	2.05	1.37	8.17	14	0.64	0.24	0.23	0.96	14
	HAMI	5.37	1.76	2.85	7.77	14	0.73	0.25	0.35	1.23	14
Vacant Land	LOSS	7.09	5.70	2.07	25.59	14	0.66	0.48	0.12	1.89	14
	BILL	4.42	2.06	1.89	9.07	14	0.54	0.17	0.26	0.79	14
	VAND	4.68	1.91	1.93	9.73	14	0.53	0.27	0.10	0.94	14
	SWLC	3.50	1.94	1.82	8.96	14	0.45	0.32	0.05	1.19	14
	NWCP	3.83	1.55	1.40	7.22	14	0.53	0.33	0.04	1.37	14
	CRAI	6.61	2.75	2.53	11.28	14	0.68	0.35	0.08	1.15	14
	THUN	4.33	1.77	2.18	8.58	14	0.57	0.35	0.05	1.44	14
	LASV	5.24	2.32	1.89	9.54	14	0.71	0.30	0.19	1.27	14

industrial site. Maximum sulfur concentrations are also similar in magnitude, in the range of 0.8 to 1.2 $\mu g/m^3$.

Average b_{abs} concentrations varied by a factor of two from site to site. The highest b_{abs} average of 32.4 ± 7.5 Mm^{-1} was recorded at the MICH commercial site. This site is located in the parking lot of a convenience store near a gas station with frequent truck traffic. Maximum b_{abs} of 69.6 ± 10.8 Mm^{-1} was found at the East Charleston commercial site on 01/27/96, where heavy vehicle traffic is expected. Vehicle exhaust from these sites resulted in the elevated b_{abs} values.

Figure 6-18 compares the site-to-site variations in material balance on: 1) a windy day (06/05/95) with highest average all-site PM_{10} concentration of 52.8 ± 19.1 $\mu g/m^3$, and 2) a low-wind day (09/11/95) with second-highest average all-site PM_{10} concentration of 47.3 ± 15.8 $\mu g/m^3$. Although the wind speeds on 06/05/95 (average and maximum wind speeds were 11 and 17.5 m/s, respectively) were a factor of three to four higher than those observed on 09/11/95 (average and maximum wind speeds were 3 and 4.5 m/s, respectively), the site averages for PM_{10} mass only vary by approximately 10%.

The material balance in Figure 6-18 exhibits a 59% to 83% crustal abundance on 06/05/95 and 52% to 71% crustal abundance on 09/11/95. PM_{10} secondary sulfate ranged from 3% to 11% and combustion byproducts ranged from 1% to 5% on these two days. This illustration shows that the incremental PM_{10} mass from the windy day can be attributed to contributions from geological material. The absolute difference in crustal abundances among all satellite sites on these two days is approximately 60 $\mu g/m^3$, which varies by approximately a factor of four on a low-wind day (09/11/95) to a factor of seven on a windy day (06/05/95). This analysis also demonstrates that site-to-site variations are significantly greater than day-to-day variations with respect to PM_{10} mass and chemistry in the saturation monitoring network. Besides the meteorology, local source impacts are superimposed to enhance the site-to-site variations.

6.6   Homogeneity Measurements

Several types of analysis can be applied to quantify how well measurements at a single site represent concentrations measured at the other sites. These are termed "homogeneity measurements" (Watson *et al.*, 1995). Within the study domain, the centrally-located BEMI (Bemis) monitoring site is selected a as a benchmark, to which all other site data are compared on a record-by-record basis. This analysis examines the spatial homogeneity of the PM_{10} mass concentration distribution.

To quantitatively evaluate the homogeneity within the study domain, a variance-weighted regression-based comparison is made, which is analogous to applications in
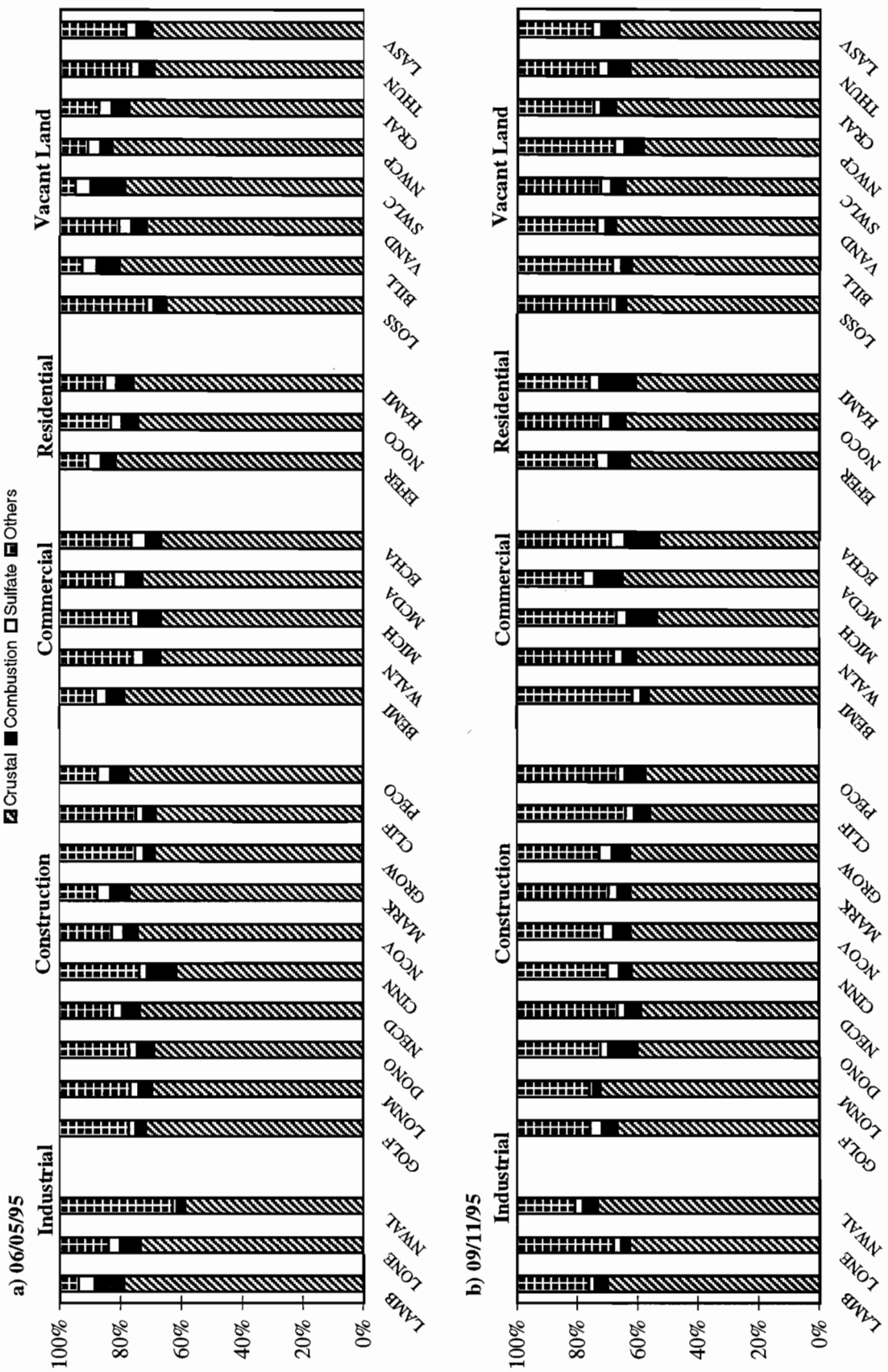
Figure 6-18 Material balance for PM_{10} measurements aquired at the saturation monitoring network on: a) a high wind speed day (06/05/95), and b) a low wind speed day (09/11/95).

collocated sampler comparisons discussed in Section 5.5. These comparisons are summarized in Table 6-11.

The slopes, intercepts, and correlation coefficients were derived from the effective-variance-weighted least-squares linear regression algorithm (Watson *et al.*, 1984). The effective-variance method incorporates the precisions of both X and Y variables into the weighing of each value. It also propagates the precisions to provide the standard errors which are reported with each slope and intercept in Table 6-11. These linear regression parameters provide a means to calculate one measurement from another within a few intervals of measurement precision.

Table 6-11 shows that PM_{10} mass correlations between Bemis and the satellite sites were lowest at the CINN construction site ($r = 0.65$), with high correlations ($r > 0.8$) at two construction sites (i.e., NCOV, CLIF), four commercial sites (i.e., BEMI, WALN, MICH, MCDA), two residential sites (i.e., EFER, NOCO), and four vacant land sites (i.e., BILL, VAND, NWCP, THUN). Moderate correlations ($0.6 < r < 0.8$) were found at all the other sites. The slopes were equal to unity within the standard errors for only 43% of the sites. The intercepts are often associated with large standard errors.

The average Y/X ratio is a factor of two higher than unity for the industrial sites (i.e., LAMB, LONE, NWAL) and two construction site (i.e., LONM, GROW). This implies that the PM_{10} concentrations found at the Bemis site are, on average, 50% to 240% lower than these sites. The large variability associated with the average ratios at these sites is attributable to a few extremely high PM_{10} concentrations.

The average of the pair differences (Y-X) between the Bemis and satellite sites, the collocated precision (the standard deviation of the paired differences), and the root mean squared (RMS) precision (the square root of the mean squared precision) in Table 6-10 can be used to test the hypothesis that no difference was found between the X and Y pairs. This table shows that differences in PM_{10} mass were found at all sites, and they are not considered to be equivalent.

The percent difference of the data pairs whose difference (Bemis [X] minus satellite site [Y]) is less than 1σ, between 1σ and 2σ, between 2σ and 3σ, and greater than 3σ. Here, σ is the measurement uncertainty of "X-Y", which is the square root of the sum of the squared uncertainties ($\sigma_X^2 + \sigma_Y^2$), where σ_X and σ_Y are the PM_{10} measurement uncertainties for the Bemis and satellite sites, respectively.

Over 90% of the sample pairs are within $\pm 1\sigma$ for one commercial site (i.e., WALN), one residential site (i.e., ERER), and four vacant land sites (i.e., BILL, VAND, NWCP, THUN). Except for the BILL vacant land site (approximately 0.35 km northwest-west

Table 6-11

Intersampler Comparison of PM$_{10}$ Concentrations at the Bemis and East Charleston Sites

Sampler[a] Y	X	Slope[b] (μg/m³)	Intercept[c] (μg/m³)	Correlation Coefficient[d] (r)	No. of Pairs	Avg. Ratio[e]	Distribution[f] <1σ	1-2σ	2-3σ	>3σ	Average[g] Difference (μg/m³)	Std.Dev. Avg.Diff (μg/m³)	Precision (μg/m³) RMSE$_Y$	RMSE$_X$
LAMB	BEMI	1.37 ± 0.09	5.01 ± 2.31	0.72	26	1.79 ± 1.02	13	6	2	5	14.271 ±	15.588	3.444	2.911
LONE	BEMI	1.07 ± 0.08	8.12 ± 1.98	0.69	25	1.70 ± 1.07	15	3	6	1	11.215 ±	13.702	3.231	2.891
NWAL	BEMI	1.76 ± 0.11	5.41 ± 2.75	0.71	26	2.17 ± 0.89	7	9	3	7	24.740 ±	21.214	3.850	2.911
GOLF	BEMI	1.21 ± 0.08	-6.26 ± 2.19	0.77	25	1.00 ± 0.49	15	7	3	0	0.620 ±	11.211	3.825	2.897
LONM	BEMI	1.93 ± 0.12	10.33 ± 3.03	0.65	26	2.40 ± 1.20	11	3	1	11	29.513 ±	27.357	4.084	2.911
DONO	BEMI	1.01 ± 0.08	5.05 ± 1.98	0.78	25	1.40 ± 0.68	19	4	2	0	6.246 ±	9.349	3.332	2.891
NECD	BEMI	0.99 ± 0.07	5.09 ± 1.93	0.77	26	1.33 ± 0.42	17	7	2	0	7.152 ±	9.964	3.729	2.911
CINN	BEMI	0.47 ± 0.06	12.88 ± 1.45	0.43	26	1.37 ± 0.84	18	6	2	0	3.377 ±	14.882	3.005	2.911
NCOV	BEMI	1.34 ± 0.09	-0.47 ± 2.23	0.83	25	1.21 ± 0.42	18	2	3	2	5.426 ±	10.671	3.159	2.933
MARK	BEMI	0.74 ± 0.07	7.62 ± 1.72	0.62	25	1.25 ± 0.82	18	5	1	1	1.916 ±	10.893	3.003	2.895
GROW	BEMI	0.76 ± 0.07	9.14 ± 1.78	0.66	25	1.57 ± 2.24	21	2	0	2	4.026 ±	10.600	3.061	2.896
CLIF	BEMI	1.33 ± 0.09	-0.72 ± 2.21	0.81	26	1.46 ± 0.64	17	6	2	1	9.182 ±	12.956	3.250	2.911
PECO	BEMI	1.26 ± 0.08	0.49 ± 2.14	0.78	26	1.25 ± 0.51	19	2	2	3	5.436 ±	11.504	3.095	2.911
WALN	BEMI	0.91 ± 0.07	3.13 ± 1.78	0.87	26	1.16 ± 0.46	24	2	0	0	1.617 ±	6.121	2.948	2.911
MICH	BEMI	1.04 ± 0.08	5.22 ± 1.91	0.83	26	1.41 ± 0.45	21	3	1	1	7.249 ±	7.309	3.100	2.911
MCDA	BEMI	0.91 ± 0.07	4.24 ± 1.80	0.80	26	1.10 ± 0.36	22	2	2	0	0.973 ±	6.971	2.997	2.911
ECHA	BEMI	0.84 ± 0.07	2.89 ± 1.71	0.63	25	1.09 ± 0.71	20	3	1	1	0.484 ±	14.504	3.073	2.937
EFER	BEMI	0.74 ± 0.06	3.37 ± 1.65	0.87	26	0.97 ± 0.37	23	3	0	0	-2.476 ±	5.134	2.952	2.911
NOCO	BEMI	0.97 ± 0.07	2.61 ± 1.84	0.85	26	1.09 ± 0.38	22	4	0	0	0.897 ±	6.210	2.998	2.911
HAMI	BEMI	0.81 ± 0.07	9.02 ± 1.77	0.72	26	1.26 ± 0.43	21	2	2	1	3.965 ±	7.769	3.066	2.911
LOSS	BEMI	1.10 ± 0.08	2.20 ± 2.07	0.66	26	1.41 ± 0.83	18	5	1	2	7.108 ±	15.884	3.435	2.911
BILL	BEMI	0.85 ± 0.07	1.84 ± 1.73	0.89	26	0.98 ± 0.37	24	2	0	0	-2.050 ±	5.072	2.934	2.911
VAND	BEMI	0.91 ± 0.07	1.35 ± 1.77	0.85	25	1.01 ± 0.28	23	1	1	0	-0.579 ±	5.733	3.034	2.884
SWLC	BEMI	0.59 ± 0.06	5.27 ± 1.58	0.72	26	0.96 ± 0.46	23	2	1	0	-3.612 ±	6.825	3.041	2.911
NWCP	BEMI	0.72 ± 0.06	2.98 ± 1.70	0.88	26	0.95 ± 0.43	23	3	0	0	-3.296 ±	4.993	3.033	2.911
CRAI	BEMI	1.04 ± 0.08	4.02 ± 1.94	0.78	26	1.30 ± 0.47	19	5	1	1	5.410 ±	9.581	3.354	2.911
THUN	BEMI	0.89 ± 0.07	0.96 ± 1.92	0.89	26	0.98 ± 0.27	24	2	0	0	-1.311 ±	5.287	3.507	2.911
LASV	BEMI	0.85 ± 0.07	5.34 ± 1.78	0.75	26	1.10 ± 0.42	21	2	2	1	0.862 ±	7.895	3.050	2.911

[a] POR=Low-volume Portable PM$_{10}$ Survey Sampler; SFS=Medium-volume Sequential Filter Sampler; POR(A)=PM$_{10}$ samples from collocated ABEM site; POR(B)=PM$_{10}$ samples from collocated BEMI site; BAM=Beta Attenuation Monitor.

[b] Regression slope with standard error.

[c] Regression intercept with standard error.

[d] Correlation coefficient.

[e] Average of Y/X and standard deviation of this ratio.

[f] Number of data pairs falling into the specified precision intervals, where each precision interval is equal to root mean square (RMS) of the sum of the squared precisions of the X and Y samplers.

[g] Average of X minus Y.

6-51

of the Bemis site), all of these sites are located within 2.5 km to the northeast, east, southeast, and south-southeast of the Bemis site.

Extending the percent difference of the data pairs to ±2σ, an additional 11 sites meet the criteria for over 90% of the data pairs. They include two residential sites (i.e., NOCO, HAMI), three commercial sites (i.e., MICH, MCDA, ECHA), three vacant land sites (i.e., LOSS, CRAI, LAST), and five construction sites (i.e., DONO, NECD, CINN, GROW, CLIF). All of these sites are situated northwest, west, southwest, and south of the Bemis site, within a distance of 9 km.

The greatest variations were found for the three industrial sites (i.e., LAMB, LONE, NWAL) with 4% to 25% of the data pairs falling beyond ±3σ, and for the LONM construction site where 42% of the data pairs exceeded ±3σ. These are also the sites with average ratios which were a factor of two greater than the Bemis site. Three construction sites (i.e., NCOV, GROW, PECO) and one vacant land site (i.e., LOSS) also reported that 8% to 11% of the data pairs falling beyond ±3σ.

Distributions in absolute PM_{10} concentration differences between the Bemis and satellite sites were also examined for the various intervals between 5 and 20 $\mu g/m^3$. Over 70% of the sample pairs at two residential sites (i.e., EFER, NOCO), one commercial site (i.e., WALN), and two vacant land sites (i.e., VAND, THUN) reported PM_{10} concentrations within ±5 $\mu g/m^3$ of the Bemis PM_{10} concentrations. These sites are within 2.5 km northwest and southwest of the Bemis site. Twenty out of the 29 sites exhibited PM_{10} concentration variations within ±10 $\mu g/m^3$ in 70% of the cases. The largest variation was found at the NWAL industrial site and LONM construction site, where 50% of the sample pairs differed by more than ±20 $\mu g/m^3$.

This homogeneity measure indicates that for over 90% of the cases, PM_{10} concentrations measured at the Bemis site can represent commercial, residential, and vacant land sites up to 2.5 km northeast to south-southeast of the site to within ±1σ of measurement uncertainty. Over 70% of the sample pairs found at two residential, one commercial, and two vacant land sites within 2.5 km northwest and southwest of the Bemis site reported PM_{10} concentrations within ±5 $\mu g/m^3$ of the Bemis PM_{10} concentrations. The same homogeneity distributions do not apply to the nearby industrial or construction sites where fugitive dust emissions are suspected to be high. The sand/gravel operation 0.5 km (i.e., LONE), and 1.5 km (i.e., LAMB) northeast of the Bemis site yielded average PM_{10} concentrations 70% and 79% higher, respectively, than observed at the Bemis site. PM_{10} concentrations at the LONM construction site (2.8 km west of the Bemis site) and the NWAL industrial site (2.6 km southwest of the Bemis site) differed by more than ±20 $\mu g/m^3$ from the Bemis measurements for 50% of the samples. These two sites also reported the highest average ratios, with average

PM_{10} concentrations being a factor of 2.4 and 2.2 higher than the Bemis site for the LONM and NWAL sites, respectively.

Due to intermittent fugitive dust sources interspersed in the study area, this homogeneity analysis shows that PM_{10} measurements at the Bemis site do not represent the general population exposure within the neighborhood scale (1 to 10 km) (Federal Register, 1979). If sufficient control measures can be applied on the locally-generated fugitive dust sources, PM_{10} measurements at the Bemis site can be representative of the surrounding mixture of land uses.

7.0 SOURCE/RECEPTOR MODELING

Various data analysis methods and source/receptor modeling approaches applied to the Las Vegas Valley PM_{10} Study are presented in this section to apportion PM_{10} to sources. Correlation matrices are generated, and multivariate statistical modeling and cluster analyses are performed to examine the spatial patterns of the saturation monitoring network. The source profiles compiled in Section 4, along with the ambient PM_{10} mass and chemical measurements acquired at the Bemis and East Charleston sites, are used as input to the Chemical Mass Balance (CMB) receptor model. CMB modeling was performed for each individual day to identify and quantify major source-type contributions.

Fugitive dust emission rates assembled in Section 3 are used as input to the Industrial Source Complex Short-Term Version 3 (ISCST-3) Gaussian plume dispersion model to calculate the source sub-type contributions from the major fugitive dust sources. The results from various modeling efforts is discussed in this section to reconcile their differences.

7.1 Spatial Receptor Modeling for the Saturation Monitoring Network

The spatial patterns of PM_{10} mass and chemical species acquired at the 30 satellite sites during the spring, summer, fall, and winter intensive monitoring periods are examined. Correlation matrices are developed and cluster analyses are performed to deduce the spatial variations of the PM_{10} components and to illustrate the zones of influence within the saturation monitoring network.

7.1.1 Correlations Among the Satellite Sites

Inter-site correlation coefficients for PM_{10} mass, silicon (Si), sulfur (S), and light absorption (b_{abs}), are displayed in Tables 7-1 to 7-4, respectively. The sites were arranged by their site-type classification in the same north-south and west-east sequences as listed in Section 6 for the time series analysis.

These correlation coefficients show which concentrations changed in the same way over time. Coefficients which exceed 0.80 show a fairly strong covariation; coefficients between 0.50 and 0.80 show a moderate covariation; and coefficients which were less than 0.50 were not considered to be physically significant (though they may be statistically significant). High correlation coefficients were observed when pairs of variables originated from the same source, were equally affected by transport and dispersion, or underwent related chemical transformations.

With respect to PM_{10} mass and silicon concentrations, the highest correlations $(r > 0.80)$ were found for the three residential sites (i.e., EFER, NOCO, HAMI).

Table 7-1

Correlation Matrix for PM$_{10}$ Mass Measurements from the Saturation Monitoring Network

	Industrial							Construction						Commercial					Residential			Vacant Land							
	LAMB	LONE	NWAL	GOLF	LONM	DONO	NECD	CINN	NCOV	MARK	GROW	CLIF	PECO	BEMI	WALN	MICH	MCDA	ECHA	EFER	NOCO	HAMI	LOSS	BILL	VAND	SWLC	NWCP	CRAI	THUN	LASV
LAMB	1.000																												
LONE	0.711	1.000																											
NWAL	0.562	0.266	1.000																										
GOLF	0.487	0.425	0.764	1.000																									
LONM	0.614	0.482	0.522	0.314	1.000																								
DONO	0.292	0.307	0.160	0.409	0.120	1.000																							
NECD	0.527	0.594	0.512	0.625	0.390	0.489	1.000																						
CINN	0.281	0.139	0.212	0.146	0.205	0.144	0.301	1.000																					
NCOV	0.584	0.392	0.805	0.645	0.533	0.197	0.328	0.105	1.000																				
MARK	0.715	0.443	0.490	0.394	0.526	0.170	0.379	0.268	0.385	1.000																			
GROW	0.539	0.472	0.542	0.585	0.531	0.197	0.433	0.170	0.395	0.469	1.000																		
CLIF	0.422	0.453	0.658	0.717	0.345	0.153	0.648	0.534	0.418	0.373	0.572	1.000																	
PECO	0.799	0.663	0.673	0.605	0.808	0.236	0.538	0.334	0.635	0.561	0.689	0.625	1.000																
BEMI	0.697	0.672	0.747	0.784	0.640	0.381	0.811	0.340	0.619	0.592	0.612	0.811	0.783	1.000															
WALN	0.637	0.457	0.746	0.697	0.596	0.284	0.679	0.183	0.477	0.652	0.597	0.651	0.713	0.865	1.000														
MICH	0.586	0.623	0.660	0.711	0.549	0.488	0.872	0.372	0.432	0.504	0.634	0.784	0.703	0.869	0.736	1.000													
MCDA	0.734	0.616	0.734	0.691	0.809	0.265	0.599	0.177	0.650	0.575	0.738	0.617	0.929	0.831	0.767	0.740	1.000												
ECHA	0.558	0.543	0.520	0.443	0.691	0.167	0.412	0.131	0.488	0.428	0.596	0.475	0.740	0.572	0.446	0.647	0.773	1.000											
EFER	0.730	0.739	0.661	0.808	0.627	0.461	0.815	0.217	0.584	0.596	0.687	0.681	0.810	0.893	0.796	0.888	0.845	0.688	1.000										
NOCO	0.752	0.670	0.680	0.677	0.772	0.276	0.665	0.345	0.655	0.582	0.724	0.662	0.917	0.862	0.750	0.782	0.935	0.747	0.881	1.000									
HAMI	0.687	0.607	0.659	0.554	0.800	0.310	0.719	0.198	0.570	0.485	0.639	0.567	0.841	0.790	0.649	0.795	0.909	0.738	0.812	0.875	1.000								
LOSS	0.438	0.407	0.550	0.716	0.399	0.365	0.468	0.149	0.583	0.518	0.416	0.510	0.442	0.671	0.513	0.605	0.550	0.332	0.615	0.552	0.448	1.000							
BILL	0.794	0.770	0.627	0.705	0.726	0.323	0.682	0.348	0.582	0.594	0.724	0.699	0.919	0.895	0.788	0.787	0.918	0.691	0.895	0.956	0.814	0.583	1.000						
VAND	0.711	0.595	0.622	0.575	0.740	0.420	0.698	0.334	0.593	0.593	0.516	0.554	0.700	0.877	0.778	0.740	0.700	0.487	0.793	0.768	0.709	0.572	0.787	1.000					
SWLC	0.602	0.568	0.563	0.496	0.749	0.270	0.682	0.209	0.456	0.542	0.625	0.515	0.660	0.799	0.733	0.703	0.766	0.561	0.717	0.745	0.741	0.545	0.776	0.853	1.000				
NWCP	0.610	0.603	0.691	0.808	0.581	0.289	0.718	0.121	0.514	0.561	0.777	0.757	0.760	0.899	0.850	0.792	0.867	0.595	0.888	0.839	0.773	0.561	0.868	0.722	0.757	1.000			
CRAI	0.825	0.637	0.548	0.580	0.549	0.521	0.717	0.275	0.526	0.670	0.565	0.419	0.681	0.772	0.673	0.673	0.752	0.434	0.765	0.760	0.746	0.578	0.786	0.758	0.749	0.696	1.000		
THUN	0.653	0.629	0.723	0.816	0.553	0.312	0.772	0.125	0.559	0.540	0.683	0.696	0.708	0.900	0.817	0.773	0.827	0.496	0.873	0.768	0.772	0.604	0.810	0.734	0.756	0.930	0.772	1.000	
LASV	0.638	0.578	0.651	0.559	0.864	0.191	0.626	0.064	0.608	0.545	0.660	0.474	0.793	0.794	0.701	0.690	0.898	0.712	0.784	0.855	0.901	0.533	0.810	0.785	0.869	0.797	0.723	0.799	1.000

Table 7-2

Correlation Matrix for PM$_{10}$ Silicon Measurements from the Saturation Monitoring Network

| | Industrial | | | | | | Construction | | | | | | Commercial | | | | | Residential | | | | | | Vacant Land | | | | |
	LAMB	LONE	NWAL	GOLF	LONM	DONO	NECD	CINN	NCOV	MARK	GROW	CLIF	PECO	BEMI	WALN	MICH	MCDA	ECHA	EFER	NOCO	HAMI	LOSS	BILL	VAND	SWLC	NWCP	CRAI	THUN	LASV
LAMB	1.000																												
LONE	0.628	1.000																											
NWAL	0.523	-0.017	1.000																										
GOLF	0.547	0.525	0.565	1.000																									
LONM	0.216	-0.096	0.263	-0.080	1.000																								
DONO	0.338	0.320	0.238	0.683	-0.253	1.000																							
NECD	0.348	0.429	0.271	0.870	-0.096	0.811	1.000																						
CINN	0.402	0.349	0.176	0.288	0.219	0.440	0.177	1.000																					
NCOV	0.379	0.026	0.673	0.457	-0.069	0.210	0.179	0.122	1.000																				
MARK	0.551	0.420	0.569	0.760	0.063	0.506	0.658	0.423	0.209	1.000																			
GROW	0.604	0.471	0.544	0.868	0.255	0.556	0.827	0.216	0.185	0.777	1.000																		
CLIF	0.583	0.530	0.459	0.929	-0.106	0.535	0.808	0.163	0.309	0.728	0.858	1.000																	
PECO	0.831	0.533	0.548	0.709	0.341	0.391	0.533	0.511	0.355	0.613	0.754	0.752	1.000																
BEMI	0.484	0.477	0.530	0.963	-0.048	0.683	0.903	0.222	0.360	0.803	0.900	0.914	0.631	1.000															
WALN	0.344	0.355	0.463	0.785	-0.004	0.599	0.813	0.227	0.083	0.866	0.854	0.771	0.524	0.887	1.000														
MICH	0.428	0.338	0.412	0.852	0.049	0.768	0.933	0.291	0.143	0.788	0.845	0.808	0.629	0.873	0.828	1.000													
MCDA	0.614	0.437	0.443	0.828	0.251	0.594	0.823	0.366	0.186	0.704	0.916	0.873	0.858	0.848	0.792	0.855	1.000												
ECHA	0.528	0.344	0.120	0.395	0.264	0.265	0.482	0.253	0.169	0.398	0.418	0.482	0.686	0.359	0.287	0.572	0.620	1.000											
EFER	0.469	0.466	0.430	0.901	0.000	0.705	0.918	0.356	0.225	0.826	0.850	0.877	0.715	0.916	0.882	0.951	0.896	0.605	1.000										
NOCO	0.591	0.498	0.356	0.716	0.364	0.471	0.710	0.466	0.144	0.729	0.857	0.711	0.832	0.714	0.729	0.749	0.880	0.640	0.806	1.000									
HAMI	0.345	0.133	0.541	0.778	0.076	0.631	0.766	0.096	0.188	0.544	0.857	0.753	0.546	0.808	0.760	0.751	0.801	0.121	0.710	0.601	1.000								
LOSS	0.283	0.157	0.368	0.635	-0.050	0.413	0.497	0.305	0.401	0.558	0.453	0.541	0.291	0.620	0.393	0.539	0.434	0.149	0.505	0.284	0.424	1.000							
BILL	0.739	0.646	0.411	0.864	0.139	0.684	0.811	0.494	0.208	0.758	0.909	0.860	0.844	0.863	0.769	0.816	0.934	0.512	0.857	0.865	0.743	0.503	1.000						
VAND	0.317	0.367	0.290	0.662	-0.013	0.653	0.734	0.344	0.281	0.711	0.618	0.577	0.352	0.794	0.760	0.680	0.618	0.308	0.722	0.561	0.473	0.548	0.671	1.000					
SWLC	0.306	0.284	0.312	0.698	0.013	0.654	0.819	0.264	0.126	0.722	0.747	0.693	0.455	0.842	0.893	0.778	0.793	0.357	0.826	0.647	0.693	0.489	0.752	0.894	1.000				
NWCP	0.419	0.437	0.402	0.898	-0.020	0.649	0.933	0.071	0.198	0.713	0.913	0.911	0.615	0.953	0.880	0.889	0.878	0.435	0.910	0.745	0.832	0.436	0.835	0.717	0.826	1.000			
CRAI	0.502	0.383	0.395	0.721	0.184	0.812	0.777	0.463	0.163	0.622	0.809	0.571	0.540	0.752	0.693	0.750	0.735	0.200	0.683	0.696	0.781	0.499	0.837	0.674	0.707	0.704	1.000		
THUN	0.397	0.405	0.476	0.906	0.002	0.645	0.902	0.077	0.217	0.678	0.923	0.888	0.591	0.956	0.877	0.848	0.858	0.289	0.869	0.689	0.904	0.465	0.825	0.673	0.809	0.975	0.747	1.000	
LASV	0.249	0.045	0.361	0.472	0.450	0.141	0.572	-0.109	0.091	0.485	0.717	0.560	0.485	0.607	0.674	0.570	0.735	0.478	0.607	0.657	0.601	0.225	0.534	0.527	0.727	0.696	0.415	0.671	1.000

Table 7-3

Correlation Matrix for PM$_{10}$ Sulfur Measurements from the Saturation Monitoring Network

	Industrial			Construction										Commercial					Residential						Vacant Land				
	LAMB	LONE	NWAL	GOLF	LONM	DONO	NECD	CINN	NCOV	MARK	GROW	CLIF	PECO	BEMI	WALN	MICH	MCDA	ECHA	EFER	NOCO	HAMI	LOSS	BILL	VAND	SWLC	NWCP	CRAI	THUN	LASV
LAMB	1.000																												
LONE	0.853	1.000																											
NWAL	0.844	0.761	1.000																										
GOLF	0.956	0.868	0.843	1.000																									
LONM	0.912	0.801	0.801	0.927	1.000																								
DONO	0.948	0.723	0.800	0.920	0.878	1.000																							
NECD	0.954	0.767	0.747	0.936	0.881	0.930	1.000																						
CINN	0.741	0.784	0.770	0.850	0.789	0.743	0.630	1.000																					
NCOV	0.933	0.921	0.868	0.978	0.913	0.873	0.896	0.845	1.000																				
MARK	0.947	0.860	0.896	0.953	0.876	0.884	0.887	0.819	0.932	1.000																			
GROW	0.886	0.884	0.791	0.924	0.832	0.816	0.843	0.799	0.949	0.911	1.000																		
CLIF	0.950	0.868	0.844	0.972	0.860	0.915	0.927	0.814	0.954	0.937	0.893	1.000																	
PECO	0.913	0.815	0.886	0.913	0.820	0.880	0.857	0.797	0.921	0.880	0.857	0.957	1.000																
BEMI	0.963	0.851	0.840	0.979	0.955	0.942	0.942	0.812	0.949	0.950	0.893	0.949	0.876	1.000															
WALN	0.878	0.716	0.701	0.884	0.814	0.851	0.933	0.597	0.838	0.881	0.872	0.859	0.760	0.905	1.000														
MICH	0.972	0.836	0.888	0.972	0.933	0.946	0.935	0.816	0.951	0.977	0.914	0.946	0.910	0.977	0.897	1.000													
MCDA	0.953	0.844	0.885	0.946	0.925	0.927	0.873	0.860	0.938	0.927	0.882	0.947	0.955	0.947	0.804	0.960	1.000												
ECHA	0.611	0.566	0.448	0.575	0.625	0.550	0.562	0.537	0.598	0.539	0.534	0.588	0.649	0.534	0.369	0.603	0.656	1.000											
EFER	0.972	0.855	0.841	0.987	0.934	0.945	0.948	0.829	0.954	0.968	0.913	0.964	0.906	0.988	0.910	0.989	0.958	0.592	1.000										
NOCO	0.926	0.896	0.884	0.967	0.927	0.895	0.875	0.880	0.981	0.948	0.931	0.944	0.913	0.958	0.831	0.967	0.960	0.630	0.962	1.000									
HAMI	0.949	0.827	0.899	0.943	0.947	0.943	0.900	0.800	0.936	0.915	0.851	0.922	0.903	0.971	0.837	0.959	0.964	0.526	0.953	0.952	1.000								
LOSS	0.928	0.805	0.837	0.965	0.914	0.930	0.933	0.814	0.923	0.943	0.870	0.943	0.871	0.979	0.908	0.969	0.917	0.506	0.978	0.937	0.939	1.000							
BILL	0.976	0.865	0.852	0.976	0.913	0.950	0.949	0.798	0.964	0.957	0.944	0.966	0.923	0.978	0.917	0.984	0.957	0.578	0.985	0.964	0.954	0.962	1.000						
VAND	0.871	0.749	0.710	0.906	0.911	0.886	0.863	0.790	0.850	0.887	0.850	0.852	0.745	0.952	0.900	0.916	0.871	0.459	0.934	0.889	0.887	0.942	0.917	1.000					
SWLC	0.860	0.687	0.637	0.848	0.863	0.898	0.859	0.698	0.787	0.830	0.808	0.817	0.728	0.910	0.897	0.881	0.854	0.476	0.901	0.836	0.860	0.893	0.896	0.970	1.000				
NWCP	0.958	0.829	0.790	0.968	0.925	0.928	0.965	0.739	0.933	0.940	0.889	0.935	0.843	0.981	0.941	0.963	0.908	0.518	0.978	0.935	0.940	0.954	0.967	0.930	0.902	1.000			
CRAI	0.947	0.781	0.846	0.942	0.908	0.965	0.943	0.747	0.919	0.917	0.886	0.913	0.871	0.966	0.912	0.970	0.918	0.488	0.960	0.925	0.958	0.966	0.974	0.915	0.899	0.949	1.000		
THUN	0.942	0.845	0.827	0.959	0.932	0.931	0.920	0.805	0.932	0.939	0.894	0.938	0.860	0.992	0.917	0.961	0.938	0.475	0.975	0.949	0.965	0.972	0.972	0.964	0.932	0.972	0.961	1.000	
LASV	0.863	0.788	0.753	0.885	0.940	0.854	0.853	0.755	0.877	0.861	0.862	0.841	0.781	0.939	0.879	0.908	0.894	0.522	0.913	0.915	0.918	0.913	0.915	0.957	0.939	0.914	0.909	0.956	1.000

Table 7-4

Correlation Matrix for PM$_{10}$ b$_{abs}$ Measurements from the Saturation Monitoring Network

	Industrial								Construction						Commercial					Residential						Vacant Land				
	LAMB	LONE	NWAL	GOLF	LONM	DONO	NECD	CINN	NCOV	MARK	GROW	CLIF	PECO	BEMI	WALN	MICH	MCDA	ECHA	EFER	NOCO	HAMI	LOSS	BILL	VAND	SWLC	NWCP	CRAI	THUN	LASV
LAMB	1.000																												
LONE	0.547	1.000																											
NWAL	0.709	0.224	1.000																										
GOLF	0.727	0.434	0.443	1.000																									
LONM	0.287	0.237	0.697	0.244	1.000																								
DONO	0.658	0.426	0.093	0.618	-0.122	1.000																							
NECD	0.673	0.515	0.554	0.788	0.542	0.387	1.000																						
CINN	0.467	0.522	0.564	0.274	0.689	0.093	0.633	1.000																					
NCOV	0.516	-0.183	0.806	0.277	0.531	0.091	0.269	0.245	1.000																				
MARK	0.348	0.198	0.551	0.420	0.631	0.120	0.380	0.506	0.430	1.000																			
GROW	0.176	-0.029	0.598	-0.027	0.719	-0.025	0.217	0.232	0.579	0.407	1.000																		
CLIF	0.769	0.359	0.481	0.771	0.098	0.643	0.458	0.211	0.427	0.463	0.019	1.000																	
PECO	0.393	-0.245	0.684	0.154	0.511	0.170	0.303	0.268	0.734	0.252	0.745	0.291	1.000																
BEMI	0.573	0.361	0.578	0.625	0.469	0.192	0.806	0.464	0.395	0.415	0.200	0.235	0.144	1.000															
WALN	0.458	0.436	0.473	0.693	0.586	0.369	0.774	0.431	0.220	0.671	0.470	0.502	0.313	0.595	1.000														
MICH	0.624	0.548	0.407	0.526	0.359	0.570	0.661	0.484	0.275	0.330	0.353	0.579	0.401	0.341	0.590	1.000													
MCDA	0.468	-0.096	0.774	0.175	0.654	0.120	0.355	0.375	0.791	0.339	0.774	0.311	0.952	0.230	0.334	0.444	1.000												
ECHA	0.153	-0.004	0.066	0.039	0.366	0.212	0.253	0.162	0.208	-0.161	0.393	0.033	0.470	-0.107	0.095	0.436	0.510	1.000											
EFER	0.381	0.460	0.693	0.400	0.808	0.043	0.546	0.574	0.434	0.604	0.593	0.342	0.406	0.465	0.719	0.388	0.546	0.067	1.000										
NOCO	0.637	0.159	0.854	0.327	0.654	0.301	0.441	0.480	0.792	0.618	0.791	0.521	0.809	0.385	0.572	0.566	0.842	0.236	0.648	1.000									
HAMI	0.187	-0.018	0.645	-0.146	0.707	-0.197	0.198	0.408	0.474	0.286	0.863	-0.037	0.760	0.078	0.320	0.211	0.793	0.388	0.567	0.721	1.000								
LOSS	0.316	0.268	0.189	0.490	0.185	0.178	0.712	0.460	-0.045	0.268	-0.139	0.127	-0.057	0.755	0.549	0.144	-0.070	-0.209	0.260	0.081	-0.090	1.000							
BILL	0.614	0.267	0.476	0.877	0.399	0.571	0.709	0.175	0.397	0.473	0.289	0.609	0.304	0.629	0.777	0.389	0.291	0.134	0.475	0.474	0.088	0.449	1.000						
VAND	0.316	0.432	0.254	0.549	0.329	0.088	0.409	0.307	-0.039	0.421	-0.180	0.247	-0.282	0.480	0.406	-0.166	-0.145	-0.275	0.454	-0.026	-0.106	0.480	0.519	1.000					
SWLC	0.374	0.531	0.379	0.600	0.455	0.174	0.762	0.360	0.092	0.267	0.231	0.297	0.093	0.670	0.785	0.359	0.168	0.014	0.734	0.285	0.184	0.661	0.620	0.523	1.000				
NWCP	0.743	0.425	0.569	0.667	0.569	0.642	0.615	0.424	0.555	0.522	0.480	0.719	0.504	0.365	0.646	0.731	0.588	0.544	0.537	0.715	0.328	0.086	0.722	0.216	0.379	1.000			
CRAI	0.627	0.301	0.789	0.424	0.584	0.187	0.580	0.489	0.442	0.338	0.494	0.185	0.513	0.633	0.453	0.197	0.565	0.034	0.555	0.598	0.586	0.372	0.528	0.458	0.435	0.392	1.000		
THUN	0.618	0.467	0.742	0.655	0.700	0.305	0.745	0.558	0.567	0.608	0.495	0.571	0.471	0.666	0.793	0.602	0.592	0.115	0.901	0.710	0.385	0.419	0.652	0.397	0.780	0.692	0.549	1.000	
LASV	0.178	-0.096	0.701	0.171	0.841	-0.201	0.449	0.459	0.624	0.512	0.788	0.126	0.744	0.365	0.586	0.250	0.785	0.296	0.772	0.723	0.806	0.212	0.376	0.107	0.489	0.422	0.520	0.691	1.000

Concentrations were moderately correlated ($r > 0.60$) among the five commercial sites (i.e., BEMI, WALN, MICH, MCDA, ECHA). Moderate to high correlations were also observed among the commercial, residential, and vacant land sites, with higher ($r > 0.90$) correlations between the commercial and residential sites (i.e., MCDA versus NOCO, MCDA versus HAMI for PM_{10} mass, BEMI versus EFER, and MICH versus EFER for PM_{10} silicon). PM_{10} mass and silicon concentrations measured within the industrial and construction sites were generally not correlated with each other, but there were a few exceptions (e.g., NCOV construction site versus NWAL industrial site for mass [$r = 0.81$], PECO construction site versus LAMB industrial site for silicon [$r = 0.83$]). As shown in Table 7-2, PM_{10} silicon at the LONE and NWAL industrial sites, LONM, CINN, and NCOV construction sites, and LOSS vacant land site show almost no correlation ($r < 0.5$) with any of the other satellite sites, implying that crustal abundances at these sites are mostly affected by local sources.

PM_{10} sulfur concentrations experienced high correlation coefficients ($r > 0.80$) at all the sites except for the East Charleston (ECHA) commercial site. As shown in Table 7-3, the ECHA commercial site is moderately correlated ($r \approx 0.6$) with most of the other sites with a few exceptions. This analysis shows that secondary sulfates are homogeneously distributed among the sites within the study area.

Table 7-4 shows that high PM_{10} light absorption (b_{abs}) correlations were more dependent upon geographical location in the vicinity of heavily-traveled roads than site type. For example, the sites close to Interstate 15 (e.g., GOLF, DONO, and NECD construction sites, BILL vacant land site) were moderately to highly correlated with the sites along Las Vegas Boulevard (e.g., MCDA commercial site, NOCO residential site, LASV and THUN vacant land sites). The East Charleston (ECHA) commercial site, the southernmost site within the study area, showed no correlation ($r < 0.5$) with any of the satellite sites. These phenomena corresponded to the emission density (e.g., population, restaurant, vegetative burning) as well as vehicular traffic volume in the area.

These correlation matrices show that clusters of high correlation coefficients were often found among the sites in close proximity of each other. The pair correlations often exceeded or were close to 0.8. These inter-site correlations confirm the observation that meteorology along with anthropogenic activities surrounding the satellite sites affected the PM_{10} mass and chemical concentrations in a similar way throughout the valley. Sampling sites with the greatest local source influences do not correlate with any other sites.

7.1.2 Cluster Analysis

Cluster analysis is a multivariate statistical procedure for detecting natural groupings in data without a *prior* knowledge of the group characteristics. This procedure has been used to determine the cluster of different chemical species with similar sampling intervals (Saucy

et al, 1987). Alternately, cluster analysis can be used to determine the grouping of chemical species based on their geographic locations. The distribution of chemical species among the satellite sites may be a result of a recurring meteorological condition or source emissions.

For a spatial cluster analysis, the data must be presented in a two-dimensional matrix consisting of the concentration measurement of a specific species for each date and site. For an unnormalized data matrix, species with high concentrations will dominate the resulting clusters. To overcome this bias, the mass and chemical data from the three intensive study periods were transformed by centering to the mean and then scaling to the standard deviation using the following equation:

$$C_n = \frac{C_i - \overline{C_i}}{\sigma_i} \tag{7-1}$$

where:

C_i = the concentration of the species *i* at a site

$\overline{C_i}$ = the average concentration of the species *i* at a site

σ_i = the standard deviation of the species concentration at a site

Normalizing the data to the standard deviation allows the usage of a wide range of chemical concentrations since each trace species is given as much weight as a major component.

Several key species indicative of the potential emission source in the study area were selected for this exercise. PM_{10} mass and silicon were used to represent geological material. PM_{10} b_{abs} measurements were chosen to represent motor vehicle and vegetative burning emissions. PM_{10} sulfur was selected to represent secondary sulfate aerosol (Hopke *et al.*, 1976a, 1976b).

The statistical software package used for cluster analyses was SYSTAT Version 5.02 (SYSTAT Inc., Evanston, IL), which includes the JOIN and KMEANS clustering methodology (Wilkinson, 1990) to examine the aerosol data from the three intensive periods combined. KMEANS clustering separates the data set into a selected number of sub-groups by maximizing the variations between groups and within each group. This method is similar to one-way analysis of variance (ANOVA) where groups are unknown, and the largest F-value is sought by reassigning members to each group.

Cluster analysis using KMEANS follows a procedure designed to isolate the most realistic cluster groupings which have real physical meaning. It is necessary to predetermine

the number of possible groupings for each of the species being examined. In this study, the KMEANS clustering was initially set to six possible groupings for each of the species examined. This analysis resulted in a pattern of one, two, or three groupings with isolated single-site clusters, from which it is difficult to extract conclusive results.

Another means of cluster analysis uses JOIN, which embraces hierarchical, tree, or linkage methodologies. JOIN computes a normalized distance between the sites for its clustering metric. The normalized distance is equal to the root mean squared distances among the sites. Various methods were tested to compute the distance of one site or cluster from another and to determine whether the two clusters should be merged into a given step. Ward's Method (Ward, 1963) returned the clearest separation of clusters and was selected for use in this study. The Ward Method uses the average value of all sites, but adjusts for its covariance in a cluster as the reference point to other clusters.

Figure 7-1 illustrates the north-south clustering pattern for normalized PM_{10} mass concentrations. As a first approximation, three main clusters were defined. The north cluster represents the vacant land sites (e.g., VAND, SWLC) and industrial sites (e.g., LAMB, WALN) in the northeast corner of the study area, which is interspersed with construction sites (e.g., CINN) and commercial sites (e.g., BEMI, WALN). The south cluster includes eight sites in the south-southwest portion of the study area with a mixture of construction, commercial, and residential sites. The center cluster includes sites located adjacent to and northwest, west, and southeast of the Bemis site.

PM_{10} silicon concentrations in Figure 7-2 displays a southwest to northeast grouping similar to the prevailing wind direction. A distinguishing cluster was found for one industrial site (i.e., NWAL) and two construction sites (i.e., LONM, NCOV) on the west side of the study domain. The largest cluster is found to center around Las Vegas Boulevard following the prevailing southwest-to-northeast wind pattern. Most of the construction sites (e.g., GOLF, DONO, NECD) are found in the north cluster.

The PM_{10} sulfur measurements exhibited decentralized clusters which spread the satellite sites into several overlapping groupings, as illustrated in Figure 7-3. This cluster pattern supports the fact that most sulfur measurements are highly correlated and it is difficult to discern separate clusters. No distinguishable pattern was found for PM_{10} b_{abs} measurements, as shown in Figure 7-4. Two northwest to southeast clusters were perpendicular to Interstate 15 and Las Vegas Boulevard.

Cluster analysis for this study is hampered by significant site-to-site and day-to-day variability in a small data set. However, cluster analysis does support the absence of concentration gradients in the mass and chemical measurements. In addition, it illustrates
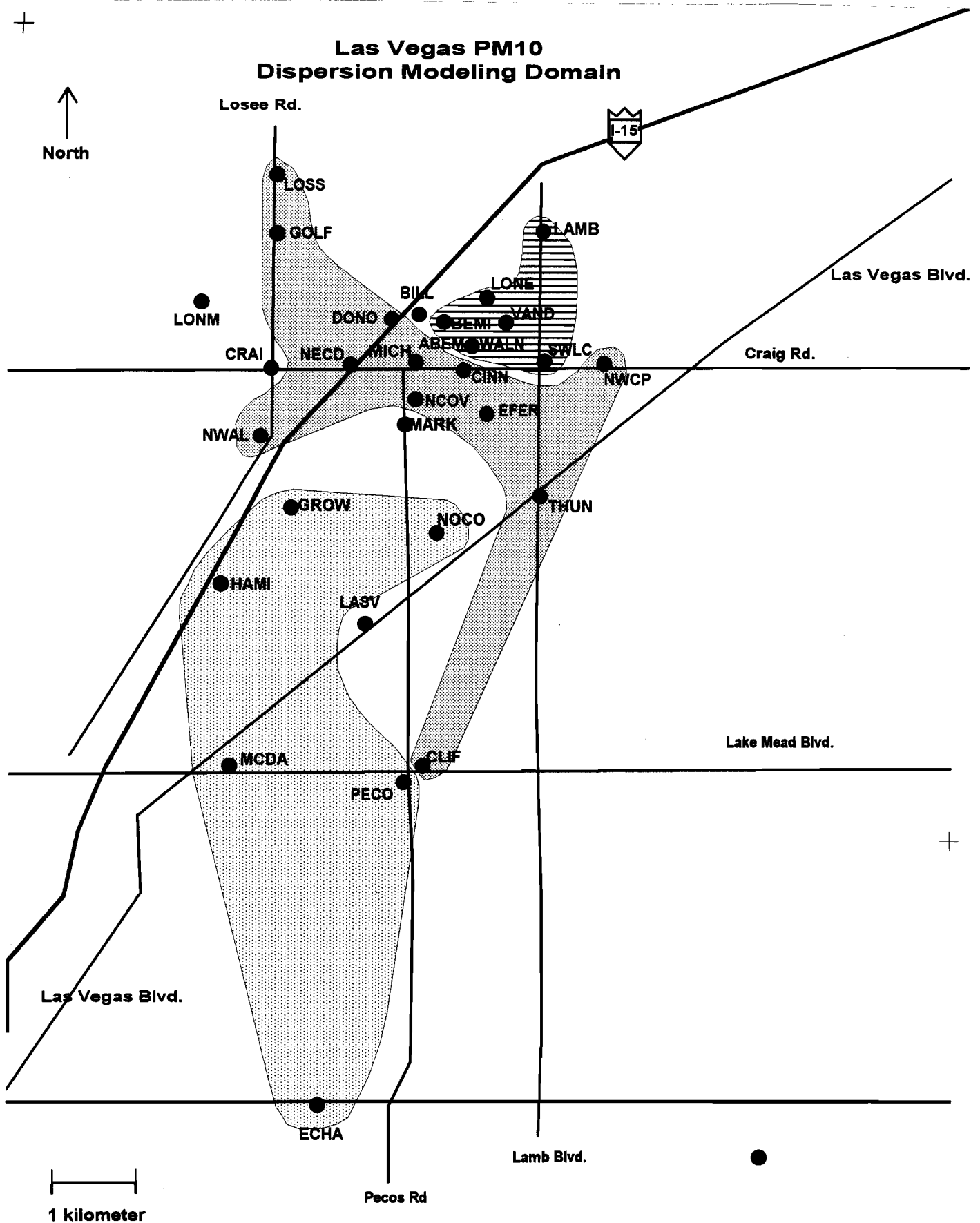
Figure 7-1   Distribution of PM$_{10}$ mass concentrations (various shades of gray represent different clusters).

Figure 7-2   Distribution of PM_{10} silicon concentrations (various shades of gray represent different clusters).
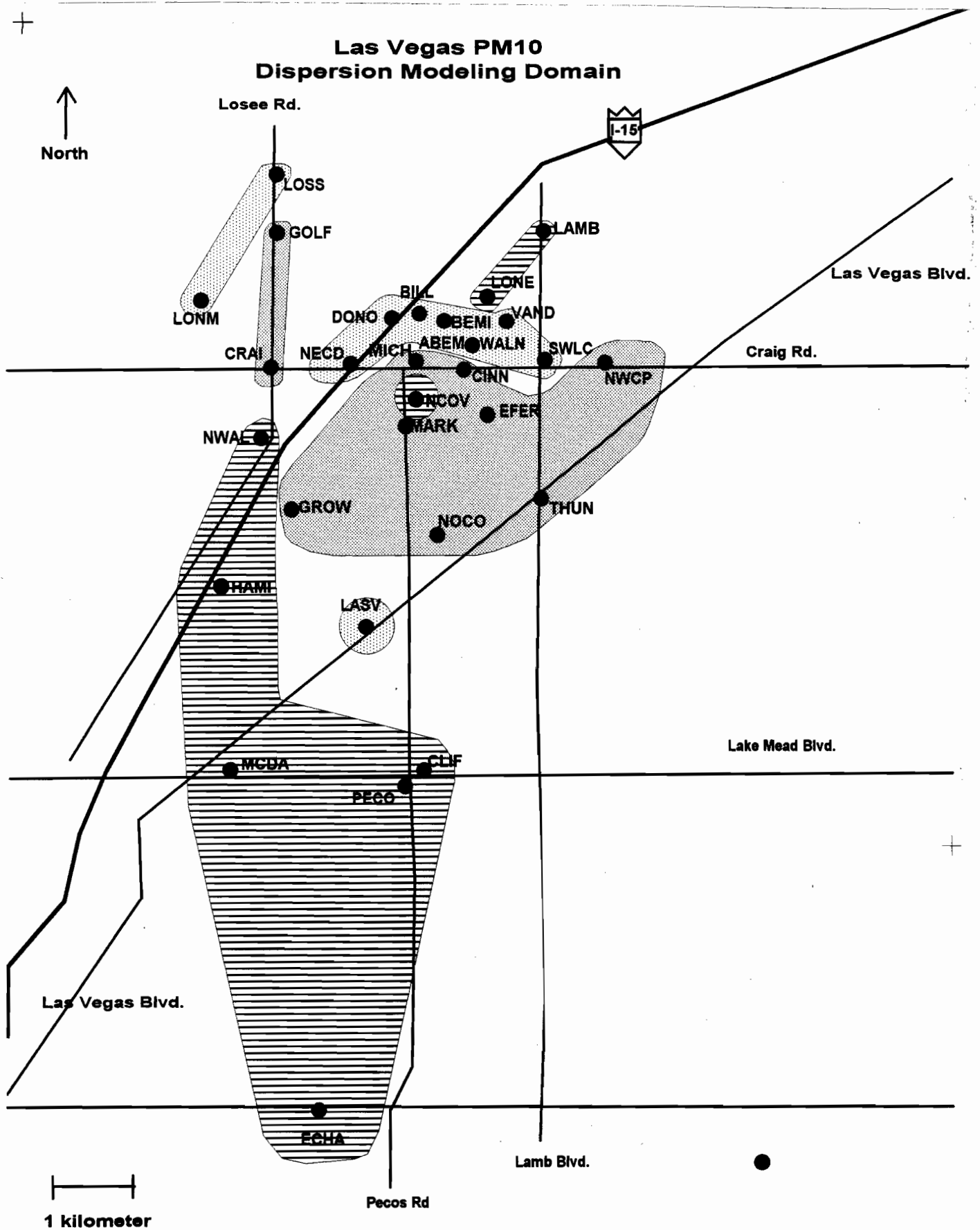
Figure 7-3   Distribution of PM_{10} sulfur concentrations (various shades of gray represent different clusters).
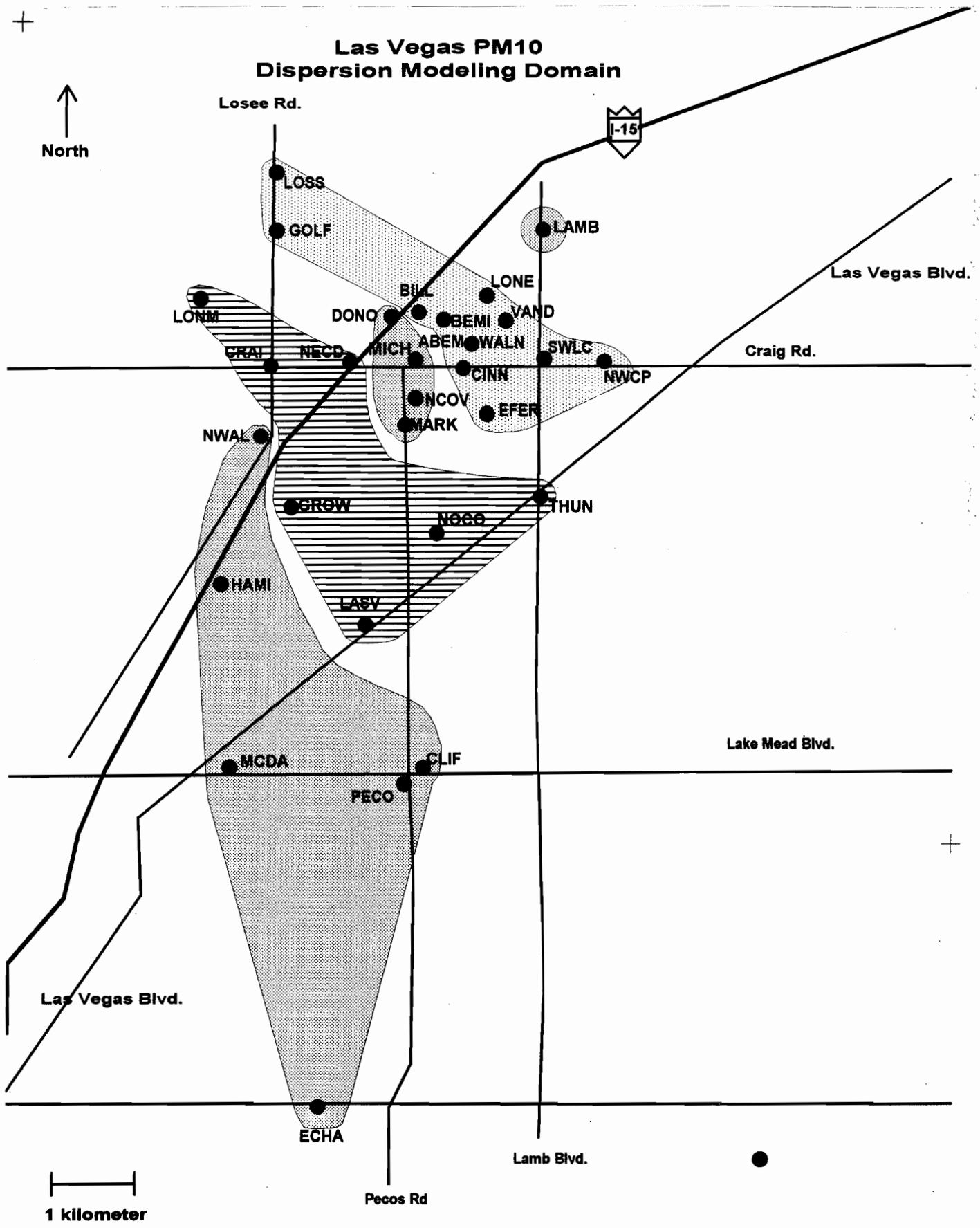
Figure 7-4   Distribution of PM_{10} b_{abs} measurements (various shades of gray represent different clusters).

that some secondary sulfate seems to have affected the study area on a scale that was greater than the spatial distribution of the two base sites.

7.2 Chemical Mass Balance Receptor Modeling

The CMB model consists of a least-squares solution to a set of linear equations which expresses each receptor concentration of a chemical species as a linear sum of products of source profile species and source contributions. The source profile species (the fractional amount of the species in the emissions from each source type) and the receptor concentrations, each with realistic uncertainty estimates, serve as input data to the CMB model. The output consists of the contributions for each source type to the total ambient aerosol mass as well as to individual chemical species concentrations. The model calculates values for contributions from each source and the uncertainties of those values. Input data uncertainties are used both to weight the relative importance of the input data to the model solution and to estimate uncertainties of the source contributions.

Current CMB software (Watson *et al.*, 1990a; 1990b) applies the effective variance solution developed and tested by Watson *et al.* (1984) because: 1) it calculates realistic uncertainties of source contributions from both the source and receptor uncertainties; and 2) chemical species measured more precisely in both source and receptor samples are given greater influence in the solution than are less precisely-measured species.

Watson (1979) observed that individual sources with similar source profiles, such as different soils and road dusts, would yield unreliable source contribution estimates if used in the same CMB. Henry (1982; 1992) proposed a quantitative method of identifying this interference among similar source compositions, which is known as "collinearity." Henry's "singular value decomposition" defines an "estimable space in which resolvable sources should lie" (Henry, 1982; 1992). The source types which do not fall into this estimable space are collinear, or too similar to be resolved from a combination of one or more of the source types which lie within the estimable space. Henry (1982; 1992) further proposed that linear combinations of source contributions resulting from collinear source compositions would be more representative of the summed contributions of these sources. Analytical measures of collinearity are available in the U.S. EPA/DRI Version 7.0 of the CMB model (Watson *et al.*, 1990a).

7.2.1 CMB Model Application and Validation

The CMB modeling procedure requires: 1) identification of the contributing source types; 2) selection of chemical species to be included; 3) estimation of the fractions of each chemical species contained in each source type (i.e., the source profiles); 4) estimation of the uncertainties of both ambient concentrations and source compositions; and 5) solution of the CMB equations.

These procedures are described in an applications and validation protocol (Watson *et al.*, 1991a) which has been assembled for PM_{10} source assessment. The protocol provides a regimen which makes the results from this source apportionment study comparable to those from other PM_{10} non-attainment areas.

The CMB applications and validation protocol consists of seven steps: 1) determination of model applicability; 2) estimation of initial source contribution; 3) examination of model outputs and performance measures; 4) identification of deviations from model assumptions; 5) identification and correction of model input errors; 6) verification of the consistency and stability of source contribution estimates; and 7) evaluation of the results of the CMB analysis with respect to other source assessment methods. The activities carried out for each of these steps are described in this section.

7.2.2   CMB Model Applicability

The requirements for CMB model applicability are as follows: 1) a sufficient number of receptor samples are taken with an accepted method to evaluate compliance with standards; 2) samples are analyzed for chemical species which are also present in source emissions; 3) potential source contributors have been identified and chemically characterized; and 4) the number of non-collinear source types is less than the number of measured species. All of these criteria have been met for the present study. Samples were taken through well-characterized PM_{10} samples. Samples from SFSs were subjected to analysis for mass, b_{abs}, elements, carbon, and ion concentrations. All major source types in the study area have been identified in Section 4 and their emissions were sampled and chemically characterized.

The number of non-collinear source profiles is less than the number of measured species. Examination of the chemical profiles shows significant differences among profiles for major source types such as primary geological material, primary motor vehicle exhaust, primary residential wood combustion, and secondary sulfates and nitrates. However, because of the similarity among the motor vehicle and wood combustion profiles, it may be difficult in many cases to distinguish these emissions using CMB modeling when the source contributions are small relative to the uncertainties of the source profiles.

7.2.3   CMB Model Outputs and Performance Measures

Watson *et al.* (1991b) defined several performance measures which are examined with each CMB to eliminate source profile combinations from further consideration. The most important of these are: 1) the source contributions estimates (SCEs) and their uncertainties; 2) "CHI SQUARE," the weighted sum of the squares of the differences between calculated and measured species concentrations. Values between one and two indicate acceptable fits; values less than one indicate very good fits to the data; 3) "R SQUARE," the fraction of the variance in the measured concentrations accounted for by

the variance in the calculated species concentrations. Values of "R SQUARE" greater than 0.9 indicate a good fit to the measured data; and 4) "PERCENT MASS," or the percent of total mass accounted for by the source contribution estimates. Values between 80% and 120% are considered to be acceptable.

The CMB output also contains the ratios of calculated to measured concentration (C/M) and the ratio of the difference between calculated and measured concentration divided by the uncertainty of this difference (R/U) for each chemical species. These indices allow the user to examine fits of individual species; for example, EC, OC, and Pb, which are important for distinguishing motor vehicle emissions from other combustion emissions, and soluble potassium (K^+), which is a marker for vegetative burning emissions. It is often found that the "C/M ratio" is significantly different from unity, but the "R/U ratio" is small (less than unity, for example). Under these conditions, a bad fit for a particular species does not significantly affect the source contribution estimates. Finally, collinearity or similarity between source profiles is indicated in the CMB output by the presence of two or more profiles in an "UNCERTAINTY/SIMILARITY CLUSTER." This condition may also result in part by small source contribution estimates with relatively large uncertainties.

7.2.4 Initial Source Contribution Estimates

Initial tests with different combinations of source profiles were done to determine which profiles best explain the data at the Bemis and East Charleston sites. Several test CMB runs were performed at each site for 24-hour samples collected on 12/27/95. On this day PM_{10} mass concentrations at the Bemis and East Charleston sites were 53.7 ± 2.7 $\mu g/m^3$ and 95.3 ± 4.8 $\mu g/m^3$, respectively. CMB performance measurements were examined to determine how well the ambient concentrations were explained by the CMB source contribution estimates and the sensitivity of these estimates to changes in the mix of profiles. The results of these initial trials were used as guidance in CMB analysis of the entire sample set.

Primary geological material was expected to be the largest contributor to PM_{10} at both sites. This was suggested by the high ambient concentrations of crustal species (e.g., Al, Si, Ca, Fe) relative to combustion-derived OC and EC. Secondary ammonium nitrate, ammonium sulfate, and ammonium bisulfate were used to explain nitrate, sulfate, and ammonium, which were unaccounted for by the primary emissions profiles. It should be noted that Ca was enriched relative to other crustal species in most of the geological source profiles with respect to the ambient samples. For example, the average ratio of Ca/Si in the 28 nonintensive samples was 1.43 ± 0.21 while the ratio in the geological profiles ranged from 1.48 (LVGPLOTC, paved parking lot dust) to 2.9 (LVGUPRDC, unpaved road dust). Only chemical species with concentrations above the lower quantifiable limits (LQL) listed in Table 5-6 were included in the CMB fit. Copper and zinc frequently appear to be contaminated in medium-volume

samples and were not used in the fit. Also excluded from the CMB fit were elemental Na and Mg, which are determined by XRF with large uncertainty intervals due to their low atomic numbers and coarse particle correction factors. PM_{10} $SO_4^=$ was used in place of S, and Cl⁻ was used in place of Cl in the CMB fit.

The test results of the source apportionments at each site are presented by a series of trials representing different combinations of source profiles in Tables 7-5a and 7-5b for the Bemis and East Charleston sites, respectively. The "best fit" or "default fit" is presented first as a reference. The source contribution estimates (SCEs) and CMB performance measurements are shown for each trial. The actual CMB outputs corresponding to the "best fit" cases in Tables 7-5a and 7-5b for the Bemis and East Charleston sites are presented in Tables 7-6a and 7-6b, respectively.

The "Best Fit" in Table 7-6a indicates that primary geological material was the largest contributor at the Bemis site, followed by primary motor vehicle emissions. The best fit was obtained using a composite geological profile (LVGEOLC), a composite motor vehicle profile (LVMVC2), and profiles representing secondary ammonium sulfate and secondary ammonium nitrate. The CMB performance measures were good, with R SQUARE of 0.96, PERCEN MASS of 100.2%, and CHI SQUARE of 0.68. In Trial 1, the composite parking lot dust source profile (LVGPLOTC) was substituted for the geological composite profile (LVGEOLC). This CMB trial underestimated the source contribution from geological material. The CHI SQUARE in Trial 1 was also higher (1.34), and the percent mass accounted for decreased from 100.2% to 78.8%. In Trial 2, the paved road dust profile (LVGPVRDC) was substituted for LVGEOLC. As in Trial 1, the geological source contribution was apparently underestimated with this profile. The CHI SQUARE in Trial 2 was also higher (1.53) and the percent of mass accounted for was 79.9%. In Trial 3, the residential wood combustion composite profile LVRWCC3 was added to the "Best Fit" solution. The wood combustion source contribution estimate (0.21 ± 0.46 µg/m³) was not statistically significant. In Trial 4, a different residential wood combustion profile (LVRWCC1) was used and the results were similar to those obtained in Trial 3. In Trial 5, the motor vehicle composite profile LVMVEC was substituted for LVMVC2. This solution was nearly identical to that of the "Best Fit" case. These tests show that over 86% of the measured PM_{10} can be attributed to primary geological contributions in this sample. Contributions from motor vehicle exhaust, secondary ammonium sulfate, and secondary ammonium nitrate accounted for 7.4%, 1.5%, and 5.4% of PM_{10}, respectively. Residential wood combustion, even if present, was too small to be resolved by CMB for the sample collected at the Bemis site on 12/27/95.

At the East Charleston site, the "Best Fit" (Table 7-6b) was obtained using the composite parking lot dust profile (LVGPLOTC), the motor vehicle composite profile (LVMVC2), and the composite residential wood combustion profile (LVRWCC3). The R

Table 7-5a

Sensitivity of Source Contribution Estimates to Changes in Source Profiles

for the Sample Acquired at the Bemis Site on 11/23/95

Source Contribution Estimates ($\mu g/m^3$)

Profile[a]	Best Fit	Trial 1	Trial 2	Trial 3	Trial 4	Trial 5
LVGPVRDC	24.80 ± 2.00		24.64 ± 2.52	24.2 ± 2.05	24.5 ± 2.01	24.3 ± 2.320
LVGEOLC		30.2 ± 3.22				
LVMVE951			0.10 ± 1.32			
LVMVC2						0.24 ± 1.39
LVRWCC3				0.21 ± 0.25		
LVRWCC1					0.31 ± 0.58	0.27 ± 0.61
NH4HSO4	1.14 ± 0.19	1.16 ± 0.20	1.14 ± 0.19	1.14 ± 0.19	1.13 ± 0.19	1.12 ± 0.19
NH4NO3	0.57 ± 0.07	0.58 ± 0.08	0.57 ± 0.07	0.57 ± 0.07	0.57 ± 0.07	0.57 ± 0.07

Performance Measures

	Best Fit	Trial 1	Trial 2	Trial 3	Trial 4	Trial 5
CHI-SQUARE[b]	0.83	0.54	0.89	0.85	0.87	0.95
R-SQUARE[c]	0.97	0.97	0.97	0.97	0.97	0.97
PERCENT MASS[d]	98.10	118.50	98.10	96.90	98.40	98.30
CLUSTERS[e]	---	---	LVGPVRDC LVMVE951	---	---	LVGPVRDC LVRWCC1 LVMVC2

[a] See Tables 4-1 to 4-8 for source profile descriptions.

[b] CHI-SQUARE measures the agreement between calculated and measured concentrations.

[c] R-SQUARE measures the correlation between calculated and measured concentrations. The closer the value of R-SQUARE to unity, the better the correlation.

[d] PERCENT MASS is the sum of source contributions divided by measured mass. The target value is 100. Values significantly less than 100 indicate missing sources, while values significantly exceeding 100 indicate sources which do not belong.

[e] CLUSTERS refers to UNCERTAINTY/SIMILARITY CLUSTERS which identify the potential for collinearity among the profiles which are contained in the CLUSTER. When source profile mnemonics are listed, they appeared together in one or more clusters and are probably collinear.

Table 7-5b

Sensitivity of Source Contribution Estimates to Changes in Source Profiles for the Sample Acquired at the East Charleston Site on 11/23/95

Source Contribution Estimates ($\mu g/m^3$)

Profile[a]	Best Fit	Trial 1	Trial 2	Trial 3	Trial 4
LVGPLOTC	97.78 ± 14.46		5.62 ± 14.80	121.9 ± 9.44	95.90 ± 11.4
LVGEOLC		8.50 ± 18.2			
LVMVE951	32.00 ± 11.7	42.10 ± 14.1	35.96 ± 12.5		
LVMVC2					43.3 ± 8.23
LVRWCC3	4.95 ± 2.29	4.84 ± 2.62		7.31 ± 2.16	3.83 ± 1.84
(NH4)2SO4	2.77 ± 1.38	3.45 ± 1.67	2.79 ± 1.52	0.26 ± 0.66	-0.46 ± 1.07
NH4NO3	3.28 ± 0.84	3.35 ± 1.05	3.34 ± 0.92	0.42 ± 0.42	2.99 ± 0.71

Performance Measures

	Best Fit	Trial 1	Trial 2	Trial 3	Trial 4
CHI-SQUARE[b]	0.74	0.5	1.02	3.66	0.62
R-SQUARE[c]	0.96	0.95	0.93	0.88	0.97
PERCENT MASS[d]	118.20	136.20	124.00	111.50	122.30
CLUSTERS[e]	---	---	---	(NH4)2SO4 NH4NO3	(NH4)2SO4 NH4NO3

[a] See Tables 4-1 to 4-8 for source profile descriptions.
[b] CHI-SQUARE measures the agreement between calculated and measured concentrations.
[c] R-SQUARE measures the correlation between calculated and measured concentrations. The closer the value of R-SQUARE to unity, the better the correlation.
[d] PERCENT MASS is the sum of source contributions divided by measured mass. The target value is 100. Values significantly less than 100 indicate missing sources, while values significantly exceeding 100 indicate sources which do not belong.
[e] CLUSTERS refers to UNCERTAINTY/SIMILARITY CLUSTERS which identify the potential for collinearity among the profiles which are contained in the CLUSTER. When source profile mnemonics are listed, they appeared together in one or more clusters and are probably collinear.

Table 7-6a
Sensitivity of Source Contribution Estimates to Changes in Source Profiles
for Samples Acquired at the Bemis Site on 12/27/95

Profile[a]	Source Contribution Estimates ($\mu g/m^3$)					
	Best Fit	Trial 1	Trial 2	Trial 3	Trial 4	Trial 5
LVGEOLC	46.10 ± 5.70			45.50 ± 5.80	45.80 ± 5.70	46.40 ± 5.90
LVGPLOTC		35.40 ± 2.90				
LVGPVRDC			35.60 ± 3.40			
LVRWCC3				0.21 ± 0.46		
LVRWCC1					0.53 ± 1.11	
LVMVC2	4.00 ± 2.40	3.40 ± 1.60	3.70 ± 2.00	3.70 ± 2.50	3.60 ± 2.50	
LVMVEC						4.00 ± 2.50
$(NH_4)_2SO_4$	0.83 ± 0.49	0.70 ± 0.41	0.81 ± 0.44	0.85 ± 0.48	0.86 ± 0.48	0.82 ± 0.52
NH_4NO_3	2.90 ± 0.30	2.80 ± 0.30	2.80 ± 0.30	2.90 ± 0.30	2.90 ± 0.30	2.90 ± 0.30
			Performance Measures			
CHI-SQUARE[b]	0.68	1.34	1.53	0.73	0.72	0.66
R-SQUARE[c]	0.96	0.96	0.94	0.96	0.96	0.96
PERCENT MASS[d]	100.20	78.80	79.90	98.90	99.90	100.60
CLUSTERS[e]			LVGPVRDC LVMVC2		LVRWCC1 LVMVC2	

[a] See Tables 4-1 to 4-8 for source profile descriptions.

[b] CHI-SQUARE measures the agreement between calculated and measured concentrations.

[c] R-SQUARE measures the correlation between calculated and measured concentrations. The closer the value of R-SQUARE to unity, the better the correlation.

[d] PERCENT MASS is the sum of source contributions divided by measured mass. The target value is 100. Values significantly less than 100 indicate missing sources, while values significantly exceeding 100 indicate sources which do not belong.

[e] CLUSTERS refers to UNCERTAINTY/SIMILARITY CLUSTERS which identify the potential for collinearity among the profiles which are contained in the CLUSTER. When source profile mnemonics are listed, they appeared together in one or more clusters and are probably collinear.

Table 7-6b

**Sensitivity of Source Contribution Estimates to Changes in Source Profiles
from the Samples Acquired at the East Charleston Site on 12/27/95**

Source Contribution Estimates ($\mu g/m^3$)

Profile[a]	Best Fit	Trial 1	Trial 2	Trial 3	Trial 4	Trial 5
LVGEOLC	82.10 ± 8.50					
LVGPLOTC		90.00 ± 12.70		85.50 ± 8.60	86.00 ± 8.60	83.20 ± 9.30
LVGPVRDC			85.70 ± 9.50			
LVRWCC3	2.30 ± 1.10	2.40 ± 1.10	2.40 ± 1.00			1.80 ± 1.30
LVRWCC1				1.30 ± 2.60		
LVMVC2	14.90 ± 4.70	18.70 ± 5.40	14.30 ± 5.30	17.00 ± 4.80	17.50 ± 4.70	
LVMVEC						14.70 ± 5.40
$(NH_4)_2SO_4$						
NH_4NO_3	2.30 ± 0.30	2.40 ± 0.30	2.30 ± 0.30	2.30 ± 0.30	2.40 ± 0.30	2.50 ± 0.40
			Performance Measures			
CHI-SQUARE[b]	0.95	1.00	1.01	1.29	1.19	0.58
R-SQUARE[c]	0.97	0.96	0.97	0.96	0.96	0.98
PERCENT MASS[d]	106.50	119.10	109.90	111.30	111.10	107.30
CLUSTERS[e]				LVGPLOTC LVRWCC1 LVMVC2		

[a] See Tables 4-1 to 4-8 for source profile descriptions.

[b] CHI-SQUARE measures the agreement between calculated and measured concentrations.

[c] R-SQUARE measures the correlation between calculated and measured concentrations. The closer the value of R-SQUARE to unity, the better the correlation.

[d] PERCENT MASS is the sum of source contributions divided by measured mass. The target value is 100. Values significantly less than 100 indicate missing sources, while values significantly exceeding 100 indicate sources which do not belong.

[e] CLUSTERS refers to UNCERTAINTY/SIMILARITY CLUSTERS which identify the potential for collinearity among the profiles which are contained in the CLUSTER. When source profile mnemonics are listed, they appeared together in one or more clusters and are probably collinear.

SQUARE, CHI SQUARE, and percent of mass accounted for were 0.97, 0.95, and 106.5%, respectively. In Trial 1, the composite geological profile (LVGEOLC) was substituted for the composite parking lot dust profile (LVGPLOTC). While the CHI SQUARE increased slightly from 0.95 to 1.00, the percent of mass accounted for increased from 106.5% to 119.1%. This was caused by an increase in the geological source contribution from 82.1 ± 8.5 to 90.0 ± 12.7 µg/m^3. In Trial 2, the paved road dust composite geological profile (LVGPVRDC) was substituted for the composite parking lot dust profile (LVGPLOTC). While the CHI SQUARE increased slightly from 0.95 to 1.01 and the percent of mass accounted for increased from 106.5% to 109.9%, this solution was similar to that in the "Best Fit" case. In Trial 3, the residential wood combustion profile LVRWCC1 was substituted for LVRWCC3. The CHI SQUARE increased from 0.95 to 1.29 and the percent of mass accounted for increased from 106.5% to 111.3%. Note that the wood combustion source contribution estimate was smaller than its uncertainty (1.3 ± 2.6 µg/m^3). This is consistent with the formation of an UNCERTAINTY/SIMILARITY cluster containing LVGPLOTC, LVRWCC1, AND LVMVC2. In Trial 4, the residential wood combustion source was removed completely. The CHI SQUARE and percent of mass accounted for were both larger than those of the "Best Fit" case. The fit to measured soluble potassium (Table 7-7b) was also worse than in the "Best Fit" case. Removing the wood combustion profile resulted in an increase in the motor vehicle source contribution estimate from 14.9 ± 4.7 to 17.0 ± 4.8 µg/m^3. In Trial 5, the motor vehicle composite profile LVMVEC was substituted for LVMVC2. Again, this solution was nearly identical to that of the "Best Fit" case. These sensitivity tests show that the East Charleston sample from 12/27/95 was dominated by geological material and motor vehicle exhaust, with detectable contributions from residential wood combustion, secondary ammonium sulfate, and secondary ammonium nitrate.

7.2.5 Deviations from Model Assumptions

One of the most important assumptions of the CMB model (Watson et al., 1984) is that the source profiles are linearly independent (i.e., they are statistically different). The degree to which this assumption can be met in practice depends to a large extent on the types and quality of chemical measurements made at the sources and receptor. The CMB model has been subjected to a number of tests to determine its ability to tolerate deviations from the model assumptions (e.g., Watson, 1979; Gordon et al., 1981; Henry, 1982, 1992; Currie et al., 1984; Dzubay et al., 1984; DeCesar et al., 1985; Javitz and Watson, 1988; Lowenthal et al., 1992). The impacts of collinearities among the source profiles vary from case to case. These collinearities tend to inflate the variances of the source contribution estimates. An example of the collinearity effect can be illustrated by the instability of the source contribution estimates between paved road dust and motor vehicle exhaust shown in Table 7-6a for the Trial 2 CMB run.

Table 7-7a
Example of CMB Source Contribution Estimates
for the Sample Collected at the Bemis Site on 12/27/95

```
Best Fit

SOURCE CONTRIBUTION ESTIMATES -  SITE: BEMIS        DATE: 12/27/95    CMB7 33889
SAMPLE DURATION       24      START HOUR       00        SIZE:    10
        R SQUARE      .96   PERCENT MASS     100.2
       CHI SQUARE     .68              DF      12

    SOURCE
        * TYPE     SCE(UG/M3)     STD ERR      TSTAT
    -------------------------------------------------
6        LVGEOLC      46.0857      5.7287      8.0446
19       (NH4)2SO       .8339       .4905      1.6999
20       NH4NO3        2.8650       .3389      8.4545
23       LVMVC2        4.0475      2.4005      1.6861
    -------------------------------------------------


MEASURED CONCENTRATION FOR SIZE: 10
        53.7+-     2.7

        UNCERTAINTY/SIMILARITY CLUSTERS    CMB7 33889    SUM OF CLUSTER SOURCES
    -----------------------------------------------------------------------------


    -----------------------------------------------------------------------------


SPECIES CONCENTRATIONS -  SITE: BEMIS        DATE: 12/27/95    CMB7 33889
SAMPLE DURATION       24      START HOUR       00        SIZE:    10
        R SQUARE      .96   PERCENT MASS     100.2
       CHI SQUARE     .68              DF      12

SPECIES-------I---MEAS-----------------CALC-------------RATIO C/M----RATIO R/U
MSGC    MSGU   T  53.73070+-  2.71900  53.83216+-  4.95066   1.00+-  .11     .0
CLIC    CLIU   *     .11520+-   .02260    .06667+-   .03815    .58+-  .35   -1.1
N3IC    N3IU   *    2.30860+-   .12510   2.30860+-   .23035   1.00+-  .11     .0
S4IC    S4IU   *    1.26390+-   .06780   1.26390+-   .34035   1.00+-  .27     .0
N4CC    N4CU         .36470+-   .02810    .95885+-   .07637   2.63+-  .29    7.3
KPAC    KPAU   *     .08490+-   .00570    .09026+-   .02567   1.06+-  .31     .2
OCTC    OCTU   *    5.76290+-   .41880   6.68927+-  1.78961   1.16+-  .32     .5
ECTC    ECTU   *    3.24370+-   .36780   2.76366+-  1.08025    .85+-  .35   - .4
TCTC    TCTU       8.97400+-   .55630   9.22122+-  2.33827   1.03+-  .27     .1
NAXC    NAXU         .00000<    .10400    .01614<    .02483    .00<   .00     .2
MGXC    MGXU         .97650+-   .05470   1.45826+-   .30422   1.49+-  .32    1.6
ALXC    ALXU   *    1.28650+-   .38330    .66632+-   .17197    .52+-  .20   -1.5
SIXC    SIXU   *    5.08420+-  1.61810   3.59598+-   .69129    .71+-  .26   - .8
PHXC    PHXU         .00600<    .01610    .01240<    .00975   2.07<  5.78     .3
SUXC    SUXU         .48010+-   .16810    .42388+-   .09950    .88+-  .37   - .3
CLXC    CLXU   *     .00960<    .05590    .02988<    .02644   3.11< 18.33     .3
KPXC    KPXU   *     .43050+-   .08860    .47672+-   .09672   1.11+-  .32     .4
CAXC    CAXU   *    9.63140+-  1.62470   7.54170+-  1.21586    .78+-  .18   -1.0
TIXC    TIXU   *     .04810+-   .01530    .08027+-   .02394   1.67+-  .73    1.1
CRXC    CRXU   *     .00500+-   .00220    .00322+-   .00138    .64+-  .40   - .7
MNXC    MNXU   *     .01620+-   .00150    .01830+-   .00433   1.13+-  .29     .5
FEXC    FEXU   *     .75420+-   .03990    .87484+-   .23367   1.16+-  .32     .5
NIXC    NIXU         .00390+-   .00070    .00174+-   .00064    .45+-  .18   -2.3
CUXC    CUXU         .01470+-   .00100    .00553+-   .00243    .38+-  .17   -3.5
ZNXC    ZNXU         .05470+-   .00290    .03108+-   .02104    .57+-  .39   -1.1
BRXC    BRXU         .00180+-   .00070    .00217+-   .00098   1.21+-  .72     .3
```

```
RBXC    RBXU          .00160+-    .00060    .00240+-    .00060    1.50+-   .68        .9
SRXC    SRXU          .03510+-    .00190    .05556+-    .01455    1.58+-   .42       1.4
YTXC    YTXU          .00060<     .00120    .00089<     .00028    1.48<   2.99        .2
ZRXC    ZRXU          .00220+-    .00110    .00311+-    .00089    1.41+-   .81        .6
MOXC    MOXU          .00000<     .00250    .00080<     .00061     .00<    .00        .3
BAXC    BAXU          .04750+-    .04010    .01297+-    .01360     .27+-   .37       -.8
PBXC    PBXU    *     .00530+-    .00200    .00680+-    .00482    1.28+-  1.03        .3
        ------------------------------------------------------------------------------
```

Trial 1

```
SOURCE CONTRIBUTION ESTIMATES -  SITE: BEMIS         DATE: 12/27/95    CMB7 33889
SAMPLE DURATION          24       START HOUR        00       SIZE:     10
         R SQUARE        .96     PERCENT MASS      78.8
        CHI SQUARE      1.34                DF        12

     SOURCE
       * TYPE      SCE(UG/M3)    STD ERR      TSTAT
     ----------------------------------------------------
2        LVGPLOTC     35.4597     2.9409      12.0576
19       (NH4)2SO       .7019      .4111       1.7071
20       NH4NO3        2.8413      .3324       8.5475
23       LVMVC2        3.3576     1.5948       2.1053
     ----------------------------------------------------
```

```
MEASURED CONCENTRATION FOR SIZE: 10
       53.7+-      2.7

           UNCERTAINTY/SIMILARITY CLUSTERS    CMB7 33889     SUM OF CLUSTER SOURCES
     ----------------------------------------------------------------------------

     ----------------------------------------------------------------------------
```

```
SPECIES CONCENTRATIONS -  SITE: BEMIS          DATE: 12/27/95    CMB7 33889
SAMPLE DURATION          24       START HOUR        00       SIZE:     10
         R SQUARE        .96     PERCENT MASS      78.8
        CHI SQUARE      1.34                DF        12

SPECIES-------I---MEAS----------------CALC-------------RATIO C/M----RATIO R/U
MSGC    MSGU    T  53.73070+-   2.71900  42.36044+-   2.49403    .79+-   .06    -3.1
CLIC    CLIU    *    .11520+-    .02260    .08187+-    .04857    .71+-   .44     -.6
N3IC    N3IU    *   2.30860+-    .12510   2.30860+-    .22496   1.00+-   .11      .0
S4IC    S4IU    *   1.26390+-    .06780   1.26390+-    .28566   1.00+-   .23      .0
N4CC    N4CU         .36470+-    .02810    .91311+-    .07379   2.50+-   .28     6.9
KPAC    KPAU    *    .08490+-    .00570    .07337+-    .02013    .86+-   .24     -.6
OCTC    OCTU    *   5.76290+-    .41880   6.77405+-   1.79197   1.18+-   .32      .5
ECTC    ECTU    *   3.24370+-    .36780   3.07972+-    .48603    .95+-   .18     -.3
TCTC    TCTU        8.97400+-    .55630   9.64560+-   1.58455   1.07+-   .19      .4
NAXC    NAXU         .00000<     .10400    .01793<     .06511    .00<    .00      .1
MGXC    MGXU         .97650+-    .05470    .88307+-    .20935    .90+-   .22     -.4
ALXC    ALXU    *   1.28650+-    .38330    .66776+-    .05481    .52+-   .16    -1.6
SIXC    SIXU    *   5.08420+-   1.61810   3.23707+-    .16607    .64+-   .21    -1.1
PHXC    PHXU         .00600<     .01610    .01762<     .01229   2.94<   8.14      .6
SUXC    SUXU         .48010+-    .16810    .44559+-    .05050    .93+-   .34     -.2
CLXC    CLXU    *    .00960<     .05590    .05277<     .03249   5.50<  32.19      .7
KPXC    KPXU    *    .43050+-    .08860    .43375+-    .03929   1.01+-   .23      .0
CAXC    CAXU    *   9.63140+-   1.62470   4.76207+-    .91806    .49+-   .13    -2.6
TIXC    TIXU    *    .04810+-    .01530    .09272+-    .02644   1.93+-   .82     1.5
CRXC    CRXU    *    .00500+-    .00220    .00307+-    .00155    .61+-   .41     -.7
MNXC    MNXU    *    .01620+-    .00150    .01615+-    .00140   1.00+-   .13     -.0
FEXC    FEXU    *    .75420+-    .03990    .84919+-    .08583   1.13+-   .13     1.0
NIXC    NIXU         .00390+-    .00070    .00140+-    .00047    .36+-   .14    -3.0
```

```
CUXC    CUXU        .01470+-    .00100    .00544+-    .00081    .37+-   .06    -7.2
ZNXC    ZNXU        .05470+-    .00290    .05025+-    .00242    .92+-   .07    -1.2
BRXC    BRXU        .00180+-    .00070    .00178+-    .00068    .99+-   .54     -.0
RBXC    RBXU        .00160+-    .00060    .00242+-    .00047   1.51+-   .64     1.1
SRXC    SRXU        .03510+-    .00190    .03031+-    .00226    .86+-   .08    -1.6
YTXC    YTXU        .00060<     .00120    .00069<     .00085   1.14<  2.69      .1
ZRXC    ZRXU        .00220+-    .00110    .00332+-    .00079   1.51+-   .84      .8
MOXC    MOXU        .00000<     .00250    .00034<     .00174    .00<    .00      .1
BAXC    BAXU        .04750+-    .04010    .00535+-    .04055    .11+-   .86     -.7
PBXC    PBXU    *   .00530+-    .00200    .00786+-    .00509   1.48+-  1.11      .5
-------------------------------------------------------------------------------
```

Trial 2

```
SOURCE CONTRIBUTION ESTIMATES -  SITE: BEMIS        DATE: 12/27/95   CMB7 33889
SAMPLE DURATION        24       START HOUR        00        SIZE:     10
      R SQUARE         .94    PERCENT MASS       79.9
      CHI SQUARE      1.53              DF            12

     SOURCE
         * TYPE     SCE(UG/M3)    STD ERR     TSTAT
----------------------------------------------------
3       LVGPVRDC     35.5859     3.3747    10.5451
19      (NH4)2SO       .8069      .4454     1.8117
20      NH4NO3        2.8526      .3347     8.5229
23      LVMVC2        3.7112     1.9917     1.8633
----------------------------------------------------


MEASURED CONCENTRATION FOR SIZE: 10
       53.7+-      2.7

        UNCERTAINTY/SIMILARITY CLUSTERS    CMB7 33889    SUM OF CLUSTER SOURCES
-------------------------------------------------------------------------------

        3      23                                          39.297+-     2.814
        3      23                                          39.297+-     2.814
-------------------------------------------------------------------------------

SPECIES CONCENTRATIONS -  SITE: BEMIS        DATE: 12/27/95    CMB7 33889
SAMPLE DURATION        24       START HOUR        00        SIZE:     10
      R SQUARE         .94    PERCENT MASS       79.9
      CHI SQUARE      1.53              DF            12

SPECIES-------I---MEAS-----------------CALC-------------RATIO C/M----RATIO R/U
MSGC    MSGU   T 53.73070+-  2.71900  42.95661+-  2.80099    .80+-   .07    -2.8
CLIC    CLIU   *   .11520+-   .02260    .05561+-   .02354    .48+-   .23    -1.8
N3IC    N3IU   *  2.30860+-   .12510   2.30860+-   .22686   1.00+-   .11     .0
S4IC    S4IU   *  1.26390+-   .06780   1.26390+-   .30994   1.00+-   .25     .0
N4CC    N4CU       .36470+-   .02810    .94436+-   .07303   2.59+-   .28    7.4
KPAC    KPAU   *   .08490+-   .00570    .07888+-   .02346    .93+-   .28    -.2
OCTC    OCTU   *  5.76290+-   .41880   6.17867+-  1.42086   1.07+-   .26     .3
ECTC    ECTU   *  3.24370+-   .36780   3.00909+-   .85909    .93+-   .28    -.3
TCTC    TCTU      8.97400+-   .55630   8.96607+-  1.83371   1.00+-   .21     .0
NAXC    NAXU       .00000<    .10400    .01872<    .03638    .00<    .00     .2
MGXC    MGXU       .97650+-   .05470    .96514+-   .14768    .99+-   .16    -.1
ALXC    ALXU   *  1.28650+-   .38330    .58506+-   .04951    .45+-   .14    -1.8
SIXC    SIXU   *  5.08420+-  1.61810   3.02763+-   .27520    .60+-   .20    -1.3
PHXC    PHXU       .00600<    .01610    .01326<    .00772   2.21<  6.07     .4
SUXC    SUXU       .48010+-   .16810    .42468+-   .05992    .88+-   .33    -.3
CLXC    CLXU   *   .00960<    .05590    .03200<    .01604   3.33< 19.48     .4
KPXC    KPXU   *   .43050+-   .08860    .39751+-   .04544    .92+-   .22    -.3
CAXC    CAXU   *  9.63140+-  1.62470   5.34439+-   .95178    .55+-   .14    -2.3
```

7-24

```
TIXC   TIXU   *   .04810+-   .01530   .07272+-   .00721   1.51+-   .50     1.5
CRXC   CRXU   *   .00500+-   .00220   .00342+-   .00116    .68+-   .38     -.6
MNXC   MNXU   *   .01620+-   .00150   .01675+-   .00214   1.03+-   .16      .2
FEXC   FEXU   *   .75420+-   .03990   .83544+-   .10595   1.11+-   .15      .7
NIXC   NIXU       .00390+-   .00070   .00171+-   .00054    .44+-   .16    -2.5
CUXC   CUXU       .01470+-   .00100   .00676+-   .00162    .46+-   .11    -4.2
ZNXC   ZNXU       .05470+-   .00290   .04042+-   .00965    .74+-   .18    -1.4
BRXC   BRXU       .00180+-   .00070   .00232+-   .00114   1.29+-   .81      .4
RBXC   RBXU       .00160+-   .00060   .00179+-   .00040   1.12+-   .49      .3
SRXC   SRXU       .03510+-   .00190   .04408+-   .01629   1.26+-   .47      .5
YTXC   YTXU       .00060<   .00120   .00066<   .00047   1.09<  2.32      .0
ZRXC   ZRXU       .00220+-   .00110   .00263+-   .00062   1.20+-   .66      .3
MOXC   MOXU       .00000<   .00250   .00071<   .00100    .00<   .00      .3
BAXC   BAXU       .04750+-   .04010   .01425+-   .02296    .30+-   .55     -.7
PBXC   PBXU   *   .00530+-   .00200   .00885+-   .00212   1.67+-   .75     1.2
    ---------------------------------------------------------------------------
```

Trial 3

```
SOURCE CONTRIBUTION ESTIMATES  -  SITE: BEMIS        DATE: 12/27/95   CMB7 33889
SAMPLE DURATION          24      START HOUR       00          SIZE:    10
         R SQUARE        .96   PERCENT MASS      98.9
         CHI SQUARE      .73          DF          11

     SOURCE
         * TYPE     SCE(UG/M3)    STD ERR    TSTAT
    -----------------------------------------------
6          LVGEOLC    45.5139     5.8074     7.8372
17         LVRWCC3     .2124      .4562      .4657
19         (NH4)2SO    .8547      .4833     1.7684
20         NH4NO3     2.8667      .3382     8.4773
23         LVMVC2     3.7099     2.4798     1.4960
    -----------------------------------------------

MEASURED CONCENTRATION FOR SIZE: 10
         53.7+-     2.7


              UNCERTAINTY/SIMILARITY CLUSTERS     CMB7 33889     SUM OF CLUSTER SOURCES
    ----------------------------------------------------------------------------

    ----------------------------------------------------------------------------

SPECIES CONCENTRATIONS  -  SITE: BEMIS        DATE: 12/27/95   CMB7 33889
SAMPLE DURATION          24      START HOUR       00          SIZE:    10
         R SQUARE        .96   PERCENT MASS      98.9
         CHI SQUARE      .73          DF          11

SPECIES-------I---MEAS-----------------CALC-------------RATIO C/M----RATIO R/U
MSGC   MSGU   T  53.73070+-  2.71900  53.15758+-  5.11138    .99+-   .11     -.1
CLIC   CLIU   *    .11520+-   .02260    .08050+-   .03820    .70+-   .36     -.8
N3IC   N3IU   *   2.30860+-   .12510   2.30860+-   .22971   1.00+-   .11      .0
S4IC   S4IU   *   1.26390+-   .06780   1.26390+-   .33354   1.00+-   .27      .0
N4CC   N4CU        .36470+-   .02810    .96416+-   .07596   2.64+-   .29     7.4
KPAC   KPAU   *    .08490+-   .00570    .09560+-   .02539   1.13+-   .31      .4
OCTC   OCTU   *   5.76290+-   .41880   6.53332+-  1.76546   1.13+-   .32      .4
ECTC   ECTU   *   3.24370+-   .36780   2.67473+-  1.06404    .82+-   .34     -.5
TCTC   TCTU       8.97400+-   .55630   8.98527+-  2.30880   1.00+-   .26      .0
NAXC   NAXU        .00000<   .10400    .01880<   .02422    .00<   .00      .2
MGXC   MGXU        .97650+-   .05470   1.43992+-   .30042   1.47+-   .32     1.5
ALXC   ALXU   *   1.28650+-   .38330    .65755+-   .16982    .51+-   .20    -1.5
SIXC   SIXU   *   5.08420+-  1.61810   3.55055+-   .68267    .70+-   .26     -.9
PHXC   PHXU        .00600<   .01610    .01217<   .00961   2.03<  5.68      .3
```

SUXC	SUXU		.48010+-	.16810	.42268+-	.09646	.88+- .37	-.3
CLXC	CLXU	*	.00960<	.05590	.04383<	.02687	4.57< 26.73	.6
KPXC	KPXU	*	.43050+-	.08860	.47995+-	.09552	1.11+- .32	.4
CAXC	CAXU	*	9.63140+-	1.62470	7.44809+-	1.20072	.77+- .18	-1.1
TIXC	TIXU	*	.04810+-	.01530	.07904+-	.02362	1.64+- .72	1.1
CRXC	CRXU	*	.00500+-	.00220	.00314+-	.00134	.63+- .38	-.7
MNXC	MNXU	*	.01620+-	.00150	.01805+-	.00427	1.11+- .28	.4
FEXC	FEXU	*	.75420+-	.03990	.86094+-	.23059	1.14+- .31	.5
NIXC	NIXU		.00390+-	.00070	.00171+-	.00063	.44+- .18	-2.3
CUXC	CUXU		.01470+-	.00100	.00528+-	.00238	.36+- .16	-3.6
ZNXC	ZNXU		.05470+-	.00290	.03073+-	.02078	.56+- .38	-1.1
BRXC	BRXU		.00180+-	.00070	.00215+-	.00096	1.20+- .71	.3
RBXC	RBXU		.00160+-	.00060	.00238+-	.00060	1.49+- .67	.9
SRXC	SRXU		.03510+-	.00190	.05484+-	.01436	1.56+- .42	1.4
YTXC	YTXU		.00060<	.00120	.00087<	.00028	1.45< 2.94	.2
ZRXC	ZRXU		.00220+-	.00110	.00306+-	.00087	1.39+- .80	.6
MOXC	MOXU		.00000<	.00250	.00079<	.00061	.00< .00	.3
BAXC	BAXU		.04750+-	.04010	.01268+-	.01352	.27+- .36	-.8
PBXC	PBXU	*	.00530+-	.00200	.00669+-	.00476	1.26+- 1.02	.3

Trial 4

SOURCE CONTRIBUTION ESTIMATES - SITE: BEMIS   DATE: 12/27/95   CMB7 33889
SAMPLE DURATION   24   START HOUR   00   SIZE: 10
        R SQUARE   .96   PERCENT MASS   99.9
       CHI SQUARE   .72   DF   11

SOURCE * TYPE	SCE(UG/M3)	STD ERR	TSTAT
6 LVGEOLC	45.8181	5.7180	8.0130
15 LVRWCC1	.5262	1.1149	.4720
19 (NH4)2SO	.8578	.4850	1.7687
20 NH4NO3	2.8689	.3383	8.4806
23 LVMVC2	3.6205	2.5326	1.4296

MEASURED CONCENTRATION FOR SIZE: 10
     53.7+-   2.7

UNCERTAINTY/SIMILARITY CLUSTERS CMB7 33889	SUM OF CLUSTER SOURCES
15 23	4.147+- 2.401

SPECIES CONCENTRATIONS - SITE: BEMIS   DATE: 12/27/95   CMB7 33889
SAMPLE DURATION   24   START HOUR   00   SIZE: 10
        R SQUARE   .96   PERCENT MASS   99.9
       CHI SQUARE   .72   DF   11

SPECIES		I	MEAS		CALC		RATIO C/M	RATIO R/U
MSGC	MSGU	T	53.73070+-	2.71900	53.69153+-	4.93048	1.00+- .10	.0
CLIC	CLIU	*	.11520+-	.02260	.08303+-	.04076	.72+- .38	-.7
N3IC	N3IU	*	2.30860+-	.12510	2.30860+-	.22977	1.00+- .11	.0
S4IC	S4IU	*	1.26390+-	.06780	1.26390+-	.33460	1.00+- .27	.0
N4CC	N4CU		.36470+-	.02810	.97197+-	.07622	2.67+- .29	7.5
KPAC	KPAU	*	.08490+-	.00570	.09010+-	.02546	1.06+- .31	.2
OCTC	OCTU	*	5.76290+-	.41880	6.74304+-	1.77778	1.17+- .32	.5
ECTC	ECTU	*	3.24370+-	.36780	2.61666+-	1.06994	.81+- .34	-.6
TCTC	TCTU		8.97400+-	.55630	9.14068+-	2.32509	1.02+- .27	.1

```
NAXC   NAXU          .00000<    .10400    .01504<    .02421    .00<   .00      .1
MGXC   MGXU          .97650+-   .05470   1.44899+-   .30241   1.48+-  .32     1.5
ALXC   ALXU    *    1.28650+-   .38330    .66155+-   .17095    .51+-  .20    -1.5
SIXC   SIXU    *    5.08420+-  1.61810   3.57245+-   .68722    .70+-  .26    -.9
PHXC   PHXU          .00600<    .01610    .01207<    .00967   2.01<  5.63     .3
SUXC   SUXU          .48010+-   .16810    .42204+-   .09635    .88+-  .37    -.3
CLXC   CLXU    *     .00960<    .05590    .04740<    .03050   4.94< 28.93     .6
KPXC   KPXU    *     .43050+-   .08860    .47603+-   .09611   1.11+-  .32     .3
CAXC   CAXU    *    9.63140+-  1.62470   7.49568+-  1.20872    .78+-  .18    -1.1
TIXC   TIXU    *     .04810+-   .01530    .07940+-   .02376   1.65+-  .72     1.1
CRXC   CRXU    *     .00500+-   .00220    .00314+-   .00133    .63+-  .38    -.7
MNXC   MNXU    *     .01620+-   .00150    .01811+-   .00429   1.12+-  .28     .4
FEXC   FEXU    *     .75420+-   .03990    .86503+-   .23206   1.15+-  .31     .5
NIXC   NIXU          .00390+-   .00070    .00170+-   .00063    .44+-  .18    -2.3
CUXC   CUXU          .01470+-   .00100    .00517+-   .00239    .35+-  .16    -3.7
ZNXC   ZNXU          .05470+-   .00290    .03007+-   .02091    .55+-  .38    -1.2
BRXC   BRXU          .00180+-   .00070    .00207+-   .00096   1.15+-  .70     .2
RBXC   RBXU          .00160+-   .00060    .00238+-   .00060   1.49+-  .67     .9
SRXC   SRXU          .03510+-   .00190    .05517+-   .01445   1.57+-  .42     1.4
YTXC   YTXU          .00060<    .00120    .00088<    .00028   1.46<  2.96     .2
ZRXC   ZRXU          .00220+-   .00110    .00308+-   .00088   1.40+-  .81     .6
MOXC   MOXU          .00000<    .00250    .00079<    .00060    .00<   .00     .3
BAXC   BAXU          .04750+-   .04010    .01263+-   .01349    .27+-  .36    -.8
PBXC   PBXU    *     .00530+-   .00200    .00668+-   .00479   1.26+- 1.02     .3
------------------------------------------------------------------------------------
```

Trial 5

```
SOURCE CONTRIBUTION ESTIMATES -  SITE: BEMIS        DATE: 12/27/95   CMB7 33889
SAMPLE DURATION        24      START HOUR       00         SIZE:    10
        R SQUARE       .96    PERCENT MASS    100.6
        CHI SQUARE     .66                     DF       12

    SOURCE
     * TYPE     SCE(UG/M3)    STD ERR      TSTAT
    --------------------------------------------------
6      LVGEOLC    46.3648      5.8976      7.8617
14     LVMVEC      4.0028      2.5152      1.5915
19     (NH4)2SO     .8230       .5191      1.5853
20     NH4NO3      2.8673       .3433      8.3524
    --------------------------------------------------

MEASURED CONCENTRATION FOR SIZE: 10
      53.7+-     2.7

        UNCERTAINTY/SIMILARITY CLUSTERS    CMB7 33889      SUM OF CLUSTER SOURCES
------------------------------------------------------------------------------------


------------------------------------------------------------------------------------

SPECIES CONCENTRATIONS -  SITE: BEMIS        DATE: 12/27/95    CMB7 33889
SAMPLE DURATION        24      START HOUR       00         SIZE:    10
        R SQUARE       .96    PERCENT MASS    100.6
        CHI SQUARE     .66                     DF       12

SPECIES-------I---MEAS----------------CALC-------------RATIO C/M----RATIO R/U
MSGC   MSGU    T  53.73070+- 2.71900  54.05793+- 5.11796   1.01+-  .11      .1
CLIC   CLIU    *    .11520+-  .02260    .06706+-  .04009    .58+-  .37    -1.0
N3IC   N3IU    *   2.30860+-  .12510   2.30860+-  .23425   1.00+-  .12     .0
S4IC   S4IU    *   1.26390+-  .06780   1.26390+-  .36027   1.00+-  .29     .0
N4CC   N4CU        .36470+-  .02810    .95865+-  .08500   2.63+-  .31     6.6
KPAC   KPAU    *    .08490+-  .00570    .09175+-  .03299   1.08+-  .40     .2
```

```
OCTC   OCTU   *   5.76290+-   .41880    6.67857+-  1.82010    1.16+-    .33        .5
ECTC   ECTU   *   3.24370+-   .36780    2.73420+-  1.13603     .84+-    .36       -.4
TCTC   TCTU       8.97400+-   .55630    9.18953+-  2.37248    1.02+-    .27        .1
NAXC   NAXU        .00000<    .10400     .01923<   .03094     .00<     .00        .2
MGXC   MGXU        .97650+-   .05470    1.47188+-   .30699    1.51+-    .33       1.6
ALXC   ALXU   *   1.28650+-   .38330     .67118+-   .17354     .52+-    .21      -1.5
SIXC   SIXU   *   5.08420+-  1.61810    3.62077+-   .69709     .71+-    .26       -.8
PHXC   PHXU        .00600<    .01610     .01203<   .00990     2.00<    5.63        .3
SUXC   SUXU        .48010+-   .16810     .42096+-   .10808     .88+-    .38       -.3
CLXC   CLXU   *    .00960<    .05590     .03174<   .02949     3.31<   19.49        .4
KPXC   KPXU   *    .43050+-   .08860     .48144+-   .09941    1.12+-    .33        .4
CAXC   CAXU   *   9.63140+-  1.62470    7.60004+-  1.22602     .79+-    .18      -1.0
TIXC   TIXU   *    .04810+-   .01530     .08030+-   .02490    1.67+-    .74       1.1
CRXC   CRXU   *    .00500+-   .00220     .00315+-   .00158     .63+-    .42       -.7
MNXC   MNXU   *    .01620+-   .00150     .01843+-   .00447    1.14+-    .30        .5
FEXC   FEXU   *    .75420+-   .03990     .87798+-   .23803    1.16+-    .32        .5
NIXC   NIXU        .00390+-   .00070     .00170+-   .00068     .44+-    .19      -2.3
CUXC   CUXU        .01470+-   .00100     .00554+-   .00335     .38+-    .23      -2.6
ZNXC   ZNXU        .05470+-   .00290     .03090+-   .02136     .56+-    .39      -1.1
BRXC   BRXU        .00180+-   .00070     .00214+-   .00104    1.19+-    .74        .3
RBXC   RBXU        .00160+-   .00060     .00241+-   .00068    1.51+-    .71        .9
SRXC   SRXU        .03510+-   .00190     .05658+-   .01562    1.61+-    .45       1.4
YTXC   YTXU        .00060<    .00120     .00089<   .00051     1.48<    3.09        .2
ZRXC   ZRXU        .00220+-   .00110     .00318+-   .00101    1.45+-    .86        .7
MOXC   MOXU        .00000<    .00250     .00084<   .00107     .00<     .00        .3
BAXC   BAXU        .04750+-   .04010     .01364+-   .02481     .29+-    .58       -.7
PBXC   PBXU   *    .00530+-   .00200     .00670+-   .00497    1.26+-   1.05        .3
------------------------------------------------------------------------------------
```

Table 7-7b

Example of CMB Source Contribution Estimates
for the Sample Collected at the East Charleston Site on 12/27/95

```
Best Fit

SOURCE CONTRIBUTION ESTIMATES - SITE: ECHARLES     DATE: 12/27/95   CMB7 33889
SAMPLE DURATION        24      START HOUR       00        SIZE:    10
       R SQUARE       .97   PERCENT MASS      106.5
       CHI SQUARE     .95              DF         10

   SOURCE
       * TYPE    SCE(UG/M3)    STD ERR     TSTAT
---------------------------------------------------
2      LVGPLOTC   82.0770      8.4865      9.6715
17     LVRWCC3     2.2555      1.1496      1.9620
20     NH4NO3      2.3462       .3102      7.5629
23     LVMVC2     14.8464      4.6651      3.1825
---------------------------------------------------

MEASURED CONCENTRATION FOR SIZE: 10
       95.3+-      4.8


       UNCERTAINTY/SIMILARITY CLUSTERS    CMB7 33889    SUM OF CLUSTER SOURCES
------------------------------------------------------------------------------


------------------------------------------------------------------------------


SPECIES CONCENTRATIONS - SITE: ECHARLES      DATE: 12/27/95    CMB7 33889
SAMPLE DURATION        24      START HOUR       00        SIZE:    10
       R SQUARE       .97   PERCENT MASS      106.5
       CHI SQUARE     .95              DF         10

SPECIES-------I---MEAS-----------------CALC-------------RATIO C/M----RATIO R/U
MSGC   MSGU   T  95.29530+-  4.79070 101.52530+-  7.26847   1.07+-   .09      .7
CLIC   CLIU   *    .26170+-   .03090    .38517+-   .13924   1.47+-   .56      .9
N3IC   N3IU   *   2.54310+-   .13960   2.14165+-   .25119    .84+-   .11    -1.4
S4IC   S4IU   *   2.29700+-   .13010   2.06210+-   .75387    .90+-   .33     -.3
N4CC   N4CU   *    .53550+-   .03720    .78306+-   .11409   1.46+-   .24     2.1
KPAC   KPAU   *    .31680+-   .01770    .27466+-   .05608    .87+-   .18     -.7
OCTC   OCTU   *  17.31630+-  1.04070  20.13814+-  4.21354   1.16+-   .25      .7
ECTC   ECTU   *  11.51400+-  1.29040  10.41613+-  1.32237    .90+-   .15     -.6
TCTC   TCTU     28.79470+-  1.55680  29.83289+-  3.70125   1.04+-   .14      .3
NAXC   NAXU       .00000<    .14840    .10189<    .15564    .00<    .00      .5
MGXC   MGXU      1.52800+-   .08350   2.06358+-   .48609   1.35+-   .33     1.1
ALXC   ALXU   *   1.90550+-   .56750   1.56725+-   .12838    .82+-   .25     -.6
SIXC   SIXU   *   8.58740+-  2.72850   7.55432+-   .38924    .88+-   .28     -.4
PHXC   PHXU       .05480+-   .02470    .04717+-   .02902    .86+-   .66     -.2
SUXC   SUXU      1.19010+-   .41500    .77246+-   .19918    .65+-   .28     -.9
CLXC   CLXU   *    .33230+-   .10000    .28696+-   .10341    .86+-   .41     -.3
KPXC   KPXU   *   1.07730+-   .21620   1.12449+-   .10048   1.04+-   .23      .2
CAXC   CAXU   *  12.44950+-  2.09950  11.08295+-  2.12718    .89+-   .23     -.5
TIXC   TIXU       .09760+-   .01940    .22232+-   .06230   2.28+-   .78     1.9
CRXC   CRXU       .00300<    .00550    .00807<    .00436   2.69<   5.14      .7
MNXC   MNXU       .03220+-   .00240    .03941+-   .00376   1.22+-   .15     1.6
FEXC   FEXU   *   1.95020+-   .09880   2.05322+-   .21364   1.05+-   .12      .4
NIXC   NIXU       .00150+-   .00080    .00385+-   .00132   2.57+-  1.63     1.5
CUXC   CUXU       .03220+-   .00180    .01873+-   .00308    .58+-   .10    -3.8
ZNXC   ZNXU       .08420+-   .00430    .13853+-   .00673   1.65+-   .12     6.8
```

```
BRXC   BRXU        .00900+-   .00100    .00734+-   .00216    .82+-  .26     -.7
RBXC   RBXU        .00300+-   .00080    .00585+-   .00113   1.95+-  .64     2.1
SRXC   SRXU        .04710+-   .00250    .07159+-   .00708   1.52+-  .17     3.3
YTXC   YTXU        .00080<    .00150    .00169<    .00202   2.12<  4.70      .4
ZRXC   ZRXU        .00490+-   .00140    .00789+-   .00192   1.61+-  .60     1.3
MOXC   MOXU        .00000<    .00320    .00099<    .00412    .00<   .00      .2
BAXC   BAXU        .11400+-   .04860    .01780+-   .09610    .16+-  .85     -.9
PBXC   PBXU    *   .02580+-   .00280    .02124+-   .01192    .82+-  .47     -.4
-----------------------------------------------------------------------------
```

Trial 1

```
SOURCE CONTRIBUTION ESTIMATES -  SITE: ECHARLES    DATE: 12/27/95    CMB7 33889
SAMPLE DURATION         24       START HOUR        00        SIZE:    10
        R SQUARE        .96    PERCENT MASS     119.1
        CHI SQUARE     1.00               DF         10

    SOURCE
        * TYPE     SCE(UG/M3)    STD ERR     TSTAT
----------------------------------------------------
6       LVGEOLC     90.0298     12.7336      7.0702
17      LVRWCC3      2.3843      1.1233      2.1226
20      NH4NO3       2.3622       .3435      6.8773
23      LVMVC2      18.7082      5.3658      3.4866
----------------------------------------------------


MEASURED CONCENTRATION FOR SIZE: 10
      95.3+-      4.8


        UNCERTAINTY/SIMILARITY CLUSTERS    CMB7 33889    SUM OF CLUSTER SOURCES
-----------------------------------------------------------------------------


-----------------------------------------------------------------------------

SPECIES CONCENTRATIONS -  SITE: ECHARLES     DATE: 12/27/95    CMB7 33889
SAMPLE DURATION         24       START HOUR        00        SIZE:    10
        R SQUARE        .96    PERCENT MASS     119.1
        CHI SQUARE     1.00               DF         10

SPECIES-------I---MEAS-----------------CALC-------------RATIO C/M----RATIO R/U
MSGC   MSGU   T  95.29530+-  4.79070 113.48440+- 11.40457   1.19+-  .13    1.5
CLIC   CLIU   *    .26170+-   .03090    .35023+-   .11711   1.34+-  .47     .7
N3IC   N3IU   *   2.54310+-   .13960   2.10956+-   .28527    .83+-  .12   -1.4
S4IC   S4IU   *   2.29700+-   .13010   1.74926+-   .82984    .76+-  .36    -.7
N4CC   N4CU   *    .53550+-   .03720    .79070+-   .12669   1.48+-  .26    1.9
KPAC   KPAU   *    .31680+-   .01770    .29904+-   .06166    .94+-  .20    -.3
OCTC   OCTU   *  17.31630+-  1.04070  19.49776+-  3.63149   1.13+-  .22     .6
ECTC   ECTU   *  11.51400+-  1.29040  10.14322+-  2.30215    .88+-  .22    -.5
TCTC   TCTU     28.79470+-  1.55680  28.83543+-  4.61187   1.00+-  .17     .0
NAXC   NAXU      .00000<    .14840    .10522<    .06993    .00<   .00     .6
MGXC   MGXU     1.52800+-   .08350   2.87673+-   .59652   1.88+-  .40    2.2
ALXC   ALXU   *   1.90550+-   .56750   1.33335+-   .33696    .70+-  .27    -.9
SIXC   SIXU   *   8.58740+-  2.72850   7.11302+-  1.35293    .83+-  .31    -.5
PHXC   PHXU      .05480+-   .02470    .03332+-   .02053    .61+-  .46    -.7
SUXC   SUXU     1.19010+-   .41500    .63244+-   .29281    .53+-  .31   -1.1
CLXC   CLXU   *    .33230+-   .10000    .23682+-   .09184    .71+-  .35    -.7
KPXC   KPXU   *   1.07730+-   .21620   1.06637+-   .19543    .99+-  .27    -.0
CAXC   CAXU   *  12.44950+-  2.09950  14.81667+-  2.37874   1.19+-  .28     .7
TIXC   TIXU      .09760+-   .01940    .16832+-   .04902   1.72+-  .61    1.3
CRXC   CRXU      .00300<    .00550    .00774<    .00423   2.58<  4.94     .7
MNXC   MNXU      .03220+-   .00240    .03860+-   .00883   1.20+-  .29     .7
FEXC   FEXU   *   1.95020+-   .09880   1.84100+-   .46848    .94+-  .24    -.2
```

```
NIXC    NIXU          .00150+-    .00080    .00432+-    .00160    2.88+- 1.87      1.6
CUXC    CUXU          .03220+-    .00180    .01994+-    .00577    :62+-   .18     -2.0
ZNXC    ZNXU          .08420+-    .00430    .09136+-    .04137    1.08+-  .49       .2
BRXC    BRXU          .00900+-    .00100    .00866+-    .00273     .96+-  .32      -.1
RBXC    RBXU          .00300+-    .00080    .00500+-    .00124    1.67+-  .61      1.3
SRXC    SRXU          .04710+-    .00250    .11064+-    .02913    2.35+-  .63      2.2
YTXC    YTXU          .00080<     .00150    .00189<     .00072    2.36<  4.52      .7
ZRXC    ZRXU          .00490+-    .00140    .00638+-    .00187    1.30+-  .53      .6
MOXC    MOXU          .00000<     .00320    .00187<     .00153     .00<   .00      .5
BAXC    BAXU          .11400+-    .04860    .03326+-    .03500     .29+-  .33     -1.3
PBXC    PBXU    *     .02580+-    .00280    .01757+-    .00970     .68+-  .38      -.8
-----------------------------------------------------------------------------------
```

Trial 2

```
SOURCE CONTRIBUTION ESTIMATES -  SITE: ECHARLES    DATE: 12/27/95    CMB7 33889
SAMPLE DURATION          24      START HOUR        00         SIZE:   10
        R SQUARE        .97    PERCENT MASS     109.9
        CHI SQUARE     1.01                DF        10

     SOURCE
        * TYPE    SCE(UG/M3)    STD ERR     TSTAT
-----------------------------------------------------
3        LVGPVRDC    85.7402     9.4778      9.0464
17       LVRWCC3      2.3671     1.0404      2.2752
20       NH4NO3       2.3018      .3018      7.6275
23       LVMVC2      14.2947     5.2719      2.7115
-----------------------------------------------------

MEASURED CONCENTRATION FOR SIZE: 10
        95.3+-     4.8

        UNCERTAINTY/SIMILARITY CLUSTERS    CMB7 33889    SUM OF CLUSTER SOURCES
-----------------------------------------------------------------------------------

-----------------------------------------------------------------------------------

SPECIES CONCENTRATIONS -  SITE: ECHARLES    DATE: 12/27/95    CMB7 33889
SAMPLE DURATION          24      START HOUR        00         SIZE:   10
        R SQUARE        .97    PERCENT MASS     109.9
        CHI SQUARE     1.01                DF        10

SPECIES-------I---MEAS----------------CALC-------------RATIO C/M----RATIO R/U
MSGC    MSGU    T  95.29530+-  4.79070 104.70380+-  8.01796    1.10+-  .10     1.0
CLIC    CLIU    *    .26170+-   .03090    .33115+-   .10177    1.27+-  .42      .7
N3IC    N3IU    *   2.54310+-   .13960   2.08396+-   .24779     .82+-  .11    -1.6
S4IC    S4IU    *   2.29700+-   .13010   1.88500+-   .80651     .82+-  .35     -.5
N4CC    N4CU    *    .53550+-   .03720    .77100+-   .10375    1.44+-  .22     2.1
KPAC    KPAU    *    .31680+-   .01770    .29264+-   .06460     .92+-  .21     -.4
OCTC    OCTU    *  17.31630+-  1.04070  18.49526+-  3.48676    1.07+-  .21      .3
ECTC    ECTU    *  11.51400+-  1.29040   9.90903+-  2.16105     .86+-  .21     -.6
TCTC    TCTU       28.79470+-  1.55680  27.68092+-  4.44198     .96+-  .16     -.2
NAXC    NAXU         .00000<    .14840    .10234<    .09458     .00<   .00      .6
MGXC    MGXU        1.52800+-   .08350   2.34141+-   .35743    1.53+-  .25     2.2
ALXC    ALXU    *   1.90550+-   .56750   1.42684+-   .12054     .75+-  .23     -.8
SIXC    SIXU    *   8.58740+-  2.72850   7.34501+-   .66526     .86+-  .28     -.4
PHXC    PHXU         .05480+-   .02470    .03719+-   .01930     .68+-  .47     -.6
SUXC    SUXU        1.19010+-   .41500    .65813+-   .20012     .55+-  .26    -1.2
CLXC    CLXU    *    .33230+-   .10000    .24745+-   .08352     .74+-  .34     -.7
KPXC    KPXU    *   1.07730+-   .21620   1.07943+-   .11739    1.00+-  .23      .0
CAXC    CAXU    *  12.44950+-  2.09950  12.92767+-  2.29478    1.04+-  .25      .2
TIXC    TIXU         .09760+-   .01940    .18120+-   .02053    1.86+-  .42     3.0
```

```
CRXC    CRXU        .00300<    .00550    .00896<    .00355    2.99<  5.60      .9
MNXC    MNXU        .03220+-   .00240    .04202+-   .00542    1.31+-  .19     1.7
FEXC    FEXU    *  1.95020+-   .09880   2.08034+-   .26450    1.07+-  .15      .5
NIXC    NIXU        .00150+-   .00080    .00461+-   .00147    3.08+- 1.91     1.9
CUXC    CUXU        .03220+-   .00180    .02109+-   .00447     .66+-  .14    -2.3
ZNXC    ZNXU        .08420+-   .00430    .11623+-   .02352    1.38+-  .29     1.3
BRXC    BRXU        .00900+-   .00100    .00832+-   .00306     .92+-  .36     -.2
RBXC    RBXU        .00300+-   .00080    .00455+-   .00101    1.52+-  .53     1.2
SRXC    SRXU        .04710+-   .00250    .10732+-   .03947    2.28+-  .85     1.5
YTXC    YTXU        .00080<    .00150    .00167<    .00120    2.08<  4.18      .5
ZRXC    ZRXU        .00490+-   .00140    .00649+-   .00160    1.33+-  .50      .8
MOXC    MOXU        .00000<    .00320    .00186<    .00257     .00<   .00      .5
BAXC    BAXU        .11400+-   .04860    .03862+-   .05925     .34+-  .54    -1.0
PBXC    PBXU    *   .02580+-   .00280    .02385+-   .00536     .92+-  .23     -.3
    -----------------------------------------------------------------------------
```

Trial 3

```
SOURCE CONTRIBUTION ESTIMATES -  SITE: ECHARLES     DATE: 12/27/95    CMB7 33889
SAMPLE DURATION         24        START HOUR        00         SIZE:    10
        R SQUARE        .96     PERCENT MASS      111.3
       CHI SQUARE      1.29            DF           10

     SOURCE
        * TYPE      SCE(UG/M3)     STD ERR     TSTAT
    -----------------------------------------------
    2      LVGPLOTC     85.4707     8.6210      9.9143
    15     LVRWCC1       1.3268     2.6230       .5058
    20     NH4NO3        2.3290      .3295      7.0679
    23     LVMVC2       16.9641     4.8115      3.5257
    -----------------------------------------------
```

```
MEASURED CONCENTRATION FOR SIZE: 10
        95.3+-      4.8
```

```
        UNCERTAINTY/SIMILARITY CLUSTERS     CMB7 33889     SUM OF CLUSTER SOURCES
    --------------------------------------------------------------------------------

        2       15      23                              103.762+-     7.313
                15      23                               18.291+-     4.846
    --------------------------------------------------------------------------------
```

```
SPECIES CONCENTRATIONS -  SITE: ECHARLES    DATE: 12/27/95    CMB7 33889
SAMPLE DURATION         24        START HOUR        00        SIZE:    10
        R SQUARE        .96     PERCENT MASS      111.3
       CHI SQUARE      1.29            DF           10

SPECIES-------I---MEAS-----------------CALC------------RATIO C/M----RATIO R/U
MSGC    MSGU    T  95.29530+-  4.79070 106.09050+-  7.28539    1.11+-  .09    1.2
CLIC    CLIU    *    .26170+-   .03090    .27869+-   .12843    1.06+-  .51     .1
N3IC    N3IU    *   2.54310+-   .13960   2.13216+-   .26600     .84+-  .11   -1.4
S4IC    S4IU    *   2.29700+-   .13010   2.16517+-   .81265     .94+-  .36    -.2
N4CC    N4CU    *    .53550+-   .03720    .79786+-   .12398    1.49+-  .25    2.0
KPAC    KPAU    *    .31680+-   .01770    .21317+-   .05275     .67+-  .17   -1.9
OCTC    OCTU    *  17.31630+-  1.04070  21.67151+-  4.40514    1.25+-  .27    1.0
ECTC    ECTU    *  11.51400+-  1.29040  10.86986+-  1.41425     .94+-  .16    -.3
TCTC    TCTU       28.79470+-  1.55680  31.77156+-  3.85789    1.10+-  .15     .7
NAXC    NAXU         .00000<   .14840    .06997<    .16235     .00<   .00     .3
MGXC    MGXU        1.52800+-   .08350   2.14814+-   .50659    1.41+-  .34    1.2
ALXC    ALXU    *   1.90550+-   .56750   1.63352+-   .13408     .86+-  .26    -.5
SIXC    SIXU    *   8.58740+-  2.72850   7.86441+-   .40673     .92+-  .29    -.3
PHXC    PHXU         .05480+-   .02470    .04880+-   .03035     .89+-  .68    -.2
```

```
SUXC    SUXU        1.19010+-   .41500   .81597+-   .22675    .69+-   .31    -.8
CLXC    CLXU    *    .33230+-   .10000   .18436+-   .08925    .55+-   .32   -1.1
KPXC    KPXU    *   1.07730+-   .21620  1.07360+-   .09961   1.00+-   .22    -.0
CAXC    CAXU    *  12.44950+-  2.09950 11.53191+-  2.21577    .93+-   .24    -.3
TIXC    TIXU         .09760+-   .01940   .23246+-   .06475   2.38+-   .81    2.0
CRXC    CRXU         .00300<    .00550   .00860<    .00468   2.87<  5.48     .8
MNXC    MNXU         .03220+-   .00240   .04086+-   .00404   1.27+-   .16    1.8
FEXC    FEXU    *   1.95020+-   .09880  2.15203+-   .22666   1.10+-   .13     .8
NIXC    NIXU         .00150+-   .00080   .00406+-   .00140   2.71+- 1.72    1.6
CUXC    CUXU         .03220+-   .00180   .02018+-   .00347    .63+-   .11   -3.1
ZNXC    ZNXU         .08420+-   .00430   .14036+-   .00692   1.67+-   .12    6.9
BRXC    BRXU         .00900+-   .00100   .00713+-   .00233    .79+-   .27    -.7
RBXC    RBXU         .00300+-   .00080   .00594+-   .00115   1.98+-   .65    2.1
SRXC    SRXU         .04710+-   .00250   .07465+-   .00782   1.58+-   .19    3.4
YTXC    YTXU         .00080<    .00150   .00178<    .00206   2.22<  4.90     .4
ZRXC    ZRXU         .00490+-   .00140   .00825+-   .00196   1.68+-   .63    1.4
MOXC    MOXU         .00000<    .00320   .00107<    .00421    .00<   .00     .2
BAXC    BAXU         .11400+-   .04860   .01882+-   .09819    .17+-   .86    -.9
PBXC    PBXU    *    .02580+-   .00280   .02196+-   .01241    .85+-   .49    -.3
        -----------------------------------------------------------------------


Trial 4

SOURCE CONTRIBUTION ESTIMATES -  SITE: ECHARLES    DATE: 12/27/95    CMB7 33889
SAMPLE DURATION         24       START HOUR        00       SIZE:    10
        R SQUARE       .96    PERCENT MASS     111.1
        CHI SQUARE    1.19                    DF        11

    SOURCE
      * TYPE      SCE(UG/M3)    STD ERR     TSTAT
    ------------------------------------------------
2       LVGPLOTC    85.9844     8.6221      9.9725
20      NH4NO3       2.3568      .3321      7.0963
23      LVMVC2      17.5213     4.6834      3.7411
    ------------------------------------------------


MEASURED CONCENTRATION FOR SIZE: 10
        95.3+-     4.8

        UNCERTAINTY/SIMILARITY CLUSTERS    CMB7 33889    SUM OF CLUSTER SOURCES
    ---------------------------------------------------------------------------

    ---------------------------------------------------------------------------

SPECIES CONCENTRATIONS -  SITE: ECHARLES    DATE: 12/27/95    CMB7 33889
SAMPLE DURATION         24       START HOUR        00       SIZE:    10
        R SQUARE       .96    PERCENT MASS     111.1
        CHI SQUARE    1.19                    DF        11

SPECIES-------I---MEAS-----------------CALC-------------RATIO C/M----RATIO R/U
MSGC    MSGU   T 95.29530+-  4.79070 105.86260+-  7.31610   1.11+-   .09    1.2
CLIC    CLIU   *    .26170+-   .03090    .23564+-   .12344    .90+-   .48    -.2
N3IC    N3IU   *   2.54310+-   .13960   2.15766+-   .27171    .85+-   .12   -1.3
S4IC    S4IU   *   2.29700+-   .13010   2.19063+-   .82621    .95+-   .36    -.1
N4CC    N4CU   *    .53550+-   .03720    .78648+-   .12566   1.47+-   .26    1.9
KPAC    KPAU   *    .31680+-   .01770    .21151+-   .05317    .67+-   .17   -1.9
OCTC    OCTU   *  17.31630+-  1.04070  21.27317+-  4.43384   1.23+-   .27     .9
ECTC    ECTU   *  11.51400+-  1.29040  11.05034+-  1.43817    .96+-   .16    -.2
TCTC    TCTU      28.79470+-  1.55680  31.53734+-  3.87889   1.10+-   .15     .7
NAXC    NAXU         .00000<    .14840    .07128<    .16370    .00<   .00     .3
MGXC    MGXU        1.52800+-   .08350   2.16184+-   .50977   1.41+-   .34    1.2
ALXC    ALXU   *   1.90550+-   .56750   1.64411+-   .13502    .86+-   .27    -.4
```

```
SIXC    SIXU    *    8.58740+-   2.72850    7.91445+-    .40963    .92+-    .30    -.2
PHXC    PHXU         .05480+-    .02470     .04936+-     .03058    .90+-    .69    -.1
SUXC    SUXU        1.19010+-    .41500     .82732+-     .23398    .70+-    .31    -.8
CLXC    CLXU    *    .33230+-    .10000     .13986+-     .08072    .42+-    .27   -1.5
KPXC    KPXU    *   1.07730+-    .21620    1.07348+-     .10041   1.00+-    .22    -.0
CAXC    CAXU    *  12.44950+-   2.09950   11.60348+-    2.22929    .93+-    .24    -.3
TIXC    TIXU         .09760+-    .01940     .23431+-     .06520   2.40+-    .82    2.0
CRXC    CRXU         .00300<     .00550     .00871<      .00476   2.90<   5.55     .8
MNXC    MNXU         .03220+-    .00240     .04121+-     .00410   1.28+-    .16    1.9
FEXC    FEXU    *   1.95020+-    .09880    2.17022+-     .22935   1.11+-    .13     .9
NIXC    NIXU         .00150+-    .00080     .00412+-     .00142   2.75+-   1.75    1.6
CUXC    CUXU         .03220+-    .00180     .02065+-     .00357    .64+-    .12   -2.9
ZNXC    ZNXU         .08420+-    .00430     .14209+-     .00703   1.69+-    .12    7.0
BRXC    BRXU         .00900+-    .00100     .00722+-     .00238    .80+-    .28    -.7
RBXC    RBXU         .00300+-    .00080     .00597+-     .00116   1.99+-    .66    2.1
SRXC    SRXU         .04710+-    .00250     .07517+-     .00801   1.60+-    .19    3.3
YTXC    YTXU         .00080<     .00150     .00179<      .00208   2.24<   4.94     .4
ZRXC    ZRXU         .00490+-    .00140     .00832+-     .00197   1.70+-    .63    1.4
MOXC    MOXU         .00000<     .00320     .00109<      .00424    .00<    .00     .2
BAXC    BAXU         .11400+-    .04860     .01922+-     .09880    .17+-    .87    -.9
PBXC    PBXU    *    .02580+-    .00280     .02210+-     .01250    .86+-    .49    -.3
-------------------------------------------------------------------------------------
```

Trial 5

```
SOURCE CONTRIBUTION ESTIMATES -  SITE: ECHARLES      DATE: 12/27/95     CMB7 33889
SAMPLE DURATION         24       START HOUR        00         SIZE:    10
       R SQUARE         .98      PERCENT MASS    107.3
       CHI SQUARE       .58      DF               10

     SOURCE
       * TYPE     SCE(UG/M3)     STD ERR     TSTAT
    ----------------------------------------------------
    2      LVGPLOTC     83.1655      9.3360      8.9080
    14     LVMVEC       14.7056      5.4172      2.7146
    17     LVRWCC3       1.8505      1.3204      1.4014
    20     NH4NO3        2.5168       .3850      6.5362
    ----------------------------------------------------


MEASURED CONCENTRATION FOR SIZE: 10
       95.3+-      4.8

        UNCERTAINTY/SIMILARITY CLUSTERS     CMB7 33889     SUM OF CLUSTER SOURCES
-------------------------------------------------------------------------------------

-------------------------------------------------------------------------------------

SPECIES CONCENTRATIONS -  SITE: ECHARLES     DATE: 12/27/95    CMB7 33889
SAMPLE DURATION         24       START HOUR        00         SIZE:    10
       R SQUARE         .98      PERCENT MASS    107.3
       CHI SQUARE       .58      DF               10

SPECIES-------I---MEAS-----------------CALC-------------RATIO C/M----RATIO R/U
MSGC    MSGU    T  95.29530+-   4.79070  102.23830+-   8.04940   1.07+-    .10     .7
CLIC    CLIU    *    .26170+-    .03090     .35758+-     .14013   1.37+-    .56     .7
N3IC    N3IU    *   2.54310+-    .13960    2.26482+-     .30225    .89+-    .13    -.8
S4IC    S4IU    *   2.29700+-    .13010    2.09222+-     .86746    .91+-    .38    -.2
N4CC    N4CU    *    .53550+-    .03720     .82645+-     .17966   1.54+-    .35    1.6
KPAC    KPAU    *    .31680+-    .01770     .26612+-     .09316    .84+-    .30    -.5
OCTC    OCTU    *  17.31630+-   1.04070   20.01919+-    4.37820   1.16+-    .26     .6
ECTC    ECTU    *  11.51400+-   1.29040   10.23976+-    1.80394    .89+-    .19    -.6
TCTC    TCTU       28.79470+-   1.55680   29.57204+-    3.91403   1.03+-    .15     .2
```

NAXC	NAXU		.00000<	.14840	.10636<	.17104	.00<	.00	.5
MGXC	MGXU		1.52800+-	.08350	2.10755+-	.50018	1.38+-	.34	1.1
ALXC	ALXU	*	1.90550+-	.56750	1.59032+-	.13931	.83+-	.26	-.5
SIXC	SIXU	*	8.58740+-	2.72850	7.66257+-	.43110	.89+-	.29	-.3
PHXC	PHXU		.05480+-	.02470	.04582+-	.02980	.84+-	.66	-.2
SUXC	SUXU		1.19010+-	.41500	.77251+-	.25084	.65+-	.31	-.9
CLXC	CLXU	*	.33230+-	.10000	.26676+-	.10702	.80+-	.40	-.4
KPXC	KPXU	*	1.07730+-	.21620	1.12586+-	.12467	1.05+-	.24	.2
CAXC	CAXU	*	12.44950+-	2.09950	11.27248+-	2.17671	.91+-	.23	-.4
TIXC	TIXU		.09760+-	.01940	.22339+-	.06715	2.29+-	.82	1.8
CRXC	CRXU		.00300<	.00550	.00785<	.00517	2.62<	5.10	.6
MNXC	MNXU		.03220+-	.00240	.03991+-	.00530	1.24+-	.19	1.3
FEXC	FEXU	*	1.95020+-	.09880	2.07079+-	.25605	1.06+-	.14	.4
NIXC	NIXU		.00150+-	.00080	.00369+-	.00155	2.46+-	1.67	1.3
CUXC	CUXU		.03220+-	.00180	.01875+-	.00896	.58+-	.28	-1.5
ZNXC	ZNXU		.08420+-	.00430	.13749+-	.01241	1.63+-	.17	4.1
BRXC	BRXU		.00900+-	.00100	.00703+-	.00246	.78+-	.29	-.7
RBXC	RBXU		.00300+-	.00080	.00587+-	.00159	1.96+-	.74	1.6
SRXC	SRXU		.04710+-	.00250	.07499+-	.02121	1.59+-	.46	1.3
YTXC	YTXU		.00080<	.00150	.00171<	.00255	2.14<	5.12	.3
ZRXC	ZRXU		.00490+-	.00140	.00819+-	.00261	1.67+-	.72	1.1
MOXC	MOXU		.00000<	.00320	.00113<	.00526	.00<	.00	.2
BAXC	BAXU		.11400+-	.04860	.02003+-	.12302	.18+-	1.08	-.7
PBXC	PBXU	*	.02580+-	.00280	.02084+-	.01268	.81+-	.50	-.4

7.2.6 Source Contribution Estimates for Nonintensive SFS PM$_{10}$ Samples

Source contributions were estimated for 28 samples collected on 14 nonintensive days at the Bemis and East Charleston sites between 04/09/95 and 01/16/96. The individual source contribution estimates for each sample are listed in Table 7-8. Average source contributions at each site are presented as pie charts in Figure 7-5. On average, calculated and measured PM$_{10}$ mass agreed well within their uncertainties at both sites. On average, primary geological material accounted for 92% (37.7 ± 5.6 μg/m^3) and 79% (47.2 ± 5.0 μg/m^3) of the calculated PM$_{10}$ mass at the Bemis and East Charleston sites, respectively. Large geological source contributions of up to 70% were also found in the Imperial Valley, CA, where resuspended dust was found to be one of the main causes of elevated PM$_{10}$ concentrations (Chow and Watson, 1997b).

Primary motor vehicle exhaust was the second-largest contributor, accounting for 4% (1.6 ± 1.5 μg/m^3) and 16% (9.9 ± 4.1 μg/m^3) of average PM$_{10}$ mass at the Bemis and East Charleston sites, respectively. On average, secondary ammonium sulfate and ammonium nitrate accounted for less than 5% of PM$_{10}$ mass at both sites.

On average, the contribution from residential wood combustion was small, with 0.13 ± 0.25 μg/m^3 (0.3% of PM$_{10}$ mass) at the Bemis site and 1.73 ± 0.81 μg/m^3 (3% of PM$_{10}$ mass) at the East Charleston site. This is consistent with the land uses surrounding the two base sites, where more residential neighborhoods are close by to the East Charleston site. As discussed in Section 4, soluble potassium is enriched in wood-combustion and vegetative-burning emissions. The ratio of soluble to total potassium in Las Vegas geological material is 0.17 ± 0.01. In the residential wood combustion source profiles, this ratio ranges from 0.57 to 0.76. In order to detect the source contribution from residential wood combustion, the soluble to total potassium ratio in the ambient aerosol must be significantly larger than its value in geological material. This was especially the case for all of the nonintensive samples collected during November, December, and January at the East Charleston site.

Table 7-8 shows that contributions from residential wood combustion were only detected at the Bemis site during the holiday season on 12/25/95, 01/01/96, and 01/02/96, with the highest contribution found on Christmas Day (0.35 ± 0.18 μg/m^3, 2% of PM$_{10}$ mass). These source contributions were small, accounting for 2% to 4% of the PM$_{10}$ mass on those days.

At the East Charleston site, contributions from residential wood combustion were found during the Christmas/New Year week (12/24/95 to 01/02/96), accounting for 1% to 9% of the PM$_{10}$ mass. The highest residential wood combustion source contribution was found to be 4.1 ± 1.1 μg/m^3 (9% of PM$_{10}$ mass) on Christmas Day (12/25/95).

Table 7-8

Individual Source Contribution Estimates to PM$_{10}$ Mass (μg/m^3) at the Bemis and East Charleston Sites

during the Non-Intensive Monitoring Periods between 04/09/95 and 01/26/96

Site	Date	Primary Geological	Motor Vehicle	Residential Wood Combustion	Secondary Ammonium Sulfate	Secondary Ammonium Nitrate	Measured Mass	Calculated Mass	Unexplained Mass
Bemis	04/09/95	61.7640 ± 6.2902	0.0000 ± 0.0000	0.0000 ± 0.0000	0.0000 ± 0.0000	0.1333 ± 0.0774	54.7460 ± 2.7831	61.8973 ± 6.2907	-7.1513 ± 4.5086
Bemis	04/27/95	45.8310 ± 5.5126	2.6272 ± 2.0414	0.0000 ± 0.0000	1.1733 ± 0.2778	0.7215 ± 0.1079	42.0120 ± 2.1595	50.3530 ± 5.8860	-8.3410 ± 4.0541
Bemis	11/23/95	24.3200 ± 2.3204	0.4543 ± 1.3146	0.0000 ± 0.0000	1.1293 ± 0.1925	0.5679 ± 0.0729	26.9780 ± 1.4077	26.4715 ± 2.6748	0.5065 ± 2.7076
Bemis	12/24/95	5.8946 ± 0.8714	0.9085 ± 0.3967	0.2202 ± 0.1302	1.5751 ± 0.1527	0.3484 ± 0.0486	7.1504 ± 0.5475	8.9468 ± 0.9795	-1.7964 ± 1.5029
Bemis	12/25/95	14.1650 ± 1.9942	1.1881 ± 0.8064	0.3546 ± 0.1780	0.9966 ± 0.1405	0.4384 ± 0.0587	15.2840 ± 0.8803	17.1427 ± 2.1638	-1.8587 ± 2.2589
Bemis	12/26/95	22.7290 ± 3.0325	1.2876 ± 1.2498	0.1842 ± 0.2609	0.7550 ± 0.1705	0.6766 ± 0.0818	25.1550 ± 1.3260	25.6324 ± 3.2957	-0.4774 ± 2.8896
Bemis	12/27/95	45.5140 ± 5.8074	3.7099 ± 2.4798	0.2124 ± 0.4562	0.8547 ± 0.4834	2.8667 ± 0.3382	53.7310 ± 2.7190	53.1577 ± 6.3586	0.5733 ± 4.4844
Bemis	12/28/95	44.2590 ± 5.5578	4.1127 ± 2.4458	0.0497 ± 0.4396	0.8817 ± 0.4795	2.6613 ± 0.3169	45.3940 ± 2.3089	51.9644 ± 6.1151	-6.5704 ± 4.1906
Bemis	12/29/95	50.1660 ± 6.2956	3.2084 ± 2.7107	0.0201 ± 0.4909	0.3562 ± 0.5100	1.5073 ± 0.1905	49.0540 ± 2.4878	55.2580 ± 6.8935	-6.2040 ± 4.4695
Bemis	12/30/95	22.3900 ± 2.9590	2.3476 ± 1.2722	0.1109 ± 0.2523	0.3631 ± 0.2466	1.0484 ± 0.1295	21.8960 ± 1.1716	26.2600 ± 3.2427	-4.3640 ± 2.8032
Bemis	12/31/95	32.0930 ± 3.8477	0.5890 ± 1.6154	0.0000 ± 0.0000	0.3911 ± 0.3171	0.9856 ± 0.1231	26.9510 ± 1.4117	34.0587 ± 4.1869	-7.1077 ± 3.2197
Bemis	01/01/96	8.2052 ± 1.2412	0.2974 ± 0.4793	0.3249 ± 0.1512	0.0316 ± 0.0617	0.0455 ± 0.0299	8.0177 ± 0.5988	8.9046 ± 1.3408	-0.8869 ± 1.7436
Bemis	01/02/96	7.8557 ± 1.0443	1.8818 ± 0.5854	0.3502 ± 0.1670	0.0947 ± 0.0789	0.0653 ± 0.0405	-99.0000 ± -99.0000	10.2477 ± 1.2120	-99.0000 ± -99.0000
Bemis	01/16/96	143.0200 ± 14.8790	0.0000 ± 0.0000	0.0000 ± 0.0000	1.2768 ± 1.3676	1.1892 ± 0.2241	123.5500 ± 6.1916	145.4860 ± 14.9434	-21.9360 ± 8.2597
East Char	04/09/95	33.5670 ± 2.3577	0.0000 ± 0.0000	0.0000 ± 0.0000	1.0749 ± 0.3766	0.1014 ± 0.0503	35.4010 ± 1.8413	34.7433 ± 2.3881	0.6577 ± 2.8577
East Char	04/27/95	36.2050 ± 2.8658	1.4577 ± 1.4647	0.0000 ± 0.0000	1.7524 ± 0.4422	0.6285 ± 0.0913	36.5660 ± 1.9141	40.0436 ± 3.2499	-3.4776 ± 3.1880
East Char	12/24/95	18.5910 ± 2.3127	8.6286 ± 1.7840	2.8722 ± 0.7696	1.0866 ± 0.2530	0.8960 ± 0.1594	33.7470 ± 1.7581	32.0744 ± 3.0353	1.6726 ± 3.0268
East Char	12/25/95	31.2570 ± 3.6059	9.0304 ± 2.3457	4.0664 ± 1.0650	0.6370 ± 0.2696	0.9466 ± 0.1713	46.4040 ± 2.3722	45.9374 ± 4.4431	0.4666 ± 3.8097
East Char	12/26/95	54.6830 ± 5.8030	12.4010 ± 3.2890	3.9958 ± 1.2397	0.44467 ± 0.4006	2.0308 ± 0.2901	65.5560 ± 3.3144	73.5573 ± 6.8025	-8.0013 ± 4.9589
East Char	12/27/95	81.0590 ± 8.3313	16.1150 ± 4.2194	2.2781 ± 1.1516	0.0000 ± 0.0000	2.3414 ± 0.3180	95.2950 ± 4.7907	101.7935 ± 9.4149	-6.4985 ± 6.4638
East Char	12/28/95	63.6440 ± 5.6481	13.8160 ± 3.5641	2.4902 ± 1.0057	1.3401 ± 0.9163	4.1919 ± 0.5279	80.3320 ± 4.0466	85.4822 ± 6.8362	-5.1502 ± 5.4815
East Char	12/29/95	53.0680 ± 4.5533	8.3616 ± 2.5865	1.6074 ± 0.7507	0.3034 ± 0.6644	2.3632 ± 0.3020	64.1160 ± 3.2422	65.7036 ± 5.3403	-1.5876 ± 4.6035
East Char	12/30/95	50.6830 ± 4.7056	11.9160 ± 2.8997	1.9515 ± 0.7900	0.2850 ± 0.7374	3.3066 ± 0.4222	66.0940 ± 3.3411	68.1421 ± 5.6477	-2.0481 ± 4.7390
East Char	12/31/95	51.8330 ± 6.5813	5.7228 ± 2.5120	0.5716 ± 0.5227	0.7891 ± 0.5677	1.6243 ± 0.2147	55.7580 ± 2.8313	60.5408 ± 7.0898	-4.7828 ± 4.7112
East Char	01/01/96	7.2269 ± 1.0848	3.2449 ± 0.6953	0.8779 ± 0.2530	0.1586 ± 0.1636	0.0543 ± 0.0569	9.9985 ± 0.7158	11.5626 ± 1.3245	-1.5641 ± 1.7780
East Char	01/02/96	29.7890 ± 3.1553	6.6329 ± 1.8757	0.8286 ± 0.4469	0.0000 ± 0.0000	0.1665 ± 0.1067	37.5840 ± 1.9425	37.4170 ± 3.6994	0.1670 ± 3.3425
East Char	01/16/96	102.5700 ± 7.7005	9.1139 ± 4.6327	0.9208 ± 1.0813	3.1815 ± 1.2236	3.3201 ± 0.4327	123.8900 ± 6.2164	119.1063 ± 9.1440	4.7837 ± 7.5453

Sec. Sulfate
0.70±0.46 (2%)

Sec. Nitrate
0.95±0.16 (2%)

Motor Vehicle
1.6±1.5 (4%)

Wood Burn
0.13±0.25 (0%)

Geol. 38±6 (92%)

Bemis

Motor Vehicle
8.2±2.8 (14%)

Sec. Sulfate
0.85±0.58 (1%)

Sec. Nitrate
1.69±0.28 (3%)

Wood Burn
1.73±0.81 (3%)

Geol. 47±5 (79%)
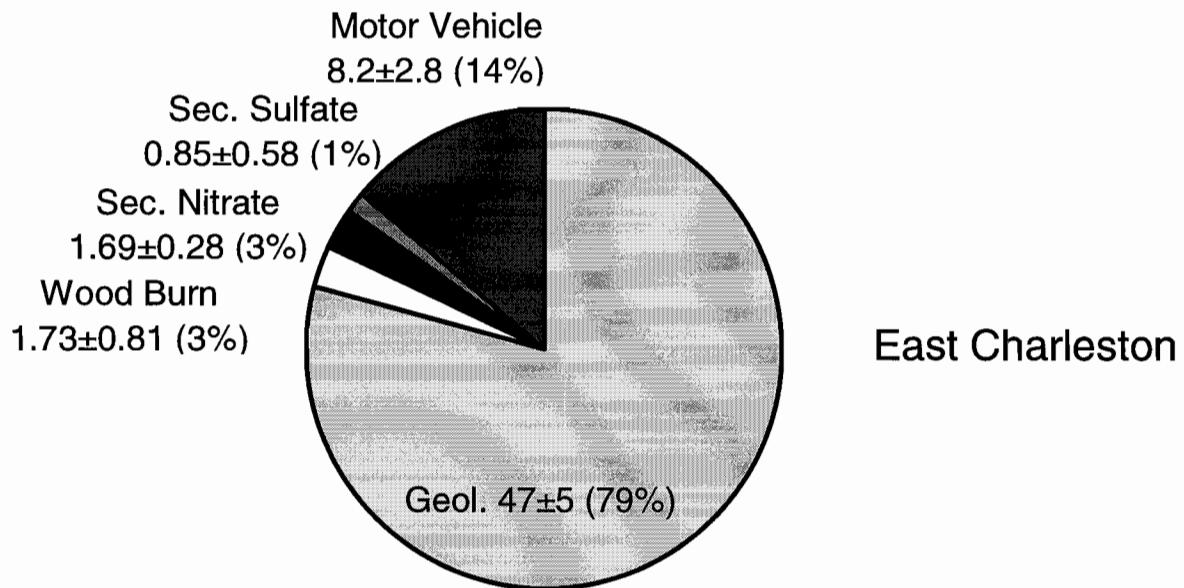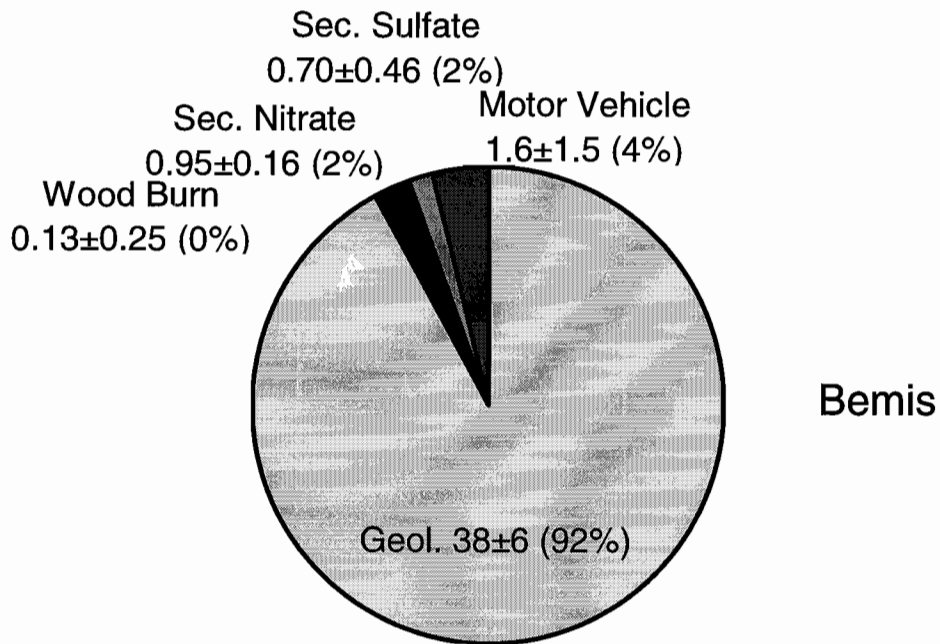
East Charleston

Figure 7-5   Average source contributions to 24-hour PM_{10} mass performed by Chemical Mass Balance receptor modeling at the Bemis and East Charleston sites during the nonintensive monitoring period between 04/09/95 and 01/16/96.

Table 7-8 shows that motor vehicle contributions were always larger at the East Charleston site than at the Bemis site, with the largest source contribution estimate being 14.8 $\pm$ 4.7 $\mu g/m^3$ (15% of PM_{10} mass) on 12/27/95. Elevated motor vehicle exhaust contributions were found at the East Charleston site during the last week of 1995, between 12/26/95 and 12/28/95, as well as on 12/30/95, where source contribution estimates from motor vehicle exhaust ranged from 20% to 60% above its site average. A similar phenomenon was observed for the motor vehicle exhaust contributions at the Bemis site between 12/27/95 and 12/30/95, when the source contribution estimates from motor vehicle exhaust were a factor of 1.8 to 2.6 higher than its site average. The highest motor vehicle contribution at the Bemis site was found to be 4.1 $\pm$ 2.4 $\mu g/m^3$ (8% of PM_{10} mass) on 12/28/95. Increased travel volume in the Las Vegas Valley during the Christmas and New Year holidays apparently had a major impact on PM_{10} concentrations.

As discussed in Section 4, it is not possible to distinguish different types of geological sources using CMB because their chemical compositions are too similar. In geological profiles assembled over the course of numerous PM_{10} and visibility studies, the average Ca/Si ratio is typically less than one. The average Ca/Si ratio at both the Bemis and East Charleston sites was 1.43. An average Ca/Si ratio of 2.1 (LVGEOLC) was found in the Las Vegas geological source profile. The enrichment of calcium in the source material and ambient aerosol in the Las Vegas Valley suggests the influence of the gypsum mine in the southwestern part of the Valley and/or of construction activities, where calcium would be expected to be associated with limestone or gypsum.

The largest geological contributions at both sites were estimated for the samples collected on 01/16/96, when the highest PM_{10} concentrations occurred at both sites. Individual source contributions for geological material varied by a factor of 25 at the Bemis site, ranging from 5.9 $\pm$ 0.8 $\mu g/m^3$ (66% of PM_{10} mass) on 12/24/95 to 143.0 $\pm$ 14.9 $\mu g/m^3$ (98% of PM_{10} mass) on 01/16/96. Large variations in geological source contributions are also found at the East Charleston site, ranging from 7.2 $\pm$ 1.1 $\mu g/m^3$ (63% of PM_{10} mass) on 01/01/96 to 102.6 $\pm$ 7.7 $\mu g/m^3$ (86% of PM_{10} mass) on 01/16/96. Less variation was found for secondary aerosol contributions. Table 7-8 shows that secondary sulfate accounted for 1% to 3% of PM_{10} mass, whereas secondary nitrate accounted for 2% to 4% of the PM_{10} mass for the 14 selected nonintensive days.

7.2.7 Source Contribution Estimates for Intensive SFS PM_{10} Samples

Source contributions were estimated for 25 samples collected on 14 intensive days at the Bemis and East Charleston sites between 09/07/95 and 01/30/96. Three samples collected on those days (09/10/95 and 09/11/95 at the Bemis site, and 01/28/96 at the East Charleston site) were invalidated during the Level II data validation process. The individual source contribution estimates for each sample are listed in Table 7-9. Average source

Table 7-9

Individual Source Contribution Estimates to PM$_{10}$ Mass (µg/m^3) at the Bemis and East Charleston Sites
during the Intensive Monitoring Periods between 06/05/95 and 01/30/96

Site	Date	Primary Geological	Motor Vehicle	Residential Wood Combustion	Secondary Ammonium Sulfate	Secondary Ammonium Nitrate	Measured Mass	Calculated Mass	Unexplained Mass
Bemis	06/05/95	71.0840 ±5.8157	0.0000 ±0.0000	0.0000 ±0.0000	1.2172 ±0.8120	0.8679 ±0.1368	70.4750 ±3.5504	73.1691 ±5.8737	-2.6941 ±6.8634
Bemis	06/06/95	36.1370 ±4.3014	0.0000 ±0.0000	0.0000 ±0.0000	0.5881 ±0.3551	0.3852 ±0.0716	34.0560 ±1.7636	37.1103 ±4.3166	-3.0543 ±4.6630
Bemis	06/07/95	19.5470 ±2.2820	0.0000 ±0.0000	0.0000 ±0.0000	0.4244 ±0.1979	0.1635 ±0.0459	17.8560 ±0.9917	20.1349 ±2.2910	-2.2789 ±2.4964
Bemis	09/07/95	29.6040 ±2.6001	0.0000 ±0.0000	0.0000 ±0.0000	2.4423 ±0.4435	0.4196 ±0.0666	27.6390 ±1.4283	32.4659 ±2.6385	-4.8269 ±3.0003
Bemis	09/08/95	34.4680 ±2.8740	0.0000 ±0.0000	0.0000 ±0.0000	1.1851 ±0.4160	0.5682 ±0.0809	32.5720 ±1.6503	36.2213 ±2.9051	-3.6493 ±3.3411
Bemis	09/09/95	20.5630 ±2.0201	0.0000 ±0.0000	0.8927 ±0.3110	0.9661 ±0.2635	0.3782 ±0.0568	20.7890 ±1.0925	22.8000 ±2.0616	-2.0110 ±2.3332
Bemis	09/12/95	33.6280 ±4.5551	1.3033 ±1.7715	0.0000 ±0.0000	0.8512 ±0.3500	0.1902 ±0.0593	29.8430 ±1.5356	35.9727 ±4.9003	-6.1297 ±5.1353
Bemis	01/26/96	21.4890 ±1.8985	0.0000 ±0.0000	0.0000 ±0.0000	0.0000 ±0.0000	0.1808 ±0.0438	21.5250 ±1.1362	21.6698 ±1.8990	-0.1448 ±2.2130
Bemis	01/27/96	29.0170 ±3.4439	0.0000 ±0.0000	0.0000 ±0.0000	0.1155 ±0.2788	0.3112 ±0.0584	26.9320 ±1.3954	29.4437 ±3.4557	-2.5117 ±3.7268
Bemis	01/28/96	25.6310 ±3.0286	0.0000 ±0.0000	0.0000 ±0.0000	0.3422 ±0.2506	0.3514 ±0.0588	22.6770 ±1.1928	26.3246 ±3.0395	-3.6476 ±3.2652
Bemis	01/29/96	20.5080 ±1.8894	0.0000 ±0.0000	0.0000 ±0.0000	0.4838 ±0.2404	0.5939 ±0.0787	21.8300 ±1.1511	21.5857 ±1.9063	0.2443 ±2.2269
Bemis	01/30/96	35.3280 ±3.6613	0.6931 ±1.9443	0.0000 ±0.0000	0.3987 ±0.4104	0.6890 ±0.0968	38.6470 ±1.9667	37.1088 ±4.1669	1.5382 ±4.6077
East Char	06/05/95	41.5640 ±3.5256	0.0000 ±0.0000	0.0000 ±0.0000	0.7859 ±0.4531	0.4633 ±0.0756	37.6770 ±1.9098	42.8132 ±3.5554	-5.1362 ±4.0359
East Char	06/06/95	26.0230 ±2.3263	0.0000 ±0.0000	0.0000 ±0.0000	0.3281 ±0.2857	0.4460 ±0.0841	26.4860 ±1.5720	26.7971 ±2.3453	-0.3111 ±2.8234
East Char	06/07/95	11.3090 ±1.0273	0.0000 ±0.0000	0.0000 ±0.0000	0.6878 ±0.1511	0.1419 ±0.0393	11.7720 ±0.7965	12.1387 ±1.0391	-0.3667 ±1.3093
East Char	09/07/95	29.4750 ±2.4475	0.0000 ±0.0000	0.0000 ±0.0000	3.1879 ±0.4974	0.5987 ±0.0841	26.2900 ±1.3841	33.2616 ±2.4989	-6.9716 ±2.8566
East Char	09/08/95	31.1470 ±2.5619	0.0000 ±0.0000	0.0000 ±0.0000	1.5772 ±0.3860	0.4410 ±0.0708	25.1850 ±1.3317	33.1652 ±2.5918	-7.9802 ±2.9139
East Char	09/09/95	34.2140 ±2.7791	0.0000 ±0.0000	0.0000 ±0.0000	1.7430 ±0.4213	0.4543 ±0.0735	26.3310 ±1.3861	36.4113 ±2.8118	-10.0803 ±3.1349
East Char	09/10/95	33.8810 ±2.7297	0.0000 ±0.0000	0.0000 ±0.0000	1.3527 ±0.3983	0.2544 ±0.0529	30.0710 ±1.5303	35.4881 ±2.7591	-5.4171 ±3.1551
East Char	09/11/95	35.6620 ±2.9447	0.0000 ±0.0000	0.0000 ±0.0000	1.3691 ±0.4210	0.1946 ±0.0845	29.4480 ±1.7371	37.2257 ±2.9758	-7.7777 ±3.4457
East Char	09/12/95	52.1880 ±4.1852	0.0000 ±0.0000	0.0000 ±0.0000	1.9352 ±0.6056	0.3684 ±0.0794	48.6900 ±2.4720	54.4916 ±4.2295	-5.8016 ±4.8989
East Char	01/26/96	30.3100 ±3.1247	2.6736 ±1.8864	1.3954 ±0.5173	0.1243 ±0.3471	0.2814 ±0.0707	32.5690 ±1.6787	34.7847 ±3.7034	-2.2157 ±4.0661
East Char	01/27/96	48.2480 ±4.7681	0.5557 ±2.4013	1.3615 ±0.6416	0.3723 ±0.5171	0.7724 ±0.1124	48.8020 ±2.4746	51.3099 ±5.4030	-2.5079 ±5.9427
East Char	01/29/96	32.5550 ±3.2769	2.4364 ±1.8918	0.7211 ±0.4251	0.6960 ±0.3781	1.1061 ±0.1432	33.6750 ±1.7334	37.5146 ±3.8290	-3.8396 ±4.2031
East Char	01/30/96	37.3280 ±3.7071	0.9586 ±1.9291	0.7030 ±0.4459	1.1518 ±0.4307	1.6010 ±0.1981	35.2350 ±1.8083	41.7424 ±4.2294	-6.5074 ±4.5998
East Char	01/01/96	7.2269 ±1.0848	3.2449 ±0.6953	0.8779 ±0.2530	0.1586 ±0.1636	0.0543 ±0.0569	9.9985 ±0.7158	11.5626 ±1.3245	-1.5641 ±1.7780
East Char	01/02/96	29.7890 ±3.1553	6.6329 ±1.8757	0.8286 ±0.4469	0.0000 ±0.0000	0.1665 ±0.1067	37.5840 ±1.9425	37.4170 ±3.6994	0.1670 ±3.3425
East Char	01/16/96	102.5700 ±7.7005	9.1139 ±4.6327	0.9208 ±1.0813	3.1815 ±1.2236	3.3201 ±0.4327	123.8900 ±6.2164	119.1063 ±9.1440	4.7837 ±7.5453

contributions at each site are presented as pie charts in Figure 7-6. On average, calculated and measured PM_{10} mass were in agreement within their measurement uncertainties at both sites. On average, geological material accounted for 96% (31.4 ± 3.4 $\mu g/m^3$) and 93% (34.1 ± 3.2 $\mu g/m^3$) of the calculated PM_{10} mass at the Bemis and East Charleston sites, respectively. Geological material was thus a relatively larger contributor in the intensive samples than in the nonintensive samples.

Both PM_{10} concentrations and geological source contributions were more similar at the Bemis and East Charleston sites in the intensive samples, which represented mostly summer and fall periods, than in the nonintensive samples, which represented mainly fall and winter periods. PM_{10} mass concentrations and the geological source contribution estimates decreased between 06/05/95 and 06/07/95 at both sites, suggesting a decrease in wind-blown dust over this period. Contributions from residential wood combustion were detected mainly at the East Charleston site from 01/26/96 to 01/30/96. However, emissions from residential wood combustion contribution were detected in the sample collected on 09/09/95 (0.89 ± 0.31 $\mu g/m^3$) at the Bemis site. This sample exhibited high chloride concentrations and a high ratio of soluble to total potassium which could not be accounted for without including a residential wood combustion profile in the CMB fit. It is suspected some vegetative burning took place in the vicinity of the Bemis site which resulted in elevated chloride and soluble potassium concentrations.

Source contributions from residential wood combustion, primary motor vehicle exhaust, and secondary sulfate and nitrate were each less than 3% at the two base sites. Secondary ammonium sulfate accounted for 2% and 3% of PM_{10} mass at the Bemis and East Charleston sites, respectively. Secondary ammonium nitrate accounted for 1% and 2% of PM_{10} mass at the Bemis and East Charleston sites, respectively. Motor vehicle exhaust contributed less than 0.5% and 1% of PM_{10} mass at the Bemis and East Charleston sites, respectively.

7.3   ISCST-3 Dispersion Modeling

7.3.1   Industrial Source Complex Short-Term Version 3 Model Overview

The ISCST-3 model is a steady-state Gaussian plume model designed for assessing pollutant concentrations from a wide variety of sources associated with an industrial source complex. The ISCST-3 dispersion model was used since it has been sanctioned by the U.S. EPA for use in regulatory PM_{10} applications (U.S. Environmental Protection Agency, 1986). In the area source option, the model is designated by the U.S. EPA as a preferred model for use in rural and urban areas, flat or rolling terrain, transport distances less than 50 kilometers, and one hour to annual averaging times. It is capable of modeling either gaseous species

Sec. Sulfate
0.75±0.38 (2%)

Sec. Nitrate
0.42±0.08 (1%)

Motor Vehicle
0.17±0.76 (1%)

Wood Burn
0.07±0.09 (0%)

Geol. 31±3 (96%)

Bemis

Sec. Sulfate
1.18±0.42 (3%)

Sec. Nitrate
0.55±0.1 (2%)

Motor Vehicle
0.51±1.13 (1%)

Wood Burn
0.32±0.28 (1%)

Geol. 34±3 (93%)
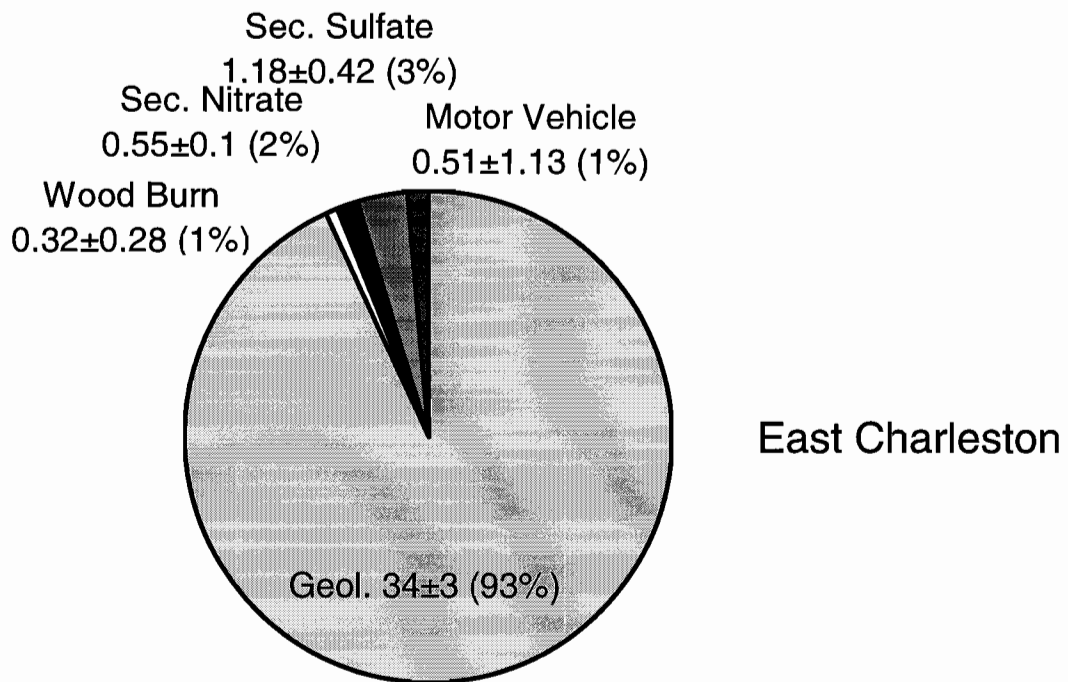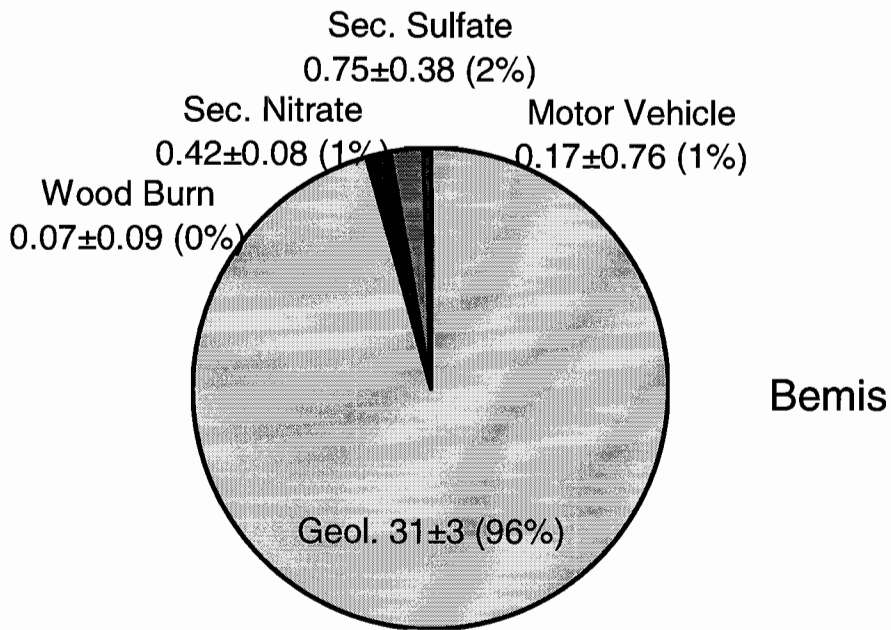
East Charleston

Figure 7-6   Average source contributions to 24-hour PM_{10} mass performed by Chemical Mass Balance receptor modeling at the Bemis and East Charleston sites during the intensive monitoring period between 09/07/95 and 01/30/96.

(e.g., SO_2, NO_x, CO, toxic and hazardous waste pollutants) or particulate matter (e.g., PM_{10} or TSP). For particulate matter, gravitational settling and wet/dry deposition can be treated.

The model requires the specification of the source type, spatial extent, location, and emission characteristics. Up to 300 sources and 1,200 receptors in four groups are allowed with the supplied code from the U.S. EPA Support Center for Regulatory Air Models (SCRAM) World Wide Web site (U.S. Environmental Protection Agency, 1997). The number of sources, receptors, and groups can be increased by modifying the FORTRAN source code and recompiling with a 32-bit extended memory compiler. This technique is outlined in the ISCST-3 User's Manual (U.S. Environmental Protection Agency, 1995).

This study used a commercial version of the ISCST-3 code called Breeze purchased from Trinity Consultants, Inc. (Dallas, TX), which accommodates up to 1,000 sources and 10,000 receptors. The allowed types of sources include points, areas, volumes, and open pits. The location and orientation of each source in a Cartesian coordinate system (x, y, z) is specified in the input file along with the source emission rate. The source emission rate will have different units depending on the type of source. For this study, the area source uses units of grams per square meter per second. Although not used in this application, the ISCST-3 is well suited to model emissions from a stack. In this case, the stack height, gas exit velocity, inside diameter, and gas exit temperature need to be entered in the input file. The model requires various meteorological parameters depending on the modeling options. In this effort, wind speeds, wind directions, and surface temperatures were the only required parameters to describe the meteorology. The ISCST-3 model requires the specification of receptor coordinates either in the form of a user-defined polar or Cartesian grid or a set of discretized point locations.

The ISCST-3 model provides ASCII text output depending on the option chosen in the input file. The model can provide concentration, dry and/or wet deposition estimates over various averaging periods for each receptor. The model has the ability to assess the contributions from groups of sources. The highest, second highest, and third highest concentrations or depositions are available in a tabular format depending on the choice of output parameters.

7.3.2 Assumptions and Limitations in Modeling

As in all numerical models, the user must understand the model assumptions and limitations in order to interpret the modeling results. The first assumption is that the atmosphere is in a steady state over the time period. This is important in interpreting transient events such as bursts of reentrained dust from large construction or disturbed areas. In this modeling effort, an assumption was made that the atmosphere is in a steady state

condition over a period of one hour. Other assumptions associated with the ISCST-3 model include:

- The plume behaves according to the Briggs plume rise equations (Briggs, 1969, 1971, 1975).

- Stability is parameterized by discrete Pasquill-Gifford (P-G) stability.

- A constant stability is assumed to occur throughout the mixing layer.

- The model assumes a constant, uniform wind for each hour.

- The plume travels in a straight-line fashion from the source.

- Vertical wind components are assumed to be zero.

- No chemical transformation occurs in the particle, but can be modeled using an exponential decay time constant.

An important limitation in this study was that the material diffused is chemically inert and remains suspended over the travel time involved and is not depleted other than through diffusion. The additional requirement for deposition calculations make run times long due to the size of the modeling domain and number of sources. Run times ranged from 4 hours to 30 hours on a 133-MHz Pentium-processor computer depending on the type of source. Due to resource limitations, the deposition calculation was not performed for this study. Sensitivity tests were performed, however, to observe the effect of turning the particle dry deposition and gravitational settling on and off. The conclusions are that the ISCST-3 particle removal algorithms do limit the zone of influence and peak concentration downwind but the general spatial patterns remain constant for both cases.

7.3.3 Conversion of GIS to Dispersion Model Input Format

PM_{10} emissions per section (~1.6 km × 1.6 km) were supplied by Clark County's Department of Comprehensive Planning as dBase and Microsoft Excel files (Jacquart, 1997). The data was organized in terms of township-range-section (TRS), and emissions for each section were expressed in tons per year. Clark County's Geographic Information System Management Office (GISMO) provided an Arc/Info section coverage of all of Clark County and a Bureau of Land Management (BLM) disposal area coverage. The TRS coverage includes 7,330 sections for a total of approximately 20,976 km^2. Since the study is interested in the PM_{10} concentrations within the BLM disposal area, the section coverage was chosen to only include those sections neighboring the disposal boundary. For this study, the two areas were chosen as rectangular regions enclosing the northern and southern BLM area (Figure 7-7). The north region contained 264 sections covering an area of approximately
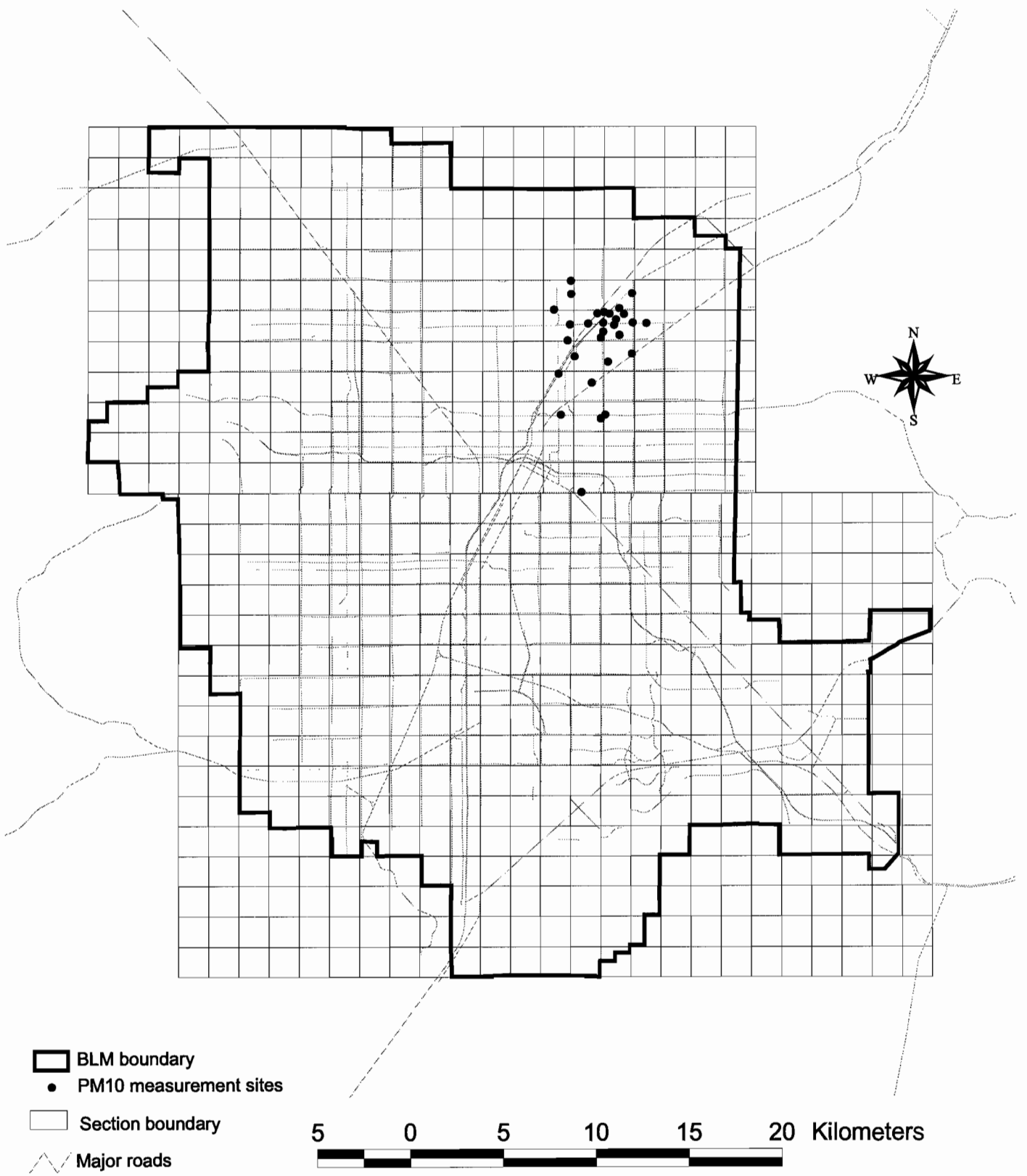
Figure 7-7   ISCST-3 model domain and monitoring site locations.

705.0 km^2. The south region contained 400 sections covering an area of approximately 1,048.4 km^2. The total horizontal and vertical extent of both north and south sections were 45.5 km and 45.4 km, respectively. Figure 7-8 shows the BLM disposal area section coverage, major roads, and the configuration of the PM$_{10}$ saturation monitoring network.

Nine source types were input into the dispersion model which included: 1) controlled construction, 2) controlled construction track-out, 3) controlled construction wind erosion, 4) mobile sources, 5) unpaved roads, 6) paved roads, 7) stationary sources, 8) disturbed land, and 9) residential wood combustion. Since the ISCST-3 model requires the source emission rate to have units of grams per square meter per second, the section emission data base was converted to these units using the area in each section.

To model the temporal variation of the various source types, a multiplication factor was introduced to allow sources to vary in time while keeping the total amount of PM$_{10}$ emitted constant. These multiplication factors should be taken as approximations to the actual emission behavior since the ISCST-3 does not provide enough flexibility to model complex temporal variations. The stationary sources and controlled construction were allowed to be emitting from 8 am to 5 pm. The paved roads, unpaved roads, and mobile sources were allowed to emit on a 24-hour basis but according to a smoothly varying function with a maximum in the daylight hours and a minimum at night. This function was created by observing the traffic counts as a function of time of day for several locations in town. The controlled construction track-out, wind erosion, and disturbed land operated at a threshold of 5 m/s. At wind speeds less than 5 m/s, the emissions from these three sources were set to be zero. For wind speeds greater than 5 m/s, the emission factor remained constant. This approximation may overestimate the amount of particles emitted since measurements have been empirically fit to a power-law dependence as a function of wind speed. The residential wood burning varied on the season, only emitting during the months of January, February, November, and December.

7.3.4 Meteorological Input

The ISCST-3 model requires the specification of a surface wind vector and mixing height for each case. Hourly wind speed and wind direction data acquired at 17 locations in the CCHD meteorological monitoring network were averaged to represent a general wind pattern within the modeling domain. These average winds vectors were computed by separating the u and v component at each site and taking the average of all u and v for each hour. In this modeling effort, the average wind speed over the entire valley was used over all of the sources. The ISCST-3 model has the limitation of requiring a constant wind field (a single wind speed and wind direction over the source or modeling domain). With regard to the sensitivity of the individual wind speed measurements, little change was found in the average as measurements from a specific site were included or excluded. For example,
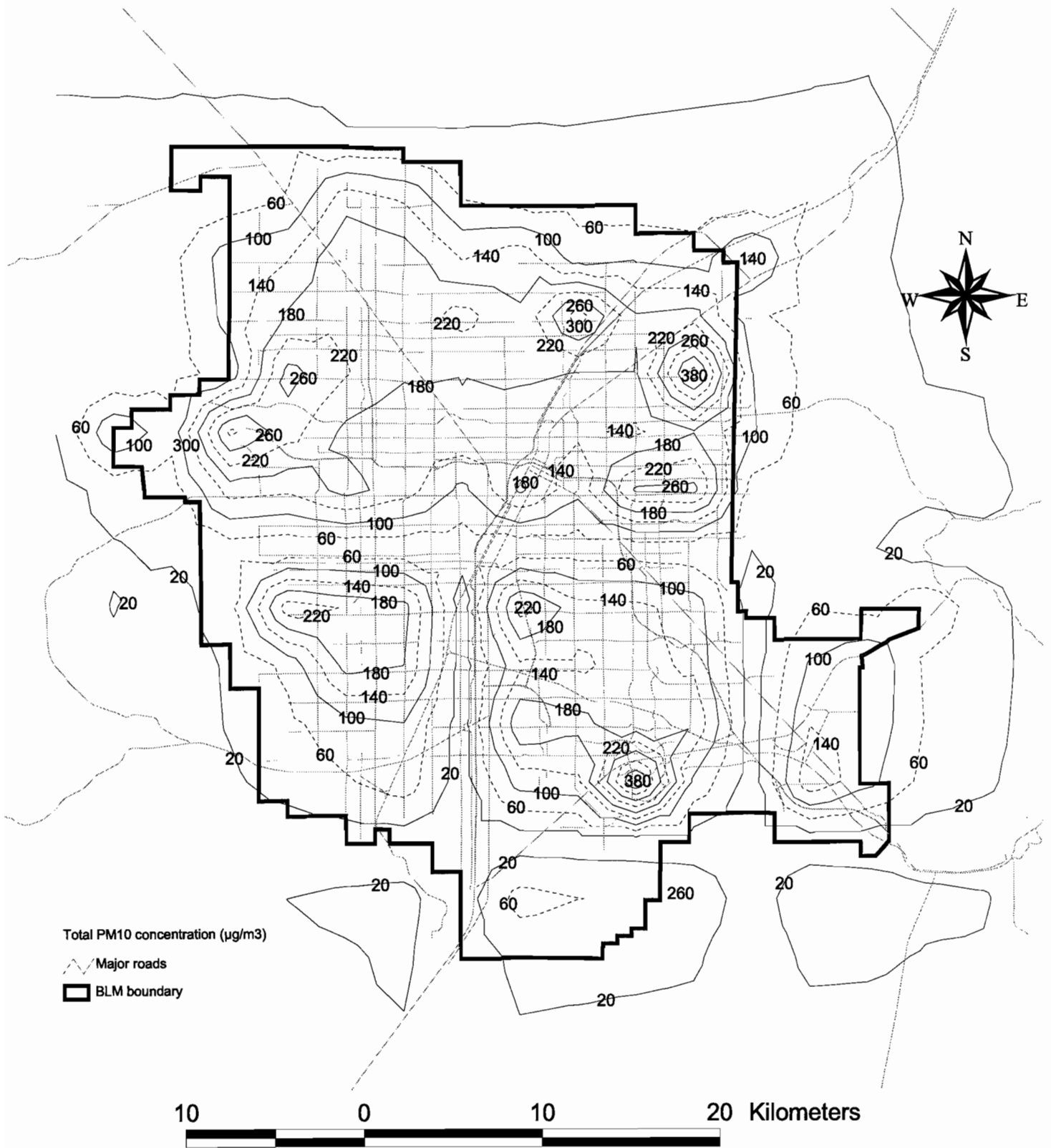
Figure 7-8   ISCST-3 dispersion model calculated annual-average PM_{10} concentrations.

excluding wind measurements from the East Charleston site will typically alter the average wind speed no more than 0.3 m/s. Test cases also indicated that the model calculations are insensitive to mixing height and stability class.

The Gaussian plume dispersion equation in the ISCST-3 is not well suited for stagnant conditions and as a result, wind speeds less than 1.0 m/s were eliminated from the calculation of the average particulate concentrations. This method is known as the US EPA "calms policy" from the Guideline of Air Quality Models (U.S. Environmental Protection Agency, 1986).

7.3.5 Summary of ISCST-3 Calculations

Annual average PM_{10} concentrations were calculated in the Las Vegas Valley using 1995 meteorological data and 1995 base year emissions estimates. Calculations for each of nine different source types were performed separately to estimate the individual source contributions to total PM_{10} within the BLM disposal area. Since the ISCST-3 model does not treat all of the aerosol transport mechanisms fully, the absolute magnitude of the PM_{10} concentrations should not be relied upon to compare with actual field measurements. Instead, the ISCST-3 model output is useful in that it captures the overall average spatial distribution of PM_{10} in the valley.

The most influential source of PM_{10} within the modeling domain was from controlled construction, with controlled construction wind erosion in second. Figure 7-8 represents the resulting annual average PM_{10} concentration by summing all of the nine source types. The highest PM_{10} concentrations are found in the northeast and southeast portions of the modeling domain.

Figure 7-10 presents the ISCST-3 modeling results for the northeast portion of the modeling area, as well as the annual emission rates in tons per year per section. PM_{10} measurements acquired at the satellite sites are superimposed on Figure 7-9 for comparison. Each pie in Figure 7-9 represents an ISCST-3 receptor location and shows the contribution from three source types: geological, mobile sources, and residential wood combustion. Elevated PM_{10} concentrations in the northeast corner of the modeling domain are mainly due to a large quantity of controlled construction at TRS number of 206215 shown in Figure 7-9. According to the 1995 emissions estimate, this section emits 865 tons of PM_{10} per year, 83% of which can be attributed to controlled construction. Other sections affected by this source have TRS values of 206209, 206210, and 206216 as shown in Figure 7-9.

The source influence from construction activities falls off to half of its maximum value in approximately 1.45 km in the east-west direction, and in approximately 1.60 km in the north-south direction. The nearest PM_{10} monitors, the THUN site (Lamb Blvd and Las
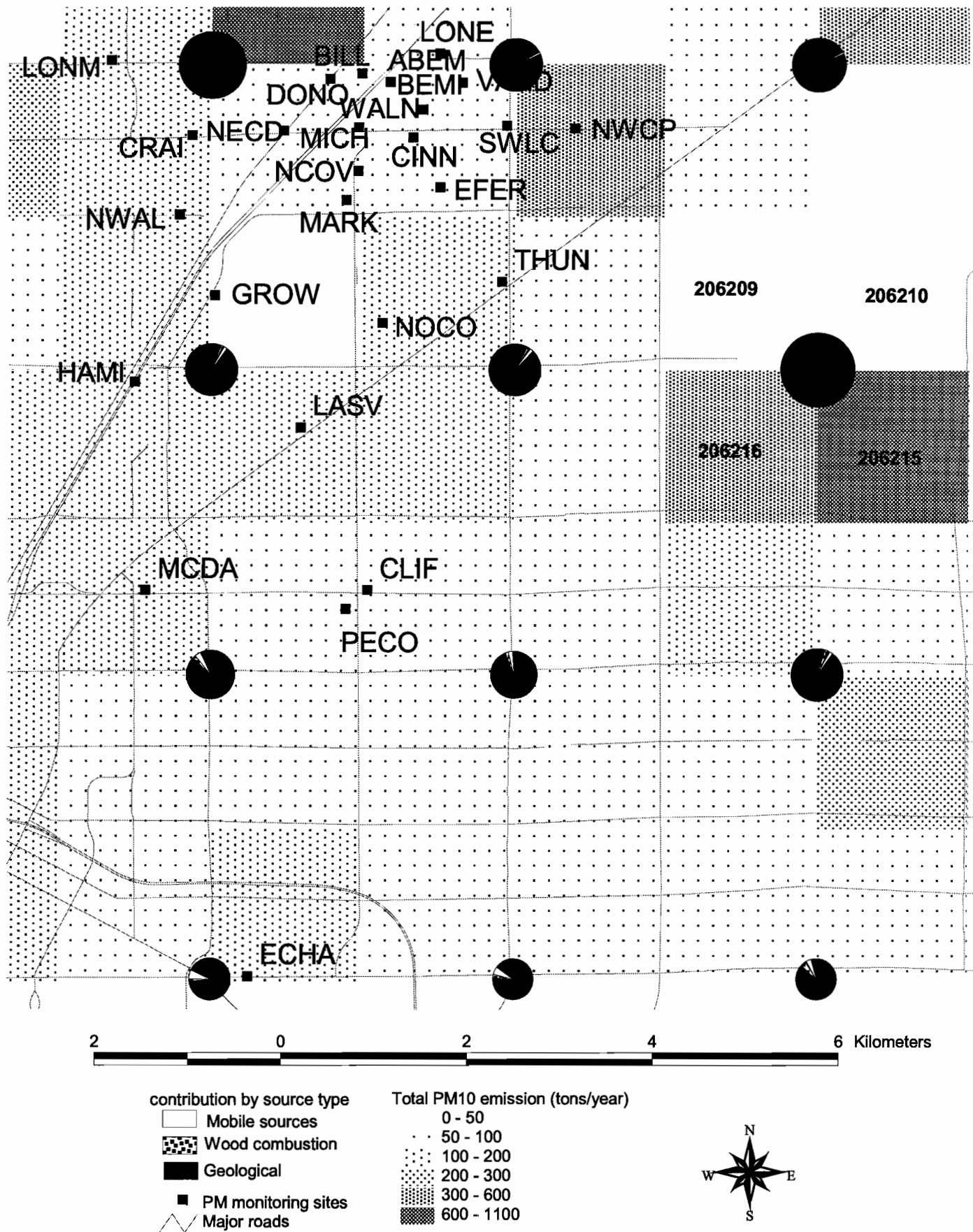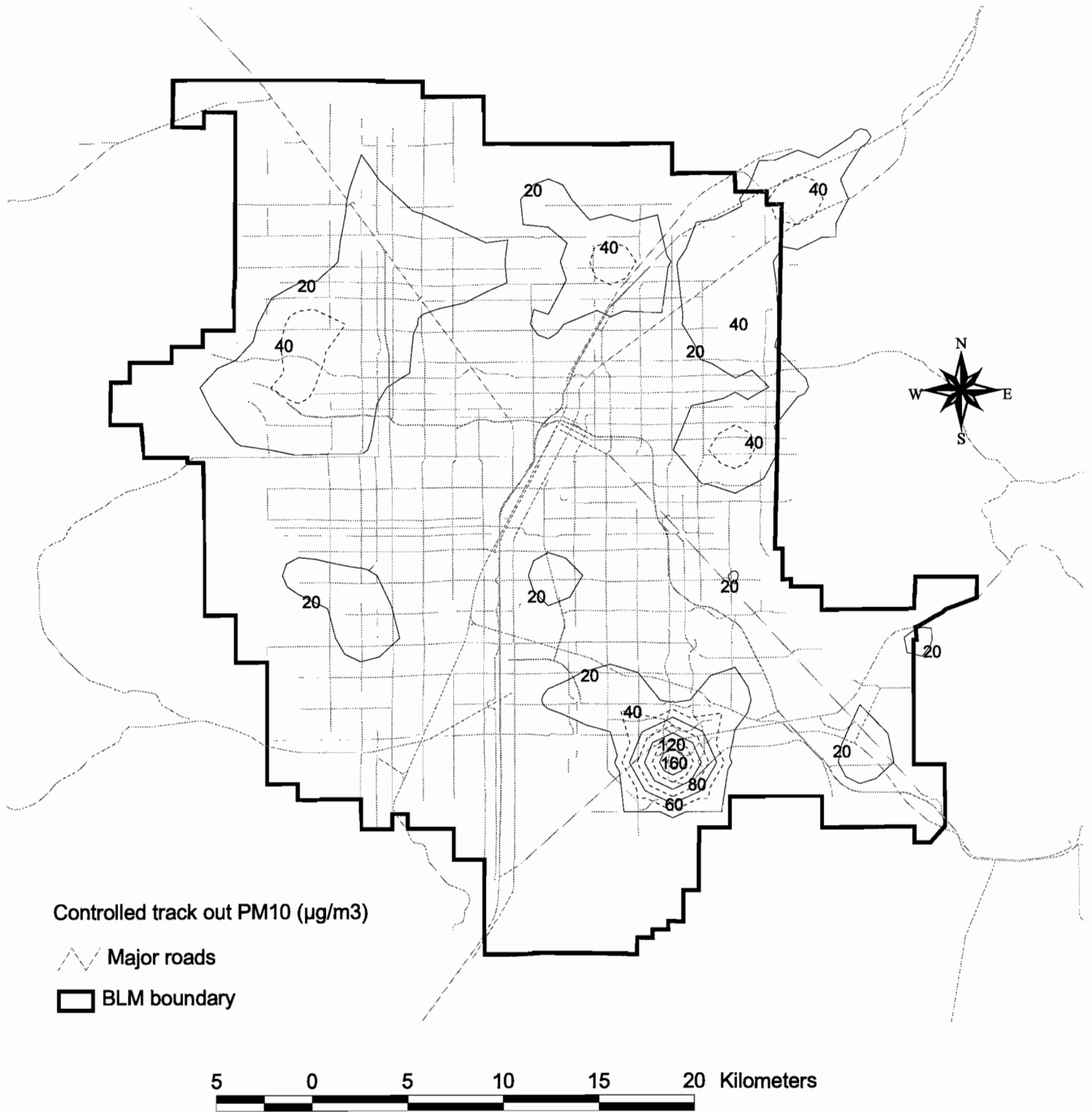
Figure 7-9   ISCST-3 dispersion model calculated PM$_{10}$ source contributions.
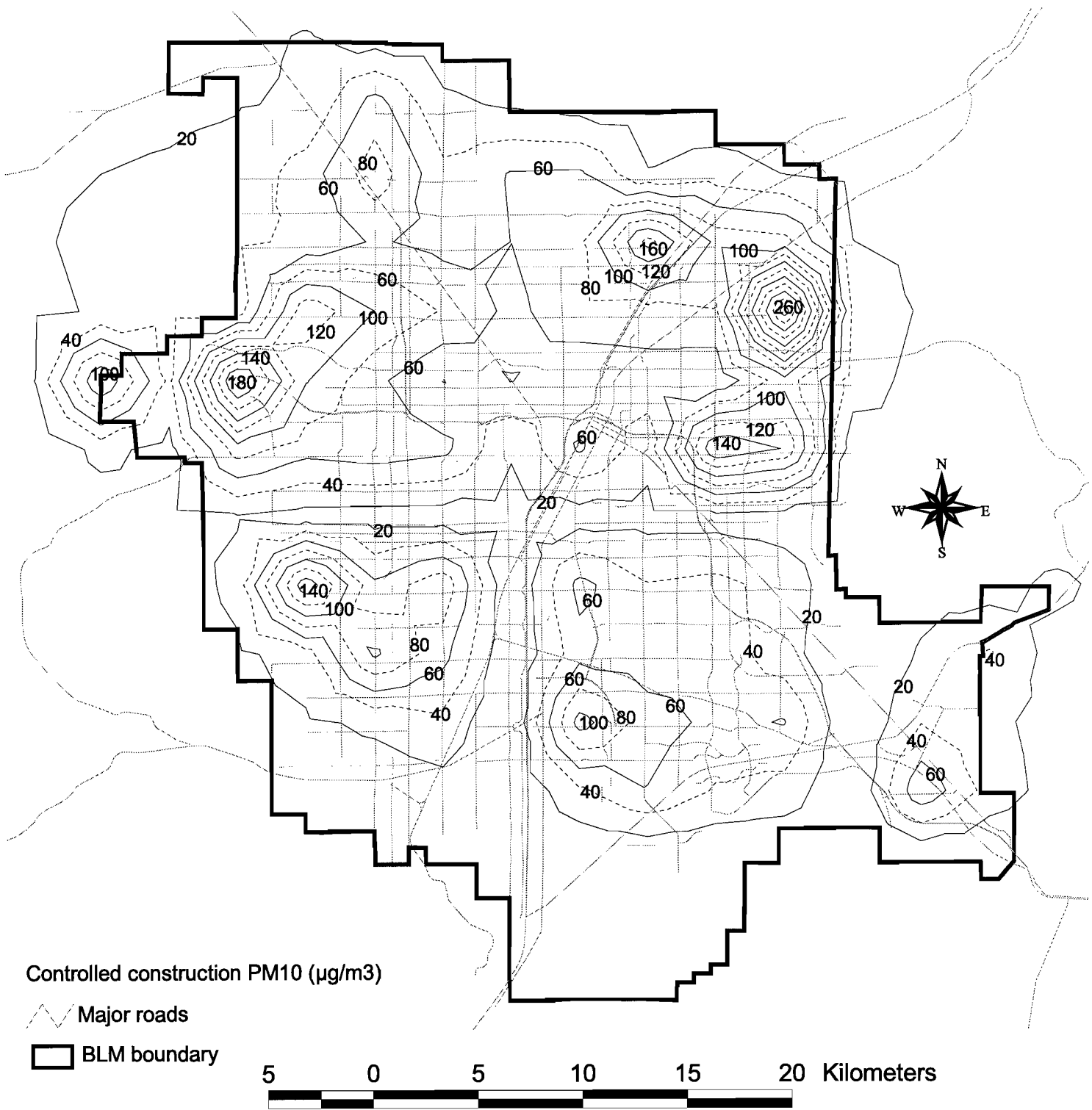
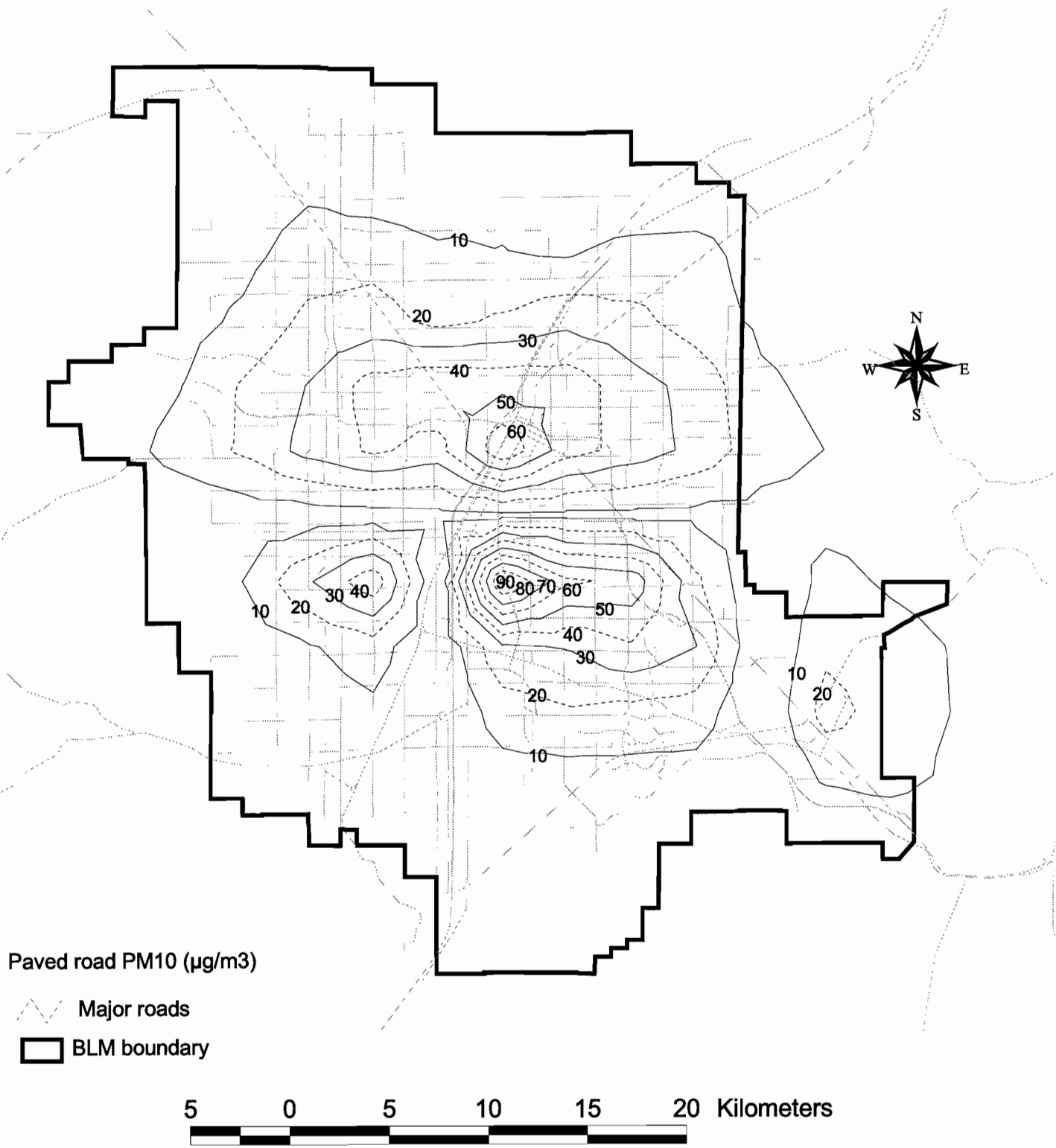Figure 7-10 ISCST-3 dispersion model calculated annual-average PM$_{10}$ contribution from controlled construction.

Vegas Blvd) and the NWCP site (Puebla Street and Craig Blvd), were both 3.5 km away from the maximum calculated concentration. At a distance of 3.5 km downwind, PM_{10} concentrations at the THUN and NWCP sites are minimally affected by that source. The remaining saturation monitoring sites are heavily influenced by controlled construction activity in the general area and to the northwest just above the DONO and BILL sites.

Comparing the contributions from construction track-out and construction wind erosion in Figure 7-10 through Figure 7-12, controlled construction demonstrated the most significant impact on the total PM_{10} in the northeast area. Construction wind erosion and construction track-out were most prominent in the southeast valley as indicated in Figure 7-11. The dispersion model calculated a peak concentration of over 100 $\mu g/m^3$ for both categories.

Figure 7-13 shows the impact of paved roads on PM_{10} concentrations in the valley. A peak contribution of approximately 90 $\mu g/m^3$ occurs near the center of the valley in the vicinity of the intersection between Paradise Road and Tropicana Avenue. Unpaved roads primarily affect the northwest portion of the valley as shown in Figure 7-14. The peak unpaved road PM_{10} contribution of 100 $\mu g/m^3$ was located about 5.5 km from the Lone Mountain II (LONM) site which is the nearest PM_{10} monitoring site. For this particular area, the source influence of unpaved road dust falls off to half its maximum value at approximately 2.7 km.

Stationary sources (e.g., sand and gravel operations) contribute little to the valley except at one particular region southwest of the urban center as shown in Figure 7-15. The region around the peak stationary source exhibits a sharp concentration gradient because of the strength of the emission relative to the surrounding area. The peak contribution of 59 $\mu g/m^3$ decreased by half in approximately 1.6 km. The concentration then falls to less than 1 $\mu g/m^3$ within 3 km of the peak.

PM_{10} contributions from disturbed land are well distributed throughout the perimeter of BLM disposal area, but the largest impact occurs in the southeastern area. Since the emissions from disturbed land covers such a large area, there are no sharp concentration gradients as exhibited in Figure 7-16.

The effect of mobile sources on PM_{10} is shown in Figure 7-17. The highest concentration of PM_{10} is located at the center of the city with a maximum of approximately 10 $\mu g/m^3$. The overall level of PM_{10} from mobile sources is very small for areas greater than 10 km from downtown.

Annual average PM_{10} from residential wood combustion is shown in Figure 7-18. The peak residential wood combustion levels occur in the southeastern part of the valley,
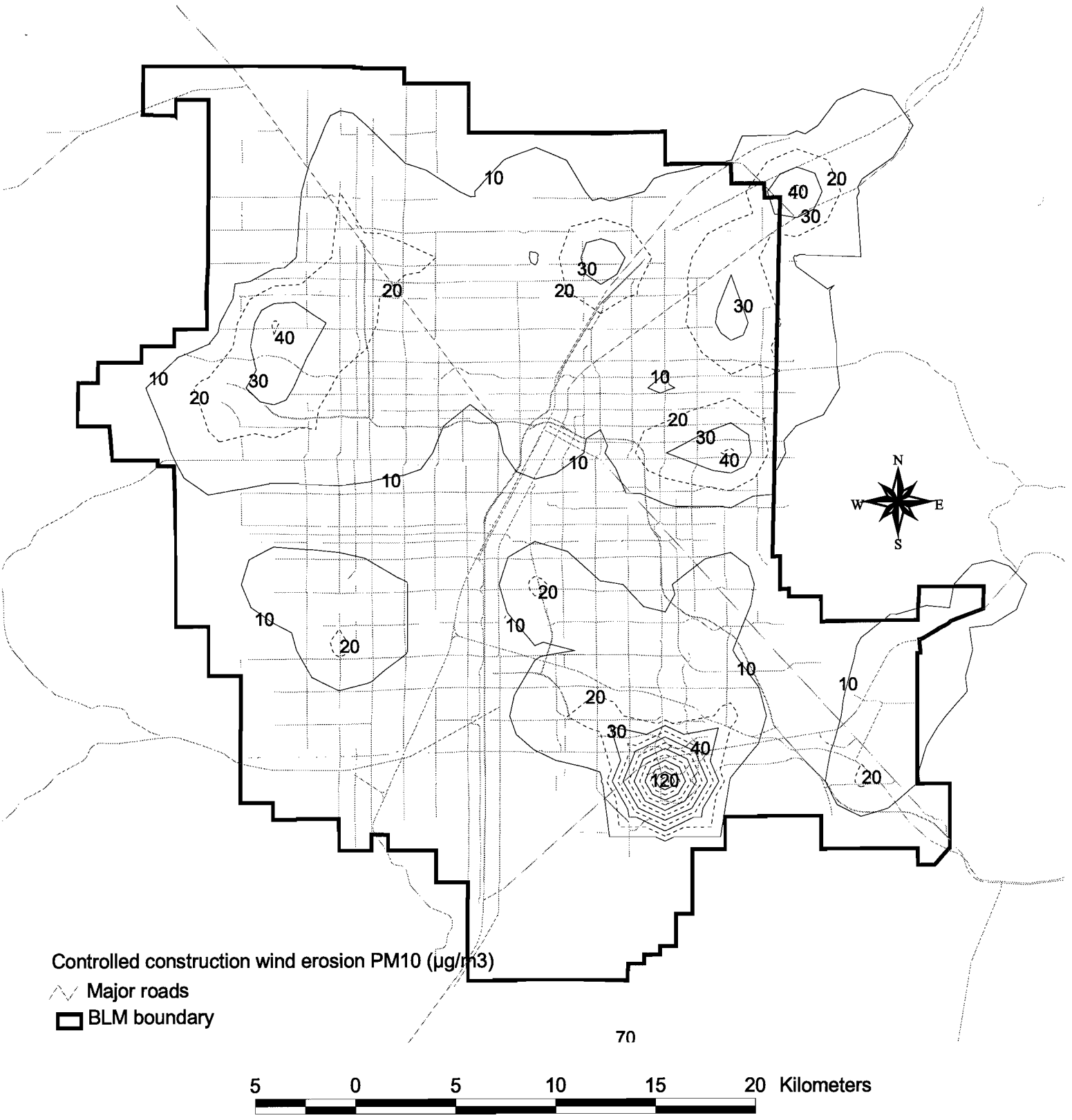
Figure 7-11 ISCST-3 dispersion model calculated annual-average PM_{10} contribution from controlled construction wind erosion.

Figure 7-12 ISCST-3 dispersion model calculated annual-average PM_{10} contribution from controlled construction track-out.
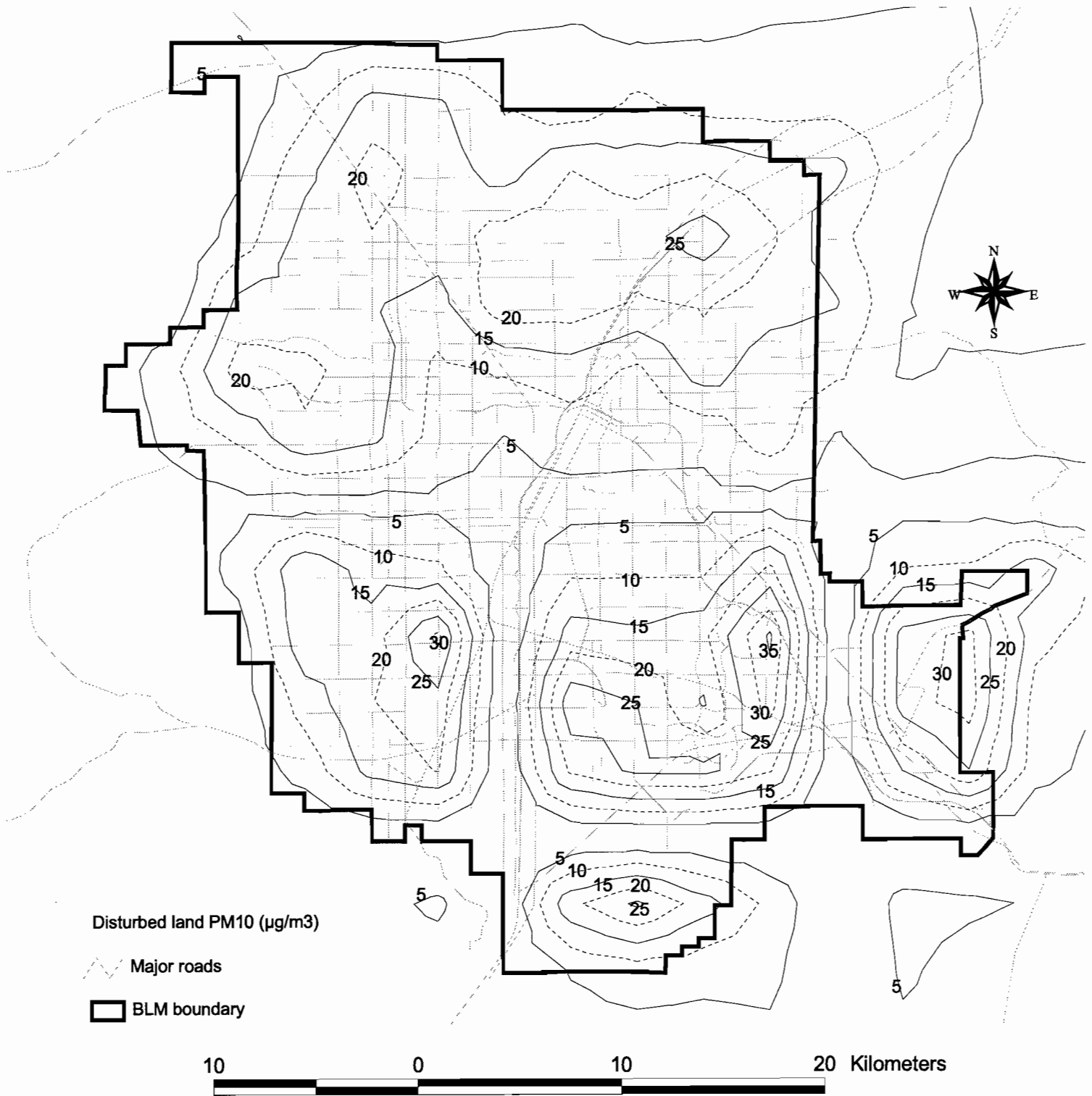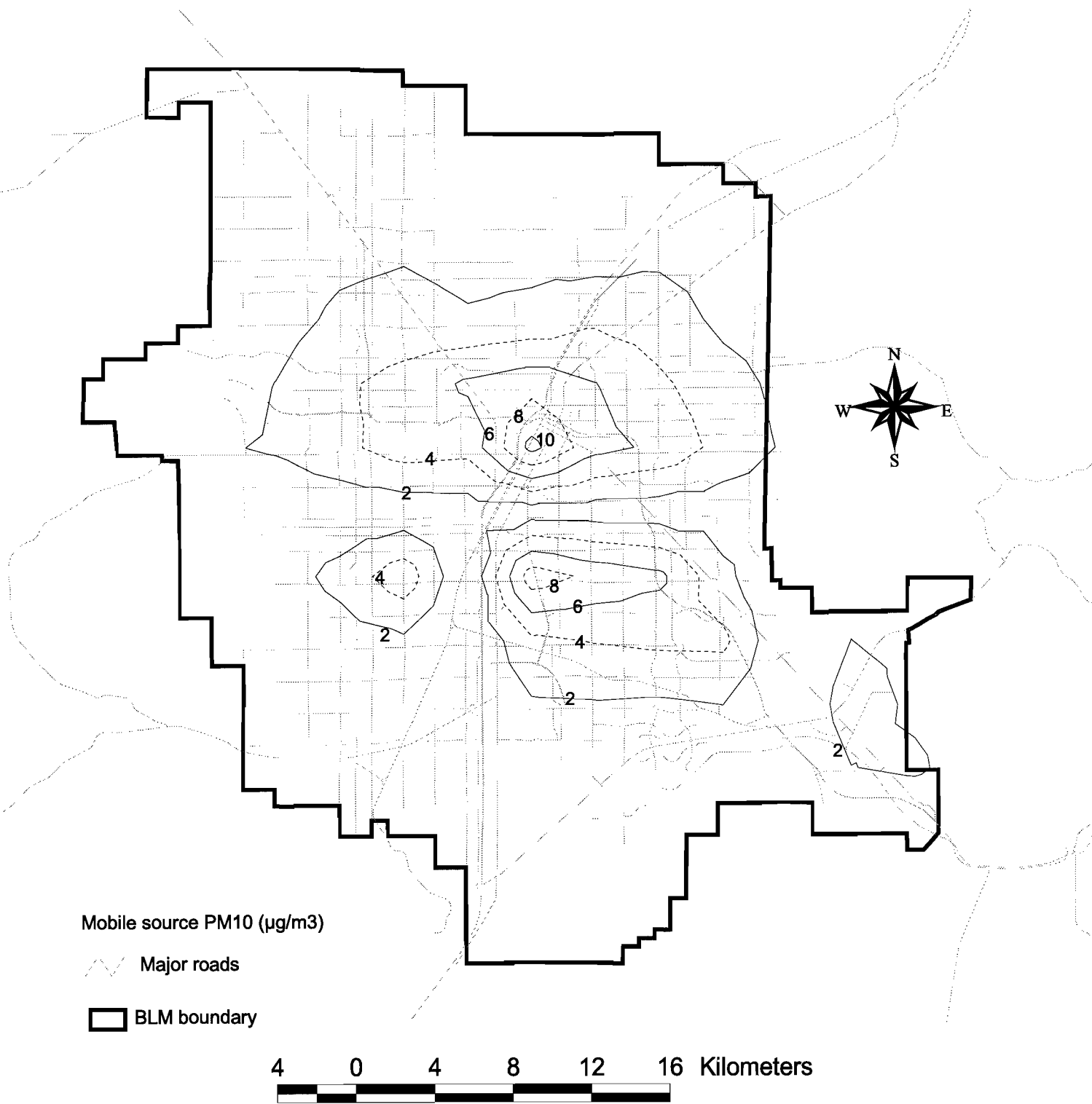
Figure 7-13 ISCST-3 dispersion model calculated annual-average PM$_{10}$ contribution from paved roads.
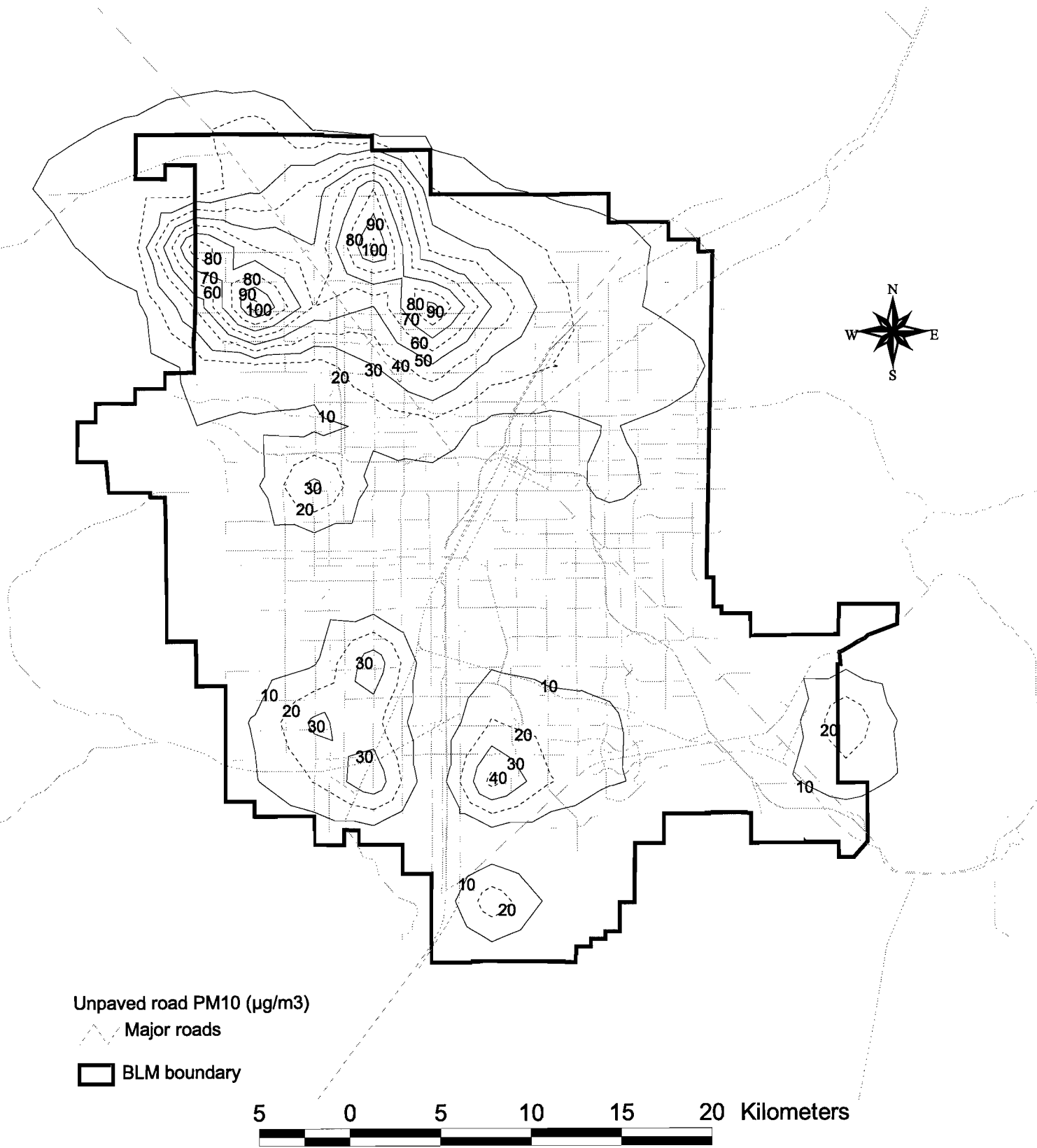
Figure 7-14 ISCST-3 dispersion model calculated annual-average PM_{10} contribution from unpaved roads.
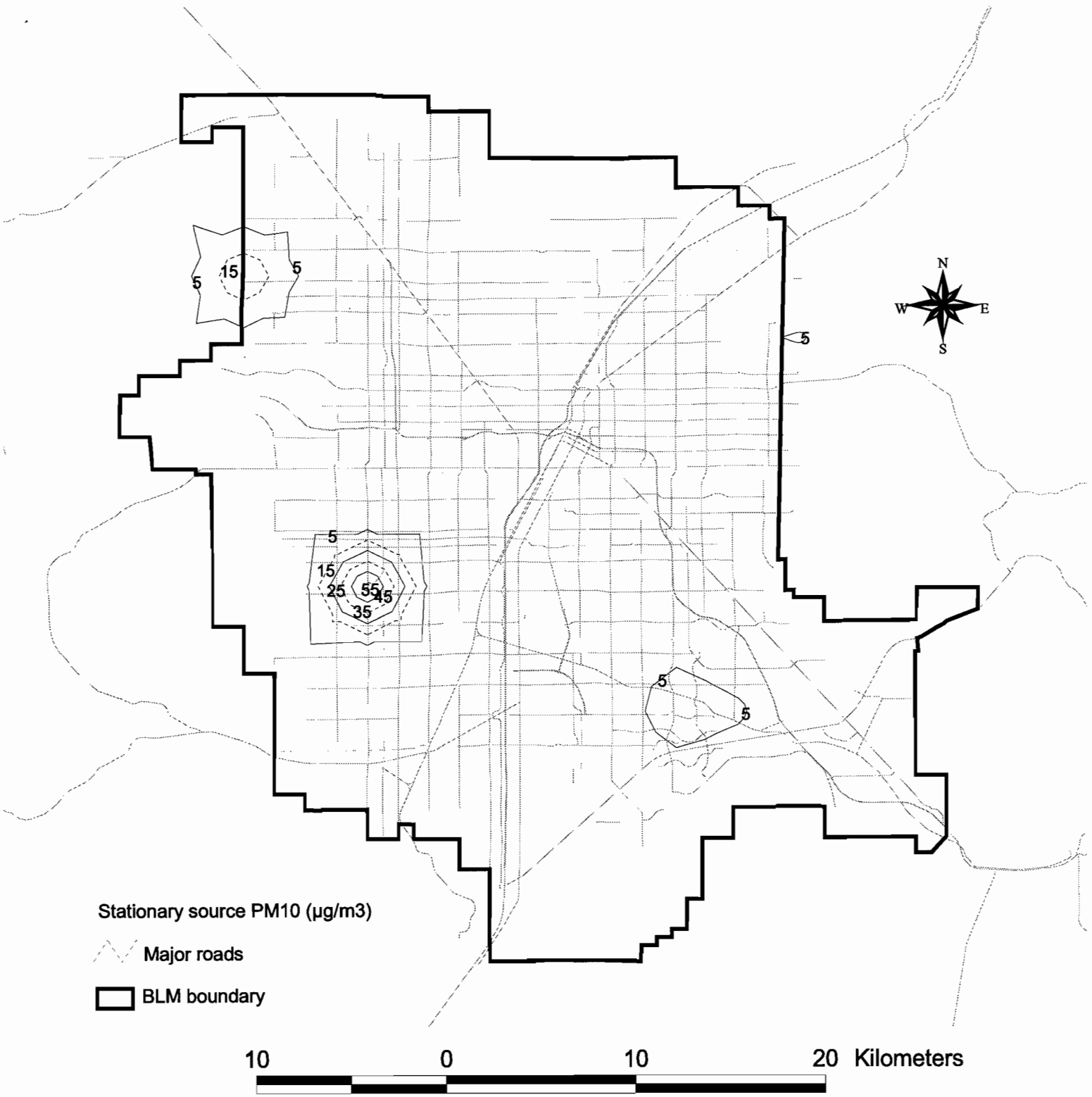
Figure 7-15 ISCST-3 dispersion model calculated annual-average PM$_{10}$ contribution from stationary sources.

Figure 7-16 ISCST-3 dispersion model calculated annual-average PM$_{10}$ contribution from disturbed land.

Figure 7-17 ISCST-3 dispersion model calculated annual-average PM_{10} contribution from mobile sources.
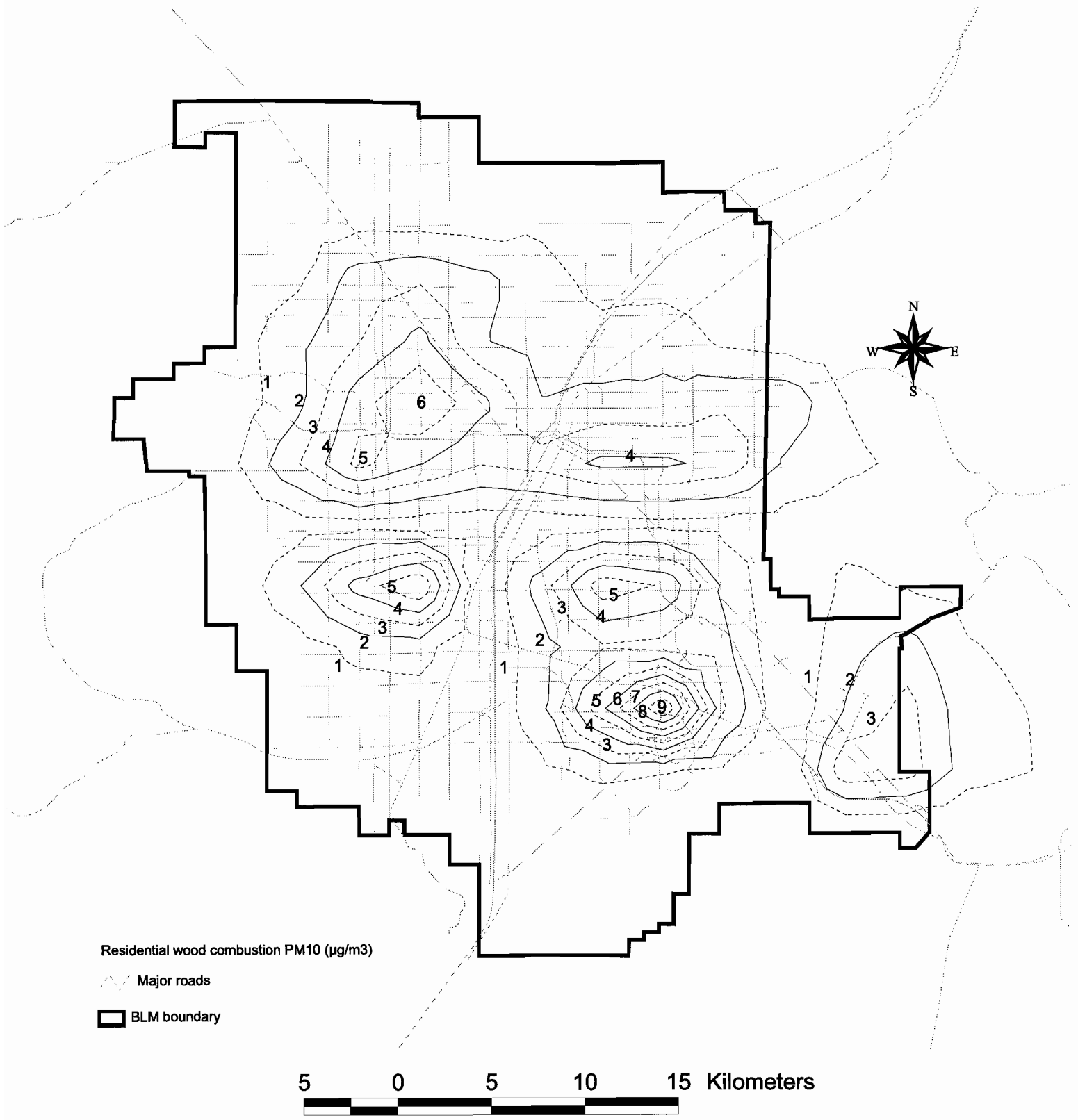
Figure 7-18 ISCST-3 dispersion model calculated annual-average PM_{10} contribution from residential wood combustion.

having a magnitude of approximately 10 $\mu g/m^3$. This peak falls off to half of the maximum with 3.8 km in the east-west direction and with 1.8 km in the north-south direction.

7.4   Source/Receptor Model Reconciliation

Table 7-10 compares average PM_{10} source contributions from the CMB receptor model with those from the ISCST-3 dispersion model. Although the magnitudes of the PM_{10} mass in the CMB and ISCST-3 varied by a factor of 2 to 4, the distribution of their relative source contributions were quite similar. Both the CMB and ISCST-3 models clearly show that geological material is the dominant source at the Bemis and East Charleston base sites. At the Bemis site, CMB reported that 86% of the PM_{10} mass can be attributed to geological material, which is comparable to the 99% calculated by the ISCST-3 model. At the East Charleston site, geological source contribution was 86% calculated by CMB and 91% calculated by ISCST-3.

Since the ISCST-3 model cannot simulate gas-to-particle transformations, the secondary particle contributions in Table 7-10 for the dispersion model are not available. Agreements in percentage of total mass are found in residential wood combustion for both sites. Contributions from residential wood combustion are relatively small, ranging from 0.2% to 0.3% of PM_{10} mass at the Bemis site and 1% to 3% of PM_{10} mass at the East Charleston site. This implies that over the period of a year, the average emission rate and activity levels for wood burning during the months of January, February, November, and December applied in the dispersion model compare well with the PM_{10} measurements during the intensive and non-intensive periods.

For mobile sources, the dispersion model's calculation is equivalent to the average source contribution derived from the CMB model between intensive and nonintensive periods. Table 7-10 shows that CMB modeling resulted in 0.5% to 4% of PM_{10} mass, whereas ISCST-3 modeling resulted in 1% of PM_{10} mass for motor vehicle exhaust contribution at the Bemis site. Source contributions for motor vehicle exhaust are much higher at the East Charleston site, ranging from 1% to 14% by CMB modeling to 7% by ISCST-3 modeling.

This comparison of the source/receptor models shows that source and receptor modeling complement each other. The 1995 preliminary emissions inventory may have overestimated the fugitive dust emission rate, resulting in higher source contribution estimates. Emission estimates for mobile sources and residential wood combustion were similar between the two models. The ISCST-3 dispersion model provides insight with respect to sub-sources of fugitive dust.

Table 7-10

Comparison of Source and Receptor Modeling Results

	Emission Estimates at the Bemis Site						Emission Estimates at the East Charleston Site					
	CMB[a]		CMB[b]		ISCST-3[c]		CMB[a]		CMB[b]		ISCST-3[c]	
Source Type	(µg/m³)	% of Mass	(µg/m³)	% of Mass	(µg/m³)	% of Mass	(µg/m³)	% of Mass	(µg/m³)	% of Mass	(µg/m³)	% of Mass
Residential Wood Combustion	0.13	0.3%	0.07	0.2%	0.56	0.3%	1.73	3%	0.32	1%	2.02	2%
Mobile Sources	1.60	4%	0.17	0.5%	1.62	1%	8.2	14%	0.51	1%	6.64	7%
Geological Material	38	92%	31	96%	181.2	99%	47	79%	34	93%	88.6	91%
Construction activity	NA[d]		NA[d]		93.68	51%	NA[d]		NA[d]		22.55	23%
Construction track-out	NA[d]		NA[d]		18.88	10%	NA[d]		NA[d]		7.21	7%
Construction wind erosion	NA[d]		NA[d]		14.64	8%	NA[d]		NA[d]		5.82	6%
Paved roads	NA[d]		NA[d]		13.16	7%	NA[d]		NA[d]		42.22	43%
Unpaved roads	NA[d]		NA[d]		12.37	7%	NA[d]		NA[d]		4.01	4%
Disturbed land	NA[d]		NA[d]		27.51	15%	NA[d]		NA[d]		6.64	7%
Stationary Sources	NA[d]		NA[d]		0.96	0.5%	NA[d]		NA[d]		0.15	0.2%
Secondary Nitrates	0.95	2%	0.42	1%	NA[d]		1.69	3%	0.55	2%	NA[d]	
Secondary Sulfates	0.7	2%	0.75	2%	NA[d]		0.85	1%	1.18	3%	NA[d]	
Total Mass	41.38		32.41		183.38		59.47		36.56		97.26	

[a] Nonintensive monitoring on selected 14 days (04/09/95 to 01/16/96) calculated by Chemical Mass Balance (CMB) receptor model.

[b] Intensive monitoring period (09/07/95 to 01/30/96) calculated by Chemical Mass Balance (CMB) receptor model.

[c] Average over 1995 calculated by ISCST-3 dispersion model.

[d] Not available.

Land uses near the sampling site can significantly impact ambient measurements. At the Bemis site, construction activity was the largest PM_{10} contributor, accounting for 51% of PM_{10} mass, followed by disturbed land (15%) and track-out from construction sites (10%). At the East Charleston site, paved road dust was the largest contributor, accounting for 43% of PM_{10} mass, followed by construction activity (23%). The zones of influence of fugitive dust from construction activity sources are small, ranging from 0.75 to 1.5 km based on either descriptive data analysis or ISCST-3 modeling.

8.0 METEOROLOGY

Excess PM_{10} concentrations result from a combination of emissions, transport, transformation, and accumulation of pollutants. Meteorological characteristics must be coupled with the transport and deposition of the particles in the atmosphere in order to better understand the causes of elevated PM_{10}. This section discusses the wind conditions in the Las Vegas Valley, establishes the relationship between PM_{10} and wind speed, explores the diurnal variations of PM_{10} concentrations, and characterizes the meteorological conditions during the PM_{10} exceedance days and over the intensive and mini-intensive monitoring periods.

8.1 Wind Conditions in the Las Vegas Valley

Wind conditions in the Las Vegas Valley are influenced over a wide range of meteorological scales. Synoptic-scale flows, such as high- and low-pressure systems, influence relatively large geographic areas, such as the western United States, at one time. Mesoscale influences, such as the Las Vegas Valley, modify the synoptic-scale flows. For example, winds usually flow along, rather than across valleys. Especially during light wind conditions, local influences cause small-scale variations in winds in the Las Vegas Valley. Within the Las Vegas Valley, the East Charleston monitoring site frequently experiences very light winds; the dynamics affecting wind flow at this location are not fully understood. McCarran Airport often records relatively strong winds. It is in an open area at a higher elevation than East Charleston.

During most of the period from May to September, prevailing regional wind flows are from the southwest. High pressure over the eastern Pacific Ocean and lower pressure over the Colorado Plateau causes this southwesterly flow. This flow is occasionally interrupted by synoptic-scale storms moving through the area, most often in late spring. During July and August, moist, southeasterly monsoonal flows alternate with the dry southwesterly flows. Northerly flows are not common during summer, but occur on infrequent occasions. Strong winds in summer are usually associated with thunderstorms; they tend to be localized and may be from any direction.

During October or early November, there is usually a transition from prevailing southwesterly flow to prevailing northerly (northwesterly or northeasterly flow). The Colorado Plateau and Great Basin are cold compared to the lower Colorado River Valley, and this cold, dense air flows down off the higher areas, giving a prevailing northeasterly wind during winter months in the Las Vegas Valley. Winds in the afternoon are usually from the northeast under these conditions; however at night, flow is typically from higher to lower terrain. At McCarran Airport, nighttime drainage flows are from the southwest. During the winter, the prevailing flows are interrupted by synoptic-scale storms moving through the

region. These usually give southerly or southwesterly flow that increases in speed as a cold front approaches. After the front passes, winds become strong northwesterly, and gradually subside.

A cumulative frequency distribution of daily average wind speed at McCarran Airport for the study period (from 01/01/95 to 01/31/96) is shown in Figure 8-1. The median (fiftieth percentile) daily average wind speed was about 3.3 m/s. About 15% of the days had average wind speed less than 2 m/s; 8% of the days had average wind speeds greater than 7 m/s.

8.2   Relationships between Wind Speed and PM_{10}

The relationships between wind speed and PM_{10} concentrations acquired with beta attenuation monitors (BAM) are explored in this section. In the Imperial Valley PM_{10} study (Chow and Watson, 1997b), it was found that at low wind speeds, PM_{10} was high due to buildup of locally-generated pollutants. At moderate wind speeds, increased dispersion gave substantially lower PM_{10} concentrations. At yet higher wind speeds, above 5 to 6 m/s, PM_{10} increased due to wind-raised dust. Meteorology and PM_{10} data from three sites (Bemis/Craig Road, East Charleston, and Jean) were examined to determine whether there was a relationship between wind speed and PM_{10} mass concentrations in the Las Vegas Valley. Figure 8-2a through Figure 8-2f show 20th, 50th, and 80th percentile PM_{10} BAM as a function of hourly average wind speed at the three sites for the summer (April to September) and winter (November to April) periods. At the Bemis/Craig Road site, a similar pattern was found as noted for the Imperial Valley, CA (Chow and Watson, 1997b). As wind speed increased, PM_{10} concentrations initially decreased, then increased sharply as wind speed exceeded about 7 m/s. The increase at higher wind speeds is most noticeable at the 80th percentile in both summer and winter and the 50th percentile in summer. Not all high wind conditions were associated with high PM_{10}; the 20th percentile in summer and the 20th and 50th percentile in winter did not show very high PM_{10} levels. An examination of the meteorology on 24-hour PM_{10} standard exceedance days shows that initial increases in wind speeds give very high PM_{10}, but when winds subside only slightly, PM_{10} concentrations may decrease substantially. This suggests that the "reservoir" of dust available for suspension may become depleted after a few hours of high winds. Very high PM_{10} BAM concentrations occurred only for about four hours during windy days, with peak concentrations lasting about two hours. The duration of high concentrations may be expected to be dependent upon two primary factors: 1) the length of time for all available dust to be raised at a local area (depends on wind speed and thickness of local dust reservoir); and 2) the dimensions of the area contributing transport of dust downwind (for the Las Vegas Valley, the size of the area with dust-producing activities). For example, it may take one to two hours for dust raised from disturbed soil at the south end of the Las Vegas Valley during strong southerly winds to reach the northern Valley.
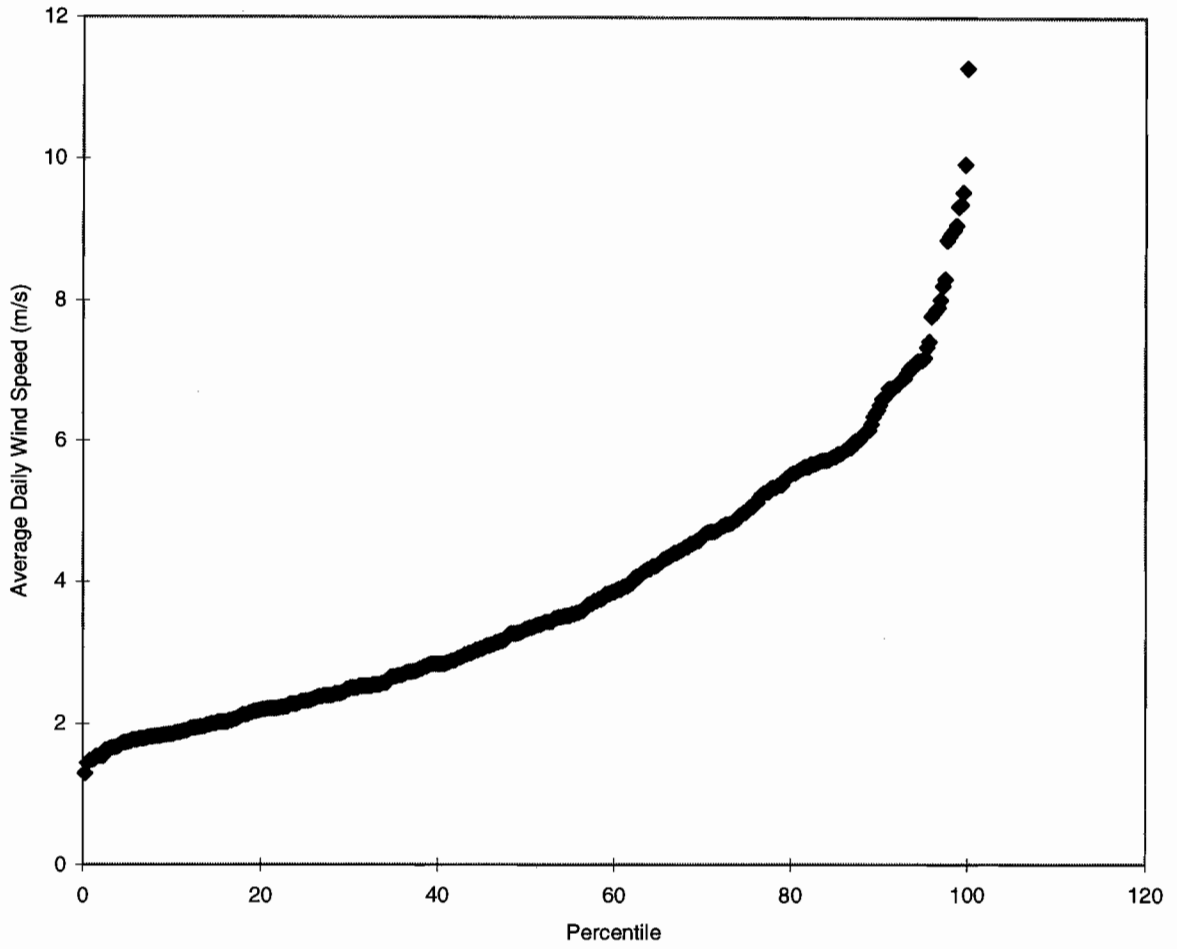
Figure 8-1   Daily mean wind speed cumulative frequency during the period from January
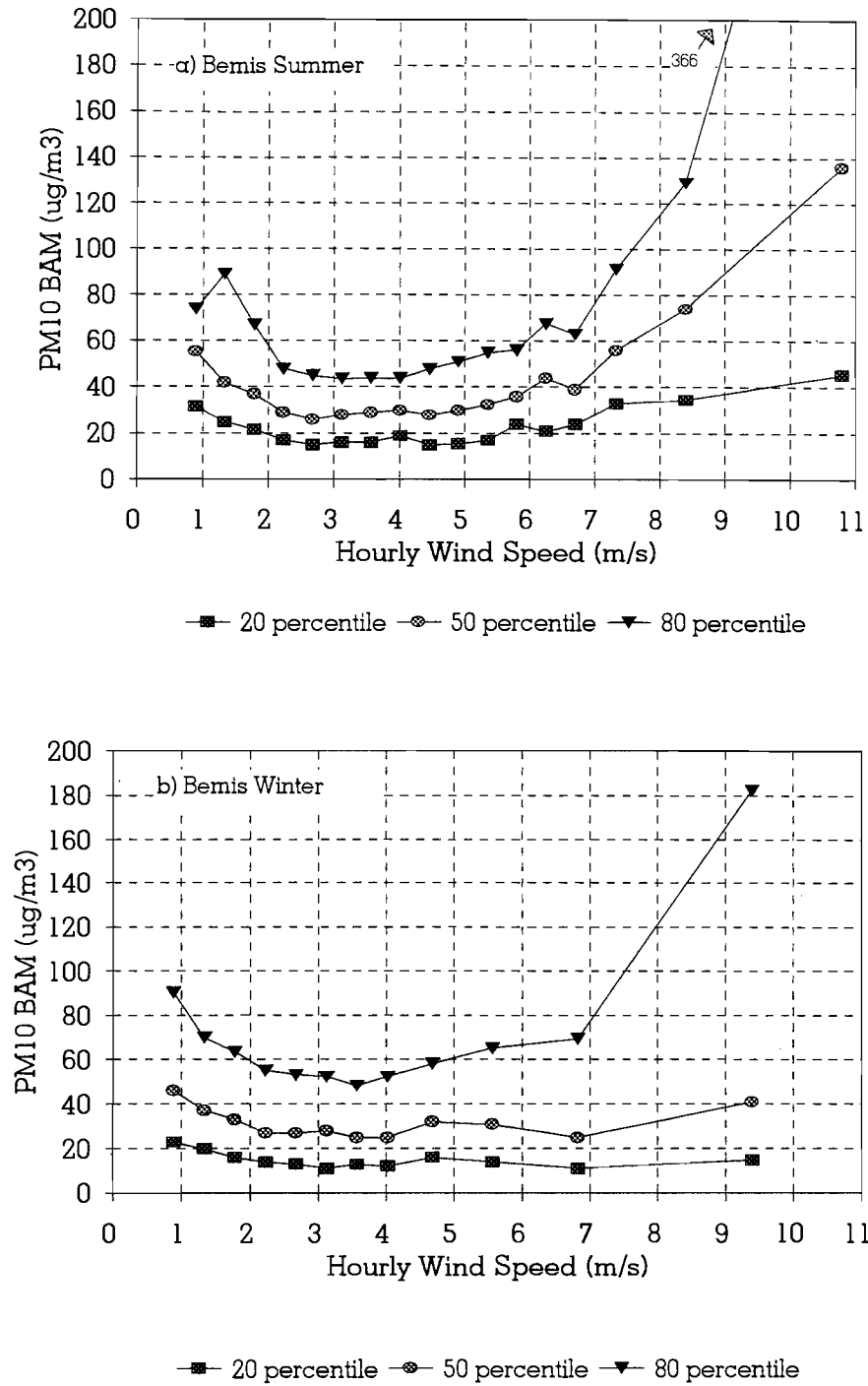1995 through January 1996 at the McCarran Airport site.

Figure 8-2   Distribution of hourly PM$_{10}$ BAM as a function of wind speeds during the: a) summer (April to September), and b) winter (November to April) periods at the Bemis/Craig Road site.
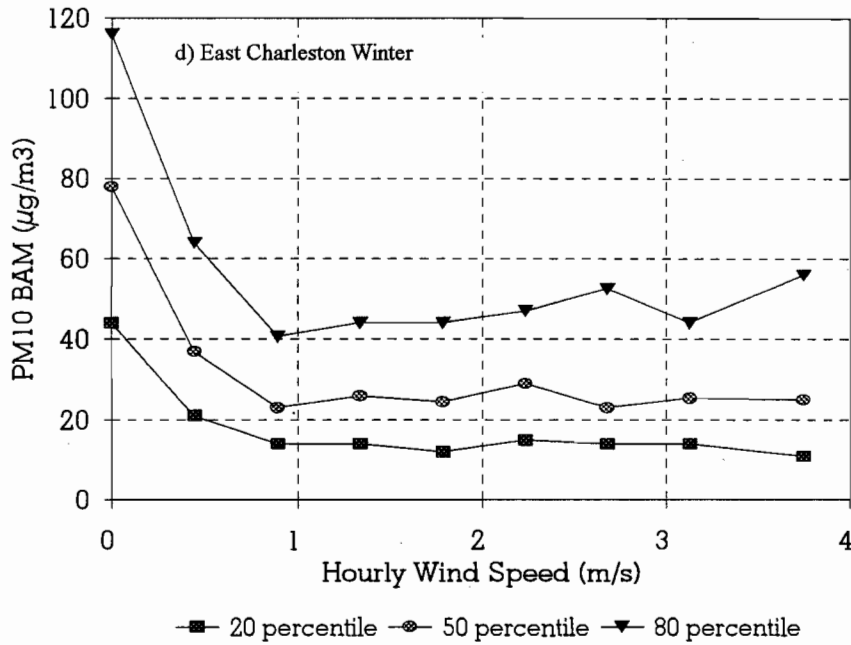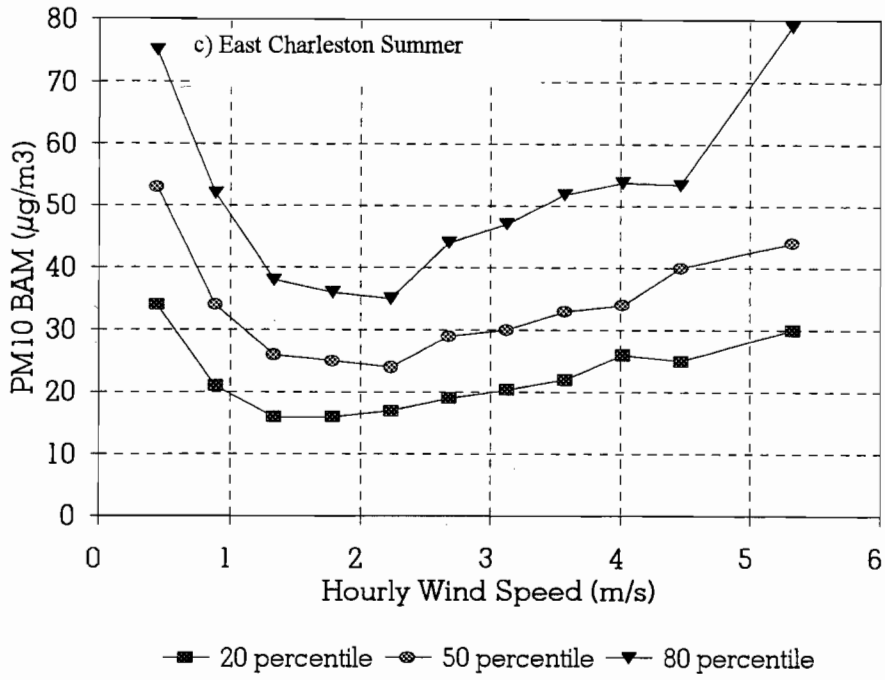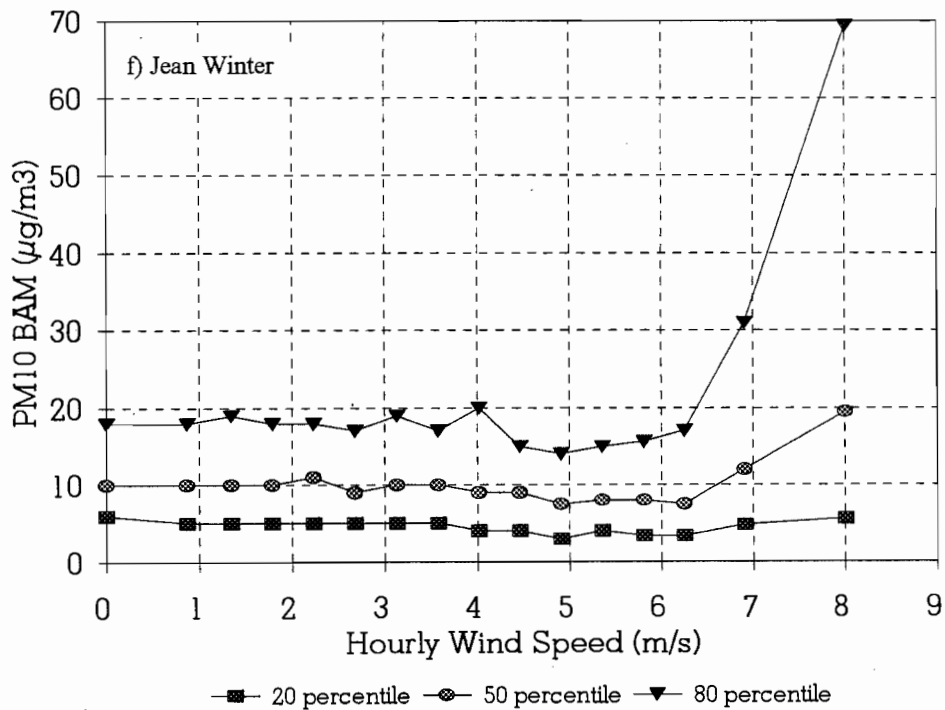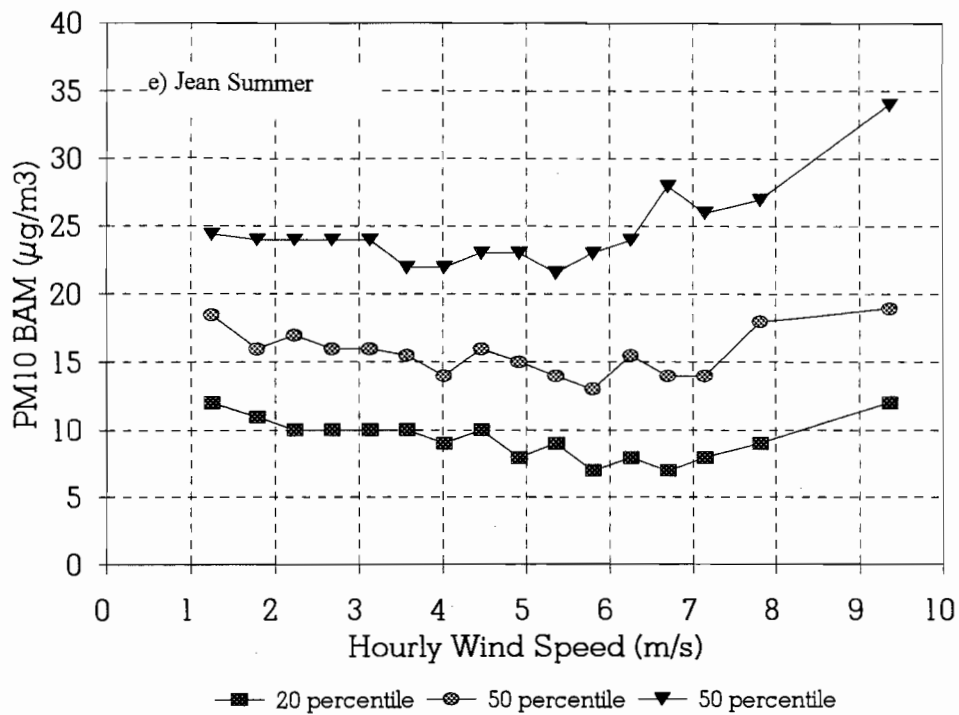
Figure 8-2   (continued)

e) Jean Summer

—■— 20 percentile —⊗— 50 percentile —▼— 50 percentile

f) Jean Winter

—■— 20 percentile —⊗— 50 percentile —▼— 80 percentile

Figure 8-2   (continued)

At the East Charleston microscale site, high PM_{10} values occurred with light winds (50th percentile of 80 $\mu g/m^3$ in winter). As winds speeds increased, PM_{10} decreased. Few strong winds were recorded at East Charleston; during summer, some increases in PM_{10} occurred as winds exceeded 5 m/s.

At the Jean site, high PM_{10} concentrations are not associated with low wind speeds as at the other sites. This is most probably because there are no significant local sources of PM_{10} at the Jean site to build up pollution during stagnant conditions. PM_{10} concentrations observed at the Jean site represent the regional background concentrations. Even as wind speeds increased to 8 or 9 m/s, 50th-percentile PM_{10} was still only around 20 $\mu g/m^3$ (summer and winter). Eightieth-percentile PM_{10} at these higher speed was about 35 $\mu g/m^3$ in winter and 70 $\mu g/m^3$ in summer. The much lower PM_{10} concentrations at the Jean site than at the Bemis/Craig Road site during high winds demonstrates that the high PM_{10} values during windy periods are not caused primarily from the fact that Las Vegas is in a desert. Relatively undeveloped desert areas such as Jean do not exceed the PM_{10} standard. It is the additional sources of PM_{10} within the Las Vegas urban area that cause violations of the PM_{10} standard.

To establish a threshold wind speed typical of the Las Vegas Valley, above which dust is suspended, data from all PM_{10} BAM sites was grouped together. By grouping all sites, a better statistical confidence is achieved because there are many more PM_{10} data points for each wind speed. For each wind speed, twentieth, fiftieth and eightieth percentile values of PM_{10} were determined. Figure 8-3 shows the results of this analysis (note that the y-axis is on a logarithmic scale). The pattern noted above at the Bemis/Craig Road site appears in this composite analysis for all sites. PM_{10} is lowest for wind speeds of 3 to 5 m/s. Below 3 m/s, PM_{10} increases with decreasing wind speed due to poor dispersion conditions. Above 5 m/s, PM_{10} increases with increasing wind speed, due to wind-raised dust. At wind speeds below 2 m/s and above 7 m/s, the PM_{10} increases are exponential functions of wind speed. This means that small increases in wind speeds above 7 m/s can cause large increases in PM_{10} concentrations and the higher the wind speed, the greater the increase in PM_{10} concentrations for each meter per second increase in wind speed. In summary, while no set threshold can be established between wind speed and PM_{10} concentration for the Las Vegas Valley, as wind speeds exceed 7 m/s, substantial increases in PM_{10} typically occur with each meter per second increase in wind speed.

8.3   Diurnal Patterns in PM_{10} Concentrations

Hourly PM_{10} BAM concentrations from the 13 locations in the CCHD's compliance monitoring network were examined to illustrate their diurnal patterns. Because diurnal patterns vary by time of year, two periods were used: 1) October through March (cool season, short days), and 2) April through September (warm season, long days).
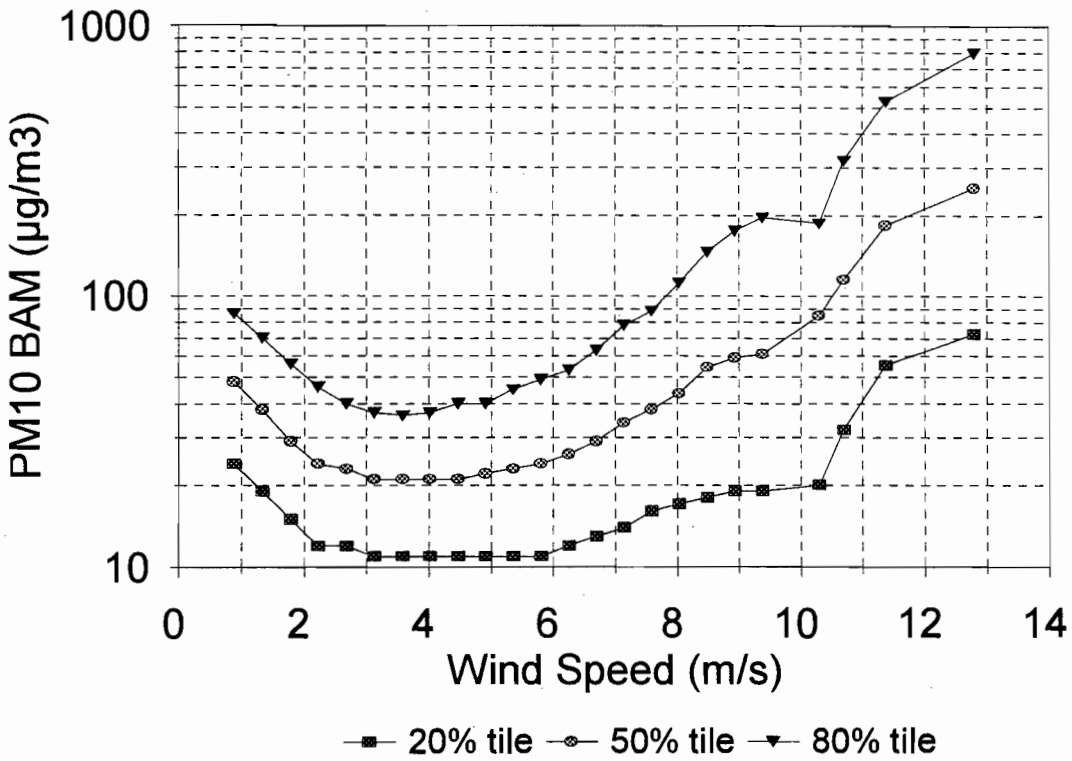
Figure 8-3   Distribution of hourly PM_{10} BAM (displayed on a logarithmic scale) as a function of wind speed at all meteorological sites.

8.3.1 Diurnal Variations of PM$_{10}$ Concentrations

Figure 8-4 to Figure 8-16 show diurnal variations of the 20th, 50th, and 80th percentile values of PM$_{10}$ concentrations for the 13 sites by time of day. These percentiles are not substantially affected by a few very low or very high concentrations, and thus represent the range of typical concentrations. Percentiles as low as 5 and 95 were also calculated; in most cases, the diurnal patterns were not much different than the 20 and 80 percentile patterns. It should be noted that, on any given day, hourly PM$_{10}$ concentrations may not follow the diurnal pattern of the percentile concentrations, although a majority of the days will follow a similar pattern.

Figure 8-4 to Figure 8-16 illustrate typical diurnal PM$_{10}$ concentration patterns with the following characteristics:

- A rise from an early morning minimum to a middle-to-late-morning peak;

- A decrease from the morning peak to an afternoon minimum; and

- A rise from the afternoon minimum to an evening maximum, and then a slow decrease to the morning minimum.

In addition, some sites (e.g., Flamingo, Jean) show an apparent rise in PM$_{10}$ concentration at midnight. The Boulder City site shows a drop at midnight, followed by a rise at 0100 PST. These are probably the times when daily instrument calibration was performed. No validation flags can be found in the BAM PM$_{10}$ data base relating to these data points. These data for midnight and 0100 PST should be used carefully, if at all, especially at the following sites: McDaniel, Flamingo, Jean, East Charleston, and Boulder City.

At all sites, the summer evening peak is less pronounced than the summer morning peak, but many sites (e.g., Bemis/Craig Road, East Charleston, Maycliff, McDaniel, City Center) have winter evening peaks higher than winter morning peaks. Table 8-1 shows, for each site, time of day at which the morning peak, afternoon minimum, and evening peak PM$_{10}$ concentrations at the 50th percentile occurred for summer and winter months. Also shown are the corresponding 50th percentile values. The following patterns can be noted:

- Summer morning peaks occur earlier than winter morning peaks (0600 or 0700 PST, compared to 0700, 0800, or 0900 PST for winter);

- Summer afternoon concentrations are relatively low for more hours than in winter, and occur in late afternoon, as compared to early afternoon (typically 1300 PST) for winter; and
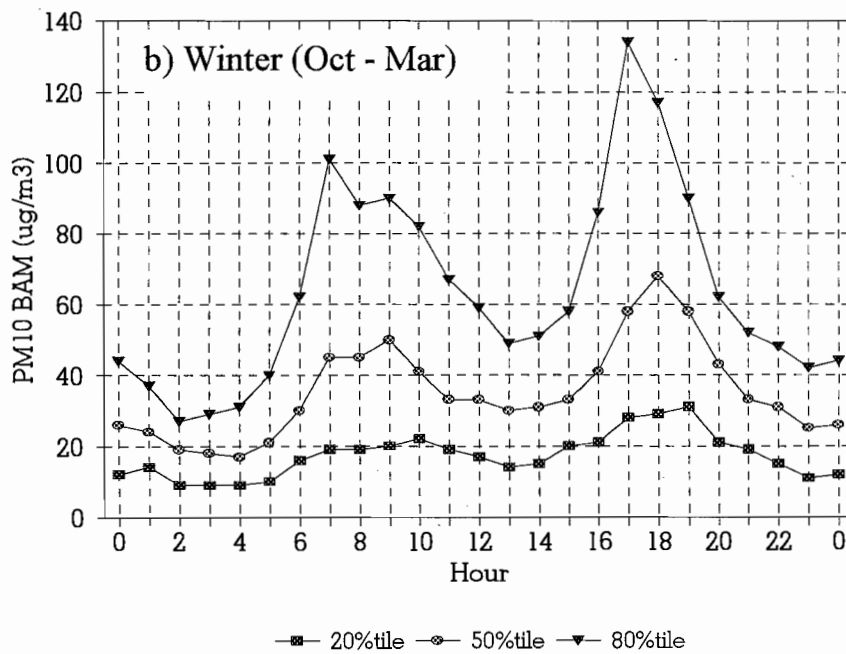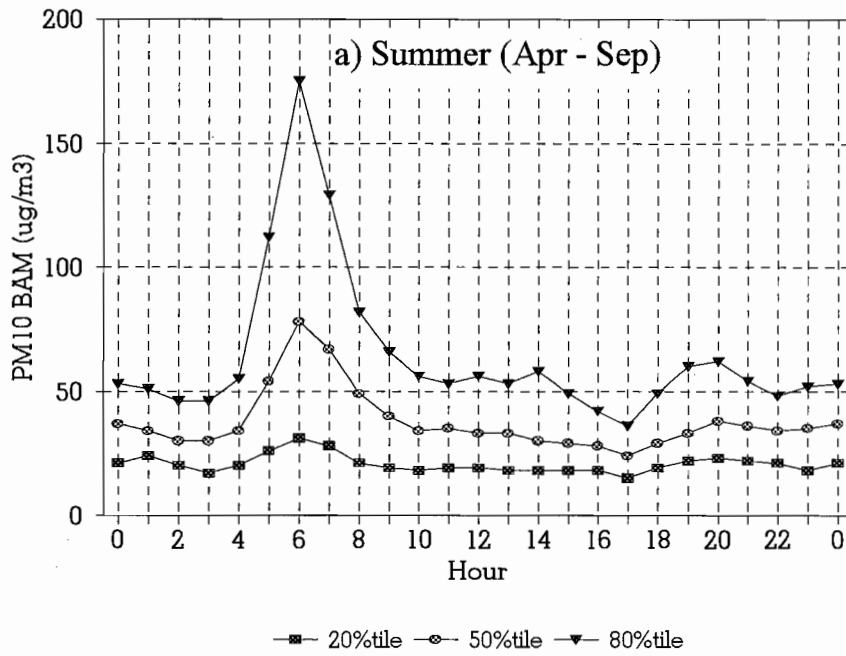
Figure 8-4   Diurnal variations of PM_{10} BAM concentrations during the: a) summer
(April to September), and b) winter (October to March) periods at the
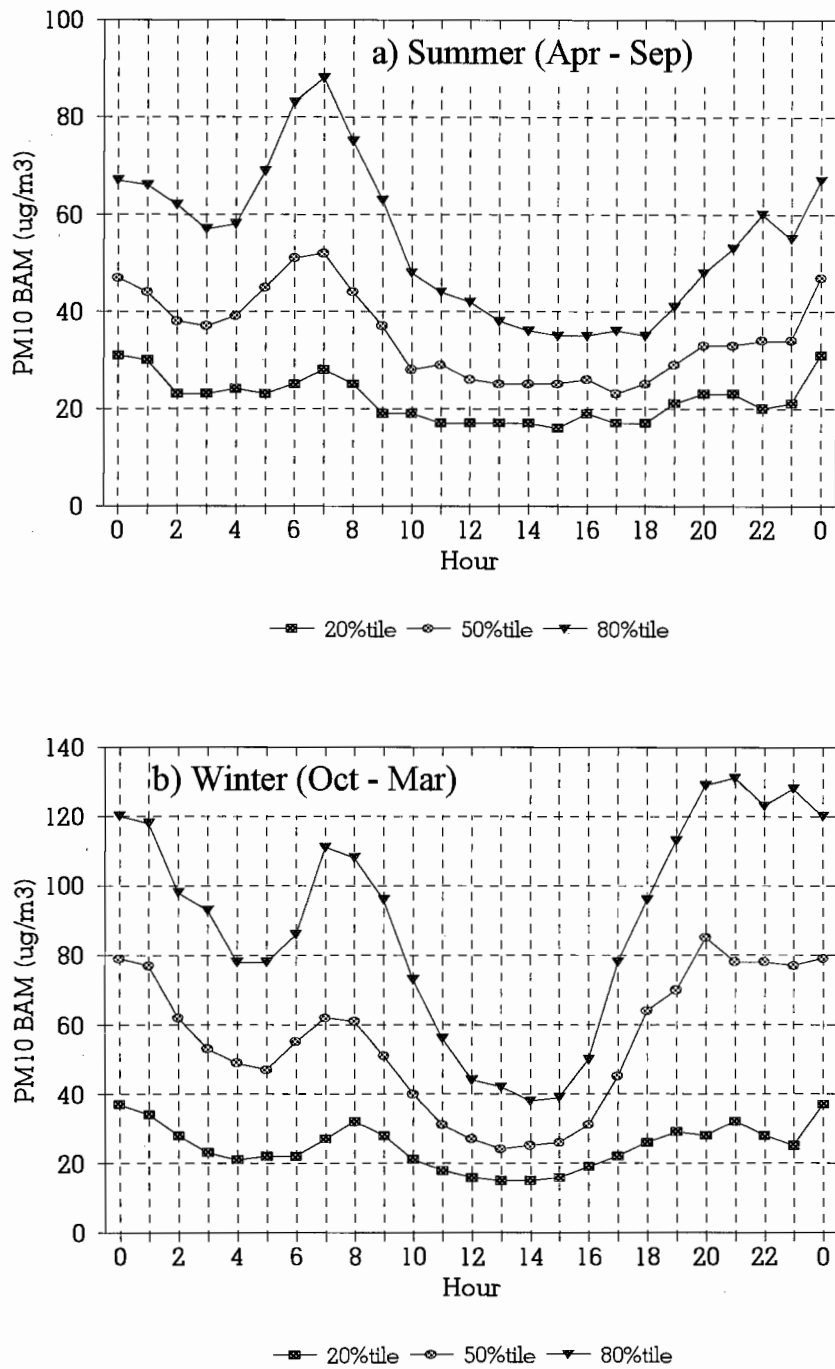East Charleston (Microscale) site.

Figure 8-5   Diurnal variations of PM_{10} BAM concentrations during the: a) summer (April to September), and b) winter (October to March) periods at the Bemis/Craig Road site.
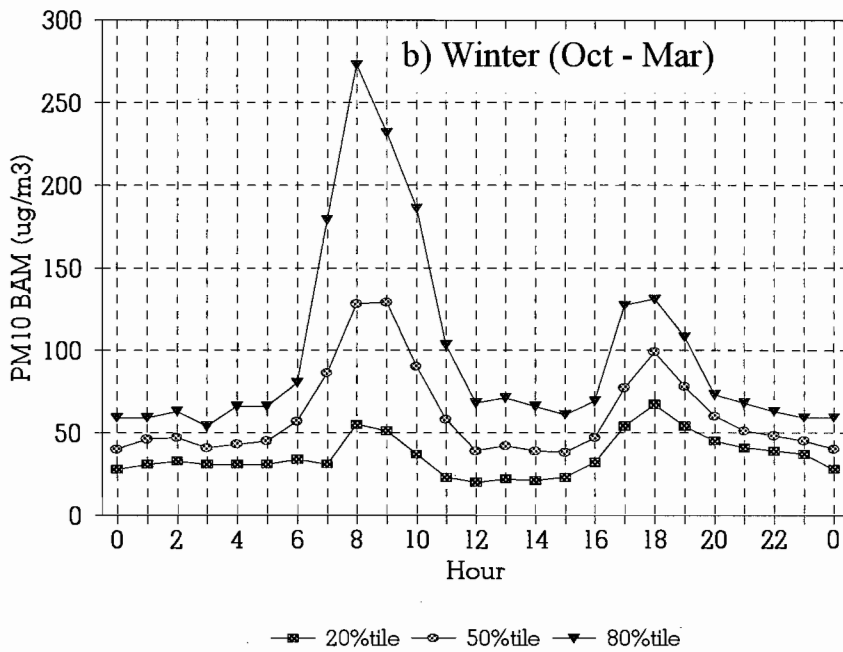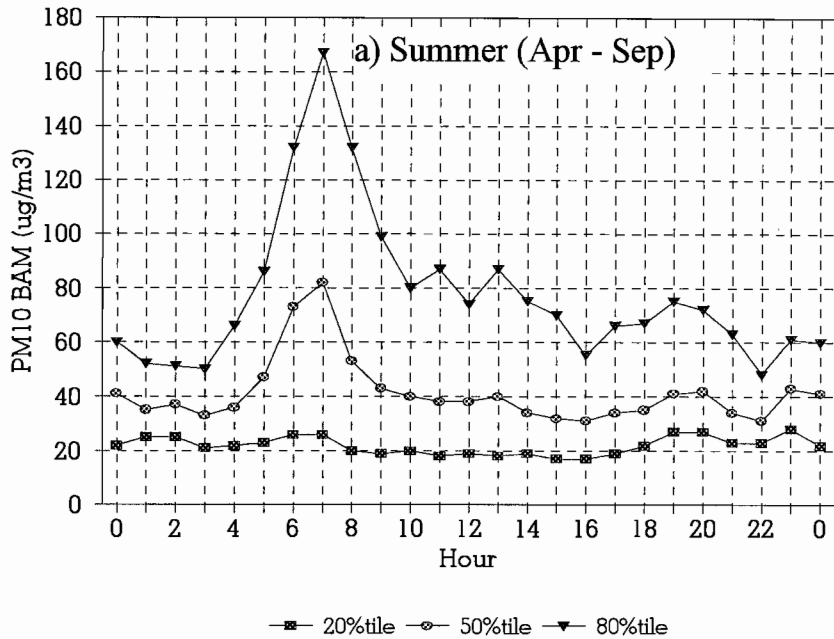
Figure 8-6   Diurnal variations of PM_{10} BAM concentrations during the: a) summer (April to September), and b) winter (October to March) periods at the Green Valley (Arroyo Grande) site.
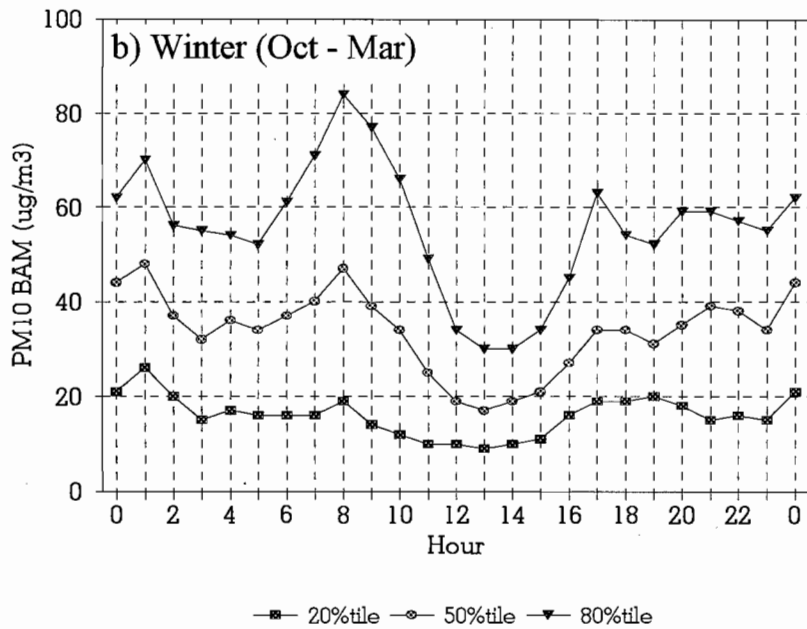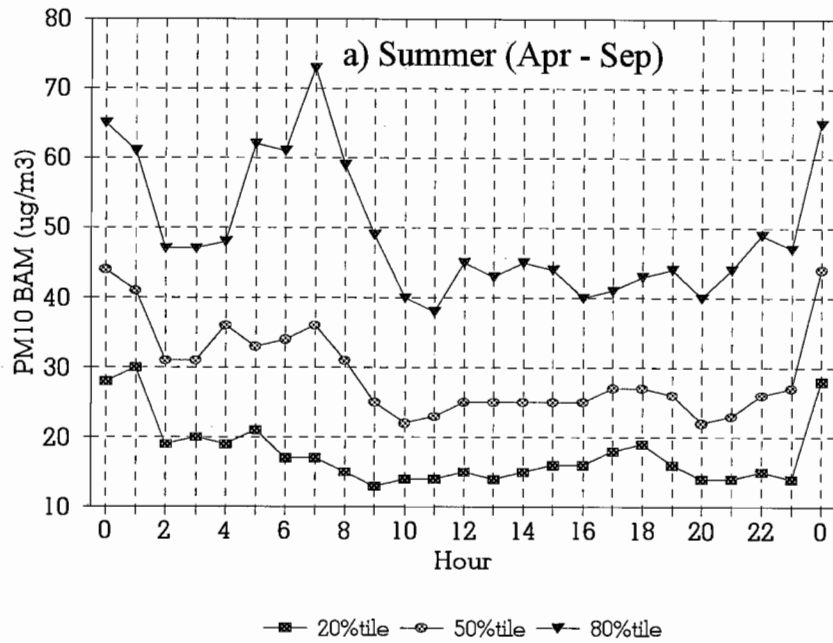
Figure 8-7   Diurnal variations of PM_{10} BAM concentrations during the: a) summer (April to September), and b) winter (October to March) periods at the Powerline site.

Figure 8-8   Diurnal variations of PM_{10} BAM concentrations during the: a) summer (April to September), and b) winter (October to March) periods at the Maycliff site.

Figure 8-9   Diurnal variations of PM_{10} BAM concentrations during the: a) summer (April to September), and b) winter (October to March) periods at the McDaniels (Lake Mead Boulevard) site.

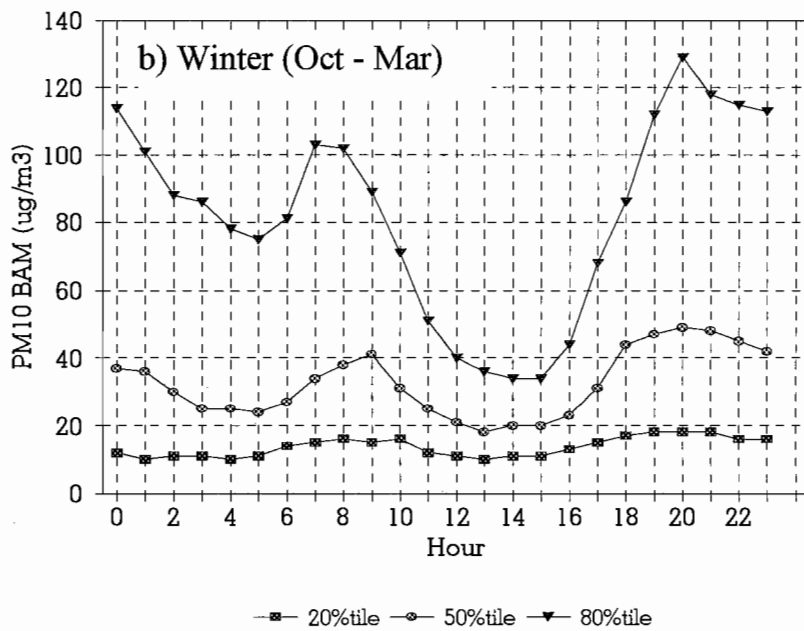Figure 8-10   Diurnal variations of PM_{10} BAM concentrations during the: a) summer (April to September), and b) winter (October to March) periods at the City Center site.
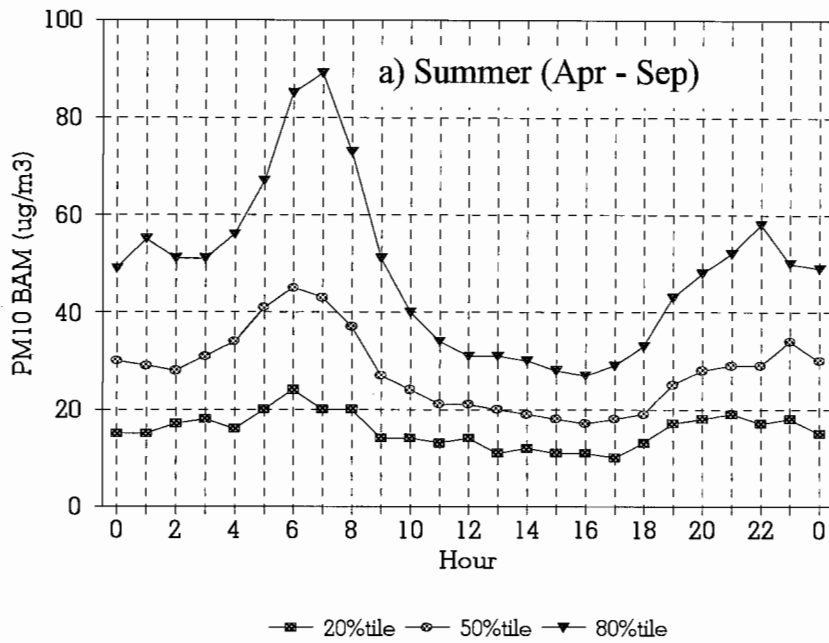
Figure 8-11   Diurnal variations of PM_{10} BAM concentrations during the: a) summer (April to September), and b) winter (October to March) periods at the Pittman site.

Figure 8-12   Diurnal variations of PM_{10} BAM concentrations during the: a) summer (April to September), and b) winter (October to March) periods at the Flamingo Road site.
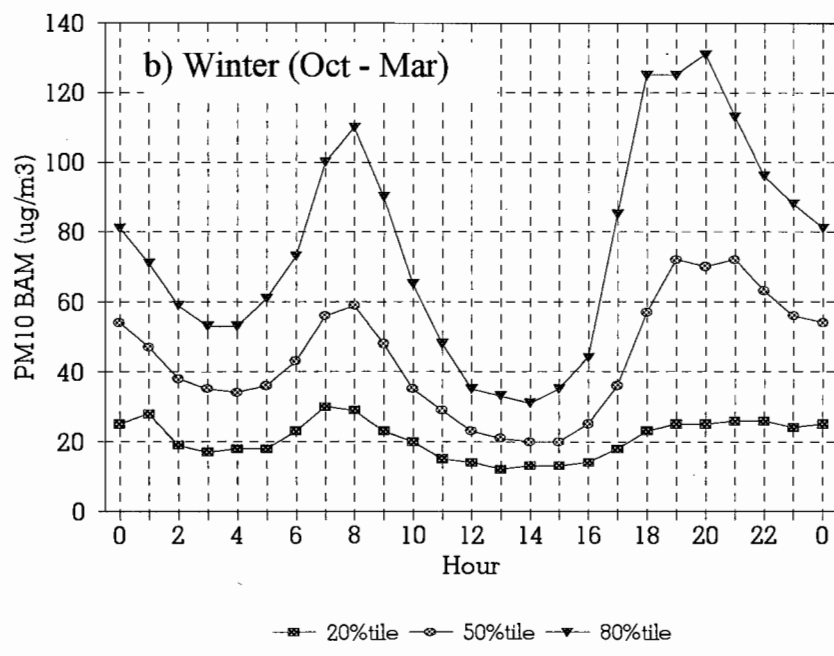
Figure 8-13   Diurnal variations of PM_{10} BAM concentrations during the: a) summer (April to September), and b) winter (October to March) periods at the Jean site.
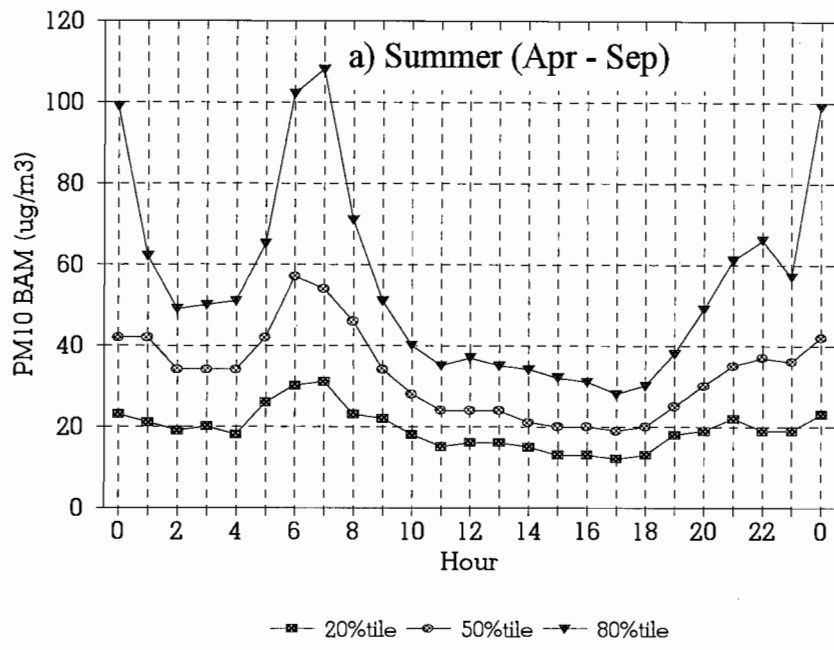
Figure 8-14   Diurnal variations of PM_{10} BAM concentrations during the: a) summer (April to September), and b) winter (October to March) periods at the Boulder City site.

Figure 8-15   Diurnal variations of PM_{10} BAM concentrations during the: a) summer (April to September), and b) winter (October to March) periods at the Paul Meyer site.
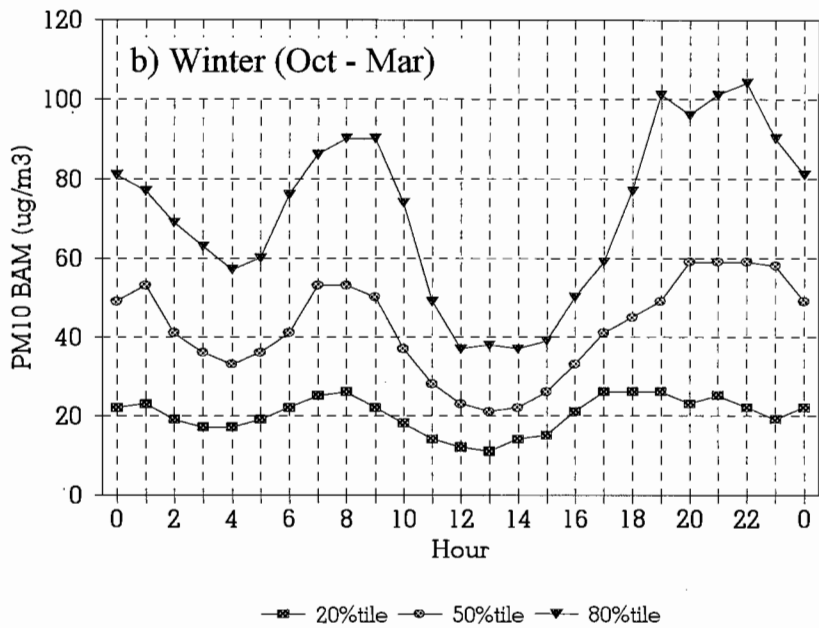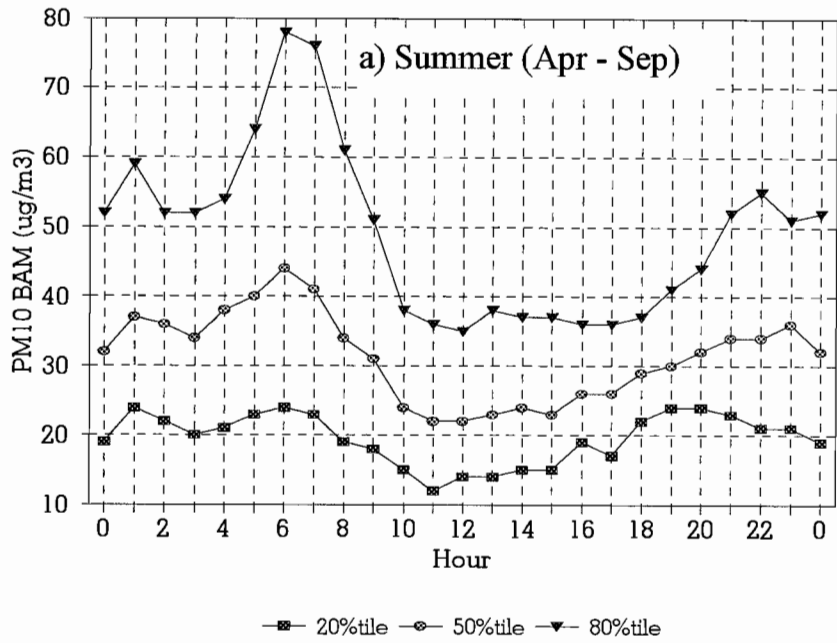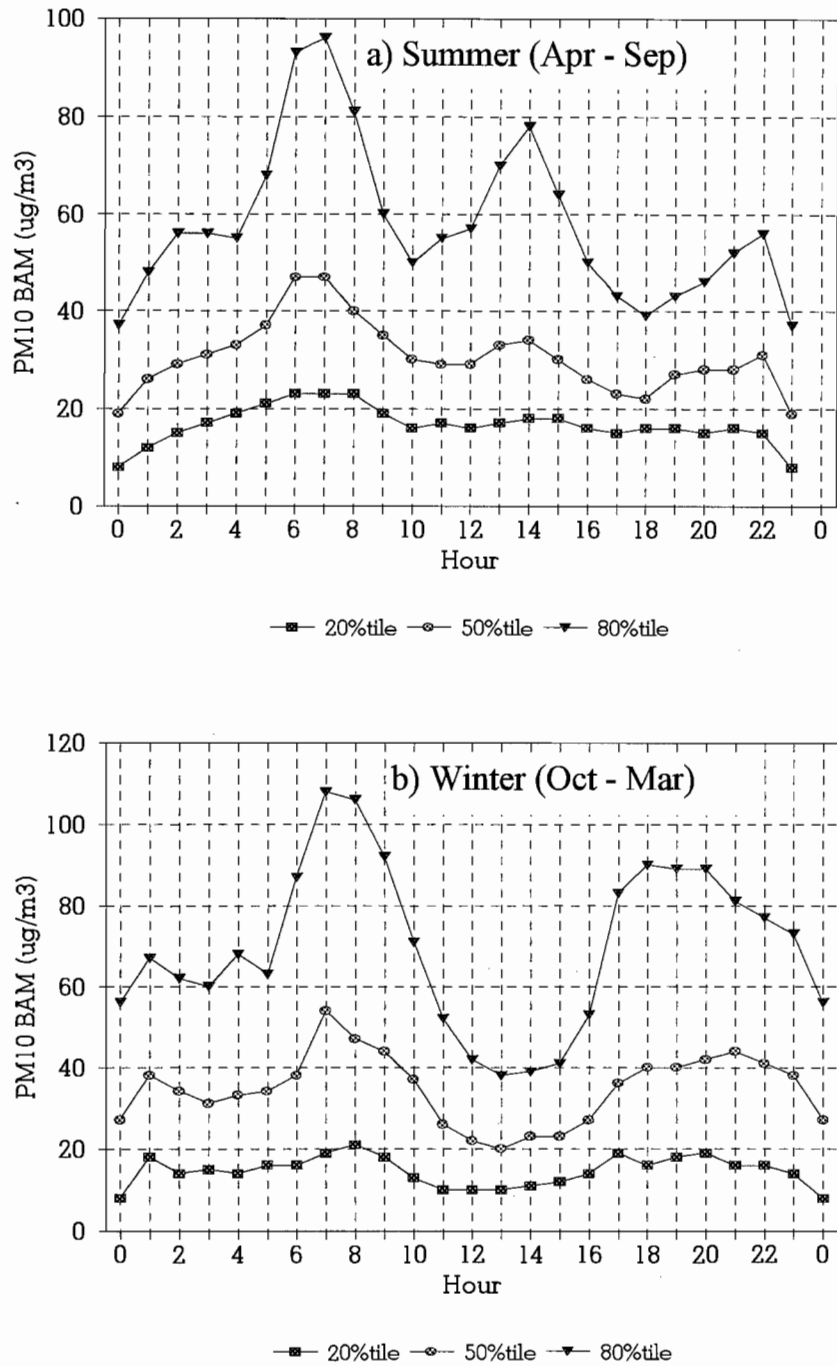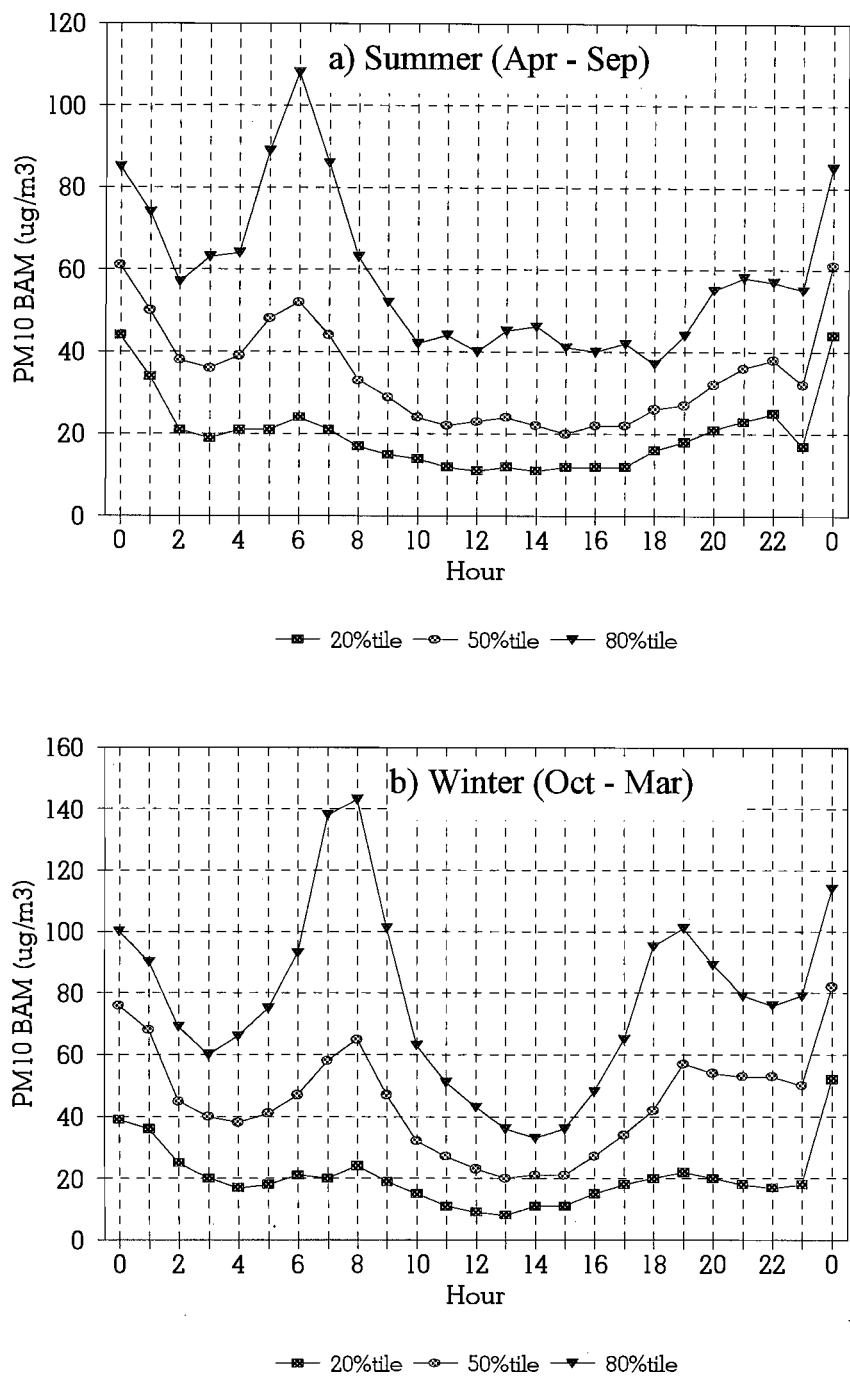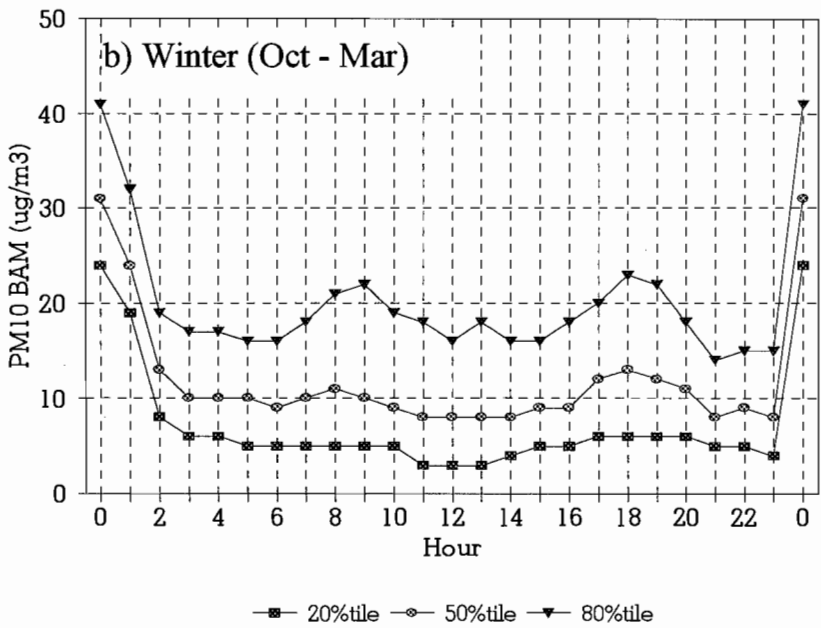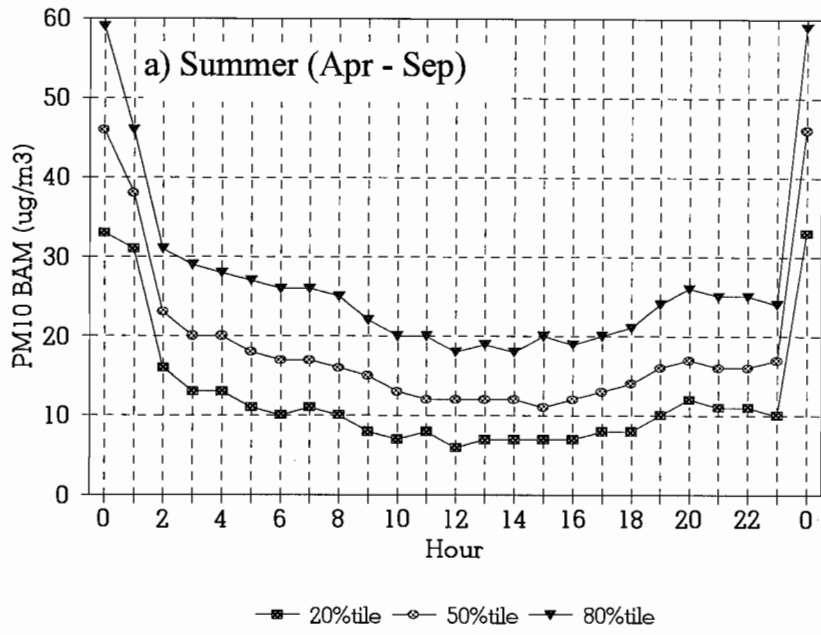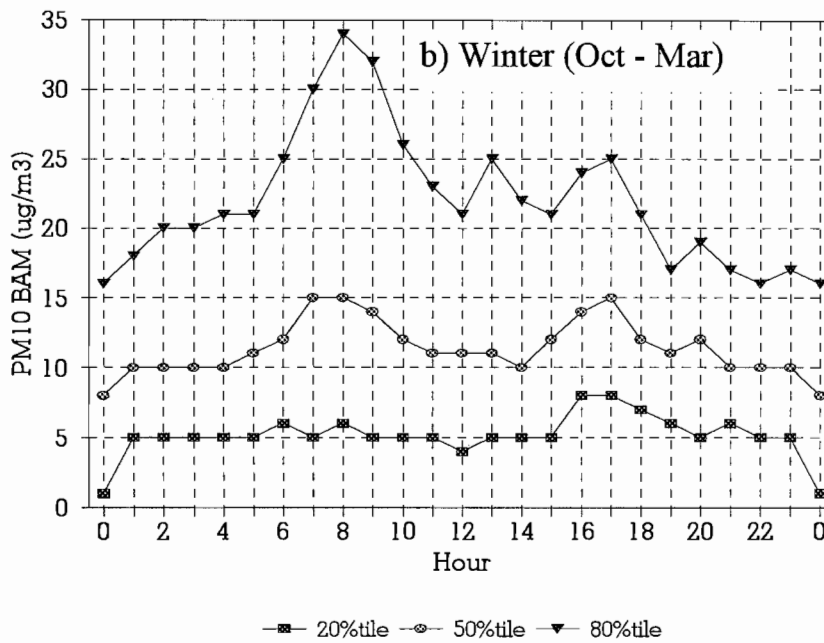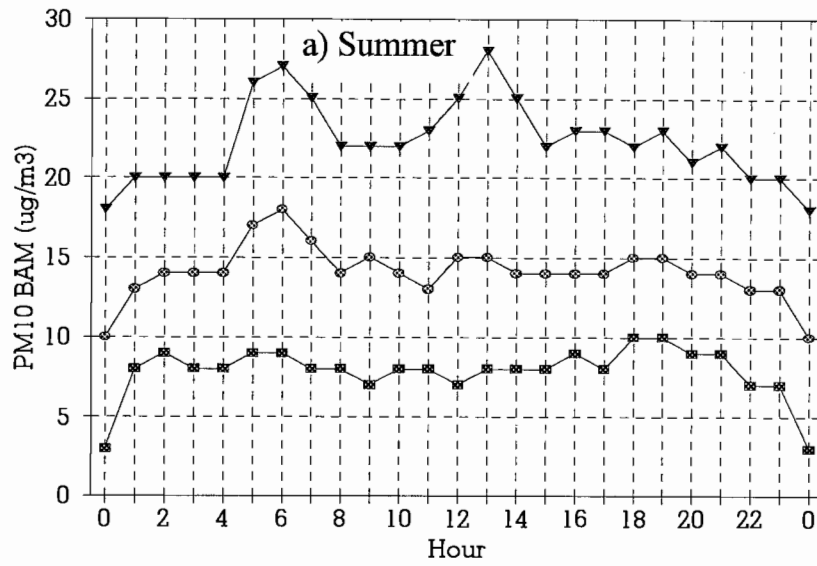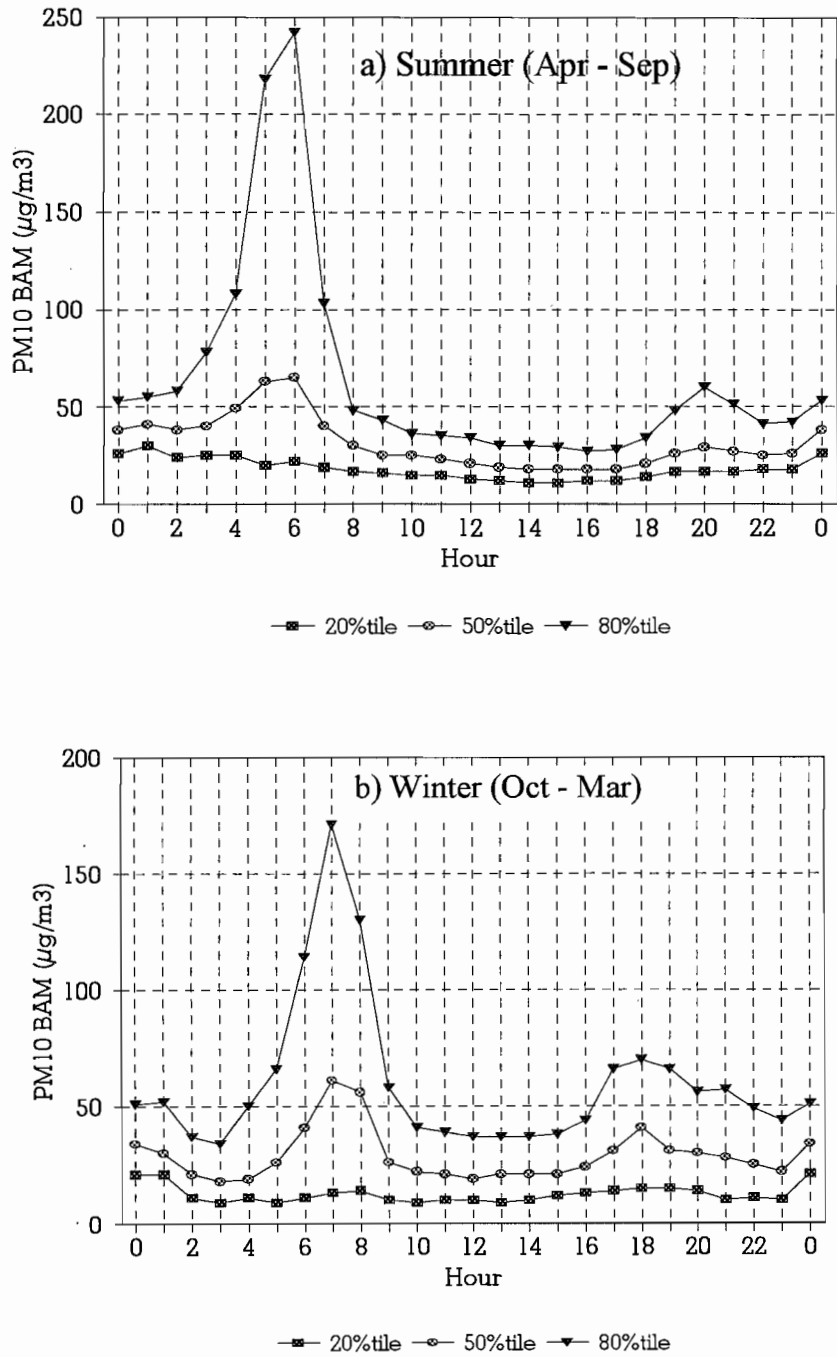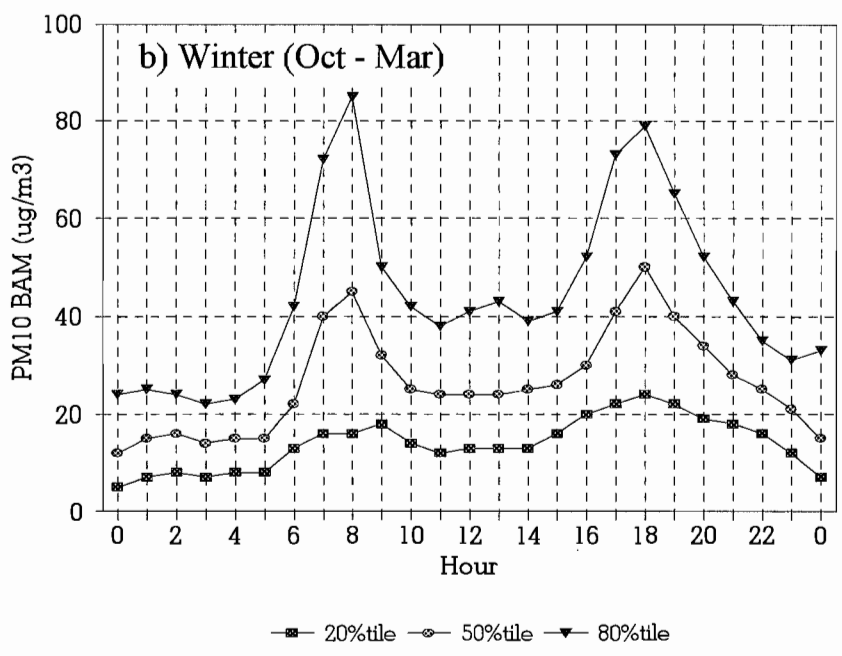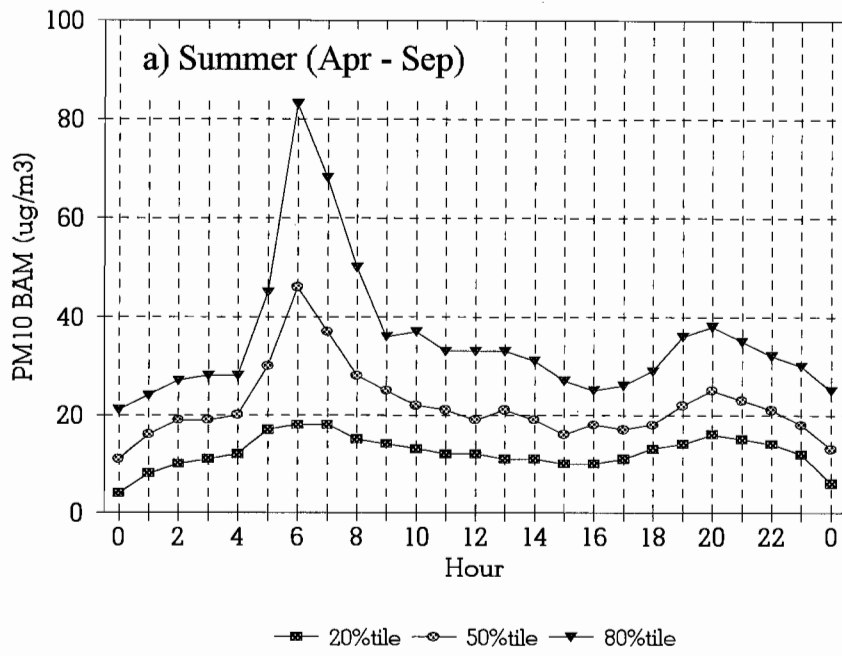
Figure 8-16   Diurnal variations of PM_{10} BAM concentrations during the: a) summer (April to September), and b) winter (October to March) periods at the Walter Johnson site.

Table 8-1
Time of Day at which Peak and Minimum PM$_{10}$ Concentrations in the 50th Percentile Occurred for the Summer (April to September) and Winter (October to March) Periods

	Time of Day Peak/Minimum PM$_{10}$ Concentrations Occurred					
Sampling Site	Summer[a] morning peak	Summer afternoon minimum	Summer evening peak	Winter[b] morning peak	Winter afternoon minimum	Winter evening peak
Craig/Bemis	0600 PST	1700 PST	2000 PST	0900 PST	1300 PST	1800 PST
East Charleston (Microscale)	0700 PST	1700 PST		0700 PST	1300 PST	2000 PST
Green Valley	0700 PST	1200 PST, 1500 PST	2000 PST, 2300 PST	0900 PST	1500 PST	1800 PST
Powerline	0700 PST	1000 PST, 2000 PST		0800 PST	1300 PST	1900 PST
Maycliff	0600 PST	1300 PST	2300 PST	0900 PST	1300 PST	2000 PST
McDaniel	0600 PST	1700 PST	2200 PST	0900 PST	1300 PST	2100 PST
City Center	0600 PST	1200 PST	2300 PST	0700-0800 PST	1300 PST	1900-2100 PST
Pittman	0700 PST	1800 PST	2000 PST	0700 PST	1300 PST	2100 PST
Flamingo Road	0600 PST	1500 PST	2200 PST	0800 PST	1300 PST	1900 PST
Jean		1100-1400 PST	2000 PST	0800 PST	1100-1300 PST	1800 PST
Boulder City	0600 PST	1400 PST	1800-1900 PST	0700-0800 PST	1400 PST	1700 PST
Paul Meyer	0600 PST	1200 PST	2000 PST	0700 PST	1200 PST	1800 PST
Walter Johnson	0600 PST	1500 PST	2000 PST	0800 PST	1100-1300 PST	1800 PST

	Corresponding 50th Percentile PM$_{10}$ Concentrations					
Sampling Site	Summer morning peak	Summer afternoon minimum	Summer evening peak	Winter morning peak	Winter afternoon minimum	Winter evening peak
Craig/Bemis	78	24	38	50	30	68
East Charleston (Microscale)	52	23		62	24	85
Green Valley	82	31	43	128	38	99
Powerline	36	22		47	17	39
Maycliff	45	17	34	41	18	49
McDaniel	57	19	37	36	16	42
City Center	44	22	36	53	21	59
Pittman	47	22	31	54	20	44
Flamingo Road	52	20	38	65	20	57
Jean		11	17	11	8	13
Boulder City	18	13	15	15	10	15
Paul Meyer	65	18	29	61	19	41
Walter Johnson	46	16	25	45	24	50

[a] Summer includes the months of April to September.
[b] Winter includes the months of October to March.

- Summer evening peaks at all sites occur later than winter evening peaks (typically 2000 to 2300 PST in summer and 1800 to 2100 PST in winter).

These patterns can be explained by diurnal meteorological and source emissions patterns during summer and winter. Because much of the PM_{10} (on typical days) is directly or indirectly related to the emissions from motor vehicle exhaust, peaks in PM_{10} concentration during the morning and evening rush hour(s) would be expected. Highest PM_{10} emissions are expected during these hours. However, ambient concentrations depend not only on source emissions, but also on the ability for the atmosphere to disperse pollutants as well. As shown in the previous section, moderate winds prevent buildup of pollutants that occurs under light wind speed conditions. Deep mixing depths, typically caused by strong solar heating during daytime, increase the vertical dispersion of pollutants and similarly prevent buildup of pollutants which occurs under inversion (low mixing depth) conditions. The product of mixing depth and wind speed, called *ventilation,* is a simple measure of the ability of the atmosphere to disperse a given amount of pollutant emissions.

During the daytime, solar radiation heats the ground, warming the layer of air next to the ground. This warm (or hot) air is buoyant and rises, mixing with the air above it. As the day progresses, air is well mixed typically to 1,000 m above the ground in winter, and to 3,000 to 4,000 m above the ground in summer. This also mixes pollutants within the mixing layer, which lowers PM_{10} concentrations at the monitoring stations, which are near ground level. Wind speeds near the ground also increase due to vertical mixing. Wind speeds usually increase with height above the ground; the mixing brings air with higher wind speeds down towards the ground. Ventilation then reaches a peak in the afternoon as mixing depths and wind speed are at their maximum. This explains the afternoon minimum in PM_{10} concentrations. In winter, lower sun angles and shorter days causes maximum mixing depths to occur earlier in the afternoon than in summer; thus PM_{10} concentrations are at a minimum earlier in the day.

At night, the ground cools due to long-wave radiation to space, causing the air in contact with it to cool as well. This creates a layer of cool air next to the ground, with warmer air above it; this is called a *temperature inversion* or *inversion* for short. Because cool, dense air lies below warmer, lighter air, vertical mixing is inhibited. Mixing depths and wind speeds are usually low, and pollutants tend to accumulate, causing elevated ground level concentrations. Inversions are typically present from just after sunset to shortly after sunrise. During winter in the Las Vegas Valley, surface-based inversions may form as early as 1600 to 1700 PST and last until the next morning around 0800 PST. During summer, with longer days, inversions will begin to dissipate by 0600 PST and not form again until at least 2000 to 2100 PST. In the urban area, heat from streets, parking lots, etc., may further delay cooling of the ground needed to form inversions.

During winter, maximum morning PM_{10} concentrations occur between 0700 and 0900 PST. This corresponds to the morning rush hour period and associated pollutant emissions. Since mixing depths and wind speeds are low at this time, ventilation is low and pollutants rapidly build up. In contrast, the summer peak in PM_{10} concentrations occurs between 0600 and 0700 PST, which is earlier than the peak in traffic. By 0800 or 0900 PST, PM_{10} concentrations are significantly lower, even though traffic levels are similar. This is because by 0800 or 0900 PST, solar heating has causing increased mixing depths and pollutants are mixed through a deeper layer, with lower concentrations recorded at the monitoring stations. During winter, PM_{10} levels are typically highest near the end of the evening rush hour, due to high emissions and low mixing depths (due to early sunset). In contrast, summertime rush hour PM_{10} levels are relatively low because ventilation is near its daily maximum (high mixing depths), even though emissions are high. Maximum PM_{10} concentrations occur later in the evening when mixing depths are much less and emissions have decreased, but are still significant. Concentrations later at the night decrease as emissions decrease. In winter, morning and evening PM_{10} peaks are similar in magnitude because of low mixing heights during the rush hours. In summer, morning PM_{10} peaks are much higher than the evening PM_{10} peaks because mixing depths are much lower during the morning rush hour than during the evening rush hour.

8.3.2 Weekday/Weekend Patterns in PM_{10} Concentrations

Hourly PM_{10} patterns for weekdays and weekends are compared for selected sites. Figure 8-17 shows the diurnal pattern in PM_{10} concentrations at the Bemis/Craig Road site for weekdays and weekends for the summer (April to September) and winter (October to March) periods. The most striking difference between weekdays and weekends is the large reduction in the size of the morning peak on weekends. This occurs in both winter and summer and can be explained by less motor-vehicle-exhaust-related emissions as fewer people are commuting to work. The early evening peak can also be seen to be somewhat lower, especially in winter.

Winter weekend and weekday diurnal PM_{10} patterns for the East Charleston and City Center sites are shown in Figure 8-18. A similar pattern was found with distinguished morning (0800 PST) and evening (2000 to 2100 PST) peaks during weekdays. Apparent carryover of PM_{10} concentrations were found during weekends between 2100 PST to early morning of the next day (0100 PST)

Figure 8-19 shows the 50th percentile PM_{10} concentrations for weekdays and weekends at the Bemis/Craig Road, East Charleston, City Center, and Walter Johnson sites. For both weekdays and weekends, the Bemis/Craig Road and Walter Johnson sites exhibited similar patterns, and the East Charleston and City Center sites exhibited similar patterns. All four sites showed a pronounced decrease in the size of the morning peak on weekends. The
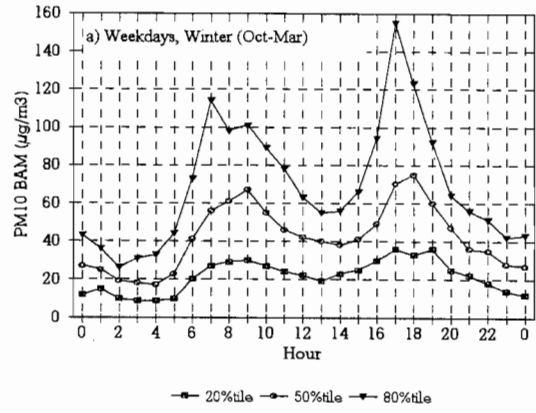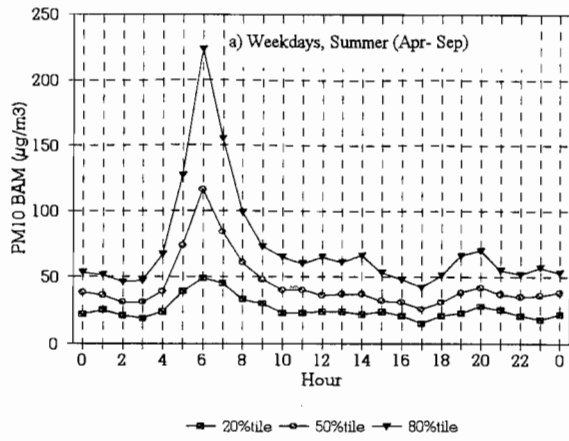
Figure 8-17   Winter weekday and weekend patterns in PM_{10} concentrations during summer (April to September) and winter (October to March) periods at the Bemis/Craig Road site.

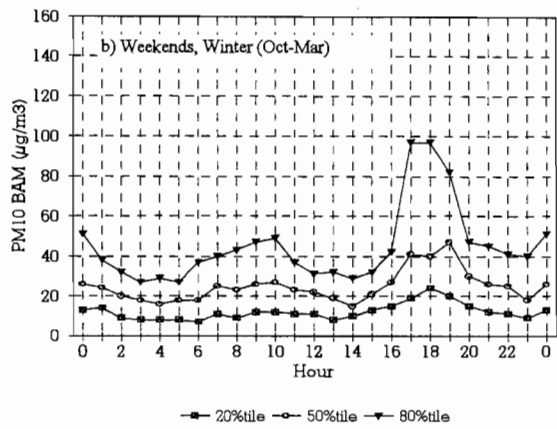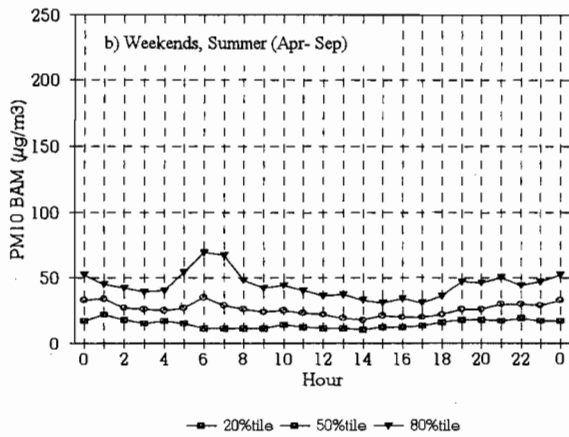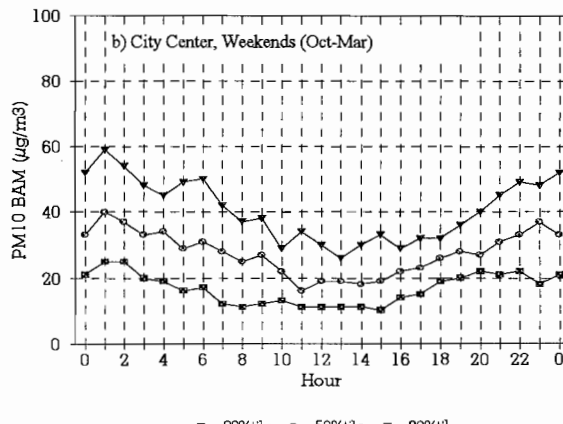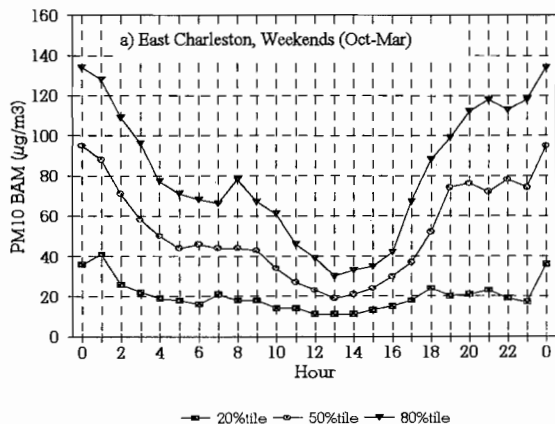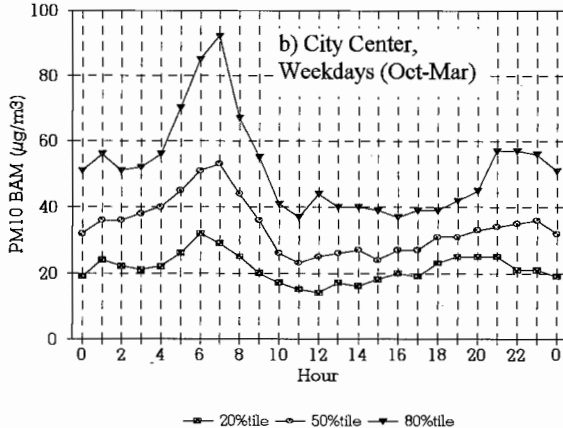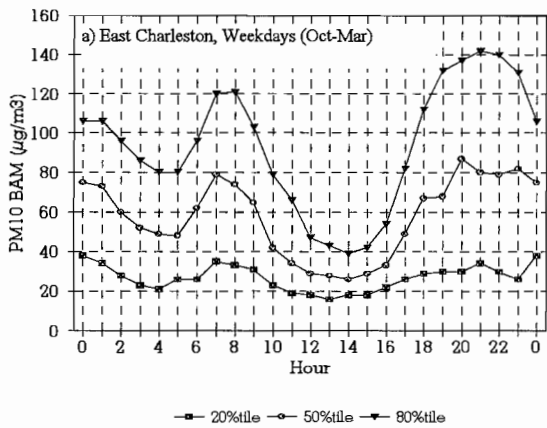Figure 8-18   Winter weekday and weekend patterns in PM_{10} concentrations during summer (April to September) and winter (October to March) periods at the a) East Charleston (Microscale) and b) City Center sites.
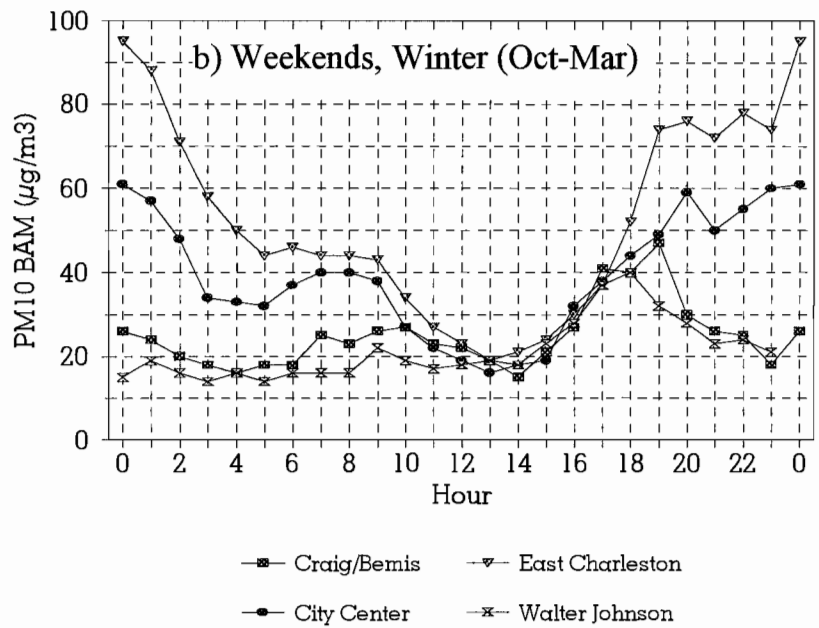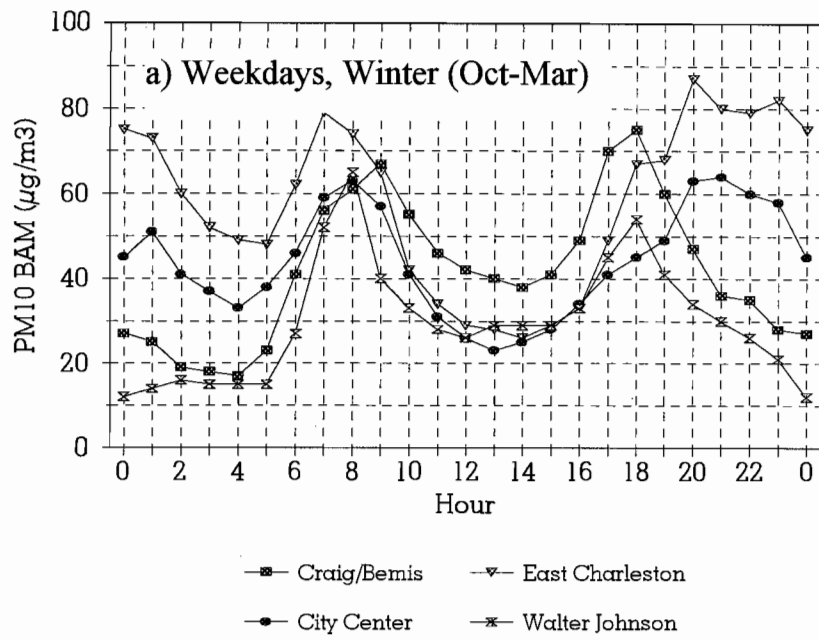
Figure 8-19   Winter weekday and weekend patterns for 50th percentile PM$_{10}$ concentrations at the Bemis/Craig, East Charleston (Microscale), City Center, and Walter Johnson sites.

East Charleston and City Center site show concentrations peaking later than the other two sites and remaining high into the early morning hours both weekdays and weekends. In the early afternoon on weekends, all sites have similar 50th percentile concentrations of about 20 $\mu g/m^3$. The East Charleston and City Center sites are near the center of the Las Vegas urban area, while the Bemis/Craig Road and Walter Johnson sites are near the edges of the urban area. The PM_{10} concentration decreases quickly during late evening at the less-urban sites, which is expected as people have returned to their homes after work. However, at the more-urban sites, traffic volume may be continued through the late evening at casinos, restaurants, etc. This increased activity, in conjunction with low mixing heights and light winds at this time of day may be largely responsible for the high PM_{10} concentrations into the early morning hours at these sites. It may also be that wind speeds are particularly light at night at the East Charleston and City Center sites, which would be conducive to elevated PM_{10} concentrations. These sites also have somewhat higher PM_{10} concentrations at midnight to 0200 PST on weekends, compared to weekdays. Because more people would typically be out on weekends at these times, this supports the argument that greater activity is responsible for higher nighttime values at the East Charleston and City Center sites.

8.4   Meteorological Conditions during PM_{10} Exceedances at the Bemis/Craig Site

Table 6-1 shows that 24-hour PM_{10} concentrations were exceeded six times (i.e., 04/09/95, 04/13/95, 06/05/95, 11/26/95, 12/12/95, 01/16/96) at the Bemis/Craig Road site during the study period. Section 6.1 discusses the meteorological conditions on 11/26/95 and 01/16/96 when Valley-wide elevated PM_{10} concentrations were found. Meteorological conditions for the remaining days are discussed here.

04/09/95

On 04/09/95, strong winds occurred following the passage of a cold front. Strong surface pressure gradients and the jet stream located over southern Nevada contributed to the high winds. A cold front passed through between 2100 and 2200 PST on 04/08/95. Winds increased from the north after 2200 PST and peaked at 0400 PST on 04/09/95, with hourly average speeds of 13 m/s and gusts to 20 m/s at the airport. PM_{10} exceedances occurred at four monitoring sites, including the Bemis/Craig Road site. PM_{10} BAM at the Bemis/Craig Road site began increasing after 2200 PST and peaked to about 1,100 $\mu g/m^3$ at 0400 PST. PM_{10} concentrations decreased rapidly to the 100 to 200 $\mu g/m^3$ range by 0600 PST and decreased to more typical levels by afternoon. The relationship between wind speed and PM_{10} at Bemis/Craig Road site for the 04/09/95 episode is shown in Figure 8-20.

Figure 8-20   Relationship between hourly averaged wind speed and PM_{10} concentrations during the period 04/08/95 to 04/09/95 at the Bemis/Craig Road site.

04/13/95

On 04/13/95, a strong surface-low-pressure system moved from British Columbia into the northern Intermountain region. High winds were caused by a strong pressure gradient between the surface low and a surface high pressure over the eastern Pacific Ocean. A cold front passed through the Las Vegas Valley between 2100 and 2200 PST. Winds started out southerly and increased as shifted to southwesterlies before the frontal passage. After frontal passage, wind became northwesterly and gradually subsided. The highest wind recorded at the Bemis/Craig Road site, 14.7 m/s, occurred during this day. Wind speed and BAM PM_{10} by hour of day for 04/13/95 and part of 04/14/95 are shown in Figure 8-21. From the late morning to early evening, somewhat elevated PM_{10} accompanied the increased wind speeds. At 2000 PST, wind speed peaked at 14.7 m/s and BAM PM_{10} jumped to 1,152 $\mu g/m^3$. PM_{10} remained high for three more hours and then dropped to less than 20 $\mu g/m^3$ early on 04/14/95, even though wind speeds remained about 7 to 10 m/s.

Summer Intensive Monitoring Period (06/05/95 to 06/07/95)

On 06/05/95, a cold front from the Pacific Northwest approached and passed through the Las Vegas Valley. As is typical for these conditions, the winds were from the southwest and increased in intensity during the approach of the front and shifted to the northwest and remained strong before gradually decreasing several hours after the frontal passage. Hourly wind speed and PM_{10} at the Bemis/Craig Road site for this period are shown in Figure 8-22. Wind speed began increasing in the late morning and reached 15 m/s at 1500 PST. After wind speeds became greater than 10 m/s, a rapid increase in PM_{10} occurred and reached 712 $\mu g/m^3$ at 1500 PST. Winds and PM_{10} then decreased for a couple of hours before the cold front passed (between 1800 and 1900 PST), after which the winds became northwesterly and increased in speed and were accompanied by increasing PM_{10} concentrations. High PM_{10} values occurred for about four hours before decreasing a winds subsided to less than 5 m/s.

Winds and PM_{10} stayed low until late in the day on 06/06/95, when a second front passed through the Las Vegas Valley, briefly increasing wind and PM_{10} levels. From 1200 PST to 1300 PST on 06/07/95, PM_{10} values of 1,453 and 452 $\mu g/m^3$ were recorded. These values occurred during light wind conditions and would therefore be expected to result from nearby activity.

12/12/95

PM_{10} BAM reached its second-highest 24-hour average concentration of 318 $\mu g/m^3$ at the Bemis/Craig Road site on 12/12/95. An unusually strong Pacific storm moved into the Pacific Northwest on this day, resulting in strong south to north pressure gradients over the western United States. At upper levels, winds were strong westerly. Figure 8-23 shows the
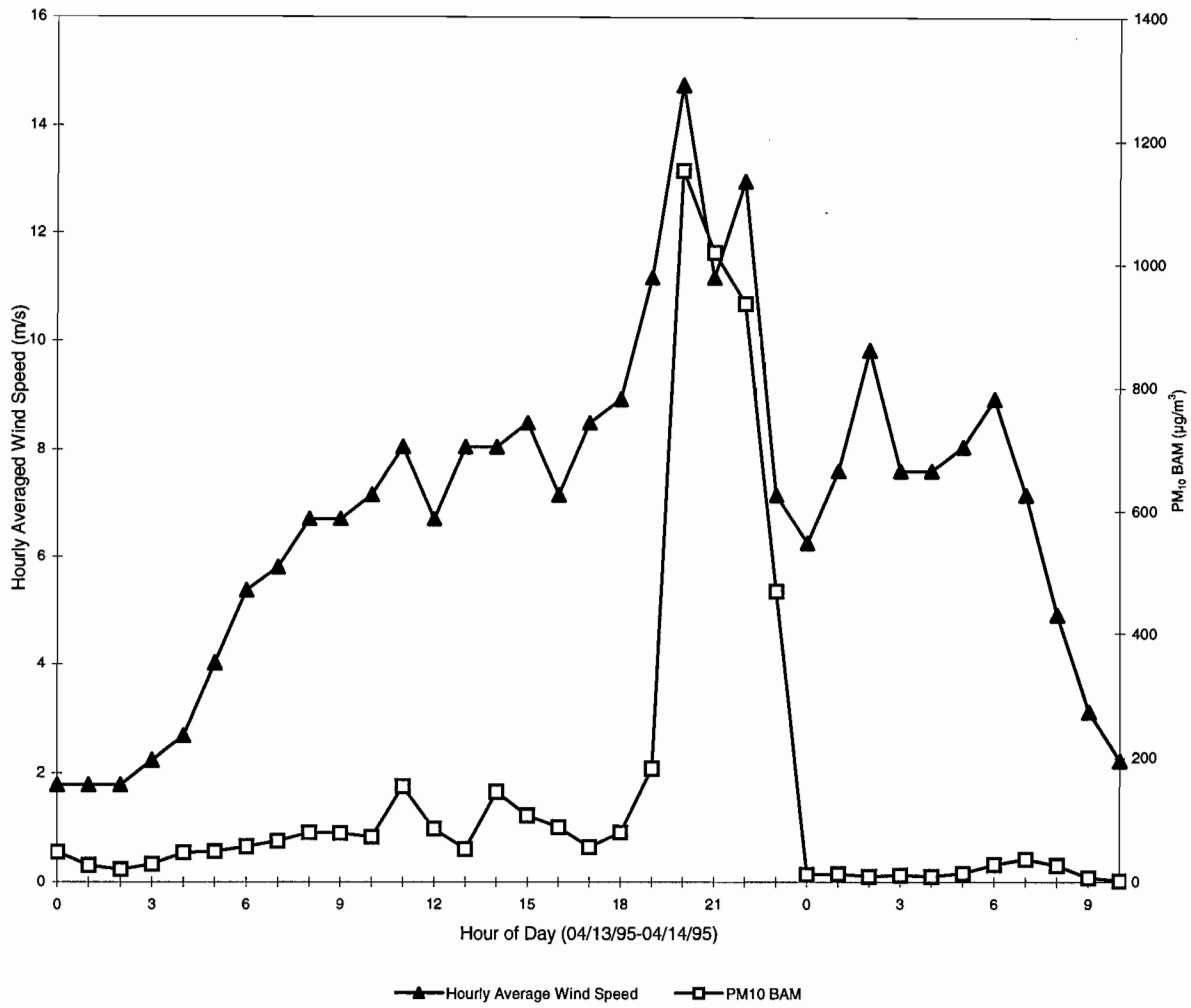
Figure 8-21   Relationship between hourly averaged wind speed and PM_{10} concentrations during the period 04/13/95 to 04/14/95 at the Bemis/Craig Road site.
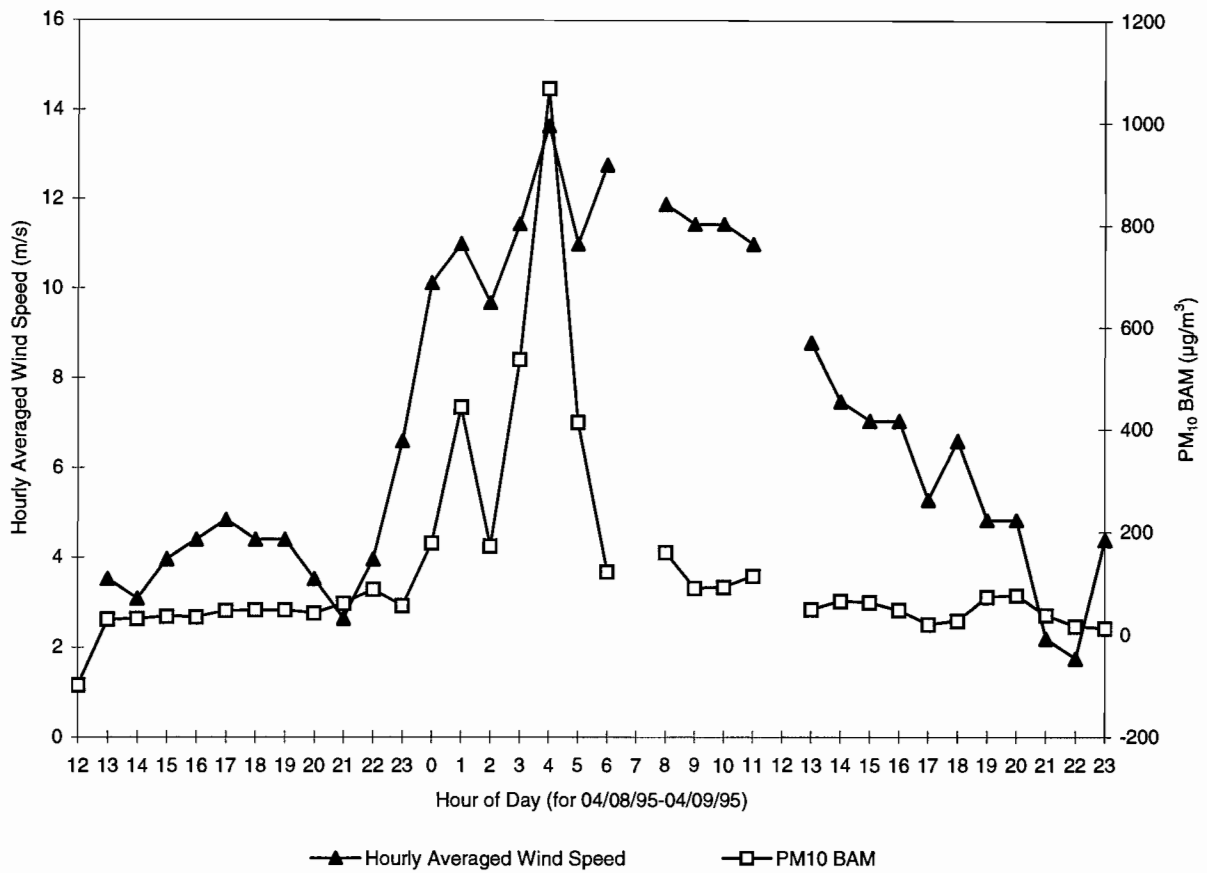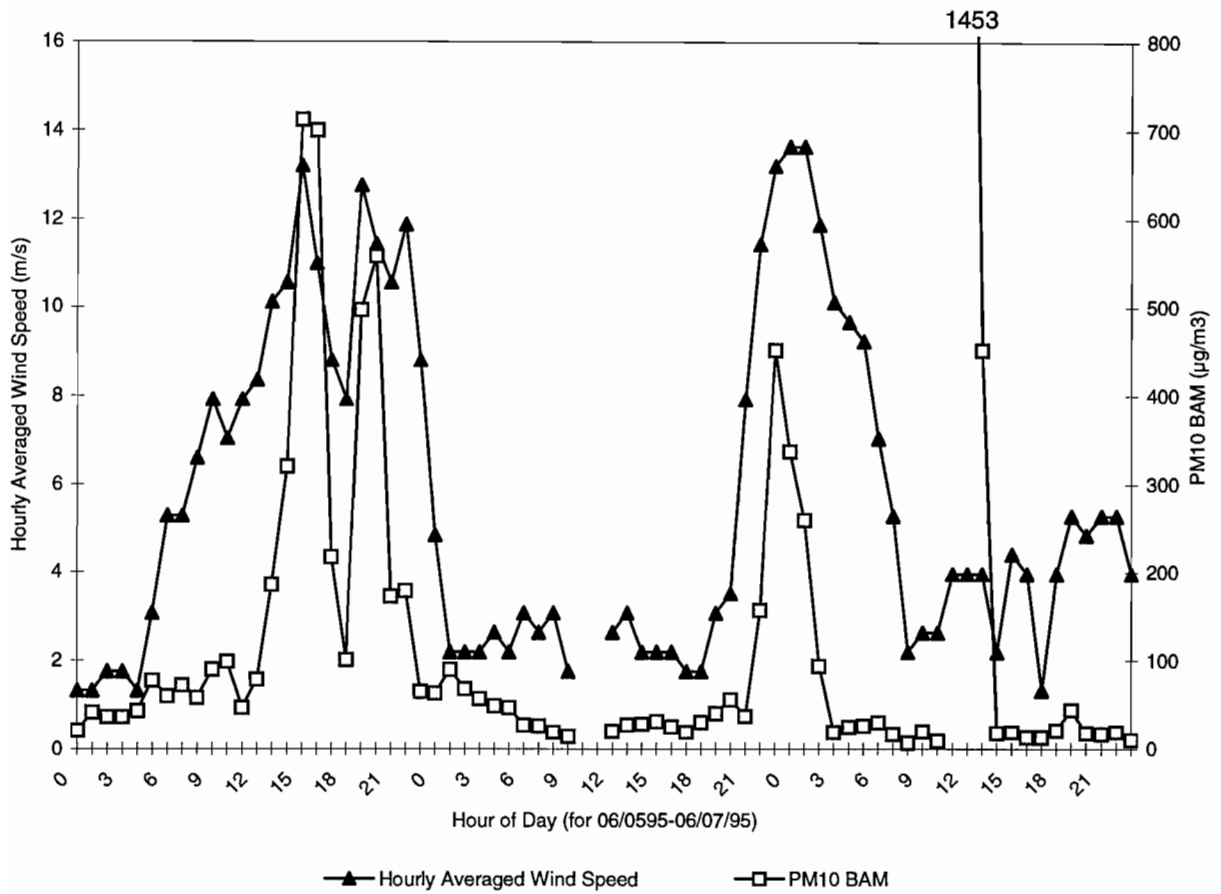
Figure 8-22   Relationship between hourly averaged wind speed and PM_{10} concentrations during the period 06/05/95 to 06/07/95 at the Bemis/Craig Road site.
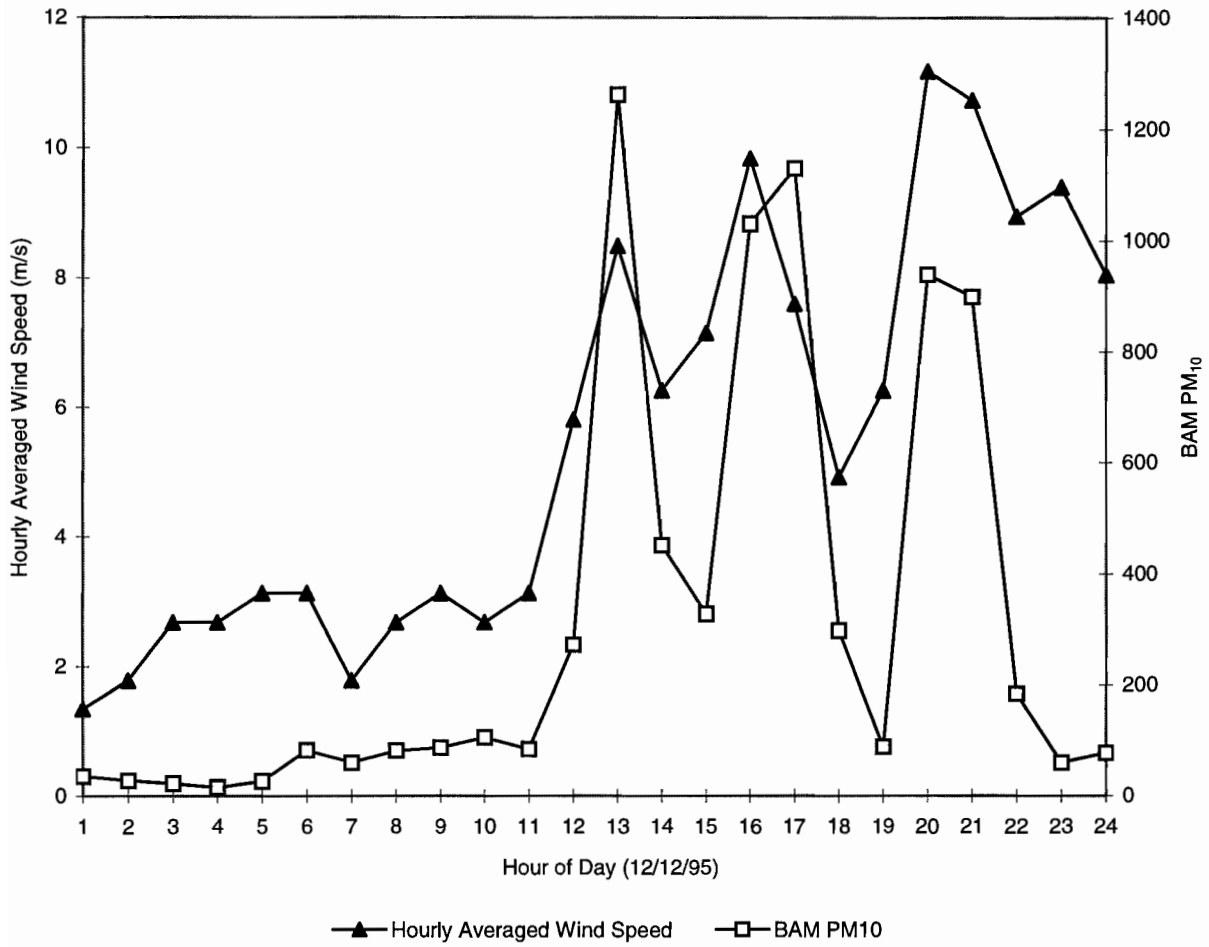
Figure 8-23   Relationship between hourly averaged wind speed and PM_{10} concentrations on 12/12/95 at the Bemis/Craig Road site.

relationship between hourly wind speed and PM_{10} concentrations for 12/12/95. Wind direction was southeasterly, becoming southwesterly during the evening. Except for the rapid decrease in PM_{10} late in the day, a good relationship between wind speed and PM_{10} exists. PM_{10} peaked at 1,261 $\mu g/m^3$ at 1200 PST with a wind speed of 8.5 m/s. Most elevated PM_{10} concentrations occur with higher wind speeds than this. This day had the 15th-highest hourly wind speed and the 25th-highest daily average wind speed of the 396-day study period, yet one of the highest PM_{10} BAM concentrations. While the wind speeds were high enough to expect elevated PM_{10} levels, PM_{10} would not be expected to be this high from the meteorology on 12/12/95. Also, PM_{10} exceedances did not occur at any other sites. This suggests that sources near the Bemis/Craig Road site contributed substantially to these high levels.

8.5   Meteorological Conditions during Intensive Study Periods

Spring Intensive Monitoring Period (04/15/95 to 04/21/95)

This period had three weather systems move across the southwestern United States. Table 8-2 shows daily wind data for this period at the Bemis/Craig Road and McCarran Airport sites. The maximum wind speed at the Bemis/Craig Road site refers to the maximum one-hour average wind speed. The maximum wind speed at McCarran Airport refers to the maximum of the reported hourly observations, which is a one-minute average taken at 10 minutes before the hour. The strongest winds occurred with frontal passages on 04/17/95 and 04/20/95, and on 04/21/95 due to moderate post-frontal pressure gradients. PM_{10} levels were low throughout this intensive study period, although winds were sufficiently strong on 04/20/95 and 04/21/95 to potentially lead to high PM_{10}.

Spring Intensive Monitoring Period (05/12/95 to 05/16/95)

During this period, an upper-level low-pressure system from the Pacific Northwest dropped southward into southern California and gradually weakened. At the surface, a widespread area of low pressure developed across the western United States by 05/13/95. Surface pressure gradually rose in conjunction with the weakening upper level low. Because surface pressure gradients were less strong than expected, winds were generally moderate in the Las Vegas Valley, with brief periods of relatively high winds. Table 8-3 gives the average wind speed and maximum hourly wind speed observed each day at the Bemis/Craig Road site.

Summer Intensive Monitoring Period (06/05/95 to 06/07/95)

(See Section 8.4)

Table 8-2
Daily Wind Data from 04/15/95 to 04/21/95 for Bemis/Craig Road and McCarran Airport

Date	Craig Road Average Wind Speed (m/s)	Craig Road Maximum Wind Speed (m/s)	McCarran Average Wind Speed (m/s)	McCarran Maximum Wind Speed (m/s)
04/15/95	3.3	5.8	4.4	7.2
04/16/95	4.6	7.6	5.0	8.2
04/17/95	4.1	7.2	4.2	10.3
04/18/95	3.3	4.9	5.4	8.2
04/19/95	2.6	6.3	3.0	8.7
04/20/95	5.8	10.7	7.9	13.9
04/21/95	6.0	9.8	6.9	10.3

Table 8-3
Daily Wind Data from 05/12/95 to 05/16/95 for Bemis/Craig Road and McCarran Airport

Date	Craig Road Average Wind Speed (m/s)	Craig Road Maximum Wind Speed (m/s)	McCarran Average Wind Speed (m/s)	McCarran Maximum Wind Speed (m/s)	McCarran Maximum Gust (m/s)
05/12/95	6.1	9.4	6.4	11.3	
05/13/95	6.0	10.3	9.2	12.8	17.5
05/14/95	4.2	8.5	6.1	9.3	13.4
05/15/95	3.5	4.5	4.5	8.7	
05/16/95	2.8	8.9	3.4	10.3	

Fall Intensive Monitoring Period (09/06/95 to 09/12/95)

This intensive monitoring period started out with above-normal temperatures and moisture for the first two days, followed by near-normal temperatures and drier conditions. Winds speeds were moderate, and peaked on 09/08/95 as weak surface and upper-level low-pressure systems passed by to the north. Wind speed at the Bemis/Craig Road and McCarran Airport sites are summarized in Table 8-4.

Winter Mini-Intensive Monitoring Period (12/24/95-1/04/96)

This period demonstrated how PM_{10} concentrations can build up over a period of a few days under light wind speed conditions. Figure 6-5 shows daily average SFS PM_{10} at the Bemis/Craig Road and East Charleston sites for the period between 12/24/95 and 01/04/96. At the East Charleston site, PM_{10} steadily increased until 12/27/95, then gradually declined through 12/31/95. Winds speeds were light, averaging 1.8 m/s to 2.5 m/s at the McCarran Airport site from 12/24/95 to 12/30/95. High surface pressure was present, which normally reduces vertical mixing, but it began to weaken after 12/27/95, allowing somewhat more vertical mixing and a decrease in PM_{10} concentrations. A frontal passage late in the day on 12/31/95, caused an increase in PM_{10} late in the day. Concentrations were low on 01/01/96 along with moderate wind speeds (good dispersion). As pressure gradients and winds weakened, a buildup of PM_{10} began with highest values occurring on 01/03/96. On 01/04/96, moderate winds again provided good dispersion and PM_{10} levels decreased.

Winter Intensive Monitoring Period (01/26/96-01/30/96)

The 01/26/96 to 01/30/96 intensive study period was representative of typical "non-extreme" winter conditions, with neither very high winds nor stagnation conditions. A weak front passed through the Las Vegas Valley in the early morning hours on 01/28/96; increased wind speeds occurred for a few hours on 01/27/96 and 01/28/96 due to this front. Table 8-5 summarizes the winds for this period.

Table 8-4
Daily Wind Data from 09/06/95 to 09/12/95 for Bemis/Craig Road and McCarran Airport

Date	Craig Road Average Wind Speed (m/s)	Craig Road Maximum Wind Speed (m/s)	McCarran Average Wind Speed (m/s)	McCarran Maximum Wind Speed (m/s)
09/06/95	3.6	8.5	3.6	7.2
09/07/95	3.6	8.0	4.3	9.8
09/08/95	3.7	6.7	6.5	11.3
09/09/95	2.7	6.7	4.6	9.8
09/10/95	1.9	3.6	4.2	7.7
09/11/95	1.9	3.6	2.5	4.1
09/12/95	2.2	4.0	1.8	6.2

Table 8-5
Daily Wind Data from 01/26/96 to 01/30/96 for Bemis/Craig Road and McCarran Airport

Date	Craig Road Average Wind Speed (m/s)	Craig Road Maximum Wind Speed (m/s)	McCarran Average Wind Speed (m/s)	McCarran Maximum Wind Speed (m/s)
01/26/96	2.5	5.8	2.3	4.6
01/27/96	3.4	8.0	3.8	8.7
01/28/96	3.3	8.9	4.5	9.8
01/29/96	2.2	3.6	2.8	6.2
01/30/96	2.4	4.9	1.7	4.1

9.0 CONTROL MEASURES

Temporal and spatial variations of PM_{10} as well as the source/receptor modeling results confirm the findings that fugitive dust is the major contributor to elevated PM_{10} in the Las Vegas Valley. This section examines the key factors that affect the magnitude of dust emissions, reviews the past fugitive dust demonstration studies, and evaluates the effectiveness of different control measures. Application of these control measures in the Las Vegas Valley to reduce PM_{10} fugitive dust emissions is also discussed.

9.1 Variables that Affect Emissions

The suspension of dust by natural wind and anthropogenic activities depends on a number of physical properties of both the atmosphere and the erodible surface. The key properties affecting the magnitude of dust emissions are: 1) surface loadings of suspendable material, 2) size distributions of the surface particulate matter, 3) moisture, 4) surface roughness, 5) wind speed and wind direction, and 6) vehicular dust suspension mechanisms. Many of these factors provide explicit or implicit inputs to the U.S. EPA's AP-42 empirical dust emission model. The following subsection reports the current status of knowledge of each of these properties with respect to their influence on the dust emission process.

9.1.1 Surface Loading

The amount of suspendable dust on a surface influences how much dust might be resuspended in the atmosphere. Most surfaces are limited reservoirs, and the suspendable dust is depleted after a short time period. Theoretical considerations of the time dependence of resuspension by wind suggest that it may be represented either as a negative exponential function (Anspaugh et al.; 1975; Linsley, 1978), or as an inverse relationship between suspension and time (Reeks et al., 1985; Garland, 1979). Nicholson (1993), in an empirical wind tunnel study of resuspension processes from concrete surfaces, found that the decay rate of particle emissions from surfaces was not well-represented by a negative exponential relationship, but appeared to follow an inverse time relationship. This relationship could be complicated in a natural environment due to the large range of surface and environmental conditions (James, 1996).

On exposed vacant land, deflation of fine particles often results in the exposure of larger nonerodible sediments which act as a shield to minimize particle resuspension by the wind. These larger nonerodible sediments also absorb momentum and decrease the erosive power of the wind that reaches the potentially erodible surface (Marshall, 1971; Raupach, 1992). When surfaces are continually disturbed by very intense winds or by vehicular movement or other anthropogenic activities, they may become "unlimited reservoirs" which emit dust whenever winds exceed threshold suspension velocities.

9.1.2 Particle Size Distribution

The current air quality standard applies to particles which are less than 10 μm in aerodynamic diameter (PM_{10}). (The "aerodynamic diameter" is defined as the diameter of a sphere of unit density [1.0 g/cm^3]; therefore, for soil particles, the aerodynamic diameter corresponds to actual, geometric diameters less than 7 μm because the density of soil particles is approximately 2.65 g/cm^3, and the aerodynamic diameter varies inversely with the square root of the density [Hinds, 1986]). The concern with PM_{10} is health-related, because it represents the upper limit of the aerodynamic particle size range which may enter the human respiratory system. The dust particle size distribution is an important variable for determining its emission and transport.

The size distribution of dust particles affects the suspension process. A flat bed of particles with diameters less than 20 μm is very difficult to be resuspended by wind. Bagnold (1937) demonstrated that fine cement particles could not be entrained by wind friction velocities in excess of 1.0 m/s. As the size of the particles are small, there is no large cross section for wind to act on. In addition, adhesive forces such as van der Walls, electrostatic, and the surface tension of adsorbed liquid films (Hinds, 1986) increase the external force required to entrain the particles. These adhesive forces increase with relative humidity and surface roughness, but decrease with increasing particle size (Corn and Stein, 1965).

Suspension of fine particles is also mitigated by the presence of larger nonerodible particles if they are present in sufficient quantities. Particles that exceed 840 μm in size are considered too large to be entrained by normal wind velocities (Chepil, 1942) and can act to shelter smaller particles in their lee. Gillette and Stockton (1989) sprinkled glass spheres with diameters ranging from 2,400 to 11,200 μm onto a bed of glass spheres with sizes from 107 to 575 μm and found major reductions in the horizontal flux of the smaller particles. In contrast, Logie (1982) found that erosion of a sand surface was enhanced when low concentrations of larger nonerodible roughness elements were present on the surface. It was suspected that the increased erosion was due to acceleration of the wind flow around the isolated elements which scoured the loose sand. Bagnold (1941) estimated that 800 μm particles are the most susceptible to suspension by wind, even though their large masses cause them to settle to the surface very rapidly.

The role of saltating particles in dust emission processes is complex. In a controlled wind tunnel experiment, Fairchild and Tillery (1982) found that resuspension was enhanced by saltation. They found saltating particles increased the resuspension rate. Resuspension rate was defined as the fraction of a surface species removed in unit time (Λ, g/s). These resuspension rates increased by a factor of two to three and reached values as high as six to seven times the nonsaltating rate for certain bed configurations. Fairchild and Tillery (1982) explained this as a more efficient utilization of wind energy by the saltation mechanism.

There is more kinetic energy transferred to the bed during saltation than in clear air flow. The relationship between saltating particles and fine particle emissions was found to be dependent upon the wind power (u_*) and the size of the saltating particles. The vertical flux of particles (F, $\mu g/m^2$-s), which is a measure of the potential for long range transport, was found to increase rapidly: 1) with increasing size of saltating particles, and 2) with decreasing size of surface sediment particles on which the particles are saltating (Fairchild and Tillery, 1982). The ratio of fine particles to particles available for saltation may have a considerable effect on the magnitude of the emission rate.

9.1.3 Moisture

In most natural systems, moisture content is the most important variable in controlling the initiation and transport of sediment by wind. Water adheres to individual soil particles, thus increasing their mass and mitigating suspension and transport. It also increases the cohesive forces among individual particles. Substantially greater wind forces are needed when soil surface moisture is increased by less than 1% from its dry state (Chepil, 1956; Belly, 1964; Bisal and Hsieh, 1966; Svasek and Terwindt, 1974). Several studies have reported that 4% moisture content is a limiting value for which erosion by wind is effectively halted (Belly, 1964; Azizov, 1977; Logie, 1982).

Due to the formation of aggregates and surface crusts, cohesion of the wetted particles often persists after the water has evaporated. Even when soil surface moisture is increased by less than 1% from its dry state, the threshold velocity required to initiate soil particle movement is significantly increased, thereby reducing the erosion potential by wind (Chepil, 1956; Belly 1964; Bisal and Hsieh, 1966; Svasek and Terwindt, 1974). The surface-moisture content is also important in enhancing the strength characteristics of surface crusts and the stability of aggregates (Bradford and Grossman, 1982; Lehrsch and Jolley, 1992).

9.1.4 Wind Speed and Surface Roughness

Wind often resuspends dust from disturbed surfaces. The amount of soil which can be suspended by wind depends on: 1) the particle size distribution, 2) wind velocity at the soil surface, 3) the roughness of the surface, 4) the relative fractions of erodible (<1,000 μm diameter) and nonerodible (>1,000 μm diameter) material (Gillette et al., 1980), and 5) the cohesion of the soil particles with one another (Chepil and Woodruff, 1963; Gillette and Hanson, 1989). In general, the stronger the wind, the greater is the horizontal shearing force exerted by the wind on the surface. This shearing force, if it is of sufficient magnitude, will entrain the loose erodible material and eject fine particles into the atmosphere. The magnitude of the shearing stress will be dependent on the rate of change of wind speed with height and the type of roughness present on the surface.

The presence of nonerodible roughness elements strongly attenuates wind erosion of soil. The roughness elements can be of several kinds including large aggregates of pebble size, bushes, shrubs, or trees. The basic suppression mechanism is the same regardless of the type of element present. The roughness elements decrease the wind stress on the erodible surface by absorbing a significant fraction of the downward momentum flux from the air flow above (Raupach *et al.*, 1993). Momentum partitioning effects should be considered when estimating wind erosion from surfaces covered by large roughness elements, such as low vegetation (≤ 1 m). Two issues remain unresolved (Raupach, 1992). First, given a surface with specified roughness element height, width, spacing, areal extent and porosity, what is the total drag on the surface? Second, what is the partition of drag between the roughness elements and the underlying surface? Further research is needed with respect to calculating drag coefficients of porous, three-dimensional objects in isolation as well as in arrays. Better estimation of the momentum loss to the large roughness elements will allow for more precise estimation of the shear stress that acts on the intervening surface where resuspension occurs.

9.1.5 Dust Suspension by Vehicles

Dust on paved roads, unpaved roads, parking lots, and construction sites is suspended by natural winds and vehicular movement. Vehicular traffic in these areas adds to particle resuspension because tire contact creates a shearing force with the road that lifts particles into the air (Nicholson *et al.*, 1989). Moving vehicles also create turbulent wakes which act much like natural winds to raise particles.

Dust on paved roads must be continually replenished; reducing the deposition of fresh dust onto these surfaces is a viable method for reducing their PM_{10} emissions. Dust loadings on a paved road surface build up by being tracked out from unpaved areas such as construction sites, unpaved roads, parking lots, and shoulders; by spills from trucks carrying dirt and other particulate materials; by transport of dirt collected on vehicle undercarriages; by wear of vehicle components such as tires, brakes, clutches, and exhaust system components; by wear of the pavement surface; by deposition of suspended particles from many emissions sources; and by water and wind erosion from adjacent areas (Chow *et al.*, 1990; Chow and Watson, 1992). The relative contribution from each of these sources is unknown. Axetell and Zell (1977) estimated typical deposition rates of 67.8 kg/km of curb for a 24-hour period for particles of all sizes from the following sources: 1) 42% from mud and dirt carryout; 2) 17% from litter; 3) 8% from biological debris; 4) 8% from ice control compounds (in areas with cold winters); 5) 8% from erosion of shoulders and adjacent areas; 6) 7% from motor vehicles; 7) 4% from atmospheric dustfall; 8) 4% from pavement wear; and 9) less than 1% from spills. These proportions are highly uncertain for the PM_{10} fraction because they apply to the TSP size fraction and because these investigators did not consider all of the sources cited above. Axetell and Zell (1977) cite these fractions without describing

the methodology used to estimate them; their paper constitutes the only publication that provides quantitative apportionments of paved road dust loadings to their sources.

Unpaved roads and other unpaved areas with vehicular activity are unlimited reservoirs of dust loading when vehicles are moving. These surfaces are always being disturbed, and wind erosion seldom has an opportunity to deflate the fine surface sediment and increase the surface roughness sufficiently to attenuate particle suspension. The grinding of particles by tires against the road surface shifts the size distribution toward smaller particles, especially those in the PM_{10} fraction. Pinnick *et al.* (1985) found the distribution of particle sizes within a vehicle-created dust plume was bimodal, with a coarse mode of approximately 50 μm and a fine mode of 2.5 μm. Patterson and Gillette (1977) reported a similar distribution for naturally generated dust plumes; however, there were proportionately fewer large particles in the natural plume dust in comparison to the vehicular case. The bimodal distribution was attributed to grinding processes caused by tires for the vehicle dust (Pinnick *et al.*, 1985) and to a sandblasting process for wind-generated dust (Patterson and Gillette, 1977). According to Nicholson *et al.* (1989), the size of the particles and the amount of dust resuspended by vehicles are dependent on the velocity of the vehicle. Nicholson *et al.* (1989) found that larger particles were more readily suspended than smaller ones and wind speeds of 24 to 32 km/h were required to suspend particles between 4.2 and 9.5 μm in diameter.

Nicholson and Branson (1990) report that a minimum velocity of 22 km/h is necessary to suspend dust from a paved road surface. It is more likely that the velocities required to entrain particles on unpaved roads is significantly less than for paved roads. An important process occurring on unpaved roads is the activation of larger particle sizes by the tires. These particles are effective in mobilizing dust particles upon impact with the surface and mirror the effect of saltating particles in a natural erosion system (Gillette, 1977; Gomes *et al.*, 1990). These bouncing particles impact on the surface and eject a range of particle sizes into the air stream, and may also shed micron- or sub-micron-sized secondary particles on impact with the surface or another object (Rosinski *et al.*, 1976; Gillette, 1977). The physics of saltation for sand-sized particles in natural erosion systems is reasonably well understood (Anderson *et al.* 1990). However, the ejection of dust-sized particles by the saltation process is still poorly understood (John *et al.*, 1991).

Other than the information inferred from the chemical composition of road dust and from multivariate relationships between downwind concentrations and vehicle variables, there is no detailed physical understanding of the effects of tire contact with particles and their suspension into the atmosphere. This knowledge is essential to understanding how these particles are suspended and how far they are transported.

Several other vehicle-related factors have been identified as contributing to the amount of particulates that are ejected from road surfaces. Dyck and Stukel (1976) suggested that vehicle weight and road type influenced dust emissions. Mollinger *et al.* (1993) found that the shape of vehicles can have a large impact on the amount of resuspension; a cylinder, an elliptical cylinder, and a rectangular solid were mounted on a pendulum which swung back and forth over dust-covered test areas. After twenty passes by the cylinder and elliptical cylinder, 65% and 45% of the dust remained in the test area, respectively. After twenty passes by the rectangular solid traveling at the same velocity, less than 20% of the dust remained. Vehicle shape appears to affect the turbulent structure of the wake shed by the vehicle, creating conditions which favor or reduce the entrainment of dust (Mollinger *et al.*, 1993). This study would suggest that it is possible to reduce suspension from road surfaces by altering the shape of vehicles.

9.2 Fugitive Dust Demonstration Studies

Various mitigation methods have been developed to control emissions from fugitive dust sources. The most common control measure is the application of suppressant onto a dust-emitting surface that effectively binds the particles within the sediment matrix. This can be accomplished either by spraying water on the dust-emitting surface or by adding chemicals which serve as an adhesive agent to bond the surface particles together. Other control measures involve the removal of loose surface material with various types of street sweepers. Soil resuspension by wind erosion can be minimized by altering the surface to decrease its erosion potential, or by adding vegetative covers to protect the susceptible soils. A viable option to reduce fugitive emissions from anthropogenic activities such as vehicles moving over unpaved roads and construction sites is to reduce the activity levels. The following subsections summarize the effectiveness of five types of fugitive dust control measures applied in past experiments.

9.2.1 Surface Watering

Surface watering is often applied on disturbed land such as construction sites or unpaved surfaces to reduce particle resuspension by vehicles. Moisture content on unpaved roads can: 1) reduce the strength of the road bed, 2) enhance the road bed's ability to deform under vehicle loading, and 3) reduce the chance of brittle failure which produces small particles that may be further crushed by tires (Rosbury and Zimmer, 1983). Flocchini *et al.* (1994) found that the addition of sufficient water to increase the surface moisture content from 0.56% to 2% can achieve greater than 86% reduction in PM_{10} emissions. Kinsey and Cowherd (1992) found immediate dust reductions at construction sites as a result of surface watering; however, the effectiveness of this measure did not increase as more water was applied to the site. Ultimately, control efficiency is limited by the evaporation potential. Low humidity levels will hasten effectiveness reduction through moisture loss, and grading

operations are continually exposing dry earth and burying the moistened topsoil. Figure 9-1 shows the effects of moisture content on downwind TSP concentrations measured near an active construction site, including heavy equipment moving at a rate of one vehicle pass per minute.

Washing vehicles as they depart from work areas can minimize dust track-out and carry-out. Track-out refers to the sediment that is attached to vehicle tires and subsequently transferred to the road surface. Carry-out is the sediment attached to the vehicle that may eventually fall off and become resuspended by other vehicles (Axetell and Zell, 1977; Brookman, 1983). Axetell and Zell (1977) found that TSP concentrations ($\sim$84 $\mu g/m^3$) were increased by 40 to 60 $\mu g/m^3$ due to uncontrolled mud track-out. Immediate cleanup with shovel and broom reduced TSP by 10 to 20 $\mu g/m^3$, and daily cleanup reduced TSP by about 5 to 10 $\mu g/m^3$. These values correspond to control efficiencies of about 30% for immediate cleanup and 15% for daily cleanup. Besides wheel washing, other cleaning procedures include street sweeping, manual broom and shovel cleanup, and water flushing to remove mud and dirt from paved surfaces after it has been tracked out. Covering haul trucks while in transit eliminates spillage and wind-generated soil loss.

9.2.2 Chemical Suppression

The application of chemical suppressants on unpaved surfaces can reduce fugitive dust emissions. Table 9-1 enumerates the commercially-available dust suppressants. These products are classified into seven categories according to their chemical composition and the suppressant mechanism they employ:

- **Salts**: These are hygroscopic compounds such as magnesium chloride or calcium chloride. They adsorb water as ambient relative humidity exceeds 50%. Water improves the adherence of the soil particles to each other, thereby reducing dust emissions. Since salts are water soluble, precipitation tends to wash them away.

- **Resin or petroleum emulsions**: These are non-water-soluble organic carbon compounds which are "emulsified" or suspended in water. When these emulsions are sprayed onto soil, they stick the soil particles together, and eventually harden to form a solid mass. Several emulsion products are based on tree resin, petroleum, or asphalt compounds.

- **Polymers**: These are long-chain molecular compounds which act as adhesives to bond soil particles together. In theory, polymers may be able to stick to more particles than ordinary resins, or bridge larger particle-to-particle gaps.
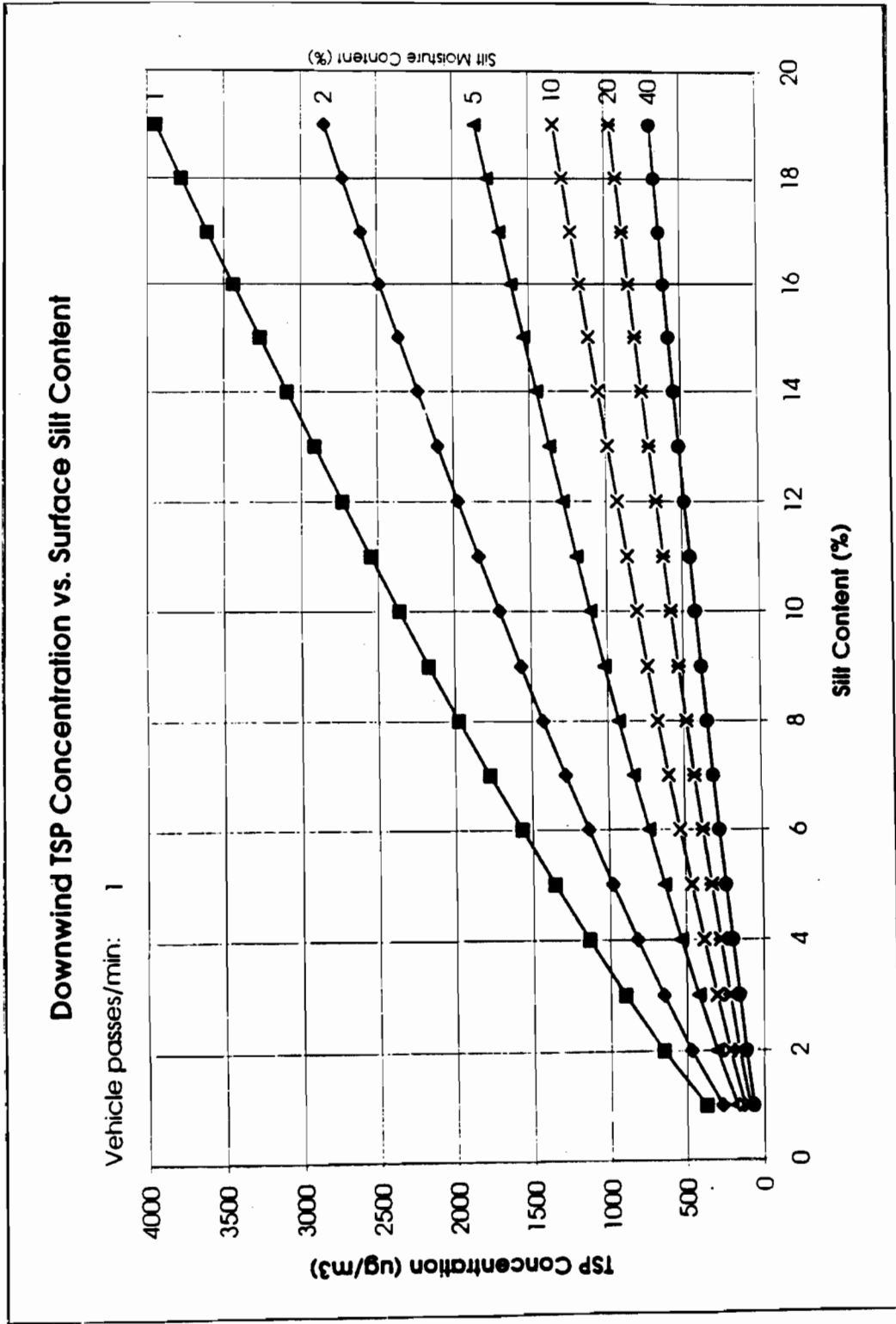
Figure 9-1   TSP emissions versus silt content for different moisture levels (Kinsey and Englehart, 1984). Applies to concentrations 50 m downwind of the emission point for TSP.

Table 9-1
Suppressants and Vendors

Product Name and Active Ingredient | Vendor Information

I. SALTS

Calcium Chloride

Lee Chemical, Inc.
21250 Box Springs Road
Moreno Valley, CA 92387
Attn: Bud Bardsley
(909) 369-5292

Calcium Chloride

Hill Brothers Chemical Company
1675 N. Main Street
Orange, CA 92667
Attn: Alfred McCarthy
(714) 998-8800

Magnesium Chloride

Western Spreading and Transportation, Inc.
641 Rock Springs Road
Escondido, CA 92025
Attn: Nick Izzi
(909) 784-7411

Magnesium Chloride

Jim Good Marketing
P.O. Box 717
Shafter, CA 93263
Attn: Jim Good
(805) 746-3783

Magnesium Chloride

Chemical Distributors, Inc.
201 Bryce Court
Henderson, NV 89105
Attn: Carrie Burgess
(702) 565-4904

Table 9-1 (continued)
Suppressants and Vendors

Product Name and Active Ingredient	Vendor Information

I. SALTS (continued)

Magnesium Chloride	Soil Stabilization Products Co. P.O. Box 2779 Merced, CA 95344 Attn: Glen Gates or Marsh Pitman (800) 523-9992
Magnesium Chloride	Dustpro, Inc. 2432 W. Peoria Ave. Suite #1160 Phoenix, AZ 85029 Attn: Greg Frey (602) 944-8411
Magnesium Chloride ("Dust-Off")	South Western Sealcoating, Inc. 23644 Adams Ave. Murietta, CA 92562 (909) 677-6228
Magnesium Chloride ("Dust-Off")	California-Fresno Oil Company PO Box 527 Fresno, CA 93709 (209) 486-0220
"Brine"	Leslie Salt Co. 7200 Central Ave. Newark, CA 94560 (415) 790-8169

II. ASPHALT/PETROLEUM EMULSIONS

Coherex (Petroleum resin emulsion)	WITCO, Golden Bear Division P.O. Box 456 Chandler, AZ 85244-0161 Attn: Roy McNeal (602) 963-2267

Table 9-1 (**continued**)
Suppressants and Vendors

Product Name and Active Ingredient   Vendor Information

Retain (asphalt emulsion)   Diversey Corp
Attn: Linda Coffee or Randy Bryan
(818) 961-6305

II. ASPHALT/PETROLEUM EMULSIONS (continued)

Asphotac (asphalt emulsion)   Pragma, Inc.
P.O. Box 1658
Sutter Creek, CA 95685
Attn: Ray Hunter
(209) 267-5072

Dust Oil Emulsion (asphalt emulsion)   Morgan Emultech, Inc.
7200 Pit Road
P.O. Box 1500
Redding, CA 96099
(916) 241-1364

Pennzsuppress D   Pennzoil Products Company
12070 Telegraph Road
Suite #324
Santa Fe Springs, CA 90670
Attn: Brad Welshans
(310) 906-4300

FlowPro 1505 (petroleum resin emulsion)   Betz Water Management Group
Big Valley District Office
4201 Ardmore Way ,#7
Bakersfield, CA 93309
(805) 835-9194

III. OTHER EMULSIONS

Table 9-1 (continued)
Suppressants and Vendors

Product Name and Active Ingredient   Vendor Information

Road Oyl (tree resin emulsion)   Soil Stabilization Products Co.
                                          P.O. Box 2779
                                          Merced, CA 95344
                                          Attn: Glen Gates or Marsh Pitman
                                          (800) 523-9992

Pineseal (tall oil pitch, tall oil rosin, and   Western Emulsions Inc.
lignin)   Dust Control Division
                                          22155 Big Timer Road
                                          Moreno Valley, CA 92557
                                          Attn: Nicolas J. Izzi
                                          (909) 784-7411

III. OTHER EMULSIONS (continued)

Enduraseal 100 and 200 (organic, water-   Cascadia Technologies Ltd.
based emulsions)   602-626 West Pander St.
                                          Vancouver, B.C., Canada V6B1V9
                                          Attn: Glenn Coward
                                          (800) 665-2994

                                          Environmental Products and Applications
                                          Co.
                                          15017 Notnil Way
                                          Lake Elsinore, CA 92530
                                          Attn: John Vermillion
                                          (909) 674-9174

Entac (organic emulsion)   Diversified Services, Inc.
                                          P.O. Box 337
                                          Elizabethton, TN 37644
                                          Attn: John McDonnell
                                          (615) 542-9100

IV. LIGNIN SULFONATE

Table 9-1 (continued)
Suppressants and Vendors

Product Name and Active Ingredient	Vendor Information
Lignin Sulfonate	RBJ Transport, Inc 1735 N. Ashby Road Merced, CA Attn: Tim Prothro (209) 722-2731
Lignin Sulfonate	Midwest Industrial Supply, Inc. P.O. Box 8431 Canton, OH 44711 Attn: Frank Elswick (805) 937-7157
Lignin Sulfonate ("Calbinder")	California-Fresno Oil Company PO Box 527 Fresno, CA 93709 (209) 486-0220
DUSTAC	Georgia Pacific Monrovia, CA (800) 955-5498

V. POLYMERS

Coherex PM (petroleum emulsion with polymer)	WITCO, Golden Bear Division P.O. Box 456 Chandler, AZ 85244-0161 Attn: Roy McNeal (602) 963-2267 Reed and Graham, Inc. 8280 14th Ave. Sacramento, CA 95826 Attn: Steve Aguirre (916) 454-2560

Table 9-1 (continued)
Suppressants and Vendors

Product Name and Active Ingredient	Vendor Information
Soil Sement (polymer emulsion)	Midwest Industrial Supply, Inc. P.O. Box 8431 Canton, OH 44711 Attn: Frank Elswick (805) 937-7157
Soil Master WR (co-polymer with "Tripolycate")	Environmental Soil Systems Inc. 13234 Whistler Ave. Granada Hills, CA 91344 Attn: Rick Granard (800) 368-4115
DC-1000	Native Soil Technology, Inc. P.O. Box 502 Danville, CA 94526 Attn: Bob Crandall (510) 837-5362
DSS-40 (acrylic co-polymer)	S&S Seeds P.O. Box 1275 Carpenteria, CA 93013 Attn: Victor Schaff (805) 684-0436
DSS-40 (acrylic co-polymer)	Karleskint-Crum, Inc. PO Box 5358 San Luis Obispo, CA 93403 (805) 543-3304

V. POLYMERS (continued)

DSS-40 (acrylic co-polymer)	J&M Land Restoration, Inc. 1640 James Rd. Bakersfield, CA 93308 (805) 872-7039

Table 9-1 (continued)
Suppressants and Vendors

Product Name and Active Ingredient	Vendor Information
Eco-Polymer	Eco-Polymers, Inc. P.O. Box 4860 Cerritos, CA 90703-4860 Attn: Ron Reed (310) 407-3090
Marloc (co-polymer)	Reclamare Company 20727 - 7th Avenue S. Seattle, WA 98198 Attn: Edward R. Johston (206) 824-2385
Soil Seal	Soil Seal Corporation 3015 Supply Avenue Los Angeles, CA 90040 (213) 727-0654
Terrafirma	AET Group 655 Lewelling Blvd., Suite 315 San Leandro, CA 94579 Attn: Regan Jones (209) 836-4884
ECO-110 and C-50	Dynaguard, Inc. 1034 N. Lemon Street Orange, CA 92667 Attn: Craig Hoad (714) 771-7411

Table 9-1 (continued)
Suppressants and Vendors

Product Name and Active Ingredient   Vendor Information

V. POLYMERS (continued)

Blend R40 Series (polymer emulsions)   Rohm and Haas Company
                                            Toxicology Department
                                            727 Norristown Road
                                            P.O. Box 904
                                            Spring House, PA 19477-0904
                                            Attn: J.D. Hamilton
                                            (215) 641-7000

Polymers/Enzymes   Boston/ASTC
                                            521 Westminster Ave.
                                            Newport Beach, CA 92663
                                            (714) 646-1207

VI. FIBERS AND MULCHES

Agri-Fiber   Precision Hydroseeding Company
                                            P.O. Box 12336
                                            Palm Desert, CA 92255
                                            Attn: Jim Sullivan
                                            (619) 360-2851

A/F 2000   American Fiber Company
                                            10820 Beverly Blvd., Suite 322
                                            Whittier, CA 90601
                                            (310) 693-4072

Fiberwood (hydroseeding mulch)   Fiberwood
                                            5854 88th Street
                                            Sacramento, CA 95828
                                            Attn: Rob Rischback
                                            (800) 655-9754

Fibercraft (hydromulch cellolose fiber)   Dynamis, Inc.
                                            P.O. Box 397
                                            Sanger, CA 93657
                                            (209) 875-0800

Table 9-1 (continued)
Suppressants and Vendors

Product Name and Active Ingredient	Vendor Information

VI. FIBERS AND MULCHES (continued)

Stabilizer (organic binder)	Stabilizer, Inc. 4832 East Indian School Phoenix, AZ 85018 Attn: Tim Myers (602) 952-8009
Dewatered Residual Wood Fiber	C.E.T.I. 15568 Slover Ave. Fontana, CA 92334 Attn: Steve McGuire (909) 428-6861
Dewatered Residual Wood Fiber	Envirosorb 1815 Wright Ave. La Verne, CA 91750 Attn: Steve McGuire (909) 392-5878
Soil Guard (bonded fiber matrix)	S&S Seeds P.O. Box 1275 Carpenteria, CA 93013 Attn: Victor Schaff (805) 684-0436
Excel-Fibermulch II (Aspen wood mulch)	American Excelsior Company 8320 Canford Street Pico Rivera, CA 90660-3702 Attn: Larry Halweg (310) 949-2461
Cellulose Fiber (Ecology Controls "M-Binder")	Sanders Hydroseeding, Inc. 1708 South Santa Fe Santa Ana, CA 92705 (714) 973-TURF

Table 9-1 (continued)
Suppressants and Vendors

Product Name and Active Ingredient   Vendor Information

Cellulose Fiber (Ecology Controls "M-Binder")

S&S Seeds
P.O. Box 1275
Carpenteria, CA 93013
Attn: Victor Schaff
(805) 684-0436

VI. FIBERS AND MULCHES (continued)

Hydrophilic colloid derived from seed husks ("Sentinel")

Albright Seed Company
487 Dawson Drive Bay 55
Camarillo, CA 93012
(805) 484-0551

Ecotak-OP and Ecotak-SAT

Elloitt Landscaping
68-315 Durango Road
Cathedral City, CA 92234
Attn: Mukul Joisher
(619) 320-0176

H. UNCLASSIFIED

AGRI-LOCK and DUST-LOCK (synthetic resin and organic compound)

SWIFT Adhesives
2400 Ellis Road
Durham, NC 27703-5543
Attn: Wes McCoy
(800) 213-4804

Calcium sulfate hemihydrate (plaster) and cellulose or wood fiber mixture ("Airtrol Plaster")

United States Gypsum Company
Industrial Gypsum Division
PO Box 803871
Chicago, IL 60680-3871

P.E.P. (liquid asphalt)

Environmental Products & Applications
15017 Notnil Way
Lake Elsinore, CA 92530
Attn: John Vermillion
(909) 674-9174

Table 9-1 (continued)
Suppressants and Vendors

<u>Product Name and Active Ingredient</u>   <u>Vendor Information</u>

Product Name and Active Ingredient	Vendor Information
EnviroCycle (solid material: hydrocarbon-soil mix)	EnviroCycle, Inc. 21992 Hiway 33 McKittrick, CA 93251 Attn: John Webb, President (800) 324-4484
Dust Buster Systems (chemical suppressants and application equipment)	Martin Marietta Magnesia Specialties, Inc. 9308 Nickam Court Bakersfield, CA 93311 Attn: Robert Samson Jr. (805) 663-0625

H. UNCLASSIFIED (continued)

Dust Sorb 1118 (acrylic resin)	Aqua Chem Ltd. P.O. Box 1138 Bakersfield, CA 93389 (805) 323-8308
Biocatalyst ("EMC Squared")	Ophir Oil Company PO Box 898 Newcastle, CA 95658 (916) 885-0491
DC 300 (non-ionic surfactant)	Compaction Compounds, Inc. 101 First Street, Suite 402 Los Altos, CA 94022 Attn: Mary Anne Rosenthal (415) 948-5900
Organic Soil Stabilizer (soil additive)	Desert Rock Supply P.O. Box 924 La Quinta, CA 92253 Attn: Jim Marquardt (619) 360-1345

Table 9-1 (continued)
Suppressants and Vendors

Product Name and Active Ingredient   Vendor Information

Lime mixture ("POZ-O-CAP")

Metamorphosis Hydroseeding, Inc.
1022A San Andreas Rd.
La Selva, CA 95076
(800) 99-4SEED

Sandcastles Dust Control Mix

Sandcastle Hydroseeding
42529 8th St. East
Lancaster, CA 93535
Attn: Betty McWilliams
(805) 723-0515

Endosperm product ("Hydroshield")

Chem Shield
1475 E. Greg Street
Sparks, NV 89434
Attn: Richard L. Maile
(702) 323-4540

H. UNCLASSIFIED (continued)

Sodium Silicate

PQ Corporation
ICD Sales Department
8401 Quartz Ave.
South Gate, CA 90280-2589
(213) 560-4891

Raybinder

ITT Rayonier
P.O. Box C-68967, Suite 900
Seattle, WA 98188
(800) 228-0604

- **Surfactants**: These are chemicals which reduce water surface tension and allow available moisture to more effectively wet the particles and aggregates in the surface layer.

- **Bitumens**: These are materials such as asphalt or road oil which act as adhesives to bond soil particles together.

- **Adhesives**: These are a paper mill byproducts, such as lignin sulfonate (a syrupy wood product), which form a sticky but water-soluble layer on unpaved surfaces.

- **Solid Materials**: These are petroleum industry byproducts made by mixing recycled materials with soil.

Most suppressants require repeated application at frequencies on the order of weeks or months. The effectiveness of chemical suppressants depends on road surface conditions, soil composition, application intensity, traffic volume, vehicle weight, and environmental factors such as precipitation and temperature. Prior to suppressant application, the road surface often needs to be gridded or wetted. Most products can be dispensed as liquids by a truck equipped with a tank and spray bar. The spraying process injects the suppressant into the road material. Solid materials can be spread and mixed into the soil or road bed with a grader.

Several studies have examined the effectiveness of different chemical suppressants on various types of unpaved roads. The control efficiency percentage is used as a measure of suppressant effectiveness between untreated and treated surfaces. Rosbury and Zimmer (1983) found considerable variability in dust emission rates for the untreated and chemical-suppressant-treated surfaces. Much of this variation was attributed to the effects of ambient meteorological conditions (especially precipitation), the types of vehicles traveling on the road, and the initial road conditions. Comparisons of chemical suppressant control efficiencies and costs/benefits are summarized in Tables 9-2 and 9-3, respectively. Control efficiency varies from 7% to 54% for well-mixed suppressant applications, from insignificant to 80% for topical suppressant applications. Suppressant cost varied from $3,000 to $11,000 per mile of application per year, assuming four applications per year. To achieve 50% control efficiency, surface watering is also required on a monthly basis, at an additional cost of $1,000 to $3,000 per mile of application per week.

Muleski and Cowherd (1987) evaluated the effectiveness of chemical suppressants on unpaved roads used by the iron and steel industry. Particles in three size fractions (<15 μm, <10 μm, and <2.5 μm) were acquired at heights up to 6 m above the surface to assess the suppressant efficiencies. Characteristics of unpaved road surfaces (such as percent silt and moisture content and the amount of loose surface material [kg/m^2]) were measured. Muleski

Table 9-2
Comparison of Chemical Suppressant Efficiencies[a]

				Calculated Average Control Efficiency						
				Mine 2			Mine 3			
				Application Method			Application Method			
Control	Particle Size (μm)	Height (m)	Isokinetic Flow	Well-Mixed	Topical	Time (weeks)	Well-Mixed	Topical	Time (Weeks)
Salt	30	1-9	yes	44%	58%	1-4	10%	21%	2-3
	15	1.5	no	52%	56%		7%	10%	
	2.5	1-9	yes	43%	41%		24%	8%	
	3.0	1.0	no	44%	46%		6%	0%	
Surfactant	30	1-9	yes		33%	1-5		19%	1-2
	15	1.5	no		19%			25%	
	2.5	1-9	yes		25%			33%	
	3.0	1.0	no		46%			28%	
Adhesive	30	1-9	yes	54%	35%	1-4	38%		1-3
	15	1.5	no	47%	29%		49%		
	2.5	1-9	yes	37%	30%		46%		
	3.0	1.0	no	36%	48%		27%		
Bitumen	30	1-9	yes	20%	24%	1-4	44%	56%	
	15	1.5	no	22%	36%		55%	80%	
	2.5	1-9	yes	26%	28%		33%	73%	
	3.0	1.0	no	54%	51%		50%		

[a] All typical applications.

Table 9-3
Comparison of Cost Effectiveness[a] of Chemical Suppressant Efficiencies[b]

| Control Measure | Cost of Suppressant Application per Mile[c] | | Cost of Grading and Watering per Week | | | Total Cost of Suppressant per Week per Mile | |
| | Location | | | | | | |
	Southern Illinois	Rock Spring	Grading	Water	Applications Required to Achieve 50% Control Efficiency[d]	Southern Illinois	Rock Spring
Salt							
Well-Mixed	$7,240	$11,263	$0	$143	once every 4 weeks	$1,953	$2,959
Topical	$3,260	$5,058	$0	$143	once every 4 weeks	$958	$1,408
Adhesive							
Well-Mixed	$4,813	$7,644	$0	$143	once every 4 weeks	$1,346	$2,054
Water			$375	$1,710	120 times per week	$2,085	$2,085

[a] Rosbury and Zimmer (1983).

[b] Achieve 50% control efficiency.

[c] Includes surface preparation, material cost, and application. Material cost includes the delivery cost to Southern Illinois and Rock Springs. Material cost for Liquidow is $0.36/gallon in the west (Rock Spring). Material cost for Flambinder is $0.33/gallon in the east (Southern Illinois) and $0.47/gallon in the west (Rock Spring). Assumes application to 15-m-wide and 18-m-wide sections of road in Southern Illinois and Rock Spring, respectively.

[d] Required application intervals could not be estimated for adhesive-topical, surfactant, or bitumens. Comparative costs could not be calculated.

and Cowherd (1987) report unpaved road emission rates similar to those found by Rosbury and Zimmer (1983). Average control efficiencies of approximately 50% or more were found within the first 30 days of suppressant application. In addition, the study reports no differences in suppressant control efficiencies 30 days after suppressant application.

Grau (1993) conducted laboratory tests on suppressant performance. Suppressant-treated soil specimens were prepared under controlled laboratory conditions to determine their performance when subjected to simulated field conditions. The screening tests included repeated air impingement tests (one-minute blasts from 80 km/h and 160 km/h air jets at 20° from the horizontal) with simulated rainfall or jet fuel spills. Forty-nine suppressants were tested, and suppressant effectiveness was determined based on visual observations. As a result, eleven suppressants were accepted and subjected to field tests.

Flocchini *et al.* (1994) estimated PM_{10} fugitive dust emissions from agricultural unpaved roads and evaluated the effectiveness of chemical suppressants in the San Joaquin Valley, CA. The relative effectiveness of control measures such as surface watering, gravel cover, lignin sulfonate, magnesium chloride, oiling, and nonhazardous crude oil were assessed. PM_{10} and size-segregated particle mass concentrations were measured at upwind and downwind locations. Vertical concentration gradients for particles above and below $PM_{2.5}$ were acquired (Cahill *et al.*, 1990). Mass concentrations at 10 m downwind and 3.3 m in height were corrected for background concentrations to assess the effect of vehicles traveling on the unpaved roads. Surface characteristics, soil type, surface loading per unit area, moisture content, and silt content (< 75 μm particle diameter) were measured. Surface samples were resuspended in the laboratory (Chow *et al.*, 1994a) to determine their relative potentials for PM_{10} emissions.

A summary of suppressant control efficiencies reported by Flocchini *et al.* (1994) is presented in Table 9-4. Percent of PM_{10} emissions varied from 98% to ~99% as different types of chemical suppressants were applied. Surface watering and road oiling reduced PM_{10} emissions by $87 \pm 6\%$ and $59 \pm 12\%$, respectively. Reducing vehicle travel speeds on unpaved roads from 40 km/h to 16 to 24 km/h can effectively reduce PM_{10} emissions by $58 \pm 3\%$ and $42 \pm 35\%$, respectively.

The effectiveness of chemical suppressants on reducing dust emissions has not been evaluated over a long time period. Watson *et al.* (1996) undertook a year-long study to assess changes in suppressant effectiveness in reducing PM_{10} emissions from unpaved public roads in the San Joaquin Valley, CA. Vehicle-induced vertical PM_{10} concentration profiles were measured. Three different types of chemical suppressants were applied on the unpaved roads: an acrylic co-polymer, a bitumen with co-polymer additive, and a "bio-catalyst". Watson *et al.* (1996) found that within a week of application the bitumen and acrylic co-polymer showed over 95% emission reduction as compared to the untreated surface. The

Table 9-4
Summary of the Effectiveness of Different Control Measures
Applied on Unpaved Roads[a]

Effectiveness Rank	Type of Treatment or Control	Percent of PM_{10} Emission Reduction
1	Recycled Oil Mix	~99%
2	Lignin Sulfonate	99%
3	Magnesium Chloride	98%
4	Water	$87 \pm 6\%$
5	Oiled Road	$59 \pm 12\%$
6	Speed Reduction (from 40 to 16 km/h)	$58 \pm 3\%$
7	Speed Reduction (from 40 to 24 km/h)	$42 \pm 35\%$
None	Gravel	Emissions from the gravel test section appeared to exceed those of the untreated section.

[a] Flocchini *et al.* (1994).

"bio-catalyst" had an effectiveness of only 39%. After three months, the efficiency of the bitumen and bio-catalyst had decreased by 20% and 30%, respectively, while the efficiency of the acrylic co-polymer remained constant. After 11 months, the control effectiveness had been reduced to 53% for the bitumen, 85% for the acrylic co-polymer and 0% for the "bio-catalyst" (Watson et al., 1996).

9.2.3 Chemical Suppression

Watson et al. (1996) also examined the relationships between surface characteristics and PM_{10} emissions on unpaved roads. Percent silt content (particles <75 μm) and silt loading (kg/m^2) are determined using sweep and vacuum sampling methods. A relatively good relationship between PM_{10} emissions and surface silt content was found. Stronger relationships were found between PM_{10} emissions and actual silt loading (kg/m^2). As silt content is subdivided into three size fractions (<75 to 38 μm, <38 to 25 μm, and <25 μm), the relationships between particle size and PM_{10} emissions became indistinguishable. This may be primarily due to the methodology that was used to size-segregate the silt fractions. A hard-sieving technique was employed, which mechanically shook the sediment nito a series of nested sieves. The efficiency of this process reduced rapidly as particle size decreased. Particles less than 38 μm tend to agglomerate to each other and to larger particles because of van der Walls forces and electrostatic attraction. The electrostatic charges would be increased further by the vibrating process during mechanical sieving.

9.2.4 Street Sweeping

Mechanical broom and vacuum street sweeping have been applied in urban areas to remove street debris, litter, and dirt rather. Water droplets are often sprayed onto the road surface prior to sweeping to minimize dust resuspension induced by the sweeper. Sweeping schedules vary from weekly to monthly. Sweeping for aesthetic purposes is confined to the curb lanes in commercial and/or residential areas. Major highways and freeways are rarely swept.

Mechanical broom sweepers use large rotating brooms to lift the material from the street onto a conveyer belt. The conveyer discharges street debris into a collection hopper. Circular gutter brooms direct the debris into the path of the rotating broom. Mechanical broom sweeping has been discounted as a means of air pollution control on paved urban streets (Axetell and Zell, 1977; U.S. EPA, 1982; Gatz et al., 1983). Chow et al. (1990) found that the brushes resuspend as many small particles as they remove.

Commercially-available vacuum sweepers use pure vacuum suction, regenerative-air suction, or blow-air/suction recirculation (Calvert et al., 1984; Duncan et al., 1985; Cowherd and Kinsey, 1986; Cowherd et al., 1988; Loete, 1989). Vacuum sweepers use a gutter broom

to loosen dirt and debris from the road surface and direct this material to a vacuum nozzle which sucks it into a hopper. The hopper usually consists of a chamber into which particles are collected by gravitational settling. The air passing through this chamber can be exhausted directly to the environment, through a bag-filter or precipitator, or to the collection nozzle for recirculation. No quantitative measurements of PM_{10} emissions from sweeper exhaust have been reported.

Pure vacuum sweepers create a strong vacuum within the pickup head which draws air from outside the head, through a duct, and into a hopper. The air movement across the road surface removes particles from the pavement and entrains them in the air flow. The vacuumed air is exhausted to ambient air after a brief residence time in the hopper. This residence time is usually insufficient to allow gravitational settling of particles in the PM_{10} size fraction.

Regenerative-air vacuum sweepers direct the exhaust air back to one end of the pickup head at velocities between 50 and 200 m/s. This blast air is directed perpendicular to the pavement where it is intended to dislodge dirt particles. The blast air and its entrained particles move across the pickup head to a suction nozzle which transports the debris to the collection hopper. The pickup head must seal with the pavement using a flexible rubber curtain to prevent blast air from escaping the collection nozzle and to maintain a negative air pressure within the nozzle.

The blow-air/suction recirculation sweeper directs a portion of the exhaust air to a blast nozzle located immediately behind the pickup head. This blast air is directed at an angle to the pavement to blow particles from the road surface into the airstream caused by suction through the head. The suction flow rate exceeds the blast flow rate so that ambient air is always being drawn into the pickup head, thereby minimizing the escape of recirculated particles to the air. The nonrecirculated portion of the exhaust air is vented into a separated settling chamber before it escapes to ambient air.

Water flushing uses pressurized sprays from a water truck to dislodge road dust and transport it to the curb, where much of the particulate is washed into the drain system. A combination of water flushing followed immediately by broom sweeping has been widely used as a means of street cleaning.

Water flushing generally results in more consistent and higher efficiencies than the sweeping methods, with source measurements of 30% to 80% control efficiency, and receptor measurements of 0 to 18 $\mu g/m^3$ reduction in TSP (Axetell and Zell, 1977; Cowherd, 1982; U.S. EPA, 1982; Cuscino et al., 1983a). The source measurements are generally taken shortly after flushing, however, or no time frame is specified, or essential information such as particle size and measurement method is missing.

Flushing can be expected to reduce particle resuspension dramatically while the road surface is still wet, but its effect on average emissions during a typical cleaning cycle cannot be ascertained from the data reported. Results of the receptor-oriented studies again are mixed and are based on TSP measurements. Flushing is generally considered to be more effective in reducing fine particle loadings on the street surface than broom or vacuum sweeping, although there are few data to support this, and the results of studies based on TSP measurements should not be considered applicable to PM_{10}.

The combination of water flushing and broom sweeping has the highest reported control efficiencies, from 47% to 90% for PM_{15} particles and 48% to 83% for $PM_{2.5}$ particles (Cowherd, 1982; Cuscino et al., 1983a, 1983b). However, the time frame of these measurements is either not specified or very short – less than three hours, when the road surface may still be wet. The large changes in control efficiency over a short time period, e.g., 30% change in control efficiency of $PM_{2.5}$ particles over a 12-minute period, suggest that measurement uncertainty is high relative to control effectiveness. Again, all measurements were made on industrial paved roads; applicability to public roads has not been demonstrated.

Seton et al. (1983a; 1983b) describe a six-month street-sweeping study conducted in Portland, OR, in 1981. Geological source contributions to chemically-speciated TSP, PM_{15}, and $PM_{2.5}$ concentrations at a nearby sampling site were compared for sweeping and nonsweeping periods. No reductions in geological source contributions were detected with daily vacuum sweeping of the curb lane of industrial-area streets.

Hewitt (1981) reported a four-year study conducted in Bangor, ME, where uncontrolled street-sweeping data over two-year periods were compared with the following two-year's routine street-sweeping data. Nearly 800 TSP measurements were obtained and a 20% reduction in TSP as a result of vacuum street cleaning was reported. Factors concerning meteorological conditions and traffic patterns were not addressed, however.

PEDCo Environmental (1981b) also measured TSP, PM_{15}, and $PM_{2.5}$ concentrations near paved roads in Denver, CO, at two sites which had been sanded during snowstorms. One site had the sand removed by sweeping while the other site had no sand removal. Though a slight decrease in TSP and $PM_{2.5}$ was observed at the site where sand was removed, the difference was not statistically significant.

The most rigorous evaluations of vacuum sweeping have been performed by Cuscino et al. (1983a). This study made size-resolved vertical profile measurements near paved roads before and after sweeping. For PM_{15} mass concentrations, emissions reductions were estimated to be 16% two hours after sweeping, 51% three hours after sweeping, 0% four hours after sweeping, and 58% 24 hours after sweeping. Cuscino et al. (1983a) note that meteorological variability may have played a large role in the differences in ambient mass

concentrations among the measurement periods. In earlier studies, Cowherd, (1982) reported efficiencies of about 45% for PM_{15} and 35% for $PM_{2.5}$ when vacuum sweeping was used. Both of these vacuum-sweeping studies were performed on industrial paved roads, where initial street loadings and amount of material tracked on is typically much higher than on public streets.

Chow *et al.* (1990) conducted a street-sweeping study specific to PM_{10}. Receptor models were used to determine the contributions from dust and from primary motor vehicle exhaust. The ratio of these two contributions is less sensitive to meteorological and emission rate differences between sweeping and nonsweeping study periods than the absolute source contributions from either source. Chow *et al.* (1990) found that daily street sweeping with a regenerative-air vacuum sweeper resulted in no detectable reductions in geological contributions to ambient PM_{10} measured in the sweeping area and that the street-sweeper design used in this study cannot possibly reduce PM_{10} on pavements.

Fitz and Bumiller (1996) investigated the effectiveness of street sweepers in reducing loose "blowsand" material on paved roads. "Blowsand" is defined as material deposited on roadways after large-scale wind erosion events in the Coachella Valley. Fitz and Bumiller (1996) found some street sweepers can successfully remove 97% to 99% of the loose surface material, whereas other sweepers in fact resuspend as many PM_{10} particles as they remove due to the exhaust from their diesel engines.

While recently-improved sweepers seem to effectively deplete the reservoir of material from which PM_{10} particles can be generated, none of these studies conclusively demonstrates the effectiveness of street sweeping on ambient concentrations of suspended PM_{10} particles. Suspended particle concentrations are affected by many variables and differences caused by street sweeping may not be detectable at nearby monitoring sites. The variables which appear to influence emissions reduction efficiencies are: 1) loading of dirt on the street before and after sweeping; 2) particle size distribution of dirt on the street; 3) sweeper efficiency in removing dust from the street surface; 4) sweeper exhaust emission rates for small particles; 5) portion of roadway which is swept; 6) length of roadway which is swept; 7) sweeping frequency; and 8) meteorological variables such as precipitation, wind speed, wind direction, and relative humidity. The previous studies offer little guidance on the quantitative effects of changes in these variables on geological contributions to PM_{10} concentrations measured near paved roads.

9.2.5 Suppression of Wind Erosion Derived Fugitive Dust

Fugitive dust emissions introduced by wind erosion can be mitigated by: 1) altering the surface (such as increasing its roughness with tillage implements and practices), 2) sufficient vegetative stubble or mulch coverage, or 3) using windbreaks. Applying tillage

implements to ridge the soil or create large nonerodible clods is a standard practice in wind erosion control where the establishment of vegetative coverage is difficult. This method results in large nonerodible roughness elements that absorb momentum from the erodible soil and trap the erodible soil in larger cracks and crevices.

No-till and minimum-till planting procedures have been developed to minimize topsoil erosion, conserve water, and reduce dust emissions (Rice, 1983). During farming practice, new seeds are planted into stubble from the last crop or into a cropped field by cutting through the surface vegetation and inserting the seed directly into the ground. This type of low- or no-till farming operation reduces wind-generated fugitive emissions because vegetative cover (e.g., standing stubble or mulch) is left on the soil surface. Vegetation protects the soil by absorbing the energy of the surface wind, reducing the wind velocity, and sheltering the resuspendable particles. The percentage of vegetative cover along with its shape and density of coverage determine the effectiveness of wind-blown dust control (Leys, 1991). Annual crops can be interplanted in narrow strips or rows which minimize the ground-level soil movement. Interplanting is often supplemented with other practices such as protecting the strips with other vegetative coverage to more efficiently reduce dust emissions.

Windbreaks or other surface barriers absorb or deflect wind energy and minimize soil movement or particle resuspension from unprotected surfaces. The length of a windbreak needs to be six to ten times its height to effectively mitigate dust emissions. In general, the shape, width, height, and porosity of the barrier, along with the surface wind speed and wind direction, affect the efficiency of the windbreak.

9.2.6 Minimization of Activity

Fugitive emissions caused by construction activity or agriculture practice can be reduced by minimizing their activity level. Vehicle-related resuspended dust can be reduced by regulating vehicle travel speeds, prohibiting road use by vehicles with more than four wheels, and reducing vehicle volume by providing perimeter parking and mass transit to industrial sites. Traffic controls are often supplemented with other control measures, such as surface watering and wheel washing, to minimize dust emissions induced by anthropogenic activities.

9.3   Application of Fugitive Dust Control Measures in the Las Vegas Valley

The application of different fugitive dust control measures and the effectiveness of these control measures in reducing ambient PM_{10} levels are discussed. Most of these fugitive dust demonstration studies were conducted in a small geographical area which assessed the changes in control efficiencies over a short (< one year) period of time. Because of

variabilities in meteorology, soil composition, particle size distribution, and activity level, it is difficult to evaluate the costs/benefits of each control measure.

Street sweeping in commercial and/or residential areas is more for aesthetic purposes than for reducing the ambient PM_{10} levels. To assure the reduction of ambient PM_{10} concentrations, the type of sweeper and the condition of the road surface need to be assessed prior to sweeper application. As surface loading accumulates on access roads near construction sites or sand and gravel operations, street sweepers can be used to deplete the reservoir of surface material to minimize particle carry-out or track-out.

Analysis of these results shows that the zones of influence of intermittent fugitive dust from construction activities or sand and gravel operations are relatively small. Since most of the particles originating from these sources require significant external force to resuspend them in the atmosphere, installation of temporary windbreaks inside of construction sites or on disturbed vacant land should be considered to effectively attenuate wind erosion of surface soil. Control measures such as surface watering of haul roads and areas of cut-and-fill operations, and treatment with inexpensive hygroscopic chemical stabilizers (e.g., lignon sulfonate) to less-frequently-traveled areas, can be used to minimize dust emissions from construction sites and sand/gravel operations. Frequent application of chemical suppressants may be necessary to compensate for breakdown under heavy vehicle movement. Traffic controls such as reducing vehicle travel speeds and traffic volume can minimze dust resuspension. Covering of haul trucks as well as cleaning vehicles and washing vehicle wheels as vehicles leave construction sites can reduce particle track-out or carry-out.

Chemical dust suppressants can be used to control fugitive dust emissions from unpaved roads, disturbed vacant land, and desert surfaces. Watson *et al.* (1996) demonstrated that polymer-type suppressants (e.g., Soil Sement, Midwest Industrial Supplies Inc.) can be used effectively on infrequently-traveled (~17 vehicles/day) unpaved roads. Eleven months after application, this suppressant yielded 85% reduction in PM_{10} emissions as compared to the untreated section. For application in the Las Vegas Valley, soil type, soil moisture, silt content, silt loading, surface characteristics, traffic volume, and environmental conditions (e.g., wind velocity, precipitation) need to be assessed prior to suppressant application.

A combination of these control measures should be applied to effectively reduce dust emissions from various fugitive dust sources. Analysis of local meteorology, soil composition, soil moisture, particle size distribution, surface silt loading, surface roughness, and activity levels need to be conducted prior to application of any control measures. Continued monitoring of ambient concentrations is essential to evaluate the long-term effectiveness of control measures in reducing PM_{10} fugitive dust emissions.

10.0 SUMMARY, CONCLUSIONS, AND RECOMMENDATIONS

The project objectives were to acquire an air quality and meteorological database of specified accuracy, precision, and validity for data analysis and modeling; to examine spatial and temporal patterns of PM_{10}; to apportion PM_{10} to its sources; to estimate fugitive dust contributions to PM_{10}; and to reconcile difference between source and receptor models. These objectives have been met, as described in the previous sections of this report. This section summarizes the conclusions from these measurement and modeling efforts and provides recommendations with respect to control strategy development and long-term air quality monitoring.

10.1 Summary

10.1.1 Data Validity

PM_{10} mass, ions, (e.g., chloride, nitrate, sulfate, ammonium), crustal-related species (e.g., aluminum, silicon, potassium, calcium, manganese, iron, copper, zinc), and combustion-related species (e.g., organic carbon, elemental carbon, light absorption, soluble potassium, chlorine) were found above the lower quantifiable limits (LQLs) in more than 95% of the samples. PM_{10} bromine and lead were detected in 82% and 68% of the samples, respectively. Rare-earth and other trace elements (e.g., cobalt, gallium, yttrium, molybdenum, palladium, indium, tin, antimony, thallium) were not detected in most of the samples, which is consistent with findings in other U.S. urban areas.

Industrial-source-related toxic species such as selenium, cadmium, and mercury were not detected in any of the samples with the exception of arsenic, which was found above the LQLs in approximately 5% of the samples. The maximum concentration of 0.0052 $\mu g/m^3$ was far below those levels that might be hazardous to human health. These specifications indicate that PM_{10} samples acquired in this study had adequate sample loadings for chemical analysis. Furthermore, the minimum detection limits (MDLs) of the selected chemical analysis methods were sufficiently low to establish a valid measurement with associated uncertainties.

Laboratory system and performance audits as well as laboratory intercomparisons were conducted during the study period to evaluate the accuracy, precision, and validity of the aerosol measurements. Thin-film standards comparisons for x-ray fluorescence analysis show that over 90% of the comparison are within ±15% of the standard value, with 64% of the elements reporting percent difference within ±10%. This yielded an overall average difference of –9%. The average difference of laboratory spike samples are well within ±10% for organic carbon, chloride, nitrate, and sulfate and within ±15% for ammonium. These comparisons confirm the consistent quality of the laboratory analyses.

Comparison of collocated PM_{10} measurements among three different aerosol samplers (i.e., medium-volume sequential filter sampler [SFS], low-volume portable PM_{10} survey sampler [POR], and low-volume PM_{10} beta attenuation monitor [BAM]) showed that the SFS and portable PM_{10} survey samplers acquired equivalent measurements, with correlation coefficients exceeding 0.8 in every pairwise comparison. In most cases, the differences between the paired samples were within the measurement uncertainties (σ). Overall, 80% of the paired differences were found within $\pm 2\sigma$, and more than 90% of the measurements differed by no more than $\pm 3\sigma$. That is, in most cases, the differences between the samplers are within the measurement precisions. Only the PM_{10} BAM measurements displayed a positive bias ranging from 30% to 200%, on average.

The sum of measured chemical concentrations accounted for 66% of the PM_{10} mass, with high correlation coefficients ($r > 0.97$). The remaining portion of measured PM_{10} can be accounted for by unmeasured metal oxides in crustal material.

Tests of physical consistency were performed for: 1) sulfate versus total sulfur; 2) chloride versus chlorine; 3) soluble potassium versus potassium; and 4) light absorption versus elemental carbon. These comparisons identified a few outliers that were either invalidated, corrected, or flagged. Correlation coefficients exceeded 0.9 for all comparisons.

Particle absorption (b_{abs}) was highly correlated with elemental carbon ($r = 0.96$). Elemental carbon concentrations on portable PM_{10} survey samples were estimated using the relationships established with the SFS. Reasonable correlation ($r = 0.96$) was found between the calculated and measured ammonium, with calculated ammonium being a factor of two higher than the measured ammonium. This implies that aerosol in the study area is either acidic or trace amounts of some mineral products are present in the atmosphere. Given that sulfur emissions are low in the Las Vegas Valley and there is little moisture to engender conversion to sulfuric acid, the excess sulfate is probably of geological origin (e.g., $CaSO_4$).

Anion/cation balances with good correlations ($r = 0.8$) support the accuracy and precision of: 1) ion chromatographic (IC) measurements for chloride, nitrate, and sulfate; 2) automated colorimetric (AC) measurements for ammonium; and 3) atomic absorption spectrophotometric (AAS) measurements for soluble potassium. The lower-than-unity ratio (0.35) of cations versus anions suggests that soluble magnesium and soluble calcium might provide the needed cations from soluble fractions of magnesium sulfate ($MgSO_4$), gypsum ($CaSO_4$), and/or lime (CaO). Soluble magnesium and calcium were not measured in this study.

Comparisons of nonvolatilized particulate nitrate versus nitric-acid-denuded total PM_{10} particulate nitrate show excellent correlation ($r = 0.93$), with approximately 40% of the particulate nitrate volatilized from the front quartz-fiber filter. Volatilized nitrate is not part

of the measured PM_{10} mass, so this loss does not show up in the sum of species comparison. Without a backup absorbent filter, particulate nitrate would be greatly underestimated.

10.1.2 Characteristics of PM_{10} Mass and Chemistry at the Two Base Sites

During the study period between 01/01/95 and 01/31/96, the 24-hour PM_{10} standard of 150 $\mu g/m^3$ at the Clark County beta attenuation compliance monitoring network was exceeded on 17 days at one or more of the measurement locations, for a total of 38 site-days. The beta attenuation monitors operated by CCHD acquire hourly average PM_{10} concentrations every day of the year. Filter samples for PM_{10} are obtained by DRI every sixth day, except during special study periods. In the every day compliance monitoring network, PM_{10} concentrations were exceeded 12 times at the Green Valley site, six times at the Bemis/Craig Road site, four times each at the Maycliff, McDaniel, and City Center sites, three times each at the East Charleston (microscale) and Pittman sites, and once each at the Powerline and Flamingo sites. The highest PM_{10} concentration of 388 $\mu g/m^3$ was reported at the McDaniel site on 01/17/96.

In the sixth-day and special-study filter sampling network operated by DRI, no 24-hour standard exceedances were encountered at the Bemis and East Charleston sites. The highest PM_{10} concentrations in the Las Vegas Valley PM_{10} Study network were found on 01/16/96 with 123.6 ± 6.2 $\mu g/m^3$ at the Bemis site and 123.9 ± 6.2 $\mu g/m^3$ at the East Charleston site. The second-highest PM_{10} concentration was found at the East Charleston site with PM_{10} mass being 119.1 ± 6.6 $\mu g/m^3$. The concurrent measurement at the Bemis site on this day was only 27.0 ± 1.4 $\mu g/m^3$. In 1995, seasonally-stratified annual averages at the Bemis and East Charleston sites were well below the annual PM_{10} standard of 50 $\mu g/m^3$, with 28.8 ± 0.5 $\mu g/m^3$ at the Bemis site and 32.4 ± 7.1 $\mu g/m^3$ at the East Charleston site.

PM_{10} mass concentrations at the Bemis base site were only moderately correlated (r = 0.51) with PM_{10} measured at the East Charleston base site. This implies that local sources within a few kilometers of one or both sites had a major impact on PM_{10} measurements. PM_{10} mass concentrations at the East Charleston site were approximately 20% higher than those observed at the Bemis site.

The sum of crustal elements (i.e., aluminum, silicon, calcium, potassium, titanium, iron, and zinc, unweighted for mineral oxides) constituted 45% and 43% of PM_{10} mass at the Bemis and East Charleston sites, respectively. Total carbon, on average, is a factor of two higher at the East Charleston site (37% of PM_{10} mass) than at the Bemis site (18% of PM_{10} mass). Levels of ions (i.e., sulfate, nitrate, ammonium) and trace species (i.e., species other than soil-related crustal species) were generally low at both sites, ranging from 1% to 6% of PM_{10} mass.

10-3

Average PM_{10} calcium concentrations were 6.3 ± 5.1 $\mu g/m^3$ at the Bemis site and 6.2 ± 3.6 $\mu g/m^3$ at the East Charleston site. The highest PM_{10} calcium concentrations were found on 01/16/95, with 27.4 ± 4.6 $\mu g/m^3$ at the Bemis site and 17.9 ± 3.0 $\mu g/m^3$ at the East Charleston site. These PM_{10} concentrations are a factor of two to eight higher than those observed in other U.S. urban areas. The gypsum mine in the southwestern part of the Valley, along with frequent construction activities in Las Vegas and widespread alkaline soils, may have contributed to these elevated calcium concentrations.

10.1.3 Temporal and Spatial Variations of the Saturation Monitoring Network

Each of the satellite monitoring sites was classified into one of five site types according to the primary land use in the close vicinity of the site. Besides the collocated Bemis site, the saturation monitoring network included three industrial sites (mainly sand/gravel operations), ten active/inactive construction sites, five commercial sites, three residential sites, and eight disturbed/undisturbed vacant land sites.

Material balances constructed for over 400 samples measured at the satellite sites showed that crustal material (including oxides associated with crustal elements) was the largest contributor, accounting for 60% to 70% of PM_{10} mass. Combustion byproducts and secondary sulfate accounted for 5% and 8% of PM_{10} mass, respectively. The enrichment of crustal components was similar among the commercial, residential, and vacant land sites with highest concentrations found in industrial sites. PM_{10} sulfur concentrations were homogeneously distributed within the study domain.

Significant temporal and spatial variations were found in the saturation monitoring network. Daily average PM_{10} concentrations varied by a factor of five, ranging from 9.6 ± 3.9 $\mu g/m^3$ on 05/14/95 to 52.8 ± 19.1 $\mu g/m^3$ on 06/05/95. Daily maximum concentrations varied by a factor of ten, ranging from 21.3 ± 3.5 $\mu g/m^3$ on 04/18/95 at the NWAL industrial site to 208.4 ± 11.7 $\mu g/m^3$ on 06/06/95 at the DONO construction site. During the study period, daily maximum PM_{10} concentrations occurred 14 times at construction sites, 10 times at industrial sites, and twice at vacant land sites; none were recorded at commercial or residential sites.

Among the five site types, average PM_{10} mass concentrations varied from 23.0 ± 13.8 $\mu g/m^3$ at the vacant land sites to 39.4 ± 24.0 $\mu g/m^3$ at the industrial sites, with an overall average of 27.9 ± 19.7 $\mu g/m^3$. Average PM_{10} concentrations by site type show that the industrial and construction sites tend to deviate from the general pattern with elevated PM_{10} concentrations, while the commercial, residential, and vacant land sites overlapped one another within one standard deviation of the average. This analysis shows that meteorology is the major driving force for the temporal variations of commercial, residential, and vacant land sites. Temporal variations of industrial and construction sites were dominated by local

fugitive dust sources, irrespective of the changes in daily meteorology. Analysis of variance confirms that significant differences were found between the industrial and all other site types except for the construction sites.

A majority of the elevated PM_{10} concentrations were found during the fall intensive monitoring period, with average PM_{10} concentrations being 40% to 50% above their site averages. Average PM_{10} concentrations were lowest during the first spring intensive monitoring period, and were often 40% to 50% below their corresponding site averages.

10.1.4 Zones of Influence and Spatial Homogeneity

Elevated PM_{10} concentrations were found to be associated with local construction activities (e.g., housing development or road construction), industrial processes (sand/gravel operations), or excess surface street dust loadings. When potential fugitive dust sources were identified within 0.5 km of a sampling site, PM_{10} concentrations were often up to four times higher than PM_{10} concentrations at nearby sites that were not adjacent to the source. Most of these elevated PM_{10} concentrations corresponded with dust-generating activities that were identified during each of the intensive monitoring periods.

Average PM_{10} concentrations among the satellite sites varied by a factor of three, with 19.1 ± 9.1 $\mu g/m^3$ at the SWLC undisturbed desert site to 52.2 ± 33.9 $\mu g/m^3$ at the LONM construction site. The site-specific maximum PM_{10} concentrations varied by a factor of five during the intensive monitoring periods, ranging from 43.8 ± 2.7 $\mu g/m^3$ at the SWLC vacant land site on 09/11/95 to 208.4 ± 11.7 $\mu g/m^3$ at the DONO construction site on 06/06/95. Site-to-site PM_{10} crustal component concentrations varied by a factor of four on a light-wind day (e.g., 09/11/95) to a factor of seven on a windy day (e.g., 06/05/95). Overall, site-to-site variations were significantly greater than the day-to-day variations with respect to PM_{10} mass and chemistry in the saturation monitoring network. Besides the meteorology, local source impacts were superimposed to enhance the site-to-site variations. During this study, there was no evidence that winds caused any significant amounts of dust to be suspended from undisturbed vacant land. There is ample evidence that large quantities of dust were suspended by wind when desert crusts were broken or natural vegetation was removed.

High winds occurred on only 50% of the site-days where the saturation monitoring network reported PM_{10} concentrations exceeding 100 $\mu g/m^3$. Case studies show that on a windy day such as 06/06/95, elevated PM_{10} concentrations ranging between 9% to 70% above the corresponding site average were found within a 0.75 km radius from the DONO construction site. The zone of influence can be pronounced to 1.5 km downwind of the source over relatively flat terrain without any wind barriers. Upwind sites within 1.5 km of the source do not show any detectable impact.

On a low-wind day, the zone of influence from an active construction site was mainly within one kilometer downwind from the source. The zone of influence could extend up to 2 km from a dust source, with the concentration gradient decreasing by 10% to 40% during low-wind periods.

Homogeneity measures show that for over 90% of the cases, PM_{10} concentrations measured at the Bemis site can represent commercial, residential, and vacant land sites up to 2.5 km northeast to southeast of the site to within $\pm 1\sigma$ of measurement uncertainty. Over 70% of the sample pairs found at two residential, one commercial, and two vacant land sites within 2.5 km northwest and southwest of the Bemis site reported PM_{10} concentrations within ± 5 $\mu g/m^3$ of the Bemis PM_{10} concentration.

The same homogeneity does not apply to nearby (0.5 to 1.5 km) industrial sites, however, with PM_{10} concentrations ranging from 70% to 80% above the Bemis site. PM_{10} concentrations at the LONM construction site, 2.8 km west of the Bemis site, differed by more than 20 $\mu g/m^3$ from the Bemis PM_{10} concentration for 50% of the samples.

10.1.5 Diurnal Variations of PM_{10} Concentrations

The statistical distribution of hourly PM_{10} concentrations at most of the PM_{10} BAM sites showed a distinct and reproducible diurnal pattern, with elevated peaks appearing around 0600 to 0700 PST and 2000 to 2200 PST during the summer (April to September), and around 0700 to 0900 PST and 1700 to 2000 PST during the winter (October to March). This is consistent with the diurnal meteorology and source emission patterns. On any given day, in particular high wind days, the diurnal variation in PM_{10} concentrations may be significantly different than the statistical distribution over all days.

Peaks in PM_{10} concentrations occurred during the morning and evening rush hours. In winter, morning and evening PM_{10} peaks are similar in magnitude because of low mixing heights during the rush hour. In summer, morning PM_{10} peaks were much higher than the evening PM_{10} peaks because mixing heights were lower during the morning rush hour than during the evening rush hour.

Weekday and weekend patterns in PM_{10} concentrations were also compared for the summer (April to September) and winter (October to March) periods. Large reductions in the size of the morning peak were found on weekends, with lower early-evening peaks during winter. This is consistent with levels of motor vehicle emissions, which are reduced during weekends as fewer people are commuting to work.

10.1.6 Receptor Modeling

PM_{10} mass and silicon were moderately correlated ($r > 0.6$) among the commercial, residential, and vacant land sites, with high correlations ($r > 0.9$) found between the residential and commercial sites. Hardly any correlation was found for PM_{10} mass and silicon measured among industrial or construction sites, or between these two site types.

Correlations of PM_{10} light absorption, indicative of carbon content, were more dependent upon geographical location in the vicinity of heavily-traveled roads (e.g., Interstate 15, Las Vegas Boulevard) than upon their site types. The East Charleston commercial site, the southernmost site within the study area, showed no correlations with any of the other site locations. This is consistent with the different emission densities (e.g., population, restaurants, vegetative burning) as well as the traffic volume in the area.

PM_{10} sulfur concentrations experienced high correlation coefficients ($r > 0.8$) among all sites except for the East Charleston commercial site. This demonstrates the homogenous distribution of secondary aerosol.

Cluster analysis did not provide additional insight into spatial patterns due to significant site-to-site and day-to-day variability in a small data set. Chemical mass balance (CMB) receptor modeling results show that the relative source contribution at the Bemis and East Charleston sites was only similar for secondary aerosol contributions, which accounted for 5% of PM_{10} mass.

For the nonintensive sampling periods, primary geological material was the single largest contributor during all periods, accounting for over 92% (37.7 ± 5.6 $\mu g/m^3$) and 79% (47.2 ± 5.0 $\mu g/m^3$) of the PM_{10} mass, on average, at the Bemis and East Charleston sites, respectively. Significant day-to-day variations were found in geological material source contributions. On a windy day (e.g., 01/16/95), geological material accounted for over 98% (146.0 ± 14.9 $\mu g/m^3$) of calculated PM_{10} mass at the Bemis site and for 86% (102.6 ± 7.7 $\mu g/m^3$) of calculated PM_{10} mass at the East Charleston site. 01/16/95 was also the date of the highest PM_{10} at both sites.

Primary motor vehicle exhaust was the second-largest contributor, typically contributing 4% (1.6 ± 1.5 $\mu g/m^3$) and 14% (8.2 ± 2.8 $\mu g/m^3$) of ambient PM_{10} mass at the Bemis and East Charleston sites, respectively. Maximum motor vehicle exhaust contributions were found on 12/27/95 at the East Charleston site (14.8 ± 4.7 $\mu g/m^3$, 15% of PM_{10} mass), and on 12/28/95 at the Bemis site (4.1 ± 2.4 $\mu g/m^3$, 8% of PM_{10} mass). Elevated motor vehicle exhaust contributions were found at both sites during the last week of 1995, when the Las Vegas Valley experienced enhanced tourist traffic during the Christmas and New Year holidays.

The highest residential wood combustion contributions were found at the East Charleston site with 4.1 ± 1.1 $\mu g/m^3$ (9% of PM_{10} mass) on Christmas Day. At the East Charleston site, elevated contributions from residential wood combustion were found during the Christmas/New Year week (12/24/95 to 01/02/96), accounting for 1% to 9% of PM_{10} mass. At the Bemis site, contributions from residential wood combustion were found only on 12/25/95, 01/01/96, and 01/02/96, with the highest contribution occurring on Christmas Day (0.35 ± 0.18 $\mu g/m^3$, 2% of PM_{10} mass). Residential wood combustion contributions at the Bemis site were negligible throughout the rest of the year.

Contributions from geological material were relatively larger in the intensive samples than in the nonintensive samples. During the intensive sampling periods, geological material accounted for 96% (31.4 ± 3.4 $\mu g/m^3$) and 93% (34.1 ± 3.2 $\mu g/m^3$) of the PM_{10} mass, on average, for the Bemis and East Charleston sites, respectively. Other source contributions during the intensive monitoring periods were similar at both sites, with primary motor vehicle exhaust, residential wood combustion, secondary ammonium sulfate, and secondary ammonium nitrate each accounting for 1% to 3% of the PM_{10} mass.

10.1.7 Dispersion Modeling

ISCST-3 modeling results show that the most influential source of PM_{10} within the modeling domain was from controlled construction. On average, construction activity was the single largest contributor at the Bemis site, accounting for 51% of modeled PM_{10} mass, followed by disturbed land (15%), construction track-out (10%), construction wind erosion (8%), paved and unpaved roads (7% each), mobile sources (1%), stationary sources (0.5%), and residential wood combustion (0.3%). At the East Charleston site, paved road dust was the largest contributor, accounting for 43% of PM_{10} mass, followed by construction activity (23%), construction track-out, disturbed land, and mobile sources (7% each), construction wind erosion (6%), unpaved road dust (4%), residential wood combustion (2%), and stationary sources (0.2%).

The highest PM_{10} concentrations were found in the northeast and southeast portions of the modeling domain. Maximum modeled source impacts were 260 $\mu g/m^3$ from controlled construction in the northeast, 170 $\mu g/m^3$ from controlled construction track-out in the south-southeast, 125 $\mu g/m^3$ from controlled construction wind erosion in the southeast, 100 $\mu g/m^3$ from unpaved roads in the northwest, 90 $\mu g/m^3$ from paved roads in the southeast near city center, 59 $\mu g/m^3$ from stationary sources in the southwest, 35 $\mu g/m^3$ from disturbed land in the southeast, 10 $\mu g/m^3$ from mobile sources at city center, and 10 $\mu g/m^3$ from residential wood combustion in the southeast.

The influences from geological material often decrease to half of their maximum values in a short distance from the source. As examples, 50% lower PM_{10} concentrations

were observed at a distance of approximately 1.45 km (east-west direction) to 1.6 km (north-south direction) for controlled construction, and at a distance of approximately 2.7 km for unpaved roads. ISCST-3 also shows that the source influence for other source types are also confined to small areas. PM_{10} concentrations were 50% lower at 1.6 km from stationary sources (mainly sand and gravel operations), and at 1.8 km (north-south direction) to 3.8 km (east-west direction) from residential wood combustion sources.

10.1.8 Source/Receptor Model Reconciliation

The average PM_{10} source contributions from the CMB receptor model were compared with those from the ISCST-3 dispersion model. Although the magnitudes of PM_{10} mass from CMB and ISCST-3 differed by two- to sixfold, the distributions of their relative source contributions are quite similar. Geological material was the most dominant source type at the Bemis and East Charleston sites, accounting for an average of 94% of PM_{10} mass calculated by CMB and 99% of PM_{10} mass calculated by ISCST-3 at the Bemis site, and accounting for 86% of PM_{10} mass calculated by CMB and 91% of PM_{10} mass calculated by ISCST-3 at the East Charleston site. Mobile sources were the second-largest contributor, accounting for 1% (ISCST-3) to 2.2% (CMB) of PM_{10} mass at the Bemis site, and 7% (ISCST-3) to 7.5% (CMB) at the East Charleston site. ISCST-3 cannot compute gas-to-particle transformation; therefore no comparisons can be made. Since secondary aerosol accounts for less than 5% of PM_{10} mass based on CMB, it is not expected to have a major impact on the percent mass distribution.

10.2   Conclusions

Several conclusions can be drawn from this analysis of PM_{10} concentrations in the Las Vegas Valley with respect to emissions, measurements, source contributions, and modeling.

The current county-wide primary PM_{10} emissions inventory agrees well with the Chemical Mass Balance (CMB) receptor modeling results with respect to relative contributions to emissions from major source categories. Fugitive dust sources account for up to 90% of primary PM_{10} emissions by both methods. The spatial distribution of PM_{10} also shows substantial variability in the geological source contribution over very short distances (< 1 km).

With respect to ambient measurements, a validated data base with specified accuracy, precision, and validity have been established. The satellite monitoring sites were strategically located to examine the spatial variations of PM_{10} concentrations within the study domain (12 km east-west × 13 km north-south), and to identify potential pollutant transport following the prevailing wind direction. Pollution impacts from specific fugitive dust emitters were

examined. It was found that the zones of influence from construction activities were very small, within a 0.75 to 1 km radius from the source. Elevated PM_{10} concentrations were found up to 1.5 to 2 km downwind from the source. No apparent impact was found at the upwind sites, however.

Homogeneity measures show that PM_{10} measurements at the Bemis site do not represent the general population exposure within the neighborhood-scale domain (1 to 10 km radius) of the site. This is mainly due to intermittent fugitive dust sources interspersed in the study area.

Elevated PM_{10} concentrations were found to be associated with local construction activities, industrial processes, or excessive surface street loading. When a potential fugitive dust emitter was located within 0.5 km of the sampling site, PM_{10} concentrations can be increased by a factor of four depending on the activity level and local meteorology.

With respect to 24-hour PM_{10} standard exceedances, not all high-wind conditions resulted in high PM_{10} concentrations. Several Valley-wide elevated PM_{10} concentrations were observed on high-wind days, however. The threshold wind velocity is about 7.5 m/s to effectively resuspend PM_{10} particles. The cumulative frequency distribution shows that average wind speeds greater than 7 m/s occurred on only 8% of the days throughout the year.

With respect to average source contributions, fugitive dust or geological material was the major contributor, accounting for 92% to 96% and 79% to 93% of the PM_{10} mass at the Bemis and East Charleston sites, respectively. Primary motor vehicle exhaust was the second-largest contributor, accounting for 0.5% to 14% of the PM_{10} mass, with increasing contributions during the last week of 1995. Contributions from residential wood combustion were only detectable during the Christmas and New Year holiday season, accounting for 1% to 9% of the PM_{10} mass over a 24-hour period. Contributions from secondary ammonium sulfate and ammonium nitrate were small, accounting for less than 5% of the PM_{10} mass.

Source modeling with a homogeneous wind field and Gaussian plume dispersion could not accurately reproduce measured PM_{10} on a quantitative basis. The relative impacts among major source types were quite similar between CMB receptor modeling and ISCST-3 dispersion modeling, however.

This comparison of the source/receptor models shows that source and receptor modeling complement each another. The 1995 preliminary emissions inventory may have overestimated the fugitive dust emission rate, resulting in higher source contribution estimates. Emission estimates for mobile sources and residential wood combustion were similar between the two models. The ISCST-3 dispersion model provides insight with respect to sub-sources of fugitive dust.

Land uses near the sampling site can significantly impact the ambient measurements. At the Bemis site, construction activity was the largest PM_{10} contributor, accounting for 51% of PM_{10} mass, followed by disturbed land (15%) and track-out from construction sites (10%). At the East Charleston site, paved road dust was the largest contributor, accounting for 43% of PM_{10} mass, followed by construction activity (23%). The zones of influence of fugitive dust from construction activity sources are small, ranging from 0.75 to 1.5 km based on either descriptive data analysis or ISCST-3 modeling.

10.3   Recommendations

This study has provided an important step toward stating and solving PM_{10} problems in the Las Vegas Valley. However, this study is incremental rather than definitive. It has eliminated questions about insignificant contributors and has raised questions about how to control significant and major contributors.

With respect to improving the emissions estimates, further studies need to be conducted to:

- Conduct additional evaluations of emission factors for unpaved roads and disturbed/undisturbed vacant land. Conduct spatially dense monitoring to re-estimate these emission factors. Emission factors developed in the Las Vegas Valley for unpaved desert surfaces may overestimate the actual emissions. Additional wind tunnel studies, featuring side-by-side statistical calibrations of different wind tunnel designs on the same desert surface, could help resolve these differences.

- Create a schedule and procedure to update activity levels with more recent information. Develop guidelines for permitting construction activities. Construction activities should be updated on a quarterly basis with information such as amount of cut/fill, the number and types of earth-moving vehicles, the length of average round-trip distances traveled, and the density of the materials being moved.

- Develop separate VKT data bases for paved and unpaved roads, morning and evening rush hours, and weekends and weekdays. Vehicle-kilometers-traveled (VKT) traffic modeling should also be updated on an annual basis.

- Characterize soil properties for different land use areas. Assemble data bases for silt loading, silt content, soil type, soil moisture, particle size distribution, and surface characteristics.

With respect to long-term ambient monitoring, measurements need to be made to:

- Provide chemically-speciated PM_{10} monitoring on an every-sixth-day schedule at sites which have shown high PM_{10} concentrations in the past. Perform chemical analysis and source apportionment modeling on those samples which exceed 24-hour PM_{10} standards. Continue this sampling and analysis indefinitely to evaluate effects of emission control measures on source contributions.

- Perform continuous hourly monitoring of PM_{10}, wind speed, and wind direction within specific fugitive dust emitters (e.g., large construction site, sand/gravel operations) to assure proper control measures are enforced at these potential fugitive dust emission sources. Perform periodic independent audits of these measurements to assure their accuracy and precision.

- Conduct spatially-dense saturation monitoring within specific fugitive dust sources to better estimate their zones of influence.

- Measure wind speed and wind direction at both 2 m and 10 m heights for selected sampling locations to establish the relationship between threshold wind velocity and elevated PM_{10} concentrations.

With respect to the control measures, a combination of strategies should be applied to assure reduction of ambient PM_{10} concentrations. Regulations and implementation plans need to be developed to:

- Enforce periodic street sweeping with recently improved vacuum sweepers on access roads near construction sites or sand/gravel operations, and on paved roads adjacent to frequently-traveled unpaved roads to deplete the reservoir of surface material and to minimize particle carry-out or track-out.

- Ensure daily surface watering of haul roads and areas of cut and fill operations within construction areas. Apply inexpensive hygroscopic chemical stabilizers to less-frequently-traveled areas. Enforce traffic controls such as reducing vehicle travel speeds and installing temporary speed bumps on frequently traveled roads. Covering haul trucks, as well as washing vehicles and vehicle tires as they leave construction sites, can mitigate particle track-out or carry-out.

- Install temporary windbreaks at construction sites, surrounding open storage piles, or on disturbed vacant land, to attenuate wind erosion of surface soil.

- Evaluate soil type, soil moisture, silt content, silt loading, surface characteristics, traffic volume, and environmental conditions in different parts of the Las Vegas Valley. Apply chemical suppressants on frequently traveled unpaved roads and susceptible unpaved shoulders of frequently-traveled paved roads.

11.0 REFERENCES

Anderson, R.S., M. Sorensen, and B.B. Willetts (1990). A Review of Recent Progress in Our Understanding of Aeolian Sediment Transport. Research Report No. 213. Dept. of Theoretical Statistics, Institute of Mathematics, University of Aarhus.

Anspaugh, L.R., J.H. Shinn, P.L. Phelps, and N.C. Kennedy (1975). Resuspension and Redistribution of Plutonium in Soils. *Hlth. Phys.* **29**:571-582.

Ashbaugh, L.L., L.O. Myrup, and R.G. Flocchini (1984). A Principal Component Analysis of Sulfur Concentrations in the Western United States. *Atmos. Environ.* **18**(4):783-791.

Ashbaugh, L.L., R.T. Matsumura, T. James, O. Caravacho and R. Flocchini (1995). Modeling Dust Emissions from Field Harvest Operations. In *Proceedings, International Conference on Air Pollution from Agricultural Operations*, Feb. 7-9, 1995, Kansas City, MO, pp. 155-159.

Axetell, K., and J. Zell (1977). Control of Reentrained Dust from Paved Streets. EPA-907/977-007-007. U.S. Environmental Protection Agency, Region VII, Kansas City, MO.

Azizov, A. (1977). Influence of Soil Moisture on the Resistance of Soil to Wind Erosion. *Sov. Soil Sci.* **9**:105-108.

Bagnold, R.A. (1937). The Transport of Sand by Wind . *Geog. J.*, **89**:409-438.

Bagnold, R.A. (1941). The Physics of Blown Sands and Desert Dunes. Methuen, London, 265 p.

Belly, P.Y. (1964). Sand Movement by Wind. U.S. Army Coastal Eng. Res. Center Tech. Mem. 1.

Berkson, J. (1950). Are There Two Regressions? *J. Am. Statist. Assoc.* **45**:164-180.

Bevington, P.R. (1969). Data Reduction and Error Analysis for the Physical Sciences. McGraw Hill, New York, NY.

Bisal, F., and J. Hsieh (1966). Influence of Moisture on Erodibility of Soil by Wind. *Soil Sci.* **102**:143-146.

Bradford, J.M., and R.B. Grosman (1982). In-Situ Measurement of Near-Surface Soil Strength by the Fall-Cone Device. *Soil Sci. Soc. Am. J.* **46**:685-688.

Briggs, G.A. (1969). U.S. Atomic Energy Commission Critical Review Series: Plume Rise. TID-25075. National Technical Information Service, Springfield, VA.

Briggs, G.A. (1971). Some Recent Analysis of Plume Rise Observations. In *Proceedings of the Second International Clean Air Act Congress*, H.M. Englund and W.T. Berry, Eds. Academic Press, New York, NY.

Briggs, G.A. (1975). Plume Rise Predictions. In *Lectures on Air Pollution and Environmental Impact Analysis*. American Meteorological Society, Boston, MA, pp. 59-111.

Brookman, E.T. (1983). Linn County, Iowa, Non-Traditional Fugitive Dust Study. EPA-907/9-83-002. U.S. Environmental Protection Agency, Kansas City, MO.

Cahill, T.A., R.A. Eldred, P.J. Feeney, P.J. Beveridge, and L.K. Wilkinson (1990). The Stacked Filter Unit Revisited. In *Transactions, Visibility, and Fine Particles*, C.V. Mathai, Ed. Air & Waste Management Association, Pittsburgh, PA, p. 213.

California Department of Transportation (1979). CALINE3 - A Versatile Dispersion Model for Predicting Air Pollutant Levels Near Highways and Arterial Streets. Office of Transportation Laboratory, Department of Transportation, State of California, Sacramento, CA.

Calvert, S., H. Brattin, S. Bhutra, and D. Ono (1984). Improved Street Sweepers for Controlling Urban Inhalable Particulate Matter. EPA-600/7-84-021. U.S. Environmental Protection Agency, Research Triangle Park, NC.

Caravacho, O.F., L.L. Ashbaugh, R.T. Matsumura, R.J. Southard, and R.G. Flocchini (1995). Measurement of PM_{10} Potential from Agricultural Soils Using a Dust Resuspension Chamber. In *Proceedings, International Conference on Air Pollution from Agricultural Operations*, Feb. 7-9, 1995, Kansas City, MO, pp. 87-92.

Chepil, W.S. (1942). Measurement of Wind Erosiveness by Dry Sieving Procedure. *Sci. Agr.* **23**:154-160.

Chepil, W.S. (1956). Influence of Moisture on Erodibility of Soil by Wind. *Soil Sci. Soc. Proc.* **20**:288-292.

Chepil, W.S., and N.P. Woodruff (1963). The Physics of Wind Erosion and Its Control. *Advances in Agronomy* **15**:211-299.

Chow, J.C., J.G. Watson, R.T. Egami, B. Wright, C. Ralph, M. Naylor, J. Smith, and R. Serdoz (1986). Program Plan for State of Nevada Air Pollution Study (SNAPS). DRI Document 8086.1D2. Prepared for State of Nevada by Desert Research Institute, Reno, NV.

Chow, J.C. (1987). Soil Sampling Protocols. In *Pacific Northwest Source Profile Library: Source Sampling and Analytical Protocols*, J. Core and J.E. Houck, Eds. Oregon Department of Environmental Quality, Portland, OR.

Chow, J.C., and J.G. Watson (1989). Summary of Particulate Data Bases for Receptor Modeling in the United States, J.G. Watson, Ed. Air & Waste Management Association, Pittsburgh, PA, pp. 108-133.

Chow, J.C., and L.W. Richards (1990). San Joaquin Valley Air Quality Study (SJVAQS)/Atmospheric Utility Signatures - Predictions and Experiment (AUSPEX), Part E: Monitoring and Analysis for Aerosols and Visibility, Vol. I: Program Plan. DRI Document 8743.1F. Prepared for Pacific Gas and Electric Company by Desert Research Institute, Reno, NV.

Chow, J.C., J.G. Watson, R.T. Egami, C.A. Frazier, Z. Lu, A. Goodrich and A. Bird (1990). Evaluation of Regenerative-Air Vacuum Street Sweeping on Geological Contributions to PM_{10}. *JAWMA*, **40**, 1134-1142.

Chow, J.C., and J.G. Watson (1992). Fugitive Emissions Add to Air Pollution. *Environ. Protection* **3**(5):26-31.

Chow, J.C., J.G. Watson, D.H. Lowenthal, P.A. Solomon, K. Magliano, S.D. Ziman, and L.W. Richards (1992a). PM_{10} Source Apportionment in California's San Joaquin Valley. *Atmos. Environ.* **26A**(18):3335-3354.

Chow, J.C., C.S. Liu, J. Cassmassi, J.G. Watson, Z. Lu, and L.C. Pritchett (1992b). A Neighborhood-Scale Study of PM_{10} Source Contributions in Rubidoux, California. *Atmos. Environ.* **26A**:693-706.

Chow, J.C., J.G. Watson, D.H. Lowenthal, C.A. Frazier, B.A. Hinsvark, L.C. Pritchett, and G.R. Neuroth (1992c). Wintertime PM_{10} and $PM_{2.5}$ Mass and Chemical Compositions in Tucson, Arizona. In *Transactions, PM_{10} Standards and Nontraditional Particulate Source Controls*, J.C. Chow, and D.M. Ono, Eds. Air & Waste Management Association, Pittsburgh, PA, pp. 231-243.

Chow, J.C., J.G. Watson, D. Lowenthal, P. Solomon, K. Magliano, S. Ziman, and L.W. Richards (1993a). PM_{10} and $PM_{2.5}$ Compositions in California's San Joaquin Valley. *Aerosol Sci. Technol.* **18**(2):105-128.

Chow, J.C., J.G. Watson, L.C. Pritchett, W.R. Pierson, C.A. Frazier, and R.G. Purcell (1993b). The DRI Thermal/Optical Reflectance Carbon Analysis System: Description, Evaluation and Applications in U.S. Air Quality Studies. *Atmos. Environ.* **27A**(8):1185-1202.

Chow, J.C., and J.G. Watson (1994a). Work Plan to Improve PM_{10} Fugitive Dust Emissions Inventory, Draft Report. DRI Document 0736.1D. Prepared for South Coast Air Quality Management District by Desert Research Institute, Reno, NV.

Chow, J.C., and J.G. Watson (1994b). Guidelines for PM_{10} Sampling and Analysis Applicable to Receptor Modeling. EPA-452/R-94-009. Prepared for the Office of Air Quality Planning and Standards, U.S. Environmental Protection Agency, Research Triangle Park, NC, by the Desert Research Institute, Reno NV.

Chow, J.C., and J.G. Watson (1994c). Contemporary Source Profiles for Geological Material and Motor Vehicle Emissions, Final Report. DRI Document 2625.2F. Prepared for Office of Air Quality Planning and Standards, U.S. Environmental Protection Agency, by the Desert Research Institute, Reno, NV.

Chow, J.C., and J.G. Watson (1994d). Guidelines for PM_{10} Sampling and Analysis Applications to Receptor Modeling, Final Report. DRI Document 2625.1F. Prepared for Office of Air Quality Planning and Standards, U.S. Environmental Protection Agency, by the Desert Research Institute, Reno, NV.

Chow, J.C., J.G. Watson, J.E. Houck, L.C. Pritchett, C.F. Rogers, C.A. Frazier, R.T. Egami, and B.M. Ball (1994a). A Laboratory Resuspension Chamber to Measure Fugitive Dust Size Distributions and Chemical Compositions. *Atmos. Environ.,* **28**(21):3463-3481.

Chow, J.C., J.G. Watson, D.H. Lowenthal, P.A. Solomon, K.L. Magliano, S.D. Ziman and L.W.Richards (1994b). PM_{10} and $PM_{2.5}$ Chemical Characteristics and Source Apportionment in the San Joaquin Valley. In *Planning and Managing Regional Air Quality Modeling and Measurement Studies,* P.A. Solomon, Ed. Lewis Publishers, Boca Raton, FL, pp. 687-698.

Chow, J.C., E.M. Fujita, J.G. Watson, Z. Lu, D.R. Lawson, and L.L. Ashbaugh (1994b). Evaluation of Filter-Based Aerosol Measurements during the 1987 Southern California Air Quality Study. *Environ. Monitor. Assess.* **30**:49-80.

Chow, J.C., J.G. Watson, E.M. Fujita, Z. Lu, D.R. Lawson, and L.L. Ashbaugh (1994c). Temporal and Spatial Variations of $PM_{2.5}$ and PM_{10} Aerosol in the Southern California Air Quality Study. *Atmos. Environ.* **28**:2061-2080.

Chow, J.C. (1995). Summary of the 1995 A&WMA Critical Review: Measurement Methods to Determine Compliance with Ambient Air Quality Standards for Suspended Particles. *Environ. Manager* **1**:12-15 (May 1995).

Chow, J.C., J.G. Watson, R.T. Egami, and F. Divita Jr. (1995). Las Vegas Valley PM_{10} Study – Volume I: Draft Program Plan. DRI Document No. 4309.1D3. Prepared for the Clark County Dept. of Comprehensive Planning, Las Vegas, NV, by the Desert Research Institute, Reno, NV (July 21, 1995).

Chow, J.C., and J.G. Watson (1997a). Ion Chromatography. In *Elemental Analysis of Airborne Particles,* S. Landsberger and M. Creatchman, Eds. Gordon and Breach Publishers, USA.

Chow, J.C., and J.G. Watson (1997b). Imperial Valley/Mexicali Cross Border PM_{10} Transport Study – Final Report. DRI Document No. 8623.2F. Prepared for the U.S. Environmental Protection Agency, Region IX, San Francisco, CA, by the Desert Research Institute, Reno, NV (January 30, 1997).

Christensen, E.R., W.J. Ferguson, A.C. Fulton, D.L. Fulton, D.G. Heindel, K.L. Nietz, S.C. Stuckey, B.M. Tallman, and C.L. Williams (1989). FoxPro: Getting Started. Fox Software, Inc., Perrysburg, OH.

Clark County Department of Comprehensive Planning (1994). PM_{10} State Implementation Plan for the Las Vegas Valley. Clark County Department of Comprehensive Planning, Air Quality Planning Committee, Las Vegas, NV.

Clark County Health District (1993). 1992 Annual SLAMS/NAMS Network Review. Clark County Health District, Air Pollution Control Division, Las Vegas, NV.

Clark County Health District (1996). Inventory of Current Estimated Emissions (Tons/Year) for the Las Vegas Valley, Apex, Boulder City, Eldorado Valley, Goodsprings, and Jean Areas. Clark County Health District, Air Pollution Control Division, Las Vegas, NV.

Core, J., and J. Houck (1987). Pacific Northwest Source Profile Library Sampling and Analytical Protocols. Oregon Department of Environmental Quality, Portland, OR.

Corn, M. and F. Stein (1965). Reentrainment of Particles from a Plane Surface. *Am. Ind. Hyg. Ass. J.* **26**:325-336.

Cowherd, C. (1982). Particulate Emission Reductions from Road Paving in California Oil Fields. Presented at the 75th Annual Meeting, New Orleans, LA. Air Pollution Control Assoc., Pittsburgh, PA.

Cowherd, C., and J.S. Kinsey (1986). Identification, Assessment and Control of Fugitive Particulate Emissions. EPA-600/8-86-023. U.S. Environmental Protection Agency, Research Triangle Park, NC.

Cowherd, C., G.E. Muleski, and J.S. Kinsey (1988). Control of Open Fugitive Dust Sources. Final Report prepared under EPA Contract No. 68-02-4395, Work Assignment 14, MRI Project 8985-14. EPA-450/3-88-008. U.S. Environmental Protection Agency, Research Triangle Park, NC.

Cowherd, C., P. Englehart, G.E. Muleski, J.S. Kinsey, and K.D. Rosbury (1990). Control of Fugitive and Hazardous Dusts. Noyes Data Corp., Park Ridge, NJ, 471 p.

Currie, L.A., R.W. Gerlach, C.W. Lewis, W.D. Balfour, J.A. Cooper, S.L. Dattner, R.T. DeCesar, G.E. Gordon, S.L. Heisler, P.K. Hopke, J.J. Shah, G.D. Thurston, and H.J. Williamson (1984). Interlaboratory Comparison of Source Apportionment Procedures: Results for Simulated Data Sets. *Atmos. Environ.* **18**:1517.

Cuscino, T., Jr., G.E. Muleski, and C. Cowherd (1983a). Determination of the Decay in Control Efficiency of Chemical Dust Suppressants. In *Proceedings, Symposium on Iron and Steel Pollution Abatement Technology for 1982*. U.S. Environmental Protection Agency, Research Triangle Park, NC.

Cuscino, T., Jr., G.E. Muleski, and C. Cowherd (1983b). Iron and Steel Plant Open Source Fugitive Emission Control Evaluation. EPA-600/2-83-110. U.S. Environmental Protection Agency, Research Triangle Park, NC (October 1983).

DeCesar, R.T., S.A. Edgerton, M.A.K. Khalil, and R.A. Rasmussen (1985). Sensitivity Analysis of Mass Balance Receptor Modeling: Methyl Chloride as an Indicator of Wood Smoke. *Chemosphere* 14(10):1495-1501.

Duncan, M., R. Jain, S.C. Yung, and R.K. Patterson (1985). Performance Evaluation of an Improved Street Sweeper. EPA-600/7-85-008. U.S. Environmental Protection Agency, Research Triangle Park, NC.

Dyck, R.I., and J.J. Stukel (1976). Fugitive Dust Emissions from Trucks on Unpaved Roads. *Environ. Sci. Technol.* 10(10):1046-1048.

Dzubay, T.G., R.K. Stevens, W.D. Balfour, H.J. Williamson, J.A. Cooper, J.E. Core, R.T. DeCesar, E.R. Crutcher, S.L. Dattner, B.L. Davis, S.L. Heisler, J.J. Shah, P.K. Hopke and D.L. Johnson (1984). Interlaboratory Comparison of Receptor Model Results for Houston Aerosol. *Atmos. Environ.* 18:1555-1566.

Ermak, D.L. (1977). An Analytical Model for Air Pollutant Transport and Deposition from a Point Source. *Atmos. Environ.* 11:231-237.

Fairchild, C.I., and M.I. Tillery (1982). Wind Tunnel Measurements of the Resuspension of Ideal Particles. *Atmos. Environ.* 16(2):229-238.

Federal Register (1987a). Revisions to the National Ambient Air Quality Standards for Particulate Matter: 40 CFR Parts 51 and 52. *Federal Register* 52:24634 (July 1, 1987).

Federal Register (1987b). Regulations for Implementing Revised Particulate Matter Standards: 40 CFR Parts 51 and 52. *Federal Register* 52:24672 (July 1, 1987).

Federal Register (1987c). Air Programs: Particulate Matter (PM_{10}) Fugitive Dust Policy: 40 CFR Parts 50 and 52. *Federal Register* 52:24716 (July 1, 1987).

Federal Register (1987d). Ambient Air Monitoring Reference and Equivalent Methods: 40 CFR Part 53. *Federal Register* 52:24724 (July 1, 1987).

Federal Register (1987e). Ambient Air Quality Surveillance for Particulate Matter: 40 CFR Part 58. *Federal Register* 52:24736 (July 1, 1987).

Federal Register (1987f). Rules and Regulations. *Federal Register* **52**:29383 (August 7, 1987).

Federal Register (1991). Designations and Classifications for Initial PM_{10} Nonattainment Areas: 40 CFR Part 81. *Federal Register* **56**:11101.

Federal Register (1993). Reclassification of Moderate PM_{10} Nonattainment Areas to Serious Areas 40 CFR Part 81. *Federal Register* **58**:3334 (January 8, 1993).

Flocchini, R.G., T.A. Cahill, R. T. Matsamura, O. Carcacho, and Z.Q. Lu (1994). Evaluation of the Emissions of PM_{10} Particulates from Unpaved Roads in the San Joaquin Valley. Final Report prepared for the San Joaquin Valley Unified Air Pollution Control District, U.S. Environmental Protection Agency, and California Air Resources Board, p. 61 (April 1994).

Fox Software, Inc. (1991). FoxPro: Getting Started. Fox Software, Inc., Perrysburg, OH.

Fryrear, D.W. (1985). Soil Cover and Wind Erosion. *Trans. ASAE* **28**:781-784.

Fryrear, D.W., J.B. Xiao, and W. Chen (1995). Wind Erosion and Dust. In *Proceedings, International Conference on Air Pollution from Agricultural Operations*, Feb. 7-9, 1995, Kansas City, MO, pp. 57-64.

Garland, J.A. (1979). Resuspension of Particulate Material from Grass and Soil. AERE-R9452, HSMO, London.

Gatz, D. E., S.T. Wiley, and L. Chu (1983). Characterization of Urban and Rural Inhalable Particulates. Illinois Department of Energy and Natural Resources, Division of Policy and Planning, Springfield, IL.

Gebhart, K.A., D.A. Latimer, and J.F. Sisler (1990). Empirical Orthogonal Function Analysis of the Particulate Sulfate Concentrations Measured during WHITEX. In *Transactions, Visibility and Fine Particles*, C.V. Mathai, Ed. Air & Waste Management Association, Pittsburgh, PA, pp. 860-871.

Gillette, D.A. (1977). Fine Particulate Emissions Due to Wind Erosion. *Trans. Am. Soc. Agric. Eng.* **20**:980-987.

Gillette, D.A., J. Adams, A. Endo, D. Smith, and R. Kihl (1980). Threshold Velocities for Input of Soil Particles into the Air by Desert Soils. *J. Geophys. Res.* **85**(C10):5621-5630.

Gillette, D.A., and K. Hanson (1989). Spatial and Temporal Variability of Dust Production Caused by Wind Erosion in the United States. *J. Geophys. Res.* **94**(D2):2197-2206.

Gillette, D.A., and P.H. Stockton (1989). The Effect of Non-Erodible Particles on Wind Erosion of Erodible Surfaces. *J. Geophys. Res.* **94**(D10):12885-12893.

Gillies, J.A. (1987). Aeolian Thresholds and Sediment Transport Rates for Three Tillage Techniques. Master Thesis. University of Guelph, 124 p.

Gillies, J.A., J.C. Chow, and W.G. Nickling (1996a). Resuspension of Particles by Wind: A Literature Review. Report prepared for California Air Resources Board, Sacramento, CA, by Desert Research Institute, Reno, NV.

Gillies, J.A., J.C. Chow, and W.G. Nickling (1996b). Resuspension of Particles by Wind: Research Initiatives. Report prepared for California Air Resources Board, Sacramento, CA, by Desert Research Institute, Reno, NV.

Gomes, L., G. Bergametti, G. Coude-Gaussen, and P. Rognon (1990). Submicron Desert Dusts: A Sandblasting Process. *J. Geophys. Res.* **95**:13927-13935.

Gordon, G.E., W.H. Zoller, G.S. Kowalczyk, and S.W. Rheingrover (1981). Composition of Source Components Needed for Aerosol Receptor Models. In *Atmospheric Aerosol-Source/Air Quality Relationships*, E.S. Macias and P.K. Hopke, Eds. American Chemical Society, Washington, DC, pp. 51-74.

Gordon, G.E. (1984). Atmospheric Tracers of Opportunity from Important Classes of Air Pollution Sources. Santa Fe, NM.

Grau, R.H. (1993). Evaluation of Methods for Controlling Dust. Technical Report GL-93-25. U.S. Army Corps of Engineers. September, 1993.

Hagen, L.J., N. Mirzamostafa, and A. Hawkins (1995). PM_{10} Generation by Wind Erosion. In *Proceedings, International Conference on Air Pollution from Agricultural Operations*, Feb. 7-9, 1995, Kansas City, MO, pp. 79-85.

Haun, J.A. (1995). Estimation of PM_{10} from Vacant Lands in the Las Vegas Valley. Unpubl. M.S. Eng. Thesis, University of Nevada, Las Vegas.

Heisler, S., D. Fitz, J. Watson, and J. Chow (1995). Tucson Urban Haze Study, Final Report. Document No. 0493-005-804. Prepared for Arizona Department of Environmental Quality, Phoenix, AZ, by ENSR, Camarillo, CA (December 1994).

Henry, R.C. (1982). Receptor Models Applied to Contemporary Air Pollution Problems, S.L. Dattner, and P.K. Hopke, Eds. Air Pollution Control Association, Pittsburgh, PA, pp. 141-162.

Henry, R.C., Y.J. Wang, and K.A. Gebhart (1991). The Relationship Between Empirical Orthogonal Functions and Sources of Air Pollution. *Atmos. Environ.* **25A**(2):503-509.

Henry, R.C. (1992). Dealing With Near Collinearity in Chemical Mass Balance Receptor Models. *Atmos. Environ.* **26A**(5):933-938.

Hewitt, T.R. (1981). The Effectiveness of Street Sweeping for Reducing Particulate Matter Background Concentration. Sirrine Environmental Consultants, Research Triangle Park, NC.

Hidy, G.M. (1985). Jekyll Island Meeting Report. *Environ. Sci. Technol.* **19**(11):1032-1033.

Hinds, W.C. (1986). Aerosol Technology. New York: Wiley Interscience.

Hopke, P.K., E.S. Gladney, G.E. Gordon, W.H. Zoller, and A.G. Jones (1976a). The Use of Multivariate Analysis to Identify Sources of Selected Elements in Boston Urban Aerosol. *Atmos. Environ.* **10**:1015-1025.

Hopke, P.K., G.E. Gordon, W.H. Zoller, and E.S. Gladney (1976b). Comparisons of Source Identification Techniques for Trace Elements in Ambient Air Particulates. San Francisco, CA.

Houck, J.E., J.C. Chow, J.G. Watson, C.A. Simons, L.C. Pritchett, J.M. Goulet, and C.A. Frazier (1989a). Determination of Particle Size Distribution and Chemical Composition of Particulate Matter from Selected Sources in California, Volume I. Contract No. A6-175-32. Prepared for California Air Resources Board, Sacramento, CA, by OMNI Environmental Services, Inc., Beaverton, OR, and the Desert Research Institute, Reno, NV.

Houck, J.E., J.C. Chow, J.G. Watson, C.A. Simons, L.C. Pritchett, J.M. Goulet, and C.A. Frazier (1989b). Determination of Particle Size Distribution and Chemical Composition of Particulate Matter from Selected Sources in California, Volume II. Contract No. A6-175-32. Prepared for California Air Resources Board, Sacramento, CA, by OMNI Environmental Services, Inc., Beaverton, OR, and the Desert Research Institute, Reno, NV.

Houck, J.E., J.C. Chow, J.G. Watson, C.A. Simons, L.C. Pritchett, J.M. Goulet, and C.A. Frazier (1989c). Determination of Particle Size Distribution and Chemical Composition of Particulate Matter from Selected Sources in California, Volume III. Contract No. A6-175-32. Prepared for California Air Resources Board, Sacramento, CA, by OMNI Environmental Services, Inc., Beaverton, OR, and the Desert Research Institute, Reno, NV.

Houck, J.E., J.C. Chow, J.G. Watson, C.A. Simons, L.C. Pritchett, J.M. Goulet, and C.A. Frazier (1989d). Determination of Particle Size Distribution and Chemical Composition of Particulate Matter from Selected Sources in California, Executive Summary. Contract No. A6-175-32. Prepared for California Air Resources Board, Sacramento, CA, by OMNI Environmental Services, Inc., Beaverton, OR, and the Desert Research Institute, Reno, NV.

Houck, J.E., J.C. Chow, J.G. Watson, C.A. Simons, L.C. Pritchett, J.M. Goulet, and C.A. Frazier (1989e). Determination of Particle Size Distribution and Chemical Composition of Particulate Matter from Selected Sources in the San Joaquin Valley, Final Report. Agreement No. A6-175-32, prepared for the San Joaquin Valley Air Pollution Study Agency and the California Air Resources Board, Sacramento, CA, by OMNI Environmental Services, Inc., Beaverton, OR, and the Desert Research Institute, Reno, NV.

Houck, J.E., L.C. Pritchett, R.B. Roholt, J.G. Watson, J.C. Chow, J.M. Goulet, and C.A. Frazier (1989f). Determination of Particle Size Distribution and Chemical Composition of Particulate Matter from Selected Sources in California. Final Report prepared for California Air Resources Board, Sacramento, CA, by Desert Research Institute, Reno, NV.

Houck, J.E. (1991). Receptor Modeling for Air Quality Management, P.K. Hopke, Ed. Elsevier, Amsterdam, The Netherlands, pp. 45-82.

Husar, R.B. (1974). Atmospheric Particulate Mass Monitoring with a Beta Radiation Detector. *Atmos. Environ.* **8**:183-188.

Jacquart, J. (1997). Personal communication. Clark County Department of Comprehensive Planning, Las Vegas, NV.

James, D.E., and J.A. Haun (1994). Estimation of PM_{10} Emissions from Unpaved Surfaces in the Las Vegas Valley, Bi-Monthly Progress Report #2. Report prepared by Clark County Health District, Las Vegas, NV, by University of Nevada, Civil and Environmental Engineering Department, Las Vegas.

James, D.E. (1996). Estimation of PM_{10} Emissions from Unpaved Surfaces in the Las Vegas Valley. Report prepared for Clark County Comprehensive Planning Department, Las Vegas, NV, by University of Nevada, Department of Civil and Environmental Engineering, Las Vegas, NV.

Javitz, H.S., and J.G. Watson (1988). Feasibility Study of Receptor Modeling for Apportioning Utility Contributions to Air Constituents, Deposition Quality and Light Extinction. SRI International, Menlo Park, CA.

John, W., D.N. Fritter, and W. Winklmayer (1991). Resuspension Induced by Impacting Particles. *J. Aerosol Sci.* **22**(6):723-736.

Kendall, M.G. (1951). Regressions, Structure and Functional Relationship, Part I. *Biometrika*, **38**:11-25.

Kendall, M.G. (1952). Regressions, Structure and Functional Relationship, Part II. *Biometrika*, **39**:96-108.

King, D.E. (1977). Evaluation of Interlaboratory Comparison Data on Linear Regression Analysis. In *Methods and Standards for Environmental Measurement*, W.H. Kirchoff, Ed. NBS Publication 464, Gaithersburg, MD.

Kinsey, J.S., and C. Cowherd, Jr. (1992). Fugitive Emissions. In *Air Pollution Engineering Manual*, A.J. Buonicore and W.T. Davis, eds. New York: Van Nostrand Reinhold, pp. 133-146.

Lee, K.W., and M. Ramamurthi (1993). Aerosol Measurement: Principles, Techniques and Applications. K. Willeke and P.A. Baron, Eds. Van Nostrand, Reinhold, New York, NY, pp. 179-205.

Lehrsch, G.A, and P.M. Jolley (1992). Temporal Changes in Wet Aggregate Stability. In *Transactions, ASAE*, **35**(2):493.

Leys, J.F. (1991). Towards a Better Model of the Effect of Prostrate Vegetation Cover on Wind Erosion. *Vegetation* **91**:49-58.

Lillienfeld, P., and J. Dulchinos (1972). Portable Instantaneous Mass Monitoring for Coal Mine Dust. *Am. Indus. Hyg. Assoc. J.,* **33**:136-145.

Lillienfeld, P. (1975). Design and Operation of Dust Measuring Instrumentation Based on the Beta-Radiation Method. *Staub-Reinhalt. Luft*, **25**:458-465.

Lillienfeld, P. (1979). GCA's Model APM-1 Ambient Particulate Monitor-Field Applications and Results. MIE Incorporated, Bedford, MA, Cincinnati, OH.

Linsley, G.S. (1978). Resuspension of the Transuranium Elements - A Review of Existing Data. NRPB-R75, HSMO, London.

Lioy, P.J., J.G. Watson, and J.D. Spengler (1980). APCA Specialty Conference Workshop on Baseline Data for Inhalable Particulate Matter. *JAPCA*, **30**(10):1126-1130.

Lippmann, M. (1989). Air Sampling Instruments for Evaluation of Atmospheric Contaminants, S.V. Hering, Ed. American Conference of Governmental Industrial Hygienists, Cincinnati, OH, pp. 305-336.

Loete, J. (1989). Street Maintenance Section, Department of Public Works, City of Reno, NV. Personal Communication.

Logie, M. (1982). Influence of Roughness Elements and Soil Moisture of Sand to Wind Erosion. *Catena Supp.* **1**:161-173.

Lowenthal, D.H., J.C. Chow, J.G. Watson, G.R. Neuroth, R.B. Robbins, B.P. Shafritz, and R.J. Countess (1992). The Effects of Collinearity on the Ability to Determine Aerosol Contributions from Diesel- and Gasoline-Powered Vehicles using the Chemical Mass Balance Model. *Atmos. Environ.* **26**A(13):2341-2351.

Macias, E.S., and R.B. Husar (1976). Fine Particles, B.Y.H. Liu, Ed. Academic Press, New York, NY, p. 536.

Madansky, A. (1959). The Fitting of Straight Lines when Both Variables are Subject to Error. *J. Am. Statist Assoc.* **54**:173-205.

Marshall, J.K. (1971). Drag Measurements in Roughness Arrays of Varying Density and Distribution. *Agr. Meteorol.* **8**:269-292.

Mathai, C.V., J.G. Watson, Jr., C.F. Rogers, J.C. Chow, I. Tombach, J. Zwicker, T. Cahill, P. Feeney, R. Eldred, M. Pitchford, and P.K. Mueller (1990). Intercomparison of Ambient Aerosol Samplers Used in Western Visibility and Air Quality Studies. *Environ. Sci. Technol.* **24**:1090-1099.

Mollinger, A.M., F.T.M. Nieuwstadt, and B. Scarlett (1993). Model Experiments of the Resuspension Caused by Road Traffic. *Aerosol Sci. Technol.* **19**(3):330-338.

MRI (1996). Improvement of Specific Emission Factors (BACM Project No.1), Final Report. Report prepared under Contract No. 9540 for South Coast Air Quality Management District Contract by Midwest Research Institute, Laramie, WY.

Muleski, G.E., and C. Cowherd (1987). Evaluation of the Effectiveness of Chemical Dust Suppressants on Unpaved Roads. EPA-600/2-87-102. Air and Energy Engineering Research Laboratory, U.S. Environmental Protection Agency, Research Triangle Park, NC.

National Climatic Data Center (1995). Local Climatological Data, Annual Summary with Comparative Data 1995, Las Vegas, NV. National Climatic Data Center, Environmental Data Information Service, National Oceanic and Atmospheric Administration, U.S. Department of Commerce, Asheville, NC.

Nicholson, K.W. (1988). A Review of Particle Resuspension. *Journal of Atmos. Environ.* 22(12):2639-2651.

Nicholson, K.W., J.R. Branson, P. Geiss, and R.J. Cannell (1989). The Effects of Vehicle Activity on Particle Resuspension. *J. Aerosol. Sci.* **20**:1425-1428.

Nicholson, K.W. and J.R. Branson (1990). Factors Affecting Resuspension. In *Highway Pollution: Proceedings of the Third International Symposium*, Munich, West Germany, R.S. Hamilton, D.M. Revitt, and R.M. Harrison, Eds. *Road Traffic* **93**:349-358.

Nicholson, K.W. (1993). Wind Tunnel Experiments on the Resuspension of Particulate Material. *Atmos. Environ.* **27A**(2):181-188.

Nickling, W.G. and J.A. Gillies (1989). Emission of Fine-Grained Particulates from Desert Soils. In *Paleoclimatology and Paleometeorology: Modern and Past Patterns of Global Atmospheric Transport*, M. Leinen and M. Sarnthein, Eds. Kluwer Academic Publishers, pp. 133-165.

Owen, P.R., and D.A. Gillette (1985). Wind Tunnel Constraints on Saltation. In *Proceedings, International Workshop on the Physics of Blown Sand*, May 28-31, 1985. O.E. Barndorff-Nielsen, J.T. Moller, K. Romer-Rasmussen, and B.B. Willetts, Eds. University of Aarhus, pp. 253-269.

Patterson, E.M., and D.A. Gillette (1977). Commonalities in Measured Size Distribution for Aerosols Having a Soil-Derived Component. *J. Geophys. Res.* **82**:2074.

PEDCo. Environmental, Inc. (1981). Study of Street Cleaning Impact on Particulate Levels in Kansas City, Kansas. Prepared under Contact No. 68-02-2535 for U.S. Environmental Protection Agency, Region VII, Kansas City, MO, by PEDCo Environmental Inc.

Peterson, J.T. (1970). Distribution of Sulfur Dioxide over Metropolitan St. Louis as Described by Empirical Orthogonal Functions, and its Relation to Meteorological Parameters. *Atmos. Environ.* **4**:501-518.

Pinnick, R.G., G. Fernandez, B.D. Hinds, C.W. Bruce, R.W. Schaefer, and J.D. Pendleton (1985). Dust Generated by Vehicular Traffic on Unpaved Roadways: Sizes and Infrared Extinction Characteristics. *Aerosol Sci. Techol.* **4**:99-121.

Raupach, M.R. (1992). Drag and Drag Partition on Rough Surfaces. *Boundary-Layer Meteorology* **60**:375-395.

Raupach, M.R., D.A. Gillette, and J.F.Leys (1993). The Effect of Roughness Elements on Wind Erosion Threshold. *J. Geophys. Res.* **98**(D2):3023-3029.

Reeks, M.W., J. Reed, and D. Hall (1985). The Long Term Suspension of Small Particles by a Turbulent Flow – Part III: Resuspension for Rough Surfaces. TPRD/B/0640/N85. CEGB Berkeley Nuclear Labs, Gloucestershire, U.K.

Rice, R.W. (1983). Fundamentals of No-Till Farming. American Association for Vocational Instructional Materials, Athens, GA.

Richmond, K., and D. Ono (1992). An Evaluation of Dispersion Modeling Techniques for the Prediction of Windblown PM_{10} Concentrations within the Mono Lake Air Basin. In *Transactions, PM_{10} Standards and Nontraditional Particulate Source Controls*, J.C. Chow, and D.M. Ono, eds. Air & Waste Management Association, Pittsburgh, PA, pp. 455-473.

Rosbury, K.D., and R.A. Zimmer (1983). Cost-Effectiveness of Dust Controls Used on Unpaved Haul Roads, Volume 1: Results, Analysis, and Conclusions. Report prepared under USBM Contract # J0218021 for the Bureau of Mines, United States Department of the Interior, by PEDCo Environmental, Inc.

Rosinski, J., G. Langer, C.T. Nagamoto, and J.S. Bogard (1976). Generation of Secondary Particles from Single Large Soil Particles upon Impact. In *Proceedings of the Atmosphere-Surface Exchange of Particulate and Gaseous Pollutants*, Richland, WA, 4-6 Sept. 1974. Energy Res. and Dev. Admin. Symp. Ser. CONF740921. Nat. Tech. Inf. Serv., Springfield, VA, pp. 638-647.

Roth, P.M., and J.G. Watson (1993). A Proposed PM_{10} Program Plan for the San Joaquin Valley. Prepared for the San Joaquin Valleywide Air Pollution Study Agency, Fresno, CA, by ENVAIR, San Anselmo, CA, and the Desert Research Institute, Reno, NV. April 1993.

Saucy, D.A., J.R. Anderson, and P.R. Buseck (1987). Cluster Analysis Applied to Atmospheric Aerosol Samples from the Norwegian Arctic. *Atmos. Environ.* **21**:1649-1657.

Seton, Johnson, and Odell Inc. (1983a). Portland Road Dust Demonstration Project. Final Report. Prepared for Department of Public Works, City of Portland, OR.

Seton, Johnson, and Odell Inc. (1983b). Portland Road Dust Demonstration Project. Appendix to Final Report. Prepared for Department of Public Works, City of Portland, OR.

Shao, Y., M.R.. Raupach, and P.A.Findlater (1993). Effect of Saltation Bombardment on the Entrainment of Dust by Wind. *J. Geophys. Res.* **98**(D7):12719-12726.

Solomon, P.A., T. Fall, L. Salmon, G.R. Cass, H.A. Gray, and A. Davidson (1989). Chemical Characteristics of PM_{10} Aerosols Collected in the Los Angeles Area. *JAPCA* **39**:154-163.

Svasek, T.N., and J.H. Terwindt (1974). Measurement of Sand Transport by Wind on a Natural Beach. *Sedimentology* **21**:311-322.

Trijonis, J., M. McGown, M. Pitchford, D. Blumenthal, P. Roberts, W. White, E. Macias, R. Weiss, A. Waggoner, J.G. Watson, J.C. Chow, and R.G. Flocchini (1988). The RESOLVE Project: Visibility Conditions and Causes of Visibility Degradation in the Mojave Desert of California. Santa Fe Research Corporation, Santa Fe, NM.

U.S. Environmental Protection Agency (1978). Guideline on Air Quality Models. EPA-450/2-78-027. U.S. Environmental Protection Agency, Research Triangle Park, NC.

U.S. Environmental Protection Agency (1982). Control Techniques for Particulate Emissions from Stationary Sources. EPA-450/3-81-005. U.S. Environmental Protection Agency, Research Triangle Park, NC.

U.S. Environmental Protection Agency (1986). Guideline on Air Quality Models (Revised). EPA-450/2-78-027R. 40 CFR Part 51, Appendix W. U.S. Environmental Protection Agency, Office of Air Quality Planning and Standards, Research Triangle Park, NC. July 1986.

U.S. Environmental Protection Agency (1987a). PM_{10} SIP Development Guidelines. EPA-450/2-86-001. U.S. Environmental Protection Agency, Research Triangle Park, NC.

U.S. Environmental Protection Agency (1987b). Protocol for Reconciling Differences Among Receptor and Dispersion Models. EPA 450/4-87-008. U.S. Environmental Protection Agency, Research Triangle Park, NC.

U.S. Environmental Protection Agency (1992). PM_{10} Saturation Sampler O&M/QA Manual. U.S. Environmental Protection Agency, Region X, Research Triangle Park, NC.

U.S. Environmental Protection Agency (1994). Compilation of Air Pollution Emission Factors (AP-42), 5th ed. U.S. Environmental Protection Agency, Research Triangle Park, NC.

U.S. Environmental Protection Agency (1995). User's Guide for the Industrial Source Complex (ISC-3) Dispersion Models – Volume II: Description of Model Algorithms. EPA-454/B-95-003b. U.S. Environmental Protection Agency, Office of Air Quality Planning and Standards, Research Triangle Park, NC. September 1995.

U.S. Environmental Protection Agency (1997). World Wide Web Home Page http://www.epa.gov/scram001/index.htm for the Support Center for Regulatory Air Models (SCRAM). U.S. Environmental Protection Agency, Research Triangle Park, NC.

U.S. Government Printing Office (1991). Clean Air Act Amendments of 1990. Conference Report to Accompany S. 1630. House of Representatives, Superintendent of Documents. U.S. Government Printing Office, Washington, DC

Wagner, A. (1987). Industrial Source Complex (ISC) Dispersion Model User's Guide - 2nd ed. (Revised), Volume 1. EPA-450/4-88-002a. U.S. Environmental Protection Agency, Research Triangle Park, NC.

Ward, J.H. (1963). Hierarchical Grouping to Optimize an Objective Function. *J. of the American Statistical Association* **58**:236-244.

Watson, J.G. (1979). Chemical Element Balance Receptor Model Methodology for Assessing the Sources of Fine and Total Particulate Matter. Ph.D. Dissertation, Oregon Graduate Center, Beaverton, OR. University Microfilms International.

Watson, J.G., J.A. Cooper, and J.J. Huntzicker (1984). The Effective Variance Weighting for Least Squares Calculations Applied to the Mass Balance Receptor Model. *Atmos. Environ.* **18**:1347.

Watson, J.G., P.J. Lioy, and P.K. Mueller (1989). The Measurement Process: Precision, Accuracy, and Validity. In *Air Sampling Instruments for Evaluation of Atmospheric Contaminants*, 7th ed., S.V. Hering, Ed. American Conference of Governmental Industrial Hygienists, Cincinnati, OH, pp. 51-57.

Watson, J.G., J.C. Chow, J.E. Core, D.A. Dubose, P.L. Hanraham, R.C. Henry, T.G. Pace, N.F. Robinson, H.J. Williamson, and L. Wijnberg (1990a). Receptor Model Technical Series, Volume III (User's Update), CMB User's Manual, Version 7.0. U.S. Environmental Protection Agency, Research Triangle Park, NC.

Watson, J.G., N.F. Robinson, J.C. Chow, R.C. Henry, B.M. Kim, T.G. Pace, E.L. Meyer, and Q. Nguyen (1990b). The USEPA/DRI Chemical Mass Balance Receptor Model, CMB 7.0. *Environ. Software* **5**(1):38-49.

Watson, J.G., J.C. Chow, and T.G. Pace (1991a). Chemical Mass Balance. In *Data Handling in Science and Technology - Volume 7: Receptor Modeling for Air Quality Management*, P.K. Hopke, Ed. Elsevier Press, New York, NY, pp. 83-116.

Watson, J.G., and J.C. Chow (1992). Data Bases for PM_{10} and $PM_{2.5}$ Chemical Compositions and Source Profiles. In *Transactions, PM_{10} Standards and Nontraditional Particulate Source Controls*, J.C. Chow, and D.M. Ono, Eds. Air & Waste Management Association, Pittsburgh, PA, pp. 61-91.

Watson, J.G., and J.C. Chow (1993). Ambient Air Sampling. In *Aerosol Measurement: Principles, Techniques and Applications*. K. Willeke and P. Baron, Eds. Van Nostrand Reinhold, New York, NY, pp. 622-639.

Watson, J.G., J.C. Chow, Z. Lu, E.M. Fujita, D.H. Lowenthal, D.R. Lawson and L.L. Ashbaugh (1994a). Chemical Mass Balance Source Apportionment of PM_{10} During the Southern California Air Quality Study. *Aerosol Sci. Technol.* **21**:1-36.

Watson, J.G., J.C. Chow, F. Lurmann and S. Musarra (1994b). Ammonium Nitrate, Nitric Acid, and Ammonia Equilibrium in Wintertime Phoenix, Arizona. *J. Air Waste Management Assoc.* **44**:405-412.

Watson, J.G., P.J. Lioy, and P.K. Mueller (1995). The Measurement Process: Precision, Accuracy, and Validity. In *Air Sampling Instruments for Evaluation of Atmospheric Contaminants*, S.V. Hering, Ed. American Conference of Governmental Industrial Hygienists, Cincinnati, OH.

Watson, J.G., J.C. Chow, J.A. Gillies, H. Moosmüller, C.F. Rogers, D. DuBois, and J. Derby (1996). Effectiveness Demonstration of Fugitive Dust Control Methods for Public Unpaved Roads and Unpaved Shoulders on Paved Roads. Final Report. DRI Document No. 685-5200.1F1. Prepared for the San Joaquin Valley Unified Air Pollution Control District, Fresno, CA, by the Desert Research Institute, Reno, NV.

Watson, J.G., J.C. Chow, and C.A. Frazier (1997). X-Ray Fluorescence Analysis of Ambient Air Samples. In *Elemental Analysis of Airborne Particles*, S. Landsberger and M. Creatchman, Eds. Gordon and Breach Publishers, USA.

White, B.R., and H. Mounla (1991). Froude Number Constraints on Saltation in Wind Tunnels. In *Aeolian Grain Transport, Vol. 1*, O.E. Barnddorff-Neilsen and B.B. Willetts, Eds. *Acta Mechanica Suppl.* **2**:145-157.

Wilkinson, L. (1990). SYSTAT: The System for Statistics. SYSTAT Inc., Evanston, IL, p. 677.

Winges, K.D. (1990a). User's Guide for the Fugitive Dust Model (FDM), Volume 1: User's Instructions. Prepared for U.S. Environmental Protection Agency, Region X, Seattle, WA, by TRC Environmental Consultants, Inc., Mountlake Terrace, WA.

Winges, K.D. (1990b). Fugitive Dust Model (FDM) Third Validation Study. Prepared for U.S. Environmental Protection Agency, Region X, Seattle, WA, by TRC Environmental Consultants, Inc., Mountlake Terrace, WA.

Winges, K.D., and F.J. Gombar (1990a). Fugitive Dust Model (FDM) First Validation Study. Prepared for U.S. Environmental Protection Agency, Region X, Seattle, WA, by TRC Environmental Consultants, Inc., Mountlake Terrace, WA.

Winges, K.D., and F.J. Gombar (1990b). Fugitive Dust Model (FDM) Second Validation Study. Prepared for U.S. Environmental Protection Agency, Region X, Seattle, WA, by TRC Environmental Consultants, Inc., Mountlake Terrace, WA.

Zimmer, R, W. Reeser, and P. Cummins (1992). Evaluation of PM_{10} Emission Factors for Paved Streets. In *Transactions: PM_{10} Standards and Nontraditional Particulate Source Controls*, J.C. Chow and D. Ono, Eds. Air & Waste Management Assoc., Pittsburgh, PA, pp. 311-323.

Zobeck, T.M. (1989). Fast-Vac: A Vacuum System to Rapidly Sample Loose Granular Material. In *Transactions of the ASAE*, No. 32, pp. 1316-1318.

APPENDIX A
Data Base Structures

Fugitive Dust and Other Source Contributions to PM_{10}
in Nevada's Las Vegas Valley

Volume II – Final Report

April 18, 1997

Table A-1
Data Base Structure for the Las Vegas Valley PM$_{10}$ Study
Site Description, Location, and Observables
(File: LVSITE.DBF)

Number of data records: 48
Date of last update: 12/05/95

Field	Field Name	Type	Width	Dec	Description
1	SITE	Character	4		Site identification code
2	NAME	Character	27		Site name
3	LOCATION	Character	45		Site address or location
4	COUNTRY	Character	3		Country where site is located
5	LATD	Numeric	2		Latitude, degrees
6	LATM	Numeric	2		Latitude, minutes
7	LATS	Numeric	2		Latitude, seconds
8	LOND	Numeric	3		Longitude, degrees
9	LONM	Numeric	2		Longitude, minutes
10	LONS	Numeric	2		Longitude, seconds
11	ELVM	Numeric	4		Site elevation, meters above mean sea level
12	LATF	Numeric	8	4	Latitude fractional
13	LONF	Numeric	8	4	Longitude fractional
14	UTMN	Numeric	9	4	UTM northing coordinate, Zone 11
15	UTME	Numeric	8	4	UTM easting coordinate, Zone 11
16	TYPE	Character	1		Field available to classify sites
17	TAC	Character	1		Temperature
18	RHP	Character	1		Relative humidity
19	WSM	Character	1		Scalar wind speed
20	WDS	Character	1		Scalar wind direction
21	SGD	Character	1		Standard deviation of wind direction
22	WVM	Character	1		Vector wind speed
23	WDV	Character	1		Vector wind direction
24	WHM	Character	1		Maximum instantaneous wind speed in a given hour
25	WLM	Character	1		Minimum instantaneous wind speed in a given hour
26	O3B	Character	1		Ozone concentration
27	SRW	Character	1		Solar radiation
28	TSC	Character	1		Shelter temperature
29	PTMM	Character	1		Precipitation
30	SCT	Character	1		Turner's stability class
31	SIN	Character	1		Ion concentrations measured on SFS samples

Table A-1
Data Base Structure for the Las Vegas Valley PM$_{10}$ Study
Site Description, Location, and Observables
(File: LVSITE.DBF)

Number of data records: 48
Date of last update: 12/05/95

Field	Field Name	Type	Width	Dec	Description
32	SEL	Character	1		Elemental concentrations measured on SFS samples
33	SCA	Character	1		Carbon concentrations measured on SFS samples
34	SAB	Character	1		Light absorption (b_{abs}) measured on SFS samples
35	SMS	Character	1		PM$_{10}$ mass concentrations measured on SFS samples
36	PEL	Character	1		Elemental concentrations measured on portable PM$_{10}$ samples
37	PAB	Character	1		Light absorption (b_{abs}) measured on portable PM$_{10}$ samples
38	PMS	Character	1		PM$_{10}$ mass concentrations measured on portable PM$_{10}$ samples
39	DEL	Character	1		Elemental concentrations measured on dichotomous samples
40	DMS	Character	1		PM$_{10}$ mass concentrations measured on dichotomous samples
41	HMS	Character	1		PM$_{10}$ mass concentrations measured on size selective inlet high-volume samples
42	BMS	Character	1		Hourly PM$_{10}$ mass concentrations measured on beta-attenuation samples
43	AGENCY	Character	8		Agency Providing data
44	MICRO_MAP	General	10		Map with satellite monitoring site
45	MAP	General	10		Map with base site
46	SITE_DESC	Memo	10		Description of site
47	CMO	Character	1		
48	NOX	Character	1		Nitrogen Oxides
44	COMMENT	Memo	10		Comments about a site or a measurement

Table A-2
Data Base Structure for the FoxPro Field
Descriptions, Naming Conventions, and Measurement
Units Used in the Las Vegas Valley PM10 Study
(File: LVFLDNAM.DBF)

Number of data records: 167
Date of last update: 08/30/96

Field	Field Name	Type	Width	Dec	Description
1	FIELD_NAME	Character		10	The name of the field as it appears in the data base files
2	FIELD_TYPE	Character		1	The code that identifies the type of field in the data base
3	FIELD_LEN	Numeric		3	The width of the field
4	FIELD_DEC	Numeric		3	The number of decimal places used in numeric fields.
5	EXPL	Character		60	Field code definition
6	UNITS	Character		25	measurement units
7	MEMO	Memo		10	A memo field with descriptive supplemental information

Table A-3
Data Base Structure for the Las Vegas Valley PM$_{10}$ Study
Base Site Mass Concentations
(File: AMB_SFS1.DBF)

Number of data records: 191
Date of last update: 09/09/96

Field	Field Name	Type	Width	Dec	Description
1	SITE	Character	10		Site identification number
2	DATE	Date	8		Sampling date
3	SIZE	Character	3		Particle fraction:
					$10 = PM_{10}$ (0-10 μm)
4	STRTHHMM	Character	4		Sample start time
5	STOPHHMM	Character	4		Sample stop time
6	TDURATION	Numeric	5	1	Sample duration (hours for sequential filter sampling system)
7	TID	Character	10		Teflon filter ID
8	QID	Character	10		Quartz filter ID
9	TFFLG	Character	5		Teflon filter flag
10	QFFLG	Character	5		Quartz filter flag
11	MSGF	Character	5		Gravimetry chemical analysis flags
12	BBDF	Character	5		Light absorbtion analysis flag
13	TVOC	Numeric	10	4	Teflon filter volume, (m^3)
14	TVOU	Numeric	10	4	Teflon filter volume uncertainty, (m^3)
15	QVOC	Numeric	10	4	Quartz filter volume, (m^3)
16	QVOU	Numeric	10	4	Quartz filter volume uncertainty, (m^3)
17	MSGC	Numeric	10	4	Mass by gravimetry, (μg/m^3)
18	BBDC	Numeric	10		B_{abs} by transmission densitometry, (Mm^{-1})
19	BBDU	Numeric	10	4	B_{abs} uncertainty by transmission densitometry, (Mm^{-1})
20	SPSUMC	Numeric	10	4	Sum of measured species concentrations, (μg/m^3)
21	SPSUMU	Numeric	10	4	Sum of measured species uncertainty, (μg/m^3)
22	MSGU	Numeric	10	4	Mass uncertainty, (μg/m^3)
23	COMMENT	Memo	10		Comments

Table A-4
Data Base Structure for the Las Vegas Valley PM_{10} Study
Base Site Chemical Analysis Concentrations
(File: AMB_SFS2.DBF)

Number of data records: 37
Date of last update: 06/26/96

Field	Field Name	Type	Width	Dec	Description
1	SITE	Character	10		Site identification number
2	DATE	Date	8		Sampling date
3	SIZE	Character	3		Particle fraction:
					$10 = PM_{10}$ (0-10 μm)
4	STRTHHMM	Character	4		Sample start time
5	STOPHHMM	Character	4		Sample stop time
6	TDURATION	Numeric	5	1	Duration (minutes)
7	TID	Character	10		Teflon filter ID
8	QID	Character	10		Quartz filter ID
9	TFFLG	Character	5		Teflon filter flag
10	QFFLG	Character	5		Quartz filter flag
11	MSGF	Character	5		Gravimetry chemical analysis flags
12	BBDF	Character	5		Light absorbtion analysis flag
13	HNIF	Character	5		Volatilized nitrate analysis flag
14	ANIF	Character	5		Anion chemical analysis flags
15	N4CF	Character	5		Ammonium chemical analysis flags
16	KPAF	Character	5		Potassium ion chemical analysis flags
17	OETF	Character	5		Carbon chemical analysis flags
18	ELXF	Character	5		Element chemical analysis flags
19	TVOC	Numeric	10	4	Teflon filter volume (m^3)
20	TVOU	Numeric	10	4	Teflon filter volume (m^3) uncertainty
21	QVOC	Numeric	10	4	Quartz filter volume, (m^3)
22	QVOU	Numeric	10	4	Quartz filter volume uncertainty, (m^3)
23	MSGC	Numeric	10	4	Mass by gravimetry, (μg/m^3)
24	MSGU	Numeric	10	4	Mass uncertainty, (μg/m^3)
25	BBDC	Numeric	10	4	B_{abs} by transmission densitometry, (Mm^{-1})
26	BBDU	Numeric	10	4	B_{abs} uncertainty by transmission densitometry, (Mm^{-1})
27	HNIC	Numeric	10	4	Volitalized Nitrate by ion chromatography, (μg/m^3)
28	HNIU	Numeric	10	4	Volitalized Nitrate uncertainty by ion chromatography, (μg/m^3)
29	CLIC	Numeric	10	4	Chloride concentration by ion chromatography, (μg/m^3)
30	CLIU	Numeric	10	4	Chloride uncertainty, (μg/m^3)
31	N3IC	Numeric	10	4	Nitrate concentration by ion chromatography, (μg/m^3)
32	N3IU	Numeric	10	4	Nitrate uncertainty, (μg/m^3)
33	S4IC	Numeric	10	4	Sulfate concentration by ion chromatography, (μg/m^3)
34	S4IU	Numeric	10	4	Sulfate uncertainty, (μg/m^3)
35	N4CC	Numeric	10	4	Ammonium concentration by automated colorimetry, (μg/m^3)
36	N4CU	Numeric	10	4	Ammonium uncertainty, (μg/m^3)
37	KPAC	Numeric	10	4	Potassium ion concentration by atomic absorbtion, (μg/m^3)
38	KPAU	Numeric	10	4	Potassium ion concentration uncertainty by atomic absorbtion, (μg/m^3)

Table A-4
Data Base Structure for the Las Vegas Valley PM$_{10}$ Study
Base Site Chemical Analysis Concentrations
(File: AMB_SFS2.DBF)

Number of data records: 37
Date of last update: 06/26/96

Field	Field Name	Type	Width	Dec	Description
39	OCTC	Numeric	10	4	Organic carbon concentration by thermal/optical reflectance, (μg/m^3)
40	OCTU	Numeric	10	4	Organic carbon uncertainty, (μg/m^3)
41	ECTC	Numeric	10	4	Elemental carbon concentration by thermal/optical reflectance, (μg/m^3)
42	ECTU	Numeric	10	4	Elemental carbon uncertainty, (μg/m3)
43	TCTC	Numeric	10	4	Total carbon concentration by thermal/optical reflectance, (μg/m^3)
44	TCTU	Numeric	10	4	Total carbon uncertainty, (μg/m3)
45	NAXC	Numeric	10	4	Sodium concentration by x-ray fluorescence, (μg/m^3)
46	NAXU	Numeric	10	4	Sodium uncertainty, (μg/m^3)
47	MGXC	Numeric	10	4	Magnesium concentration by x-ray fluorescence, (μg/m^3)
48	MGXU	Numeric	10	4	Magnesium uncertainty, (μg/m^3)
49	ALXC	Numeric	10	4	Aluminum concentration by x-ray fluorescence, (μg/m^3)
50	ALXU	Numeric	10	4	Aluminum uncertainty, (μg/m^3)
51	SIXC	Numeric	10	4	Silicon concentration by x-ray fluorescence, (μg/m^3)
52	SIXU	Numeric	10	4	Silicon uncertainty, (μg/m^3)
53	PHXC	Numeric	10	4	Phosphorous concentration by x-ray fluorescence, (μg/m^3)
54	PHXU	Numeric	10	4	Phosphorous uncertainty, (μg/m^3)
55	SUXC	Numeric	10	4	Sulfur concentration by x-ray fluorescence, (μg/m^3)
56	SUXU	Numeric	10	4	Sulfur uncertainty, (μg/m^3)
57	CLXC	Numeric	10	4	Chlorine concentration by x-ray fluorescence, (μg/m^3)
58	CLXU	Numeric	10	4	Chlorine uncertainty, (μg/m^3)
59	KPXC	Numeric	10	4	Potassium concentration by x-ray fluorescence, (μg/m^3)
60	KPXU	Numeric	10	4	Potassium uncertainty, (μg/m^3)
61	CAXC	Numeric	10	4	Calcium concentration by x-ray fluorescence, (μg/m^3)
62	CAXU	Numeric	10	4	Calcium uncertainty, (μg/m^3)
63	TIXC	Numeric	10	4	Titanium concentration by x-ray fluorescence, (μg/m^3)
64	TIXU	Numeric	10	4	Titanium uncertainty, (μg/m^3)
65	VAXC	Numeric	10	4	Vanadium concentration by x-ray fluorescence, (μg/m^3)
66	VAXU	Numeric	10	4	Vanadium uncertainty, (μg/m^3)
67	CRXC	Numeric	10	4	Chromium concentration by x-ray fluorescence, (μg/m^3)
68	CRXU	Numeric	10	4	Chromium uncertainty, (μg/m^3)
69	MNXC	Numeric	10	4	Manganese concentration by x-ray fluorescence, (μg/m^3)
70	MNXU	Numeric	10	4	Manganese uncertainty, (μg/m^3)
71	FEXC	Numeric	10	4	Iron concentration by x-ray fluorescence, (μg/m^3)
72	FEXU	Numeric	10	4	Iron uncertainty, (μg/m^3)
73	COXC	Numeric	10	4	Cobalt concentration by x-ray fluorescence, (μg/m^3)
74	COXU	Numeric	10	4	Cobalt uncertainty, (μg/m^3)
75	NIXC	Numeric	10	4	Nickel concentration by x-ray fluorescence, (μg/m^3)
76	NIXU	Numeric	10	4	Nickel uncertainty, (μg/m^3)

Table A-4
Data Base Structure for the Las Vegas Valley PM$_{10}$ Study
Base Site Chemical Analysis Concentrations
(File: AMB_SFS2.DBF)

Number of data records: 37
Date of last update: 06/26/96

Field	Field Name	Type	Width	Dec	Description
77	CUXC	Numeric	10	4	Copper concentration by x-ray fluorescence, (μg/m^3)
78	CUXU	Numeric	10	4	Copper uncertainty, (μg/m^3)
79	ZNXC	Numeric	10	4	Zinc concentration by x-ray fluorescence, (μg/m^3)
80	ZNXU	Numeric	10	4	Zinc uncertainty, (μg/m^3)
81	GAXC	Numeric	10	4	Gallium concentration by x-ray fluorescence, (μg/m^3)
82	GAXU	Numeric	10	4	Gallium uncertainty, (μg/m^3)
83	ASXC	Numeric	10	4	Arsenic concentration by x-ray fluorescence, (μg/m^3)
84	ASXU	Numeric	10	4	Arsenic uncertainty, (μg/m^3)
85	SEXC	Numeric	10	4	Selenium concentration by x-ray fluorescence, (μg/m^3)
86	SEXU	Numeric	10	4	Selenium uncertainty, (μg/m^3)
87	BRXC	Numeric	10	4	Bromine concentration by x-ray fluorescence, (μg/m^3)
88	BRXU	Numeric	10	4	Bromine uncertainty, (μg/m^3)
89	RBXC	Numeric	10	4	Rubidium concentration by x-rayfluorescence, (μg/m3)
90	RBXU	Numeric	10	4	Rubidium uncertainty, (μg/m^3)
91	SRXC	Numeric	10	4	Strontium concentration by x-ray fluorescence, (μg/m^3)
92	SRXU	Numeric	10	4	Strontium uncertainty, (μg/m^3)
93	YTXC	Numeric	10	4	Yttrium concentration by x-ray fluorescence, (μg/m^3)
94	YTXU	Numeric	10	4	Yttrium uncertainty, (μg/m^3)
95	ZRXC	Numeric	10	4	Zirconium concentration by x-ray fluorescence, (μg/m^3)
96	ZRXU	Numeric	10	4	Zirconium uncertainty, (μg/m^3)
97	MOXC	Numeric	10	4	Molybdenum concentration by x-ray fluorescence, (μg/m^3)
98	MOXU	Numeric	10	4	Molybdenum uncertainty, (μg/m^3)
99	PDXC	Numeric	10	4	Palladium concentration by x-ray fluorescence, (μg/m^3)
100	PDXU	Numeric	10	4	Palladium uncertainty, (μg/m^3)
101	AGXC	Numeric	10	4	Silver concentration by x-ray fluorescence, (μg/m^3)
102	AGXU	Numeric	10	4	Silver uncertainty, (μg/m^3)
103	CDXC	Numeric	10	4	Cadmium concentration by x-ray fluorescence, (μg/m^3)
104	CDXU	Numeric	10	4	Cadmium uncertainty, (μg/m^3)
105	INXC	Numeric	10	4	Indium concentration by x-ray fluorescence, (μg/m^3)
106	INXU	Numeric	10	4	Indium uncertainty, (μg/m^3)
107	SNXC	Numeric	10	4	Tin concentration by x-ray fluorescence,(μg/m^3)
108	SNXU	Numeric	10	4	Tin uncertainty, (μg/m^3)
109	SBXC	Numeric	10	4	Antimony concentration by x-ray fluorescence, (μg/m^3)
110	SBXU	Numeric	10	4	Antimony uncertainty, (μg/m^3)
111	BAXC	Numeric	10	4	Barium concentration by x-ray fluorescence, (μg/m^3)
112	BAXU	Numeric	10	4	Barium uncertainty, (μg/m^3)
113	LAXC	Numeric	10	4	Lanthanum concentration by x-ray fluorescence, (μg/m^3)
114	LAXU	Numeric	10	4	Lanthanum uncertainty, (μg/m^3)

Number of data records: 37
Date of last update: 06/26/96

Field	Field Name	Type	Width	Dec	Description
115	AUXC	Numeric	10	4	Gold concentration by x-ray fluorescence, (μg/m^3)
116	AUXU	Numeric	10	4	Gold uncertainty, (μg/m^3)
117	HGXC	Numeric	10	4	Mercury concentration by x-ray fluorescence, (μg/m^3)
118	HGXU	Numeric	10	4	Mercury uncertainty, (μg/m^3)
119	TLXC	Numeric	10	4	Thallium concentration by x-ray fluorescence, (μg/m^3)
120	TLXU	Numeric	10	4	Thallium uncertainty, (μg/m^3)
121	PBXC	Numeric	10	4	Lead concentration by x-ray fluorescence, (μg/m^3)
122	PBXU	Numeric	10	4	Lead uncertainty, (μg/m^3)
123	URXC	Numeric	10	4	Uranium concentration by x-ray fluorescence, (μg/m^3)
124	URXU	Numeric	10	4	Uranium uncertainty, (μg/m3)
125	SPSUMC	Numeric	10	4	Sum of measured species concentrations, (μg/m^3)
126	SPSUMU	Numeric	10	4	Sum of measured species uncertainty, (μg/m^3)
127	COMMENT	Memo	10		Comments

Table A-5
Data Base Structure for the Las Vegas Valley PM$_{10}$ Study
Satellite Site Mass Concentrations
(File: AMB_POR1.DBF)

Number of data records: 781
Date of last update: 08/21/96

Field	Field Name	Type	Width	Dec	Description
1	SITE	Character	10		Site identification number
2	DATE	Date	8		Sampling date
3	SIZE	Character	3		Particle fraction:
					$10 = PM_{10}$ (0-10 μm)
4	STRTHHMM	Character	4		Sample start time
5	STOPHHMM	Character	4		Sample stop time
6	TDURATION	Numeric	5	1	Sample duration (hours for portable sampling system)
7	TID	Character	10		Teflon filter ID
8	TFFLG	Character	5		Teflon filter flag
9	MSGF	Character	5		Gravimetry chemical analysis flags
10	BBDF	Character	5		Light absorbtion analysis flag
11	TVOC	Numeric	10	4	Teflon filter volume, (m^3)
12	TVOU	Numeric	10	4	Teflon filter volume uncertainty, (m^3)
13	MSGC	Numeric	10	4	Mass by gravimetry, (μg/m^3)
14	MSGU	Numeric	10	4	Mass uncertainty, (μg/m^3)
15	BBDC	Numeric	10	4	b_{abs} by transmission densitometry, (Mm^{-1})
16	BBDU	Numeric	10	4	b_{abs} uncertainty by transmission densitometry, (Mm^{-1})
17	SPSUMC	Numeric	10	4	Sum of measured species concentrations, (μg/m^3)
18	SPSUMU	Numeric	10	4	Sum of measured species uncertainty, (μg/m^3)
19	COMMENT	Memo	10		Comments

Table A-6
Data Base Structure for the Las Vegas Valley PM$_{10}$ Study
Satellite Site Chemical Analysis Concentrations
(File: AMB_POR2.DBF)

Number of data records: 424
Date of last update: 06/27/96

Field	Field Name	Type	Width	Dec	Description
1	SITE	Character	10		Site identification number
2	DATE	Date	8		Sampling date
3	SIZE	Character	3		Particle fraction:
					$10 = PM_{10}$ (0-10 μm)
4	STRTHHMM	Character	4		Sample start time
5	STOPHHMM	Character	4		Sample stop time
6	TDURATION	Numeric	5	1	Duration (minutes)
7	TID	Character	10		Teflon filter ID
8	TFFLG	Character	5		Teflon filter flag
9	MSGF	Character	5		Gravimetry chemical analysis flags
10	BBDF	Character	5		Light absorbtion analysis flag
11	ELXF	Character	5		Element chemical analysis flags
12	TVOC	Numeric	10	4	Teflon filter volume (m^3)
13	TVOU	Numeric	10	4	Teflon filter volume (m^3) uncertainty
14	MSGC	Numeric	10	4	Mass by gravimetry, (μg/m^3)
15	MSGU	Numeric	10	4	Mass uncertainty, (μg/m^3)
16	BBDC	Numeric	10	4	B$_{abs}$ by transmission densitometry, (Mm^{-1})
17	BBDU	Numeric	10	4	B$_{abs}$ uncertainty by transmission densitometry, (Mm^{-1})
18	ALXC	Numeric	10	4	Aluminum concentration by x-ray fluorescence, (μg/m^3)
19	ALXU	Numeric	10	4	Aluminum uncertainty, (μg/m^3)
20	SIXC	Numeric	10	4	Silicon concentration by x-ray fluorescence, (μg/m^3)
21	SIXU	Numeric	10	4	Silicon uncertainty, (μg/m^3)
22	SUXC	Numeric	10	4	Sulfur concentration by x-ray fluorescence, (μg/m^3)
23	SUXU	Numeric	10	4	Sulfur uncertainty, (μg/m^3)
24	KPXC	Numeric	10	4	Potassium concentration by x-ray fluorescence, (μg/m^3)
25	KPXU	Numeric	10	4	Potassium uncertainty, (μg/m^3)
26	CAXC	Numeric	10	4	Calcium concentration by x-ray fluorescence, (μg/m^3)
27	CAXU	Numeric	10	4	Calcium uncertainty, (μg/m^3)
28	FEXC	Numeric	10	4	Iron concentration by x-ray fluorescence, (μg/m^3)
29	FEXU	Numeric	10	4	Iron uncertainty, (μg/m^3)
30	SPSUMC	Numeric	10	4	Sum of measured species concentrations, (μg/m^3)
31	SPSUMU	Numeric	10	4	Sum of measured species uncertainty, (μg/m^3)
32	COMMENT	Memo	10		Comments

Table A-7
Data Base Structure for the Las Vegas Valley PM$_{10}$ Study
Composite and Specific Source Profile Data in Percent of Total Mass
(File: LVSORPCT.DBF)

Number of data records: 88
Date of last update: 08/13/96

Field	Field Name	Type	Width	Dec	Description
1	SN	Character	6		Source identification code
2	MNEMONIC	Character	8		Mnemonic site identifier
3	SIZE	Character	2		Particle fraction:
					$\quad$ 10=PM$_{10}$ (0-10 μm)
					$\quad$ F=PM$_{2.5}$ (0-2.5 μm)
4	CLIC	Numeric	10	6	Chloride concentration by ion chromatography, (percent of mass)
5	CLIU	Numeric	10	6	Chloride uncertainty, (percent of mass)
6	N3IC	Numeric	10	6	Nitrate concentration by ion chromatography, (percent of mass)
7	N3IU	Numeric	10	6	Nitrate uncertainty, (percent of mass)
8	S4IC	Numeric	10	6	Sulfate concentration by ion chromatography, (percent of mass)
9	S4IU	Numeric	10	6	Sulfate uncertainty, (percent of mass)
10	N4CC	Numeric	10	6	Ammonium concentration by automated chromatography, (percent of mass)
11	N4CU	Numeric	10	6	Ammonium uncertainty, (percent of mass)
12	NAAC	Numeric	10	6	Soluble sodium concentration by atomic absorption, (percent of mass)
13	NAAU	Numeric	10	6	Soluble sodium uncertainty, (percent of mass)
14	KPAC	Numeric	10	6	Potassium concentration by atomic absorption, (percent of mass)
15	KPAU	Numeric	10	6	Potassium uncertainty, (percent of mass)
16	OCTC	Numeric	10	6	Organic carbon concentration by thermal/ optical reflectance, (percent of mass)
17	OCTU	Numeric	10	6	Organic carbon uncertainty, (percent of mass)
18	ECTC	Numeric	10	6	Elemental carbon concentration by thermal/ optical reflectance, (percent of mass)
19	ECTU	Numeric	10	6	Elemental carbon uncertainty, (percent of mass)
20	NAXC	Numeric	10	6	Sodium concentration by x-ray fluorescence, (percent of mass)
21	NAXU	Numeric	10	6	Sodium uncertainty
22	MGXC	Numeric	10	6	Magnesium concentration by x-ray fluorescence, (percent of mass)
23	MGXU	Numeric	10	6	Magnesium uncertainty
24	ALXC	Numeric	10	6	Aluminum concentration by x-ray fluorescence, (percent of mass)
25	ALXU	Numeric	10	6	Aluminum uncertainty, (percent of mass)
26	SIXC	Numeric	10	6	Silicon concentration by x-ray fluorescence, (percent of mass)
27	SIXU	Numeric	10	6	Silicon uncertainty, (percent of mass)
28	PHXC	Numeric	10	6	Phosphorous concentration by x-ray fluorescence, (percent of mass)

Table A-7
Data Base Structure for the Las Vegas Valley PM$_{10}$ Study
Composite and Specific Source Profile Data in Percent of Total Mass
(File: LVSORPCT.DBF)

Number of data records: 88
Date of last update: 08/13/96

Field	Field Name	Type	Width	Dec	Description
29	PHXU	Numeric	10	6	Phosphorous uncertainty, (percent of mass)
30	SUXC	Numeric	10	6	Sulfur concentration by x-ray fluorescence, (percent of mass)
31	SUXU	Numeric	10	6	Sulfur uncertainty, (percent of mass)
32	CLXC	Numeric	10	6	Chlorine concentration by x-ray fluorescence, (percent of mass)
33	CLXU	Numeric	10	6	Chlorine uncertainty, (percent of mass)
34	KPXC	Numeric	10	6	Potassium concentration by x-ray fluorescence, (percent of mass)
35	KPXU	Numeric	10	6	Potassium uncertainty, (percent of mass)
36	CAXC	Numeric	10	6	Calcium concentration by x-ray fluorescence, (percent of mass)
37	CAXU	Numeric	10	6	Calcium uncertainty, (percent of mass)
38	TIXC	Numeric	10	6	Titanium concentration by x-ray fluorescence, (percent of mass)
39	TIXU	Numeric	10	6	Titanium uncertainty, (percent of mass)
40	VAXC	Numeric	10	6	Vanadium concentration by x-ray fluorescence, (percent of mass)
41	VAXU	Numeric	10	6	Vanadium uncertainty, (percent of mass)
42	CRXC	Numeric	10	6	Chromium concentration by x-ray fluorescence, (percent of mass)
43	CRXU	Numeric	10	6	Chromium uncertainty, (percent of mass)
44	MNXC	Numeric	10	6	Manganese concentration by x-ray fluorescence, (percent of mass)
45	MNXU	Numeric	10	6	Manganese uncertainty, (percent of mass)
46	FEXC	Numeric	10	6	Iron concentration by x-ray fluorescence, (percent of mass)
47	FEXU	Numeric	10	6	Iron uncertainty, (percent of mass)
48	COXC	Numeric	10	6	Cobalt concentration by x-ray fluorescence, (percent of mass)
49	COXU	Numeric	10	6	Cobalt uncertainty, (percent of mass)
50	NIXC	Numeric	10	6	Nickel concentration by x-ray fluorescence, (percent of mass)
51	NIXU	Numeric	10	6	Nickel uncertainty, (percent of mass)
52	CUXC	Numeric	10	6	Copper concentration by x-ray fluorescence, (percent of mass)
53	CUXU	Numeric	10	6	Copper uncertainty, (percent of mass)
54	ZNXC	Numeric	10	6	Zinc concentration by x-ray fluorescence, (percent of mass)
55	ZNXU	Numeric	10	6	Zinc uncertainty, (percent of mass)
56	GAXC	Numeric	10	6	Gallium concentration by x-ray fluorescence, (percent of mass)
57	GAXU	Numeric	10	6	Gallium uncertainty, (percent of mass)
58	ASXC	Numeric	10	6	Arsenic concentration by x-ray fluorescence, (percent of mass)
59	ASXU	Numeric	10	6	Arsenic uncertainty, (percent of mass)
60	SEXC	Numeric	10	6	Selenium concentration by x-ray fluorescence, (percent of mass)
61	SEXU	Numeric	10	6	Selenium uncertainty, (percent of mass)
62	BRXC	Numeric	10	6	Bromine concentration by x-ray

Table A-7
Data Base Structure for the Las Vegas Valley PM$_{10}$ Study
Composite and Specific Source Profile Data in Percent of Total Mass
(File: LVSORPCT.DBF)

Number of data records: 88
Date of last update: 08/13/96

Field	Field Name	Type	Width	Dec	Description
					fluorescence, (percent of mass)
63	BRXU	Numeric	10	6	Bromine uncertainty, (percent of mass)
64	RBXC	Numeric	10	6	Rubidium concentration by x-ray fluorescence, (percent of mass)
65	RBXU	Numeric	10	6	Rubidium uncertainty, (percent of mass)
66	SRXC	Numeric	10	6	Strontium concentration by x-ray fluorescence, (percent of mass)
67	SRXU	Numeric	10	6	Strontium uncertainty, (percent of mass)
68	YTXC	Numeric	10	6	Yttrium concentration by x-ray fluorescence, (percent of mass)
69	YTXU	Numeric	10	6	Yttrium uncertainty, (percent of mass)
70	ZRXC	Numeric	10	6	Zirconium concentration by x-ray fluorescence, (percent of mass)
71	ZRXU	Numeric	10	6	Zirconium uncertainty, (percent of mass)
72	MOXC	Numeric	10	6	Molybdenum concentration by x-ray fluorescence, (percent of mass)
73	MOXU	Numeric	10	6	Molybdenum uncertainty, (percent of mass)
74	PDXC	Numeric	10	6	Palladium concentration by x-ray fluorescence, (percent of mass)
75	PDXU	Numeric	10	6	Palladium uncertainty, (percent of mass)
76	AGXC	Numeric	10	6	Silver concentration by x-ray fluorescence, (percent of mass)
77	AGXU	Numeric	10	6	Silver uncertainty, (percent of mass)
78	CDXC	Numeric	10	6	Cadmium concentration by x-ray fluorescence, (percent of mass)
79	CDXU	Numeric	10	6	Cadmium uncertainty, (percent of mass)
80	INXC	Numeric	10	6	Indium concentration by x-ray fluorescence, (percent of mass)
81	INXU	Numeric	10	6	Indium uncertainty, (percent of mass)
82	SNXC	Numeric	10	6	Tin concentration by x-ray fluorescence, (percent of mass)
83	SNXU	Numeric	10	6	Tin uncertainty, (percent of mass)
84	SBXC	Numeric	10	6	Antimony concentration by x-ray fluorescence, (percent of mass)
85	SBXU	Numeric	10	6	Antimony uncertainty, (percent of mass)
86	BAXC	Numeric	10	6	Barium concentration by x-ray fluorescence, (percent of mass)
87	BAXU	Numeric	10	6	Barium uncertainty, (percent of mass)
88	LAXC	Numeric	10	6	Lanthanum concentration by x-ray fluorescence, (percent of mass)
89	LAXU	Numeric	10	6	Lanthanum uncertainty, (percent of mass)
90	AUXC	Numeric	10	6	Gold concentration by x-ray fluorescence, (percent of mass)
91	AUXU	Numeric	10	6	Gold uncertainty, (percent of mass)
92	HGXC	Numeric	10	6	Mercury concentration by x-ray fluorescence, (percent of mass)
93	HGXU	Numeric	10	6	Mercury uncertainty, (percent of mass)
94	TLXC	Numeric	10	6	Thallium concentration by x-ray fluorescence, (percent of mass)

Table A-7
Data Base Structure for the Las Vegas Valley PM_{10} Study
Composite and Specific Source Profile Data in Percent of Total Mass
(File: LVSORPCT.DBF)

Number of data records: 88
Date of last update: 08/13/96

Field	Field Name	Type	Width	Dec	Description
95	TLXU	Numeric	10	6	Thallium uncertainty, (percent of mass)
96	PBXC	Numeric	10	6	Lead concentration by x-ray fluorescence, (percent of mass)
97	PBXU	Numeric	10	6	Lead uncertainty, (percent of mass)
98	URXC	Numeric	10	6	Uranium concentration by x-ray fluorescence, (percent of mass)
99	URXU	Numeric	10	6	Uranium uncertainty, (percent of mass)

Table A-8
Data Base Structure for the Las Vegas Valley PM_{10} Study
Composite and Specific Source Profile Data in Fraction of Total Mass
(File: LVSORFRC.DBF)

Number of data records: 88
Date of last update: 09/04/96

Field	Field Name	Type	Width	Dec	Description
1	SN	Character	6		Source identification code
2	MNEMONIC	Character	8		Mnemonic site identifier
3	SIZE	Character	2		Particle fraction: $10 = PM_{10}$ (0-10 μm) $F = PM_{2.5}$ (0-2.5 μm)
4	CLIC	Numeric	10	6	Chloride concentration by ion chromatography, (fraction of mass)
5	CLIU	Numeric	10	6	Chloride uncertainty, (fraction of mass)
6	N3IC	Numeric	10	6	Nitrate concentration by ion chromatography, (fraction of mass)
7	N3IU	Numeric	10	6	Nitrate uncertainty, (fraction of mass)
8	S4IC	Numeric	10	6	Sulfate concentration by ion chromatography, (fraction of mass)
9	S4IU	Numeric	10	6	Sulfate uncertainty, (fraction of mass)
10	N4CC	Numeric	10	6	Ammonium concentration by automated chromatography, (fraction of mass)
11	N4CU	Numeric	10	6	Ammonium uncertainty, (fraction of mass)
12	NAAC	Numeric	10	6	Soluble sodium concentration by atomic absorption, (fraction of mass)
13	NAAU	Numeric	10	6	Soluble sodium uncertainty, (fraction of mass)
14	KPAC	Numeric	10	6	Potassium concentration by atomic absorption, (fraction of mass)
15	KPAU	Numeric	10	6	Potassium uncertainty, (fraction of mass)
16	OCTC	Numeric	10	6	Organic carbon concentration by thermal/ optical reflectance, (fraction of mass)
17	OCTU	Numeric	10	6	Organic carbon uncertainty, (fraction of mass)
18	ECTC	Numeric	10	6	Elemental carbon concentration by thermal/ optical reflectance, (fraction of mass)
19	ECTU	Numeric	10	6	Elemental carbon uncertainty, (fraction of mass)
20	NAXC	Numeric	10	6	Sodium concentration by x-ray fluorescence, (fraction of mass)
21	NAXU	Numeric	10	6	Sodium uncertainty
22	MGXC	Numeric	10	6	Magnesium concentration by x-ray fluorescence, (fraction of mass)
23	MGXU	Numeric	10	6	Magnesium uncertainty
24	ALXC	Numeric	10	6	Aluminum concentration by x-ray fluorescence, (fraction of mass)
25	ALXU	Numeric	10	6	Aluminum uncertainty, (fraction of mass)
26	SIXC	Numeric	10	6	Silicon concentration by x-ray fluorescence, (fraction of mass)
27	SIXU	Numeric	10	6	Silicon uncertainty, (fraction of mass)
28	PHXC	Numeric	10	6	Phosphorous concentration by x-ray fluorescence, (fraction of mass)

Table A-8
Data Base Structure for the Las Vegas Valley PM$_{10}$ Study
Composite and Specific Source Profile Data in Fraction of Total Mass
(File: LVSORFRC.DBF)

Number of data records: 88
Date of last update: 09/04/96

Field	Field Name	Type	Width	Dec	Description
29	PHXU	Numeric	10	6	Phosphorous uncertainty, (fraction of mass)
30	SUXC	Numeric	10	6	Sulfur concentration by x-ray fluorescence, (fraction of mass)
31	SUXU	Numeric	10	6	Sulfur uncertainty, (fraction of mass)
32	CLXC	Numeric	10	6	Chlorine concentration by x-ray fluorescence, (fraction of mass)
33	CLXU	Numeric	10	6	Chlorine uncertainty, (fraction of mass)
34	KPXC	Numeric	10	6	Potassium concentration by x-ray fluorescence, (fraction of mass)
35	KPXU	Numeric	10	6	Potassium uncertainty, (fraction of mass)
36	CAXC	Numeric	10	6	Calcium concentration by x-ray fluorescence, (fraction of mass)
37	CAXU	Numeric	10	6	Calcium uncertainty, (fraction of mass)
38	TIXC	Numeric	10	6	Titanium concentration by x-ray fluorescence, (fraction of mass)
39	TIXU	Numeric	10	6	Titanium uncertainty, (fraction of mass)
40	VAXC	Numeric	10	6	Vanadium concentration by x-ray fluorescence, (fraction of mass)
41	VAXU	Numeric	10	6	Vanadium uncertainty, (fraction of mass)
42	CRXC	Numeric	10	6	Chromium concentration by x-ray fluorescence, (fraction of mass)
43	CRXU	Numeric	10	6	Chromium uncertainty, (fraction of mass)
44	MNXC	Numeric	10	6	Manganese concentration by x-ray fluorescence, (fraction of mass)
45	MNXU	Numeric	10	6	Manganese uncertainty, (fraction of mass)
46	FEXC	Numeric	10	6	Iron concentration by x-ray fluorescence, (fraction of mass)
47	FEXU	Numeric	10	6	Iron uncertainty, (fraction of mass)
48	COXC	Numeric	10	6	Cobalt concentration by x-ray fluorescence, (fraction of mass)
49	COXU	Numeric	10	6	Cobalt uncertainty, (fraction of mass)
50	NIXC	Numeric	10	6	Nickel concentration by x-ray fluorescence, (fraction of mass)
51	NIXU	Numeric	10	6	Nickel uncertainty, (fraction of mass)
52	CUXC	Numeric	10	6	Copper concentration by x-ray fluorescence, (fraction of mass)
53	CUXU	Numeric	10	6	Copper uncertainty, (fraction of mass)
54	ZNXC	Numeric	10	6	Zinc concentration by x-ray fluorescence, (fraction of mass)
55	ZNXU	Numeric	10	6	Zinc uncertainty, (fraction of mass)
56	GAXC	Numeric	10	6	Gallium concentration by x-ray fluorescence, (fraction of mass)
57	GAXU	Numeric	10	6	Gallium uncertainty, (fraction of mass)
58	ASXC	Numeric	10	6	Arsenic concentration by x-ray fluorescence, (fraction of mass)
59	ASXU	Numeric	10	6	Arsenic uncertainty, (fraction of mass)
60	SEXC	Numeric	10	6	Selenium concentration by x-ray fluorescence, (fraction of mass)
61	SEXU	Numeric	10	6	Selenium uncertainty, (fraction of mass)
62	BRXC	Numeric	10	6	Bromine concentration by x-ray

Table A-8
Data Base Structure for the Las Vegas Valley PM$_{10}$ Study
Composite and Specific Source Profile Data in Fraction of Total Mass
(File: LVSORFRC.DBF)

Number of data records: 88
Date of last update: 09/04/96

Field	Field Name	Type	Width	Dec	Description
					fluorescence, (fraction of mass)
63	BRXU	Numeric	10	6	Bromine uncertainty, (fraction of mass)
64	RBXC	Numeric	10	6	Rubidium concentration by x-ray fluorescence, (fraction of mass)
65	RBXU	Numeric	10	6	Rubidium uncertainty, (fraction of mass)
66	SRXC	Numeric	10	6	Strontium concentration by x-ray fluorescence, (fraction of mass)
67	SRXU	Numeric	10	6	Strontium uncertainty, (fraction of mass)
68	YTXC	Numeric	10	6	Yttrium concentration by x-ray fluorescence, (fraction of mass)
69	YTXU	Numeric	10	6	Yttrium uncertainty, (fraction of mass)
70	ZRXC	Numeric	10	6	Zirconium concentration by x-ray fluorescence, (fraction of mass)
71	ZRXU	Numeric	10	6	Zirconium uncertainty, (fraction of mass)
72	MOXC	Numeric	10	6	Molybdenum concentration by x-ray fluorescence, (fraction of mass)
73	MOXU	Numeric	10	6	Molybdenum uncertainty, (fraction of mass)
74	PDXC	Numeric	10	6	Palladium concentration by x-ray fluorescence, (fraction of mass)
75	PDXU	Numeric	10	6	Palladium uncertainty, (fraction of mass)
76	AGXC	Numeric	10	6	Silver concentration by x-ray fluorescence, (fraction of mass)
77	AGXU	Numeric	10	6	Silver uncertainty, (fraction of mass)
78	CDXC	Numeric	10	6	Cadmium concentration by x-ray fluorescence, (fraction of mass)
79	CDXU	Numeric	10	6	Cadmium uncertainty, (fraction of mass)
80	INXC	Numeric	10	6	Indium concentration by x-ray fluorescence, (fraction of mass)
81	INXU	Numeric	10	6	Indium uncertainty, (fraction of mass)
82	SNXC	Numeric	10	6	Tin concentration by x-ray fluorescence, (fraction of mass)
83	SNXU	Numeric	10	6	Tin uncertainty, (fraction of mass)
84	SBXC	Numeric	10	6	Antimony concentration by x-ray fluorescence, (fraction of mass)
85	SBXU	Numeric	10	6	Antimony uncertainty, (fraction of mass)
86	BAXC	Numeric	10	6	Barium concentration by x-ray fluorescence, (fraction of mass)
87	BAXU	Numeric	10	6	Barium uncertainty, (fraction of mass)
88	LAXC	Numeric	10	6	Lanthanum concentration by x-ray fluorescence, (fraction of mass)
89	LAXU	Numeric	10	6	Lanthanum uncertainty, (fraction of mass)
90	AUXC	Numeric	10	6	Gold concentration by x-ray fluorescence, (fraction of mass)
91	AUXU	Numeric	10	6	Gold uncertainty, (fraction of mass)
92	HGXC	Numeric	10	6	Mercury concentration by x-ray fluorescence, (fraction of mass)
93	HGXU	Numeric	10	6	Mercury uncertainty, (fraction of mass)
94	TLXC	Numeric	10	6	Thallium concentration by x-ray fluorescence, (fraction of mass)

Table A-8
Data Base Structure for the Las Vegas Valley PM$_{10}$ Study
Composite and Specific Source Profile Data in Fraction of Total Mass
(File: LVSORFRC.DBF)

Number of data records: 88
Date of last update: 09/04/96

Field	Field Name	Type	Width	Dec	Description
95	TLXU	Numeric	10	6	Thallium uncertainty, (fraction of mass)
96	PBXC	Numeric	10	6	Lead concentration by x-ray fluorescence, (fraction of mass)
97	PBXU	Numeric	10	6	Lead uncertainty, (fraction of mass)
98	URXC	Numeric	10	6	Uranium concentration by x-ray fluorescence, (fraction of mass)
99	URXU	Numeric	10	6	Uranium uncertainty, (fraction of mass)

Table A-9
Data Base Structure for the Las Vegas Valley PM$_{10}$ Study
Source Profile Data for CMB Model Input
(File: LVSORCMB.DBF)

Number of data records: 88
Date of last update: 09/03/96

Field	Field Name	Type	Width	Dec	Description
1	ORDER	Character	10		Defines the source category: geologic, motor vehicle, vegetative burning, etc...
2	SNO	Numeric	3		Source number coding for source category
3	SID	Character	8		Source identification code
4	DESC	Character	50		Specific source type description
5	SIZE	Character	2		Particle fraction: $10 = PM_{10}$ (0-10 μm) $F = PM_{2.5}$ (0-2.5 μm)
6	CLIC	Numeric	10	6	Chloride concentration by ion chromatography, (fraction of mass)
7	CLIU	Numeric	10	6	Chloride uncertainty, (fraction of mass)
8	N3IC	Numeric	10	6	Nitrate concentration by ion chromatography, (fraction of mass)
9	N3IU	Numeric	10	6	Nitrate uncertainty, (fraction of mass)
10	S4IC	Numeric	10	6	Sulfate concentration by ion chromatography, (fraction of mass)
11	S4IU	Numeric	10	6	Sulfate uncertainty, (fraction of mass)
12	N4CC	Numeric	10	6	Ammonium concentration by automated chromatography, (fraction of mass)
13	N4CU	Numeric	10	6	Ammonium uncertainty, (fraction of mass)
14	NAAC	Numeric	10	6	Soluble sodium concentration by atomic absorption, (fraction of mass)
15	NAAU	Numeric	10	6	Soluble sodium uncertainty, (fraction of mass)
16	KPAC	Numeric	10	6	Potassium concentration by atomic absorption, (fraction of mass)
17	KPAU	Numeric	10	6	Potassium uncertainty, (fraction of mass)
18	OCTC	Numeric	10	6	Organic carbon concentration by thermal/ optical reflectance, (fraction of mass)
19	OCTU	Numeric	10	6	Organic carbon uncertainty, (fraction of mass)
20	ECTC	Numeric	10	6	Elemental carbon concentration by thermal/ optical reflectance, (fraction of mass)
21	ECTU	Numeric	10	6	Elemental carbon uncertainty, (fraction of mass)
22	NAXC	Numeric	10	6	Sodium concentration by x-ray fluorescence, (fraction of mass)
23	NAXU	Numeric	10	6	Sodium uncertainty
24	MGXC	Numeric	10	6	Magnesium concentration by x-ray fluorescence, (fraction of mass)

Table A-9
Data Base Structure for the Las Vegas Valley PM$_{10}$ Study
Source Profile Data for CMB Model Input
(File: LVSORCMB.DBF)

Number of data records: 88
Date of last update: 09/03/96

Field	Field Name	Type	Width	Dec	Description
25	MGXU	Numeric	10	6	Magnesium uncertainty
26	ALXC	Numeric	10	6	Aluminum concentration by x-ray fluorescence, (fraction of mass)
27	ALXU	Numeric	10	6	Aluminum uncertainty, (fraction of mass)
28	SIXC	Numeric	10	6	Silicon concentration by x-ray fluorescence, (fraction of mass)
29	SIXU	Numeric	10	6	Silicon uncertainty, (fraction of mass)
30	PHXC	Numeric	10	6	Phosphorous concentration by x-ray fluorescence, (fraction of mass)
31	PHXU	Numeric	10	6	Phosphorous uncertainty, (fraction of mass)
32	SUXC	Numeric	10	6	Sulfur concentration by x-ray fluorescence, (fraction of mass)
33	SUXU	Numeric	10	6	Sulfur uncertainty, (fraction of mass)
34	CLXC	Numeric	10	6	Chlorine concentration by x-ray fluorescence, (fraction of mass)
35	CLXU	Numeric	10	6	Chlorine uncertainty, (fraction of mass)
36	KPXC	Numeric	10	6	Potassium concentration by x-ray fluorescence, (fraction of mass)
37	KPXU	Numeric	10	6	Potassium uncertainty, (fraction of mass)
38	CAXC	Numeric	10	6	Calcium concentration by x-ray fluorescence, (fraction of mass)
39	CAXU	Numeric	10	6	Calcium uncertainty, (fraction of mass)
40	TIXC	Numeric	10	6	Titanium concentration by x-ray fluorescence, (fraction of mass)
41	TIXU	Numeric	10	6	Titanium uncertainty, (fraction of mass)
42	VAXC	Numeric	10	6	Vanadium concentration by x-ray fluorescence, (fraction of mass)
43	VAXU	Numeric	10	6	Vanadium uncertainty, (fraction of mass)
44	CRXC	Numeric	10	6	Chromium concentration by x-ray fluorescence, (fraction of mass)
45	CRXU	Numeric	10	6	Chromium uncertainty, (fraction of mass)
46	MNXC	Numeric	10	6	Manganese concentration by x-ray fluorescence, (fraction of mass)
47	MNXU	Numeric	10	6	Manganese uncertainty, (fraction of mass)
48	FEXC	Numeric	10	6	Iron concentration by x-ray fluorescence, (fraction of mass)
49	FEXU	Numeric	10	6	Iron uncertainty, (fraction of mass)
50	COXC	Numeric	10	6	Cobalt concentration by x-ray fluorescence, (fraction of mass)

Table A-9
Data Base Structure for the Las Vegas Valley PM$_{10}$ Study
Source Profile Data for CMB Model Input
(File: LVSORCMB.DBF)

Number of data records: 88
Date of last update: 09/03/96

Field	Field Name	Type	Width	Dec	Description
51	COXU	Numeric	10	6	Cobalt uncertainty, (fraction of mass)
52	NIXC	Numeric	10	6	Nickel concentration by x-ray fluorescence, (fraction of mass)
52	NIXU	Numeric	10	6	Nickel uncertainty, (fraction of mass)
54	CUXC	Numeric	10	6	Copper concentration by x-ray fluorescence, (fraction of mass)
55	CUXU	Numeric	10	6	Copper uncertainty, (fraction of mass)
56	ZNXC	Numeric	10	6	Zinc concentration by x-ray fluorescence, (fraction of mass)
57	ZNXU	Numeric	10	6	Zinc uncertainty, (fraction of mass)
58	GAXC	Numeric	10	6	Gallium concentration by x-ray fluorescence, (fraction of mass)
59	GAXU	Numeric	10	6	Gallium uncertainty, (fraction of mass)
60	ASXC	Numeric	10	6	Arsenic concentration by x-ray fluorescence, (fraction of mass)
61	ASXU	Numeric	10	6	Arsenic uncertainty, (fraction of mass)
62	SEXC	Numeric	10	6	Selenium concentration by x-ray fluorescence, (fraction of mass)
63	SEXU	Numeric	10	6	Selenium uncertainty, (fraction of mass)
64	BRXC	Numeric	10	6	Bromine concentration by x-ray fluorescence, (fraction of mass)
65	BRXU	Numeric	10	6	Bromine uncertainty, (fraction of mass)
66	RBXC	Numeric	10	6	Rubidium concentration by x-ray fluorescence, (fraction of mass)
67	RBXU	Numeric	10	6	Rubidium uncertainty, (fraction of mass)
68	SRXC	Numeric	10	6	Strontium concentration by x-ray fluorescence, (fraction of mass)
69	SRXU	Numeric	10	6	Strontium uncertainty, (fraction of mass)
70	YTXC	Numeric	10	6	Yttrium concentration by x-ray fluorescence, (fraction of mass)
71	YTXU	Numeric	10	6	Yttrium uncertainty, (fraction of mass)
72	ZRXC	Numeric	10	6	Zirconium concentration by x-ray fluorescence, (fraction of mass)
73	ZRXU	Numeric	10	6	Zirconium uncertainty, (fraction of mass)
74	MOXC	Numeric	10	6	Molybdenum concentration by x-ray fluorescence, (fraction of mass)
75	MOXU	Numeric	10	6	Molybdenum uncertainty, (fraction of mass)
76	PDXC	Numeric	10	6	Palladium concentration by x-ray fluorescence, (fraction of mass)
77	PDXU	Numeric	10	6	Palladium uncertainty, (fraction of mass)
78	AGXC	Numeric	10	6	Silver concentration by x-ray fluorescence, (fraction of mass)
79	AGXU	Numeric	10	6	Silver uncertainty, (fraction of mass)
80	CDXC	Numeric	10	6	Cadmium concentration by x-ray

Table A-9
Data Base Structure for the Las Vegas Valley PM$_{10}$ Study
Source Profile Data for CMB Model Input
(File: LVSORCMB.DBF)

Number of data records: 88
Date of last update: 09/03/96

Field	Field Name	Type	Width	Dec	Description
					fluorescence, (fraction of mass)
81	CDXU	Numeric	10	6	Cadmium uncertainty, (fraction of mass)
82	INXC	Numeric	10	6	Indium concentration by x-ray fluorescence, (fraction of mass)
83	INXU	Numeric	10	6	Indium uncertainty, (fraction of mass)
84	SNXC	Numeric	10	6	Tin concentration by x-ray fluorescence, (fraction of mass)
85	SNXU	Numeric	10	6	Tin uncertainty, (fraction of mass)
86	SBXC	Numeric	10	6	Antimony concentration by x-ray fluorescence, (fraction of mass)
87	SBXU	Numeric	10	6	Antimony uncertainty, (fraction of mass)
88	BAXC	Numeric	10	6	Barium concentration by x-ray fluorescence, (fraction of mass)
89	BAXU	Numeric	10	6	Barium uncertainty, (fraction of mass)
90	LAXC	Numeric	10	6	Lanthanum concentration by x-ray fluorescence, (fraction of mass)
91	LAXU	Numeric	10	6	Lanthanum uncertainty, (fraction of mass)
92	AUXC	Numeric	10	6	Gold concentration by x-ray fluorescence, (fraction of mass)
93	AUXU	Numeric	10	6	Gold uncertainty, (fraction of mass)
94	HGXC	Numeric	10	6	Mercury concentration by x-ray fluorescence, (fraction of mass)
95	HGXU	Numeric	10	6	Mercury uncertainty, (fraction of mass)
96	TLXC	Numeric	10	6	Thallium concentration by x-ray fluorescence, (fraction of mass)
97	TLXU	Numeric	10	6	Thallium uncertainty, (fraction of mass)
98	PBXC	Numeric	10	6	Lead concentration by x-ray fluorescence, (fraction of mass)
99	PBXU	Numeric	10	6	Lead uncertainty, (fraction of mass)
100	URXC	Numeric	10	6	Uranium concentration by x-ray fluorescence, (fraction of mass)
101	URXU	Numeric	10	6	Uranium uncertainty, (fraction of mass)
102	SPSUMC	Numeric	10	6	Sum of measured species concentrations, (fraction of mass)

Table A-10
Common Data Base Structure for Meteorological and
Beta Attenuation Monitor (BAM) Data for the Las Vegas Valley PM$_{10}$ Study
(File: LVMETBAM.DBF)

Number of data records: 182,016
Date of last update: 06/18/96

Field Name	Type	Width	Dec	Description
1 YRCC	Character	4		Year of sample collection
2 JDAT	Numeric	3	0	Sampling date, (Julian day)
3 HEC	Numeric	4	0	Time in HHMM format at end of hourly average observation, i.e. 0500 is for data collected 0400 through 0500, (PST)
4 TAF	Numeric	5	1	Ambient temperature, (degrees F)
5 RHP	Numeric	5	1	Relative humidity, (%)
6 WSE	Numeric	5	1	Scalar windspeed, (m/s)
7 WDS	Numeric	5	1	Scalar wind direction, (degrees from north)
8 SITE	Character	4		Site identification code
9 HR	Numeric	2		Time in hours at beginning of hourly average observation, i.e. 5 is for data collected 0500 through 0600
10 DATE	Date	8		Sampling date, (calander day)
11 MONTH	Character	10		Month of sampling (i.e. January)
12 DAY	Character	2		Day of month when sample was taken
13 BMS	Numeric	6	1	Beta Attenuation Monitor (BAM) (μg/m3)
24 COMMENTS	Memo	10		Comments

Table A-11
Common Data Base Structure for the Las Vegas Valley
Beta Attenuation 24-Hour Average PM$_{10}$ Data
(File: LVBAM24H.DBF)

Number of data records: 7584
Date of last update: 09/05/96

Field	Field Name	Type	Width	Dec	Description
1	SITE	Character	4		Site identification code
2	DATE	Date	8		Sampling date
3	SIZE	Character	2		Particle fraction:
					$\quad$ 10=PM$_{10}$ (0-10 μm)
4	STSTHHMM	Character	4		Sample start time
5	STOPHHMM	Character	4		Sample stop time
6	DURATION	Numeric	2		Sample duration, (hours)
7	PERIOD	Character	1		Sample period:
					$\quad$ 1) 0001 to 0600 PST
					$\quad$ 2) 0601 to 1200 PST
					$\quad$ 3) 1201 to 1800 PST
					$\quad$ 4) 1801 to 2400 PST
					$\quad$ 0) 0001 to 2400 PST
8	MSGC	Numeric	6	1	PM$_{10}$ mass concentration measured by beta attenuation, (μg/m^3)
9	MSGU	Numeric	6	1	PM$_{10}$ mass concentration uncertainty, (μg/m^3)

Table A-12
Ambient and Source Field Sampling Data Validation Flags[a]
Applied to the Las Vegas Valley PM10 Study
(File: AMBFLAG.DOC)

Validation Flag	Sub Flag	Description
A		Sampler adjustment or maintenance.
	A1	Sampler audit during sample period.
	A2	Sampler cleaned prior to sample period.
	A3	Particle size cut device regreased or replaced prior to sample period.
B		Field Blank.
D		Sample dropped.
	D1	Sample dropped after sampling.
	D2	Filter dropped during unloading.
F		Filter damaged or ripped.
	F1	Filter damaged in the field.
	F2	Filter damaged when removed from holder.
	F3	Filter wrinkled.
	F4	Filter torn due to over-tightened filter holder.
	F5	Teflon membrane separated from support ring.
	F6	Pinholes in filter.
G		Filter deposit damaged.
	G1	Deposit scratched or scraped, causing a thin line in the deposit.
	G2	Deposit smudged, causing a large area of deposit to be displaced.
	G3	Filter returned to lab with deposit side down in PetriSlide.
	G4	Part of deposit appears to have fallen off; particles on inside of PetriSlide.
	G5	Finger touched filter in the field (without gloves).
	G6	Finger touched filter in the lab (with gloves).
H		Filter holder assembly problem.
	H1	Filter misaligned in holder - possible air leak.
	H2	Filter holder loose in sampler - possible air leak.
	H3	Filter holder not tightened sufficiently - possible air leak.
	H4	Filter support grid upside down.
	H5	Two substrates loaded in place of one.
I		Inhomogeneous sample deposit.
	I1	Evidence of impaction - deposit heavier in center of filter.
	I2	Random areas of darker or lighter deposit on filter.
	I3	Light colored deposit with dark specks.
	I4	Non-uniform deposit near edge - possible air leak.
L		Sample loading error.
	L1	Teflon and quartz filters were loaded reversely in SFS.

Rev. 6/7/95

Table A-12 (Cont.)
Ambient and Source Field Sampling Data Validation Flags[a]
Applied to the Las Vegas Valley PM10 Study
(File: AMBFLAG.DOC)

Validation Flag	Sub Flag	Description
	L2	$PM_{2.5}$ and PM_{10} filter pack switched.
	L3	Fine and Coarse filters were loaded reversely in dichotomous sampler.
	L4	Filter loaded in wrong port.
M		Sampler malfunction.
N		Foreign substance on sample.
	N1	Insects on deposit, removed before analysis.
	N2	Insects on deposit, not all removed.
	N3	Metallic particles observed on deposit.
	N4	Many particles on deposit much larger than cut point of inlet.
	N5	Fibers or fuzz on filter.
	N6	Oily-looking droplets on filter.
	N7	Shiny substance on filter.
	N8	Particles on back of filter.
	N9	Discoloration on deposit.
O		Sampler operation error.
	O1	Pump was not switched on after changing samples.
	O2	Timer set incorrectly.
	O3	Dichotomous sampler assembled with virtual impactor 180° out of phase; only PM_{10} data reported.
P		Power failure during sampling.
Q		Flow rate error.
	Q1	Initial or final flow rate differed from nominal by $> \pm 10\%$.
	Q2	Initial or final flow rate differed from nominal by $> \pm 15\%$.
	Q3	Final flow rate differed from initial by $> \pm 15\%$.
	Q4	Initial or final flow rate not recorded, used estimated flow rate.
	Q5	Nominal flow rate assumed.
R		Replacement filter used.
	R1	Filter that failed flow rate or QC checks replaced with spare.
	R2	Filter sampling sequence changed from order designated on field data sheet.
S		Sample validity is suspect.
T		Sampling time error.
	T1	Sampling duration error of $> \pm 10\%$.
	T2	Sample start time error of $> \pm 10\%$ of sample duration.

Rev. 6/7/95

Table A-12 (Cont.)
Ambient and Source Field Sampling Data Validation Flags[a]
Applied to the Las Vegas Valley PM10 Study
(File: AMBFLAG.DOC)

Validation Flag	Sub Flag	Description
	T3	Elapsed time meter reading not recorded or recorded incorrectly. Sample duration estimated based on readings from previous or subsequent sample.
	T4	Nominal sample duration assumed.
	T5	Sample ran during prescribed period, plus part of next period.
	T6	More than one sample was run to account for the prescribed period.
U		Unusual local particulate sources during sample period.
	U1	Local construction activity.
	U2	Forest fire or slash or field burning.
V		Invalid sample (Void).
W		Wet Sample.
	W1	Deposit spotted from water drops.
	W2	Filter damp when unloaded.
	W3	Filter holder contained water when unloaded.
X		No sample was taken this period, sample run was skipped.

[a] Samples are categorized as valid, suspect, or invalid. Unflagged samples, or samples with any flag except 'S' or 'V' indicate valid results. The 'S' flag indicates samples of suspect validity. The 'V' flag indicates invalid samples. Field data validation flags are all upper case.

Table A-13
Chemical Analysis Data Validation Flags[a]
Applied in the Las Vegas Valley PM$_{10}$ Study
(File: CHEMFLAG.DOC)

Validation Flag	Sub Flag	Description
b		Blank.
	b1	Field/dynamic blank.
	b2	Laboratory blank.
	b3	Distilled-deionized water blank.
	b4	Method blank.
	b5	Extract/solution blank.
	b6	Transport blank.
c		Analysis result reprocessed or recalculated.
	c1	XRF spectrum reprocessed using manually adjusted background.
d		Sample dropped.
f		Filter damaged or ripped.
	f1	Filter damaged, outside of analysis area.
	f2	Filter damaged, within analysis area.
	f3	Filter wrinkled.
	f4	Filter stuck to PetriSlide.
	f5	Teflon membrane separated from support ring.
	f6	Pinholes in filter.
g		Filter deposit damaged.
	g1	Deposit scratched or scraped, causing a thin line in the deposit.
	g2	Deposit smudged, causing a large area of deposit to be displaced.
	g3	Filter deposit side down in PetriSlide.
	g4	Part of deposit appears to have fallen off; particles on inside of PetriSlide.
	g5	Ungloved finger touched filter.
	g6	Gloved finger touched filter.
h		Filter holder assembly problem.
	h1	Deposit not centered.
	h2	Sampled on wrong side of filter.
	h4	Filter support grid upside down- deposit has widely spaced stripes or grid pattern.
	h5	Two filters in PetriSlide- analyzed separately.
i		Inhomogeneous sample deposit.
	i1	Evidence of impaction - deposit heavier in center of filter.
	i2	Random areas of darker or lighter deposit on filter.
	i3	Light colored deposit with dark specks.
	i4	Non-uniform deposit near edge - possible air leak.

Validation Flag	Sub Flag	Description
m		Analysis results affected by matrix effect.
	m1	Organic/elemental carbon split undetermined due to an apparent color change of non-carbon particles during analysis; all measured carbon reported as organic.
	m2	Non-white carbon punch after carbon analysis, indicative of mineral particles in deposit.
	m3	A non-typical, but valid, laser response was observed during TOR analysis. This phenomena may result in increased uncertainty of the organic/elemental carbon split. Total carbon measurements are likely unaffected.
n		Foreign substance on sample.
	n1	Insects on deposit, removed before analysis.
	n2	Insects on deposit, not all removed.
	n3	Metallic particles observed on deposit.
	n4	Many particles on deposit much larger than cut point of inlet.
	n5	Fibers or fuzz on filter.
	n6	Oily-looking droplets on filter.
	n7	Shiny substance on filter.
	n8	Particles on back of filter.
	n9	Discoloration on deposit.
q		Standard.
	q1	Quality control standard.
	q2	Externally prepared quality control standard.
	q3	Second type of externally prepared quality control standard.
	q4	Calibration standard.
r		Replicate analysis.
	r1	First replicate analysis on the same analyzer.
	r2	Second replicate analysis on the same analyzer.
	r3	Third replicate analysis on the same analyzer.
	r4	Sample re-analysis.
	r5	Replicate on different analyzer.
	r6	Sample re-extraction and re-analysis.
	r7	Sample re-analyzed with same result, original value used.
s		Suspect analysis result.
v		Invalid (void) analysis result.
	v1	Quality control standard check exceeded ± 10% of specified concentration range.
	v2	Replicate analysis failed acceptable limit specified in SOP.

Table A-13 (continued)
Chemical Analysis Data Validation Flags[a]
Applied in the Las Vegas Valley PM$_{10}$ Study
(File: CHEMFLAG.DOC)

Validation Flag	Sub Flag	Description
	v3	Potential contamination.
	v4	Concentration out of expected range.
w		Wet Sample.
	w1	Deposit spotted from water drops.

[a] Analysis results are categorized as valid, suspect, or invalid. Unflagged samples, or samples with any flag except 's' or 'v' indicate valid results. The 's' flag indicates results of suspect validity. The 'v' flag indicates invalid analysis results. Chemical analysis data validation flags are all lower case.

APPENDIX B
Las Vegas Valley Source Composition Library

Fugitive Dust and Other Source Contributions to PM$_{10}$
in Nevada's Las Vegas Valley

Volume II – Final Report

April 18, 1997

Table B-1
Individual Geological Source Profiles (Weight Percent by Mass)
Acquired in the Las Vegas PM$_{10}$ Study

	LVGCONS1	LVGCONS2	LVGCONS3	LVGCONS4	LVGCONS5
Mass	100.000% ± 7.104%	100.000% ± 7.479%	100.000% ± 7.136%	100.000% ± 7.142%	100.000% ± 7.137%
Cl$^-$	0.189% ± 0.039%	0.056% ± 0.073%	0.110% ± 0.039%	0.156% ± 0.045%	0.083% ± 0.038%
NO$_3^-$	0.115% ± 0.025%	0.084% ± 0.071%	0.067% ± 0.034%	0.169% ± 0.037%	0.036% ± 0.034%
SO$_4^=$	1.441% ± 0.108%	0.552% ± 0.082%	0.948% ± 0.077%	0.447% ± 0.048%	0.645% ± 0.058%
NH$_4^+$	0.054% ± 0.024%	0.172% ± 0.074%	0.085% ± 0.035%	0.106% ± 0.037%	0.064% ± 0.034%
K$^+$	0.216% ± 0.026%	0.251% ± 0.059%	0.111% ± 0.028%	0.194% ± 0.032%	0.166% ± 0.030%
OC	12.048% ± 1.907%	6.485% ± 1.701%	8.865% ± 1.532%	9.111% ± 1.582%	8.214% ± 1.442%
EC	0.166% ± 0.190%	1.969% ± 0.858%	0.000% ± 0.259%	1.076% ± 0.447%	0.010% ± 0.261%
TC	12.122% ± 1.733%	8.166% ± 2.163%	8.734% ± 1.476%	10.050% ± 1.645%	8.087% ± 1.410%
Na	0.000% ± 0.135%	0.000% ± 0.252%	0.000% ± 0.165%	0.000% ± 0.166%	0.000% ± 0.168%
Mg	3.055% ± 0.219%	2.930% ± 0.225%	3.927% ± 0.283%	3.237% ± 0.234%	3.716% ± 0.268%
Al	1.263% ± 0.091%	2.345% ± 0.176%	0.885% ± 0.066%	1.258% ± 0.092%	1.214% ± 0.089%
Si	7.102% ± 0.504%	10.788% ± 0.793%	5.722% ± 0.407%	6.830% ± 0.486%	6.537% ± 0.465%
P	0.000% ± 0.013%	0.043% ± 0.009%	0.003% ± 0.014%	0.016% ± 0.005%	0.001% ± 0.015%
S	0.249% ± 0.018%	0.196% ± 0.016%	0.234% ± 0.017%	0.118% ± 0.009%	0.188% ± 0.014%
Cl	0.063% ± 0.081%	0.039% ± 0.095%	0.028% ± 0.088%	0.048% ± 0.096%	0.030% ± 0.101%
K	1.090% ± 0.085%	1.519% ± 0.120%	0.768% ± 0.067%	0.958% ± 0.081%	1.000% ± 0.084%
Ca	14.959% ± 1.061%	16.598% ± 1.227%	16.161% ± 1.150%	17.738% ± 1.263%	18.631% ± 1.326%
Ti	0.135% ± 0.017%	0.245% ± 0.044%	0.107% ± 0.020%	0.135% ± 0.022%	0.130% ± 0.021%
V	0.007% ± 0.010%	0.013% ± 0.025%	0.009% ± 0.012%	0.008% ± 0.013%	0.008% ± 0.013%
Cr	0.005% ± 0.002%	0.008% ± 0.005%	0.003% ± 0.002%	0.005% ± 0.003%	0.004% ± 0.002%
Mn	0.036% ± 0.003%	0.056% ± 0.005%	0.025% ± 0.002%	0.033% ± 0.003%	0.031% ± 0.003%
Fe	1.578% ± 0.112%	2.520% ± 0.185%	1.154% ± 0.082%	1.487% ± 0.106%	1.486% ± 0.106%
Co	0.001% ± 0.024%	0.000% ± 0.039%	0.000% ± 0.018%	0.002% ± 0.023%	0.000% ± 0.023%
Ni	0.003% ± 0.001%	0.002% ± 0.002%	0.004% ± 0.001%	0.003% ± 0.001%	0.004% ± 0.001%
Cu	0.001% ± 0.001%	0.002% ± 0.002%	0.000% ± 0.001%	0.001% ± 0.001%	0.001% ± 0.001%
Zn	0.010% ± 0.001%	0.017% ± 0.002%	0.007% ± 0.001%	0.011% ± 0.001%	0.007% ± 0.001%
Ga	0.001% ± 0.002%	0.000% ± 0.004%	0.000% ± 0.002%	0.000% ± 0.002%	0.000% ± 0.002%
As	0.001% ± 0.002%	0.001% ± 0.005%	0.001% ± 0.003%	0.001% ± 0.003%	0.000% ± 0.003%
Se	0.000% ± 0.001%	0.000% ± 0.002%	0.000% ± 0.001%	0.000% ± 0.001%	0.000% ± 0.001%
Br	0.001% ± 0.001%	0.002% ± 0.002%	0.002% ± 0.001%	0.002% ± 0.001%	0.001% ± 0.001%
Rb	0.006% ± 0.001%	0.008% ± 0.002%	0.004% ± 0.001%	0.005% ± 0.001%	0.005% ± 0.001%
Sr	0.106% ± 0.008%	0.097% ± 0.007%	0.135% ± 0.010%	0.117% ± 0.008%	0.141% ± 0.010%
Yt	0.002% ± 0.001%	0.003% ± 0.002%	0.001% ± 0.001%	0.002% ± 0.001%	0.001% ± 0.001%
Zr	0.007% ± 0.002%	0.009% ± 0.003%	0.004% ± 0.006%	0.006% ± 0.002%	0.006% ± 0.002%
Mo	0.000% ± 0.002%	0.000% ± 0.006%	0.000% ± 0.003%	0.002% ± 0.003%	0.001% ± 0.003%
Pd	0.000% ± 0.008%	0.000% ± 0.020%	0.000% ± 0.011%	0.000% ± 0.011%	0.000% ± 0.011%
Ag	0.005% ± 0.009%	0.000% ± 0.024%	0.001% ± 0.013%	0.001% ± 0.013%	0.000% ± 0.013%
Cd	0.000% ± 0.009%	0.000% ± 0.024%	0.000% ± 0.013%	0.001% ± 0.014%	0.000% ± 0.013%
In	0.000% ± 0.011%	0.006% ± 0.028%	0.000% ± 0.015%	0.000% ± 0.015%	0.000% ± 0.015%
Sn	0.000% ± 0.014%	0.000% ± 0.035%	0.002% ± 0.018%	0.000% ± 0.019%	0.005% ± 0.018%
Sb	0.001% ± 0.015%	0.001% ± 0.041%	0.000% ± 0.021%	0.000% ± 0.022%	0.004% ± 0.021%
Ba	0.035% ± 0.052%	0.030% ± 0.140%	0.014% ± 0.072%	0.013% ± 0.075%	0.019% ± 0.071%
La	0.000% ± 0.068%	0.000% ± 0.183%	0.000% ± 0.093%	0.000% ± 0.097%	0.000% ± 0.092%
Au	0.000% ± 0.003%	0.000% ± 0.007%	0.000% ± 0.003%	0.000% ± 0.004%	0.000% ± 0.003%
Hg	0.002% ± 0.002%	0.000% ± 0.005%	0.000% ± 0.003%	0.001% ± 0.003%	0.001% ± 0.003%
Tl	0.000% ± 0.002%	0.001% ± 0.005%	0.000% ± 0.003%	0.002% ± 0.003%	0.001% ± 0.003%
Pb	0.004% ± 0.002%	0.007% ± 0.005%	0.002% ± 0.004%	0.001% ± 0.004%	0.002% ± 0.004%
U	0.001% ± 0.002%	0.003% ± 0.005%	0.001% ± 0.003%	0.001% ± 0.003%	0.001% ± 0.003%
Sum of Species	43.304% ± 2.275%	46.551% ± 2.459%	38.933% ± 2.015%	42.835% ± 2.162%	41.957% ± 2.069%

	LVGPLOT1	LVGPLOT2	LVGPVRD1	LVGPVRD2	LVGPVRD3
Mass	100.000% ± 7.359%	100.000% ± 7.503%	100.000% ± 7.344%	100.000% ± 7.563%	100.000% ± 7.231%
Cl$^-$	0.289% ± 0.088%	0.098% ± 0.091%	0.109% ± 0.074%	0.132% ± 0.099%	0.088% ± 0.056%
NO$_3^-$	0.171% ± 0.072%	0.284% ± 0.090%	0.120% ± 0.069%	0.118% ± 0.093%	0.131% ± 0.053%
SO$_4^=$	2.282% ± 0.184%	1.236% ± 0.127%	0.924% ± 0.097%	1.026% ± 0.121%	1.153% ± 0.100%
NH$_4^+$	0.118% ± 0.072%	0.218% ± 0.091%	0.150% ± 0.071%	0.154% ± 0.095%	0.118% ± 0.054%
K$^+$	0.212% ± 0.058%	0.134% ± 0.069%	0.148% ± 0.055%	0.179% ± 0.075%	0.133% ± 0.043%
OC	17.763% ± 3.114%	10.657% ± 2.394%	10.822% ± 2.175%	15.952% ± 3.119%	10.417% ± 1.936%
EC	4.641% ± 1.636%	5.496% ± 1.956%	5.441% ± 1.886%	1.250% ± 0.833%	3.058% ± 1.099%
TC	22.128% ± 3.536%	15.825% ± 3.155%	15.984% ± 2.837%	16.837% ± 3.366%	13.270% ± 2.270%
Na	0.000% ± 0.244%	0.045% ± 0.269%	0.090% ± 0.246%	0.062% ± 0.274%	0.000% ± 0.215%
Mg	2.053% ± 0.159%	2.887% ± 0.222%	2.887% ± 0.217%	2.630% ± 0.205%	3.177% ± 0.234%
Al	1.967% ± 0.147%	1.749% ± 0.134%	1.567% ± 0.118%	1.683% ± 0.130%	1.568% ± 0.116%
Si	9.346% ± 0.676%	8.781% ± 0.642%	8.519% ± 0.616%	8.374% ± 0.615%	8.453% ± 0.606%
P	0.067% ± 0.010%	0.019% ± 0.009%	0.044% ± 0.009%	0.059% ± 0.010%	0.013% ± 0.020%
S	0.650% ± 0.048%	0.579% ± 0.043%	0.553% ± 0.041%	0.446% ± 0.034%	0.411% ± 0.030%
Cl	0.201% ± 0.030%	0.072% ± 0.090%	0.099% ± 0.028%	0.118% ± 0.028%	0.021% ± 0.102%
K	1.278% ± 0.098%	1.124% ± 0.091%	1.129% ± 0.089%	1.137% ± 0.090%	1.023% ± 0.086%
Ca	11.543% ± 0.845%	15.203% ± 1.123%	13.258% ± 0.966%	11.623% ± 0.872%	18.390% ± 1.320%
Ti	0.304% ± 0.046%	0.199% ± 0.051%	0.201% ± 0.042%	0.216% ± 0.055%	0.184% ± 0.033%
V	0.017% ± 0.026%	0.016% ± 0.030%	0.008% ± 0.025%	0.017% ± 0.032%	0.013% ± 0.019%
Cr	0.008% ± 0.005%	0.006% ± 0.006%	0.010% ± 0.005%	0.008% ± 0.007%	0.008% ± 0.004%
Mn	0.041% ± 0.004%	0.046% ± 0.005%	0.042% ± 0.004%	0.044% ± 0.005%	0.043% ± 0.004%
Fe	2.449% ± 0.177%	2.117% ± 0.155%	2.589% ± 0.187%	2.170% ± 0.159%	2.046% ± 0.147%
Co	0.000% ± 0.038%	0.000% ± 0.033%	0.000% ± 0.040%	0.000% ± 0.034%	0.000% ± 0.032%
Ni	0.003% ± 0.002%	0.004% ± 0.002%	0.006% ± 0.002%	0.003% ± 0.002%	0.004% ± 0.001%
Cu	0.009% ± 0.002%	0.007% ± 0.002%	0.014% ± 0.002%	0.013% ± 0.002%	0.005% ± 0.001%
Zn	0.125% ± 0.009%	0.118% ± 0.009%	0.129% ± 0.010%	0.097% ± 0.008%	0.067% ± 0.005%
Ga	0.000% ± 0.004%	0.000% ± 0.005%	0.000% ± 0.004%	0.000% ± 0.006%	0.000% ± 0.003%
As	0.000% ± 0.007%	0.000% ± 0.006%	0.000% ± 0.007%	0.001% ± 0.008%	0.000% ± 0.004%
Se	0.000% ± 0.003%	0.000% ± 0.003%	0.000% ± 0.003%	0.000% ± 0.003%	0.000% ± 0.002%
Br	0.002% ± 0.002%	0.002% ± 0.003%	0.002% ± 0.003%	0.010% ± 0.002%	0.002% ± 0.001%
Rb	0.007% ± 0.002%	0.006% ± 0.002%	0.005% ± 0.002%	0.005% ± 0.002%	0.006% ± 0.001%
Sr	0.088% ± 0.007%	0.080% ± 0.006%	0.214% ± 0.016%	0.080% ± 0.006%	0.110% ± 0.008%
Yt	0.002% ± 0.003%	0.002% ± 0.004%	0.001% ± 0.003%	0.002% ± 0.004%	0.002% ± 0.002%
Zr	0.010% ± 0.003%	0.008% ± 0.003%	0.009% ± 0.004%	0.007% ± 0.003%	0.008% ± 0.002%
Mo	0.000% ± 0.006%	0.001% ± 0.008%	0.002% ± 0.006%	0.002% ± 0.008%	0.004% ± 0.005%
Pd	0.001% ± 0.020%	0.006% ± 0.025%	0.004% ± 0.020%	0.020% ± 0.027%	0.003% ± 0.017%
Ag	0.016% ± 0.024%	0.002% ± 0.029%	0.010% ± 0.024%	0.013% ± 0.031%	0.000% ± 0.019%
Cd	0.000% ± 0.025%	0.004% ± 0.030%	0.001% ± 0.024%	0.005% ± 0.032%	0.000% ± 0.020%
In	0.000% ± 0.028%	0.000% ± 0.035%	0.004% ± 0.028%	0.003% ± 0.037%	0.000% ± 0.023%
Sn	0.003% ± 0.035%	0.000% ± 0.044%	0.000% ± 0.035%	0.003% ± 0.046%	0.005% ± 0.028%
Sb	0.012% ± 0.041%	0.000% ± 0.050%	0.000% ± 0.040%	0.020% ± 0.053%	0.000% ± 0.032%
Ba	0.017% ± 0.145%	0.001% ± 0.176%	0.082% ± 0.142%	0.005% ± 0.190%	0.000% ± 0.112%
La	0.000% ± 0.190%	0.000% ± 0.230%	0.000% ± 0.184%	0.000% ± 0.248%	0.000% ± 0.147%
Au	0.000% ± 0.009%	0.000% ± 0.009%	0.000% ± 0.009%	0.000% ± 0.010%	0.000% ± 0.006%
Hg	0.000% ± 0.006%	0.000% ± 0.007%	0.002% ± 0.006%	0.000% ± 0.007%	0.000% ± 0.004%
Tl	0.000% ± 0.006%	0.000% ± 0.007%	0.001% ± 0.006%	0.000% ± 0.007%	0.001% ± 0.004%
Pb	0.029% ± 0.005%	0.009% ± 0.006%	0.029% ± 0.005%	0.025% ± 0.007%	0.012% ± 0.004%
U	0.001% ± 0.006%	0.001% ± 0.007%	0.001% ± 0.006%	0.000% ± 0.007%	0.000% ± 0.004%
Sum of Species	54.572% ± 3.715%	50.404% ± 3.397%	48.414% ± 3.138%	46.953% ± 3.446%	50.046% ± 2.697%

	LVGPVRD4	LVGPVRD5	LVGPVRD6	LVGPVRD7	LVGSOIL1
Mass	100.000% ± 7.505%	100.000% ± 7.514%	100.000% ± 8.062%	100.000% ± 7.143%	100.000% ± 7.343%
Cl$^-$	0.135% ± 0.093%	0.200% ± 0.098%	0.000% ± 0.131%	0.141% ± 0.044%	0.051% ± 0.071%
NO$_3^-$	0.322% ± 0.090%	0.314% ± 0.091%	0.165% ± 0.130%	0.191% ± 0.038%	0.105% ± 0.069%
SO$_4^=$	1.664% ± 0.153%	3.008% ± 0.243%	0.736% ± 0.142%	1.985% ± 0.150%	1.579% ± 0.136%
NH$_4^+$	0.177% ± 0.090%	0.212% ± 0.092%	0.227% ± 0.132%	0.092% ± 0.037%	0.119% ± 0.070%
K$^+$	0.175% ± 0.070%	0.326% ± 0.074%	0.170% ± 0.103%	0.160% ± 0.031%	0.169% ± 0.056%
OC	11.574% ± 2.503%	18.217% ± 3.357%	6.235% ± 2.610%	10.598% ± 1.789%	8.688% ± 1.916%
EC	5.450% ± 1.938%	8.593% ± 2.938%	4.410% ± 1.785%	3.108% ± 1.071%	1.136% ± 0.653%
TC	16.682% ± 3.242%	26.477% ± 4.291%	10.136% ± 3.632%	13.568% ± 2.046%	9.554% ± 2.228%
Na	0.000% ± 0.278%	0.000% ± 0.249%	0.000% ± 0.350%	0.000% ± 0.164%	0.000% ± 0.262%
Mg	2.975% ± 0.228%	2.073% ± 0.163%	2.890% ± 0.238%	2.193% ± 0.161%	4.504% ± 0.333%
Al	1.683% ± 0.129%	1.349% ± 0.105%	1.770% ± 0.145%	1.695% ± 0.123%	1.526% ± 0.116%
Si	8.749% ± 0.640%	6.854% ± 0.502%	9.373% ± 0.717%	8.726% ± 0.621%	10.120% ± 0.731%
P	0.010% ± 0.026%	0.027% ± 0.009%	0.050% ± 0.012%	0.006% ± 0.018%	0.016% ± 0.024%
S	0.498% ± 0.038%	0.582% ± 0.044%	0.367% ± 0.030%	0.400% ± 0.029%	0.547% ± 0.040%
Cl	0.089% ± 0.097%	0.129% ± 0.029%	0.025% ± 0.102%	0.056% ± 0.090%	0.006% ± 0.091%
K	1.133% ± 0.093%	0.852% ± 0.070%	1.121% ± 0.097%	1.255% ± 0.098%	1.188% ± 0.095%
Ca	16.559% ± 1.221%	11.855% ± 0.883%	16.752% ± 1.303%	16.254% ± 1.158%	15.809% ± 1.148%
Ti	0.193% ± 0.051%	0.166% ± 0.051%	0.187% ± 0.074%	0.209% ± 0.025%	0.168% ± 0.041%
V	0.011% ± 0.030%	0.016% ± 0.030%	0.012% ± 0.043%	0.012% ± 0.010%	0.000% ± 0.032%
Cr	0.012% ± 0.006%	0.005% ± 0.008%	0.007% ± 0.012%	0.007% ± 0.003%	0.003% ± 0.010%
Mn	0.053% ± 0.005%	0.035% ± 0.004%	0.046% ± 0.006%	0.050% ± 0.004%	0.044% ± 0.004%
Fe	2.596% ± 0.190%	1.816% ± 0.133%	2.056% ± 0.157%	2.297% ± 0.163%	1.961% ± 0.142%
Co	0.000% ± 0.041%	0.000% ± 0.029%	0.000% ± 0.033%	0.000% ± 0.035%	0.000% ± 0.031%
Ni	0.005% ± 0.002%	0.002% ± 0.003%	0.003% ± 0.004%	0.005% ± 0.001%	0.001% ± 0.002%
Cu	0.014% ± 0.002%	0.014% ± 0.002%	0.005% ± 0.003%	0.012% ± 0.001%	0.003% ± 0.002%
Zn	0.111% ± 0.008%	0.106% ± 0.008%	0.073% ± 0.006%	0.054% ± 0.004%	0.041% ± 0.003%
Ga	0.000% ± 0.005%	0.000% ± 0.005%	0.000% ± 0.008%	0.000% ± 0.002%	0.001% ± 0.004%
As	0.000% ± 0.007%	0.004% ± 0.007%	0.001% ± 0.010%	0.001% ± 0.004%	0.001% ± 0.007%
Se	0.000% ± 0.003%	0.000% ± 0.003%	0.000% ± 0.005%	0.000% ± 0.001%	0.000% ± 0.003%
Br	0.002% ± 0.003%	0.003% ± 0.002%	0.003% ± 0.004%	0.001% ± 0.001%	0.002% ± 0.002%
Rb	0.005% ± 0.002%	0.003% ± 0.002%	0.004% ± 0.003%	0.006% ± 0.001%	0.007% ± 0.002%
Sr	0.146% ± 0.011%	0.094% ± 0.007%	0.098% ± 0.008%	0.112% ± 0.008%	0.143% ± 0.011%
Yt	0.002% ± 0.004%	0.002% ± 0.004%	0.002% ± 0.005%	0.002% ± 0.001%	0.002% ± 0.003%
Zr	0.007% ± 0.004%	0.007% ± 0.003%	0.004% ± 0.008%	0.009% ± 0.002%	0.009% ± 0.003%
Mo	0.001% ± 0.008%	0.001% ± 0.008%	0.001% ± 0.011%	0.000% ± 0.003%	0.003% ± 0.006%
Pd	0.008% ± 0.025%	0.019% ± 0.025%	0.008% ± 0.036%	0.000% ± 0.011%	0.001% ± 0.021%
Ag	0.004% ± 0.029%	0.020% ± 0.029%	0.017% ± 0.042%	0.005% ± 0.013%	0.000% ± 0.024%
Cd	0.009% ± 0.030%	0.007% ± 0.029%	0.010% ± 0.043%	0.004% ± 0.013%	0.000% ± 0.024%
In	0.000% ± 0.034%	0.000% ± 0.034%	0.003% ± 0.049%	0.000% ± 0.015%	0.011% ± 0.028%
Sn	0.021% ± 0.043%	0.007% ± 0.043%	0.002% ± 0.063%	0.000% ± 0.019%	0.007% ± 0.035%
Sb	0.004% ± 0.049%	0.000% ± 0.050%	0.004% ± 0.072%	0.000% ± 0.022%	0.005% ± 0.040%
Ba	0.078% ± 0.175%	0.028% ± 0.176%	0.000% ± 0.257%	0.039% ± 0.075%	0.079% ± 0.143%
La	0.000% ± 0.227%	0.000% ± 0.230%	0.000% ± 0.338%	0.000% ± 0.097%	0.087% ± 0.189%
Au	0.000% ± 0.009%	0.000% ± 0.009%	0.000% ± 0.013%	0.000% ± 0.004%	0.000% ± 0.007%
Hg	0.000% ± 0.007%	0.000% ± 0.007%	0.001% ± 0.010%	0.002% ± 0.003%	0.001% ± 0.006%
Tl	0.001% ± 0.007%	0.001% ± 0.007%	0.000% ± 0.010%	0.001% ± 0.003%	0.000% ± 0.006%
Pb	0.021% ± 0.006%	0.019% ± 0.006%	0.027% ± 0.009%	0.019% ± 0.003%	0.027% ± 0.005%
U	0.002% ± 0.007%	0.002% ± 0.007%	0.001% ± 0.010%	0.002% ± 0.003%	0.003% ± 0.006%
Sum of Species	53.689% ± 3.501%	55.858% ± 4.607%	46.327% ± 3.566%	49.006% ± 2.495%	47.405% ± 2.505%

Individual Geological Source Profiles (Weight Percent by Mass)
Acquired in the Las Vegas PM₁₀ Study

	LVGSOIL2	LVGSOIL3	LVGSOIL4	LVGDDES1	LVGSOIL5
Mass	100.000% ± 7.124%	100.000% ± 7.538%	100.000% ± 7.408%	100.000% ± 7.118%	100.000% ± 7.262%
Cl⁻	0.000% ± 0.030%	0.063% ± 0.094%	0.005% ± 0.078%	0.041% ± 0.030%	0.086% ± 0.061%
NO₃⁻	0.000% ± 0.030%	0.000% ± 0.091%	0.000% ± 0.077%	0.037% ± 0.028%	0.073% ± 0.058%
SO₄⁼	0.352% ± 0.040%	0.568% ± 0.100%	0.461% ± 0.084%	0.575% ± 0.051%	0.654% ± 0.075%
NH₄⁺	0.057% ± 0.031%	0.210% ± 0.094%	0.153% ± 0.079%	0.061% ± 0.029%	0.122% ± 0.059%
K⁺	0.083% ± 0.025%	0.153% ± 0.072%	0.141% ± 0.061%	0.089% ± 0.023%	0.133% ± 0.046%
OC	12.468% ± 2.013%	8.364% ± 2.188%	4.681% ± 1.621%	6.990% ± 1.226%	2.276% ± 1.123%
EC	0.000% ± 0.232%	3.454% ± 1.346%	3.061% ± 1.176%	1.437% ± 0.527%	2.692% ± 0.999%
TC	12.350% ± 1.836%	11.464% ± 2.848%	7.441% ± 2.239%	8.317% ± 1.348%	4.743% ± 1.620%
Na	0.000% ± 0.150%	0.000% ± 0.262%	0.000% ± 0.241%	0.000% ± 0.144%	0.000% ± 0.216%
Mg	3.930% ± 0.282%	3.491% ± 0.266%	3.634% ± 0.272%	3.252% ± 0.234%	4.080% ± 0.299%
Al	0.841% ± 0.062%	1.195% ± 0.095%	1.364% ± 0.105%	0.940% ± 0.069%	1.053% ± 0.080%
Si	5.019% ± 0.357%	6.551% ± 0.481%	7.967% ± 0.579%	5.769% ± 0.410%	6.908% ± 0.496%
P	0.009% ± 0.012%	0.001% ± 0.021%	0.045% ± 0.008%	0.010% ± 0.013%	0.008% ± 0.018%
S	0.106% ± 0.008%	0.132% ± 0.012%	0.150% ± 0.013%	0.183% ± 0.014%	0.230% ± 0.018%
Cl	0.000% ± 0.097%	0.000% ± 0.095%	0.000% ± 0.088%	0.000% ± 0.101%	0.000% ± 0.097%
K	0.732% ± 0.068%	0.825% ± 0.074%	1.010% ± 0.084%	0.733% ± 0.069%	0.752% ± 0.069%
Ca	18.026% ± 1.281%	16.614% ± 1.228%	15.599% ± 1.141%	18.950% ± 1.346%	17.567% ± 1.265%
Ti	0.106% ± 0.019%	0.123% ± 0.051%	0.153% ± 0.044%	0.123% ± 0.018%	0.122% ± 0.034%
V	0.008% ± 0.011%	0.007% ± 0.030%	0.007% ± 0.026%	0.010% ± 0.008%	0.009% ± 0.021%
Cr	0.005% ± 0.002%	0.004% ± 0.008%	0.004% ± 0.007%	0.004% ± 0.002%	0.002% ± 0.006%
Mn	0.023% ± 0.002%	0.030% ± 0.004%	0.034% ± 0.004%	0.029% ± 0.002%	0.034% ± 0.003%
Fe	1.143% ± 0.081%	1.294% ± 0.095%	1.524% ± 0.111%	1.276% ± 0.091%	1.325% ± 0.095%
Co	0.000% ± 0.018%	0.000% ± 0.021%	0.000% ± 0.024%	0.001% ± 0.020%	0.000% ± 0.021%
Ni	0.003% ± 0.001%	0.001% ± 0.003%	0.002% ± 0.003%	0.003% ± 0.001%	0.002% ± 0.002%
Cu	0.001% ± 0.001%	0.002% ± 0.003%	0.001% ± 0.002%	0.002% ± 0.001%	0.001% ± 0.002%
Zn	0.010% ± 0.001%	0.013% ± 0.002%	0.018% ± 0.002%	0.014% ± 0.001%	0.013% ± 0.002%
Ga	0.000% ± 0.002%	0.001% ± 0.005%	0.000% ± 0.005%	0.000% ± 0.002%	0.000% ± 0.004%
As	0.000% ± 0.002%	0.002% ± 0.006%	0.000% ± 0.006%	0.000% ± 0.002%	0.001% ± 0.004%
Se	0.000% ± 0.001%	0.000% ± 0.003%	0.000% ± 0.003%	0.000% ± 0.001%	0.000% ± 0.002%
Br	0.000% ± 0.001%	0.001% ± 0.003%	0.001% ± 0.003%	0.001% ± 0.001%	0.001% ± 0.002%
Rb	0.005% ± 0.001%	0.004% ± 0.002%	0.005% ± 0.002%	0.004% ± 0.001%	0.004% ± 0.001%
Sr	0.133% ± 0.010%	0.112% ± 0.009%	0.102% ± 0.008%	0.151% ± 0.011%	0.158% ± 0.012%
Yt	0.002% ± 0.001%	0.001% ± 0.004%	0.002% ± 0.003%	0.002% ± 0.001%	0.002% ± 0.003%
Zr	0.005% ± 0.005%	0.006% ± 0.004%	0.005% ± 0.003%	0.005% ± 0.006%	0.004% ± 0.007%
Mo	0.002% ± 0.003%	0.002% ± 0.008%	0.001% ± 0.007%	0.001% ± 0.003%	0.001% ± 0.006%
Pd	0.000% ± 0.010%	0.008% ± 0.025%	0.000% ± 0.022%	0.002% ± 0.010%	0.000% ± 0.018%
Ag	0.000% ± 0.011%	0.007% ± 0.029%	0.004% ± 0.026%	0.000% ± 0.011%	0.000% ± 0.021%
Cd	0.000% ± 0.012%	0.013% ± 0.031%	0.000% ± 0.026%	0.000% ± 0.011%	0.004% ± 0.021%
In	0.000% ± 0.013%	0.000% ± 0.035%	0.000% ± 0.030%	0.000% ± 0.013%	0.000% ± 0.024%
Sn	0.002% ± 0.017%	0.009% ± 0.043%	0.006% ± 0.038%	0.000% ± 0.016%	0.000% ± 0.031%
Sb	0.004% ± 0.019%	0.000% ± 0.050%	0.009% ± 0.043%	0.000% ± 0.018%	0.000% ± 0.036%
Ba	0.000% ± 0.065%	0.000% ± 0.177%	0.000% ± 0.153%	0.013% ± 0.061%	0.000% ± 0.124%
La	0.000% ± 0.085%	0.000% ± 0.232%	0.000% ± 0.200%	0.000% ± 0.079%	0.000% ± 0.163%
Au	0.000% ± 0.003%	0.002% ± 0.008%	0.000% ± 0.007%	0.000% ± 0.003%	0.000% ± 0.006%
Hg	0.001% ± 0.003%	0.002% ± 0.007%	0.002% ± 0.006%	0.001% ± 0.003%	0.001% ± 0.005%
Tl	0.001% ± 0.003%	0.000% ± 0.007%	0.001% ± 0.006%	0.001% ± 0.002%	0.002% ± 0.005%
Pb	0.003% ± 0.002%	0.005% ± 0.009%	0.010% ± 0.005%	0.005% ± 0.002%	0.001% ± 0.006%
U	0.001% ± 0.003%	0.004% ± 0.007%	0.003% ± 0.006%	0.001% ± 0.003%	0.001% ± 0.005%
Sum of Species	42.888% ± 2.453%	42.925% ± 2.939%	39.867% ± 2.431%	40.405% ± 1.970%	37.870% ± 2.081%

Table B-1 (continued)
Individual Geological Source Profiles (Weight Percent by Mass)
Acquired in the Las Vegas PM₁₀ Study

	LVGUPRD1	LVGUPRD2
Mass	100.000% ± 7.214%	100.000% ± 7.144%
Cl⁻	0.094% ± 0.054%	0.293% ± 0.059%
NO₃⁻	0.076% ± 0.050%	0.141% ± 0.037%
SO₄⁼	1.099% ± 0.095%	0.581% ± 0.055%
NH₄⁺	0.089% ± 0.051%	0.088% ± 0.037%
K⁺	0.107% ± 0.040%	0.169% ± 0.031%
OC	9.817% ± 1.825%	9.237% ± 1.600%
EC	1.590% ± 0.652%	0.095% ± 0.276%
TC	11.220% ± 2.008%	9.193% ± 1.557%
Na	0.000% ± 0.192%	0.000% ± 0.165%
Mg	2.337% ± 0.174%	3.331% ± 0.241%
Al	1.085% ± 0.082%	1.297% ± 0.095%
Si	6.708% ± 0.480%	7.126% ± 0.507%
P	0.001% ± 0.018%	0.008% ± 0.015%
S	0.289% ± 0.022%	0.171% ± 0.013%
Cl	0.007% ± 0.123%	0.151% ± 0.035%
K	0.742% ± 0.077%	0.943% ± 0.080%
Ca	22.780% ± 1.631%	17.995% ± 1.281%
Ti	0.097% ± 0.029%	0.135% ± 0.022%
V	0.006% ± 0.017%	0.009% ± 0.013%
Cr	0.004% ± 0.004%	0.005% ± 0.003%
Mn	0.024% ± 0.003%	0.034% ± 0.003%
Fe	1.112% ± 0.080%	1.478% ± 0.105%
Co	0.001% ± 0.018%	0.000% ± 0.023%
Ni	0.004% ± 0.001%	0.003% ± 0.001%
Cu	0.001% ± 0.002%	0.001% ± 0.001%
Zn	0.012% ± 0.001%	0.013% ± 0.001%
Ga	0.000% ± 0.003%	0.000% ± 0.002%
As	0.000% ± 0.004%	0.000% ± 0.003%
Se	0.000% ± 0.002%	0.000% ± 0.001%
Br	0.001% ± 0.002%	0.002% ± 0.001%
Rb	0.005% ± 0.001%	0.005% ± 0.001%
Sr	0.106% ± 0.008%	0.096% ± 0.007%
Yt	0.003% ± 0.002%	0.002% ± 0.001%
Zr	0.005% ± 0.002%	0.006% ± 0.002%
Mo	0.003% ± 0.004%	0.002% ± 0.003%
Pd	0.000% ± 0.015%	0.003% ± 0.011%
Ag	0.000% ± 0.018%	0.000% ± 0.013%
Cd	0.007% ± 0.018%	0.000% ± 0.013%
In	0.007% ± 0.021%	0.000% ± 0.015%
Sn	0.000% ± 0.026%	0.006% ± 0.019%
Sb	0.000% ± 0.030%	0.007% ± 0.021%
Ba	0.031% ± 0.101%	0.006% ± 0.073%
La	0.000% ± 0.133%	0.000% ± 0.095%
Au	0.000% ± 0.005%	0.001% ± 0.004%
Hg	0.000% ± 0.004%	0.001% ± 0.003%
Tl	0.001% ± 0.004%	0.002% ± 0.003%
Pb	0.003% ± 0.005%	0.002% ± 0.004%
U	0.001% ± 0.004%	0.001% ± 0.003%
Sum of Species	47.764% ± 2.606%	42.813% ± 2.161%

Composite Geological Source Profiles (Weight Percent by Mass) Acquired in the Las Vegas PM$_{10}$ Study

	LVGCONSC	LVGPLOTC	LVGPVRDC	LVGSOILC	LVGUPRDC	LVGEOLC
Mass	100.000% ± 3.220%	100.000% ± 5.255%	100.000% ± 2.829%	100.000% ± 5.078%	100.000% ± 5.076%	100.000% ± 1.565%
Cl⁻	0.119% ± 0.054%	0.193% ± 0.135%	0.115% ± 0.061%	0.032% ± 0.290%	0.193% ± 0.141%	0.110% ± 0.080%
NO$_3^-$	0.094% ± 0.051%	0.227% ± 0.080%	0.194% ± 0.088%	0.028% ± 0.281%	0.108% ± 0.046%	0.123% ± 0.093%
SO$_4^=$	0.807% ± 0.401%	1.759% ± 0.740%	1.499% ± 0.795%	0.707% ± 0.496%	0.840% ± 0.366%	1.087% ± 0.677%
NH$_4^+$	0.096% ± 0.047%	0.168% ± 0.071%	0.161% ± 0.048%	0.120% ± 0.285%	0.089% ± 0.031%	0.129% ± 0.055%
K$^+$	0.187% ± 0.053%	0.173% ± 0.055%	0.184% ± 0.064%	0.127% ± 0.255%	0.138% ± 0.044%	0.164% ± 0.054%
OC	8.944% ± 2.016%	14.210% ± 5.025%	11.973% ± 3.949%	8.238% ± 2.842%	9.527% ± 1.213%	9.976% ± 3.851%
EC	0.644% ± 0.864%	5.069% ± 1.275%	4.473% ± 2.350%	1.818% ± 1.426%	0.842% ± 1.057%	2.642% ± 2.297%
TC	9.432% ± 1.697%	18.976% ± 4.457%	16.136% ± 5.140%	9.825% ± 2.083%	10.207% ± 1.433%	12.379% ± 5.065%
Na	0.000% ± 0.081%	0.022% ± 0.182%	0.022% ± 0.098%	0.000% ± 0.637%	0.000% ± 0.127%	0.009% ± 0.048%
Mg	3.373% ± 0.430%	2.470% ± 0.590%	2.689% ± 0.414%	3.762% ± 0.812%	2.834% ± 0.703%	3.145% ± 0.660%
Al	1.393% ± 0.555%	1.858% ± 0.154%	1.616% ± 0.138%	1.173% ± 0.439%	1.191% ± 0.150%	1.423% ± 0.373%
Si	7.396% ± 1.965%	9.063% ± 0.466%	8.436% ± 0.772%	7.085% ± 2.017%	6.917% ± 0.349%	7.742% ± 1.499%
P	0.013% ± 0.018%	0.043% ± 0.034%	0.030% ± 0.021%	0.016% ± 0.190%	0.005% ± 0.012%	0.021% ± 0.021%
S	0.197% ± 0.051%	0.615% ± 0.050%	0.465% ± 0.081%	0.224% ± 0.194%	0.230% ± 0.084%	0.331% ± 0.177%
Cl	0.042% ± 0.041%	0.137% ± 0.091%	0.077% ± 0.044%	0.001% ± 0.532%	0.079% ± 0.101%	0.054% ± 0.056%
K	1.067% ± 0.279%	1.201% ± 0.109%	1.093% ± 0.126%	0.897% ± 0.439%	0.843% ± 0.142%	1.014% ± 0.209%
Ca	16.817% ± 1.420%	13.373% ± 2.588%	14.956% ± 2.673%	17.000% ± 1.974%	20.387% ± 3.383%	16.312% ± 2.637%
Ti	0.150% ± 0.054%	0.252% ± 0.074%	0.194% ± 0.019%	0.134% ± 0.226%	0.116% ± 0.027%	0.165% ± 0.051%
V	0.009% ± 0.007%	0.016% ± 0.020%	0.013% ± 0.011%	0.007% ± 0.146%	0.007% ± 0.011%	0.010% ± 0.005%
Cr	0.005% ± 0.002%	0.007% ± 0.004%	0.008% ± 0.003%	0.004% ± 0.076%	0.004% ± 0.002%	0.006% ± 0.003%
Mn	0.036% ± 0.012%	0.044% ± 0.004%	0.045% ± 0.006%	0.032% ± 0.082%	0.029% ± 0.007%	0.038% ± 0.009%
Fe	1.645% ± 0.515%	2.283% ± 0.235%	2.224% ± 0.291%	1.440% ± 0.503%	1.295% ± 0.259%	1.794% ± 0.504%
Co	0.001% ± 0.012%	0.000% ± 0.025%	0.000% ± 0.013%	0.000% ± 0.234%	0.001% ± 0.014%	0.000% ± 0.006%
Ni	0.003% ± 0.001%	0.003% ± 0.001%	0.004% ± 0.001%	0.002% ± 0.044%	0.003% ± 0.001%	0.003% ± 0.001%
Cu	0.001% ± 0.001%	0.008% ± 0.001%	0.011% ± 0.004%	0.002% ± 0.044%	0.001% ± 0.001%	0.005% ± 0.005%
Zn	0.011% ± 0.004%	0.121% ± 0.006%	0.091% ± 0.027%	0.019% ± 0.058%	0.012% ± 0.001%	0.049% ± 0.046%
Ga	0.000% ± 0.001%	0.000% ± 0.003%	0.000% ± 0.002%	0.000% ± 0.071%	0.000% ± 0.002%	0.000% ± 0.001%
As	0.001% ± 0.001%	0.000% ± 0.005%	0.001% ± 0.003%	0.001% ± 0.082%	0.000% ± 0.002%	0.001% ± 0.001%
Se	0.000% ± 0.001%	0.000% ± 0.002%	0.000% ± 0.001%	0.000% ± 0.055%	0.000% ± 0.001%	0.000% ± 0.001%
Br	0.001% ± 0.000%	0.002% ± 0.002%	0.003% ± 0.003%	0.001% ± 0.058%	0.001% ± 0.001%	0.002% ± 0.002%
Rb	0.006% ± 0.002%	0.007% ± 0.001%	0.005% ± 0.001%	0.005% ± 0.044%	0.005% ± 0.001%	0.005% ± 0.001%
Sr	0.119% ± 0.018%	0.084% ± 0.005%	0.122% ± 0.046%	0.128% ± 0.173%	0.101% ± 0.007%	0.119% ± 0.031%
Yt	0.002% ± 0.001%	0.002% ± 0.002%	0.002% ± 0.001%	0.002% ± 0.050%	0.002% ± 0.001%	0.002% ± 0.001%
Zr	0.006% ± 0.002%	0.009% ± 0.002%	0.007% ± 0.002%	0.006% ± 0.129%	0.005% ± 0.001%	0.007% ± 0.002%
Mo	0.001% ± 0.002%	0.001% ± 0.005%	0.002% ± 0.003%	0.002% ± 0.087%	0.002% ± 0.003%	0.001% ± 0.001%
Pd	0.000% ± 0.006%	0.003% ± 0.016%	0.009% ± 0.009%	0.002% ± 0.163%	0.002% ± 0.010%	0.004% ± 0.006%
Ag	0.001% ± 0.007%	0.009% ± 0.019%	0.010% ± 0.011%	0.002% ± 0.175%	0.000% ± 0.011%	0.005% ± 0.006%
Cd	0.000% ± 0.007%	0.002% ± 0.019%	0.005% ± 0.011%	0.003% ± 0.177%	0.004% ± 0.011%	0.003% ± 0.005%
In	0.001% ± 0.008%	0.000% ± 0.022%	0.001% ± 0.012%	0.002% ± 0.190%	0.004% ± 0.013%	0.002% ± 0.006%
Sn	0.002% ± 0.010%	0.001% ± 0.028%	0.005% ± 0.016%	0.005% ± 0.209%	0.003% ± 0.016%	0.004% ± 0.007%
Sb	0.001% ± 0.011%	0.006% ± 0.032%	0.004% ± 0.018%	0.004% ± 0.225%	0.004% ± 0.018%	0.003% ± 0.008%
Ba	0.022% ± 0.039%	0.009% ± 0.114%	0.033% ± 0.064%	0.018% ± 0.415%	0.018% ± 0.062%	0.022% ± 0.029%
La	0.000% ± 0.051%	0.000% ± 0.149%	0.000% ± 0.084%	0.017% ± 0.473%	0.000% ± 0.081%	0.004% ± 0.038%
Au	0.000% ± 0.002%	0.000% ± 0.006%	0.000% ± 0.003%	0.000% ± 0.091%	0.001% ± 0.003%	0.000% ± 0.001%
Hg	0.001% ± 0.002%	0.000% ± 0.004%	0.001% ± 0.003%	0.001% ± 0.083%	0.001% ± 0.002%	0.001% ± 0.001%
Tl	0.001% ± 0.001%	0.000% ± 0.004%	0.001% ± 0.002%	0.001% ± 0.082%	0.001% ± 0.002%	0.001% ± 0.001%
Pb	0.003% ± 0.002%	0.019% ± 0.014%	0.021% ± 0.006%	0.010% ± 0.075%	0.003% ± 0.003%	0.012% ± 0.010%
U	0.001% ± 0.002%	0.001% ± 0.004%	0.001% ± 0.002%	0.002% ± 0.085%	0.001% ± 0.002%	0.001% ± 0.001%
Sum of Species	42.716% ± 2.737%	52.488% ± 2.947%	50.042% ± 3.517%	42.698% ± 2.980%	45.288% ± 3.501%	45.945% ± 5.046%

Table B-3
Individual Motor Vehicle Exhaust Source Profiles (Weight Percent by Mass)
Acquired in the Las Vegas PM$_{10}$ Study

	LVMVECH1	LVMVECH2	LVMVEEC1	LVMVEEC2	LVMVE951
Mass	100.000% ± 19.012%	100.000% ± 19.362%	100.000% ± 22.129%	100.000% ± 30.345%	100.000% ± 42.899%
Cl$^-$	0.664% ± 0.549%	0.509% ± 0.601%	0.411% ± 0.656%	1.285% ± 1.059%	0.121% ± 1.631%
NO$_3^-$	0.000% ± 0.780%	0.000% ± 0.894%	6.641% ± 1.343%	0.000% ± 1.857%	0.000% ± 1.826%
SO$_4^=$	5.913% ± 1.154%	14.685% ± 2.387%	3.358% ± 1.948%	3.575% ± 2.297%	0.000% ± 2.783%
NH$_4^+$	0.000% ± 0.592%	3.232% ± 0.908%	0.136% ± 0.948%	0.000% ± 1.319%	0.000% ± 1.846%
K$^+$	0.510% ± 0.098%	0.278% ± 0.084%	0.691% ± 0.141%	0.402% ± 0.151%	0.258% ± 0.201%
OC	45.631% ± 12.833%	44.652% ± 13.619%	58.759% ± 16.986%	62.601% ± 23.695%	53.629% ± 32.370%
EC	46.598% ± 9.120%	33.087% ± 6.868%	28.527% ± 6.571%	32.470% ± 9.165%	40.346% ± 14.427%
TC	90.455% ± 19.510%	75.788% ± 18.669%	85.179% ± 21.845%	91.751% ± 31.256%	88.354% ± 45.061%
Na	0.000% ± 0.900%	0.000% ± 1.052%	1.339% ± 0.598%	0.000% ± 1.799%	0.000% ± 2.441%
Mg	0.000% ± 0.159%	0.000% ± 0.196%	0.000% ± 0.210%	0.000% ± 0.315%	0.000% ± 0.460%
Al	0.044% ± 0.159%	0.353% ± 0.201%	0.212% ± 0.213%	0.000% ± 0.315%	0.342% ± 0.471%
Si	0.000% ± 0.351%	1.010% ± 0.510%	0.000% ± 0.552%	0.000% ± 0.679%	0.990% ± 0.783%
P	0.078% ± 0.125%	0.000% ± 0.156%	0.023% ± 0.164%	0.060% ± 0.248%	0.174% ± 0.314%
S	2.365% ± 0.381%	6.364% ± 0.967%	2.169% ± 0.682%	2.570% ± 0.852%	0.000% ± 0.749%
Cl	0.181% ± 0.103%	0.000% ± 0.208%	0.067% ± 0.225%	0.275% ± 0.205%	0.072% ± 0.407%
K	0.000% ± 0.103%	0.268% ± 0.128%	0.000% ± 0.134%	0.002% ± 0.210%	0.441% ± 0.322%
Ca	0.000% ± 1.085%	0.000% ± 1.388%	0.000% ± 1.762%	0.000% ± 2.205%	0.000% ± 2.026%
Ti	0.065% ± 0.468%	0.103% ± 0.478%	0.000% ± 0.564%	0.015% ± 0.969%	0.243% ± 1.409%
V	0.000% ± 0.193%	0.025% ± 0.198%	0.033% ± 0.234%	0.038% ± 0.401%	0.079% ± 0.582%
Cr	0.003% ± 0.047%	0.011% ± 0.048%	0.000% ± 0.056%	0.117% ± 0.073%	0.003% ± 0.139%
Mn	0.012% ± 0.024%	0.030% ± 0.026%	0.000% ± 0.041%	0.000% ± 0.071%	0.027% ± 0.103%
Fe	0.791% ± 0.190%	1.650% ± 0.313%	0.389% ± 0.234%	0.000% ± 0.285%	2.289% ± 0.779%
Co	0.000% ± 0.037%	0.000% ± 0.053%	0.000% ± 0.045%	0.000% ± 0.060%	0.005% ± 0.092%
Ni	0.003% ± 0.021%	0.010% ± 0.022%	0.009% ± 0.026%	0.002% ± 0.044%	0.017% ± 0.064%
Cu	0.026% ± 0.015%	0.160% ± 0.028%	0.040% ± 0.019%	0.082% ± 0.035%	0.084% ± 0.053%
Zn	0.128% ± 0.027%	0.271% ± 0.046%	0.227% ± 0.047%	0.213% ± 0.063%	0.226% ± 0.088%
Ga	0.000% ± 0.039%	0.000% ± 0.040%	0.003% ± 0.047%	0.000% ± 0.082%	0.000% ± 0.116%
As	0.006% ± 0.046%	0.013% ± 0.049%	0.011% ± 0.056%	0.015% ± 0.095%	0.010% ± 0.135%
Se	0.000% ± 0.024%	0.007% ± 0.025%	0.001% ± 0.029%	0.000% ± 0.049%	0.000% ± 0.070%
Br	0.012% ± 0.023%	0.022% ± 0.018%	0.031% ± 0.021%	0.031% ± 0.049%	0.053% ± 0.052%
Rb	0.006% ± 0.021%	0.000% ± 0.021%	0.000% ± 0.025%	0.000% ± 0.043%	0.000% ± 0.062%
Sr	0.000% ± 0.025%	0.000% ± 0.029%	0.000% ± 0.036%	0.000% ± 0.061%	0.000% ± 0.075%
Yt	0.007% ± 0.029%	0.001% ± 0.028%	0.000% ± 0.034%	0.001% ± 0.059%	0.000% ± 0.084%
Zr	0.000% ± 0.033%	0.005% ± 0.033%	0.000% ± 0.039%	0.000% ± 0.069%	0.000% ± 0.096%
Mo	0.000% ± 0.059%	0.000% ± 0.059%	0.004% ± 0.072%	0.000% ± 0.123%	0.000% ± 0.174%
Pd	0.000% ± 0.181%	0.045% ± 0.183%	0.049% ± 0.219%	0.036% ± 0.370%	0.000% ± 0.535%
Ag	0.000% ± 0.210%	0.000% ± 0.213%	0.000% ± 0.252%	0.165% ± 0.435%	0.190% ± 0.635%
Cd	0.014% ± 0.210%	0.006% ± 0.217%	0.027% ± 0.255%	0.122% ± 0.438%	0.012% ± 0.631%
In	0.167% ± 0.252%	0.133% ± 0.260%	0.057% ± 0.299%	0.170% ± 0.521%	0.694% ± 0.593%
Sn	0.142% ± 0.321%	0.108% ± 0.326%	0.035% ± 0.382%	0.000% ± 0.657%	0.000% ± 0.954%
Sb	0.000% ± 0.382%	0.000% ± 0.391%	0.000% ± 0.459%	0.000% ± 0.789%	0.000% ± 1.152%
Ba	0.153% ± 1.374%	0.000% ± 1.402%	0.000% ± 1.660%	0.000% ± 2.848%	0.000% ± 4.135%
La	0.000% ± 1.801%	0.000% ± 1.842%	0.000% ± 2.170%	0.000% ± 3.729%	0.000% ± 5.412%
Au	0.000% ± 0.064%	0.029% ± 0.069%	0.000% ± 0.078%	0.000% ± 0.134%	0.024% ± 0.192%
Hg	0.002% ± 0.054%	0.012% ± 0.054%	0.000% ± 0.065%	0.000% ± 0.111%	0.000% ± 0.157%
Tl	0.005% ± 0.053%	0.000% ± 0.052%	0.000% ± 0.062%	0.000% ± 0.108%	0.000% ± 0.154%
Pb	0.013% ± 0.069%	0.072% ± 0.053%	0.022% ± 0.084%	0.000% ± 0.143%	0.051% ± 0.204%
U	0.000% ± 0.051%	0.000% ± 0.051%	0.000% ± 0.061%	0.009% ± 0.106%	0.000% ± 0.149%
Sum of Species	100.000% ± 16.070%	100.000% ± 15.800%	100.000% ± 18.727%	100.000% ± 26.268%	100.000% ± 36.541%

Individual Motor Vehicle Exhaust Source Profiles (Weight Percent by Mass)
Acquired in the Las Vegas PM$_{10}$ Study

	LVMVELM1	LVMVELM2	LVMVELM3	LVMVELV1	LVMVELV2
Mass	100.000% ± 17.114%	100.000% ± 21.361%	100.000% ± 42.584%	100.000% ± 22.980%	100.000% ± 31.661%
Cl$^-$	0.178% ± 0.472%	0.609% ± 0.691%	0.183% ± 1.582%	0.000% ± 0.766%	0.276% ± 1.141%
NO$_3^-$	0.841% ± 0.525%	0.746% ± 0.702%	0.526% ± 1.608%	0.916% ± 0.799%	0.722% ± 1.265%
SO$_4^=$	4.035% ± 0.841%	8.763% ± 1.683%	0.000% ± 2.157%	6.341% ± 1.517%	4.167% ± 2.008%
NH$_4^+$	0.924% ± 0.522%	2.522% ± 0.844%	0.000% ± 1.660%	1.087% ± 0.837%	0.000% ± 1.237%
K$^+$	0.272% ± 0.067%	0.254% ± 0.087%	0.247% ± 0.194%	0.220% ± 0.096%	0.283% ± 0.153%
OC	42.230% ± 11.308%	53.887% ± 16.069%	71.671% ± 35.574%	52.484% ± 17.348%	46.803% ± 23.040%
EC	43.073% ± 8.005%	30.002% ± 6.514%	25.558% ± 9.783%	22.007% ± 5.413%	30.569% ± 9.121%
TC	83.725% ± 17.029%	81.582% ± 21.118%	91.786% ± 44.884%	71.882% ± 21.878%	73.584% ± 30.927%
Na	0.000% ± 0.957%	0.000% ± 1.153%	0.000% ± 2.521%	0.280% ± 1.324%	1.379% ± 1.067%
Mg	0.206% ± 0.165%	0.000% ± 0.204%	0.305% ± 0.443%	1.993% ± 0.405%	1.556% ± 0.519%
Al	0.836% ± 0.192%	0.394% ± 0.213%	0.000% ± 0.434%	0.707% ± 0.270%	1.182% ± 0.467%
Si	2.567% ± 0.495%	0.664% ± 0.377%	0.000% ± 0.673%	3.079% ± 0.724%	3.729% ± 1.254%
P	0.114% ± 0.061%	0.016% ± 0.156%	0.118% ± 0.288%	0.000% ± 0.170%	0.000% ± 0.258%
S	1.664% ± 0.258%	3.368% ± 0.575%	0.000% ± 0.469%	2.133% ± 0.427%	1.996% ± 0.616%
Cl	0.001% ± 0.157%	0.070% ± 0.209%	0.018% ± 0.379%	0.000% ± 0.246%	0.020% ± 0.383%
K	0.461% ± 0.114%	0.241% ± 0.133%	0.128% ± 0.279%	0.310% ± 0.163%	0.519% ± 0.264%
Ca	2.322% ± 1.012%	0.000% ± 1.018%	0.000% ± 2.004%	8.705% ± 2.046%	3.170% ± 2.683%
Ti	0.152% ± 0.419%	0.090% ± 0.599%	0.056% ± 1.350%	0.062% ± 0.683%	0.362% ± 1.030%
V	0.014% ± 0.173%	0.020% ± 0.247%	0.057% ± 0.557%	0.039% ± 0.282%	0.045% ± 0.425%
Cr	0.004% ± 0.042%	0.000% ± 0.059%	0.039% ± 0.137%	0.000% ± 0.067%	0.008% ± 0.104%
Mn	0.036% ± 0.022%	0.012% ± 0.044%	0.018% ± 0.098%	0.044% ± 0.036%	0.069% ± 0.056%
Fe	1.749% ± 0.271%	1.393% ± 0.275%	0.478% ± 0.338%	1.182% ± 0.276%	4.493% ± 1.100%
Co	0.000% ± 0.045%	0.000% ± 0.047%	0.022% ± 0.074%	0.014% ± 0.050%	0.018% ± 0.118%
Ni	0.002% ± 0.019%	0.000% ± 0.026%	0.005% ± 0.061%	0.001% ± 0.031%	0.001% ± 0.047%
Cu	0.036% ± 0.014%	0.100% ± 0.025%	0.023% ± 0.060%	0.035% ± 0.023%	0.154% ± 0.048%
Zn	0.201% ± 0.032%	0.334% ± 0.059%	0.215% ± 0.083%	0.103% ± 0.032%	0.155% ± 0.056%
Ga	0.001% ± 0.035%	0.000% ± 0.050%	0.002% ± 0.113%	0.003% ± 0.057%	0.000% ± 0.086%
As	0.023% ± 0.041%	0.000% ± 0.062%	0.000% ± 0.130%	0.009% ± 0.065%	0.026% ± 0.101%
Se	0.000% ± 0.021%	0.000% ± 0.030%	0.000% ± 0.068%	0.000% ± 0.035%	0.000% ± 0.053%
Br	0.027% ± 0.015%	0.021% ± 0.021%	0.039% ± 0.067%	0.027% ± 0.025%	0.038% ± 0.037%
Rb	0.001% ± 0.019%	0.000% ± 0.026%	0.000% ± 0.059%	0.000% ± 0.030%	0.000% ± 0.047%
Sr	0.000% ± 0.021%	0.012% ± 0.027%	0.000% ± 0.075%	0.023% ± 0.032%	0.000% ± 0.055%
Yt	0.006% ± 0.025%	0.000% ± 0.035%	0.000% ± 0.081%	0.002% ± 0.041%	0.005% ± 0.062%
Zr	0.003% ± 0.029%	0.000% ± 0.041%	0.000% ± 0.093%	0.002% ± 0.048%	0.018% ± 0.073%
Mo	0.003% ± 0.053%	0.000% ± 0.075%	0.000% ± 0.170%	0.000% ± 0.085%	0.000% ± 0.130%
Pd	0.039% ± 0.158%	0.016% ± 0.233%	0.000% ± 0.518%	0.097% ± 0.261%	0.104% ± 0.396%
Ag	0.000% ± 0.186%	0.144% ± 0.267%	0.000% ± 0.597%	0.132% ± 0.302%	0.108% ± 0.462%
Cd	0.000% ± 0.189%	0.189% ± 0.271%	0.107% ± 0.604%	0.031% ± 0.303%	0.000% ± 0.467%
In	0.036% ± 0.223%	0.146% ± 0.315%	0.313% ± 0.728%	0.130% ± 0.363%	0.065% ± 0.550%
Sn	0.000% ± 0.283%	0.115% ± 0.402%	0.193% ± 0.917%	0.139% ± 0.457%	0.198% ± 0.696%
Sb	0.000% ± 0.344%	0.000% ± 0.485%	0.092% ± 1.112%	0.014% ± 0.549%	0.000% ± 0.837%
Ba	0.048% ± 1.229%	0.000% ± 1.761%	0.000% ± 3.968%	0.000% ± 1.989%	0.000% ± 3.011%
La	0.000% ± 1.606%	0.000% ± 2.278%	0.000% ± 5.212%	0.000% ± 2.611%	0.270% ± 3.955%
Au	0.000% ± 0.058%	0.000% ± 0.083%	0.000% ± 0.184%	0.000% ± 0.093%	0.000% ± 0.141%
Hg	0.000% ± 0.047%	0.000% ± 0.067%	0.000% ± 0.153%	0.000% ± 0.077%	0.000% ± 0.117%
Tl	0.004% ± 0.047%	0.000% ± 0.066%	0.000% ± 0.150%	0.000% ± 0.075%	0.000% ± 0.115%
Pb	0.006% ± 0.061%	0.106% ± 0.066%	0.000% ± 0.197%	0.002% ± 0.099%	0.000% ± 0.149%
U	0.000% ± 0.045%	0.000% ± 0.064%	0.019% ± 0.145%	0.000% ± 0.072%	0.044% ± 0.113%
Sum of Species	100.000% ± 14.150%	100.000% ± 17.802%	100.000% ± 37.838%	100.000% ± 18.790%	100.000% ± 25.716%

Table B-3 (continued)
Individual Motor Vehicle Exhaust Source Profiles (Weight Percent by Mass)
Acquired in the Las Vegas PM$_{10}$ Study

	LVMVELV3	LVMVELV4	LVMVELV5	LVMVELV6	LVMVEPE1
Mass	100.000% ± 29.054%	100.000% ± 32.493%	100.000% ± 26.836%	100.000% ± 26.257%	100.000% ± 29.694%
Cl⁻	0.622% ± 0.897%	1.295% ± 1.142%	0.000% ± 0.965%	0.634% ± 0.733%	0.000% ± 0.908%
NO₃⁻	0.000% ± 0.973%	0.000% ± 1.122%	1.701% ± 1.058%	0.000% ± 0.851%	0.000% ± 1.125%
SO₄⁼	4.302% ± 1.789%	0.000% ± 1.769%	11.588% ± 2.528%	0.000% ± 1.558%	0.000% ± 1.987%
NH₄⁺	0.000% ± 0.936%	0.000% ± 1.127%	3.200% ± 1.182%	0.000% ± 0.791%	0.000% ± 1.081%
K⁺	0.045% ± 0.126%	2.550% ± 0.619%	0.209% ± 0.118%	0.076% ± 0.120%	0.166% ± 0.140%
OC	64.464% ± 22.954%	55.153% ± 24.335%	41.721% ± 19.050%	46.757% ± 17.830%	35.758% ± 19.019%
EC	30.065% ± 8.667%	37.291% ± 11.172%	35.047% ± 8.876%	50.952% ± 12.732%	59.859% ± 15.904%
TC	91.918% ± 29.689%	88.988% ± 33.357%	73.469% ± 26.415%	95.628% ± 27.250%	92.704% ± 30.795%
Na	0.000% ± 1.308%	0.000% ± 1.895%	0.971% ± 0.828%	1.304% ± 0.701%	1.086% ± 0.931%
Mg	0.000% ± 0.306%	0.946% ± 0.417%	0.000% ± 0.288%	0.000% ± 0.273%	0.000% ± 0.355%
Al	0.000% ± 0.306%	0.000% ± 0.355%	0.573% ± 0.308%	0.000% ± 0.273%	0.209% ± 0.358%
Si	0.000% ± 1.014%	0.000% ± 1.007%	0.266% ± 0.512%	0.000% ± 1.098%	0.000% ± 1.212%
P	0.000% ± 0.183%	0.065% ± 0.223%	0.113% ± 0.197%	0.139% ± 0.092%	0.064% ± 0.216%
S	1.199% ± 0.378%	0.000% ± 0.360%	4.296% ± 0.854%	0.000% ± 0.304%	0.533% ± 0.513%
Cl	0.500% ± 0.205%	1.506% ± 0.417%	0.185% ± 0.175%	0.107% ± 0.154%	0.042% ± 0.289%
K	0.000% ± 0.216%	2.481% ± 0.652%	0.252% ± 0.185%	0.000% ± 0.209%	0.060% ± 0.249%
Ca	0.000% ± 3.383%	0.000% ± 3.398%	0.000% ± 1.506%	0.000% ± 3.748%	0.000% ± 3.863%
Ti	0.000% ± 0.743%	0.000% ± 0.918%	0.139% ± 0.827%	0.000% ± 0.600%	0.127% ± 0.782%
V	0.034% ± 0.307%	0.024% ± 0.379%	0.064% ± 0.342%	0.005% ± 0.250%	0.007% ± 0.323%
Cr	0.003% ± 0.073%	0.027% ± 0.092%	0.000% ± 0.082%	0.000% ± 0.061%	0.003% ± 0.078%
Mn	0.000% ± 0.041%	0.010% ± 0.049%	0.023% ± 0.045%	0.000% ± 0.033%	0.017% ± 0.043%
Fe	0.031% ± 0.408%	0.076% ± 0.418%	2.497% ± 0.546%	0.000% ± 0.441%	1.560% ± 0.589%
Co	0.008% ± 0.072%	0.000% ± 0.076%	0.012% ± 0.073%	0.000% ± 0.073%	0.012% ± 0.096%
Ni	0.005% ± 0.033%	0.011% ± 0.042%	0.011% ± 0.037%	0.000% ± 0.027%	0.031% ± 0.027%
Cu	0.092% ± 0.032%	0.093% ± 0.037%	0.088% ± 0.032%	0.059% ± 0.023%	0.274% ± 0.065%
Zn	0.158% ± 0.056%	0.191% ± 0.066%	0.355% ± 0.078%	0.129% ± 0.051%	0.323% ± 0.086%
Ga	0.011% ± 0.062%	0.008% ± 0.076%	0.000% ± 0.067%	0.000% ± 0.050%	0.014% ± 0.064%
As	0.000% ± 0.072%	0.000% ± 0.090%	0.004% ± 0.079%	0.000% ± 0.060%	0.007% ± 0.078%
Se	0.000% ± 0.037%	0.003% ± 0.046%	0.000% ± 0.040%	0.000% ± 0.030%	0.000% ± 0.039%
Br	0.015% ± 0.041%	0.061% ± 0.036%	0.039% ± 0.031%	0.034% ± 0.023%	0.047% ± 0.030%
Rb	0.000% ± 0.033%	0.000% ± 0.040%	0.000% ± 0.035%	0.000% ± 0.027%	0.000% ± 0.035%
Sr	0.000% ± 0.063%	0.634% ± 0.165%	0.000% ± 0.039%	0.000% ± 0.068%	0.000% ± 0.071%
Yt	0.000% ± 0.044%	0.000% ± 0.054%	0.000% ± 0.048%	0.000% ± 0.035%	0.000% ± 0.046%
Zr	0.000% ± 0.051%	0.000% ± 0.071%	0.034% ± 0.057%	0.001% ± 0.042%	0.000% ± 0.053%
Mo	0.005% ± 0.092%	0.015% ± 0.114%	0.000% ± 0.101%	0.016% ± 0.077%	0.000% ± 0.097%
Pd	0.042% ± 0.284%	0.045% ± 0.355%	0.015% ± 0.312%	0.000% ± 0.229%	0.107% ± 0.304%
Ag	0.134% ± 0.329%	0.239% ± 0.409%	0.183% ± 0.369%	0.000% ± 0.274%	0.091% ± 0.353%
Cd	0.036% ± 0.333%	0.389% ± 0.324%	0.000% ± 0.363%	0.056% ± 0.277%	0.048% ± 0.358%
In	0.000% ± 0.399%	0.331% ± 0.496%	0.163% ± 0.440%	0.060% ± 0.318%	0.048% ± 0.419%
Sn	0.000% ± 0.496%	0.091% ± 0.624%	0.210% ± 0.563%	0.159% ± 0.413%	0.034% ± 0.534%
Sb	0.000% ± 0.607%	0.000% ± 0.749%	0.000% ± 0.665%	0.000% ± 0.490%	0.000% ± 0.642%
Ba	0.000% ± 2.171%	0.000% ± 2.692%	0.478% ± 2.429%	0.183% ± 1.768%	0.077% ± 2.297%
La	0.000% ± 2.866%	0.267% ± 3.529%	0.000% ± 3.177%	0.000% ± 2.318%	0.000% ± 2.994%
Au	0.010% ± 0.102%	0.000% ± 0.123%	0.020% ± 0.115%	0.000% ± 0.084%	0.000% ± 0.107%
Hg	0.028% ± 0.084%	0.000% ± 0.102%	0.000% ± 0.092%	0.016% ± 0.070%	0.000% ± 0.086%
Tl	0.000% ± 0.081%	0.000% ± 0.100%	0.000% ± 0.089%	0.000% ± 0.068%	0.000% ± 0.086%
Pb	0.033% ± 0.108%	0.045% ± 0.135%	0.048% ± 0.120%	0.005% ± 0.088%	0.079% ± 0.086%
U	0.025% ± 0.080%	0.000% ± 0.098%	0.000% ± 0.086%	0.017% ± 0.066%	0.018% ± 0.082%
Sum of Species	100.000% ± 25.227%	100.000% ± 27.612%	100.000% ± 21.739%	100.000% ± 22.576%	100.000% ± 25.600%

	LVMVEPE2	LVMVEPE3	LVMVESA1	LVMVESA2	LVMVESA3
Mass	100.000% ± 14.785%	100.000% ± 22.706%	100.000% ± 21.591%	100.000% ± 32.316%	100.000% ± 19.999%
Cl$^-$	0.156% ± 0.275%	0.552% ± 0.761%	0.166% ± 0.616%	0.218% ± 1.146%	0.168% ± 0.583%
NO$_3^-$	0.240% ± 0.299%	1.855% ± 0.908%	0.000% ± 0.757%	0.000% ± 1.217%	0.412% ± 0.610%
SO$_4^=$	2.629% ± 0.534%	7.246% ± 1.875%	0.000% ± 1.227%	0.000% ± 1.524%	4.143% ± 1.004%
NH$_4^+$	0.493% ± 0.310%	1.350% ± 0.927%	0.000% ± 0.731%	0.000% ± 1.193%	0.746% ± 0.620%
K$^+$	0.024% ± 0.033%	0.412% ± 0.116%	0.235% ± 0.086%	0.341% ± 0.153%	0.285% ± 0.082%
OC	46.822% ± 9.357%	45.653% ± 16.298%	49.897% ± 15.036%	60.012% ± 25.198%	47.239% ± 13.867%
EC	48.294% ± 8.263%	29.171% ± 6.844%	48.980% ± 10.356%	36.920% ± 10.545%	45.188% ± 9.116%
TC	94.210% ± 15.087%	72.346% ± 21.776%	96.859% ± 22.758%	93.025% ± 34.152%	90.487% ± 20.617%
Na	0.000% ± 0.496%	0.000% ± 1.477%	0.000% ± 0.950%	0.719% ± 0.921%	0.444% ± 0.509%
Mg	0.000% ± 0.087%	1.840% ± 0.394%	0.000% ± 0.183%	0.000% ± 0.307%	0.000% ± 0.169%
Al	0.000% ± 0.087%	0.967% ± 0.304%	0.000% ± 0.183%	0.000% ± 0.307%	0.000% ± 0.169%
Si	0.000% ± 0.204%	3.312% ± 0.864%	0.000% ± 0.462%	0.000% ± 0.509%	0.000% ± 0.366%
P	0.034% ± 0.069%	0.077% ± 0.176%	0.000% ± 0.128%	0.138% ± 0.210%	0.000% ± 0.121%
S	1.037% ± 0.159%	2.827% ± 0.608%	0.000% ± 0.326%	0.000% ± 0.313%	1.358% ± 0.250%
Cl	0.000% ± 0.086%	0.174% ± 0.147%	0.001% ± 0.162%	0.195% ± 0.201%	0.003% ± 0.151%
K	0.000% ± 0.057%	0.418% ± 0.178%	0.000% ± 0.124%	0.043% ± 0.203%	0.000% ± 0.113%
Ca	0.000% ± 0.626%	4.319% ± 1.990%	0.000% ± 1.524%	0.000% ± 1.667%	0.000% ± 1.197%
Ti	0.000% ± 0.264%	0.375% ± 0.482%	0.006% ± 0.529%	0.032% ± 0.984%	0.000% ± 0.522%
V	0.000% ± 0.109%	0.044% ± 0.268%	0.030% ± 0.219%	0.042% ± 0.406%	0.000% ± 0.282%
Cr	0.000% ± 0.026%	0.008% ± 0.064%	0.000% ± 0.052%	0.004% ± 0.097%	0.000% ± 0.086%
Mn	0.011% ± 0.013%	0.123% ± 0.040%	0.016% ± 0.028%	0.006% ± 0.071%	0.000% ± 0.042%
Fe	0.585% ± 0.112%	2.179% ± 0.446%	0.344% ± 0.205%	1.024% ± 0.347%	0.302% ± 0.167%
Co	0.004% ± 0.023%	0.001% ± 0.069%	0.003% ± 0.040%	0.020% ± 0.062%	0.006% ± 0.034%
Ni	0.000% ± 0.012%	0.016% ± 0.029%	0.005% ± 0.024%	0.000% ± 0.043%	0.003% ± 0.022%
Cu	0.017% ± 0.008%	0.047% ± 0.022%	0.046% ± 0.019%	0.096% ± 0.039%	0.058% ± 0.019%
Zn	0.250% ± 0.032%	0.164% ± 0.040%	0.146% ± 0.034%	0.297% ± 0.080%	0.120% ± 0.028%
Ga	0.000% ± 0.022%	0.031% ± 0.054%	0.009% ± 0.044%	0.025% ± 0.083%	0.000% ± 0.041%
As	0.008% ± 0.026%	0.000% ± 0.062%	0.000% ± 0.052%	0.007% ± 0.093%	0.005% ± 0.048%
Se	0.000% ± 0.014%	0.010% ± 0.033%	0.000% ± 0.027%	0.000% ± 0.049%	0.000% ± 0.025%
Br	0.012% ± 0.009%	0.038% ± 0.024%	0.024% ± 0.020%	0.010% ± 0.047%	0.021% ± 0.018%
Rb	0.000% ± 0.011%	0.000% ± 0.028%	0.005% ± 0.023%	0.010% ± 0.043%	0.000% ± 0.021%
Sr	0.000% ± 0.014%	0.034% ± 0.039%	0.000% ± 0.037%	0.000% ± 0.055%	0.000% ± 0.031%
Yt	0.000% ± 0.016%	0.005% ± 0.038%	0.000% ± 0.031%	0.000% ± 0.059%	0.000% ± 0.029%
Zr	0.000% ± 0.018%	0.017% ± 0.045%	0.000% ± 0.037%	0.000% ± 0.067%	0.004% ± 0.034%
Mo	0.000% ± 0.033%	0.023% ± 0.080%	0.000% ± 0.066%	0.008% ± 0.122%	0.000% ± 0.061%
Pd	0.005% ± 0.100%	0.127% ± 0.250%	0.000% ± 0.204%	0.050% ± 0.376%	0.000% ± 0.191%
Ag	0.025% ± 0.116%	0.114% ± 0.291%	0.008% ± 0.237%	0.059% ± 0.440%	0.024% ± 0.224%
Cd	0.000% ± 0.115%	0.162% ± 0.296%	0.094% ± 0.240%	0.031% ± 0.446%	0.144% ± 0.226%
In	0.088% ± 0.139%	0.000% ± 0.342%	0.124% ± 0.282%	0.171% ± 0.527%	0.126% ± 0.262%
Sn	0.005% ± 0.176%	0.000% ± 0.432%	0.123% ± 0.361%	0.000% ± 0.663%	0.035% ± 0.336%
Sb	0.000% ± 0.213%	0.068% ± 0.519%	0.000% ± 0.434%	0.043% ± 0.812%	0.000% ± 0.406%
Ba	0.472% ± 0.765%	0.000% ± 1.901%	0.035% ± 1.555%	0.000% ± 2.886%	0.203% ± 1.458%
La	0.000% ± 0.996%	0.000% ± 2.467%	0.061% ± 2.041%	0.000% ± 3.778%	0.713% ± 1.923%
Au	0.000% ± 0.037%	0.004% ± 0.088%	0.006% ± 0.073%	0.011% ± 0.134%	0.016% ± 0.068%
Hg	0.000% ± 0.030%	0.000% ± 0.072%	0.005% ± 0.060%	0.000% ± 0.109%	0.011% ± 0.056%
Tl	0.000% ± 0.030%	0.000% ± 0.070%	0.000% ± 0.058%	0.000% ± 0.108%	0.000% ± 0.054%
Pb	0.007% ± 0.039%	0.028% ± 0.093%	0.028% ± 0.078%	0.016% ± 0.141%	0.029% ± 0.072%
U	0.001% ± 0.029%	0.000% ± 0.068%	0.003% ± 0.056%	0.012% ± 0.104%	0.003% ± 0.052%
Sum of Species	100.000% ± 12.603%	100.000% ± 18.329%	100.000% ± 18.629%	100.000% ± 27.955%	100.000% ± 16.906%

Table B-4
Composite Motor Vehicle Exhaust Source Profiles (Weight Percent by Mass)
Acquired in the Las Vegas PM$_{10}$ Study

	LVMVECHC	LVMVEECC	LVMVELMC	LVMVELVC	LVMVEPEC
Mass	100.000% ± 13.568%	100.000% ± 18.778%	100.000% ± 16.874%	100.000% ± 11.595%	100.000% ± 13.399%
Cl$^-$	0.586% ± 0.407%	0.848% ± 0.623%	0.323% ± 0.597%	0.471% ± 0.492%	0.236% ± 0.405%
NO$_3^-$	0.000% ± 0.593%	3.320% ± 4.696%	0.704% ± 0.610%	0.556% ± 0.692%	0.698% ± 1.009%
SO$_4^=$	10.299% ± 6.203%	3.467% ± 1.506%	4.266% ± 4.386%	4.400% ± 4.341%	3.292% ± 3.668%
NH$_4^+$	1.616% ± 2.285%	0.068% ± 0.812%	1.149% ± 1.276%	0.715% ± 1.293%	0.614% ± 0.683%
K$^+$	0.394% ± 0.164%	0.547% ± 0.205%	0.257% ± 0.074%	0.564% ± 0.977%	0.201% ± 0.197%
OC	45.142% ± 9.356%	60.680% ± 14.577%	55.929% ± 14.826%	51.230% ± 8.550%	42.744% ± 8.912%
EC	39.842% ± 9.553%	30.498% ± 5.639%	32.877% ± 9.104%	34.322% ± 9.693%	45.775% ± 15.499%
TC	83.121% ± 13.502%	88.465% ± 19.066%	85.698% ± 17.482%	82.578% ± 11.630%	86.420% ± 13.541%
Na	0.000% ± 0.692%	0.669% ± 0.948%	0.000% ± 0.978%	0.656% ± 0.640%	0.362% ± 0.627%
Mg	0.000% ± 0.126%	0.000% ± 0.189%	0.171% ± 0.172%	0.749% ± 0.885%	0.613% ± 1.062%
Al	0.199% ± 0.219%	0.106% ± 0.190%	0.410% ± 0.418%	0.410% ± 0.493%	0.392% ± 0.509%
Si	0.505% ± 0.714%	0.000% ± 0.437%	1.077% ± 1.333%	1.179% ± 1.739%	1.104% ± 1.912%
P	0.039% ± 0.100%	0.042% ± 0.149%	0.082% ± 0.111%	0.053% ± 0.079%	0.058% ± 0.096%
S	4.364% ± 2.828%	2.369% ± 0.546%	1.677% ± 1.684%	1.604% ± 1.612%	1.466% ± 1.205%
Cl	0.091% ± 0.128%	0.171% ± 0.152%	0.030% ± 0.154%	0.386% ± 0.578%	0.072% ± 0.112%
K	0.134% ± 0.189%	0.001% ± 0.124%	0.277% ± 0.170%	0.594% ± 0.946%	0.159% ± 0.226%
Ca	0.000% ± 0.881%	0.000% ± 1.411%	0.774% ± 1.341%	1.979% ± 3.530%	1.440% ± 2.493%
Ti	0.084% ± 0.334%	0.008% ± 0.560%	0.099% ± 0.512%	0.094% ± 0.332%	0.167% ± 0.318%
V	0.013% ± 0.138%	0.036% ± 0.232%	0.031% ± 0.211%	0.035% ± 0.137%	0.017% ± 0.145%
Cr	0.007% ± 0.033%	0.058% ± 0.083%	0.014% ± 0.052%	0.006% ± 0.033%	0.004% ± 0.035%
Mn	0.021% ± 0.018%	0.000% ± 0.041%	0.022% ± 0.037%	0.024% ± 0.027%	0.050% ± 0.063%
Fe	1.220% ± 0.607%	0.194% ± 0.275%	1.207% ± 0.656%	1.380% ± 1.811%	1.441% ± 0.804%
Co	0.000% ± 0.032%	0.000% ± 0.038%	0.007% ± 0.033%	0.009% ± 0.033%	0.006% ± 0.040%
Ni	0.006% ± 0.015%	0.005% ± 0.025%	0.002% ± 0.023%	0.005% ± 0.015%	0.016% ± 0.016%
Cu	0.093% ± 0.095%	0.061% ± 0.030%	0.053% ± 0.041%	0.087% ± 0.040%	0.112% ± 0.141%
Zn	0.200% ± 0.101%	0.220% ± 0.039%	0.250% ± 0.073%	0.182% ± 0.090%	0.246% ± 0.079%
Ga	0.000% ± 0.028%	0.002% ± 0.047%	0.001% ± 0.043%	0.004% ± 0.028%	0.015% ± 0.029%
As	0.010% ± 0.034%	0.013% ± 0.055%	0.008% ± 0.050%	0.007% ± 0.032%	0.005% ± 0.034%
Se	0.004% ± 0.017%	0.000% ± 0.028%	0.000% ± 0.026%	0.001% ± 0.017%	0.003% ± 0.018%
Br	0.017% ± 0.015%	0.031% ± 0.026%	0.029% ± 0.024%	0.036% ± 0.015%	0.032% ± 0.018%
Rb	0.003% ± 0.015%	0.000% ± 0.025%	0.000% ± 0.022%	0.000% ± 0.015%	0.000% ± 0.015%
Sr	0.000% ± 0.019%	0.000% ± 0.036%	0.004% ± 0.027%	0.109% ± 0.257%	0.011% ± 0.027%
Yt	0.004% ± 0.020%	0.001% ± 0.034%	0.002% ± 0.030%	0.001% ± 0.020%	0.002% ± 0.021%
Zr	0.003% ± 0.023%	0.000% ± 0.040%	0.001% ± 0.035%	0.009% ± 0.024%	0.006% ± 0.024%
Mo	0.000% ± 0.042%	0.002% ± 0.071%	0.001% ± 0.064%	0.006% ± 0.041%	0.008% ± 0.043%
Pd	0.022% ± 0.129%	0.043% ± 0.215%	0.018% ± 0.196%	0.050% ± 0.127%	0.079% ± 0.135%
Ag	0.000% ± 0.149%	0.082% ± 0.251%	0.048% ± 0.226%	0.133% ± 0.148%	0.077% ± 0.157%
Cd	0.010% ± 0.151%	0.075% ± 0.253%	0.099% ± 0.229%	0.085% ± 0.150%	0.070% ± 0.159%
In	0.150% ± 0.181%	0.114% ± 0.300%	0.165% ± 0.275%	0.125% ± 0.178%	0.045% ± 0.186%
Sn	0.125% ± 0.229%	0.017% ± 0.380%	0.103% ± 0.347%	0.133% ± 0.225%	0.013% ± 0.236%
Sb	0.000% ± 0.273%	0.000% ± 0.456%	0.031% ± 0.420%	0.002% ± 0.269%	0.023% ± 0.284%
Ba	0.076% ± 0.982%	0.000% ± 1.648%	0.016% ± 1.504%	0.110% ± 0.972%	0.183% ± 1.026%
La	0.000% ± 1.288%	0.000% ± 2.157%	0.000% ± 1.970%	0.089% ± 1.276%	0.000% ± 1.335%
Au	0.014% ± 0.047%	0.000% ± 0.078%	0.000% ± 0.070%	0.005% ± 0.045%	0.001% ± 0.048%
Hg	0.007% ± 0.038%	0.000% ± 0.064%	0.000% ± 0.058%	0.007% ± 0.037%	0.000% ± 0.039%
Tl	0.003% ± 0.037%	0.000% ± 0.062%	0.001% ± 0.057%	0.000% ± 0.036%	0.000% ± 0.038%
Pb	0.043% ± 0.044%	0.011% ± 0.083%	0.037% ± 0.072%	0.022% ± 0.048%	0.038% ± 0.044%
U	0.000% ± 0.036%	0.004% ± 0.061%	0.006% ± 0.055%	0.014% ± 0.036%	0.006% ± 0.037%
Sum of Species	100.000% ± 11.268%	100.000% ± 16.130%	100.000% ± 14.715%	100.000% ± 9.712%	100.000% ± 11.305%

	LVMVESAC	LVMVC2
Mass	100.000% ± 14.570%	100.000% ± 21.341%
Cl$^-$	0.184% ± 0.475%	0.396% ± 0.238%
NO$_3^-$	0.137% ± 0.519%	0.774% ± 1.079%
SO$_4^=$	1.381% ± 2.392%	3.872% ± 3.010%
NH$_4^+$	0.249% ± 0.510%	0.630% ± 0.549%
K$^+$	0.287% ± 0.065%	0.358% ± 0.136%
OC	52.383% ± 10.818%	51.677% ± 5.684%
EC	43.696% ± 6.167%	38.194% ± 5.313%
TC	93.457% ± 15.309%	86.870% ± 3.426%
Na	0.388% ± 0.473%	0.296% ± 0.279%
Mg	0.000% ± 0.132%	0.219% ± 0.300%
Al	0.000% ± 0.132%	0.266% ± 0.153%
Si	0.000% ± 0.260%	0.694% ± 0.484%
P	0.046% ± 0.091%	0.071% ± 0.044%
S	0.453% ± 0.784%	1.705% ± 1.312%
Cl	0.067% ± 0.111%	0.127% ± 0.113%
K	0.014% ± 0.088%	0.231% ± 0.204%
Ca	0.000% ± 0.852%	0.599% ± 0.763%
Ti	0.013% ± 0.411%	0.101% ± 0.077%
V	0.024% ± 0.180%	0.033% ± 0.020%
Cr	0.001% ± 0.047%	0.013% ± 0.019%
Mn	0.007% ± 0.029%	0.022% ± 0.015%
Fe	0.557% ± 0.405%	1.184% ± 0.621%
Co	0.010% ± 0.027%	0.005% ± 0.004%
Ni	0.003% ± 0.018%	0.008% ± 0.006%
Cu	0.067% ± 0.026%	0.080% ± 0.019%
Zn	0.188% ± 0.096%	0.216% ± 0.025%
Ga	0.011% ± 0.034%	0.005% ± 0.006%
As	0.004% ± 0.039%	0.008% ± 0.003%
Se	0.000% ± 0.020%	0.001% ± 0.002%
Br	0.018% ± 0.018%	0.031% ± 0.011%
Rb	0.005% ± 0.018%	0.001% ± 0.002%
Sr	0.000% ± 0.024%	0.018% ± 0.038%
Yt	0.000% ± 0.024%	0.001% ± 0.001%
Zr	0.001% ± 0.028%	0.003% ± 0.003%
Mo	0.003% ± 0.051%	0.003% ± 0.003%
Pd	0.017% ± 0.156%	0.033% ± 0.025%
Ag	0.030% ± 0.182%	0.080% ± 0.059%
Cd	0.090% ± 0.185%	0.063% ± 0.034%
In	0.141% ± 0.218%	0.205% ± 0.203%
Sn	0.053% ± 0.276%	0.063% ± 0.052%
Sb	0.014% ± 0.335%	0.010% ± 0.012%
Ba	0.079% ± 1.196%	0.067% ± 0.062%
La	0.258% ± 1.568%	0.050% ± 0.091%
Au	0.011% ± 0.056%	0.008% ± 0.008%
Hg	0.005% ± 0.046%	0.003% ± 0.003%
Tl	0.000% ± 0.045%	0.001% ± 0.001%
Pb	0.024% ± 0.059%	0.032% ± 0.013%
U	0.006% ± 0.043%	0.005% ± 0.005%
Sum of Species	100.000% ± 12.536%	100.396% ± 8.523%

Table B-5
Individual Residential Wood Combustion Source Profiles (Weight Percent by Mass)
Acquired in the Las Vegas PM₁₀ Study

	LVRWCAD1	LVRWCAD2	LVRWCAD3	LVRWCAD4	LVRWCAD5
Mass	100.000% ± 7.103%	100.000% ± 7.251%	100.000% ± 7.064%	100.000% ± 7.278%	100.000% ± 8.627%
Cl⁻	6.117% ± 0.792%	7.874% ± 1.010%	0.440% ± 0.062%	1.494% ± 0.200%	1.505% ± 0.198%
NO₃⁻	0.127% ± 0.020%	0.203% ± 0.054%	0.036% ± 0.027%	0.137% ± 0.065%	0.080% ± 0.038%
SO₄⁼	0.657% ± 0.051%	0.626% ± 0.070%	0.077% ± 0.028%	0.380% ± 0.070%	0.199% ± 0.041%
NH₄⁺	2.796% ± 0.270%	3.487% ± 0.308%	0.437% ± 0.047%	0.810% ± 0.097%	0.773% ± 0.082%
K⁺	0.019% ± 0.002%	0.951% ± 0.069%	0.175% ± 0.013%	0.261% ± 0.020%	0.307% ± 0.025%
OC	52.050% ± 6.679%	66.728% ± 8.726%	59.569% ± 7.656%	73.010% ± 9.579%	34.793% ± 4.743%
EC	4.331% ± 0.609%	6.074% ± 0.870%	2.585% ± 0.372%	5.720% ± 0.834%	3.297% ± 0.490%
TC	56.318% ± 6.028%	72.620% ± 7.949%	62.056% ± 6.653%	78.496% ± 8.637%	37.947% ± 4.396%
Na	0.000% ± 0.085%	0.012% ± 0.179%	0.000% ± 0.047%	0.134% ± 0.056%	0.028% ± 0.077%
Mg	0.000% ± 0.033%	0.000% ± 0.073%	0.018% ± 0.022%	0.039% ± 0.050%	0.022% ± 0.034%
Al	0.053% ± 0.008%	0.049% ± 0.018%	0.014% ± 0.007%	0.032% ± 0.017%	0.016% ± 0.011%
Si	0.023% ± 0.005%	0.044% ± 0.012%	0.013% ± 0.004%	0.052% ± 0.011%	0.014% ± 0.006%
P	0.004% ± 0.013%	0.003% ± 0.027%	0.004% ± 0.007%	0.000% ± 0.017%	0.009% ± 0.012%
S	0.132% ± 0.010%	0.132% ± 0.013%	0.027% ± 0.003%	0.123% ± 0.011%	0.080% ± 0.008%
Cl	5.790% ± 0.411%	8.111% ± 0.583%	0.476% ± 0.035%	1.365% ± 0.100%	1.558% ± 0.124%
K	0.663% ± 0.047%	1.270% ± 0.092%	0.216% ± 0.016%	0.318% ± 0.026%	0.391% ± 0.032%
Ca	0.030% ± 0.007%	0.093% ± 0.019%	0.022% ± 0.009%	0.029% ± 0.020%	0.004% ± 0.012%
Ti	0.000% ± 0.017%	0.000% ± 0.047%	0.000% ± 0.024%	0.001% ± 0.056%	0.000% ± 0.034%
V	0.000% ± 0.007%	0.001% ± 0.019%	0.000% ± 0.010%	0.000% ± 0.023%	0.000% ± 0.014%
Cr	0.000% ± 0.002%	0.000% ± 0.005%	0.000% ± 0.002%	0.000% ± 0.005%	0.000% ± 0.003%
Mn	0.000% ± 0.001%	0.000% ± 0.003%	0.000% ± 0.002%	0.001% ± 0.004%	0.000% ± 0.002%
Fe	0.007% ± 0.002%	0.028% ± 0.007%	0.005% ± 0.003%	0.009% ± 0.008%	0.003% ± 0.005%
Co	0.000% ± 0.001%	0.000% ± 0.002%	0.000% ± 0.001%	0.000% ± 0.002%	0.000% ± 0.001%
Ni	0.000% ± 0.001%	0.000% ± 0.002%	0.000% ± 0.001%	0.000% ± 0.003%	0.000% ± 0.002%
Cu	0.001% ± 0.001%	0.001% ± 0.002%	0.000% ± 0.001%	0.000% ± 0.002%	0.000% ± 0.002%
Zn	0.017% ± 0.001%	0.014% ± 0.002%	0.000% ± 0.001%	0.004% ± 0.002%	0.001% ± 0.001%
Ga	0.000% ± 0.002%	0.000% ± 0.004%	0.000% ± 0.002%	0.000% ± 0.005%	0.000% ± 0.003%
As	0.000% ± 0.003%	0.000% ± 0.007%	0.000% ± 0.002%	0.002% ± 0.005%	0.000% ± 0.003%
Se	0.000% ± 0.001%	0.000% ± 0.002%	0.000% ± 0.001%	0.000% ± 0.003%	0.000% ± 0.002%
Br	0.012% ± 0.001%	0.019% ± 0.002%	0.000% ± 0.001%	0.002% ± 0.002%	0.002% ± 0.001%
Rb	0.001% ± 0.001%	0.003% ± 0.002%	0.000% ± 0.001%	0.000% ± 0.002%	0.000% ± 0.002%
Sr	0.001% ± 0.001%	0.002% ± 0.002%	0.000% ± 0.001%	0.000% ± 0.003%	0.000% ± 0.002%
Yt	0.000% ± 0.001%	0.000% ± 0.003%	0.000% ± 0.001%	0.000% ± 0.003%	0.000% ± 0.002%
Zr	0.000% ± 0.001%	0.001% ± 0.003%	0.000% ± 0.002%	0.000% ± 0.004%	0.000% ± 0.002%
Mo	0.000% ± 0.002%	0.000% ± 0.006%	0.000% ± 0.003%	0.000% ± 0.007%	0.000% ± 0.004%
Pd	0.002% ± 0.007%	0.000% ± 0.018%	0.002% ± 0.009%	0.011% ± 0.021%	0.002% ± 0.013%
Ag	0.002% ± 0.008%	0.013% ± 0.022%	0.005% ± 0.010%	0.006% ± 0.025%	0.006% ± 0.015%
Cd	0.005% ± 0.008%	0.005% ± 0.022%	0.001% ± 0.010%	0.004% ± 0.025%	0.000% ± 0.015%
In	0.000% ± 0.009%	0.000% ± 0.025%	0.004% ± 0.012%	0.009% ± 0.029%	0.004% ± 0.018%
Sn	0.000% ± 0.012%	0.009% ± 0.032%	0.002% ± 0.016%	0.009% ± 0.038%	0.002% ± 0.023%
Sb	0.000% ± 0.014%	0.000% ± 0.038%	0.000% ± 0.019%	0.000% ± 0.045%	0.000% ± 0.027%
Ba	0.000% ± 0.051%	0.007% ± 0.139%	0.000% ± 0.070%	0.000% ± 0.163%	0.000% ± 0.099%
La	0.000% ± 0.066%	0.000% ± 0.180%	0.000% ± 0.092%	0.000% ± 0.215%	0.000% ± 0.131%
Au	0.000% ± 0.003%	0.000% ± 0.007%	0.000% ± 0.003%	0.002% ± 0.008%	0.000% ± 0.005%
Hg	0.000% ± 0.002%	0.001% ± 0.006%	0.000% ± 0.003%	0.000% ± 0.006%	0.000% ± 0.004%
Tl	0.000% ± 0.002%	0.000% ± 0.005%	0.000% ± 0.003%	0.000% ± 0.006%	0.000% ± 0.004%
Pb	0.015% ± 0.002%	0.032% ± 0.006%	0.001% ± 0.004%	0.003% ± 0.008%	0.001% ± 0.005%
U	0.000% ± 0.002%	0.001% ± 0.005%	0.000% ± 0.003%	0.000% ± 0.006%	0.000% ± 0.004%
Sum of Species	66.588% ± 6.726%	86.837% ± 8.800%	63.486% ± 7.667%	82.091% ± 9.622%	41.206% ± 4.775%

Individual Residential Wood Combustion Source Profiles (Weight Percent by Mass)
Acquired in the Las Vegas PM$_{10}$ Study

	LVRWCCA1	LVRWCCA2	LVRWCCA3	LVRWCCA4	LVRWCCA5
Mass	100.000% ± 7.523%	100.000% ± 8.428%	100.000% ± 8.379%	100.000% ± 7.099%	100.000% ± 7.365%
Cl$^-$	0.346% ± 0.103%	0.243% ± 0.166%	0.334% ± 0.167%	0.096% ± 0.023%	0.147% ± 0.078%
NO$_3^-$	0.411% ± 0.095%	0.256% ± 0.160%	0.334% ± 0.159%	0.129% ± 0.021%	0.169% ± 0.075%
SO$_4^=$	0.775% ± 0.107%	0.452% ± 0.163%	0.567% ± 0.164%	0.617% ± 0.049%	0.278% ± 0.077%
NH$_4^+$	0.456% ± 0.100%	0.354% ± 0.164%	0.459% ± 0.164%	0.198% ± 0.025%	0.175% ± 0.076%
K$^+$	0.725% ± 0.054%	0.530% ± 0.045%	0.438% ± 0.038%	0.403% ± 0.029%	0.147% ± 0.013%
OC	54.451% ± 7.418%	64.769% ± 9.334%	45.472% ± 6.914%	47.092% ± 6.051%	51.456% ± 6.922%
EC	17.324% ± 2.463%	16.656% ± 2.447%	20.290% ± 2.967%	50.754% ± 7.050%	13.121% ± 1.863%
TC	71.450% ± 8.119%	80.827% ± 9.918%	65.169% ± 8.272%	97.782% ± 10.413%	64.299% ± 7.229%
Na	0.013% ± 0.149%	0.072% ± 0.127%	0.126% ± 0.123%	0.000% ± 0.034%	0.005% ± 0.108%
Mg	0.132% ± 0.044%	0.080% ± 0.109%	0.085% ± 0.115%	0.007% ± 0.016%	0.102% ± 0.034%
Al	0.280% ± 0.034%	0.000% ± 0.062%	0.102% ± 0.042%	0.012% ± 0.005%	0.127% ± 0.021%
Si	0.355% ± 0.031%	0.164% ± 0.027%	0.355% ± 0.037%	0.167% ± 0.013%	0.294% ± 0.025%
P	0.009% ± 0.019%	0.013% ± 0.028%	0.004% ± 0.026%	0.000% ± 0.005%	0.005% ± 0.014%
S	0.222% ± 0.018%	0.165% ± 0.017%	0.139% ± 0.015%	0.227% ± 0.016%	0.140% ± 0.012%
Cl	0.237% ± 0.025%	0.126% ± 0.030%	0.164% ± 0.031%	0.071% ± 0.007%	0.040% ± 0.013%
K	0.848% ± 0.065%	0.646% ± 0.058%	0.514% ± 0.049%	0.434% ± 0.031%	0.207% ± 0.020%
Ca	0.531% ± 0.049%	0.180% ± 0.052%	0.624% ± 0.069%	0.131% ± 0.011%	0.638% ± 0.052%
Ti	0.009% ± 0.082%	0.000% ± 0.137%	0.017% ± 0.132%	0.000% ± 0.016%	0.011% ± 0.063%
V	0.000% ± 0.034%	0.000% ± 0.056%	0.008% ± 0.055%	0.000% ± 0.009%	0.005% ± 0.026%
Cr	0.001% ± 0.008%	0.000% ± 0.013%	0.004% ± 0.013%	0.000% ± 0.003%	0.000% ± 0.006%
Mn	0.003% ± 0.006%	0.001% ± 0.010%	0.005% ± 0.010%	0.000% ± 0.001%	0.003% ± 0.005%
Fe	0.107% ± 0.014%	0.049% ± 0.020%	0.267% ± 0.029%	0.020% ± 0.003%	0.120% ± 0.013%
Co	0.001% ± 0.004%	0.001% ± 0.006%	0.006% ± 0.008%	0.001% ± 0.001%	0.000% ± 0.003%
Ni	0.000% ± 0.004%	0.003% ± 0.006%	0.002% ± 0.006%	0.000% ± 0.001%	0.001% ± 0.003%
Cu	0.002% ± 0.004%	0.003% ± 0.006%	0.006% ± 0.004%	0.000% ± 0.001%	0.002% ± 0.003%
Zn	0.113% ± 0.009%	0.052% ± 0.006%	0.025% ± 0.005%	0.013% ± 0.001%	0.006% ± 0.002%
Ga	0.000% ± 0.007%	0.007% ± 0.011%	0.000% ± 0.011%	0.000% ± 0.001%	0.000% ± 0.005%
As	0.000% ± 0.009%	0.000% ± 0.013%	0.001% ± 0.013%	0.001% ± 0.002%	0.000% ± 0.006%
Se	0.000% ± 0.004%	0.000% ± 0.007%	0.002% ± 0.007%	0.000% ± 0.001%	0.000% ± 0.003%
Br	0.002% ± 0.004%	0.002% ± 0.006%	0.000% ± 0.007%	0.001% ± 0.001%	0.001% ± 0.003%
Rb	0.003% ± 0.004%	0.002% ± 0.006%	0.002% ± 0.006%	0.001% ± 0.001%	0.000% ± 0.003%
Sr	0.001% ± 0.004%	0.000% ± 0.006%	0.003% ± 0.006%	0.001% ± 0.001%	0.002% ± 0.003%
Yt	0.000% ± 0.005%	0.000% ± 0.008%	0.001% ± 0.008%	0.000% ± 0.001%	0.000% ± 0.004%
Zr	0.001% ± 0.006%	0.003% ± 0.009%	0.006% ± 0.009%	0.000% ± 0.001%	0.000% ± 0.004%
Mo	0.004% ± 0.010%	0.000% ± 0.017%	0.000% ± 0.016%	0.000% ± 0.002%	0.000% ± 0.008%
Pd	0.000% ± 0.030%	0.024% ± 0.052%	0.000% ± 0.049%	0.000% ± 0.005%	0.008% ± 0.023%
Ag	0.007% ± 0.036%	0.036% ± 0.061%	0.020% ± 0.056%	0.001% ± 0.006%	0.012% ± 0.027%
Cd	0.005% ± 0.036%	0.022% ± 0.061%	0.022% ± 0.058%	0.000% ± 0.006%	0.006% ± 0.028%
In	0.009% ± 0.043%	0.016% ± 0.071%	0.017% ± 0.070%	0.001% ± 0.008%	0.010% ± 0.033%
Sn	0.000% ± 0.054%	0.012% ± 0.091%	0.024% ± 0.090%	0.000% ± 0.010%	0.000% ± 0.042%
Sb	0.000% ± 0.065%	0.000% ± 0.110%	0.000% ± 0.107%	0.000% ± 0.012%	0.000% ± 0.051%
Ba	0.000% ± 0.237%	0.132% ± 0.400%	0.028% ± 0.388%	0.000% ± 0.044%	0.000% ± 0.185%
La	0.000% ± 0.313%	0.018% ± 0.523%	0.000% ± 0.507%	0.017% ± 0.058%	0.000% ± 0.241%
Au	0.000% ± 0.012%	0.006% ± 0.019%	0.000% ± 0.018%	0.000% ± 0.002%	0.001% ± 0.009%
Hg	0.000% ± 0.009%	0.000% ± 0.015%	0.007% ± 0.015%	0.000% ± 0.002%	0.001% ± 0.007%
Tl	0.000% ± 0.009%	0.000% ± 0.015%	0.000% ± 0.014%	0.000% ± 0.002%	0.000% ± 0.007%
Pb	0.016% ± 0.009%	0.010% ± 0.020%	0.012% ± 0.019%	0.000% ± 0.002%	0.001% ± 0.009%
U	0.000% ± 0.009%	0.000% ± 0.014%	0.001% ± 0.014%	0.000% ± 0.002%	0.000% ± 0.007%
Sum of Species	76.104% ± 7.832%	84.167% ± 9.681%	69.580% ± 7.563%	99.666% ± 9.291%	66.806% ± 7.178%

Individual Residential Wood Combustion Source Profiles (Weight Percent by Mass)
Acquired in the Las Vegas PM$_{10}$ Study

	LVRWCCH1	LVRWCCH2	LVRWCCH3	LVRWCCH4	LVRWCPI1
Mass	100.000% ± 8.121%	100.000% ± 7.130%	100.000% ± 7.380%	100.000% ± 7.402%	100.000% ± 7.884%
Cl$^-$	0.639% ± 0.169%	0.287% ± 0.047%	0.698% ± 0.118%	0.332% ± 0.089%	1.682% ± 0.252%
NO$_3^-$	0.269% ± 0.142%	0.079% ± 0.029%	0.212% ± 0.075%	0.142% ± 0.075%	0.433% ± 0.126%
SO$_4^=$	0.448% ± 0.145%	0.277% ± 0.035%	0.501% ± 0.082%	0.275% ± 0.077%	0.645% ± 0.131%
NH$_4^+$	0.233% ± 0.143%	0.361% ± 0.043%	0.343% ± 0.080%	0.375% ± 0.083%	0.544% ± 0.133%
K$^+$	0.582% ± 0.047%	0.306% ± 0.022%	0.687% ± 0.051%	0.403% ± 0.030%	0.512% ± 0.041%
OC	63.605% ± 9.009%	75.779% ± 9.746%	67.404% ± 8.944%	66.501% ± 8.837%	42.723% ± 6.227%
EC	16.173% ± 2.363%	12.444% ± 1.738%	10.810% ± 1.542%	9.210% ± 1.322%	14.157% ± 2.054%
TC	79.267% ± 9.511%	88.119% ± 9.444%	77.948% ± 8.664%	75.441% ± 8.412%	56.438% ± 6.921%
Na	0.000% ± 0.206%	0.045% ± 0.025%	0.000% ± 0.130%	0.000% ± 0.103%	0.075% ± 0.263%
Mg	0.097% ± 0.063%	0.012% ± 0.022%	0.000% ± 0.055%	0.000% ± 0.058%	0.090% ± 0.058%
Al	0.032% ± 0.057%	0.012% ± 0.008%	0.026% ± 0.019%	0.272% ± 0.030%	0.244% ± 0.039%
Si	0.217% ± 0.027%	0.018% ± 0.005%	0.056% ± 0.012%	0.117% ± 0.015%	0.466% ± 0.041%
P	0.013% ± 0.027%	0.005% ± 0.007%	0.009% ± 0.016%	0.011% ± 0.015%	0.021% ± 0.027%
S	0.158% ± 0.016%	0.094% ± 0.007%	0.159% ± 0.013%	0.114% ± 0.010%	0.207% ± 0.019%
Cl	0.570% ± 0.052%	0.292% ± 0.022%	0.706% ± 0.055%	0.269% ± 0.025%	1.479% ± 0.116%
K	0.700% ± 0.059%	0.392% ± 0.029%	0.877% ± 0.066%	0.529% ± 0.041%	0.719% ± 0.059%
Ca	0.147% ± 0.045%	0.003% ± 0.009%	0.006% ± 0.023%	0.067% ± 0.024%	0.782% ± 0.070%
Ti	0.011% ± 0.122%	0.001% ± 0.026%	0.004% ± 0.061%	0.006% ± 0.066%	0.020% ± 0.104%
V	0.002% ± 0.050%	0.000% ± 0.011%	0.002% ± 0.025%	0.002% ± 0.027%	0.005% ± 0.043%
Cr	0.000% ± 0.012%	0.000% ± 0.003%	0.002% ± 0.006%	0.000% ± 0.007%	0.003% ± 0.010%
Mn	0.021% ± 0.007%	0.000% ± 0.002%	0.008% ± 0.003%	0.004% ± 0.004%	0.006% ± 0.006%
Fe	0.051% ± 0.018%	0.006% ± 0.004%	0.015% ± 0.009%	0.034% ± 0.010%	0.143% ± 0.019%
Co	0.002% ± 0.005%	0.000% ± 0.001%	0.000% ± 0.003%	0.000% ± 0.003%	0.000% ± 0.005%
Ni	0.000% ± 0.005%	0.000% ± 0.001%	0.001% ± 0.003%	0.000% ± 0.003%	0.004% ± 0.004%
Cu	0.014% ± 0.004%	0.000% ± 0.001%	0.001% ± 0.003%	0.002% ± 0.002%	0.013% ± 0.004%
Zn	0.013% ± 0.004%	0.005% ± 0.001%	0.007% ± 0.002%	0.010% ± 0.002%	0.112% ± 0.009%
Ga	0.001% ± 0.010%	0.000% ± 0.002%	0.001% ± 0.005%	0.002% ± 0.006%	0.000% ± 0.009%
As	0.000% ± 0.012%	0.000% ± 0.003%	0.001% ± 0.006%	0.002% ± 0.006%	0.000% ± 0.010%
Se	0.000% ± 0.006%	0.000% ± 0.001%	0.000% ± 0.003%	0.000% ± 0.003%	0.002% ± 0.006%
Br	0.000% ± 0.006%	0.001% ± 0.001%	0.002% ± 0.002%	0.001% ± 0.003%	0.014% ± 0.004%
Rb	0.000% ± 0.005%	0.000% ± 0.001%	0.001% ± 0.003%	0.000% ± 0.003%	0.000% ± 0.005%
Sr	0.002% ± 0.006%	0.000% ± 0.001%	0.000% ± 0.003%	0.000% ± 0.003%	0.003% ± 0.005%
Yt	0.000% ± 0.007%	0.000% ± 0.002%	0.000% ± 0.004%	0.000% ± 0.004%	0.001% ± 0.006%
Zr	0.003% ± 0.009%	0.000% ± 0.002%	0.000% ± 0.004%	0.000% ± 0.005%	0.005% ± 0.007%
Mo	0.000% ± 0.016%	0.000% ± 0.003%	0.000% ± 0.008%	0.001% ± 0.008%	0.000% ± 0.013%
Pd	0.007% ± 0.047%	0.000% ± 0.009%	0.005% ± 0.023%	0.000% ± 0.025%	0.010% ± 0.040%
Ag	0.013% ± 0.055%	0.001% ± 0.011%	0.002% ± 0.027%	0.015% ± 0.029%	0.020% ± 0.047%
Cd	0.000% ± 0.055%	0.001% ± 0.011%	0.009% ± 0.027%	0.002% ± 0.029%	0.000% ± 0.048%
In	0.000% ± 0.065%	0.004% ± 0.014%	0.000% ± 0.032%	0.000% ± 0.034%	0.012% ± 0.056%
Sn	0.015% ± 0.083%	0.000% ± 0.017%	0.015% ± 0.041%	0.027% ± 0.045%	0.023% ± 0.072%
Sb	0.000% ± 0.099%	0.000% ± 0.021%	0.000% ± 0.049%	0.000% ± 0.053%	0.000% ± 0.086%
Ba	0.000% ± 0.358%	0.000% ± 0.075%	0.000% ± 0.181%	0.000% ± 0.193%	0.072% ± 0.306%
La	0.035% ± 0.472%	0.000% ± 0.098%	0.000% ± 0.235%	0.000% ± 0.253%	0.000% ± 0.403%
Au	0.003% ± 0.017%	0.000% ± 0.004%	0.001% ± 0.008%	0.000% ± 0.009%	0.004% ± 0.015%
Hg	0.000% ± 0.014%	0.001% ± 0.003%	0.000% ± 0.007%	0.000% ± 0.007%	0.001% ± 0.012%
Tl	0.000% ± 0.014%	0.000% ± 0.003%	0.000% ± 0.007%	0.000% ± 0.007%	0.000% ± 0.012%
Pb	0.000% ± 0.018%	0.000% ± 0.004%	0.001% ± 0.009%	0.000% ± 0.010%	0.009% ± 0.015%
U	0.000% ± 0.013%	0.000% ± 0.003%	0.000% ± 0.006%	0.000% ± 0.007%	0.000% ± 0.011%
Sum of Species	82.696% ± 9.342%	89.740% ± 9.901%	81.026% ± 9.084%	77.877% ± 8.943%	62.857% ± 6.591%

Individual Residential Wood Combustion Source Profiles (Weight Percent by Mass)
Acquired in the Las Vegas PM$_{10}$ Study

	LVRWCP12	LVRWCP13	LVRWCP14	LVRWCSI1	LVRWCSI2
Mass	100.000% ± 11.900%	100.000% ± 11.937%	100.000% ± 11.607%	100.000% ± 24.812%	100.000% ± 7.918%
Cl$^-$	2.697% ± 0.527%	9.175% ± 1.353%	10.430% ± 1.505%	1.086% ± 0.901%	0.316% ± 0.136%
NO$_3^-$	0.909% ± 0.352%	0.973% ± 0.351%	1.016% ± 0.338%	4.597% ± 1.197%	0.637% ± 0.135%
SO$_4^=$	1.514% ± 0.372%	1.918% ± 0.388%	2.388% ± 0.399%	3.873% ± 1.110%	0.578% ± 0.134%
NH$_4^+$	0.359% ± 0.344%	0.811% ± 0.352%	1.810% ± 0.383%	2.351% ± 0.969%	0.246% ± 0.129%
K$^+$	1.916% ± 0.192%	4.575% ± 0.452%	4.081% ± 0.395%	0.681% ± 0.156%	0.780% ± 0.060%
OC	39.100% ± 8.458%	27.548% ± 7.202%	40.092% ± 8.335%	43.842% ± 17.188%	33.925% ± 5.189%
EC	26.114% ± 4.218%	35.508% ± 5.656%	16.251% ± 2.717%	23.073% ± 5.650%	20.477% ± 2.945%
TC	63.981% ± 11.252%	61.832% ± 11.031%	55.169% ± 10.111%	63.821% ± 22.491%	53.945% ± 6.717%
Na	0.788% ± 0.305%	2.548% ± 0.428%	1.907% ± 0.387%	0.339% ± 0.648%	0.000% ± 0.187%
Mg	0.000% ± 0.277%	0.330% ± 0.165%	0.214% ± 0.287%	0.650% ± 0.395%	0.067% ± 0.094%
Al	0.093% ± 0.149%	0.061% ± 0.159%	0.224% ± 0.092%	0.848% ± 0.279%	0.123% ± 0.035%
Si	0.590% ± 0.080%	0.592% ± 0.082%	0.488% ± 0.072%	3.455% ± 0.647%	0.522% ± 0.045%
P	0.000% ± 0.070%	0.090% ± 0.046%	0.094% ± 0.045%	0.083% ± 0.140%	0.009% ± 0.025%
S	0.513% ± 0.057%	0.693% ± 0.076%	0.758% ± 0.080%	1.175% ± 0.222%	0.332% ± 0.027%
Cl	2.586% ± 0.266%	8.594% ± 0.853%	9.548% ± 0.926%	0.066% ± 0.204%	0.299% ± 0.034%
K	2.495% ± 0.254%	5.872% ± 0.583%	5.485% ± 0.533%	1.245% ± 0.268%	1.532% ± 0.118%
Ca	1.153% ± 0.155%	0.576% ± 0.123%	0.667% ± 0.122%	2.697% ± 0.557%	0.283% ± 0.045%
Ti	0.030% ± 0.289%	0.017% ± 0.294%	0.028% ± 0.282%	0.153% ± 0.693%	0.023% ± 0.108%
V	0.009% ± 0.119%	0.008% ± 0.121%	0.009% ± 0.116%	0.024% ± 0.286%	0.007% ± 0.045%
Cr	0.002% ± 0.028%	0.000% ± 0.029%	0.000% ± 0.028%	0.017% ± 0.068%	0.000% ± 0.011%
Mn	0.016% ± 0.016%	0.027% ± 0.016%	0.021% ± 0.015%	0.058% ± 0.040%	0.005% ± 0.008%
Fe	0.234% ± 0.048%	0.115% ± 0.043%	0.166% ± 0.043%	1.063% ± 0.221%	0.129% ± 0.018%
Co	0.000% ± 0.013%	0.006% ± 0.013%	0.001% ± 0.012%	0.010% ± 0.035%	0.003% ± 0.005%
Ni	0.004% ± 0.013%	0.003% ± 0.013%	0.001% ± 0.013%	0.241% ± 0.051%	0.002% ± 0.005%
Cu	0.028% ± 0.010%	0.034% ± 0.010%	0.007% ± 0.012%	0.163% ± 0.038%	0.003% ± 0.005%
Zn	0.282% ± 0.030%	0.427% ± 0.044%	0.215% ± 0.023%	0.223% ± 0.048%	0.028% ± 0.004%
Ga	0.000% ± 0.025%	0.003% ± 0.024%	0.003% ± 0.023%	0.000% ± 0.058%	0.003% ± 0.009%
As	0.011% ± 0.028%	0.003% ± 0.030%	0.001% ± 0.028%	0.000% ± 0.066%	0.003% ± 0.010%
Se	0.000% ± 0.015%	0.000% ± 0.015%	0.000% ± 0.014%	0.000% ± 0.034%	0.000% ± 0.005%
Br	0.017% ± 0.011%	0.062% ± 0.012%	0.058% ± 0.012%	0.007% ± 0.032%	0.004% ± 0.004%
Rb	0.001% ± 0.013%	0.010% ± 0.010%	0.011% ± 0.009%	0.000% ± 0.029%	0.003% ± 0.005%
Sr	0.007% ± 0.014%	0.005% ± 0.014%	0.010% ± 0.014%	0.029% ± 0.027%	0.004% ± 0.004%
Yt	0.001% ± 0.017%	0.000% ± 0.017%	0.000% ± 0.017%	0.000% ± 0.040%	0.000% ± 0.006%
Zr	0.001% ± 0.020%	0.000% ± 0.020%	0.000% ± 0.019%	0.038% ± 0.037%	0.001% ± 0.007%
Mo	0.000% ± 0.036%	0.000% ± 0.036%	0.000% ± 0.035%	0.032% ± 0.084%	0.000% ± 0.013%
Pd	0.001% ± 0.109%	0.000% ± 0.111%	0.000% ± 0.109%	0.000% ± 0.265%	0.000% ± 0.041%
Ag	0.060% ± 0.129%	0.035% ± 0.130%	0.000% ± 0.126%	0.079% ± 0.308%	0.000% ± 0.048%
Cd	0.050% ± 0.132%	0.052% ± 0.130%	0.000% ± 0.125%	0.139% ± 0.310%	0.024% ± 0.049%
In	0.042% ± 0.155%	0.041% ± 0.152%	0.000% ± 0.147%	0.000% ± 0.366%	0.005% ± 0.057%
Sn	0.000% ± 0.196%	0.043% ± 0.197%	0.000% ± 0.188%	0.000% ± 0.465%	0.000% ± 0.073%
Sb	0.000% ± 0.235%	0.000% ± 0.237%	0.000% ± 0.226%	0.000% ± 0.566%	0.000% ± 0.089%
Ba	0.093% ± 0.850%	0.000% ± 0.862%	0.000% ± 0.827%	0.000% ± 2.038%	0.000% ± 0.318%
La	0.000% ± 1.113%	0.000% ± 1.131%	0.000% ± 1.083%	0.000% ± 2.657%	0.000% ± 0.413%
Au	0.000% ± 0.042%	0.000% ± 0.044%	0.007% ± 0.039%	0.044% ± 0.094%	0.002% ± 0.015%
Hg	0.000% ± 0.032%	0.004% ± 0.033%	0.001% ± 0.031%	0.012% ± 0.077%	0.001% ± 0.012%
Tl	0.000% ± 0.032%	0.000% ± 0.032%	0.000% ± 0.030%	0.000% ± 0.074%	0.000% ± 0.012%
Pb	0.022% ± 0.042%	0.045% ± 0.032%	0.033% ± 0.030%	0.056% ± 0.099%	0.000% ± 0.015%
U	0.008% ± 0.031%	0.000% ± 0.031%	0.000% ± 0.030%	0.000% ± 0.071%	0.000% ± 0.011%
Sum of Species	76.617% ± 9.608%	86.358% ± 9.375%	80.753% ± 8.988%	89.506% ± 18.582%	58.948% ± 6.002%

	LVRWCSI3	LVRWCSI4
Mass	100.000% ± 8.606%	100.000% ± 7.246%
Cl$^-$	0.538% ± 0.193%	0.273% ± 0.066%
NO$_3^-$	1.188% ± 0.198%	0.423% ± 0.062%
SO$_4^=$	1.040% ± 0.193%	0.510% ± 0.066%
NH$_4^+$	0.411% ± 0.180%	0.087% ± 0.055%
K$^+$	1.545% ± 0.124%	1.498% ± 0.108%
OC	7.902% ± 3.118%	3.052% ± 0.999%
EC	28.599% ± 4.173%	14.426% ± 2.031%
TC	35.846% ± 5.704%	17.284% ± 2.267%
Na	0.000% ± 0.443%	0.157% ± 0.245%
Mg	0.194% ± 0.234%	0.060% ± 0.129%
Al	0.079% ± 0.160%	0.000% ± 0.086%
Si	30.374% ± 2.397%	33.660% ± 2.411%
P	0.000% ± 0.054%	0.000% ± 0.046%
S	0.406% ± 0.035%	0.597% ± 0.044%
Cl	0.457% ± 0.050%	0.361% ± 0.031%
K	2.313% ± 0.187%	3.061% ± 0.220%
Ca	0.401% ± 0.063%	0.067% ± 0.023%
Ti	0.029% ± 0.148%	0.005% ± 0.051%
V	0.006% ± 0.061%	0.001% ± 0.021%
Cr	0.008% ± 0.015%	0.006% ± 0.004%
Mn	0.006% ± 0.011%	0.003% ± 0.004%
Fe	0.232% ± 0.028%	0.018% ± 0.007%
Co	0.002% ± 0.008%	0.001% ± 0.002%
Ni	0.001% ± 0.007%	0.000% ± 0.002%
Cu	0.024% ± 0.005%	0.003% ± 0.002%
Zn	0.168% ± 0.014%	0.176% ± 0.013%
Ga	0.004% ± 0.012%	0.000% ± 0.004%
As	0.001% ± 0.014%	0.001% ± 0.005%
Se	0.001% ± 0.007%	0.000% ± 0.003%
Br	0.005% ± 0.005%	0.004% ± 0.002%
Rb	0.002% ± 0.006%	0.002% ± 0.002%
Sr	0.004% ± 0.007%	0.000% ± 0.003%
Yt	0.000% ± 0.009%	0.000% ± 0.003%
Zr	0.003% ± 0.010%	0.000% ± 0.004%
Mo	0.000% ± 0.018%	0.000% ± 0.006%
Pd	0.014% ± 0.057%	0.007% ± 0.020%
Ag	0.027% ± 0.066%	0.008% ± 0.023%
Cd	0.023% ± 0.067%	0.016% ± 0.024%
In	0.039% ± 0.079%	0.015% ± 0.028%
Sn	0.015% ± 0.100%	0.000% ± 0.035%
Sb	0.000% ± 0.121%	0.000% ± 0.042%
Ba	0.000% ± 0.433%	0.012% ± 0.150%
La	0.000% ± 0.568%	0.000% ± 0.195%
Au	0.001% ± 0.022%	0.000% ± 0.010%
Hg	0.000% ± 0.017%	0.000% ± 0.006%
Tl	0.000% ± 0.016%	0.000% ± 0.006%
Pb	0.009% ± 0.021%	0.004% ± 0.008%
U	0.000% ± 0.016%	0.001% ± 0.006%
Sum of Species	73.581% ± 5.822%	56.146% ± 3.340%

Table B-6
Composite Residential Wood Combustion Source Profiles (Weight Percent by Mass)
Acquired in the Las Vegas PM$_{10}$ Study

	LVRWCC1		LVRWCC2		LVRWCC3		LVRWCC4	
Mass	±		±		±		±	
Cl⁻	3.4859 ±	2.9445	0.5553 ±	0.4384	7.4338 ±	3.3886	0.4057 ±	0.1444
NO₃⁻	0.1167 ±	0.0564	0.6853 ±	1.2459	0.9658 ±	0.3468	0.8054 ±	0.3822
SO₄⁻	0.3879 ±	0.2285	0.7882 ±	0.9873	1.9400 ±	0.3863	0.7748 ±	0.2652
NH₄⁺	1.6606 ±	1.2355	0.5361 ±	0.5831	0.9930 ±	0.6062	0.2491 ±	0.1623
K⁺	0.3424 ±	0.3195	0.5264 ±	0.1841	3.5240 ±	1.1547	1.5212 ±	0.1160
OC	57.2300 ±	13.2285	55.4479 ±	12.4616	35.5797 ±	8.0181	5.4768 ±	2.4251
EC	4.4013 ±	1.3461	15.7941 ±	4.1297	25.9577 ±	7.8624	21.5129 ±	7.0865
TC	61.4875 ±	14.1027	70.6111 ±	10.4850	60.3273 ±	10.8095	26.5648 ±	9.2812
Na	0.0348 ±	0.1006	0.0613 ±	0.2447	1.7475 ±	0.7271	0.0786 ±	0.3579
Mg	0.0158 ±	0.0459	0.1195 ±	0.1729	0.1812 ±	0.2490	0.1271 ±	0.1892
Al	0.0330 ±	0.0161	0.1877 ±	0.2310	0.1259 ±	0.1366	0.0397 ±	0.1282
Si	0.0290 ±	0.0160	0.5471 ±	0.9324	0.5565 ±	0.0780	32.0173 ±	2.4040
P	0.0041 ±	0.0163	0.0166 ±	0.0469	0.0611 ±	0.0545	0.0000 ±	0.0501
S	0.0986 ±	0.0408	0.2641 ±	0.2946	0.6546 ±	0.1035	0.5015 ±	0.0952
Cl	3.4599 ±	2.9656	0.3863 ±	0.3957	6.9093 ±	3.0819	0.4088 ±	0.0478
K	0.5714 ±	0.3792	0.7462 ±	0.3599	4.6172 ±	1.5090	2.6870 ±	0.3737
Ca	0.0357 ±	0.0301	0.5415 ±	0.7308	0.7988 ±	0.2535	0.2341 ±	0.1667
Ti	0.0004 ±	0.0382	0.0230 ±	0.2284	0.0248 ±	0.2883	0.0167 ±	0.1104
V	0.0002 ±	0.0158	0.0050 ±	0.0941	0.0086 ±	0.1189	0.0031 ±	0.0456
Cr	0.0000 ±	0.0037	0.0024 ±	0.0224	0.0005 ±	0.0282	0.0067 ±	0.0108
Mn	0.0003 ±	0.0027	0.0103 ±	0.0160	0.0215 ±	0.0154	0.0044 ±	0.0080
Fe	0.0103 ±	0.0093	0.1803 ±	0.2881	0.1714 ±	0.0488	0.1249 ±	0.1069
Co	0.0001 ±	0.0016	0.0022 ±	0.0115	0.0024 ±	0.0126	0.0015 ±	0.0056
Ni	0.0001 ±	0.0017	0.0229 ±	0.0688	0.0029 ±	0.0129	0.0005 ±	0.0049
Cu	0.0004 ±	0.0016	0.0191 ±	0.0458	0.0228 ±	0.0116	0.0135 ±	0.0108
Zn	0.0073 ±	0.0071	0.0538 ±	0.0658	0.3078 ±	0.0885	0.1722 ±	0.0136
Ga	0.0000 ±	0.0032	0.0013 ±	0.0192	0.0021 ±	0.0241	0.0021 ±	0.0092
As	0.0004 ±	0.0046	0.0008 ±	0.0218	0.0048 ±	0.0284	0.0008 ±	0.0107
Se	0.0000 ±	0.0019	0.0003 ±	0.0114	0.0000 ±	0.0144	0.0003 ±	0.0055
Br	0.0072 ±	0.0072	0.0031 ±	0.0106	0.0454 ±	0.0206	0.0047 ±	0.0040
Rb	0.0009 ±	0.0015	0.0008 ±	0.0096	0.0076 ±	0.0107	0.0022 ±	0.0047
Sr	0.0004 ±	0.0019	0.0040 ±	0.0091	0.0072 ±	0.0140	0.0021 ±	0.0054
Yt	0.0000 ±	0.0023	0.0002 ±	0.0132	0.0004 ±	0.0169	0.0000 ±	0.0065
Zr	0.0001 ±	0.0027	0.0052 ±	0.0129	0.0002 ±	0.0195	0.0013 ±	0.0076
Mo	0.0000 ±	0.0048	0.0033 ±	0.0279	0.0000 ±	0.0354	0.0001 ±	0.0136
Pd	0.0036 ±	0.0144	0.0049 ±	0.0871	0.0003 ±	0.1098	0.0108 ±	0.0427
Ag	0.0062 ±	0.0171	0.0186 ±	0.1012	0.0317 ±	0.1282	0.0175 ±	0.0493
Cd	0.0031 ±	0.0171	0.0209 ±	0.1020	0.0339 ±	0.1289	0.0196 ±	0.0501
In	0.0034 ±	0.0202	0.0064 ±	0.1204	0.0273 ±	0.1511	0.0270 ±	0.0593
Sn	0.0041 ±	0.0258	0.0106 ±	0.1531	0.0142 ±	0.1936	0.0076 ±	0.0748
Sb	0.0001 ±	0.0310	0.0000 ±	0.1863	0.0000 ±	0.2330	0.0000 ±	0.0908
Ba	0.0014 ±	0.1124	0.0211 ±	0.6709	0.0311 ±	0.8467	0.0061 ±	0.3242
La	0.0000 ±	0.1475	0.0049 ±	0.8754	0.0000 ±	1.1088	0.0000 ±	0.4248
Au	0.0004 ±	0.0052	0.0055 ±	0.0309	0.0023 ±	0.0417	0.0003 ±	0.0166
Hg	0.0002 ±	0.0044	0.0021 ±	0.0254	0.0016 ±	0.0321	0.0000 ±	0.0124
Tl	0.0000 ±	0.0042	0.0000 ±	0.0246	0.0000 ±	0.0312	0.0000 ±	0.0121
Pb	0.0104 ±	0.0120	0.0095 ±	0.0326	0.0332 ±	0.0350	0.0064 ±	0.0161
U	0.0001 ±	0.0041	0.0001 ±	0.0235	0.0026 ±	0.0303	0.0006 ±	0.0117
Sum of Species	±		±		±		±	

Table B-7
Secondary Aerosol Source Profiles (Weight Percent of Mass)

Species[a]	AMSUL: PM$_{2.5}$ and coarse[b] Conc. ± Unc.[c]	AMBSUL: PM$_{2.5}$ and coarse[b] Conc. ± Unc.[c]	AMNIT: PM$_{2.5}$ and coarse[b] Conc. ± Unc.[c]	OC: PM$_{2.5}$ and coarse[b] Conc. ± Unc.[c]
Cl⁻	0.000 ± 0.000	0.000 ± 0.000	0.000 ± 0.000	0.000 ± 0.000
NO$_3^-$	0.000 ± 0.000	0.000 ± 0.000	77.5 ± 7.8	0.000 ± 0.000
SO$_4^=$	72.7 ± 7.3	83.5 ± 8.3	0.000 ± 0.000	0.000 ± 0.000
NH$_4^+$	27.3 ± 2.7	15.7 ± 1.6	22.6 ± 2.3	0.000 ± 0.000
Na$^+$	0.000 ± 0.000	0.000 ± 0.000	0.000 ± 0.000	0.000 ± 0.000
TC	0.000 ± 0.000	0.000 ± 0.000	0.000 ± 0.000	100 ± 10
OC	0.000 ± 0.000	0.000 ± 0.000	0.000 ± 0.000	100 ± 10
EC	0.000 ± 0.000	0.000 ± 0.000	0.000 ± 0.000	0.000 ± 0.000
Na	0.000 ± 0.000	0.000 ± 0.000	0.000 ± 0.000	0.000 ± 0.000
Al	0.000 ± 0.000	0.000 ± 0.000	0.000 ± 0.000	0.000 ± 0.000
Si	0.000 ± 0.000	0.000 ± 0.000	0.000 ± 0.000	0.000 ± 0.000
P	0.000 ± 0.000	0.000 ± 0.000	0.000 ± 0.000	0.000 ± 0.000
S	24.3 ± 2.4	27.9 ± 2.8	0.000 ± 0.000	0.000 ± 0.000
Cl	0.000 ± 0.000	0.000 ± 0.000	0.000 ± 0.000	0.000 ± 0.000
K	0.000 ± 0.000	0.000 ± 0.000	0.000 ± 0.000	0.000 ± 0.000
Ca	0.000 ± 0.000	0.000 ± 0.000	0.000 ± 0.000	0.000 ± 0.000
Ti	0.000 ± 0.000	0.000 ± 0.000	0.000 ± 0.000	0.000 ± 0.000
V	0.000 ± 0.000	0.000 ± 0.000	0.000 ± 0.000	0.000 ± 0.000
Cr	0.000 ± 0.000	0.000 ± 0.000	0.000 ± 0.000	0.000 ± 0.000
Mn	0.000 ± 0.000	0.000 ± 0.000	0.000 ± 0.000	0.000 ± 0.000
Fe	0.000 ± 0.000	0.000 ± 0.000	0.000 ± 0.000	0.000 ± 0.000
Ni	0.000 ± 0.000	0.000 ± 0.000	0.000 ± 0.000	0.000 ± 0.000
Cu	0.000 ± 0.000	0.000 ± 0.000	0.000 ± 0.000	0.000 ± 0.000
Zn	0.000 ± 0.000	0.000 ± 0.000	0.000 ± 0.000	0.000 ± 0.000
As	0.000 ± 0.000	0.000 ± 0.000	0.000 ± 0.000	0.000 ± 0.000
Se	0.000 ± 0.000	0.000 ± 0.000	0.000 ± 0.000	0.000 ± 0.000
Br	0.000 ± 0.000	0.000 ± 0.000	0.000 ± 0.000	0.000 ± 0.000
Sr	0.000 ± 0.000	0.000 ± 0.000	0.000 ± 0.000	0.000 ± 0.000
Mo	0.000 ± 0.000	0.000 ± 0.000	0.000 ± 0.000	0.000 ± 0.000
Cd	0.000 ± 0.000	0.000 ± 0.000	0.000 ± 0.000	0.000 ± 0.000
Sn	0.000 ± 0.000	0.000 ± 0.000	0.000 ± 0.000	0.000 ± 0.000
Sb	0.000 ± 0.000	0.000 ± 0.000	0.000 ± 0.000	0.000 ± 0.000
Ba	0.000 ± 0.000	0.000 ± 0.000	0.000 ± 0.000	0.000 ± 0.000
Hg	0.000 ± 0.000	0.000 ± 0.000	0.000 ± 0.000	0.000 ± 0.000
Pb	0.000 ± 0.000	0.000 ± 0.000	0.000 ± 0.000	0.000 ± 0.000
Sum of Species	100 ± 8	99.1 ± 8.5	100 ± 8	100 ± 10

[a] TC = OC + EC; sum does not include Na$^+$, Cl⁻, S, or TC.

[b] PM$_{10}$ minus PM$_{2.5}$.

[c] Conc. is the average abundance (percent of total mass) for several samples of emissions from the same source type. Unc. is the standard deviation of the abundances for these samples.